

**FIBRE-REINFORCED POLYMER (FRP) FOR SHEAR
REINFORCEMENT IN CONCRETE STRUCTURES**

by

EMILE F. G. SHEHATA

A Dissertation
Submitted to the Faculty of Graduate Studies
in Partial Fulfilment of the
Requirements for the Degree of

DOCTOR OF PHILOSOPHY

Structural Engineering Division
Department of Civil and Geological Engineering
University of Manitoba
Winnipeg, Manitoba

© **March 1999**



National Library
of Canada

Acquisitions and
Bibliographic Services

395 Wellington Street
Ottawa ON K1A 0N4
Canada

Bibliothèque nationale
du Canada

Acquisitions et
services bibliographiques

395, rue Wellington
Ottawa ON K1A 0N4
Canada

Your file Votre référence

Our file Notre référence

The author has granted a non-exclusive licence allowing the National Library of Canada to reproduce, loan, distribute or sell copies of this thesis in microform, paper or electronic formats.

The author retains ownership of the copyright in this thesis. Neither the thesis nor substantial extracts from it may be printed or otherwise reproduced without the author's permission.

L'auteur a accordé une licence non exclusive permettant à la Bibliothèque nationale du Canada de reproduire, prêter, distribuer ou vendre des copies de cette thèse sous la forme de microfiche/film, de reproduction sur papier ou sur format électronique.

L'auteur conserve la propriété du droit d'auteur qui protège cette thèse. Ni la thèse ni des extraits substantiels de celle-ci ne doivent être imprimés ou autrement reproduits sans son autorisation.

0-612-41626-7

Canada

THE UNIVERSITY OF MANITOBA
FACULTY OF GRADUATE STUDIES

COPYRIGHT PERMISSION PAGE

**FIBRE-REINFORCED POLYMER (FRP) FOR SHEAR REINFORCEMENT IN
CONCRETE STRUCTURES**

BY

EMILE F. G. SHEHATA

**A Thesis/Practicum submitted to the Faculty of Graduate Studies of The University
of Manitoba in partial fulfillment of the requirements of the degree
of
DOCTOR OF PHILOSOPHY**

EMILE F. G. SHEHATA ©1999

Permission has been granted to the Library of The University of Manitoba to lend or sell copies of this thesis/practicum, to the National Library of Canada to microfilm this thesis and to lend or sell copies of the film, and to Dissertations Abstracts International to publish an abstract of this thesis/practicum.

The author reserves other publication rights, and neither this thesis/practicum nor extensive extracts from it may be printed or otherwise reproduced without the author's written permission.

ACKNOWLEDGMENTS

The level of appreciation and respect that I feel towards my advisor Dr. Sami Rizkalla of the civil engineering department at the University of Manitoba cannot be expressed in any written form, but will be carried with me for the rest of my life. To him I say: "*I am really grateful, Thank you*".

I would like to thank Prof. B. Pinkney and Prof. C. Wu for serving on his Ph.D. committee. Thanks are extended to Prof. J. Glanville for reviewing the final draft of the thesis. Many thanks go to Prof. A. Nanni from the University of Missouri-Rolla for reviewing the thesis as the external examiner. The support provided by the network of centres of excellence on the Intelligent Sensing for Innovative Structures (ISIS Canada) is greatly acknowledged.

I wish to express my thanks to Messrs. M. McVey and S. Sparrow of the W.R. McQuade Structures Laboratory at the University of Manitoba for their assistance during fabrication and testing of the specimens. Special thanks are also extended to Mr. R. Morphy, Mr. B. Flisak and Mr. G. Hocezk for their assistance during the experimental phase of this study.

The patience and support of my family Irini, Fekry, Laila and Edward cannot be praised enough; to them this thesis is dedicated.

ABSTRACT

Stirrups used for shear reinforcement in concrete members are normally located as an outer reinforcement with respect to the flexural reinforcement and therefore are more susceptible to severe environmental effects because of the minimum concrete cover provided. The use of fibre-reinforced polymer (FRP) reinforcement in concrete structures has increased rapidly over the last ten years. The corrosion-free characteristics and high strength-to-weight ratio of FRP reinforcement significantly increase the service life of structures. Several experimental and analytical research programs have been conducted to investigate the flexural behavior of concrete members reinforced and/or prestressed by FRP reinforcement. The use of FRP as shear reinforcement for concrete structures has not yet been fully explored and the currently available data are insufficient to formulate rational design guidelines. Due to the diagonal nature of shear cracks, the induced tensile forces are typically oriented at an angle with respect to the stirrups and consequently the stirrups' tensile strength in the direction of the fibres cannot be developed. Bending of FRP stirrups to develop sufficient anchorage may also lead to a significant reduction in the strength capacity of the stirrups.

A two-phase experimental program undertaken at the University of Manitoba to examine the structural performance of FRP stirrups as shear reinforcement for concrete structures is reported. The first experimental phase, designed to evaluate the strength capacity of a

single FRP stirrup as influenced by bending of the FRP bars to achieve the appropriate anchorage and by the diagonal shear cracks that have an angle to the direction of the fibres, is described. The variables considered are the type of material, bar diameter, configuration of the stirrup anchorage, embedment length, tail length, and angle of the stirrups. The second experimental phase, including ten large-scale reinforced concrete beams tested to failure to investigate the behavior and contribution of the FRP stirrups in beam action, is also described. The shear deformation, crack width, and stirrup strain are reported. The variables considered are the material type of the stirrups, the material type of the flexural reinforcement, and the stirrup spacing.

An analytical investigation to describe the various factors affecting the strength capacity of FRP stirrups and the shear strength of beams reinforced with FRP is reported. The test results of the experimental program are compared to different analytical models used to predict the shear strength and behavior of the test specimens. Based on the findings of this investigation, design guidelines for concrete beams reinforced with FRP as longitudinal and/or shear reinforcement are proposed. Shear design equations for concrete beams reinforced with FRP using the American Concrete Institute (ACI) and the Canadian Standards Association (CSA) design approaches are proposed. Expressions for the minimum FRP shear reinforcement ratio are also proposed. The reliability of the proposed equations for the ACI and CSA codes is evaluated by comparing the measured and the calculated values of the tested beams and beams tested by others. Strain limits for the FRP stirrups to control the shear crack width in concrete beams are also proposed.

TABLE OF CONTENTS

ACKNOWLEDGMENTS	ii
ABSTRACT	iii
TABLE OF CONTENTS	v
LIST OF TABLES	xiv
LIST OF FIGURES	xvii
NOTATION	xxvii
ABBREVIATIONS	xxx
1. INTRODUCTION	
1.1 GENERAL	1
1.2 OBJECTIVES	3
1.3 SCOPE AND CONTENTS	3
2. SHEAR BEHAVIOR OF CONCRETE BEAMS: BACKGROUND AND REVIEW	
2.1 GENERAL	8
2.1.1 FACTORS AFFECTING SHEAR BEHAVIOUR AND CAPACITY OF CONCRETE BEAMS	9
2.1.2 INTERNAL FORCES IN A BEAM WITH SHEAR REINFORCEMENT	10

2.2 SHEAR REINFORCEMENT	11
2.2.1 ROLE OF SHEAR REINFORCEMENT IN CONCRETE BEAMS	11
2.2.2 ANCHORAGE OF STIRRUPS IN CONCRETE BEAMS	12
2.2.3 “KINKING” OF STIRRUPS AT THE SHEAR CRACK LOCATION	13
2.3 SHEAR MECHANISM IN REINFORCED CONCRETE BEAMS	14
2.3.1 HISTORICAL DEVELOPMENT OF SHEAR MODELS	14
2.3.2 MODIFIED COMPRESSION FIELD THEORY (MCFT)	16
2.3.3 SHEAR FRICTION MODEL (SFM) FOR CONCRETE BEAMS	21
2.4 STIRRUP EFFECTIVENESS	23
2.5 DESIGN PROCEDURES	25
2.5.1 AMERICAN CONCRETE INSTITUTE, ACI 318-95	26
2.5.2 CANADIAN STANDARDS ASSOCIATION, CSA-M23.3-94	27
2.5.2.1 Simplified method	27
2.5.2.2 General method	28
2.5.3 EUROCODE, EC2 PART 1	30
2.5.3.1 Standard method	31
2.5.3.2 Variable strut inclination method	32
2.5.4 BRITISH STANDARD BS8110	32
2.5.5 JAPANESE CODE, JSCE STANDARDS	33
2.6 CONTROL OF SHEAR CRACKING	34
2.6.1 DESIGN CODE APPROACHES	35

2.6.2 CALCULATION OF SHEAR CRACK WIDTH	36
3. SHEAR BEHAVIOR OF CONCRETE BEAMS REINFORCED WITH FRP: BACKGROUND AND REVIEW	
3.1 GENERAL	47
3.1.1 DEFINITION OF FRP	48
3.1.2 GENERAL CHARACTERISTICS OF FRP	49
3.1.3 APPLICATIONS OF FRP IN STRUCTURAL ENGINEERING	50
3.1.4 BEHAVIOUR OF CONCRETE MEMBERS REINFORCED WITH FRP	50
3.1.5 FACTORS AFFECTING SHEAR BEHAVIOUR OF CONCRETE BEAMS REINFORCED WITH FRP	51
3.2 BEHAVIOUR OF FRP AS SHEAR REINFORCEMENT FOR CONCRETE MEMBERS	52
3.2.1 CLASSIFICATION AND FABRICATION OF FRP SHEAR REINFORCEMENT	52
3.2.2 STRENGTH CAPACITY OF FRP STIRRUPS	55
3.2.2.1 Bend effect	55
3.2.2.2 Effect of inclined shear cracks	62
3.2.3 FRP AS SHEAR REINFORCEMENT FOR FLEXURAL MEMBERS	65
3.2.3.1 Open stirrups	66
3.2.3.2 Closed-loop stirrups	67
3.2.3.3 Pre-formed spirals	72
3.2.3.4 On-site fabricated stirrups	77

3.2.3.5 Two-dimensional grids	78
3.2.3.6 FRP diagonal bars	79
3.2.4 ANALYTICAL STUDIES	80
3.2.5 FIELD APPLICATION	87
3.3 BEHAVIOUR OF MEMBERS REINFORCED WITH FRP AS LONGITUDINAL REINFORCEMENT	89
3.3.1 REINFORCED CONCRETE MEMBERS	90
3.3.2 PRESTRESSED CONCRETE MEMBERS	91
3.4 SHEAR TRANSFER	93
3.5 DESIGN CONSIDERATIONS	94
3.5.1 JAPANESE DESIGN GUIDELINES	94
3.5.1.1 JSCE design recommendations	95
3.5.1.2 Building Research Institute (BRI)	100
3.5.2 CANADIAN HIGHWAY BRIDGE DESIGN CODE (CHBDC 1998)	103
3.5.3 EUROCRETE PROJECT	104
3.5.4 COMPARATIVE STUDIES	106
3.6 SUMMARY	107
4. THE EXPERIMENTAL PROGRAM	
4.1 GENERAL	127
4.2 MATERIALS	128

4.2.1 CFRP LEADLINE	129
4.2.2 CFRP CFCC	130
4.2.3 GFRP C-BAR™	131
4.2.4 STEEL	132
4.2.5 CONCRETE	132
4.3 EXPERIMENTAL PHASE I	133
4.3.1 TEST SPECIMENS	134
4.3.1.1 Bend specimens	134
4.3.1.2 Kink specimens	135
4.3.2 TEST SETUP	136
4.3.2.1 Bend specimens	136
4.3.2.2 Kink specimens	137
4.4 PHASE II	137
4.4.1 TEST SPECIMENS	138
4.4.2 FABRICATION OF THE BEAMS	140
4.4.3 TEST SETUP	140
4.4.4 INSTRUMENTATION	141
5. EXPERIMENTAL RESULTS AND ANALYSIS: PHASE I	
 PANEL SPECIMENS	
5.1 GENERAL	165

5.2 BEND CAPACITY	166
5.2.1 CFRP LEADLINE STIRRUPS	167
5.2.2 CFRP CFCC STIRRUPS	168
5.2.3 GFRP C-BAR™ STIRRUPS	169
5.2.4 STEEL STIRRUPS	170
5.3 EFFECT OF BEND RADIUS ON BEND CAPACITY	170
5.4 EFFECT OF EMBEDMENT LENGTH ON FRP STIRRUP CAPACITY	173
5.5 EFFECT OF STIRRUP ANCHORAGE ON FRP STIRRUP CAPACITY	175
5.7 DETAILING OF FRP STIRRUPS	177
5.8 STIRRUP CAPACITY AT CRACK INTERSECTION	178
5.8.1 MODEL “A”: FULL BOND BETWEEN THE FRP STIRRUPS AND THE CONCRETE	178
5.8.2 MODEL “B”: DEBONDING LENGTH AT THE CRACK LOCATION	181
5.9 SUMMARY AND CONCLUSIONS	182
6. EXPERIMENTAL RESULTS AND ANALYSIS: PHASE II	
 BEAM SPECIMENS	
6.1 GENERAL	197
6.2 GENERAL BEHAVIOUR OF BEAM SPECIMENS	198
6.2.1 SHEAR CRACKING LOAD	199

6.2.2 BEAMS REINFORCED WITH STEEL STRANDS FOR FLEXURE	200
6.2.2.1 Control beams	200
6.2.2.2 Beams reinforced with CFRP stirrups	202
6.2.2.3 Beams reinforced with GFRP stirrups	203
6.2.3 BEAMS REINFORCED WITH CFRP STRANDS FOR FLEXURE	204
6.2.3.1 Beam reinforced with CFRP stirrups	204
6.2.3.2 BEAM REINFORCED WITH GFRP STIRRUPS	205
6.2.4 LOAD–DEFLECTION CHARACTERISTICS	205
6.3 FAILURE MODES	206
6.4 CONTRIBUTION OF FRP STIRRUPS	207
6.4.1 STRAIN IN FRP STIRRUPS	207
6.4.2 EFFECTIVENESS OF FRP STIRRUPS	212
6.5 SHEAR CRACKING	213
6.5.1 CRACK PATTERN	213
6.5.2 CRACK WIDTH	215
6.5.3 CRACK WIDTH VERSUS STIRRUP STRAIN	218
6.6 ANALYTICAL PREDICTION	220
6.6.1 SHEAR MODELS IN DESIGN CODES AND GUIDELINES	221
6.6.2 SHEAR FRICTION MODEL (SFM)	223
6.6.2.1 Analysis procedure	223
6.6.2.2 Analysis results and discussion	226

6.6.3 MODIFIED COMPRESSION FIELD THEORY (MCFT)	228
6.6.3.1 Analysis procedure	229
6.6.3.2 Analysis results and discussion	230
6.6.4 ESTIMATION OF SHEAR CRACK WIDTH	233
6.7 SUMMARY	235
7. PROPOSED PROVISION FOR FRP SHEAR REINFORCEMENT OF CONCRETE BEAMS	
7.1 GENERAL	279
7.2 PROPOSED PROVISION BASED ON ACI DESIGN APPROACH	280
7.2.1 BACKGROUND AND BASIC REMARKS	280
7.2.2 AVAILABLE EXPERIMENTAL RESULTS	282
7.2.3 INFLUENCE OF MAJOR FACTORS	284
7.2.3.1 Beams without shear reinforcement	285
7.2.3.2 FRP Stirrups	286
7.2.3.3 Concrete contribution to shear strength of beams reinforced with FRP	287
7.2.4 MAXIMUM SHEAR STRENGTH OF BEAMS REINFORCED WITH FRP	288
7.2.5 PREDICTION OF SHEAR FAILURE MODE	290
7.2.6 MINIMUM SHEAR REINFORCEMENT	291
7.2.7 RELIABILITY OF THE PROPOSED PROVISIONS	293
7.3 PROPOSED PROVISION BASED ON CSA DESIGN APPROACH	295

7.3.1 PROPOSED DESIGN GUIDELINES BASED ON THE SIMPLIFIED METHOD	296
7.3.2 PROPOSED DESIGN GUIDELINES BASED ON THE GENERAL METHOD	297
7.3.3 MINIMUM SHEAR REINFORCEMENT	298
7.3.4 RELIABILITY OF THE PROPOSED PROVISIONS	299
7.4 PROPOSED PROVISION FOR SERVICEABILITY REQUIREMENT	301
7.5 DESIGN EXAMPLE	304
8. SUMMARY AND CONCLUSIONS	
8.1 SUMMARY	329
8.2 CONCLUSIONS	331
8.2.1 STRENGTH OF A SINGLE FRP STIRRUP	332
8.2.2 BEHAVIOUR OF FRP STIRRUPS IN BEAM ACTION	334
8.2.3 ANALYSIS OF BEAM SPECIMENS	336
8.2.4 DESIGN GUIDELINES	337
8.3 RECOMMENDATIONS FOR FUTURE WORK	339
REFERENCES	340
APPENDIX A	354
APPENDIX B	360
APPENDIX C	367
APPENDIX D	375

LIST OF TABLES

Chapter 3

3-1. Characteristics of beams tested by Vijay <i>et al.</i> (1996)	109
3-2. Characteristics of beams tested by Alsayed <i>et al.</i> (1996)	110
3-3. Characteristics of beams tested by Alsayed <i>et al.</i> (1997)	110
3-4. Characteristics of beams tested by Zhao <i>et al.</i> (1995)	111
3-5. Characteristics of beams tested by Duranovi <i>et al.</i> (1997)	111
3-6. Characteristics of beams tested by Yonekura <i>et al.</i> (1993)	112
3-7. Characteristics of beams tested by Nagasaka <i>et al.</i> (1993)	112
3-8. Characteristics of beams tested by Tottori <i>et al.</i> (1993)	114
3-9. Characteristics of beams tested by Nakamura <i>et al.</i> (1995)	116

Chapter 4

4-1. Properties of FRP and steel bars used in the experimental program	143
4-2. Dimensions of stirrups used in the experimental program	143
4-3. Details of bend specimens: CFRP Leadline stirrups	144
4-4. Details of bend specimens: CFRP CFCC stirrups	145
4-5. Details of bend specimens: GFRP C-BAR TM stirrups	146
4-6. Details of bend specimens: steel stirrups	146
4-7. Details of kink specimens	147

4-8. Details of beam specimens	148
--------------------------------	-----

Chapter 5

5-1. Test results of bend specimens: CFRP Leadline stirrups	184
5-2. Test results of bend specimens: CFRP CFCC stirrups	185
(a) $d_b = 5$ mm (7-wire)	
(b) $d_b = 5$ mm (single wire)	
(c) $d_b = 7.5$ mm (7-wire)	
5-3. Test results of bend specimens: GFRP C-BAR TM stirrups	186
5-4. Test results of bend specimens: steel stirrups	186
5-5. Test results of kink specimens	187

Chapter 6

6-1. Test results of beam specimens	236
6-2. Measured versus calculated ultimate shear stress for beams tested in experimental phase II	237
6-3. Shear friction analysis of tested beams	238

Chapter 7

7-1. Basic data for 20 test beams reinforced with FRP bars for flexure and having no shear reinforcement	305
7-2. Basic data for 72 test beams reinforced with FRP bars for flexure and FRP stirrups for shear	306

7-3.	Basic data for 28 test beams reinforced with FRP stirrups for shear and steel bars for flexure	308
7-4.	Basic data for 6 test beams reinforced with FRP bars for flexure and steel stirrups for shear	308
7-5.	Measured and calculated ultimate shear stress for Group B beams, reinforced with FRP bars for flexure and FRP stirrups for shear	309
7-6.	Measured and calculated ultimate shear stress for Group C beams, reinforced with FRP stirrups for shear and steel bars for flexure	311
7-7.	Comparison between measured, v_{test} , and calculated, v_n , shear strength for Group B beams, reinforced with FRP bars for flexure and FRP stirrups for shear	312
7-8.	Comparison between measured, v_{test} , and calculated, v_n , shear strength for Group C beams, reinforced with FRP stirrups for shear and steel bars for flexure	312
7-9.	Measured and calculated ultimate shear stress for Group B beams - CSA design approaches	313
7-10.	Measured and calculated ultimate shear stress for Group C beams – CSA design approaches	315
7-11.	Comparison between measured, v_{test} , and calculated, v_n , shear strength for Group B beams – CSA and CHBDC approaches	316
7-12.	Comparison between measured, v_{test} , and calculated, v_n , shear strength for Group C beams – CSA and CHBDC approaches	316

LIST OF FIGURES

Chapter 1

- 1-1. Definition of the problem 7

Chapter 2

- 2-1. Internal forces in a cracked beam with stirrups (ASCE-ACI committee 426 - 1973) 38
- (a) Shear resisting mechanism
 - (b) Applied shear versus internal resisting shear
- 2-2. Average stress–strain relationships of mild steel bars 39
(Pang and Hsu 1995)
- 2-3. Truss model for shear in a beam panel 40
- (a) Truss Analogy
 - (b) Equilibrium for shear
 - (c) Vertical equilibrium
- 2-4. Aspects of modified compression field theory
(Collins and Mitchell 1991)
- (a) Equilibrium in terms of average stresses 41
 - (b) Equilibrium in terms of local stresses at a crack 41
 - (c) Compatibility relationships 41
 - (d) Stress–strain relationships for reinforcement 42
 - (e) Stress–strain relationships for cracked concrete in compression 42
 - (f) Stress–strain relationships for cracked concrete in tension 42
- 2-5. Modified compression field theory for a concrete beam 43
- 2-6. Different solution techniques for the MCFT modeling 44
of a beam section subjected to shear and moment
- (a) Detailed analysis
 - (b) More direct procedure

2-7.	Shear friction model in a concrete beam (Loov 1998)	44
2-8.	Values of β and θ for sections with shear reinforcement (CSA23.3-1994 general method)	45
2-9.	Values of β and θ for sections without shear reinforcement (CSA23.3-1994 general method)	46

Chapter 3

3-1.	Stress–strain relationships for typical FRP and steel shear reinforcement	117
3-2.	Different configurations of FRP shear reinforcement	117
3-3.	Photomicrograph photo of a bent fibre	118
3-4.	Test setup by Maruyama <i>et al.</i> (1993)	118
3-5.	Details of specimens by Currier <i>et al.</i> (1994)	119
3-6.	Details of specimens by Ehsani <i>et al.</i> (1995)	119
3-7.	Model of bent bar in concrete by Nakamura and Higai (1995)	120
3-8.	Test setup by Ueda <i>et al.</i> (1995)	120
3-9.	Details of specimens and test setup by Maruyama <i>et al.</i> (1989)	121
3-10.	Test setup by Kanemastu <i>et al.</i> (1993)	121
3-11.	Details of specimens by Zhao <i>et al.</i> (1995)	122
3-12.	Model of stirrup strain distribution by Zhao <i>et al.</i> (1995)	122
3-13.	Details of specimens by Yonekura <i>et al.</i> (1993)	123
3-14.	Outline of specimens and test setup by Nagasaka <i>et al.</i> (1993)	123
3-15.	CFRP grids used by Erki and Bakht (1996)	124
3-16.	Details of specimens and test setup by Sonobe <i>et al.</i> (1995)	124
3-17.	Shear resisting model by Sato <i>et al.</i> (1995)	125
3-18.	Schematic diagram of Lattice Model (Choi <i>et al.</i> 1997)	125
3-19.	Cross-section of the Taylor bridge girders (Rizkalla <i>et al.</i> 1998)	126

Chapter 4

4-1.	Carbon and Glass FRP bars used for the stirrups	149
------	---	-----

4-2.	Stress–strain relationships of reinforcing bars used as stirrups in this program	149
4-3.	Configuration of stirrups used in the experimental program	150
4-4.	Stress–strain diagrams of different batches of concrete	151
4-5.	Details of bend specimens	151
4-6.	Details of kink specimens	152
4-7.	Description of the direct shear test setup	152
4-8.	Test setup: bend specimens	153
4-9.	Test setup: kink specimens	153
4-10.	Details of beam specimens	154
4-11.	Configuration of FRP stirrups used in beam specimens	154
4-12.	Casting bed for beam specimens	155
4-13.	Test setup of beam specimens	155
4-14.	Instrumentation of beam SN-0	
	(a) Location of strain gauges	156
	(b) Location of PI and demec gauges	157
4-15.	Instrumentation of beam SS-2, SC-2 and SG-2	
	(a) Location of strain gauges	158
	(b) Location of PI and demec gauges	159
4-16.	Instrumentation of beam SC-3, SG-3, CC-3 and CG-3	
	(a) Location of strain gauges	160
	(b) Location of PI and demec gauges	161
4-17.	Instrumentation of beam SC-4 and SG-4	
	(a) Location of strain gauges	162
	(b) Location of PI and demec gauges	163
4-18.	Instrumentation for shear cracks and deformation	164
 Chapter 5		
5-1.	Failure modes of bend specimens	188
5-2.	Failure at the bend - CFRP Leadline stirrups	188

5-3.	Failure at the bend - CFRP CFCC stirrups	189
5-4.	Failure of GFRP C-BAR TM stirrups due to “waving” of fibres	189
5-5.	Effect of bend radius, r_b , on strength capacity of the bend, f_{bend}	190
	(a) Test results versus equations proposed by JSCE (1997)	
	(b) Test results versus equations proposed by Nakamura and Higai (1995; Eq. 5-3) and Ishihara <i>et al.</i> (1997; Eq. 5-4)	
5-6.	Effect of embedment length, l_d , on capacity of CFRP CFCC stirrups	191
5-7.	Effect of embedment length, l_d , on capacity of CFRP Leadline stirrups	191
5-8.	Effect of embedment length, l_d , on capacity of GFRP C-BAR TM stirrups	192
5-9.	Effect of tail length, l_d^* , on bend capacity of CFRP Leadline stirrups	192
5-10.	Effect of tail length l_d^* on capacity of CFRP CFCC stirrups	193
5-11.	Detailing of FRP stirrups	193
5-12.	Kink specimens - Modelling of load transfer	194
	(a) Model “A” : assuming Full bond between stirrups and concrete	
	(b) Model “B” : assuming long debonding length at crack location	
5-13.	Effect of stirrup angle θ on capacity of FRP stirrups subject to combined shear and tension - Model “A”	195
	(a) Test results versus available equations in the literature	
	(b) Test results versus proposed equations	
5-14.	Effect of stirrup angle, θ , on capacity of FRP stirrups	196
	(a) Stress in FRP stirrups at failure based on Model “B”	
	(b) Observed strain in FRP stirrups at failure, ε_{fr}	

Chapter 6

6-1.	Typical shear versus strain in FRP stirrups: beam specimens	240
6-2.	Typical shear versus average strains in the web: beam specimens	240
6-3.	Typical shear versus top strain in the shear span: beam specimens	241

6-4.	Shear cracking of beam SN-0	242
6-5.	Beam SN-0 at failure	242
6-6.	Shear cracking of beam SS-2	243
6-7.	Beam SS-2 at failure	243
6-8.	Shear cracking of beam SC-2	244
6-9.	Beam SC-2 at failure	244
6-10.	Shear cracking of beam SC-3	245
6-11.	Beam SC-3 at failure	245
6-12.	Shear cracking of beam SC-4	246
6-13.	Beam SC-4 at failure	246
6-14.	Shear cracking of beam SG-2	247
6-15.	Beam SG-2 at failure	247
6-16.	Shear cracking of beam SG-3	248
6-17.	Beam SG-3 at failure	248
6-18.	Shear cracking of beam SG-4	249
6-19.	Beam SG-4 at failure	249
6-20.	Shear cracking of beam CC-3	250
6-21.	Beam CC-3 at failure	250
6-22.	Shear cracking of beam CG-3	251
6-23.	Beam CG-3 at failure	251
6-24.	Load–deflection relationships: beam specimens	252
	(a) Applied load versus deflection measured at midspan	
	(b) Applied load versus deflection measured at loading point	
6-25.	Applied shear versus average strain in stirrups: beams reinforced with CFRP stirrups	253
6-26.	Applied shear versus average strain in stirrups: beams reinforced with GFRP stirrups	253
6-27.	Shear reinforcement ratio versus stirrup strain at applied shear, $V = 175$ kN	254
6-28.	Effect of flexural reinforcement on average strain in FRP stirrups	255

(a) Beams reinforced with CFRP stirrups	
(b) Beams reinforced with GFRP stirrups	
6-29. Characteristic stirrup stress $\rho_{fv} f_{fv}$ versus stirrup strain: beam specimens	256
(a) stirrup spacing = $d/2$	
(b) stirrup spacing = $d/3$	
(c) stirrup spacing = $d/4$	
6-30. Applied shear versus shear resisting components: beams with stirrup spacing = $d/2$	257
6-31. Applied shear versus shear resisting components: beams with stirrup spacing = $d/3$	257
6-32. Applied shear versus shear resisting components: beams with stirrup spacing = $d/4$	258
6-33. Effect of flexural reinforcement on shear resisting components	259
(a) Beams reinforced with CFRP stirrups	
(b) Beams reinforced with GFRP stirrups	
6-34. Effect of stirrup spacing on effective capacity of FRP stirrups	260
6-35. Determination of shear crack width	261
6-36. Applied shear versus crack width: beams reinforced with CFRP stirrups	261
6-37. Applied shear versus crack width: beams reinforced with GFRP stirrups	262
6-38. Applied shear versus crack width: beams reinforced with stirrups spaced at $d/2$	262
6-39. Effect of flexural reinforcement on shear crack width: beam specimens	263
(a) Beams reinforced with CFRP stirrups	
(b) Beams reinforced with GFRP stirrups	
6-40. Shear crack width versus average strain in stirrups: beams reinforced with CFRP stirrups	264

6-41.	Shear crack width versus average strain in stirrups: beams reinforced with CFRP stirrups	264
6-42.	Effect of stirrup material on shear crack width	265
6-43.	Effect of elastic modulus of reinforcing bar on crack width	265
6-44.	Measured ultimate shear stress versus calculated from: (a) ACI318-95 Code (1995), (b) JSCE model (1997), (c) BRI model (1997), (d) CHBDC Code (1998), and (e) Eurocrete model (1996); for tested beams	266
6-45.	Potential failure planes in beams analyzed using shear friction model (SFM)	
	(a) Beam SN-0	267
	(b) Beam SS-2	267
	(c) Beam SC-2	267
	(d) Beam SC-3	268
	(e) Beam SC-4	268
	(f) Beam SG-2	268
	(g) Beam SG-3	269
	(h) Beam SG-4	269
	(i) Beam CC-3	269
	(j) Beam CG-3	270
6-46.	Internal forces at a potential failure plane: SFM	270
6-47.	Measured shear strength versus calculated using the SFM for beams reinforced with steel strands	271
6-48.	Effect of stirrup spacing on effective capacity of FRP stirrups in beam action - Measured versus SFM	271
6-49.	Measured shear strength versus calculated using the SFM for beams reinforced with CFRP strands	272
6-50.	Stress–strain relationships used to model the longitudinal reinforcement for the Modified compression field theory (MCFT)	272

6-51.	Stress–strain relationships used to model the shear reinforcement for the MCFT	273
6-52.	Modelling of the beam section as three concrete layers for the MCFT	273
6-53.	Shear versus average strain in stirrups as predicted using MCFT for beam SS-2	274
6-54.	Shear versus average strain in stirrups as predicted using MCFT for beam SC-2	274
6-55.	Shear versus average strain in stirrups as predicted using MCFT for beam SC-3	275
6-56.	Shear versus average strain in stirrups as predicted using MCFT for beam SC-4	275
6-57.	Shear versus average strain in stirrups as predicted using MCFT for beam CC-3	276
6-58.	Measured shear strength versus calculated using the MCFT for beams reinforced with steel or CFRP stirrups	276
6-59.	Effect of stirrup spacing on effective capacity of CFRP stirrups in beam action: Measured versus MCFT	277
6-60.	Measured versus predicted shear crack width for beam SS-2	277
6-61.	Measured versus predicted shear crack width for beam SC-3	278
6-62.	Measured versus predicted shear crack width for beam SG-3	278

Chapter 7

7-1.	Effect of FRP longitudinal reinforcement on shear strength of beams without shear reinforcement	317
	(a) effect of $\rho_f E_f / E_s$	
	(b) effect of E_f / E_s	
7-2.	Effective stirrup stress at ultimate in beams reinforced with FRP stirrups	318
	(a) variation with $\rho_{fv} f_{fv}$	

	(b) variation with $\rho_{fv}(E_{fv}/E_s)$	
7-3.	Evaluation of concrete contribution to the shear strength of beams reinforced with FRP	319
	(a) based on average stirrup contribution	
	(b) based on safe stirrup contribution	
7-4.	Shear strength of beams reinforced with FRP and governed by shear-compression mode of failure	320
	(a) effect of E_{fl}	
	(b) effect of E_{fv}	
7-5.	Shear-rupture failure versus shear-compression failure	321
7-6.	Requirement of minimum shear reinforcement: ACI approach	322
	(a) diagonal tension cracking stress versus measured shear capacity	
	(b) proposed ρ_{fvmin} versus provided ρ_{fv}	
7-7.	Measured ultimate shear stress versus calculated from:	323
	(a) Proposed Design equations (7-10) and (7-13),	
	(b) ACI318-95 Code (1995), (c) JSCE method 1 (1997),	
	(d) BRI method (1997), (e) CHBDC Code (1998), and	
	(f) Eurocrete project (1996); for beams reinforced with FRP for shear and flexure and tested by many researchers	
7-8.	Measured ultimate shear stress versus calculated from:	324
	(a) Proposed Design equations (7-10) and (7-13),	
	(b) ACI318-95 Code (1995), (c) JSCE method 1 (1997),	
	(d) BRI method (1997), (e) CHBDC Code (1998), and	
	(f) Eurocrete project (1996); for beams reinforced with FRP for shear and steel for flexure and tested by many researchers	
7-9.	Requirement of minimum shear reinforcement: CSA approach	325
	(a) diagonal tension cracking stress versus measured shear capacity	
	(b) proposed ρ_{fvmin} versus provided ρ_{fv}	
7-10.	Measured ultimate shear stress versus calculated from proposed design equations based on:	326

(a) the simplified method in the CSA23.3-94 code (equation 7-18), and (b) the general method in the CSA23.3-94 code (equation 7-21); for beams reinforced with FRP for shear and flexure and tested by many researchers	
7-11. Measured ultimate shear stress versus calculated from proposed design equations based on:	327
(a) the simplified method in the CSA23.3-94 code (equation 7-18), and (b) the general method in the CSA23.3-94 code (equation 7-21); for beams reinforced with FRP for shear and steel for flexure and tested by many researchers	
7-12. Serviceability requirement: shear crack width versus average strain in stirrups	328
 Appendix A	
A-1. Potential failure planes for beam SC-3	359
A-2. Internal forces for potential failure plane 2	359
A-3. Internal forces for potential failure plane 3	359
 Appendix C	
C-1. Measured versus predicted shear crack width for beam SS-2	370
C-2. Measured versus predicted shear crack width for beam SC-2	370
C-3. Measured versus predicted shear crack width for beam SC-3	371
C-4. Measured versus predicted shear crack width for beam SC-4	371
C-5. Measured versus predicted shear crack width for beam SG-2	372
C-6. Measured versus predicted shear crack width for beam SG-3	372
C-7. Measured versus predicted shear crack width for beam SG-4	373
C-8. Measured versus predicted shear crack width for beam CC-3	373
C-9. Measured versus predicted shear crack width for beam CG-3	374
 Appendix D	
D-1. Dimensions and details of the beam	382

NOTATION

a	= shear span
a/d	= shear span-to-depth ratio, equivalent to $(M_u/V_u d)$
A_l	= cross sectional area of longitudinal reinforcement
A_v	= total cross sectional area of stirrup within distance s
A_{fl}	= cross sectional area of FRP longitudinal reinforcement
A_{fv}	= total cross sectional area of FRP stirrup within distance s
b_w	= web width of the beam
d	= effective depth of cross-section
d_a	= maximum aggregate size
d_b	= diameter of the reinforcing bar
d_e	= effective bar diameter, $\sqrt{4A_b / \pi}$
E_s	= reference elastic modulus of steel, 200 GPa
E_{fv}	= elastic modulus of FRP shear reinforcement
E_{fl}	= elastic modulus of FRP longitudinal reinforcement
f_{bend}	= strength capacity of the bend portion of the FRP stirrup
f_c'	= concrete compressive strength
f_{fu}	= guaranteed tensile strength of the FRP parallel to the fibres
f_{fuw}	= guaranteed tensile strength of the FRP stirrups parallel to the fibres
f_{syv}	= yield strength of steel stirrups
f_{fv}	= effective stress in the FRP stirrups at ultimate load
h	= overall depth of the beam cross-section
h_b	= height of the FRP bar ($h_b = d_b$ for round bar)
jd	= shear depth, defined as the distance between the compressive force and tensile force acting on the cross-section
l_d	= embedment of the bend portion of the FRP stirrup
l_d^*	= tail length beyond the bend portion of the FRP stirrup

M_o	=	the decompression moment
M_u	=	moment corresponding to ultimate shear capacity
s	=	spacing of the shear reinforcement
s_z	=	crack-spacing parameter for members without shear reinforcement (CSA Standards)
$s_{mx}, s_{mv}, s_{m\theta}$	=	crack spacing in longitudinal, transverse and inclined directions, respectively
V_{ay}	=	shear component resisted by the aggregate interlock along the shear crack
V_c	=	shear-resisting force provided by concrete
$V_{c(aci)}$	=	shear-resisting force provided by concrete, as determined using ACI equation
V_{cf}	=	shear-resisting force provided by concrete in beams reinforced with FRP for flexure
V_{cr}	=	shear force at diagonal tension cracking
V_{cz}	=	shear component resisted by the compression zone
V_{dl}	=	shear component resisted by the dowel action of longitudinal reinforcement
V_s	=	shear-resisting force provided by steel stirrups
V_{sf}	=	shear-resisting force provided by FRP stirrups
V_n	=	nominal shear strength
V_{test}	=	measured shear strength based on test results
V_u	=	factored shear force due to applied loads
v	=	shear stress, $V/b_w d$
w	=	crack width
α_s	=	angle of the stirrups with the longitudinal axis of the beam
β	=	strength factor used to determine V_c in the CSA general method
γ_b	=	member safety factor

ε_{fv}	=	strain in FRP shear reinforcement at ultimate
ϕ	=	strength reduction factor
$\phi_c, \phi_s (\gamma_c, \gamma_s)$	=	resistance safety factors for concrete and steel, respectively
ϕ_f	=	strength reduction factor for shear design of members reinforced with FRP
λ	=	1.0 for normal weight concrete (CSA Standards)
ρ_v	=	shear reinforcement ratio, $A_v/b_w s$
ρ_{fv}	=	FRP shear reinforcement ratio, $A_{fv}/b_w s$
$\rho_{fv_{min}}$	=	minimum FRP shear reinforcement
ρ_l	=	longitudinal reinforcement ratio, $A_l/b_w d$
ρ_{fl}	=	FRP longitudinal reinforcement ratio, $A_{fl}/b_w d$
ρ_v'	=	$\rho_{fv} (E_{fv}/E_s)$ = ratio of the shear reinforcement, modified by the elastic modulus ratio
ρ_l'	=	$\rho_{fl} (E_{fl}/E_s)$ = ratio of the flexural reinforcement, modified by the elastic modulus ratio
θ	=	angle of the shear crack with the longitudinal axis of the beam
χ	=	strength reduction factor for FRP stirrups
σ_N	=	average axial compressive stress on the beam section

ABBREVIATIONS

AIJ	Architectural Institute of Japan
ACI	American Concrete Institute
ASCE	American Society of Civil Engineers
ASTM	American Society for Testing and Materials
BRI	Building Research Institute in Japan
BS	British Standards
CFCC	carbon fibre composite cable
CFRP	carbon fibre-reinforced polymer
CFT	compression field theory
CHBDC	Canadian Highway Bridge Design Code
CSA	Canadian Standards Association
FA-STM	fixed-angle softening truss model
FRP	fibre-reinforced polymer
GFRP	glass fibre-reinforced polymer
JSCE	Japanese Society of Civil Engineers
MCFT	modified compression field theory
NS	Norwegian Standards
RA-STM	rotating-angle softening truss model
SFM	shear friction model

Chapter

1

Introduction

1.1 General

Deterioration of concrete structures due to the corrosion of steel reinforcement has led to the need for an alternative type of reinforcement such as fibre-reinforced-polymer (FRP) reinforcement. Stirrups used for shear reinforcement are normally located as an outer reinforcement with respect to the flexural reinforcement and therefore are more susceptible to severe environmental effects because of the minimum concrete cover provided. FRPs are corrosion-free materials and have recently been used as reinforcement to avoid the deterioration of concrete structures caused by corrosion of steel reinforcement.

Use of FRP as reinforcement for concrete structures has increased rapidly over the last ten years. FRP reinforcement is made from high-tensile-strength fibres such as carbon, glass, aramid and others embedded in polymeric matrices and produced in the form of bars, strands, ropes, tendons and grids, in a wide variety of shapes and characteristics. FRP reinforcement is used as prestressed, non-prestressed and shear reinforcement for concrete structures. Several experimental and analytical research programs have been conducted to investigate the flexural behaviour of concrete members reinforced and/or

prestressed by FRP reinforcement. The use of FRP as shear reinforcement for concrete structures has not yet been fully explored and the currently available data are not sufficient to formulate rational design guidelines.

Since FRP reinforcement is characterized by a linearly elastic stress–strain relationship up to failure, shear failure of reinforced concrete members will occur due either to rupture of FRP stirrups or to crushing of concrete in the compression zone or in the web. Failure due to rupture of FRP stirrups will occur suddenly when one or more FRP stirrups reach their strength capacity. This type of shear failure is brittle when compared to that of a beam reinforced with steel stirrups. The other mode of failure, shear-compression failure, occurs when the diagonal shear cracks propagate towards the compression chord, reducing the depth of the compression zone and causing crushing of the concrete. Such a mode of failure is much more comparable to that of a concrete beam with steel stirrups. Concrete members reinforced with steel stirrups are normally designed for shear to allow yielding of the steel stirrups before crushing of concrete.

Due to the diagonal nature of shear cracks, the induced tensile forces are typically oriented at an angle with respect to the stirrups (Figure 1-1, kink effect) and consequently the stirrups' tensile strength in the direction of the fibres may not be developed. Bending of FRP stirrups to develop sufficient anchorage (Figure 1-1, bend effect) may also lead to a significant reduction in the strength capacity of the stirrups.

1.2 Objectives

The main objective of this investigation is to examine the structural performance of FRP stirrups as shear reinforcement for concrete structures. The various specific objectives are:

1. To evaluate the strength capacity of a single FRP stirrup as influenced by:
 - i- Bending of the FRP bars to achieve the appropriate anchorage (bend effect)
 - ii- The effect of the diagonal shear cracks at an angle to the direction of the fibres (kink effect)
2. To evaluate the contribution of the FRP stirrups to the shear resisting mechanism of concrete beams.
3. To investigate the modes of failure and the shear strength of concrete beams reinforced with FRP as shear and/or longitudinal reinforcement.
4. To examine the shear cracking behaviour of concrete beams reinforced with FRP
5. To study the influence of FRP longitudinal reinforcement on the shear strength and cracking behaviour of concrete beams.
6. To propose design guidelines for the shear design of concrete members reinforced with FRP.

1.3 Scope and Contents

This study comprises experimental and analytical investigations. Based on the findings of the investigations, design guidelines are proposed to predict the shear strength of concrete beams reinforced with FRP. Equations are also proposed to control the shear

crack width in concrete beams reinforced with FRP. Each part of this study is discussed briefly in the following subsections:

Experimental Investigation: The experimental program consisted of two phases. The first experimental phase, Phase I, was designed to evaluate the strength capacity of a single FRP stirrup as influenced by bending of the FRP bars to achieve the appropriate anchorage and by the diagonal shear cracks, which are at an angle to the direction of the fibres (Figure 1-1). Ninety-three specially designed panel specimens were tested to investigate the bend effect, and twelve specially designed panel specimens were tested to investigate the kink effect. The second experimental phase, Phase II, included ten large-scale reinforced concrete beams tested to failure to investigate the modes of failure and the contribution of the FRP stirrups in the beam action mechanism. The beam specimens were designed to fail in shear without premature failure due to bond.

Analytical Modelling: This part of the investigation included analysis of the test results to describe the various factors affecting the strength capacity of the FRP stirrups. The test results of the first experimental phase were compared to different equations from the literature to evaluate the strength capacity of a single FRP stirrup as influenced by the bend and kink effects. The results of the second experimental phase were compared to different analytical models used to predict the shear strength and behaviour of reinforced concrete beams.

Design Guidelines: Based on the results for the beams tested in this study and an additional 118 beams tested by others, design guidelines are proposed for the use of FRP as shear reinforcement in concrete structures. The design guidelines cover the ultimate and serviceability limit states for concrete beams reinforced with FRP. The proposed shear provisions are provided in a convenient format for the current development of design codes for concrete members reinforced with FRP.

The following is a brief description of the contents of the thesis:

Chapter 2: This chapter presents the currently available theories for prediction of the shear behaviour and strength of concrete beams reinforced with steel. The Canadian, American, European and Japanese design approaches for shear are also presented.

Chapter 3: This chapter presents the available literature on the behaviour of FRP stirrups in concrete members. The available design guidelines for concrete members reinforced with FRP, proposed by Japanese, Canadian and European task committees are also presented.

Chapter 4: This chapter describes the experimental program conducted at the University of Manitoba to test 113 specially designed panel specimens and ten concrete beams reinforced with FRP.

Chapter 5: This chapter presents the test results and analysis for the panel specimens. Test results are compared to equations available in the literature. Design guidelines for the detailing and the strength capacity of a single FRP stirrup are presented.

Chapter 6: This chapter presents the test results and analysis for the beam specimens. The behaviour of concrete beams reinforced with FRP, in terms of FRP stirrups' contribution, modes of failure and shear cracking, are described in this chapter. Test results of the beam specimens are compared to different shear models. Recommendations are given for the analysis of concrete beams reinforced with FRP using the currently available shear theories. A simple equation is proposed to predict the shear crack width in concrete beams reinforced with FRP stirrups.

Chapter 7: This chapter presents design guidelines for the use of FRP as shear reinforcement in concrete structures. The proposed provisions are based on the design approaches in the current ACI318 and CSA23.3 codes for concrete members reinforced with steel. The chapter also proposes strain limits for the FRP stirrups to control the shear crack width in concrete beams.

Chapter 8: A summary of this investigation is given. Several conclusions are introduced to give an understanding of the behaviour of concrete members reinforced with FRP. The design guidelines for concrete members reinforced with FRP proposed in this investigation are summarized in this chapter.

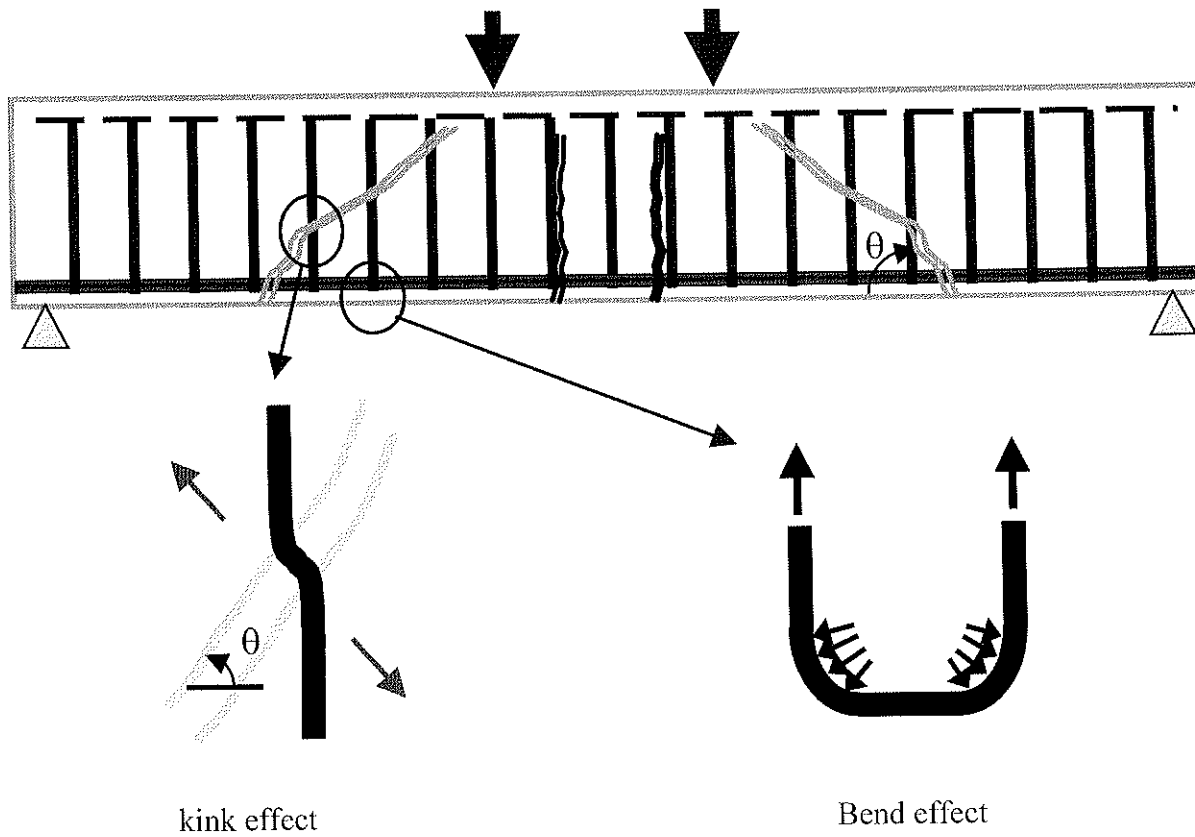


Figure 1-1. Definition of the problem

Chapter 2

Shear Behaviour of Concrete Beams: Background and Review¹

2.1 General

The flexural behaviour of reinforced and prestressed concrete members has been extensively researched and rationalized into simple equilibrium and compatibility equations in most of the current codes. However, the shear mechanism is not well defined and is considered to be one of the most complex mechanisms for rationalization into a simple model. Several models are introduced by different codes using several assumptions related to the material properties and the internal mechanism.

In general, shear failure of reinforced and prestressed concrete members is catastrophic in nature, and therefore a considerable margin of safety is typically used. In spite of many decades of experimental research and the use of highly sophisticated analytical tools, shear failure is not yet fully understood. Shear transfer in concrete beams relies heavily on the tensile and compressive strength of the concrete. Thus, it is not surprising that a failure due to shear in general is brittle. Furthermore, if shear reinforcement is not appropriately provided for reinforced or prestressed concrete beams, shear failure is

¹ All equations in chapter 2 use metric units (Newton, mm) unless otherwise specified

likely to occur suddenly, and without advance warning of distress. Therefore, concrete beams are generally reinforced with shear reinforcement to ensure that flexural failure will occur before shear failure in case of overloading conditions to ensure ductile failure.

The literature on shear behaviour of concrete beams is very extensive as it dates from the beginning of this century. Thus, it is beyond the scope of this study to encompass all preceding works related to this topic. A comprehensive review is provided by the ASCE-ACI Task Committee 426 (1973).

This chapter focuses on the role of and requirements for steel shear reinforcement in concrete members as well as new theoretical concepts that have been recently introduced to describe the shear mechanism of reinforced or prestressed concrete beams. Shear provisions in the Canadian Standard CSA A23.3-94, the American Concrete Institute Building Code ACI 318-95, Eurocode EC2 (1992), the British Standard BS8110 (1985) and the Japanese Standards JSCE (1996) are briefly reviewed to provide a bench mark to evaluate the effectiveness of the shear reinforcement in concrete members. This chapter is focussed on steel stirrups. The literature on the use of FRP as shear reinforcement is discussed in chapter 3.

2.1.1 Factors affecting shear behaviour and capacity of concrete beams

It is known that the shear behaviour and capacity of concrete beams are affected by the following parameters:

1. the shear span-to-depth ratio, a/d , which affects the shear capacity and shear mode of failure;
2. the compressive strength of the concrete, f_c' ;

3. the longitudinal reinforcement ratio, ρ_{sl} , which refers to the dowel component of the concrete contribution, V_c , and controls the opening of the flexural shear cracks
4. the shear reinforcement ratio, ρ_{sv} , which introduces the shear component, V_s , and also affects the concrete contribution, V_c ;
5. the type of loading, that affects the crack distribution in the shear-critical zones;
6. size effect of the beam cross-section: It was observed that as the beam depth increases, the ultimate shear stress reduces as a result of the increase in the dissipated fracture energy; and
7. the magnitude of effective prestressed force and the vertical component of draped tendons.

2.1.2 Internal forces in a beam with shear reinforcement

Inclined cracking may reduce the strength capacity of concrete beams; therefore, concrete beams should be reinforced with stirrups to ensure the full development of the flexural capacity. The internal forces in a typical concrete beam with steel stirrups intersecting an inclined crack are shown in Figure 2-1a. Shear is transferred across line A-B-C through the shear in the compression zone, V_{cz} , the vertical component of the shear transferred across the crack by interlock of the aggregate particles on the two faces of the crack, V_{ay} , the dowel action of the longitudinal reinforcement, V_{dl} , and the shear transferred by tension in the stirrups, V_s . The loading history of such a beam is shown qualitatively in Figure 2-1b. The components of the internal shear resistance must equal the applied shear as indicated by the upper 45° line. Prior to flexural cracking, all shear is carried by the uncracked concrete. After initiation of the flexural cracks and prior to initiation of

inclined shear cracking, the external shear is resisted by the concrete components; V_{cz} , V_{ay} , and V_{dl} . After initiation of inclined shear cracks, the external shear is resisted by the concrete, V_c , and the stirrups, V_s , as shown in Figure 2-1b. Eventually, the stirrups crossing the crack yield, and V_s remains constant for higher applied shears. Once the stirrups yield, the inclined cracks open rapidly. As the inclined crack widens, V_{ay} decreases further, forcing V_{dl} and V_{cz} to increase at an accelerated rate until either a splitting (dowel) failure occurs, or the compression zone crushes due to combined shear and compression. Another possible failure may occur by rupture of the stirrups when stirrups with low strain at ultimate are used.

Each of the shear resisting components of this process except V_s has a brittle load–deformation response. As a result, it is difficult to quantify the contributions of V_{cz} , V_{dl} , and V_{ay} at ultimate. In design, these are lumped together in V_c , referred to as “the shear carried by the concrete”. Thus the nominal strength, V_n , is assumed to be

$$V_n = V_c + V_s \quad (2-1)$$

Traditionally in North American design practice, V_c is taken equal to the shear force at the initiation of inclined shear cracking, V_{cr} .

2.2 Shear reinforcement

2.2.1 Role of shear reinforcement in concrete beams

Shear reinforcement in the form of stirrups contributes to the strength of the shear mechanisms by the following means:

1. Improving the contribution of the dowel action. A stirrup can effectively support the longitudinal reinforcement that crosses a flexural shear crack close to the stirrup.
2. Limiting the opening of inclined shear cracks, thus enhancing and preserving shear transfer by aggregate interlock.
3. Using sufficiently closely spaced stirrups provides confinement of the concrete, leading to an increase in the compressive strength and consequently enhances zones affected by arch action.
4. Enhancing the bond by reducing the splitting cracks that develop due to dowel forces.

In summary, shear reinforcement is used in concrete beams to preserve the overall integrity of the concrete contribution V_c , allowing the development of additional shear forces V_s through the well-known truss mechanism adopted by many codes.

2.2.2 Anchorage of stirrups in concrete beams

Due to the relatively short length of the stirrups, the desired tensile capacity of a steel stirrup is typically developed using appropriate anchorage length and bending of the stirrups into a 90° , 135° or 180° hook. According to section 7.1 of the ACI 318-95 code, a 90° bend plus a $6d_b$ extension at the free end of the bar is required. The inside diameter of bend, according to the ACI 318-95 code, should not be less than $4d_b$. According to section A12.2.2 of CSA Standard A23.3, either a 90° or 135° bend plus an extension of at least $6d_b$, but not less than 60 mm, is required at the free end of the bar.

2.2.3 “Kinking” of stirrups at the shear crack location

In addition to a tensile force, the stirrup is subjected further to a dowel action at its intersection with the shear crack. Opening of the inclined shear crack at the location of the stirrup induces a kinking action in the direction of the crack.

Pang and Hsu (1995) investigated experimentally the stress–strain relationship of reinforcing bars in concrete panels subjected to membrane shear. Pang and Hsu concluded that local kinking at the crack location has two effects on the average stress–strain relationship of steel bars:

1. The induced bending stress at the location of the inclined shear crack is superimposed on the tensile stress in the steel bar, leading to a decrease of the apparent yield strength and the ultimate strength of the steel bar, as illustrated in Figure 2-2.
2. The local bending of a steel bar at the crack location causes further damage of bond between concrete and steel, increasing the plastic zone of the bar at the crack. This longer plastic zone contributes additional deformation to the average elongation of a steel bar.

Based on their investigation, Pang and Hsu (1995) introduced a kinking factor to modify the typical stress–strain curve of the steel bars, as shown in Figure 2-2. The kinking factor was assumed to vary linearly with the crack angle θ from 45 to 90 degrees.

The proposed constitutive law of reinforcing bars was utilized by Pang and Hsu (1996) in the formulation of the fixed-angle softened truss model (FA-STM) that is capable of predicting the response of concrete elements subjected to membrane forces. However, the “kinking” effect has not yet been incorporated into any code of practice.

2.3 Shear mechanism in reinforced concrete beams

During the last 25 years, since ASCE-ACI Committee 426 published its report in 1973, several attempts have been made to rationalize the shear mechanism in reinforced and prestressed concrete beams. ASCE-ACI Committee 445 (1998) recently published an extensive report reviewing some of the shear models for concrete members that have evolved since 1973. The shear models for reinforced concrete members with shear reinforcement presented in the ASCE-ACI report (1998), include:

- a- compression field theory (CFT) (Collins 1978);
- b- modified compression field theory (MCFT) (Vecchio and Collins 1986);
- c- variable angle truss model (Eurocode EC2 1992);
- d- truss models with crack friction (Dei Poli *et al.* 1990);
- e- rotating-angle softened-truss model (RA-STM) (Hsu 1993); and
- f- fixed-angle softened-truss model (FA-STM) (Hsu 1993).

The historical development of the above-mentioned shear models is presented in section 2.3.1. A description of the MCFT that is currently integrated into many design codes, is given in section 2.3.2. A recently developed shear model based on the shear friction theory (Loov 1998) is described in section 2.3.3.

2.3.1 Historical development of shear models

Early shear design for reinforced concrete beams was based on a truss analogy developed by Ritter in 1899 and Morsch in 1902. This theory was based on the assumption that concrete reinforced with longitudinal and transverse steel bars would develop inclined cracks when subjected to shear as shown in Figure 2-3. These shear cracks are assumed

to be straight and at an inclined angle θ to the horizontal direction. The concrete struts between these cracks carry a compressive stress induced by the applied shear.

The web region within the effective depth jd (Figure 2-3a) is assumed to resist the shear force. Figure 2-3b shows the axial force N induced by the shear force; this is shared equally between the top and bottom chords.

Based on the equilibrium in the vertical direction (Figure 2-3c), the total shear resistance of the stirrups spaced at s with a yield force of $A_{sv}f_{sv}$ can be calculated as follows:

$$V_s = \frac{A_{sv} f_{sv} jd \cot \theta}{s} \quad (2-2)$$

Ritter and Morsch proposed that the angle θ be assumed to be 45 degrees. However, research in the past three decades has shown that the angle θ may not always be 45 degrees once cracking occurs (Nielsen 1984).

Collins (1972) introduced compatibility equations to the truss model in order to determine the angle of inclination of the concrete strut. This theory was referred to as the “compression field theory (CFT)”. In 1978, Collins hypothesized that the principal strain directions in the concrete coincided with the corresponding principal stress directions. Based on compatibility, equilibrium and constitutive material relationships, the CFT was able to predict the response of a reinforced concrete member subjected to shear. However, the CFT was based on the uniaxial compressive stress–strain curve of concrete and was found to be inaccurate in predicting the strength and deformation of reinforced concrete members.

Further tests by Vecchio and Collins (1981 and 1982) found that it is necessary to take into account the reduction of the concrete compressive capacity due to the principal

tensile strain in cracked concrete. This improvement led to the “modified compression field theory (MCFT)” (Vecchio and Collins 1986 and 1988). The MCFT takes in account the contribution of the tensile stresses in the concrete between cracks. As a consequence, a “concrete contribution” term, V_c , has been introduced to the shear resisting mechanism. The concrete contribution, V_c , was assumed to diminish as the principal tensile strain in the cracked web increases. The MCFT is integrated into the latest revision of the shear provisions in the Canadian code (CSA A23.3-94), as discussed in section 2.5.2.

Hsu (1988, 1993 and 1996) documented independent research that resulted in a theory similar to the MCFT called the “softened truss model theory”. The rotating-angle softened-truss model (RA-STM) was based on the simplifying assumption that the concrete struts are inclined at a rotating angle that varies with the applied shear (Pang and Hsu 1992). In 1996, Pang and Hsu developed the fixed-angle softened-truss model (FA-STM) on the basis of smeared cracks using a fixed angle determined by the direction of the first batch of cracks initiated at the shear cracking load. The FA-STM allows for the derivation of the concrete contribution term V_c , while the RA-STM is incapable of predicting V_c .

2.3.2 Modified compression field theory (MCFT)

Figure 2-4 summarizes the basic aspects of the MCFT. As mentioned in the previous section, the MCFT is a further development of the CFT that accounts for the influence of tensile stresses in the cracked concrete. It is recognized that the local stresses in both the concrete and the reinforcement vary from point to point in the cracked concrete, with high reinforcement stresses but low concrete tensile stresses occurring at crack locations.

The shear stress, v , applied to the cracked reinforced concrete causes tensile stresses in the longitudinal reinforcement, f_{sl} , tensile stresses in the transverse reinforcement, f_{sv} , compressive stresses in the cracked concrete, f_2 , and tensile stresses in the uncracked concrete between the cracks, f_1 . The equilibrium conditions, which relate the concrete stresses and the reinforcement stresses to the applied loads, can be derived from Figures 2-4a and 2-4b, as follows:

$$\rho_{sv} f_{sv} = f_{cy} = v \tan \theta - f_1 \quad (2-3)$$

$$\rho_{sl} f_{sl} = f_{cx} = v \cot \theta - f_1 \quad (2-4)$$

$$f_2 = v (\tan \theta + \cot \theta) - f_1 \quad (2-5)$$

where ρ_{sl} and ρ_{sv} are the ratios of the longitudinal and transverse reinforcement; respectively.

The compatibility conditions relating the strains in the cracked concrete to the strains in the reinforcement are expressed in terms of average strains, where the strains are measured over base lengths that are greater than crack spacing (Figure 2-4c). Due to the anisotropy of the cracked concrete, the principal stress direction may not be the same as the principal strain direction. However, the MCFT assumes that the angle of inclination, θ , of the diagonal compressive stress, f_1 , coincides with the angle of inclination of the principal compressive strain, ε_1 . The angle θ can be derived from Figure 2-4c, as follows:

$$\tan^2 \theta = \frac{\varepsilon_x + \varepsilon_2}{\varepsilon_y + \varepsilon_2} \quad (2-6)$$

Based on Mohr's circle in Figure 2-4c, the principal strain and the shear strain in the cracked concrete element can be derived as follows:

$$\varepsilon_1 = \varepsilon_x + \varepsilon_y + \varepsilon_2 \quad (2-7)$$

$$\gamma_{xy} = 2(\varepsilon_x + \varepsilon_2) \cot \theta \quad (2-8)$$

The stress–strain relationships for the reinforcement and the concrete are required for relating the stress components in Figure 2-4a to the strain components in Figure 2-4c. It is assumed that the reinforcement strains are related to the reinforcement stresses by the usual simple bilinear approximations shown in Figure 2-4d. Based on the test results of reinforced concrete elements in pure shear, Vecchio and Collins (1986) found that the principal compressive stress in the concrete, f_2 , is a function not only of the principal compressive strain, ε_2 , but also of the coexisting tensile strain, ε_1 . They proposed the following stress–strain relationships:

$$f_2 = f_{2max} \left[2 \left(\frac{\varepsilon_2}{\varepsilon_c} \right) - \left(\frac{\varepsilon_2}{\varepsilon_c} \right)^2 \right] \quad (2-9)$$

$$\frac{f_{2max}}{f_c'} = \frac{1}{0.8 + 170\varepsilon_1} \leq 1.0 \quad (2-10)$$

Equations (2-9) and (2-10) are presented in Figure 2-4e. It should be noted that an increase in ε_1 results in a decrease in f_{2max}/f_c' . Based on their test results, Vecchio and Collins (1986) proposed the following equations for the average tensile stress versus average tensile strain relationship:

$$f_1 = E_{ct} \varepsilon_1 \quad \text{if } \varepsilon_1 \leq \varepsilon_{cr} \quad (2-11)$$

$$f_1 = \frac{\alpha_1 \alpha_2 f_{cr}}{1 + \sqrt{500\varepsilon_1}} \quad \text{if } \varepsilon_1 \geq \varepsilon_{cr} \quad (2-12)$$

where E_{ct} is the elastic modulus of the uncracked concrete in tension ($E_{ct} = E_c$ in compression), f_{cr} and ε_{cr} are the tensile stress and strain at cracking, respectively, and α_1

and α_2 are factors accounting for the bond characteristics of the reinforcement and the type of loading; respectively. To limit the principal tensile stress in the concrete against the possibility of failure of the aggregate interlock mechanism, which is responsible for transmitting the interface shear stress, v_{ci} , across the crack surface, Bhide and Collins (1989) proposed the following equation:

$$f_1 \leq \frac{0.18\sqrt{f'_c} \tan \theta}{\left(0.3 + \frac{24w}{d_a + 16}\right)} \quad (2-13)$$

where d_a is the maximum aggregate size and w is the shear crack width. Equation (2-13) is based on the assumption that at high shear loads, the average strain in the transverse reinforcement ($\rho_{sv} < \rho_{sl}$) exceeds the yield strain and therefore $f_{sv} = f_{svcr} = f_{svy}$. The shear crack width, w , required for equation (2-13) can be determined using the following equations:

$$w = \varepsilon_1 s_{m\theta} \quad (2-14)$$

$$s_{m\theta} = 1 / \left(\frac{\sin \theta}{s_{ml}} + \frac{\cos \theta}{s_{mv}} \right) \quad (2-15)$$

$$s_{ml} = 2 \left(c_l + \frac{s_l}{10} \right) + 0.25k_1 \frac{d_{bl}}{\rho_{sl}} \quad (2-16)$$

$$s_{mv} = 2 \left(c_v + \frac{s_v}{10} \right) + 0.25k_1 \frac{d_{bv}}{\rho_{sv}} \quad (2-17)$$

where $s_{m\theta}$ is the diagonal crack spacing, s_{ml} and s_{mv} are the crack spacings indicative of the crack control characteristics of the longitudinal and transverse reinforcement; respectively; c_l and c_v are the concrete covers for the longitudinal and transverse reinforcement, respectively; s_l and s_v are the spacings between the reinforcing bars in the

longitudinal and transverse directions, respectively; d_{bl} and d_{bv} are the bar diameters of the longitudinal and transverse reinforcement, respectively; and ρ_{sl} and ρ_{sv} are the ratios of the longitudinal and transverse reinforcement, respectively (Figure 2-4a). The stress-strain relationship for the concrete in tension is presented in Figure 2-4f as given by equations (2-11), (2-12) and (2-13).

Figure 2-5 shows the equilibrium and compatibility conditions in a reinforced concrete beam subjected to shear. Equations (2-3) to (2-8), which are derived based on equilibrium and compatibility conditions for a concrete element subjected to pure shear, can be used to determine the behaviour of a reinforced concrete beam loaded in shear. However, ρ_{sl} is defined as the flexural reinforcement ratio and ρ_{sv} as the shear reinforcement ratio ($A_{sv}/b_w s$), where s is the stirrup spacing. Based on the equilibrium equation (2-3) and the free body diagram in Figure 2-5, the shear force, V , can be determined as follows:

$$V = f_1 b_w jd \cot \theta + \rho_{sv} f_{sv} b_w jd \cot \theta \quad (2-18)$$

where b_w is the web width, jd is the shear depth, f_{sv} is the average stress in the stirrups and θ is the shear cracking angle (Figure 2-5).

Collins and Mitchell (1991) described two solution techniques to predict the behaviour of a beam section subjected to shear and bending moment using the MCFT, as shown in Figure 2-6. A detailed “dual-section” analysis requires dividing the cross section into many layers, as shown in Figure 2-6a. A lengthy iterative procedure to determine the shear stress, v , the longitudinal strain, ϵ_x , the stirrup stress, f_{sv} , and the angle, θ , is performed for each layer and therefore the equilibrium conditions are examined for the whole cross section. It is reported by Collins and Mitchell (1991) that the dual-section

analysis is very time consuming. A more direct and simplified procedure was proposed by assuming an average shear stress distribution over the web of the beam, as shown in Figure 2-6b. To determine the shear stress, v , the stirrup stress, f_{sv} , and the angle, θ , Collins and Mitchell (1991) considered the longitudinal strain, ε_x , at the mid-depth of the web to apply the governing compatibility conditions. Using these simplifications, an iterative procedure consisting of five steps was implemented into a computer program "RESPONSE" to predict the behaviour of a beam section subjected to shear and bending moment. As indicated by Collins and Mitchell (1991) and Felber (1990), the "RESPONSE" program was examined against several test results and showed good performance. Further details regarding the dual-section analysis and the "RESPONSE" program can be found in the textbook authored by Collins and Mitchell (1991) and the thesis by Felber (1990).

2.3.3 Shear friction model (SFM) for concrete beams

The SFM is based on the behaviour of the shear and longitudinal reinforcement crossing a shear crack plane. As the concrete interfaces on both sides of the crack separate and slip due to loading applied to the member, the reinforcement crossing the crack will be subjected to dowel action and tension, causing the concrete interfaces to press against each other (Krauthammer 1992).

Loov (1998) proposed that the shear resistance, v_n , transferred across a crack is limited by the stress that can be sustained by bond and anchorage and can be predicted as follows:

$$v_n = k\sqrt{\sigma f'_c} \quad (2-19)$$

where σ is the normal stress on the plane and k is the shear-friction factor that equals $2.1f'_c{}^{-0.4}$, according to Loov and Peng (1998).

Loov (1998) asserted that the SFM could predict the shear strength of beams that have major shear cracks where slip could occur. Theoretical equations were derived from the free-body diagram shown in Figure 2-7.

The total normal force acting on the inclined plane is designated as R and the total shear force acting across the same plane is designated as S . The tension force in the longitudinal reinforcement is represented by T and the sum of the vertical stirrup forces crossing the inclined crack is given by T_v . The vertical shear force acting on the free body is V_n . Equilibrium equations for the free-body diagram parallel and perpendicular to the shear plane can be formulated as follows:

$$R = T \sin\theta - [V_n - T_v] \cos\theta \quad (2-20)$$

$$S = T \cos\theta + [V_n - T_v] \sin\theta \quad (2-21)$$

Equation (2-19) can be re-written as follows:

$$\frac{S}{A} = k \sqrt{\frac{R}{A} f'_c} \quad (2-22)$$

where A is the area of the inclined plane (Figure 2-7).

Hence, solving for V_n , the following equation was derived for the shear strength of a beam:

$$\frac{V_n}{C_w} = 0.5k^2 \left[\sqrt{\frac{T}{0.25k^2 C_w} + \cot^2\theta} - \cot\theta \right] (1 + \cot^2\theta) - \frac{T}{C_w} \cot\theta + \frac{T_v}{C_w} \quad (2-23)$$

where $C_w = f'_c b_w h$ is the limiting force in the concrete web based on an overall depth h , b_w is the web width of the beam and h is the overall depth of the beam as shown in Figure 2-7.

The shear strength must be determined by trial-and-error since all possible failure planes between the inside edge of the support plate and the inside edge of the load plate to a maximum angle of 90° should be checked (Loov 1998). The plane with the lowest calculated V_n value gives the governing shear strength of the beam.

Kriski and Loov (1996) and Loov (1998) performed shear-friction analyses on beams tested by Clark (1951), Kani *et al.* (1979), Sarsam and Al-Musawi (1992) and themselves in order to evaluate the accuracy of the SFM. Based on their study, they concluded that the shear friction equation (2-23) is expected to be very useful for unusual situations because it can be used where the stirrup spacing or any of the other design parameters is variable along the length of the member.

2.4 Stirrup effectiveness

Design procedures for shear provide simple superposition of stirrup capacity, V_s , and concrete contribution, V_c , hence ignoring the influence of the stirrups on the concrete contribution to the shear resisting mechanisms. Most of the design codes (such as the ACI 318-95), assume that the concrete contribution, V_c , is equal to the shear cracking force, V_{cr} . The concrete contribution, V_c , consisting of the beam action and arch action contributions, interacts with shear reinforcement in different ways. This interaction results in variable truss mechanism contributions (V_c and V_s) and in some enhancement of beam action contribution.

The stirrup effectiveness function, defined as the ratio of effective increase in shear stress due to stirrup inclusion and the conventional stirrup contribution based on the 45-deg truss model, was first introduced by Haddadin *et al.* (1971). They introduced a concept to evaluate the effectiveness of the stirrups as given in the following discussion.

The following equations were proposed to determine the ultimate shear capacity of concrete beams with stirrups:

$$\frac{V_n}{b_w d} = \frac{V_{c(aci)}}{b_w d} + 1.75 \rho_{sv} f_{sv} \quad \text{units: lb, in.} \quad (2-24)$$

for $50 \text{ psi} < \rho_{sv} f_{sv} \leq 0.06 f_c \sqrt{\frac{b_f}{b_w}} \sqrt{\frac{d}{a}}$

$$\frac{V_n}{b_w d} = \frac{V_{c(aci)}}{b_w d} + 0.5 \rho_{sv} f_{sv} + 0.075 f_c \sqrt{\frac{b_f}{b_w}} \sqrt{\frac{d}{a}} \quad \text{units: lb, in.} \quad (2-25)$$

for $0.06 f_c \sqrt{\frac{b_f}{b_w}} \sqrt{\frac{d}{a}} < \rho_{sv} f_{sv} \leq 630 \text{ psi}$

where b_f is the width of the flange of T-beams and b_f/b_w should not be taken more than 3.5. Equations (2-24) and (2-25) proposed by Haddadin *et al.* (1971) included the stirrup effectiveness factor that is affected by the shear failure modes and shear span-to-depth ratio. In these equations the concrete contribution, $V_{c(aci)}$, can be determined according to the ACI 318-71 code.

The use of the stirrup effectiveness factor was also recommended by Mphonde (1989) to account for the increase in shear capacity of beams over the capacities predicted by the current design approaches. Based on tests by Mphonde and Frantz (1985), the stirrup contribution was found to be 60 percent higher than that predicted by the ACI code. Hence, Mphonde proposed a constant effectiveness factor of 1.60 for stirrup capacity.

A rational model was recently developed by Russo and Puleri (1997), based on the interaction of shear resisting mechanisms and the stirrup effectiveness concept. The following equation was proposed to determine the shear strength of concrete beams reinforced with steel stirrups:

$$\frac{V_n}{b_w d} = 0.83\xi \chi \sqrt[3]{\rho_{sl}} + 1.67 \frac{\sqrt{f'_c}}{\chi} \rho_{sv} f_{sv} \quad (2-26)$$

$$\xi = \frac{1}{\sqrt{1 + \frac{d}{25d_a}}}$$

$$\chi = \sqrt{f'_c} + 250 \sqrt{\rho_{sl} \left(\frac{d}{a}\right)^5}$$

where d_a is the maximum aggregate size. The stirrup effectiveness function, proposed by Russo and Puleri (1997), was derived to include the effect of the flexural reinforcement ratio, the shear span-to-depth ratio and the concrete strength on the stirrup contribution to the shear capacity of concrete beams.

2.5 Design procedures

Although there are significant efforts to rationalize shear behaviour in concrete beams, many current code requirements are based on empirical formulas for estimating the shear strength of concrete beams. The following subsections present the different shear design approaches used in national and international codes of practice. Other codes of practice are similar to or slightly different from the aforementioned approaches.

2.5.1 American Concrete Institute, ACI 318-95

The ACI code adopts the 45-degree truss model with an additional term for the concrete contribution, as follows:

$$V_d = \phi V_n \quad (2-27)$$

$$V_n = V_c + V_s \quad (2-28)$$

$$V_c = \left(\sqrt{f'_c} + 120 \rho_{sl} \frac{V_u d}{M_u} \right) \frac{b_w d}{7} \leq 0.3 \sqrt{f'_c} b_w d \quad (2-29)$$

where ϕ is the strength reduction factor for shear ($\phi = 0.85$) and V_u and M_u are the applied shear force and moment at the critical section.

The $V_u d / M_u$ term is generally small. Therefore ACI 318-95 allows the use of the following simplified equation:

$$V_c = 0.17 \sqrt{f'_c} b_w d \quad (2-30)$$

Equations (2-29) and (2-30) for V_c are applied for $V_u d / M_u$ values higher than 1.0.

However, the ACI code uses a multiplier to V_c for deep flexural beams, as given by:

$$V_c = \left(3.5 - 2.5 \frac{M_u}{V_u d} \right) 0.17 \sqrt{f'_c} b_w d \quad (2-31)$$

For the stirrup contribution to shear, the conservative 45-degree truss model is used as follows:

$$V_s = \frac{A_{sv} f_{yv} d}{s} \quad (2-32)$$

The stirrup contribution, V_s , given by equation (2-32), is determined based on the 45-degree truss model assuming that all the stirrups crossing the shear crack have reached yield and hence equation (2-32) governs the shear-yield (shear-tension) mode of failure.

To avoid shear failure initiated by crushing of the concrete before utilization of the full capacity of the shear reinforcement, the ACI 318-95 limits V_s to $\frac{2}{3}\sqrt{f'_c}b_wd$; hence, the upper bound condition of ACI equation (2-28) for shear-compression failure may be rewritten as follows:

$$V_n = V_c + \left\{ \frac{2}{3}\sqrt{f'_c}b_wd \right\} \quad (2-33)$$

The 1995 ACI 318 code requires a minimum amount of shear reinforcement for nonprestressed members reinforced with steel, as given by the following equation:

$$\rho_{sv_{min}} = \frac{A_{sv_{min}}}{b_w s} = \frac{0.345}{f_{sv}} \quad (2-34)$$

2.5.2 Canadian Standards Association, CSA-M23.3-94

The Canadian code CSA-M23.3-94 permits two alternative methods of shear design of reinforced concrete beams, namely, the simplified method and the general method. The simplified method is based on the traditional “concrete plus steel contributions” approach whereas the general method is derived from the modified compression field theory.

2.5.2.1 Simplified method

The simplified method is based on the 45-degree truss model with an effective depth of d . The shear resistance V_d can be determined by the following equation:

$$V_d = V_{cd} + V_{sd} \quad (2-35)$$

The concrete contribution is given by:

$$\begin{aligned}
 V_{cd} &= 0.2\lambda\phi_c\sqrt{f'_c}b_wd & d \leq 300 \text{ mm} \\
 V_{cd} &= \frac{260}{1000+d}\lambda\phi_c\sqrt{f'_c}b_wd \geq 0.1\lambda\phi_c\sqrt{f'_c}b_wd & d > 300 \text{ mm}
 \end{aligned}
 \tag{2-36}$$

where λ equals 1.0 for normal density concrete and ϕ_c is the material safety factor for concrete ($\phi_c = 0.60$).

The steel contribution is given by:

$$V_{sd} = \frac{\phi_s A_{sv} f_{sv} d}{s} \leq 0.8\lambda\phi_c\sqrt{f'_c}b_wd
 \tag{2-37}$$

where ϕ_s is the material safety factor for steel ($\phi_s = 0.85$).

The 1994 CSA23.3 code requires a minimum amount of shear reinforcement for nonprestressed members reinforced with steel, as given by the following equation:

$$\rho_{sv_{min}} = \frac{A_{sv_{min}}}{b_w s} = \frac{0.06\sqrt{f'_c}}{f_{sv}}
 \tag{2-38}$$

2.5.2.2 General method

The general method is based on the MCFT; however, it is formulated in the form of a concrete contribution plus steel contribution approach. Designing or analyzing using the general method requires the determination of the effective shear depth jd , which is assumed in the Canadian Standard as being not less than $0.9d$.

The nominal shear strength of a beam can be determined by the following equation:

$$V_d = V_{cd} + V_{sd} \leq 0.25 f'_c b_w jd
 \tag{2-39a}$$

$$V_{cd} = 1.3 \lambda \phi_c \beta \sqrt{f'_c} b_w jd
 \tag{2-39b}$$

$$V_{sd} = \frac{\phi_s A_{sv} f_{sv}}{s} jd \cot \theta \quad (2-39c)$$

where β and θ are determined from Figure 2-8 for sections with shear reinforcement, v_f is the factored shear stress ($v_f = V_u/b_w jd$) and ε_x is the longitudinal strain of flexural tension chord of the member, which can be estimated as:

$$\varepsilon_x = \frac{M_u / jd + 0.5V_u \cot \theta}{E_s A_{st}} \quad (2-40)$$

where M_u is the moment at the critical section, A_{st} is the cross-sectional area of longitudinal steel in the flexural tension side of a beam and E_s is the elastic modulus of longitudinal steel in the flexural tension side of a beam.

The determination of ε_x is dependent on the location of the critical section that dictates the values of M_u and V_u . Visualizing the beam as a variable-angle truss, the yielding of shear reinforcement occurs over a length of $jd \cot \theta$ (Collins *et al.* 1996). It is reasonable to consider the section in the middle of this length as being critical. Therefore, the critical section may be taken at a distance of $0.5jd \cot \theta$ from a concentrated load or support. In simplifying, the distance of $0.5jd \cot \theta$ is taken as approximately equal to jd . The θ values given by Figure 2-8 have been chosen to insure that the stirrup strain ε_{sv} is at least 0.002 and to insure that, for highly stressed members, the principal compressive stress in the concrete does not exceed the crushing strength (Collins *et al.* 1996).

β and θ are determined from Figure 2-9 for sections without shear reinforcement, where s_2 is the spacing of the cracks perpendicular to the longitudinal reinforcement. This spacing is a function of the maximum distance between longitudinal bars or longitudinal bars and the flexural compression zone. For beams with less than the minimum shear

reinforcement and no intermediate layers of longitudinal crack control reinforcement, the crack spacing parameter s_z may be taken as jd (or $0.9d$).

There is no direct solution to find the shear strength of a beam using the general method. First, the applied shear load V_u has to be assumed and the design shear strength V_d can be determined by equation (2-39). This process is iterated until V_u equals V_d .

2.5.3 Eurocode, EC2 Part 1

The Eurocode (EC2 1992) is partly based on the theory of plasticity by Nielsen (1984).

Two methods of design are given:

- i. The Standard Method, which combines a concrete contribution and a stirrup contribution based on the 45-degree truss model.
- ii. The Variable Strut Inclination Method.

Shear design is based on three values of shear resistance, stated as V_{rd1} , V_{rd2} and V_{rd3} .

V_{rd1} refers to the shear capacity of a concrete member without shear reinforcement, determined from an empirical formula:

$$V_{rd1} = [\tau_{rd} k_d \beta (1.2 + 40 \rho_{sl})] b_w d \quad (2-41)$$

where τ_{rd} is the basic design shear strength ($\tau_{rd} = 0.25 f_{ctk0.05}/\gamma_c$), $f_{ctk0.05}$ is the lower 5% fractile characteristics tensile strength ($f_{ctk0.05} = 0.7 f_{ctm}$), f_{ctm} is the mean value of the tensile concrete strength ($f_{ctm} = 0.30 (f_c')^{2/3}$), γ_c is the material safety factor for concrete ($\gamma_c = 1.50$), k_d is the size effect factor ($k_d = 1.6 - 0.001d \geq 1.0$), ρ_{sl} is the ratio of the longitudinal steel reinforcement ($\rho_{sl} \leq 0.02$) and $\beta = 2.5d/a$ ($1.0 \leq \beta \leq 5.0$).

The resistance V_{rd2} is the shear capacity of a beam when web crushing occurs according to the plasticity theory (Nielsen 1984). The maximum V_{rd2} value that can be attained is limited by the effective stress in the compression strut such that:

$$\begin{aligned} V_{rd2}(max) &= 0.5\nu f_{cd} b_w (0.9d) \\ \nu &= 0.7 - \frac{f'_c}{200} \geq 0.50 \end{aligned} \quad (2-42)$$

where $f_{cd} = f'_c / \gamma_c$, and $\gamma_c = 1.50$.

The minimum shear reinforcement, ρ_{svmin} , is specified by the Eurocode2 (1992) in a table format, as a function of the concrete strength, f'_c , and yield strength of the stirrups, f_{syv} .

The difference between the Standard Method and the Variable Strut Inclination Method is in the determination of the resistance V_{rd3} . The alternative methods of calculating V_{rd3} are discussed below.

2.5.3.1 Standard method

The Standard Method is similar to the provisions of the ACI 318-95 with the total shear resistance given as follows:

$$\begin{aligned} V_{rd3} &= V_{cd} + V_{sd} \leq V_{rd2}(max) \\ V_{cd} &= V_{rd1} \\ V_{sd} &= \frac{A_{sv} (f_{syv} / \gamma_s)}{s} (0.9d) \end{aligned} \quad (2-43)$$

where V_{cd} is the design concrete contribution in shear, V_{rd1} is given by equation (2-41), $V_{rd2}(max)$ is given by equation (2-42) and γ_s is the material safety factor for steel ($\gamma_s = 1.15$).

2.5.3.2 Variable strut inclination method

The variable strut inclination method is based on a truss with an angle θ chosen within the ranges of:

- i. $0.4 < \cot \theta < 2.5$ for beams with constant longitudinal reinforcement, or
- ii. $0.5 < \cot \theta < 2.0$ for beams with curtailed longitudinal reinforcement.

The shear resistance based on the crushing of the compressive strut is:

$$V_{rd2} = \frac{b_w(0.9d)v(f'_c/\gamma_c)}{(\cot\theta + \tan\theta)} \quad (2-44)$$

The shear resistance based on a truss model with stirrups yielding is:

$$V_{rd3} = \frac{A_{sv}(f_{syv}/\gamma_s)}{s}(0.9d)\cot\theta \quad (2-45)$$

A limitation based on the plasticity theory is placed on the effectiveness of the shear reinforcement such that:

$$\frac{A_{sv}f_{syv}/\gamma_s}{b_w s} \leq 0.5v(f'_c/\gamma_c) \quad (2-46)$$

2.5.4 British standard BS8110

Similar to the ACI code, the BS8110 code adopts the 45-deg truss model with an additional term for the concrete contribution. The following equations are used for shear design of beams reinforced with steel:

$$V_d = V_{cd} + V_{sd} \leq 0.80 \sqrt{f_{cu}} b_w d \leq 5.0 b_w d \quad (2-47)$$

$$V_{cd} = 0.925(100\rho_l)^{1/3}(f_{cu}/40)^{1/3}(400/d)^{1/3} b_w d / \gamma_c \quad (2-48)$$

$$V_{sd} = \frac{A_{sv} f_{yv} d}{\gamma_s s} \quad (2-49)$$

where f_{cu} is the concrete cube strength ($f_{cu} = 1.25f_c$), γ_c is the material safety factor for concrete ($\gamma_c = 1.25$), γ_s is the material safety factor for steel ($\gamma_s = 1.15$) and $(f_{cu}/40)^{1.3}$ should not exceed 1.0.

The 1985 BS8110 code requires a minimum amount of shear reinforcement for nonprestressed members reinforced with steel, as given by the following equation:

$$\rho_{svmin} = \frac{A_{svmin}}{b_w s} = \frac{0.4}{f_{yv} / \gamma_s} \quad (2-50)$$

2.5.5 Japanese code, JSCE standards

The Japanese society for civil engineers (JSCE) standard specifications for design and construction of concrete structures (JSCE 1986) adopts the 45-degree truss model with an additional term for concrete contribution.

$$V_d = V_{cd} + V_{sd} \quad (2-51)$$

V_{cd} is the design shear capacity of beam members without shear reinforcement and is given by:

$$V_{cd} = \beta_d \beta_p \beta_n f_{vcd} b_w d / \gamma_b \quad (2-52a)$$

$$f_{vcd} = 0.2(f'_{cd})^{1.3} \quad (2-52b)$$

$$\beta_d = (1000/d)^{1.4} \quad ; \text{ if } \beta_d > 1.5 \quad \text{then } \beta_d = 1.5 \quad (2-52c)$$

$$\beta_p = (100\rho_{sl})^{1.3} \quad ; \text{ if } \beta_p > 1.5 \quad \text{then } \beta_p = 1.5 \quad (2-52d)$$

$$\begin{aligned}\beta_n &= 1 + M_o / M_d & \text{for } N_d \geq 0 \\ \beta_n &= 1 + 2M_o / M_d & \text{for } N_d < 0\end{aligned}\quad (2-52e)$$

where f'_{cd} is the design compressive strength of the concrete ($f'_{cd} = f'_c / \gamma_c$), N_d is the design axial compressive force (or prestressing force), M_d is the design bending moment, M_o is the decompression moment, γ_b is the member safety factor ($\gamma_b = 1.3$), γ_c is the material safety factor of concrete ($\gamma_c = 1.3$ for $f'_c < 50$ MPa and 1.5 otherwise) and β_n should be within the limits: $0 \leq \beta_n \leq 2.0$.

V_{sd} is the design shear capacity borne by shear reinforcement and is given by:

$$V_{sd} = [A_{sv} (f_{sv} / \gamma_s) (\sin \alpha_s + \cos \alpha_s) / s] jd / \gamma_b \quad (2-53)$$

where α_s is the angle between the shear reinforcement and the member axis, jd is the shear depth ($jd = d/1.15$), γ_s is the material safety factor for steel ($\gamma_s = 1.0$) and γ_b is the member safety factor ($\gamma_b = 1.15$).

The shear force in concrete members should not exceed the design shear capacity $V_{d,max}$, determined based on the diagonal compressive capacity of web concrete, and given by the following equation:

$$\begin{aligned}V_{d,max} &= f_{wcd} b_w d / \gamma_b \\ f_{wcd} &= 1.25 \sqrt{f'_{cd}} \leq 7.8 \text{ MPa}\end{aligned}\quad (2-54)$$

where γ_b is the member safety factor ($\gamma_b = 1.3$).

2.6 Control of shear cracking

The control of crack widths at the service load level is an important serviceability criterion for reinforced concrete structures. Although design codes include proposals for

the calculation and the control of the widths of tensile and flexural cracks, none of them contains provisions for shear cracks. However, the control of shear cracking has been introduced implicitly in the design codes by limiting design yield stress and the spacing of the stirrups.

2.6.1 Design code approaches

The ACI 318-95 code limits the design yield strength of shear reinforcement to a maximum of 420 MPa, and to 550 MPa for welded deformed wire fabric. According to the ASCE-ACI Committee 426 (1973), for stirrups having a yield strength of 420 MPa and a load factor of 1.6 and an upper limit on the stirrup contribution of $2\sqrt{f'_c}/3$, the stirrup stress at service load 1.0(D+L) will be about 220 MPa (a strain value of 0.11%), corresponding to a maximum crack width of about 0.32mm. However, in the ACI 318-95 code, the limitation on the design yield strength was raised to 550 MPa since recent research has indicated that the performance of higher strength steel as shear reinforcement has been satisfactory. The ACI 318-95 code limits the stirrup spacing to a maximum of $d/2$ (or 600mm) if $V_s < 0.33\sqrt{f'_c}b_w d$, and to $d/4$ (or 300mm) if $V_s \geq 0.33\sqrt{f'_c}b_w d$. Similarly, the CSA23.3-94 standard limits the stirrup spacing to $0.7d$ (or 600mm) if $V_u < 0.1\lambda\phi_c f'_c b_w d$, and to $0.35d$ (or 300mm) if $V_u \geq 0.1\lambda\phi_c f'_c b_w d$.

The Eurocode-92 controls the shear cracking by limiting the stirrup spacing to values between 50 and 300 mm, according to the applied shear load and the shear cracking load.

2.6.2 Calculation of shear crack width

A few researchers have attempted to compute the width of inclined shear cracks by integrating strains along a stirrup in the cracked web of a beam. The crack width, w , was determined as a function of the stirrup strain ε_{sv} and the distance between cracks along the stirrup.

Based on strain integration along the stirrup and test data, Placas and Regan (1971) proposed the following equation for the maximum shear crack width at any load stage ($V > V_{cr}$):

$$w = \frac{s \sin \alpha}{10^6 \rho_{sv} (f'_c)^{1/3}} \left(\frac{V - V_{cr}}{b_w d} \right) \quad \text{units : lb, in.} \quad (2-55)$$

where w is the shear crack width in inches and V_{cr} is the shear force causing shear cracking.

Another equation for the shear crack width was introduced by the CEB-FIP Model Code-78 (1978) as follows:

$$w = 1.7 k_w w_m \quad (2-56a)$$

$$w_m = \varepsilon_{sm} s_m$$

$$\varepsilon_{sm} = \frac{f_{sv}}{E_s} \left[1 - \left(\frac{V_{cd}}{V_{ser}} \right)^2 \right] \geq 0.4 \frac{f_{sv}}{E_s} \quad (2-56b)$$

$$f_{sv} = \frac{V_{ser} - V_{cd}}{b_w d \rho_{sv}} \geq 40 \text{ MPa} \quad (2-56c)$$

$$s_m = 2 \left(c + \frac{s}{10} \right) + k_1 k_2 \frac{d_b}{\rho_r} \leq d - x \quad (2-56d)$$

where k_w is a coefficient to take into account the inclination of the stirrups (1.2 for vertical stirrups), V_{ser} is the shear force at the service load level, $V_{cd} = 2.5 \tau_{rd} b_w d$, τ_{rd} is

given by equation (2-41), s_m is the crack spacing, c is the concrete cover, s is the spacing of the reinforcing bars, if $s > 15d_b$, take $s = 15d_b$, k_1 is a coefficient which characterizes the bond properties of the bars (0.4 for deformed bars), k_2 is a coefficient representing the influence of the form of the stress diagram (0.25 for pure tension and shear, and 0.125 for bending), $\rho_r = \frac{A_{sv}}{A_{c,ef}}$, $A_{c,ef}$ is the concrete area where reinforcing bars (A_{sv}) can effectively

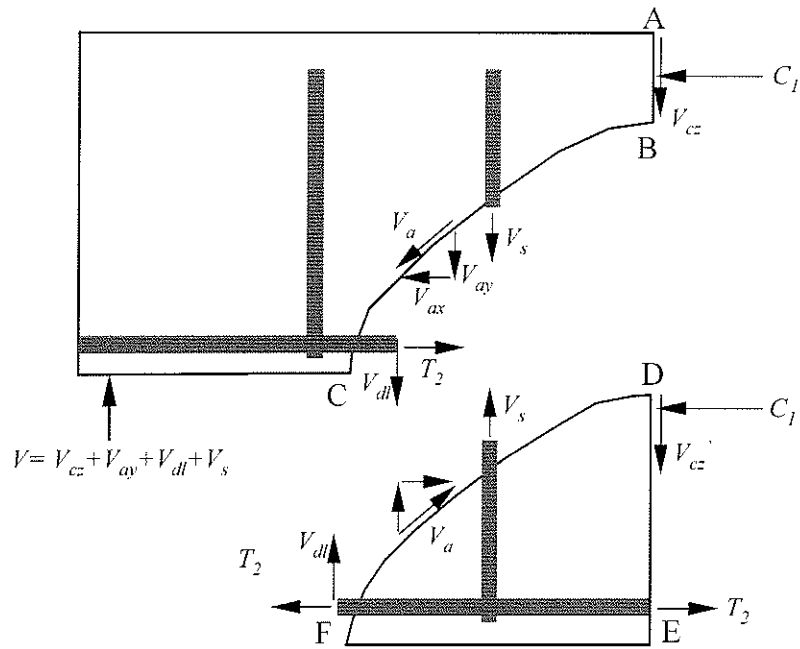
influence the crack width, and is defined in section 15.2.3 of the CEB-FIP MC-78, and x is the height of the compression zone in the cracked section. The allowable crack width given by the CEB-FIP MC-78 is 0.4 mm for mild exposure conditions.

The shear crack width can be also determined using the following equation, proposed by Hassan *et al.* (1991), as a function of the slip of the stirrup at the crack location, S_d , and the concrete compressive strength f'_c :

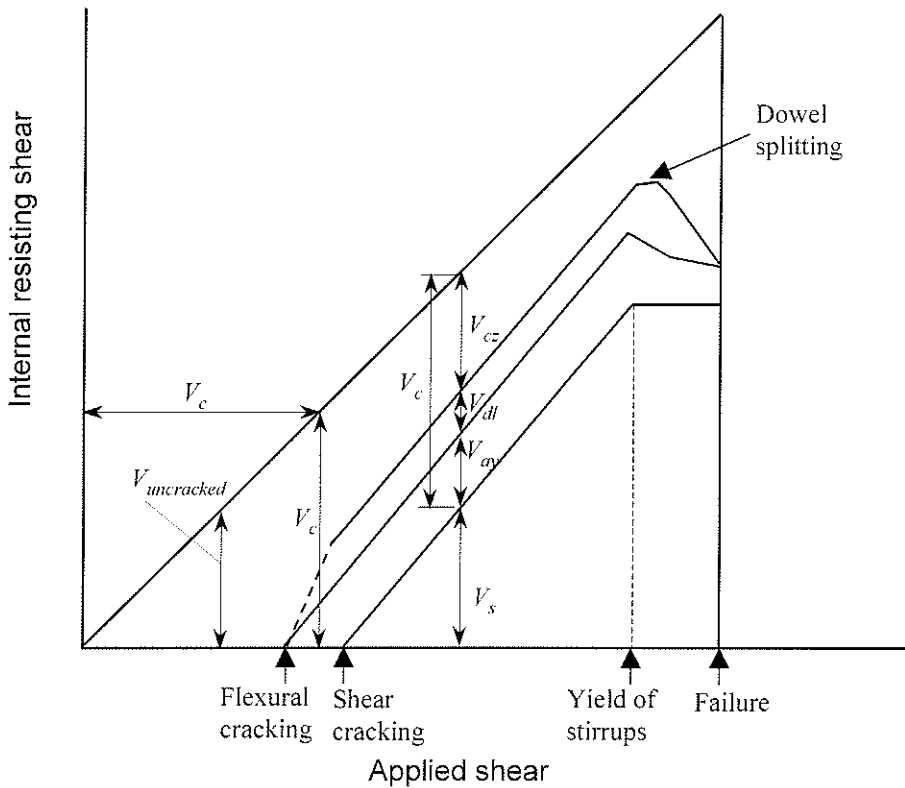
$$w = \frac{1.8S_d d_b}{10^6 (f'_c / 19.6)^{2.3} \rho_{sv}^{1.3}} \quad (2-57a)$$

$$S_d = 8 \times 10^3 \varepsilon_{sv} + 2 \times 10^6 \varepsilon_{sv}^2 \quad (2-57b)$$

where ε_{sv} is the strain in the steel stirrups and d_b is the bar diameter of the stirrup.



(a) Shear resisting mechanism



(b) Applied shear versus internal resisting shear

Figure 2-1. Internal forces in a cracked beam with stirrups (ASCE-ACI committee 426 - 1973)

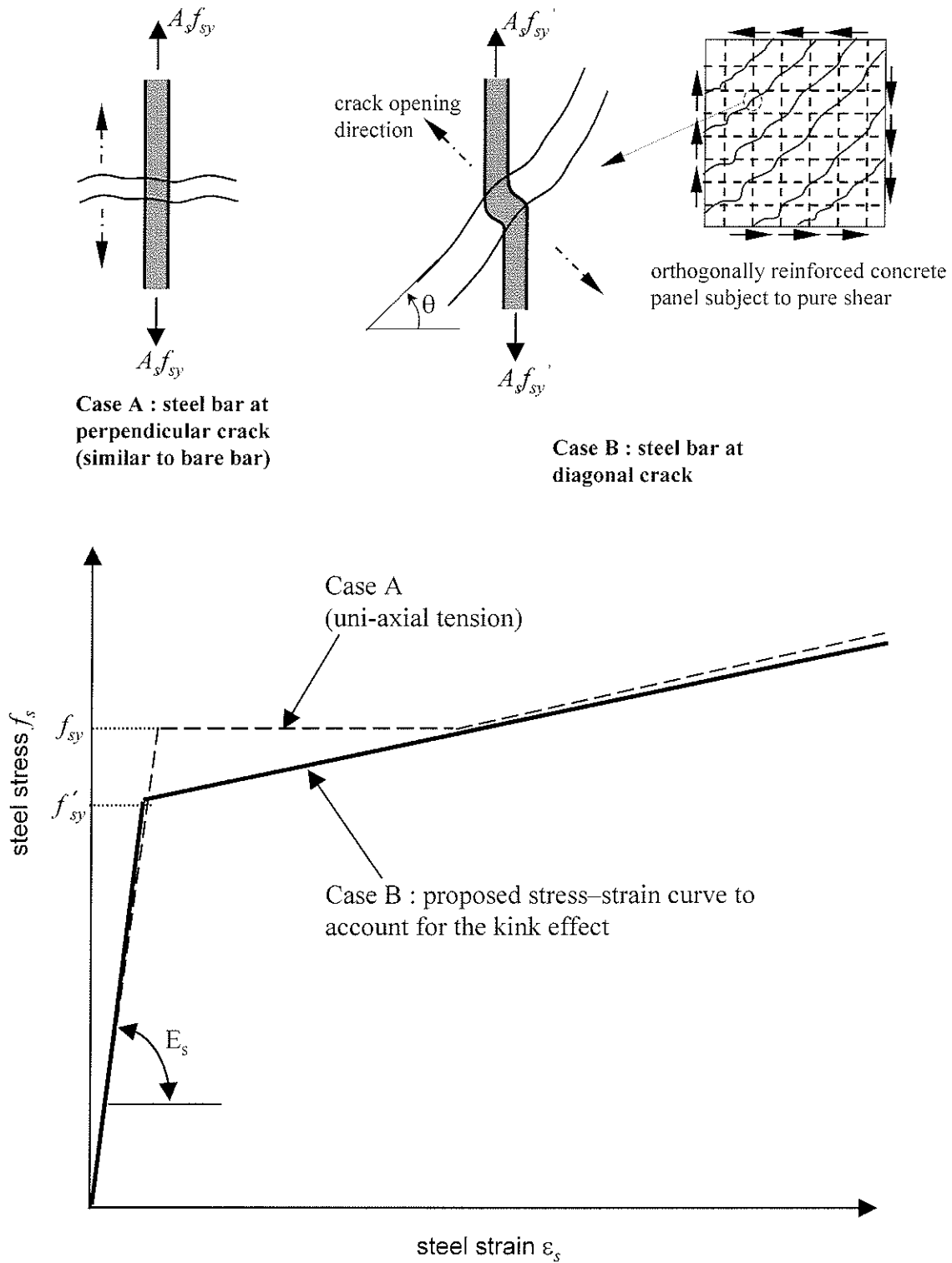


Figure 2-2. Average stress-strain relationships of mild steel bars (Pang and Hsu 1995)

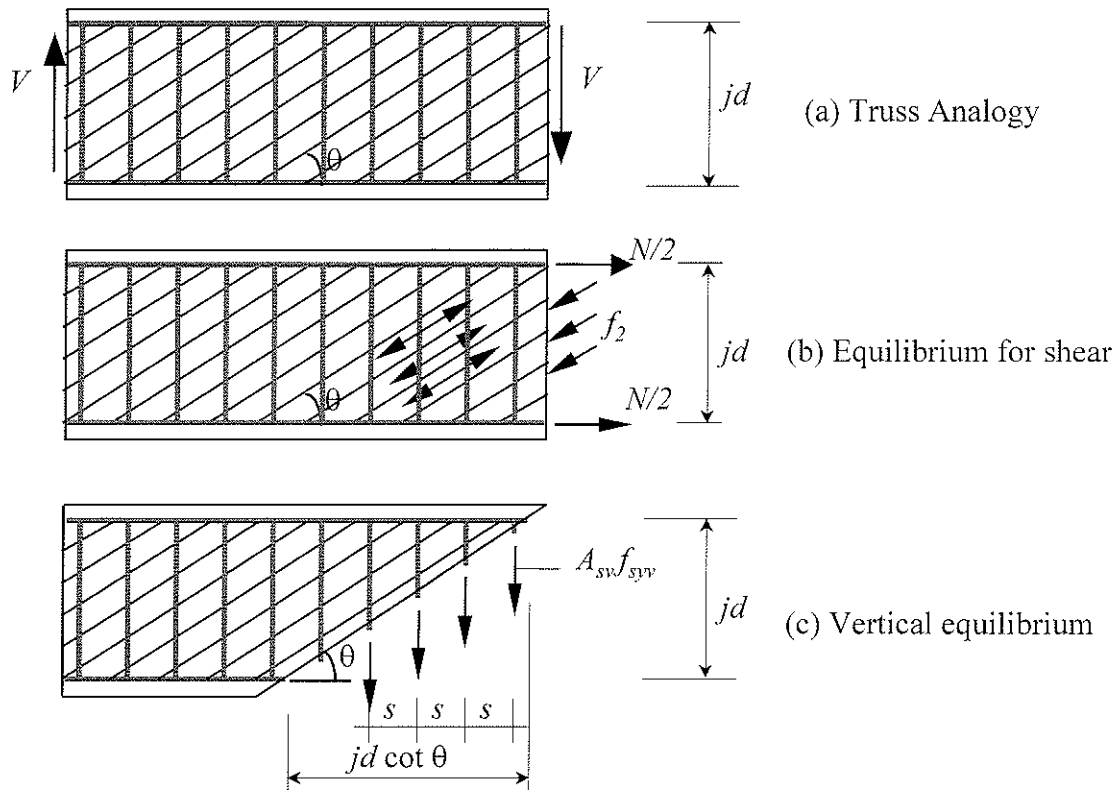
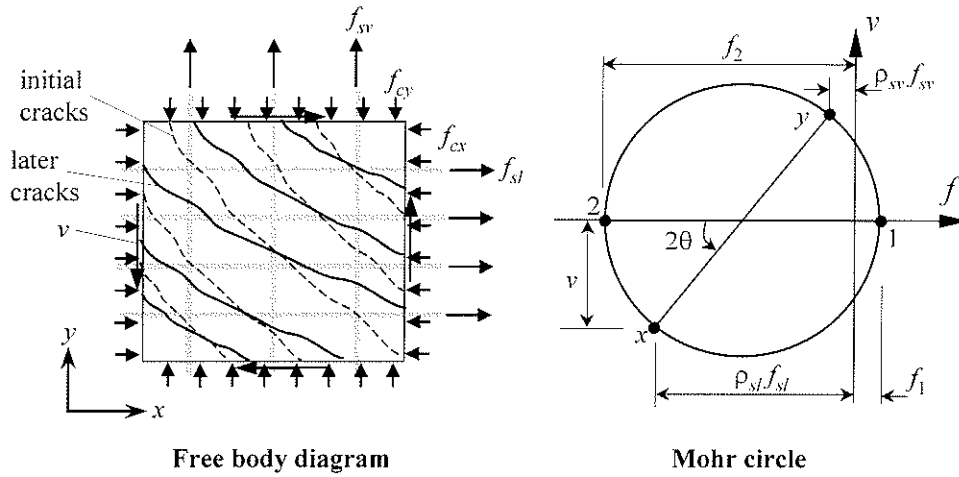
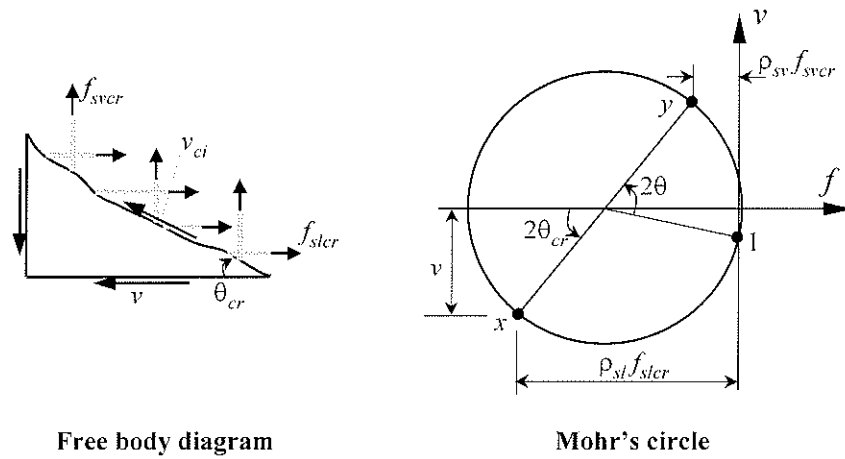


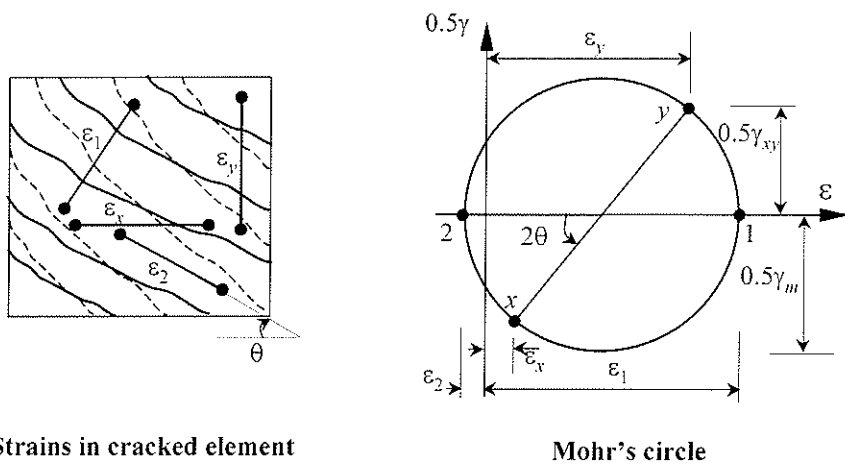
Figure 2-3. Truss model for shear in a beam panel



(a) Equilibrium in terms of average stresses

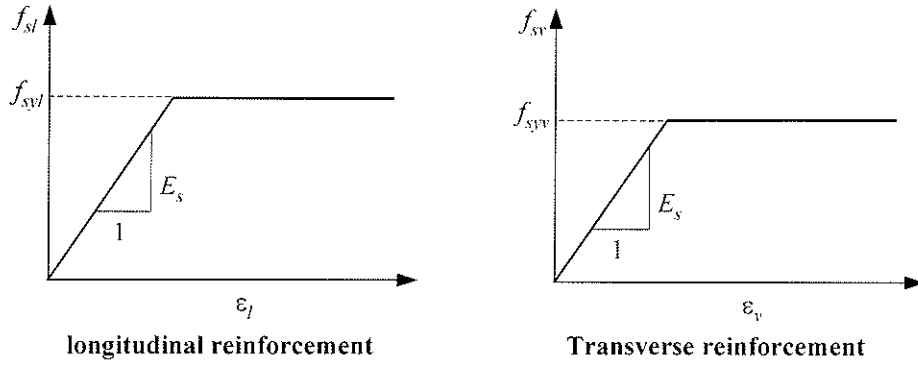


(b) Equilibrium in terms of local stresses at a crack

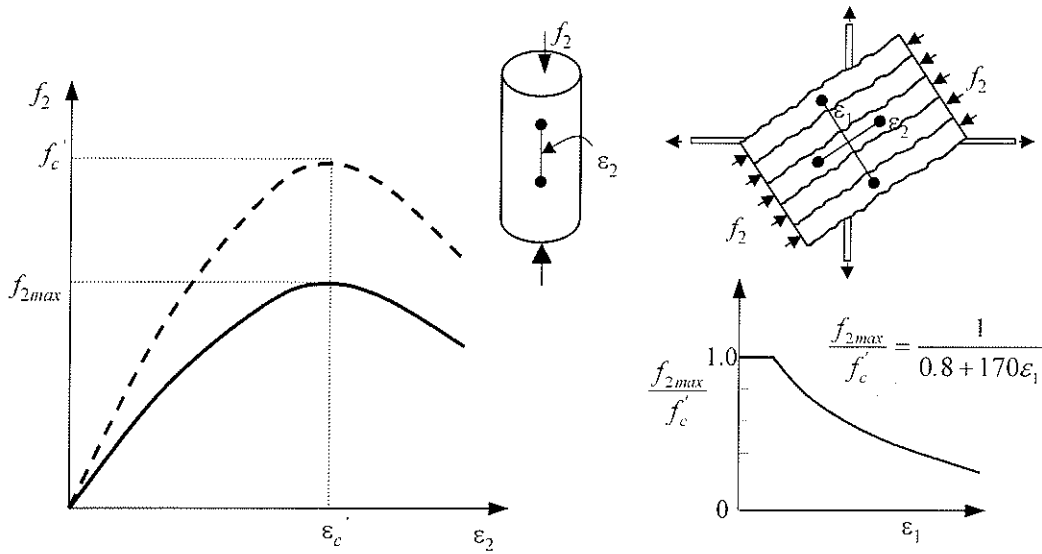


(c) Compatibility relationships

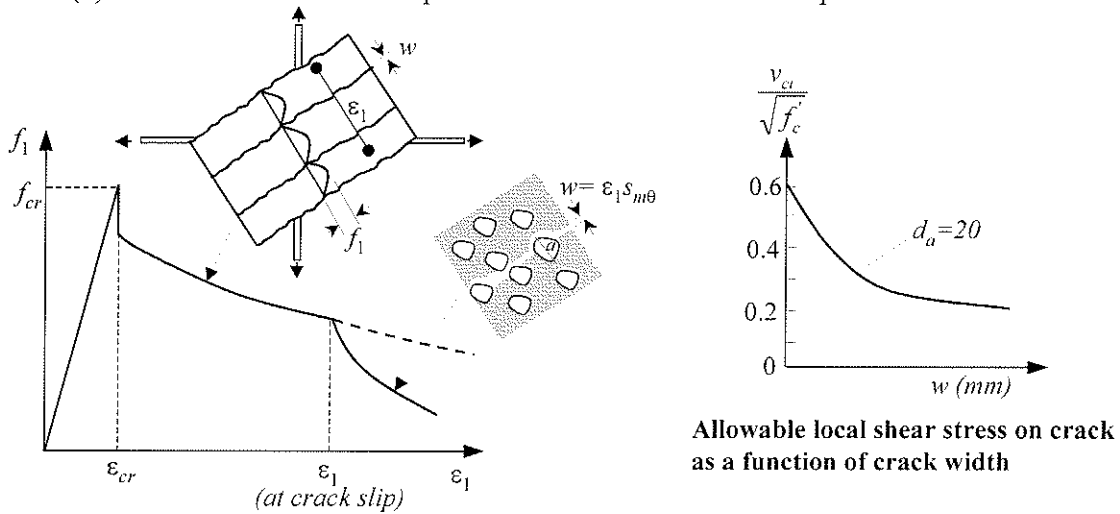
Figure 2-4. Aspects of modified compression field theory (Collins and Mitchell 1991)



(d) Stress-strain relationships for reinforcement



(e) Stress-strain relationships for cracked concrete in compression



(f) Stress-strain relationships for cracked concrete in tension

Figure 2-4(cont'd). Aspects of modified compression field theory (Collins and Mitchell 1991)

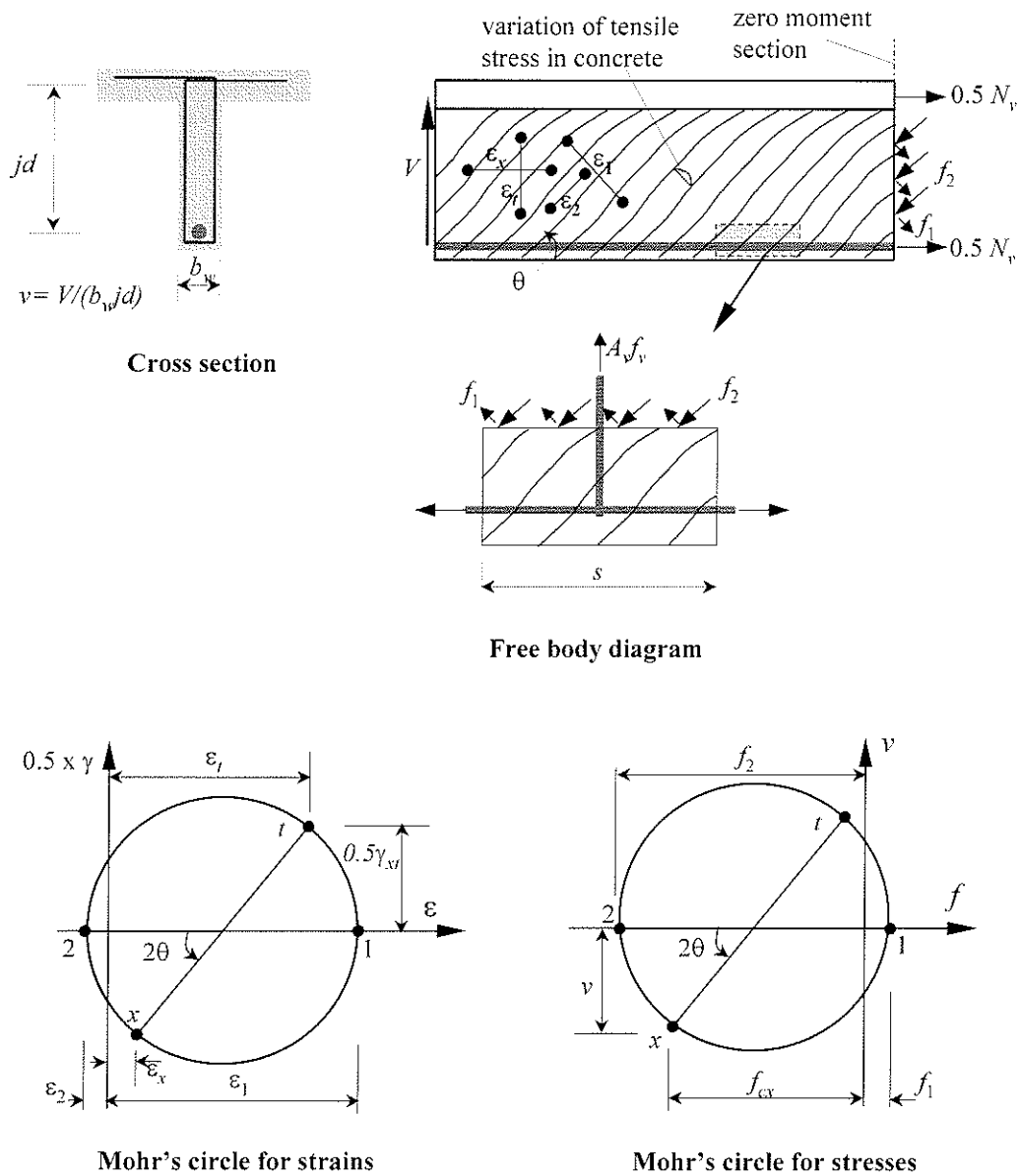
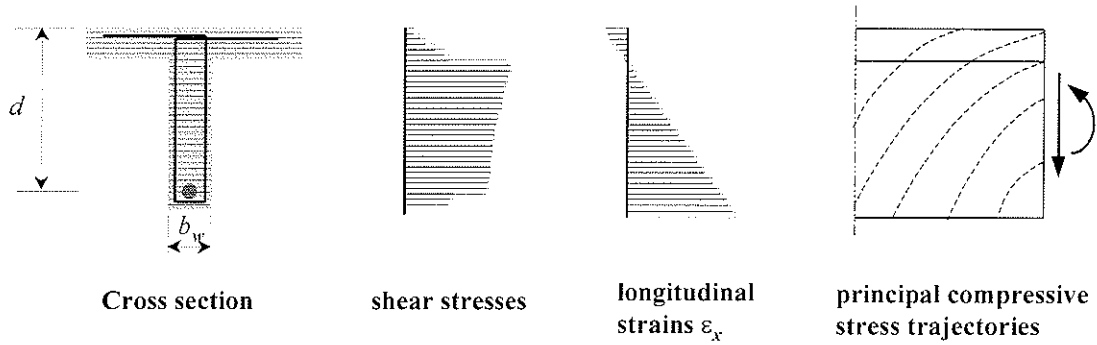
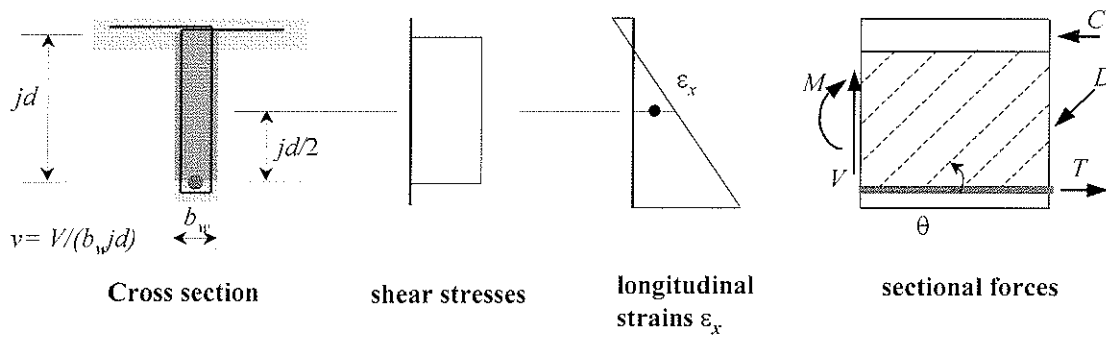


Figure 2-5. Modified compression field theory for a concrete beam



(a) Detailed analysis



(b) More direct procedure

Figure 2-6. Different solution techniques for the MCFT modeling of a beam section subjected to shear and moment

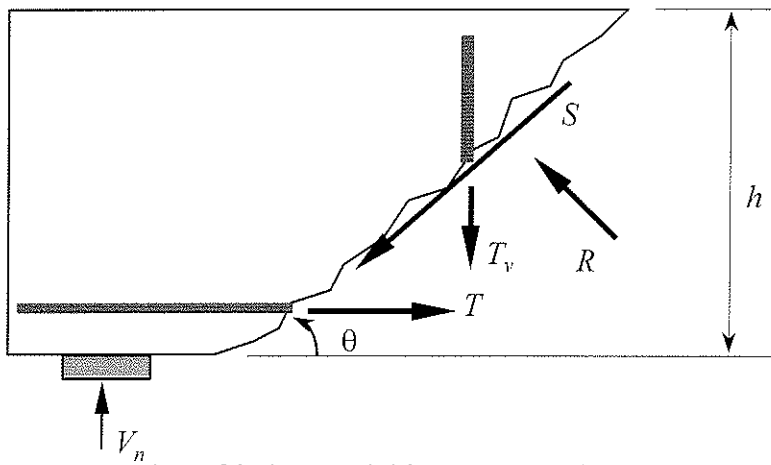


Figure 2-7. Shear friction model in a concrete beam (Loov 1998)

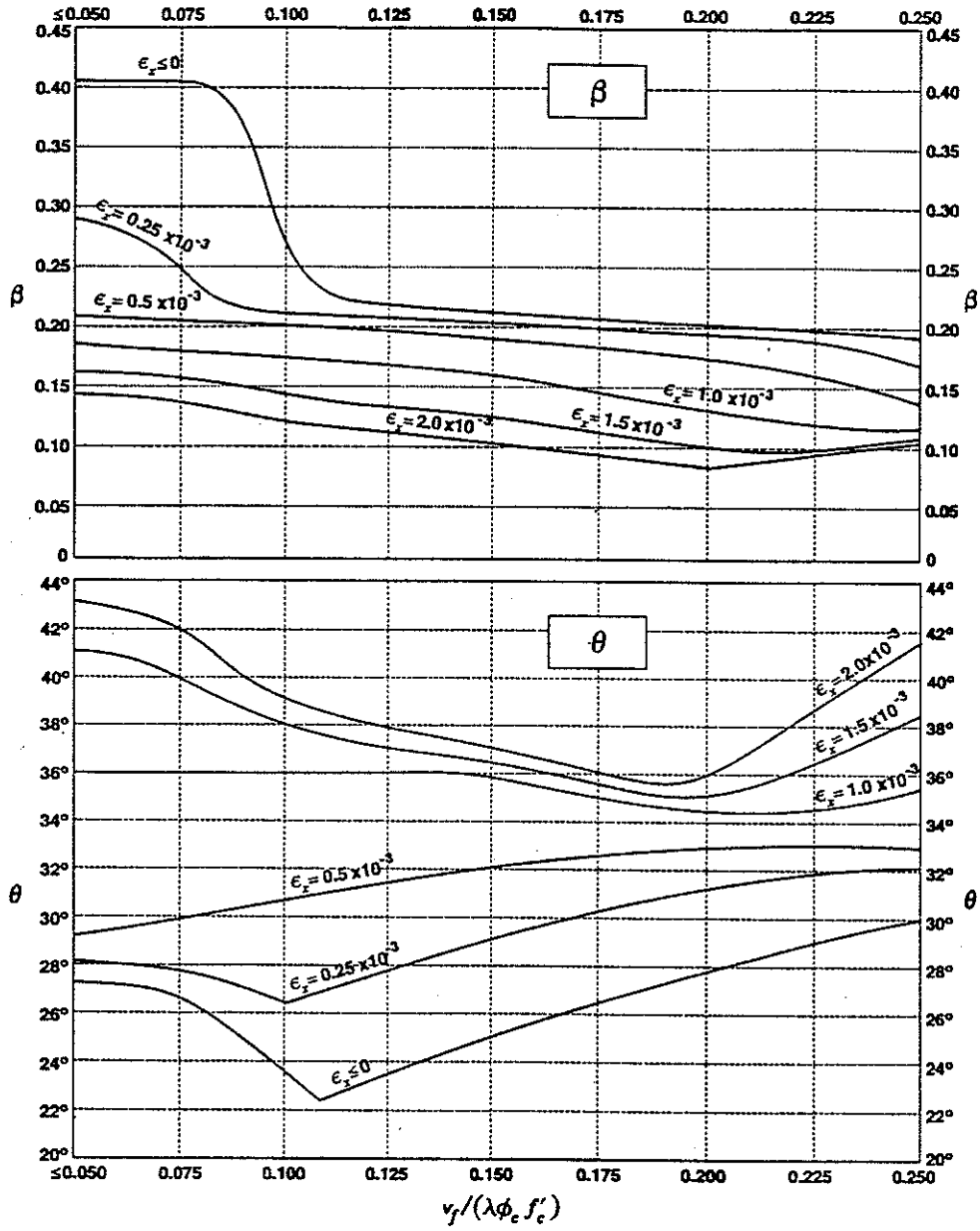


Figure 2-8. Values of β and θ for sections with shear reinforcement (CSA23.3-1994 general method)

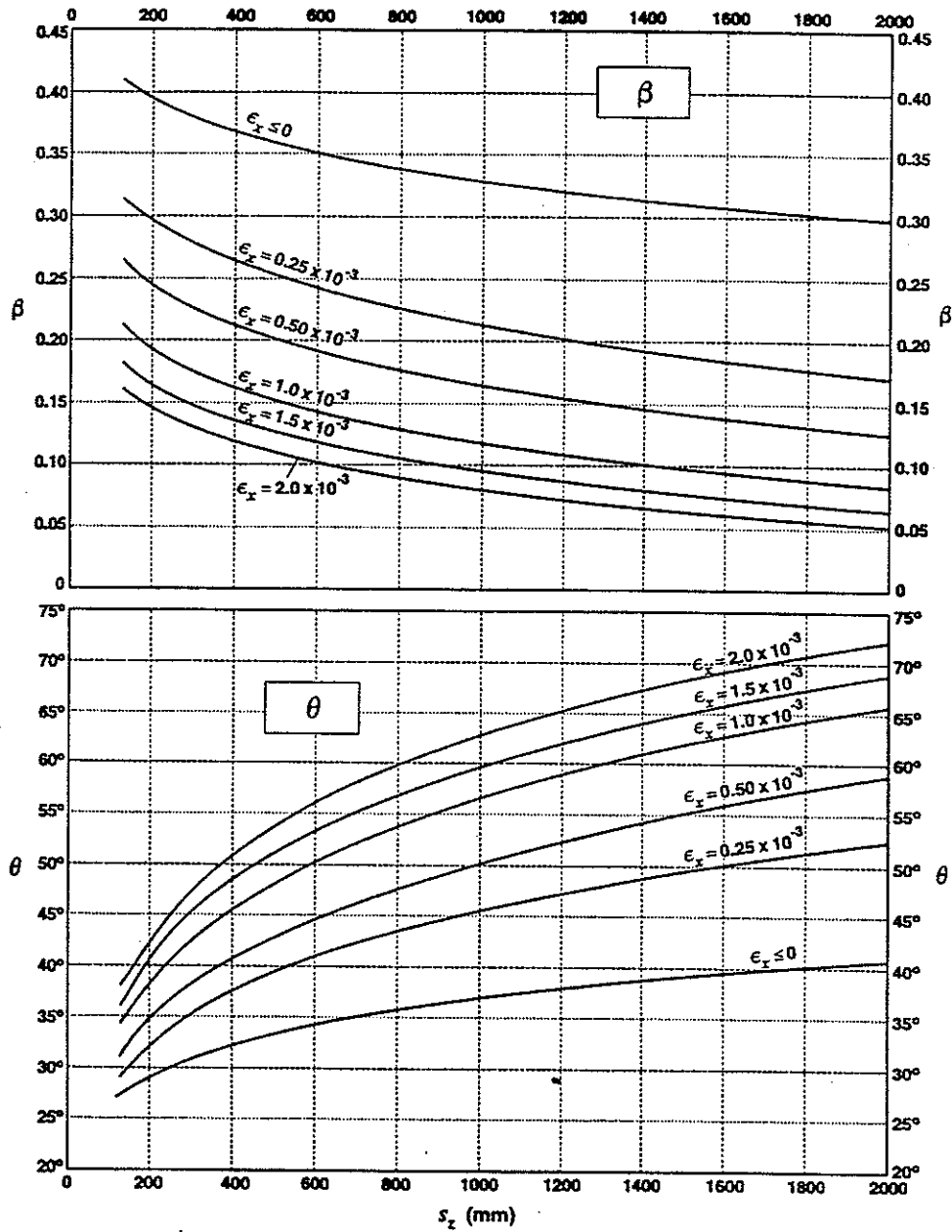


Figure 2-9. Values of β and θ for sections without shear reinforcement (CSA23.3-1994 general method)

Chapter 3

Shear Behaviour of Concrete Beams Reinforced with FRP: Background and Review¹

3.1 General

Deterioration of concrete structures has become a serious problem in the last 25 years due to corrosion of steel bars used as reinforcement for concrete structures. Cost estimates for repair and rehabilitation of existing concrete infrastructure are over billions of dollars [Bedard 1992 and Fickelhorn 1990]. As a result, there is a growing interest in building structures being more durable, having a service life exceeding 100 years. Fibre-reinforced polymers (FRP) are considered to be the materials for construction of new structures as well as for repair and strengthening of existing structures and bridges. FRP have been extensively used for aerospace and defense industries. The current challenge is to use these materials in civil engineering applications.

This chapter provides brief information on the FRP materials, their characteristics and applications in structural engineering. The chapter is focussed on the use of FRP as shear

¹ All equations in chapter 3 use metric units (Newton, mm) unless otherwise specified

reinforcement for concrete structures. The research programs conducted to investigate the strength capacity of FRP stirrups and the shear strength of concrete beams reinforced with FRP are reviewed. Design guidelines for concrete members reinforced with FRP, recently introduced in Japan, Europe and Canada, are also discussed.

3.1.1 Definition of FRP

Fibre-reinforced composite materials consist of fibres that are of high strength and modulus of elasticity embedded in a polymer matrix with distinct interfaces to achieve adequate bond. The new composite materials have unique properties that cannot be achieved with either of the constituents acting alone. In general, the fibres are the principal load-carrying members, while the surrounding matrix keeps them in the desired location and orientation, acts as a load transfer medium between them, and protects them from environmental damage due to elevated temperatures and humidity.

The various types of fibres are glass, carbon, and Kevlar 49. All these fibres are available commercially as continuous lengths. The matrix material may be polymer or ceramic. Polymers, which are commonly used, are available as two categories, thermosetting polymers such as epoxies, polyester, phenolics, and polyimides, and thermoplastic polymers such as nylons, and polyamide-imide (PAI). The chemical compositions and mechanical properties of the various types of fibres and polymers are given in many textbooks [Mallick 1993 and Murphy 1998].

3.1.2 General characteristics of FRP

Composites have become more popular and accepted by engineers, designers, manufacturers, marketing and management, due to combination of the following unique characteristics:

1. **High strength:** By proper mixing of the matrix and selection of the fibres, composite materials can provide significantly high strength properties in comparison to current conventional construction materials. However, FRP materials are also characterized by elastic behaviour up to failure, while their elastic moduli depend on the type and the volumetric ratio of the fibres. Typical stress–strain diagrams for different types of FRP materials compared to mild and high strength steel are shown in Figure 3-1.
2. **Light weight:** Composite materials have significantly higher strength-to-weight ratio than metals and other construction materials.
3. **Corrosion resistance:** Composite materials are non-corrodible. There are a number of matrix materials that can provide long-term resistance to most chemical and temperature environments.
4. **Design flexibility:** Composites can be formed into virtually any shape a designer may have in mind: complex or simple, large or small, structural or architectural.
5. **Dimensional stability:** Under severe mechanical and environmental stresses, composites are less susceptible to the viscoelastic characteristics of polymers.
6. **High dielectric strength:** Composites have outstanding electrical insulating properties.
7. **Other characteristics:** Easy finishing, low tooling cost, proven history of successful applications in aerospace industry are among the many benefits of composites.

3.1.3 Applications of FRP in structural engineering

The use of fibre-reinforced polymers in the structural engineering field has grown in the last decade. FRP comes in the form of laminates, structural sections, reinforcing bars and grids, and prestressing tendons. FRP is not intended to substitute for other materials but should be selected based on its own particular qualities. FRP encourages designers to create structural systems that could not be built using conventional materials.

One of the major factors that reduces the life of concrete structures is the corrosion of steel reinforcement. This problem is more serious in cold climates where de-icing agents accelerate the corrosion. The non-corrodible characteristics of FRP reinforcement are desirable for concrete structures in this severe cold environment. FRP has strength-to-weight ratios ranging from three to five times higher than reinforcing steel. The light weight of FRP provides easier handling and installation and reduces the assembly costs.

3.1.4 Behaviour of concrete members reinforced with FRP

Since FRP reinforcement is characterized by a linearly elastic stress–strain relationship up to failure, failure of reinforced concrete members may occur due either to rupture of the FRP reinforcing bars or to crushing of the concrete. In both cases, the failure is brittle when compared to that of a similar member reinforced with steel. Concrete members reinforced with steel are normally designed to force yielding of the steel before crushing of the concrete. To increase the margin of safety against brittle failure due to rupture of the FRP bars, the Japanese design guidelines [JSCE 1997, Machida *et al.* 1995 and

Sonobe *et al.* 1997] use a higher material safety factor, γ_m , (where design strength = nominal strength/ γ_m) for FRP reinforcement than that for steel.

Several experimental and analytical research programs have been conducted to investigate the flexural behaviour of concrete members reinforced and/or prestressed by FRP reinforcement. It was concluded that the use of fundamental principles including equilibrium of the cross section, compatibility of strains, plane sections remaining plane after deformation and constitutive behaviour of concrete and FRP material, are adequate to predict the load–deflection behaviour, the ultimate flexural capacity and the mode of failure of concrete members reinforced or prestressed by FRP reinforcement.

3.1.5 Factors affecting shear behaviour of concrete beams reinforced with FRP

Due to the unique characteristics of FRP, the following parameters may affect the behaviour of concrete members reinforced with FRP as longitudinal and/or shear reinforcement:

1. The longitudinal stiffness of the FRP flexural reinforcement, $E_{fl} A_{fl}$, which affects the flexural and shear crack width and consequently the concrete contribution in shear.
2. The transverse stiffness of the FRP flexural reinforcement which affects the dowel action component of the longitudinal bars.
3. The longitudinal stiffness of the FRP shear reinforcement, $E_{fs} A_{fs}$, which controls the width of the diagonal cracks.
4. The strength capacity of the FRP shear reinforcement, which is affected by bending the bars into stirrups and the nature of the shear cracks having an angle with the direction of the fibres.

3.2 Behaviour of FRP as shear reinforcement for concrete members

Since FRP reinforcement is non-ductile, shear failure of reinforced concrete members occurs either due to rupture of the FRP stirrups or due to crushing of the concrete in the compression zone or in the web. Failure due to rupture of FRP stirrups occurs suddenly when one or more FRP stirrups reach the ultimate capacity. This type of shear failure is brittle when compared to that of a beam reinforced with steel stirrups. The other failure mode, shear-compression failure, occurs when the diagonal shear cracks propagate diagonally toward the compression zone and cause crushing of the concrete. Such a mode of failure is comparable to that of a concrete beam with steel stirrups. However, reinforced concrete members with steel stirrups are normally designed to allow yielding of the steel stirrups before crushing of concrete.

3.2.1 Classification and fabrication of FRP shear reinforcement

FRP bars have been used as shear reinforcement for concrete beams in four different configurations, as illustrated in Figure 3-2. The fabrication process of the FRP shear reinforcement used in various experimental studies has been reported by the researchers as follows:

1. Pre-bent open stirrups: In this case the stirrups are terminated in the compression zone by a standard hook or overlapped ends. FRP stirrups are normally delivered prefabricated to the construction site or testing laboratories. The two methods of bending, reported by Maruyama *et al.* (1993), are as follows:

- i- Bend the pre-pregnated bars over metal bars to the required radius and allow the epoxy resin matrix to be hardened by heat. This process causes collapse and flattening of the bend zone.
- ii- Heat-harden the pultruded FRP bars after bending them over semi-circular grooved metal molds with a radius approximately equal to the bar diameter. This process retains the circular cross section of the bar within the bend zone.

2. Pre-bent closed-loop stirrups: These stirrups are fabricated using filament winding techniques. Duranovic *et al.* (1997) reported the fabrication of GFRP closed-loop stirrups used to reinforce concrete beams. The GFRP stirrups have a rectangular cross section of 10x4 mm. The stirrups are made by winding continuous glass fibres around a wooden mould, producing a hollow rectangular section having a wall thickness of 4 mm. After removal of the wooden mould, the GFRP hollow section is cut into the desired stirrup width (10 mm). The cutting process causes cutting of number of fibres and a consequent reduction of the effective area of the stirrup. The loss of effective area is related to the angle at which the fibres are wound during the manufacture process.

3. Pre-formed spirals: In this case, the stirrups are made by winding FRP pre-pregnated bars continuously into the desirable form according to the beam section, as shown in Figure 3-2.

4. On-site fabricated shear reinforcement: Okumura *et al.* (1993) reported a new process to fabricate CFRP bars with a curved shape. This process utilizes the joule heat of carbon fibres to cure the impregnated thermosetting resin of a rope-shaped pre-pregnated bar. The impregnated thermosetting resin used is a formulated epoxy resin

with special hardeners to provide enough latency at room temperature coupled with rapid cure at 120-150°C. The pre-pregnated bar used has a 10 mm diameter and a 60% fibre volumetric ratio. The curing process is conducted by means of an electric current of 13-15A to heat the pre-pregnated bar to about 150°C for 30 minutes. The voltage applied is 10V per metre of the bar. In their study, Okumura *et al.* (1993) used the 10-mm bar as shear reinforcement in the form of spirals.

5. Two dimensional and three dimensional grids: FRP grids, commercially named as NEFMAC (Clarke 1993) are currently produced in Japan and Canada. NEFMAC is formed into flat or curved 2-D or 3-D grid shapes by the newly developed pin-winding process, which is a kind of filament winding process. In a batch process, to form large sized 2-D or 3-D grid shapes, fibres are impregnated with a peroxide curing system, and formed into the grid shape at room temperature in successive layers. In the case of a continuous process to form a 2-D grid with a small cross-section, fibres are impregnated with a resin incorporating an ultraviolet curing system, and formed into a flat grid.

6. Diagonal FRP bars: FRP bent-up bars are permitted for use as shear reinforcement in the JSCE recommendation for FRP reinforced members. However, when bent-up reinforcement and stirrups are used together for shear reinforcement, the stirrups should not carry less than 50% of the shear force required to be borne by the shear reinforcement. Use of FRP diagonal bars was examined by Sonobe *et al.* (1995).

3.2.2 Strength capacity of FRP Stirrups

Due to the relatively low dowel resistance of FRP reinforcing bars, the strength capacity of FRP stirrups is affected by two main factors. First, bending of FRP stirrups to develop sufficient anchorage leads to a significant reduction of the stirrup capacity at the bend zone. Second, due to the diagonal nature of shear cracks, the induced forces are typically oriented at an angle with respect to the stirrups and consequently the stirrups' tensile strength parallel to the fibres cannot be fully developed. The following sections review the research completed to investigate the strength capacity of single stirrups, or bent bars compared with the tensile strength parallel to the fibres.

3.2.2.1 Bend effect

The strength reduction due to bending of FRP bars was recognized by some researchers and was found to limit the ultimate capacity of the FRP stirrups. The bend capacity of FRP bars is influenced by many factors such as the bending process, the radius of the bend, r_b , the type of the reinforcing fibres, and the bar diameter, d_b (or d_e). A photomicrograph of an individual bent fibre, shown in Figure 3-3, indicates large deformation bands around the sharp bend that might cause reduction of the strength capacity of the bend zone.

The tensile strength of FRP bent bars was investigated by Maruyama *et al.* (1993), while varying the type of material, the radius of bend, r_b , and the concrete strength, f'_c . The tested FRP bent bars were made of 7-strand CFRP bars of 7.5-mm diameter, pultruded CFRP bars of 6-mm diameter, and braided AFRP bars of 8-mm diameter. The internal

radii of the bend used in this study were 5 mm, 15 mm, and 25 mm. Both high-strength concrete of 50 MPa, and ultra-high-strength concrete of 100 MPa were used. Steel bars of 6-mm diameter were tested as control specimens. The FRP bent bar was embedded in concrete block with a 50-mm embedment length, and a tensile force was applied to the bar via a hydraulic jack, as shown in Figure 3-4. The findings of this research can be summarized as follows:

1. CFRP and AFRP bars all ruptured at the bend. The rupture occurred at the tip of the bent portion on the loading side.
2. The bend capacity of FRP bars tends to decrease as the radius of the bend, r_b , decreases. In the case of CFRP strands, for example, strength was about 65% of tensile strength parallel to the fibres for 25-mm bend radius, about 60% for 15-mm radius of bend and 50% for 5-mm radius of bend.
3. The differences in bend capacity seen for 50 MPa to 100 MPa concrete strength varied to some degree with the type of the bar and the results suggest that higher strength concrete increases the bend capacity. However, this increase in strength might be also attributed to possible improvement of the bond strength for the 50-mm straight portion prior to the bend portion (Figure 3-4).

The tensile strength of FRP bent bars was also investigated experimentally by Miyata *et al.* (1989). In this investigation, the tensile capacity of FRP bent bars and FRP grid reinforcement in concrete was examined by pullout tests. The FRP bar used in this study was composed of continuous glass fibres impregnated with epoxy resin. The nominal cross sectional area of the FRP bar was 88.4 mm^2 ($d_e=10.6 \text{ mm}$), and its strength parallel

to the fibres was 640 MPa. The variable considered was the bend radius, r_b . The FRP bars were pulled out of the concrete blocks using a centre hole jack. After failure, the concrete blocks were broken and the failure mode of the FRP bar was observed. The findings of this study can be summarized as follows:

1. The bend capacity was observed to be 60% of the strength parallel to the fibres for an inner radius of bend, r_b , of 10 mm, 70% for r_b of 15 mm, 77% for r_b of 20 mm, 75% for r_b of 25 mm and 86% for r_b of 30 mm. Clearly, the strength capacity tends to decrease as the radius of bend, r_b , decreases.
2. Rupture of the fibres at the bend zone initiated from the inside surface of the bend.
3. The FRP flat grid reinforcement failed at the transverse bar joint inside the concrete, and the tensile capacity was lower than the tensile strength parallel to the fibres.

The strength capacity and failure modes of thermoplastic FRP stirrups were investigated by Currier *et al.* (1994). Two 560x75-mm rectangular shaped stirrups, anchored to concrete blocks, were subjected to tensile force using a hydraulic jack placed between the two blocks as shown in Figure 3-5. The stirrups were formed by heating and bending the thermoplastic bands into the desired dimensions with a heat gun. Hooks and bends were shaped around a 12-mm-diameter bar. Three specimens were tested, one with both stirrups made of Nylon/Carbon, one with both stirrups made of Nylon/Aramid, and one with a stirrup of each. Strain gauges were glued to the stirrups' branches as shown in Figure 3-5. The conclusions of this study can be summarized as follows:

1. The bend capacity of the thermoplastic FRP stirrups was only about 25 percent of the tensile strength parallel to the fibres.

2. Failure for both the Nylon/Carbon and Nylon/Aramid stirrups was due mainly to the stress concentration at the bend portion of the stirrup.

The bond characteristics of hooked GFRP bars to concrete were studied by Ehsani *et al.* (1995). Thirty-six 90-degree hooked reinforcing bars embedded in concrete blocks, as shown in Figure 3-6, were tested under static loading. The specimens were tested to examine the influences of:

- a- concrete compressive strength, f_c' , that was varied between 28 and 56 MPa;
- b- bar diameter, $d_b (= d_e)$, that was 9.5, 19.0 or 28.6 mm;
- c- bend radius-to- bar diameter ratio, r_b/d_e , that was either zero or three;
- d- embedment length l_d , that was varied between 0 and $15d_e$; and
- e- tail length beyond the hook l_d^* , that was either $12d_e$ or $20d_e$.

The FRP bars used in this study the effective bar diameter $d_e (= \sqrt{4A_b/\pi})$ equals the nominal bar diameter, d_b .

The slip between the reinforcing bars and concrete was measured at the loaded end for various load levels. The tensile load was applied to the reinforcing bar until splitting of concrete or fracture of reinforcing bar occurred. The test results included the loaded-end slip, the failure load and the mode of failure. The loaded-end slip was corrected in order to exclude the elastic deformation of both unbonded part (3 in.) and that part outside the specimen (4 in.) from the measured loaded-end slip. The findings of this study can be summarized as follows:

1. For a bend radius, r_b , of $3d_e$, the strength capacity of the bend was reduced to about 70%, 70% and 64% of the strength parallel to the fibres for specimens with bar

diameters d_e of 9.5, 19.0 and 28.6 mm, respectively. For a radius of bend, r_b , of zero, these ratios further reduced to 15%, 16% and 18% for d_e of 9.5, 19.0 and 28.6 mm, respectively.

2. Higher concrete compressive strength increased the strength capacity of bent bars.
3. A minimum bend radius-to-diameter, r_b/d_e , ratio of three is recommended for GFRP hooks.
4. An additional tail length beyond $12d_e$ had no beneficial effect on the tensile strength and the slip of the bar. Therefore, use of a tail length of $12d_e$ is adequate.
5. An increase in the straight embedment length, l_d , beyond the bend increases the strength capacity and reduces the slip.

A theoretical investigation of the bend capacity of FRP stirrups was conducted by Nakamura and Higai (1995b). When a tensile force is applied to the FRP bend zone as shown in Figure 3-7, and there is no bond between FRP and concrete, the FRP bar stretches δ_x in the straight part subjected to uniform axial force (Figure 3-7). It was assumed that the cross section rotates with an angle ϕ maintaining the radius of the bend, r_b (Figure 3-7). Using the Bernoulli assumption, the strain distribution in the cross section was represented by a hyperbolic curve, and the stress distribution was therefore obtained using the product of the elastic modulus, E_f , and the strain. Integrating the stress distribution over the cross section resulted in the following equation for the strength capacity of FRP bent bars, f_{bend} :

$$f_{bend} = f_{fuv} \frac{r_b}{d_b} \ln \left(1 + \frac{d_b}{r_b} \right) \quad (3-1)$$

where d_b is the bar diameter (Figure 3-7), and f_{frv} is the tensile strength of FRP bars parallel to the fibres.

The failure criteria and capacity of FRP closed stirrups were examined experimentally and analytical by Ueda *et al.* (1995). Test specimens were designed to model a closed FRP stirrup intersecting a shear crack as shown in Figure 3-8. The closed stirrup was made of aramid FRP bar with nominal diameter and cross-sectional area of 6 mm and 25 mm², respectively. The reported tensile strength parallel to the fibres of the FRP bar was 2560 MPa. The shear crack was modelled as an artificial crack created by inserting a plastic plate of 0.5-mm thickness. The distance between the crack and bend portion was selected as a parameter and was varied to provide 10-, 60- and 110-mm lengths. Parallel to the experimental program, a 2-D nonlinear finite element analysis was carried out to investigate the local stresses at the bend portion of the FRP bar. The findings of this study can be summarized as follows:

1. The stirrup capacity was varied between 40 percent and 100 percent of the tensile strength parallel to the fibres, for specimens with embedment lengths of 10 and 60 mm, respectively. In both specimens, rupture of the FRP bar occurred at the bend zone. For the specimen with embedment length of 110 mm, the FRP bar ruptured at the artificial crack location at a stress level higher than the reported tensile strength parallel to the fibres.
2. At the bend portion, it was observed that strains at the inner surface of the bend were smaller than those at the outside surface.

Finite element analysis combined with pilot tests were undertaken by Ishihara *et al.* (1997) to evaluate the ultimate capacity of FRP stirrups as affected by the bend. The specimen and test setup used in this study were similar to those used by Ueda *et al.* (1995), as shown in Figure 3-8. The FRP bar used was “FIBRA”, which consists of twisted fibre soaked in resin and bonded sand on the surface. The two types of fibres used were aramid and carbon. The reported tensile strength parallel to the fibres of the AFRP bars was 1575 MPa and of the CFRP bars was 2260 MPa. The nominal bar diameter, $d_b (= d_e)$, was 9 mm for both the AFRP and CFRP bars. The radii of the bend, r_b , of both FRP bars were 9, 27 and 45 mm, corresponding to one, three and five times the bar diameter, respectively. The FRP bars were debonded from the location of the artificial crack to the starting point of the bend portion. Bonded and debonded bars were tested to examine the effect of bond. Four specimens reinforced with AFRP stirrups and four with CFRP stirrups, were tested. A 2-D nonlinear finite element analysis was carried out to investigate local stress in the FRP bar at the bend zone. The findings of this study can be summarized as follows:

1. It was observed that the strength increases with increase of the radius of the bend, r_b .

Based on the bonded specimens, the strength capacity ranged from 60 to 86% of the tensile strength parallel to the fibres for the AFRP stirrups and 49 to 66% for the CFRP stirrups.

2. Based on the finite element analysis, the following equation for the prediction of the bend strength, f_{bend} , was proposed:

$$f_{bend} = f_{fiv} \frac{1}{\lambda} \ln(1 + \lambda) \quad (3-2)$$

where $\ln\lambda = 0.90 + 0.73 \ln \frac{d_b}{r_b}$, and d_b is the bar diameter.

3. The experimental results indicated that the strength reduction at the bend zone is different among the different types of FRP bars. The authors concluded that the difference in the strength reduction can be attributed to the difference in the bond characteristics.

3.2.2.2 Effect of inclined shear cracks

The effect of the dowel forces induced on stirrups due to a diagonal crack, as illustrated in Figure 1-1, was considered as an important factor that might affect the capacity of FRP stirrups, and has been investigated by a few researchers, as described below.

The strength characteristics and behaviour of FRP bars were examined by Maruyama *et al.* (1989) as affected by the crack angle with the fibres. Experiments included applying concrete block specimens, containing FRP stirrups to a tension force after formation of an artificial crack at various angles with the stirrups, as shown in Figure 3-9. The three types of FRP bars used in this study were carbon, aramid, and glass and were fabricated using epoxy resin as a matrix. The reported tensile strength of the FRP bars was higher than 1500 MPa, and their nominal diameters were between five and six mm. The findings of this study can be summarized as follows:

1. The tensile capacity of various FRP bars was reduced significantly when the bars were tensioned at an angle with the fibres.

2. The reduced strength f_{fv} of the FRP bars, can be determined based on the angle θ of the crack with respect to the fibres (Figure 3-9) and the tensile strength parallel to the fibres f_{fu} , as follows:

$$f_{fv} = f_{fu} \left(1 - \frac{k}{100} \theta \right) \quad (3-3)$$

where k is the reduction factor and has a value range of 1.9 to 2.3 for CFRP bars, 1.9 for AFRP bars, 1.3 for GFRP bars, and 0.1 for steel. It should be noted that the angle θ in equation (3-3) is limited to 30 degrees.

3. According to equation (3-3), the diagonal tensile strength at a 30° angle is approximately 30% of the tensile strength parallel to the fibres for CFRP bars, 45% for AFRP bars, and 65% for GFRP bars.

The failure criteria of FRP bars subject to tensile and shear forces were investigated experimentally and analytically by Kanematsu *et al.* (1993) and Ueda *et al.* (1995). The research included Aramid FRP bars with a nominal diameter, d_b , of 8 mm, a tensile strength of 1280 MPa and an elastic modulus of 65 GPa. Specially designed concrete blocks separated into three parts by stainless steel plates, as shown in Figure 3-10, were used. The FRP bar was placed at the center. The tensile force was applied to the FRP bar by pushing the two end blocks by hydraulic jacks. After reaching the specified crack width, the two end concrete blocks were fixed to the supporting bed. While the crack width was kept constant, the central block was pushed vertically using an independent hydraulic jack to apply a shear force or a shear displacement to the FRP bar at the crack location. The variable in this study was the crack width between the end and central blocks, which was achieved by varying the initial tensile force. Four specimens were

tested by Kanematsu *et al.* (1993), and an additional eight specimens were tested by Ueda *et al.* (1995). Parallel to the experimental program, 3-D linear finite element and 2-D nonlinear finite element analyses were carried out to investigate local stresses in the FRP bar at the crack location. The findings of this study can be summarized as follows:

1. The experimental program showed that the tensile strength of the Aramid FRP bar, used in this study, was reduced significantly at the crack location under the action of combined tensile and shear forces.
2. The failure criteria of FRP bars used as reinforcement for concrete should consider not only tensile and shear forces in the FRP bar but also crack width and shear displacement.
3. Accurate estimation of the shear modulus of the FRP bar, debonding length around the FRP bar at the crack location and the bond-stress–slip relation of the FRP bar is essential for predicting the strength at the crack location using the finite element models. The shear modulus and shear strength of FRP bars are also important parameters.

A theoretical investigation was conducted by Nakamura and Higai (1995b) to evaluate the diagonal tensile strength of FRP bars. The analytical model is proposed for a given length L of a FRP bar and an applied diagonal tensile force acting on an angle θ with respect to the direction of the fibres. Based on the proposed model, the diagonal tensile strength of an FRP bar can be determined by the following equation for an FRP bar with rectangular cross-section:

$$f_{fv} = f_{fiv} / (\cos\theta + 6 \sin\theta \tan\theta) \quad (3-4)$$

For FRP bars with circular cross-sections, the following equation was proposed:

$$f_{fv} = f_{fuv} / (\cos\theta + 8 \sin\theta \tan\theta) \quad (3-5)$$

Nakamura and Higai (1995b) compared their proposed equations with experimental results conducted by Maruyama *et al.* (1989). It was concluded that the strength reduction due to diagonal tensile force can be reasonably evaluated by the proposed equations.

Based on the experimental and analytical investigations presented in the last sections, it can be concluded that the diagonal tensile strength of a FRP bar can be less than the bend capacity of an FRP stirrup. The current investigation reported in this thesis includes testing of 113 specially designed specimens to evaluate the bend capacity and the diagonal tensile strength of FRP stirrups.

3.2.3 FRP as shear reinforcement for flexural members

The use of FRP as shear reinforcement for concrete beams has been reported by various researchers in many countries. The majority of the work done has been devoted to evaluation of the shear strengthening of existing concrete members using FRP laminates as external shear reinforcement. However, the use of FRP as internal shear reinforcement in the form of stirrups has not been fully investigated. The following sections review the available results of research work conducted to evaluate the behaviour of FRP as shear reinforcement for concrete members.

3.2.3.1 Open stirrups

The shear behaviour of concrete beams reinforced with GFRP bars has been investigated by Vijay *et al.* (1996). The work addresses the shear behaviour of concrete beams reinforced with FRP bars and stirrups. The experimental program examined the applicability of ACI equations, the failure modes and the ductility factors based on energy and deformability concepts. Six beams were tested using a two-point loading system. The parameters of this study were the concrete compressive strength, f'_c , and the stirrup spacing, s . Dimensions, details and test results of beams tested by Vijay *et al.* (1996) are summarized in Table 3-1. The findings of this investigation can be summarized as follows:

1. The ACI 318-95 shear equation is conservative and adequate for the design of FRP stirrups. The following equation was used to predict the concrete contribution in shear V_{cf} :

$$V_{cf} = 0.17\sqrt{f'_c}b_wd \quad (3-6)$$

2. The permissible design stress values in FRP stirrups should be based on their bend capacity and the bond characteristics. In this study, the strength capacity of the stirrups was observed to be 248 MPa, which corresponds to about 38 percent of the strength parallel to the fibres.

A design procedure for concrete beams reinforced for shear and/or flexure with GFRP bars was proposed by Alsayed *et al.* (1996 and 1997). GFRP bars in the form of single loop stirrups with overlapping ends were used as shear reinforcement. Seven beams were designed to fail in shear and were tested under a two-point loading system. The

parameters considered were the material type of the longitudinal reinforcement and the material type of the shear reinforcement. Dimensions, details and test results of beams tested by Alsayed *et al.* (1996 and 1997) are summarized in Tables 3-2 and 3-3. The findings of this study can be summarized as follows:

1. All beams failed in shear. For the beams with GFRP stirrups, shear failure was due to the slippage of the stirrups rather than rupture.
2. The following modification to the ACI equation for shear was proposed:

$$\begin{aligned}
 V_n &= k_1 V_c + k_2 V_s \\
 V_c &= \frac{1}{6} \sqrt{f'_c} \\
 V_s &= \frac{A_v f_v d}{s}
 \end{aligned} \tag{3-7}$$

where the values of k_1 and k_2 are:

- | | |
|-------------|--|
| 1.0 and 1.0 | for beams by steel for flexure and shear |
| 0.5 and 0.5 | for beams reinforced with GFRP for flexure and shear |
| 1.0 and 0.5 | for beams reinforced with steel for flexure and GFRP for shear |
| 0.5 and 1.0 | for beams reinforced with GFRP for flexure and steel for shear |

3. The proposed modifications to the ACI equation were checked against the measured shear capacity and the results were found to be within the acceptable accuracy.

3.2.3.2 Closed-loop stirrups

The shear behaviour of concrete beams reinforced with FRP bars for flexural and shear was examined by Zhao *et al.* (1995). In particular, the contribution of FRP stirrups was studied in terms of the strain in the stirrups, shear crack opening and shear deformation. FRP stirrups were manufactured continuously in the form of a closed loop. The shape

and dimensions of beam specimens are shown in Figure 3-11. A notch was provided at the most probable location of diagonal crack initiation in one half span of the beam so as to induce a diagonal crack within the target region for measurements of crack opening and stirrup strain. Nineteen beams were tested with variation of the flexural reinforcement ratio, the location and spacing of stirrups, the material type of the stirrups and the shear span-to-depth ratio, a/d . Dimensions, details and test results of beams that failed in shear are summarized in Table 3-4. The findings of this study can be summarized as follows:

1. All beam specimens except two failed in shear. The failure was classified as shear-compression failure since none of the stirrups ruptured except in one beam.
2. When the shear-compression failure was dominant, the higher stiffness of stirrup resulted in the higher shear capacity and smaller strain at ultimate.
3. The concrete contribution, V_{cf} , for beams reinforced with FRP as longitudinal reinforcement was evaluated by the conventional code equations taking into account the ratio of the stiffness of FRP to that of steel, E_{fl}/E_s . The following expression was used in this study to predict the concrete contribution:

$$\begin{aligned}
 V_{cf} &= 0.20(1 + \beta_p + \beta_d) \left\{ 0.75 + 1.4 / (a/d) \right\} f_c^{1.3} b_w d \\
 \beta_p &= (100 \rho_{fl}^*)^{1.2} - 1 \leq 0.73 \\
 \beta_d &= (1000 / d)^{1.4} - 1 \\
 \rho_{fl}^* &= \rho_{fl} (E_{fl} / E_s)
 \end{aligned} \tag{3-8}$$

where E_{fl} is the elastic modulus of FRP longitudinal reinforcement and E_s is the elastic modulus of steel ($E_s = 200$ GPa).

4. The ratio of flexural reinforcement had insignificant effect on the shear capacity.

5. The strain distribution along a diagonal crack can be expressed by a cubic function as illustrated in Figure 3-12.
6. Taking into account the proposed strain distribution, shown in Figure 3-12, the contribution of FRP stirrups V_{sf} was determined using the following equation

$$V_{sf} = E_{fv} a_{fv} \sum (\gamma_p \gamma_w \gamma_a) (L_i / L_o)^{1/3} \quad (3-9)$$

where:

$$\gamma_p = 0.012 / (36 \rho_{fl}^* + 1),$$

$$\gamma_w = 1.7 / (520 \rho_{fv}^* + 1),$$

$$\gamma_a = 3.3 / (0.8a / d + 1),$$

$$(\gamma_p \gamma_w \gamma_a) (L_i / L_o)^{1/3} \leq \frac{f_{fv}}{E_{fv}} (L_i / L_o)^{1/3},$$

$$\rho_{fv}^* = (A_{fv} + 300) / (b_w L_o) (E_{fv} / E_s),$$

$$\rho_{fl}^* = \rho_{fl} (E_{fl} / E_s),$$

a_{fv} is the cross sectional area of a stirrup, A_{fv} is the total cross sectional area of the stirrups in the target region, and the L_i/L_o ratio is defined in Figure 3-12.

The size effect of the specimens for concrete beams reinforced with FRP was investigated by Maruyama and Zhao (1996). The contribution of FRP stirrups was studied in terms of the strain of stirrups, shear crack opening and shear deformation. Carbon FRP grids were used for flexural reinforcement and Glass FRP bars of three different sizes were used for shear reinforcement in the form of closed-loop stirrups. The configuration of beam specimens was similar to that of those tested by Zhao *et al.* (1995),

as shown in Figure 3-11. The experimental program consisted of testing of nine specimens of three different sizes of beams of rectangular cross-section, 150 x 300 mm, 300 x 600 mm and 450 x 900 mm. The beam length was selected to provide a shear span-to-depth ratio of 2.5. In addition to the effective depth, the test parameters included the amount of shear reinforcement and influence of the notch (Figure 3-11) on the shear strength. The findings of this study can be summarized as follows:

1. All beam specimens failed in shear. The failure was classified as one of the following modes of failure: a) diagonal tension failure for beams without stirrups, b) shear-compression failure for beams with large amount of stirrups, c) rupture of stirrups and d) shear-compression with rupture of stirrups (balanced mode of failure).
2. The following expression was used in this study for the concrete contribution V_{cf} ,

$$V_{cf} = 0.20\beta_p\beta_d\{0.75 + 1.4/(a/d)\}f_c^{1/3}b_wd \quad (3-10)$$

where $\beta_p = (100\rho_{fl}^*)^{1/3}$, $\beta_d = (1000/d)^{1/4}$, $\rho_{fl}^* = \rho_{fl}(E_{fl}/E_s)$, and E_{fl} is the elastic modulus of FRP longitudinal reinforcement.

3. It was observed that the difference in reinforcing materials does not significantly influence the size effect as far as the concrete contribution for shear capacity, V_{cf} is concerned. It should be mentioned that the size effect is considered in equation (3-10) by the factor β_d .
4. Based on the test results of this study, the strain distribution along a diagonal crack was assumed to be proportional to η_i which is described in Figure 3-12 and defined by the following function:

$$\eta_i = 1 - 3.3(L_i/L_o - 0.7)^2 \quad (3-11)$$

where η_i equals 1.0 at the point of intersection of the shear crack with the longitudinal reinforcement and zero at the tip of the shear crack, and L_i/L_o ratio is defined in Figure 3-12.

5. Taking into account the strain distribution of stirrups, the contribution of stirrups V_{sf} was determined using the following equation:

$$V_{sf} = A_{fv} E_{fv} \varepsilon_{fv} j d / s \quad (3-12)$$

where ε_{fv} is the ultimate strain of FRP stirrups which was formulated as a function of a/d and amount of shear reinforcement (similar to equation 3-9), and E_{fv} is the elastic modulus of the shear reinforcement.

Seven concrete beams reinforced for flexure and shear with GFRP bars were tested by Duranovic *et al.* (1997) to examine the shear strength and the mode of failure. GFRP closed-loop stirrups of 10x4-mm rectangular cross-section were used as shear reinforcement. The bend capacity of the GFRP stirrups was varied from 390 to 410MPa. Two beams reinforced with steel bars were tested as control specimens. The main variable of this study was the stirrup spacing. Dimensions, details and test results of beams failed in shear are summarized in Table 3-5. The findings of this investigation can be summarized as follows:

1. Failure of the beams was due to either diagonal shear for beams without shear reinforcement, or flexural compression or shear-rupture for beams with shear reinforcement. Two beams reinforced with GFRP stirrups failed in shear by rupture of the stirrups. However, stresses measured by means of strain gauges on the GFRP stirrups never exceeded 270 MPa.

2. The shear strength of the beams was predicted by using the modifications proposed by the Eurocrete Project (1996) to British code BS8110 (refer to section 3.5.3). The measured strain in the stirrups exceeded the design strain value of 0.0025 recommended by Eurocrete Project (1996). Therefore, the predicted values were very conservative when compared to the measured values.

3.2.3.3 Pre-formed spirals

The flexural and shear behaviour of reinforced and prestressed concrete beams using carbon or Aramid FRP bars were investigated by Yonekura *et al* (1993). The objective of this study was to examine the flexural strength, modes of failure and shear strength of reinforced and prestressed concrete beams using FRP as longitudinal and shear reinforcement. CFRP strands and AFRP bars were used as prestressing tendons and longitudinal reinforcement. Beams prestressed by conventional steel bars were tested as control specimens. AFRP spiral reinforcement was used as shear reinforcement. Twenty I-shaped beams were tested in the flexural phase of this study and 12 beams were tested in the shear phase. Details of the test specimens are shown in Figure 3-13. The parameters selected for the experimental program were the type of prestressing tendons, the type of longitudinal reinforcement, quantities of prestressing tendons, the amount of initial prestressing force and the amount of shear reinforcement provided by varying the pitch of the FRP spirals. Dimensions, details and test results of reinforced concrete beams failed in shear are summarized in Table 3-6. The following equation was used to predict the ultimate shear strength of the beams:

$$V_n = V_{cf} + V_{sf} + V_p \quad (3-13a)$$

$$V_{cf} = 0.2 \left\{ 0.75 + 1.4 / (a/d) \right\} \rho_{fl}^{*1.3} f_c^{1.3} (d/1000)^{-1.4} b_w d \quad (3-13b)$$

$$V_p = 2M_o / a \quad (3-13c)$$

$$V_{sf} = A_{fv} (E_{fv} / E_s) f_{flw} (jd/s) b_w d \quad (3-13d)$$

where $\rho_{fl}^* = \rho_{fl} (E_{fl} / E_s)$, ρ_{fl} is the reinforcement ratio of the FRP longitudinal reinforcement, and M_o is the decompression moment.

The findings of the shear phase of this investigation can be summarized as follows:

1. The beams tested for shear failed either by shear-compression or by rupture of the spiral shear reinforcement.
2. The shear strengths of prestressed concrete beams using FRP tendons and FRP spiral stirrups are smaller than those using steel tendons and steel stirrups when similar shear contribution was provided by the stirrups.
3. The proposed equation predicted safely the shear strength of reinforced and prestressed beams tested for shear. The ratios of observed to calculated shear strength were greater than 1.0 for all beams; an average of 1.23 was obtained.
4. The ultimate flexural and shear strengths of prestressed concrete beams using FRP bars were improved by increasing the prestress force.

The shear performance of specially designed concrete beams reinforced with FRP stirrups was studied by Nagasaka *et al.* (1993). The objective was to investigate the effect of pre-shaped FRP stirrups on the shear behaviour of concrete beams. Four types of bars, braided CFRP bars, braided AFRP bars, hybrid glass and carbon FRP bars, and steel bars were used as shear reinforcement. These shear reinforcements were used in the

form of rectangular spiral stirrups, except for the hybrid bars that were in the form of rectangular closed-loop stirrups. The FRP stirrups were characterized by the tensile strength parallel to the fibres, f_{fv} , and the bend capacity of the stirrup f_{bend} . Thirty-five beams of effective cross-sectional dimensions of were specially detailed and subjected to anti-symmetrical loading, as illustrated in Figure 3-14. The variables considered were the type and reinforcement ratio of stirrups, the concrete compressive strength and the clear span. Dimensions, details and test results of the beams tested by Nagasaka *et al.* (1993) are summarized in Table 3-7. The findings of this investigation can be summarized as follows:

1. Shear failure of the beams with FRP stirrups occurred due to rupture of the stirrups at the bend zone or due to crushing of a concrete strut formed between diagonal cracks.
2. The shear strength of beams that failed due to rupture of the stirrups increased almost linearly with increasing ratio of shear reinforcement and decreased almost linearly with the clear span of the beam.
3. The shear strength of beams that failed due to concrete crushing increased with increasing ratio of shear reinforcement, but the rate of increase had a tendency to reduce when the ratio was over 1%.
4. The shear strength of beams increased roughly linearly with the square root of $\rho_{fv}E_{fv}$. This demonstrates that shear strength was affected by the axial rigidity of the shear reinforcement.
5. The rupture and crushing modes were distinguished by the shear reinforcement factor $\rho_{fv}f_{bend}/f_c$, and the critical value of the factor was found to be about 0.30. For

beams with a small $\rho_{fv}f_{bend}/f'_c$ factor, a rupture mode of failure occurs, and for beams with high $\rho_{fv}f_{bend}/f'_c$ factor, crushing mode of failure occurs.

6. The ultimate shear capacity of FRP reinforced concrete beams was reasonably estimated by modifying Arakawa's formula (AIJ 1987) as follows:

For a shear-rupture mode of failure:

$$V_{n1} = 0.875b_w d \left[\frac{0.115k_u k'_p (f'_c + 180)}{(M/Vd) + 0.12} + 2.7\sqrt{\rho_{fv} f_{bend}} \right] \text{ units : kgf, cm} \quad (3-14)$$

where $k_u = 0.72$ when $d \geq 40\text{cm}$, and $k'_p = 0.82(100\rho_{fl}E_{fl}/E_s)^{0.23}$.

$$V_{n2} = 0.875b_w d \left[\frac{0.092k_u k_p (f'_c + 180)}{(M/Vd) + 0.12} + 2.7\sqrt{\rho_{fv} f_{bend}} \right] \text{ units : kgf, cm} \quad (3-15)$$

where $k_p = 0.82(100\rho_{fl})^{0.23}$.

For a shear-compression mode of failure:

$$V_{nmax} = 0.875b_w d \left[\frac{0.115k_u k'_p (f'_c + 180)}{(M/Vd) + 0.12} + 2.7\sqrt{\rho_{fv}^* f_{bend}} \right] \text{ units : kgf, cm} \quad (3-16)$$

where $\rho_{fv}^* = \rho_{fv}(E_{fv}/E_s)$.

Based on the test results, equation (3-15) for the shear capacity of beams that failed in shear-rupture resulted in a little better agreement with the measured values than equation (3-14).

The shear capacity of concrete beams using FRP as flexural and shear reinforcement was investigated experimentally by Tottori and Wakui (1993). CFRP composite cables were used as longitudinal reinforcement. GFRP, AFRP, CFRP and Vinylon FRP bars were used as shear reinforcement in the form of spirals. Specially designed specimens were

tested to evaluate the dowel capacity of CFRP flexural reinforcement. Shear tests of reinforced concrete beams were conducted on several beams with different types of shear reinforcement. The shear force contributed by the shear reinforcement was measured by means of strain gauges installed on the FRP spirals. Dimensions, details and test results for beams tested by Tottori and Wakui (1993) are summarized in Table 3-8. The findings of this study can be summarized as follows:

1. The shear force carried by the compression zone and aggregate interlock was assumed to be related to the tensile stiffness of the longitudinal reinforcement. Therefore, the shear capacity of concrete beams without shear reinforcement was proposed to be the larger of V_{cf1} and V_{cf2} , given as follows:

$$V_{cf1} = 0.2(f'_c)^{1/3}(\rho_{fl}^*)^{1/3}(1000/d)^{1/4}\left(0.75 + 1.4/a\right)b_w d \quad (3-17a)$$

$$V_{cf2} = 0.244(f'_c)^{2/3}\left(1 + \sqrt{\rho_{fl}^*}\right)\frac{\{1 + 3.33(r/d)\}}{\{1 + (a/d)^2\}}b_w d \quad (3-17b)$$

where $\rho_{fl}^* = \rho_{fl}(E_{fl}/E_s)$ and r is the length of the loading plate in the direction of the beam span.

2. The dowel capacity of the test specimens using FRP reinforcement is about 70% of those using reinforcing steel with almost the same diameter. This ratio happened to correspond to the factor $(E_{fl}/E_s)^{1/3}$, which is included in equation (3-17).
3. The stirrup strain value at ultimate was observed to be more than 1%, but did not reach the guaranteed value of the rupture strain, corresponding to f_{flw} .
4. Based on the measured shear force contributed by the FRP spirals, the contribution of concrete to the shear resisting force was observed to be equal to the shear cracking load of the beams.

5. The stirrup contribution to the shear capacity of concrete beams with FRP spirals was estimated using the following equation:

$$V_{sf} = \frac{A_{fv} E_{fv} jd}{s} \varepsilon_{fv} \quad (3-18)$$

where jd is the shear depth of the beam ($jd = d/1.15$) and ε_{fv} is the stirrup strain at ultimate. Based on the experimental results, the value of ε_{fv} was recommended to be 0.01 as far as the mode of failure is shear-rupture. There was no correlation observed between ε_{fv} obtained by shear tests and a/d , ρ_{fl} and f'_c .

3.2.3.4 On-site fabricated stirrups

A new process to fabricate CFRP stirrups with a curved shape has been reported by Okumura *et al.* (1993). Ten-mm-CFRP rope-shaped pre-pregnated bars were used as shear reinforcement in the form of spirals. The strength of the bend was evaluated experimentally to be more than $0.9f_{fu}$ for $r_b/d_b = 3.0$ and equivalent to f_{fu} for $r_b/d_b > 6.0$. Three beams reinforced for shear with CFRP spirals were tested under a two-point loading system. The beams were reinforced for flexure with steel bars. A beam without shear reinforcement was also tested as a control specimen. The variable considered was the pitch of the spirals. The shear capacity of the beams was predicted using Niwa's equation (1986) as the sum of the concrete compression, V_c , and the shear reinforcement contribution, V_{sf} , based on the truss model:

$$V_n = 0.2\rho_{sl}^{1.3}(1000/d)^{1.4}f'_c{}^{1.3}b_w d + \frac{A_{fv} f_{fv} jd}{s} \quad (3-19)$$

where jd is the shear depth ($jd = d/1.15$), ρ_{sl} is the reinforcement ratio of the steel longitudinal reinforcement and f_{fr} is the stress in the FRP spiral at ultimate.

The findings of this research can be summarized as follows:

1. Failure of beams occurred by rupture of the CFRP spirals. The spiral stress at ultimate was 65% of the tensile strength parallel to the fibres.
2. The contribution of the shear reinforcement was found to be between 55 and 70 percent of the calculated V_s . The reason for this was attributed to:
 - i- The tensile strength of the CFRP pre-pregated bars was reduced due to the kink effect at the crack location.
 - ii- The crack width was large and the concrete contribution to the shear strength was reduced.

3.2.3.5 Two-dimensional grids

The concept of using FRP planar grids for shear reinforcement in concrete beams has been investigated by Erki and Bakht (1996). Five 4-m-long beams, having a 225x500-mm cross-section, were tested to failure. Two configurations of CFRP grid, shown in Figure 3-15 and designated as Type I and Type II, were used to provide shear reinforcement for the beams. A modulus of elasticity of 71 GPa and tensile strength of 1200 MPa were obtained in laboratory testing of the CFRP grids. The cross-sectional area of the bars comprising the grids was 9.3 mm^2 . Multiple grids were stacked to provide the necessary cross-sectional area of the bars for the beams. Conventional reinforcement consisting of steel stirrups was used in one of the beams. The beams with CFRP grids were designed to provide the same tensile stiffness as the steel stirrups. One

beam was constructed using steel stirrups, two identical beams were constructed using Type I grid and two identical beams were constructed using Type II grid. All tested beams failed in flexure by concrete crushing after yielding of the flexural steel. The strains in the CFRP grids did not exceed the ultimate tensile strain, so that no failure of the shear reinforcement occurred. The cross-bars of the grids also provided sufficient anchorage for the grids, so that no pull-out occurred in these tests. Based on their study, Erki and Bakht (1996) recommended the use of FRP planar grids for shear reinforcement in concrete beams as they requires less labor for preparation and installation.

It should be mentioned that the use of FRP girds as shear reinforcement does not provide confinement for the concrete in the compression and tension sides of the beam and might permit vertical delamination of the concrete in thin-webbed beams.

3.2.3.6 FRP diagonal bars

The fundamental performance of reinforced concrete beams with diagonal FRP bars was investigated by Sonobe *et al.* (1995). Braided aramid FRP bars were used as longitudinal, diagonal reinforcement and stirrups for three specimens. The guaranteed tensile strength of the AFRP bars was 1320 MPa, and the elastic modulus was 59 GPa. Two specimens with steel reinforcement were also constructed. Details of a typical specimen and the test rig are shown in Figure 3-16. The parameters included the ratio of diagonal reinforcement to longitudinal reinforcement. The specimens were tested under antisymmetrical cyclic load. Specimens with FRP diagonal reinforcement failed by rupture of stirrups and longitudinal reinforcement. The shear strength of the beams was calculated by the following equation:

$$V_n = V_{cf} + V_{sf} + A_{f_{vD}} f_{f_{vD}} \sin \alpha_s \quad (3-20a)$$

$$f_{f_{vD}} = \frac{V_{cf} + V_{sf}}{A_{f_l} + A_{f_{vD}} \cos \alpha_s} \frac{L}{2jd} \quad (3-20b)$$

where V_{cf} and V_{sf} are the shear resisting force carried by the concrete and the stirrups, respectively, which can be determined according to the modified Arakawa's equations (3-15) and (3-16), $A_{f_{vD}}$ is the area of diagonal reinforcement, α_s is the angle between diagonal reinforcement and longitudinal axis of the member, $f_{f_{vD}}$ is the stress of diagonal reinforcement, L is the clear span length and jd is taken as $0.875d$.

The findings of this study can be summarized as follows:

1. The shear strength of FRP reinforced specimens increases as the amount of diagonal reinforcement increases.
2. The proposed method predicted well the shear strength of the specimens with FRP diagonal reinforcement.

3.2.4 Analytical studies

This section reviews the analytical work done to establish shear design guidelines for the use of FRP as reinforcement in concrete members. These investigations used either statistical analysis or theoretical models to predict the shear strength of concrete beams reinforced with FRP and tested by other researchers.

The applicability of the JSCE shear equations to shear test results of concrete beams reinforced with FRP was examined by Yokoi *et al.* (1992). The following equation was

proposed for predicting the shear strength of concrete beams reinforced with FRP bars as longitudinal and shear reinforcement:

$$V_n = \alpha V_c + \beta V_s \quad (3-21a)$$

$$V_c = 0.20(100\rho_{fl}^* f'_c)^{1/3} (1000/d)^{1/4} \left\{ 0.75 + 1.4/(a/d) \right\} b_w d \quad \text{for } a/d \geq 2.5 \quad (3-21b)$$

$$V_c = 0.77(100\rho'_{fw} f'_c)^{1/3} (1000/d)^{1/4} (a/d)^{-1.166} b_w d \quad \text{for } a/d < 2.5$$

$$V_s = A_{fv} f_{fv} (d/1.15) / s \quad (3-21c)$$

$$\alpha = -39.7 * f_{bend} / E_{fv} + 1.08 \quad \text{for } 0.002 < f_{bend} / E_{fv} < 0.013 \quad (3-21d)$$

$$\alpha = 0.80 \quad \text{for } 0.013 < f_{bend} / E_{fv}$$

$$\beta = 0.50 \quad (3-21e)$$

where the factor α was chosen to evaluate the shear force carried by concrete as a ratio of the shear cracking load V_c , the factor β was chosen to reflect the effect of bend capacity on the stirrup contribution, and $\rho_{fl}^* = \rho_{fl} (E_{fl} / E_s)$.

Non-linear finite element analysis was carried out by Sato *et al.* (1993 and 1994) to clarify the shear resisting mechanism of reinforced and prestressed concrete beams reinforced with FRP bars as flexural and shear reinforcement. Seven rectangular beams with a total depth of 300 mm and a clear span of 1400 mm were analyzed under static loading conditions. Sato *et al.* (1993 and 1994) studied the effect of the elastic modulus, E_{fv} , and the tensile strength of shear reinforcement, f_{fv} , and the prestressing force on the shear strength and the components of the shear resisting mechanism. The findings of these studies can be summarized as follows:

1. A shear-compression mode of failure mode was predicted for the analyzed beams.

2. In the case where the elastic modulus of flexural and/or shear reinforcement is low, the shear resisting component in the uncracked zone, V_{cz} , is smaller and the shear resisting component at the shear cracking zone, V_a , greater than those in a beam with high-elastic-modulus reinforcement.

An analytical model was proposed by Sato *et al.* (1995) based on finite element method (FEM) results to predict the shear strength of concrete beams which are expected to fail in either shear-compression mode or shear-rupture mode. The proposed shear resisting mechanism for beams reinforced with FRP, which is described in Figure 3-17, was based on the nonlinear finite element analysis by Sato *et al.* (1993 and 1994). From Figure 3-17, the shear strength of concrete beams reinforced with FRP was determined as follows:

$$V_n = V_{cpz} + V_{web} + V_{str} - V_{com} \quad (3-22a)$$

$$\begin{aligned} V_{cpz} &= bx_e v_{cpz} \\ v_{cpz} &= 0.65 f'_c \sin\alpha \cos\alpha \end{aligned} \quad (3-22b)$$

$$\begin{aligned} V_{web} &= \rho_{fv} bL_{web} v_{web} \\ v_{web} &= E_{fv} \varepsilon_{fv} \end{aligned} \quad (3-22c)$$

$$\varepsilon_{fv} = 0.0053 \frac{\sqrt{f'_c}}{\sqrt{a/d} + 1} e^{\left(\frac{-1000}{\rho_{fl} E_{fl}} - 0.05 \sqrt{\rho_{fl} E_{fl}} \right)}$$

$$\begin{aligned} V_{str} &= bL_{str} v_{str} \\ v_{str} &= \frac{0.77 \left(\frac{\rho_{fl} E_{fl} + 10 \rho_{fv} E_{fv}}{5000} + 0.66 \right) f_c'^{1.3}}{\sqrt{a/d} + 1} \leq \frac{1.28 f_c'^{1.3}}{\sqrt{a/d} + 1} \end{aligned} \quad (3-22d)$$

$$\begin{aligned}
 V_{com} &= bL_{com}v_{com} \\
 v_{com} &= (0.15f'_c)(d/a) \\
 x_e &= \left[\frac{1 - e^{-\alpha d}}{1 + 3.2^{-0.12}(\rho_{fv}E_{fv})^{0.4}} \right] x
 \end{aligned} \tag{3-22e}$$

where v_{cpz} is the average shear stress in the concrete in the compression zone, v_{web} is the average tensile stress in the shear reinforcement, v_{str} is the average shear stress in the concrete in the shear cracking zone, v_{com} is the average compressive stress in concrete at the horizontal zone (Figure 3-17), $\alpha = \tan^{-1}(d/a)$, x_e is the depth of the compression zone, x is the depth of the compression zone based on the bending theory and the lengths L_{web} , L_{str} and L_{com} are taken as $(h-x_e)$, $(h-x_e)$ and $(x_e a/h)$, respectively, as shown in Figure 3-17. Sato *et al.* (1995) tested their proposed model (equation 3-22) against the available experimental results. The shear strengths predicted by the proposed model agreed well with the experimental shear strengths of concrete beams not only with shear reinforcement but also without shear reinforcement.

The shear behaviour of concrete beams reinforced with FRP were predicted by Choi *et al.* (1997) using a lattice model, described in Figure 3-18. In the lattice model, the concrete is modelled as a flexural compression member, a flexural tension member, a diagonal compression member and an arch member. The reinforcement is modelled as a horizontal member and a vertical member. Based on fracture mechanics, the diagonal tension member of concrete was modelled by the one-fourth tension softening curve. The compression softening behaviour was modelled similarly to the modified compression field theory. The horizontal member in the flexural tension zone was modelled using the tension stiffening of concrete. The stress-strain relationships were assumed to be elastic

and perfectly plastic for the steel reinforcement and linearly elastic up to failure for the FRP reinforcement. To examine the applicability of the lattice model, the prediction of the applied shear-force–displacement relationship by the lattice model was compared to the experimental results of four concrete beams reinforced with either steel or FRP. The findings of this analytical investigation can be summarized as follows:

1. For beams reinforced with FRP bars, the concrete contribution for shear, V_{cf} , decreases with the increase in stress in the stirrup.
2. For beams reinforced with FRP bars, the shear strength increases with the increase in the mechanical coefficient ($\rho_{fv}f_{bend}/f_c'$) where beams fail due to the rupture of stirrups. However, with values of the mechanical coefficient higher than 0.07, the failure mode changes to the web concrete softening, and the shear strength of beams maintains almost constant value.

It should be mentioned that a limiting value for ($\rho_{fv}f_{bend}/f_c'$) of 0.30 was proposed by Nagasaka *et al.* (1993) based on an experimental investigation (see section 3.2.3.3). The ($\rho_{fv}f_{bend}/f_c'$) value proposed in the analytical study by Choi *et al.* (1997) is very small compared to that proposed by Nagasaka *et al.* (1993).

The experimental results of Duranovic *et al.* (1997) (refer to section 3.2.3.2) were compared to the results of FEM analysis using general commercial finite element packages, as well as in-house developed software, by Najjar *et al.* (1997). Four GFRP reinforced beams and four steel reinforced beams were analyzed using the ANSYS 3-D FE model. Some beams were reanalyzed using a 1-D finite element model and comparisons were made with results obtained from the 3-D FEM and experiments. In the

3-D FEM, the steel and FRP bars were modelled as smeared reinforcement within the 3-D brick element. The behaviour was predicted well for all beams except two reinforced with GFRP bars for flexure and steel or GFRP stirrups for shear. In these two beams, the FE solution stopped converging at an early stage of the analysis. Modification of the properties of the stirrups improved the situation and resulted in much better results. However, other FE software (DIANA) was used to verify the analysis of these two beams. The findings of this investigation can be summarized as follows:

1. Using commercial FE software for the analysis of FRP reinforced members can produce accurate predictions. However, 1-D approaches using simple analytical models can provide quick and accurate solutions when dealing with problems dominated by flexural behaviour.
2. The main problem of the analysis of FRP reinforced concrete was the concrete mechanical characteristics and not the FRP mechanical characteristics. In particular, the shear retention factor used by the ANSYS program to assess the capability of shear transfer along the crack was found to have a significant effect on the behaviour. It was found that the shear retention factor is affected by several parameters such as the beam size, type of reinforcement and others. Therefore, there is no direct way of establishing experimentally this particular parameter *a priori*.

The effects of the elastic modulus, E_{fl} , of the longitudinal and, E_{fv} , of the shear reinforcement on the shear strength of concrete beams were investigated analytically by Nakamura and Higai (1995b). Nakamura and Higai (1995b) proposed different equations to evaluate the bend capacity and diagonal tensile strength of FRP stirrups (equations 3-1,

3-4 and 3-5). Nakamura and Higai (1995b) complemented their study with an experimental investigation to verify the proposed analytical model. Nakamura and Higai (1995b) reported testing of ten concrete beams with stirrups, and two beams without shear reinforcement. Parameters of the experiment were:

- a- material type of the longitudinal reinforcement (GFRP or steel);
- b- material type of the stirrups (GFRP or steel);
- c- spacing of the stirrups; and
- d- radius of the bend, r_b , of GFRP stirrups.

The beams were tested under a one-point loading system with a shear span-to-depth ratio of 3.0. Dimensions, details and test results of beams tested by Nakamura and Higai (1995b) are summarized in Table 3-9. The analysis of concrete beams reinforced with FRP as longitudinal and shear reinforcement was performed using the extended modified compression field theory (Nakamura and Higai 1995a). The findings of the experimental and analytical phases can be summarized as follows:

1. Failure of beams with GFRP stirrups occurred by rupture at the bend portion of the stirrups. The radius of the bend, r_b , was an important factor for the shear strength of a concrete beam with GFRP stirrups.
2. The analytical results indicated that the shear strength is proportional to the one-fourth power of the ratio of the elastic moduli (E_{fl}/E_s). Therefore, the shear strength of the concrete beam reinforced with FRP as flexural reinforcement can be evaluated as follows:

$$V_n = V_c \left(E_{fl} / E_s \right)^{1/4} \quad (3-23)$$

where V_c is the shear strength based on Niwa's equation for concrete beams without shear reinforcement (equation 3-19).

3. The effective stress in the FRP stirrups was determined based on the bend capacity using equation (3-1) proposed by the authors. It should be noted that the authors did not utilize the design equations proposed to determine the diagonal strength of FRP bars (equations 3-4 and 3-5).
4. The contribution of FRP stirrups, V_{sf} , in the shear strength of concrete beams, V_n , was determined considering the bend capacity and the effect of shear deformation, as follows:

$$V_{sf} = \frac{A_{fv} f_{bend} jd}{s} (E_{fv} / E_s)^{0.4} \quad (3-24)$$

where jd is the shear depth ($jd = d/1.15$), and E_{fv} is the elastic modulus of the shear reinforcement.

5. Based on the analytical results, the shear strength of concrete beams reinforced with FRP stirrups was predicted as $V_n = V_{cf} + V_{sf}$, where the mode of failure was considered to be rupture of the FRP stirrups. The concrete contribution, V_{cf} , was taken as the shear strength of concrete beam without shear reinforcement (equation 3-23).

3.2.5 Field application

Carbon FRP stirrups were used for the first time as shear reinforcement for two girders of the "Taylor" bridge (Rizkalla *et al.* 1998). Construction of the Taylor bridge was completed on October 1997 in Headingley, Manitoba, Canada. CFRP was also used to prestress four girders and to reinforce part of the deck slab of Taylor bridge. Two different types of CFRP reinforcement were used. CFCC cables of 15.2-mm diameter,

produced by Tokyo Rope, Japan, were used to pretension two girders while the other two girders were pretensioned using 10-mm-diameter indented Leadline bars, produced by Mitsubishi Chemical Corporation, Japan. Two of the four girders were reinforced for shear with 15.2-mm-diameter CFCC stirrups and Leadline bars of 10x5-mm rectangular section. The other bridge girders were reinforced for shear with 15-mm-diameter epoxy coated steel stirrups. Cross-sections of the girders reinforced with CFCC, Leadline and steel bars are shown in Figure 3-19. Based on AASHTO code 1989, the girders reinforced with CFRP were designed for a stress level in the stirrups of 275 MPa at the factored load level, compared to 200 MPa stress level used for the steel stirrups. This stress in the CFRP stirrups is lower than 33 percent of the bend capacity of the stirrups, f_{bend} .

Due to a lack of design codes, several research projects were conducted to examine the performance of the bridge. One of these projects (Fam *et al.* 1997) was to examine the flexural and shear behaviour of five I-girders, 9.3 m each, reinforced for shear and prestressed by CFRP, and one beam prestressed by conventional steel strands and reinforced with steel stirrups. The test beams were 1:3.6 scale models of the Taylor bridge girders. Various stirrup sizes and configurations were used to study their effect on shear and flexural behaviour. CFCC strands of 5.0- and 7.5-mm diameter and CFCC single wire of 5-mm diameter were used as shear reinforcement in the form of double-legged open stirrups. Leadline bars of 10x5-mm rectangular section were used as shear reinforcement in the form of single- and double-legged open stirrups. The beams were subjected to four concentrated loads to simulate an equivalent truck loading condition. All beams failed in flexure except for one that failed in shear. Shear failure of the beam

with double-legged Leadline stirrups occurred due to an inappropriate configuration of the stirrups. The findings of this study can be summarized as follows:

1. The stress level induced in the stirrups and the diagonal crack width were not directly proportional to the shear reinforcement ratio.
2. Due to the relatively high elastic modulus of CFRP compared to that of other FRP reinforcement, the effect of the elastic modulus on the induced strain in the stirrups and the diagonal crack width was insignificant and was not directly proportional to the modular ratio.
3. The ACI code predicted the shear cracking load well; however, it underestimated the stirrup strain after diagonal cracking. The modified compression field theory (MCFT) predicted the entire response well.
4. For beams controlled by flexural capacity, variation of the shear reinforcement ratio did not significantly affect the flexural behaviour.

3.3 Behaviour of members reinforced with FRP as longitudinal reinforcement

The shear strength of a concrete beam reinforced with FRP as longitudinal reinforcement was found to be lower than that of a concrete beam reinforced with steel. When FRP is used as longitudinal reinforcement, shear resisting component of the compression concrete is decreased by the low rigidity of FRP reinforcement. Some researchers have proposed to resolve the problem by using FRP bars with an axial stiffness, $E_f A_{f_l}$, equal to reinforcing steel. In addition to the above-mentioned research done to evaluate the shear

strength of concrete beams with FRP as flexural and/or shear reinforcement, this section reviews other research programs devoted to concrete beams without shear reinforcement.

3.3.1 Reinforced concrete members

The shear strength of concrete beams reinforced longitudinally with FRP bars has been evaluated by many researchers as a part of the shear strength of concrete beams with FRP longitudinal and shear reinforcement. The concrete contribution, V_{cf} , given in equations (3-8), (3-10), (3-13), (3-17), (3-21) and (3-22) that was proposed by various researchers can be used for concrete members without shear reinforcement.

The size effect on the shear strength of concrete beams reinforced with FRP has been investigated analytically by Niwa *et al.* (1997). Using FEM technique and based on the fictitious crack model, Niwa *et al.* (1997) evaluated the size effect on the shear behaviour of concrete beams without shear reinforcement. Nonlinear elements perpendicular to the crack were used to represent the concrete's fracture properties. Parallel bar elements were used to account for any possible slide along the shear crack. In the analysis, the effective depth, d , of a beam was changed from 0.1 to 2 meters. In this study, the elastic modulus of FRP reinforcement was also varied as 200, 100, 67 and 50 GPa. The findings of this analytical investigation can be summarized as follows:

1. The size effect on the shear strength of concrete beams reinforced with FRP is similar to that of conventionally reinforced concrete beams.
2. The shear strength of concrete beams reinforced with FRP decreases significantly with the decrease in the elastic modulus, E_{fr} . The decreasing rate is almost proportional to $(E_{fr}/E_s)^{1/4}$.

3.3.2 Prestressed concrete members

The effect of a prestressing force on the shear strength of concrete beams reinforced with FRP tendons has been studied by Tottori and Wakui (1993). CFRP cables, commercially named as Tokyo Rope, of 12.5-mm and 15.2-mm diameter were used for prestressing. Based on their study, Tottori and Wakui proposed that the effect of prestressing on shear strength can be evaluated from the decompression moment in the case of using FRP tendons as well as in the case of using steel tendons. In this study, the shear strength was expressed as follows:

$$V_n = V_{cf} + V_p + V_{sf} \quad (3-25a)$$

$$V_p = 2.0(M_o / a) \quad (3-25b)$$

where M_o is the decompression moment, and V_{cf} , V_{sf} are given by equations (3-17) and (3-18).

Nakai *et al.* (1993) tested several beams prestressed by FRP tendons in order to investigate the influences of the prestressing force, the type of the prestressing tendons used, the elastic modulus and the reinforcement ratio on the shear strength of beams. Aramid FRP tendons (four 6-mm-diameter bars), carbon FRP cables (15.2mm) were used to prestress nine T-beams of effective depth, d , of 430 mm. The prestressing level of FRP tendons was varied between zero and 70% of the nominal tensile strength of the tendons. The beams were tested under a two-point loading system with $a/d = 2.5$. The original Niwa's equation was used to determine the shear capacity of the beams as follows:

$$V_n = V_c + V_p \quad (3-26a)$$

$$V_p = 2.0(M_o / a) \quad (3-26b)$$

where V_c is the concrete contribution as determined by Niwa's equation (3-10) without considering the effect of the elastic modulus of the longitudinal reinforcement, E_{fl} .

The findings of this study can be summarized as follows:

1. The prestressing force has a major influence on the shear strength and, for simple beams, the shear strength can be evaluated based on the decompression moment M_o and the shear span, a , as given in equation (3-26b).
2. The elastic modulus of the tendons has little influence on the shear strength of prestressed beams, and there is no need to take active steps to assess it during design.

The shear strength and failure modes of concrete beams prestressed by CFRP tendons have been investigated by Naaman and Park (1997). The main objective of the experimental program was to understand the shear behaviour of prestressed concrete beams using CFRP tendons and to compare their response with that of beams using steel tendons. CFRP cables, commercially named as Tokyo Rope, of 7.5-mm diameter and steel strands of 12.7-mm diameter were used to prestress the concrete beams. Nine beams were tested, five using CFRP tendons and four using steel strands. The beams, having dimensions of 130 x 260 x 1650 mm, were tested under a one-point loading system. The shear span-to-depth ratio, a/d , was 2.5. The crack width and differential shear (transverse) displacement at the level of the bottom reinforcement layer were measured using an infrared data acquisition system. The findings of this study can be summarized as follows:

1. Shear failure of concrete beams prestressed by FRP tendons was due to rupture of the FRP tendon at the crack location. The failure occurred by tendon rupture due to dowel forces at the critical shear crack. When steel strands were used, the shear failure mode was either shear-tension initiated by yielding of the steel strands or shear-compression initiated by crushing of the concrete.
2. The shear strength of concrete beams prestressed with FRP tendons was less than that of beams prestressed with steel strands having about the same reinforcing index.
3. The shear crack width at failure of beams prestressed with FRP tendons was about one-half that of similar beams prestressed with steel strands.

3.4 Shear Transfer

The application of the shear friction model (Kriski and Loov 1996) to reinforced concrete members requires the examination of the shear transfer mechanism, i.e., aggregate interlock and dowel action, when FRP bars used as reinforcement. This need is due to the relatively high strength of FRP combined with a low modulus of elasticity and shear strength deviating from those for steel bars. Tomaszewicz *et al.* (1997) tested push-off specimens using FRP reinforcing bars. FRP bars of glass fibre (GFRP, $d_b = 13.5$ mm, $E_f = 45$ GPa and $f_{fu} = 1000$ MPa), carbon fibre (CFRP, $d_b = 8$ mm, $E_f = 200$ GPa and $f_{fu} = 1480$ MPa) and plytron thermoplastic bars ($d_b = 9$ mm, $E_f = 23.4$ GPa and $f_{fu} = 520$ MPa) were used as reinforcement in addition to a test series of steel reinforcing bars. The push-off specimens used for the shear tests were similar to those used by Mattock (1972) and other investigators for examining the shear-friction characteristics of steel-reinforced concrete. The tests consisted of a series of specimens pre-cracked along the shear plane

prior to the shear test and another series manufactured with a smooth low-friction shear plane. Only one specimen was tested for each type of FRP reinforcing bar. A control specimen reinforced with steel bars ($d_b = 8$ mm, $E_f = 200$ GPa and $f_{sy} = 500$ MPa) was also tested. Based on this investigation, the authors concluded that the fundamental behaviour of specimens with FRP reinforcement does not appear to be very different from that of the steel reinforced specimen. However, the scope of the research was not sufficient to propose a model for the prediction of the shear transfer resistance of FRP reinforced specimens.

3.5 Design considerations

The lack of design codes and specifications is limiting the use of fibre-reinforced polymer (FRP) reinforcement for concrete structures. Numerous national efforts are completed or underway to develop design guidelines for FRP reinforced members. This section reviews the shear provisions in the proposed design guidelines for concrete structures reinforced with FRP.

3.5.1 Japanese design guidelines

Two different shear design recommendations for FRP reinforced members are presented in this section, namely, those of the Japanese society for civil engineers (JSCE) and of the Building Research Institute (BRI).

3.5.1.1 JSCE design recommendations

The JSCE recommendations for design and construction of concrete structures using FRP were first published in English in October 1997. The shear provision in these design guidelines is considered as a modified version of the JSCE (1986,1996) specifications for steel reinforced members. Two different shear design methods are proposed in the JSCE recommendation for members reinforced longitudinally and transversely with FRP bars.

Method 1:

The design shear strength, V_d , is determined by the following equation:

$$V_d = V_{cfd} + V_{sfd} + V_{ped} \quad (3-27)$$

V_{cfd} is the design shear strength of members without shear reinforcement and is given by:

$$V_{cfd} = \beta_d \beta_p \beta_n f_{vcd} b_w d / \gamma_b \quad (3-28a)$$

$$f_{vcd} = 0.2(f'_{cd})^{1/3} \quad (3-28b)$$

$$\beta_d = (1000/d)^{1/4} \leq 1.5 \quad (3-28c)$$

$$\beta_p = (100\rho_{fl}E_{fl}/E_s)^{1/3} \leq 1.5 \quad (3-28d)$$

$$\begin{aligned} \beta_n &= 1 + M_o / M_d & \text{for } N_d \geq 0 \\ \beta_n &= 1 + 2M_o / M_d & \text{for } N_d < 0 \end{aligned} \quad (3-28e)$$

where f'_{cd} is the design compressive strength of the concrete ($f'_{cd} = f'_c / \gamma_c$), N_d is the design axial compressive force (or prestressing force), M_d is the design bending moment, M_o is the decompression moment, E_s is the reference elastic modulus ($E_s = 200$ GPa), γ_b is the member safety factor ($\gamma_b = 1.3$), γ_c is the material safety factor of concrete ($\gamma_c = 1.3$ for $f'_c < 50$ MPa and 1.5 otherwise) and β_n should be within the limits $0 \leq \beta_n \leq 2.0$.

V_{sfd} is the design shear contributed by FRP shear reinforcement and is given by:

$$V_{sfd} = [A_{fv} E_{fv} \varepsilon_{fv} (\sin \alpha_s + \cos \alpha_s) / s + A_{pv} f_{pv} (\sin \alpha_p + \cos \alpha_p) / s_p] jd / \gamma_b \quad (3-29a)$$

$$\varepsilon_{fv} = 0.0001 \sqrt{f'_{mcd} \frac{\rho_{fl} E_{fl}}{\rho_{fv} E_{fv}}} \left[1 + 2 \left(\frac{\sigma_N}{f'_{mcd}} \right) \right] \leq f_{bend} / E_{fv} \quad (3-29b)$$

$$f_{bend} = \left(0.05 \frac{r_b}{d_b} + 0.3 \right) f_{fu} / \gamma_{mfb} \quad (3-29c)$$

$$f_{pv} = \sigma_{vpe} + E_{fpv} \varepsilon_{fv} \leq f_{fu} / \gamma_m \quad (3-29d)$$

$$f'_{mcd} = \left(\frac{h}{300} \right)^{-1.10} f'_{cd} \quad (3-29e)$$

$$\sigma_N = (N_d + P_{ed}) / A_g \leq 0.4 f'_{mcd} \quad (3-29f)$$

where ε_{fv} is the design value of shear reinforcement strain at ultimate limit state, f_{bend} is the design strength of the bend portion, r_b is the bend radius, d_b is the bar diameter, γ_{mfb} is the safety factor for the bend ($\gamma_{mfb} = 1.3$), α_s is the angle between the shear reinforcement and the member axis, s is the spacing of shear reinforcement, α_p and s_p are the inclination angle and spacing of draped prestressing tendons, A_{pv} is the cross-sectional area of the draped tendons, f_{pv} is the effective tensile stress in the prestressing shear reinforcement tendons, jd is the shear depth ($jd = d/1.15$), f'_{mcd} is the design compressive strength of concrete allowing for size effect, h is the total depth of the member, σ_N is the average axial compressive stress, P_{ed} is the effective prestressing force in axial tendons, and γ_b is the member safety factor ($\gamma_b = 1.15$).

V_{ped} is the component of effective tensile force of draped tendons, obtained from the following equation:

$$V_{ped} = P_{ed} \sin \alpha_p / \gamma_b \quad (3-30)$$

where γ_b is the member safety factor ($\gamma_b = 1.15$)

The shear force in concrete members should not exceed the design shear capacity V_{dmax} , determined based on the diagonal compressive capacity of web concrete, as follows:

$$\begin{aligned} V_{dmax} &= f_{wcd} b_w d / \gamma_b \\ f_{wcd} &= 1.25 \sqrt{f'_{cd}} \leq 7.8 \text{ MPa} \end{aligned} \quad (3-31)$$

where f'_{cd} is the design compressive strength of the concrete ($f'_{cd} = f'_c / \gamma_c$), and γ_b is the member safety factor ($\gamma_b = 1.3$).

Method 2:

The shear strength obtained by method 2 is generally greater than that obtained by method 1; however, it might give a lower shear strength than method 1 when the longitudinal reinforcement has high rigidity. It was reported in the JSCE design guidelines (1997) that the method given below is greatly simplified, for instance by conservatively ignoring the effect of the shear span-to-depth ratio on shear strength.

The design shear strength when shear reinforcement does not rupture is calculated as follows:

$$V_d = V_{cfd} + V_{sfd} \quad (3-32)$$

V_{cfd} is the design shear force carried by concrete, obtained from the following equation:

$$V_{cfd} = V_{czd} + V_{afd} \quad (3-33a)$$

$$V_{czd} = \beta f'_{mcd} x_e b_w / \gamma_b \quad (3-33b)$$

$$V_{aid} = \beta_P \beta_{pE} (f'_{mcd})^{1.3} (h - x_e) b_w / \gamma_b \quad (3-33c)$$

$$x_e = \left[1 + 0.8 (\rho_{fv} E_{fv})^{-0.2} \right] \left[1 + \left(\frac{\sigma_N}{f'_{mcd}} \right)^{0.7} \right] x \quad (3-33d)$$

$$\beta = 0.2 \left(\frac{\sigma_N}{f'_{mcd}} \right)^{0.7} \quad (3-33e)$$

$$\beta_P = 1 - 5 \left(\frac{\sigma_N}{f'_{mcd}} \right) \geq 0 \quad (3-33f)$$

$$\beta_{pE} = 0.24 \left(\frac{\rho_{fl} E_{fl} + 10 \rho_{fv} E_{fv}}{5000k} + 0.66 \right) \geq 0.40 \quad (3-33g)$$

$$k = 1 - \left(\frac{\sigma_N}{f'_{mcd}} \right)^{0.1} \quad (3-33h)$$

where V_{czd} is the design shear force carried by concrete in compression, V_{aid} is the design shear force carried by concrete in diagonal cracking zone, x_e is the depth of concrete compression zone at ultimate, x is the position of neutral axis according to elastic theory, σ_N is the average axial compressive stress (equation 3-29f) and γ_b is the member safety factor ($\gamma_b = 1.3$).

V_{sfd} is the design shear contributed by FRP shear reinforcement, obtained by the following equation:

$$V_{sfd} = \frac{A_{fv} E_{fv} \varepsilon_{fv} (h - x_e) b_w}{s \tan \theta_{cr}} \frac{1}{\gamma_b} \quad (3-34a)$$

$$\varepsilon_{fv} = 0.0001 \sqrt{f'_{mcd} \frac{\rho_{fl} E_{fl}}{\rho_{fv} E_{fv}}} \left[1 + 2 \left(\frac{\sigma_N}{f'_{mcd}} \right) \right] \leq f_{bend} / E_{fv} \quad (3-34b)$$

$$\theta_{cr} = 45 \left[1 - \left(\frac{\sigma_N}{f'_{mcd}} \right)^{0.7} \right] \quad (3-34c)$$

where f_{bend} is the design strength of the bend portion (equation 3-29c), ε_{fv} is the strain in the FRP shear reinforcement at ultimate limit state, and θ_{cr} is the angle of diagonal cracking.

The design shear strength when shear reinforcement breaks by fibre rupture is calculated as follows:

$$V_d = V_{co} - \beta_m (V_{co} - V_{c2d}) + \beta_m V_{aid} + \beta_m V_{sfd} \quad (3-35a)$$

$$V_{co} = \beta_o \beta_d f'_{cd} x_o b_w / \gamma_b + \beta_{po} \beta_{pleo} \beta_d (f'_{cd})^3 (h - x_o) b_w / \gamma_b \quad (3-35b)$$

$$x_o = \left[1 + \left(\frac{\sigma_N}{f'_{cd}} \right)^{0.7} \right] x \quad (3-35c)$$

$$\beta_o = 0.14 \left(\frac{\sigma_N}{f'_{cd}} \right)^{0.7} \quad (3-35d)$$

$$\beta_d = (1000 / d)^{1.4} \leq 1.5 \quad (3-35e)$$

$$\beta_{po} = 1 - 5 \left(\frac{\sigma_N}{f'_{cd}} \right) \geq 0 \quad (3-35f)$$

$$\beta_{pleo} = 0.17 \left(\frac{\rho_{fl} E_{fl}}{5000k} + 0.66 \right) \leq 0.28 \quad (3-35g)$$

$$k = 1 - \left(\frac{\sigma_N}{f'_{cd}} \right)^{0.7} \quad (3-35h)$$

$$\beta_m = \frac{f_{bend}}{E_{fv} \varepsilon_{fv}} \quad (3-35i)$$

where V_{co} is the diagonal shear cracking load, V_{czd} , V_{aid} and V_{sfd} are given by equations (3-33b), (3-33c) and (3-34a), respectively, x_o is the depth of compression zone in concrete at onset of diagonal cracking, f_{bend} is the bend capacity of FRP stirrups as given by equation (3-29c), and ε_{fv} is the strain in the FRP shear reinforcement as given by equation (3-34b).

It should be noted that the mode of failure of the beam varies depending on the rigidity of the longitudinal reinforcement and the shear reinforcement. It is implied by equations (3-34) and (3-35) that for a rigidity index $(\rho_{fl}E_{fl}+10\rho_{fv}E_{fv})$ less than 5000, shear failure occurs due to rupture of shear reinforcement and for a rigidity index $(\rho_{fl}E_{fl}+10\rho_{fv}E_{fv})$ higher than 5000, shear failure occurs due to concrete crushing.

Verification of shear cracks:

It is stated that verification of shear cracks shall be in accordance with JSCE standards for steel reinforced members. The JSCE standards indicate that for a member whose stirrup strain is not greater than 0.001 and whose service load does not exceed 0.5 to 0.7 times the ultimate load, the shear crack width does not have significant influence. The allowable crack widths set for aesthetic considerations is 0.5 mm for normal environments.

3.5.1.2 Building Research Institute (BRI)

The BRI recommendations for design of concrete structures using FRP were first published in English on August 1997 in the Journal of Composites for Construction

(Sonobe *et al.* 1997). Two different shear design methods are proposed in the BRI recommendations for members reinforced longitudinally and transversely with FRP bars.

Shear Strength Eq.(1) : Modification of Arakawa's Equation

The shear strength of members reinforced with FRP is given by:

$$v_n = \min.(0.8V_{n1}, 0.9V_{n2}) \quad (3-36a)$$

$$V_{n1} = b_w jd \left[\frac{0.115k_u k_p (f_c' + 180)}{(M/Vd) + 0.12} + 2.7 \sqrt{\rho_{fv} f_{bend}} \right] \quad \text{units: kgf, cm} \quad (3-36b)$$

$$V_{n2} = b_w jd \left[\frac{0.115k_u k_p (f_c' + 180)}{(M/Vd) + 0.12} + 2.7 \sqrt{\rho_{fv}^* f_{bend}} \right] \quad \text{units: kgf, cm} \quad (3-36c)$$

$$k_u = 0.72 \quad \text{when } d \geq 40 \text{ cm ; } k_u = 1 \quad \text{otherwise} \quad (3-36d)$$

$$k_p' = 0.82(100\rho_f \cdot E_f / E_s)^{0.23} \quad (3-36e)$$

where V_{n1} represents the shear strength when the shear reinforcement ruptures, V_{n2} represents the shear strength when the concrete undergoes compression failure, jd is the shear depth ($jd = 0.875d$), f_c' is the concrete compressive strength (kgf/cm²) and f_{bend} is the bend strength of FRP stirrups (kgf/cm²), and $\rho_{fv}^* = \rho_{fv} (E_{fv} / E_s)$.

Equation (3-36) was derived from the correspondence between the calculated and test values, since criteria for distinguishing between rupture and compression failure are not clearly established. The tested beams used to develop equation (3-36) have the following characteristics:

Concrete strength: $225 < f_c' < 500 \text{ kgf/cm}^2$

Bend capacity: $3500 < f_{bend} < 9200 \text{ kgf/cm}^2$

Shear span-to-depth ratio: $1.67 < (a/d) < 4.0$

Shear reinforcement capacity: $\rho_{fv} f_{bend} < 150 \text{ kgf/cm}^2$

Shear Strength Eq.(2) : Application of Evaluation Method of AIJ Design Guidelines

The shear strength of members reinforced with FRP is given by:

$$V_n = b_w j_t \rho_{fv} (\alpha_w f_{bend}) + \alpha_a \tan \theta (v f'_c - 2 \rho_{fv} f_{bend}) b_w h / 2 \quad \text{units : kgf, cm} \quad (3-37a)$$

$$\tan \theta = \sqrt{(Lh)^2 + 1} - L / h \quad (3-37b)$$

$$v = 0.7 - f'_c / 2000 \quad (3-37c)$$

where L is the clear span of the member (cm), h is the total depth of the member (cm), j_t is the distance between the top and bottom longitudinal reinforcements (cm), v is the effectiveness factor for compressive strength of concrete, and α_w and α_a are the effectiveness factors for truss mechanism and arch mechanism, respectively, as given below.

The reinforcement efficiency of the shear reinforcement at the ultimate state is represented by α_w , and the concrete compression section is assumed to resist shear forces up to α_a times the maximum bearable compression force. The following two alternative methods are proposed using different values for the coefficients α_w and α_a :

Alternative 1: $\alpha_w=0.50$, and $\alpha_a=1.0$; when the ultimate state takes the form of shear-

rupture failure ($\rho_{fv} f_{bend} < 0.5 v f'_c$)

Alternative 2: $\alpha_w=0.50$, and $\alpha_a=0$; when the ultimate state takes the form of shear-rupture failure

In both alternatives, when the ultimate state takes the form of shear-compression failure ($\rho_f f_{bend} > 0.5 v f'_c$), $\alpha_w = 0.50$, and $\rho_f f_{bend} = 0.5 v f'_c$ may be substituted into equation (3-37) to give:

$$V_n = b_w j_t \rho_{fv} (0.5 v f'_c) / 2 \quad (3-38)$$

Values calculated from the two alternatives were compared with the test values. While alternative 2, which ignores the arch mechanism, gives values on the safe side, the agreement between the test and calculated values is low in the range ($\rho_f f_{bend} < 50$). As ($\rho_f f_{bend}$) increases, however, the difference between alternatives 1 and 2 is reduced, the same values are given by the two alternatives for shear-compression failure (equation 3-38). The tested beams used to develop equations (3-37) and (3-38) have the following characteristics:

Concrete strength: $225 < f'_c < 500 \text{ kgf/cm}^2$

Bend capacity: $3800 < f_{bend} < 9200 \text{ kgf/cm}^2$

Span ratio: $1.6 < (L/D) < 4.0$

Shear reinforcement capacity: $25 < \rho_f f_{bend} < 150 \text{ kgf/cm}^2$

Shear reinforcement pitch: $0.09 < s/j_t < 0.5$

where j_t is the distance between the top and bottom longitudinal reinforcements.

3.5.2 Canadian Highway Bridge Design Code (CHBDC 1998)

The Canadian Highway Bridge Design Code includes a new section for fibre-reinforced structures (CHBDC 1998 and Bakht *et al.* 1996). According to the CHBDC, the shear strength of concrete members reinforced with steel is determined using the general method of the CSA23.3-94 (1994), which is based on the modified compression field

theory. The design shear capacity of concrete members reinforced with FRP is obtained by the following modification of the general method used for concrete members with steel reinforcement;

$$V_d = V_{cfd} + \phi_p V_p + V_{sfd} \leq 0.25 f'_c b_w j d \quad (3-39)$$

where $j d$ is the effective shear depth ($j d \geq 0.9 d$), V_{cfd} is the shear resistance provided by the concrete, determined by the general method (chapter 2, section 2.5.2.2), ϕ_p is the resistance factor for the prestressing tendons, V_p is the shear resistance provided by the draped tendons and V_{sfd} is the shear resistance provided by the shear reinforcement, determined by the following equation;

$$V_{sfd} = \frac{\phi_f f_{fv} A_{fv} j d (\cot \theta + \cot \alpha_s) \sin \alpha_s}{s} \quad (3-40a)$$

$$f_{fv} = E_{fv} \varepsilon_{fv} < (0.3 + 0.05 r_b / d_b) f_{fv} \quad (3-40b)$$

$$\varepsilon_{fv} = 0.0001 \sqrt{f'_c \frac{\rho_{ff} E_{ff}}{\rho_{fv} E_{fv}}} \left(1 + \left(\frac{\sigma_N}{f'_c} \right)^{0.20} \right) \leq 0.002 \quad (3-40c)$$

where ϕ_f is the material resistance factor of the FRP stirrups, θ is the angle of inclination of the principal diagonal compressive stresses to the longitudinal axis of the member, determined by the general method, α_s is the angle of inclination of the transverse reinforcement to the longitudinal axis of the member and σ_N is the average axial compressive stress.

3.5.3 Eurocrete Project

Modified design rules are being proposed by Clarke *et al.* (1996) for several European design codes (such as British code BS8110, Eurocode ENV 1992 and Norwegian code

NS 3473). The Eurocrete Project provisions for FRP shear reinforcement are the same as the provisions for steel reinforced concrete beams, the only difference being in the calculation of the concrete contribution to shear. The concrete contribution depends on the ratio of longitudinal reinforcement, which is to be multiplied by the ratio of the stiffness of the FRP to that of steel:

$$\rho_{fl}^* = \rho_{fl} (E_{fl} / E_s) \quad (3-41)$$

where $E_{fl} < E_s$, and $E_s = 200$ GPa.

The effective reinforcement ratio ρ_{fl}^* can then be used in existing expressions to obtain the shear resistance provided by the concrete.

According to Clarke *et al.* (1996), a characteristic strength of the FRP shear reinforcement should be met. The strain in the shear reinforcement at ultimate should be limited to 0.0025 (which is slightly higher than the maximum strain implied by the British standard BS 8110 which limits the stress for steel to 460 MPa). Accordingly, the limiting value of shear stress, f_{fv} , should be taken as

$$f_{fv} = 0.0025 E_{fv} \quad (3-42)$$

Furthermore, a minimum amount of shear reinforcement equivalent to a shear stress of 0.4 MPa for all grades of concrete should be provided. Test values were compared against the values predicted by BS8110, modified according to equations (3-41) and (3-42). A partial safety factor of at least 1.5 is recommended for a safe design approach.

The provision of shear reinforcement for prestressed concrete beams is the same as for reinforced beams; only the approach for obtaining the concrete contribution, V_c , to the shear strength differs. The approach proposed by the Eurocrete project for beams prestressed by FRP tendons was to treat the beam as a reinforced beam but with an axial

load. This approach was originally adopted by the Eurocode EC2 and the Norwegian standards NS3473 for prestressed concrete beams with steel tendons. The concrete contribution depends on the area of longitudinal reinforcement, which again should be modified by multiplying by the ratio of (E_{fl}/E_s) .

3.5.4 Comparative studies

Mostofinejad and Razaqpur (1997) performed a comparative study between the test data and the available FRP design recommendations and proposed an alternative procedure for shear design of RC members with FRP reinforcement. Twenty-four beams from experimental work carried out by various researchers, such as Alsayed *et al.* (1996), Vijay *et al.* (1996) and Zhao *et al.* (1995), were selected for this investigation. The JSCE and BRI design recommendations were used to predict the shear strength of the selected test beams. The findings of this study can be summarized as follows:

1. Comparison of experimental data with the results of these methods indicated that no matter which combination of FRP material and steel is used for flexural and shear reinforcement, the BRI method is highly conservative.
2. The JSCE method 1 overestimates the shear strength of FRP reinforced concrete beams in many cases.
3. The following equation proposed in this study and partially based on the ACI code, is less conservative than that of the BRI method; however, it needs a theoretical underpinning before its adoption in practice.

$$V_n = V_{c(aci)} + V_{sf} \quad (3-43a)$$

$$V_{c(aci)} = 0.166\sqrt{f'_c}b_wd \quad (3-43b)$$

$$V_{sf} = \frac{A_{fv} f_{fv} d}{s} \quad (3-43c)$$

$$f_{fv} = \frac{f_{fuw}}{\alpha d_b} \quad (3-43d)$$

$$\alpha = \frac{0.27}{1 - (f_{fuw} - 400) / 2000} \quad \text{for } f_{fuw} \leq 2000 \text{ MPa} \quad (3-43e)$$

where f_{fv} is the stress in shear reinforcement at ultimate state, f_{fuw} is the tensile strength parallel to the fibres of the FRP shear reinforcement and d_b is the bar diameter of the shear reinforcement.

It should be mentioned that equation (3-43) applies only for the shear-rupture mode of failure and cannot predict the shear-compression mode of failure.

3.6 Summary

This chapter reviews the research work, the field application project and the development of design guidelines for the use of FRP as shear reinforcement in concrete structures. It can be seen that most of the research work has been conducted in Japan and has resulted in the implementation of two different design guidelines (JSCE and BRI). The Canadian (CHBDC) and European (Eurocrete Project) codes used the experimental work carried out by Japanese researchers in their design guidelines for members reinforced with FRP.

Besides the well-known factors affecting the shear strength of reinforced concrete members, such as a/d , f_c' , ρ_{sl} , ρ_{sv} , etc., the shear strength of members reinforced with FRP is also affected by the relative stiffness (E_f/E_s) and the strength reduction of FRP stirrups due to the bend effect and the effect of the inclined shear cracks intersecting the stirrups with an angle. The use of the relative stiffness factor (E_f/E_s) to modify the shear

resistance provided by the concrete, V_c , was proposed by various researchers and code committees. The JSCE and the BRI design guidelines used the bend capacity of FRP stirrups to limit the stirrups' contribution to the shear strength of concrete beams.

It has been shown by some researchers that the diagonal tensile strength of the FRP bars is generally less than the bend capacity of FRP stirrups. However, it has been reported for beams reinforced with FRP stirrups and confirmed by many researchers that shear failure normally occurs either by concrete crushing or rupture of the FRP stirrups at the bend portion. Stirrup kinking at the crack location has not been seen to affect the capacity of FRP stirrups in beam action. Chapter 5 of the thesis presents analytical models for both bend and kink effects on the strength of FRP stirrups and proposes a rational model for each effect.

Table 3-1. Characteristics of beams tested by Vijay *et al.* (1996)

Beam no.	b_w mm	h mm	d mm	a/d (5)	f_c MPa (6)	Reinfor- -cement code (7)	Flexural reinforcement					Shear reinforcement						V_{test} kN (20)	$\frac{V_{test}}{b_w d}$ MPa (21)	Mode of failure (22)	
							type (8)	A_{fr} mm ² (9)	f_{fr} MPa (10)	E_{fr} GPa (11)	ρ_{fr} % (12)	type (13)	s mm (14)	A_{fr} mm ² (15)	f_{fr} MPa (16)	f_{fr} MPa (17)	E_{fr} GPa (18)				ρ_{fr} % (19)
1	150	300	264.5	1.89	44.8	F0	G	567	655	54	1.43	---							44.8	1.129	DT
2	150	300	264.5	1.89	44.8	FF	G	567	655	54	1.43	G	101.6	142	655	248	54	0.93	126.8	3.196	ST
3	150	300	264.5	1.89	44.8	FF	G	567	655	54	1.43	G	152.4	142	655	248	54	0.62	115	2.899	ST
4	150	300	264.5	1.89	31	F0	G	254	655	54	0.64	---							44.8	1.129	DT
5	150	300	264.5	1.89	31	FF	G	254	655	54	0.64	G	101.6	142	655	248	54	0.93	123.2	3.105	ST
6	150	300	264.5	1.89	31	FF	G	254	655	54	0.64	G	152.4	142	655	248	54	0.62	123.3	3.108	ST

column (5) a is the shear span

column (7) F0 = beams without shear reinforcement, reinforced for flexure by FRP

FF = beams with FRP shear reinforcement, reinforced for flexure by FRP

SF = beams with FRP shear reinforcement, reinforced for flexure by steel

FS = beams with steel shear reinforcement, reinforced for flexure by FRP

S0 = beams without shear reinforcement, reinforced for flexure by steel

SS = beams with steel shear reinforcement, reinforced for flexure by steel

column (8, 13) A = AFRP C = CFRP G = GFRP V = VFRP(Vynylon) H = HFRP(hybrid) S = steel

column (10, 17) f_{fr} and f_{fr} represents the guaranteed strength parallel to the fibres for FRP reinforcement and the yield strength f_{sy} for steel

column (22) DT = diagonal tension failure ST = shear failure by rupture of FRP or yield of steel SC = shear failure by concrete crushing

S = shear failure (type of failure was not identified in the corresponding reference)

Table 3-2. Characteristics of beams tested by Alsayed *et al.* (1996)

Beam no.	b_w mm	h mm	d mm	a/d	f_c MPa	Reinforcement code	Flexural reinforcement					Shear reinforcement						V_{test} kN	$v_{test} = V_{test}/b_w d$ MPa	Mode of failure	
							type	A_{fl} mm ²	f_{fl} MPa	E_{fl} GPa	ρ_{fl} %	type	s mm	A_{fv} mm ²	f_{fv} MPa	f_{bend} MPa	E_{fv} GPa				ρ_{fv} %
(1)	(2)	(3)	(4)	(5)	(6)	(7)	(8)	(9)	(10)	(11)	(12)	(13)	(14)	(15)	(16)	(17)	(18)	(19)	(20)	(21)	(22)
1	200	360	311	3.22	35.5	SS	S	603	553	200	0.97	S	150	56.6	286	n/a	200	0.19	88.9	1.430	ST
2	200	360	309.5	3.23	35.5	FF	G	851	700	36	1.37	G	150	63.3	565	n/a	42	0.21	68.5	1.107	ST
3	200	360	311	3.22	39.5	SS	S	603	553	200	0.97	S	150	56.6	286	n/a	200	0.19	100.4	1.614	ST
4	200	360	309.5	3.23	39.5	FF	G	851	700	36	1.37	G	150	63.3	565	n/a	42	0.21	57.8	0.936	ST

Table 3-3. Characteristics of beams tested by Alsayed *et al.* (1997)

Beam no.	b_w mm	h mm	d mm	a/d	f_c MPa	Reinforcement code	Flexural reinforcement					Shear reinforcement						V_{test} kN	$v_{test} = V_{test}/b_w d$ MPa	Mode of failure	
							type	A_{fl} mm ²	f_{fl} MPa	E_{fl} GPa	ρ_{fl} %	type	s mm	A_{fv} mm ²	f_{fv} MPa	f_{bend} MPa	E_{fv} GPa				ρ_{fv} %
(1)	(2)	(3)	(4)	(5)	(6)	(7)	(8)	(9)	(10)	(11)	(12)	(13)	(14)	(15)	(16)	(17)	(18)	(19)	(20)	(21)	(22)
1	200	360	309	2.36	35.7	FF	G	804	764	43	1.30	G	80	63.3	565	n/a	42	0.40	108.9	1.762	ST
2	200	360	310	2.36	35.7	SF	S	616	553	200	0.99	G	80	63.3	565	n/a	42	0.40	144.4	2.330	ST
3	200	360	309	2.36	35.2	FS	G	804	764	43	1.30	S	80	56.6	286	n/a	200	0.35	103.5	1.675	ST

Table 3-4. Characteristics of beams tested by Zhao *et al.* (1995)

Beam no.	b_w mm	h mm	d mm	a/d	f_c MPa	Reinforcement code	Flexural reinforcement					Shear reinforcement						V_{test} kN	$v_{test} = V_{test}/b_w d$ MPa	Mode of failure	
							type	A_{fl} mm ²	f_{fl} MPa	E_{fl} GPa	ρ_{fl} %	type	s mm	A_{fv} mm ²	f_{fv} MPa	f_{hend} MPa	E_{fv} GPa				ρ_{fv} %
(1)	(2)	(3)	(4)	(5)	(6)	(7)	(8)	(9)	(10)	(11)	(12)	(13)	(14)	(15)	(16)	(17)	(18)	(19)	(20)	(21)	(22)
1	150	300	250	3	34.3	F0	C	568	1124	105	1.51	---							45	1.200	DT
2	150	300	250	3	34.3	F0	C	1136	1124	105	3.03	---							46	1.227	DT
3	150	300	250	3	34.3	FF	C	1136	1124	105	3.03	G	90	56.6	1100	n/a	39	0.42	113	3.013	SC
4	150	300	250	3	34.3	FF	C	1136	1124	105	3.03	C	90	56.6	1300	n/a	100	0.42	125.9	3.357	SC
5	150	300	250	3	34.3	F0	C	852	1124	105	2.27	---							40.5	1.080	DT
6	150	300	250	3	34.3	FF	C	852	1124	105	2.27	G	90	56.6	1100	n/a	39	0.42	116.2	3.099	SC
7	150	300	250	2	34.3	FF	C	568	1124	105	1.51	G	90	56.6	1100	n/a	39	0.42	123.3	3.288	SC
8	150	300	250	4	34.3	FF	C	568	1124	105	1.51	G	90	56.6	1100	n/a	39	0.42	73.3	1.955	SC

Table 3-5. Characteristics of beams tested by Duranovi *et al.* (1997)

Beam no.	b_w mm	h mm	d mm	a/d	f_c MPa	Reinforcement code	Flexural reinforcement					Shear reinforcement						V_{test} kN	$v_{test} = V_{test}/b_w d$ MPa	Mode of failure	
							type	A_{fl} mm ²	f_{fl} MPa	E_{fl} GPa	ρ_{fl} %	type	s mm	A_{fv} mm ²	f_{fv} MPa	f_{hend} MPa	E_{fv} GPa				ρ_{fv} %
(1)	(2)	(3)	(4)	(5)	(6)	(7)	(8)	(9)	(10)	(11)	(12)	(13)	(14)	(15)	(16)	(17)	(18)	(19)	(20)	(21)	(22)
1	150	250	210	3.65	38.1	F0	G	429	1000	45	1.36	---							52.9	1.679	DT
2	150	250	210	3.65	32.9	F0	G	429	1000	45	1.36	---							43.9	1.394	DT
3	150	250	210	3.65	39.8	FF	G	429	1000	45	1.36	G	153	80	1000	n/a	45	0.35	97.9	3.110	ST
4	150	250	210	2.44	39.8	FF	G	429	1000	45	1.36	G	153	80	1000	n/a	45	0.35	133.1	4.225	ST

Table 3-6. Characteristics of beams tested by Yonekura *et al.* (1993)

Beam no.	b_w	h	d	a/d	f_c	Reinforcement code	Flexural reinforcement					Shear reinforcement						V_{test}	$v_{test} = V_{test}/b_w d$	Mode of failure	
							type	A_{fl}	f_{fl}	E_{fl}	ρ_{fl}	type	s	A_{fv}	f_{fv}	f_{bend}	E_{fv}				ρ_{fv}
(1)	(2)	(3)	(4)	(5)	(6)	(7)	(8)	(9)	(10)	(11)	(12)	(13)	(14)	(15)	(16)	(17)	(18)	(19)	(20)	(21)	(22)
1	70	220	180	2.67	62	FS	C	228	2110	145	1.81	S	40	47.2	183	---	200	1.69	98.0	7.778	SC
2	70	220	180	2.67	59.8	FS	C	307	2110	145	2.44	S	40	47.2	183	---	200	1.69	103.5	8.214	SC

Table 3-7. Characteristics of beams tested by Nagasaka *et al.* (1993)

Beam no.	b_w	h	d	a/d	f_c	Reinforcement code	Flexural reinforcement					Shear reinforcement						V_{test}	$v_{test} = V_{test}/b_w d$	Mode of failure	
							type	A_{fl}	f_{fl}	E_{fl}	ρ_{fl}	type	s	A_{fv}	f_{fv}	f_{bend}	E_{fv}				ρ_{fv}
(1)	(2)	(3)	(4)	(5)	(6)	(7)	(8)	(9)	(10)	(11)	(12)	(13)	(14)	(15)	(16)	(17)	(18)	(19)	(20)	(21)	(22)
1	250	300	253	1.19	28.9	FF	A	1200	1295	56	1.90	C	80	100	1285	903	112	0.5	246.2	3.893	ST
2	250	300	253	1.19	34.0	FF	A	1200	1295	56	1.90	C	40	100	1285	903	112	1	310.9	4.917	ST
3	250	300	253	1.19	32.8	FF	A	1200	1295	56	1.90	C	27	100	1285	903	112	1.48	359.0	5.677	ST
4	250	300	253	1.78	28.9	FF	A	1200	1295	56	1.90	C	80	100	1285	903	112	0.5	204.0	3.226	ST
5	250	300	253	1.78	28.9	FF	A	1200	1295	56	1.90	C	40	100	1285	903	112	1	276.6	4.374	ST
6	250	300	253	1.78	28.9	FF	A	1200	1295	56	1.90	C	27	100	1285	903	112	1.48	282.5	4.467	SC
7	250	300	253	2.37	32.8	FF	A	1200	1295	56	1.90	C	80	100	1285	903	112	0.5	158.9	2.513	ST
8	250	300	253	2.37	32.8	FF	A	1200	1295	56	1.90	C	40	100	1285	903	112	1	229.5	3.629	ST
9	250	300	253	1.78	33.4	FF	A	1200	1295	56	1.90	A	80	100	1373	824	60	0.5	201.1	3.179	ST
10	250	300	253	1.78	34.7	FF	A	1200	1295	56	1.90	A	40	100	1373	824	60	1	271.7	4.296	SC
11	250	300	253	1.78	33.4	FF	A	1200	1295	56	1.90	H	80	100	716	481	44	0.5	169.7	2.683	ST
12	250	300	253	1.78	33.4	FF	A	1200	1295	56	1.90	H	40	100	716	481	44	1	243.2	3.846	ST
13	250	300	253	1.78	34.7	FF	A	1200	1295	56	1.90	G	80	100	1354	608	46	0.5	175.5	2.776	ST
14	250	300	253	1.78	36.0	FF	A	1200	1295	56	1.90	G	40	100	1354	608	46	1	228.5	3.614	ST
15	250	300	253	1.78	34.1	F0	A	1200	1295	56	1.90	---							112.8	1.784	DT

Table 3-7 (cont'd). Characteristics of beams tested by Nagasaka *et al.* (1993)

Beam no.	b_w mm	h mm	d mm	a/d	f_c MPa	Reinforcement code	Flexural reinforcement					Shear reinforcement						V_{test} kN	$v_u = V_u/b_w d$ MPa	Mode of failure	
							type	A_{fl} mm ²	f_{fl} MPa	E_{fl} GPa	ρ_{fl} %	type	s mm	A_{fv} mm ²	f_{fv} MPa	f_{hend} MPa	E_{fv} GPa				ρ_{fv} %
(1)	(2)	(3)	(4)	(5)	(6)	(7)	(8)	(9)	(10)	(11)	(12)	(13)	(14)	(15)	(16)	(17)	(18)	(19)	(20)	(21)	(22)
16	250	300	253	1.78	34.1	S0	S	1020	1393	206	1.61	---							105.9	1.675	DT
17	250	300	253	1.78	22.9	F0	A	1200	1295	56	1.90	---							83.4	1.318	DT
18	250	300	253	1.78	38.2	FS	A	1200	1295	56	1.90	S	40	80	1432	---	206	0.8	270.7	4.281	SC
19	250	300	253	1.78	23.5	FF	A	1200	1295	56	1.90	C	40	100	1285	903	112	1	207.0	3.273	SC
20	250	300	253	1.78	22.5	FF	A	1200	1295	56	1.90	C	27	100	1285	903	112	1.48	221.7	3.505	SC
21	250	300	253	2.37	24.3	FF	A	1200	1295	56	1.90	C	40	100	1285	903	112	1	182.4	2.885	SC
22	250	300	253	2.37	22.9	FF	A	1200	1295	56	1.90	C	27	100	1285	903	112	1.48	191.3	3.024	SC
23	250	300	253	1.78	22.5	FF	A	1200	1295	56	1.90	A	40	100	1373	824	60	1	190.3	3.009	SC
24	250	300	253	1.78	22.5	FF	A	1200	1295	56	1.90	A	27	100	1373	824	60	1.48	203.1	3.211	SC
25	250	300	253	1.78	23.5	FF	A	1200	1295	56	1.90	H	40	100	716	481	44	1	190.3	3.009	SC
26	250	300	253	1.78	23.5	FF	A	1200	1295	56	1.90	H	27	100	716	481	44	1.48	211.9	3.350	SC
27	250	300	253	1.78	26.0	SF	S	1197	844	184	1.89	H	40	100	716	481	44	1	208.0	3.288	SC
28	250	300	253	1.78	25.2	SS	S	1197	844	184	1.89	S	40	80	1432	---	206	0.8	262.9	4.157	SC
29	250	300	253	1.78	39.5	SS	S	1197	844	184	1.89	S	40	80	1432	---	206	0.8	354.1	5.599	SC
30	250	300	253	1.78	25.3	SF	S	1197	844	184	1.89	C	80	100	1285	903	112	0.5	176.6	2.792	SC
31	250	300	253	1.78	25.4	SF	S	1197	844	184	1.89	C	40	100	1285	903	112	1	230.5	3.645	SC
32	250	300	253	1.78	27.6	SF	S	1197	844	184	1.89	C	27	100	1285	903	112	1.48	240.3	3.800	SC
33	250	300	253	1.78	39.5	FF	A	1200	1295	56	1.90	C	27	100	1285	903	112	1.48	292.3	4.622	SC
34	250	300	253	2.37	39.2	FF	A	1200	1295	56	1.90	C	27	100	1285	903	112	1.48	226.6	3.583	SC

Table 3-8. Characteristics of beams tested by Tottori *et al.* (1993)

Beam no.	b_w mm	h mm	d mm	a/d	f_c MPa	Reinforcement code	Flexural reinforcement					Shear reinforcement						V_{test} kN	$v_{test} = V_{test}/b_w d$ MPa	Mode of failure	
							type	A_f mm ²	f_{fu} MPa	E_f GPa	ρ_f %	type	s mm	A_{fv} mm ²	f_{fu} MPa	f_{bend} MPa	E_{fv} GPa				ρ_{fv} %
(1)	(2)	(3)	(4)	(5)	(6)	(7)	(8)	(9)	(10)	(11)	(12)	(13)	(14)	(15)	(16)	(17)	(18)	(19)	(20)	(21)	(22)
1	200	400	325	3.23	44.4	FF	C	456	2070	137	0.70	G	250	73.6	716	n/a	40	0.15	103.0	1.584	S
2	200	400	325	3.23	44.7	FF	C	456	2070	137	0.70	G	250	73.6	716	n/a	40	0.15	105.9	1.630	S
3	200	400	325	3.23	44.9	FF	C	456	2070	137	0.70	A	250	36	1511	n/a	69	0.07	84.9	1.305	S
4	200	400	325	2.15	44.6	FF	C	456	2070	137	0.70	C	250	34	1413	n/a	110	0.07	161.9	2.490	S
5	200	400	325	3.23	44.8	FF	C	456	2070	137	0.70	C	250	34	1413	n/a	110	0.07	83.4	1.283	S
6	200	400	325	4.31	44.6	FF	C	456	2070	137	0.70	C	250	34	1413	n/a	110	0.07	73.6	1.132	S
7	200	400	325	3.23	45.0	FF	C	456	2070	137	0.70	C	250	20.2	2040	n/a	144	0.04	98.1	1.509	S
8	200	400	325	3.23	44.7	FF	C	456	2070	140	0.70	C	175	20.2	1746	n/a	137	0.06	107.9	1.660	S
9	200	400	325	3.23	44.7	FF	C	456	2070	140	0.70	C	100	20.2	1746	n/a	137	0.10	156.9	2.415	S
10	200	400	325	3.23	39.4	FF	C	456	2070	140	0.70	A	250	60	1089	n/a	58	0.12	103.0	1.585	S
11	200	400	325	3.23	39.4	FF	A	600	1297	58	0.92	A	250	45	1236	n/a	58	0.09	83.4	1.283	S
12	200	400	325	3.23	39.4	FF	A	600	1297	58	0.92	A	175	45	1236	n/a	58	0.13	98.1	1.509	S
13	200	400	325	3.23	39.4	FF	A	600	1297	58	0.92	A	100	45	1236	n/a	58	0.23	132.4	2.037	S
14	200	400	325	3.23	39.4	FF	A	600	1297	58	0.92	A	250	60	1089	n/a	58	0.12	107.4	1.653	S
15	200	400	325	3.23	39.4	FF	A	600	1297	58	0.92	A	250	60	1089	n/a	58	0.12	78.5	1.207	S
16	200	400	325	3.23	57.8	FF	A	600	1297	58	0.92	A	250	60	1089	n/a	58	0.12	107.4	1.653	S
17	200	400	325	3.23	39.4	FF	A	600	1297	58	0.92	C	250	20.2	1746	n/a	137	0.04	86.3	1.328	S
18	200	330	285	2.11	37.2	SF	S	2323	294	206	4.07	V	75	81.4	602	n/a	36	0.54	230.5	4.044	S
19	200	330	285	2.11	37.2	SF	S	2323	294	206	4.07	V	150	81.4	602	n/a	36	0.27	221.7	3.890	S
20	200	330	285	3.16	35.3	SF	S	2323	294	206	4.07	V	75	81.4	602	n/a	36	0.54	169.7	2.977	S
21	200	330	285	3.16	35.3	SF	S	2323	294	206	4.07	V	150	81.4	602	n/a	36	0.27	137.3	2.409	S
22	200	330	285	3.16	35.3	SF	S	2323	294	206	4.07	V	225	81.4	602	n/a	36	0.18	117.7	2.065	S
23	200	330	285	4.21	31.4	SF	S	2323	294	206	4.07	V	150	81.4	602	n/a	36	0.27	115.8	2.031	S
24	200	400	325	3.23	42.2	SF	S	557	1468	192	0.86	V	100	81.4	602	n/a	36	0.41	157.9	2.430	S
25	200	400	325	3.23	71.6	SF	S	557	1468	192	0.86	V	100	81.4	602	n/a	36	0.41	165.8	2.551	S

Table 3-8 (cont'd). Characteristics of beams tested by Tottori *et al.* (1993)

Beam no.	b_w mm	h mm	d mm	a/d	f'_c MPa	Reinforcement code	Flexural reinforcement					Shear reinforcement						V_{test} kN	$v_{test} = V_{test}/b_w d$ MPa	Mode of failure	
							type	A_{fl} mm ²	f_{fl} MPa	E_{fl} GPa	ρ_{fl} %	type	s mm	A_{fv} mm ²	f_{fv} MPa	f_{bend} MPa	E_{fv} GPa				ρ_{fv} %
(1)	(2)	(3)	(4)	(5)	(6)	(7)	(8)	(9)	(10)	(11)	(12)	(13)	(14)	(15)	(16)	(17)	(18)	(19)	(20)	(21)	(22)
26	200	400	325	4.31	50.6	SF	S	557	1468	192	0.86	V	100	81.4	602	n/a	36	0.41	150.1	2.309	S
27	200	400	325	4.31	65.7	SF	S	557	1468	192	0.86	V	100	81.4	602	n/a	36	0.41	153.0	2.354	S
28	150	300	250	2.5	35.5	FF	C	206	1283	94	0.55	C	200	36.2	1283	n/a	94	0.12	57.9	1.543	S
29	150	300	250	2.5	37.6	FF	C	206	1283	94	0.55	C	100	36.2	1283	n/a	94	0.24	82.4	2.197	S
30	150	300	250	2.5	34.3	FF	C	395	1283	94	1.05	C	200	36.2	1283	n/a	94	0.12	71.4	1.903	S
31	150	300	250	2.5	34.2	FF	C	791	1283	94	2.11	C	200	36.2	1283	n/a	94	0.12	80.9	2.158	S
32	150	300	250	2.5	29.4	SF	S	774	397	206	2.06	C	200	36.2	1283	n/a	94	0.12	105.9	2.825	S
33	300	550	500	2.5	31.9	FF	C	791	1283	94	0.53	C	200	36.2	1283	n/a	94	0.06	160.4	1.069	S
34	150	300	260	3.08	38.8	SF	S	1161	369	206	2.98	A	300	56.6	1766	n/a	53	0.13	84.9	2.176	S
35	150	300	260	3.08	42.2	FF	A	1200	1278	63	3.08	A	300	56.6	1766	n/a	53	0.13	60.3	1.547	S
36	200	300	250	3.2	40.7	SF	S	2323	369	206	4.65	A	200	150	1278	n/a	64	0.38	191.8	3.836	S
37	200	300	250	2	77.5	FF	C	465	1766	137	0.93	A	100	56.5	1864	n/a	53	0.28	260.5	5.209	S
38	200	300	250	3	82.5	FF	C	465	1766	137	0.93	A	75	56.5	1864	n/a	53	0.38	172.2	3.443	S
39	200	300	250	3	84.2	FF	C	465	1766	137	0.93	C	100	30.4	1766	n/a	137	0.15	194.2	3.885	S
40	200	300	250	3	84.2	FF	C	465	1766	137	0.93	A	125	56.5	1864	n/a	53	0.27	140.3	2.806	S
41	200	300	250	3	82.5	FF	C	465	1766	137	0.93	C	125	30.4	1766	n/a	137	0.12	182.9	3.659	S
42	200	400	325	2.15	44.6	F0	C	456	2070	137	0.70	---							98.1	1.509	S
43	200	400	325	3.23	44.5	F0	C	456	2070	137	0.70	---							122.6	1.887	S
44	200	400	325	4.31	45.0	F0	C	456	2070	137	0.70	---							117.7	1.811	S
45	200	400	325	2.77	46.9	F0	S	557	1468	192	0.86	---							147.1	2.264	S
46	200	400	325	3.23	46.9	F0	S	557	1468	192	0.86	---							93.2	1.434	S
47	200	400	325	4.31	46.9	F0	S	557	1468	192	0.86	---							78.5	1.207	S
48	200	400	325	2.15	46.9	F0	A	600	1297	58	0.92	---							152.0	2.339	S
49	200	400	325	3.23	46.9	F0	A	600	1297	58	0.92	---							61.8	0.951	S
50	200	400	325	4.30	46.9	F0	A	600	1297	58	0.92	---							47.1	0.724	S

Table 3-9. Characteristics of beams tested by Nakamura *et al.* (1995)

Beam no.	b mm	h mm	d mm	a/d (5)	f_c MPa (6)	Reinforcement code (7)	Flexural reinforcement					Shear reinforcement						V_{test} kN (20)	$v_{test} = V_{test}/b_w d$ MPa (21)	Mode of failure (22)	
							type (8)	A_{fl} mm ² (9)	f_{fl} MPa (10)	E_{fl} GPa (11)	ρ_{fl} % (12)	type (13)	s mm (14)	A_{fv} mm ² (15)	f_{fv} MPa (16)	f_{bend} MPa (17)	E_{fv} GPa (18)				ρ_{fv} % (19)
1	300	200	150	4	22.7	F0	G	603	751	29	1.34	---							33.1	0.736	DT
2	300	200	150	4	27.8	F0	G	804	751	29	1.79	---							36.3	0.808	DT
3	200	300	250	3	35.4	FF	G	804	751	29	1.61	G	100	70	828	544	31	0.35	83.4	1.668	ST
4	200	300	250	3	33.4	FF	G	804	751	29	1.61	G	100	70	828	649	31	0.35	100.1	2.001	ST
5	200	300	250	3	35.2	FF	G	804	751	29	1.61	G	200	70	828	544	31	0.18	56.2	1.124	ST
6	200	300	250	3	35.2	FF	G	804	751	29	1.61	G	200	70	828	649	31	0.18	66.2	1.324	ST
7	200	300	250	3	34.7	SF	S	861	371	180	1.72	G	150	70	828	544	31	0.23	96.4	1.929	ST
8	200	300	250	3	34.4	SF	S	861	371	180	1.72	G	150	70	828	649	31	0.23	106.3	2.127	ST
9	200	300	250	3	35.6	SF	S	861	371	180	1.72	G	250	70	828	544	31	0.14	79.8	1.596	ST
10	200	300	250	3	35.8	SF	S	861	371	180	1.72	G	250	70	828	649	31	0.14	79.8	1.596	ST
11	200	300	250	3	38.6	FS	G	804	751	29	1.61	S	150	64	370	---	180	0.21	77.2	1.543	ST
12	200	300	250	3	37.1	FS	G	804	751	29	1.61	S	250	64	370	---	180	0.13	54.7	1.095	ST

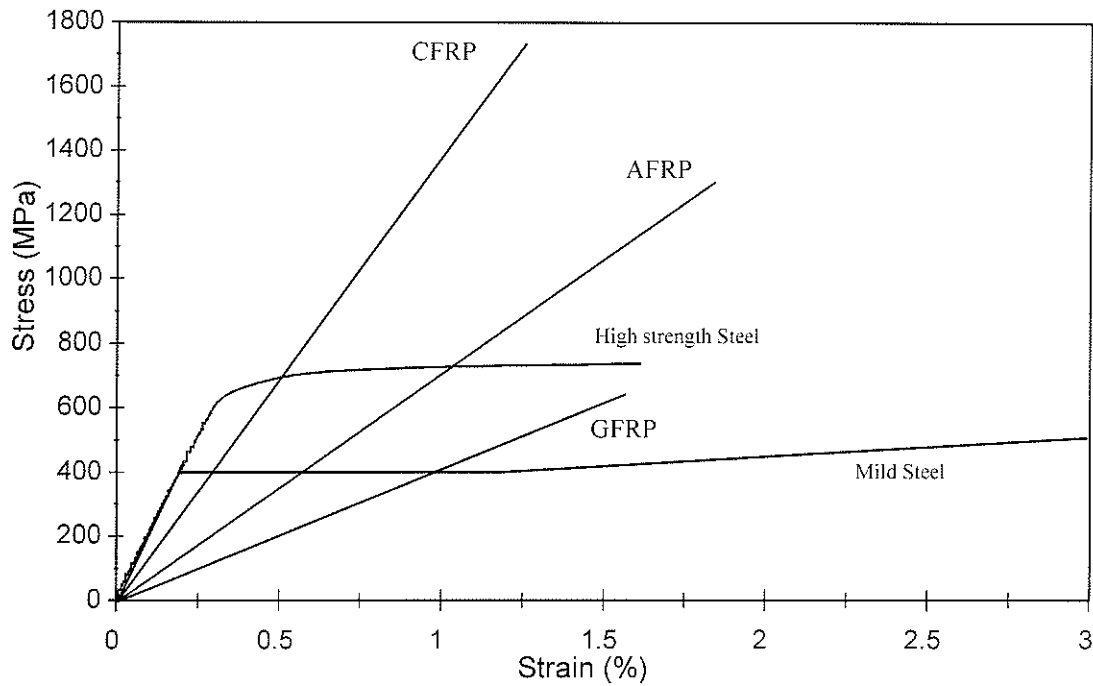


Figure 3-1. Stress-strain relationships for typical FRP and steel shear reinforcement

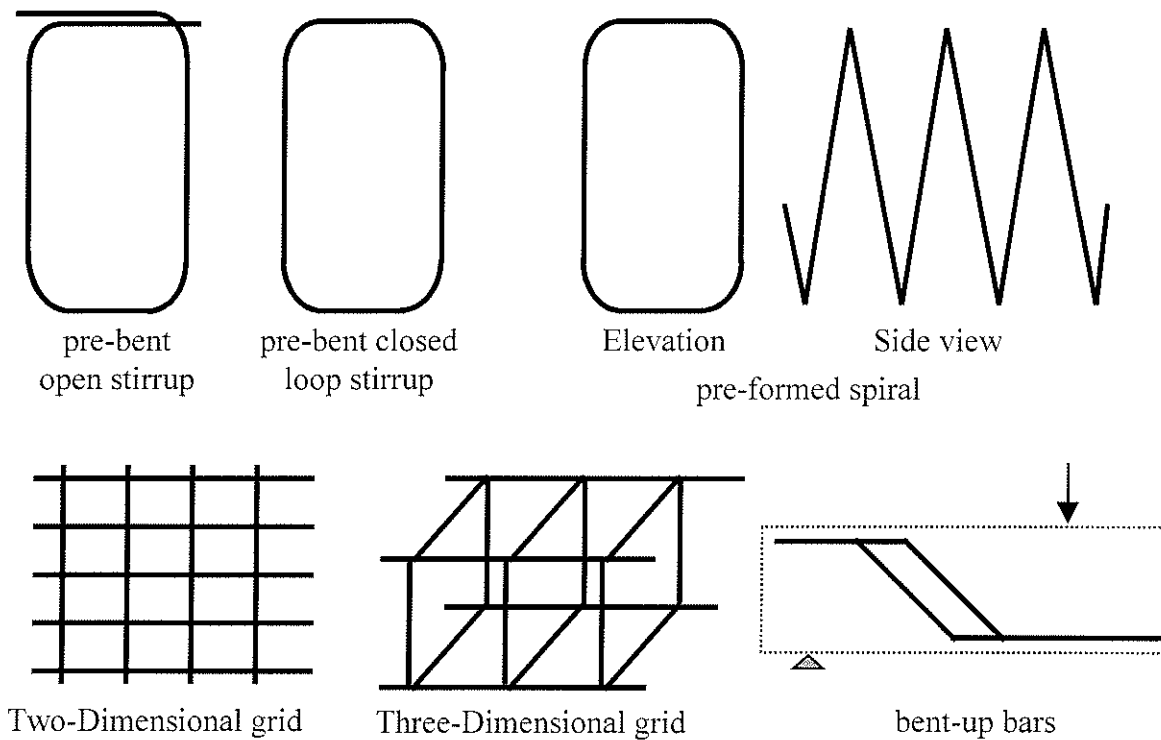


Figure 3-2. Different configurations of FRP shear reinforcement

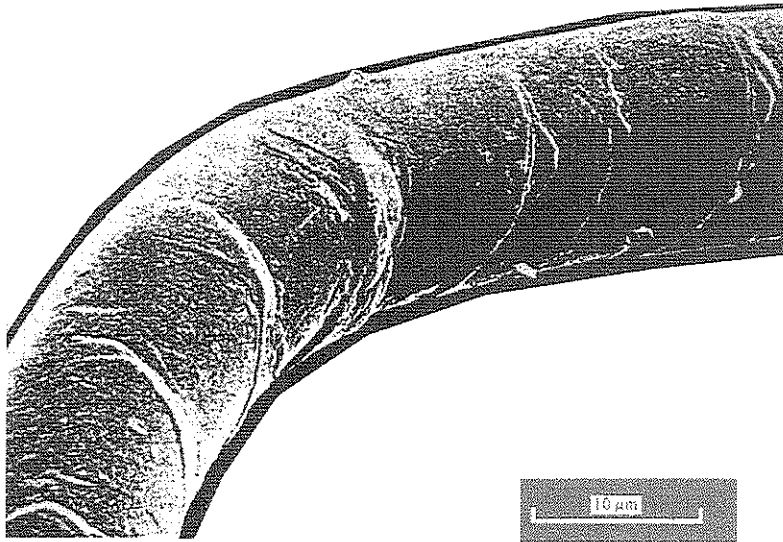


Figure 3-3. Photomicrograph photo of a bent fibre

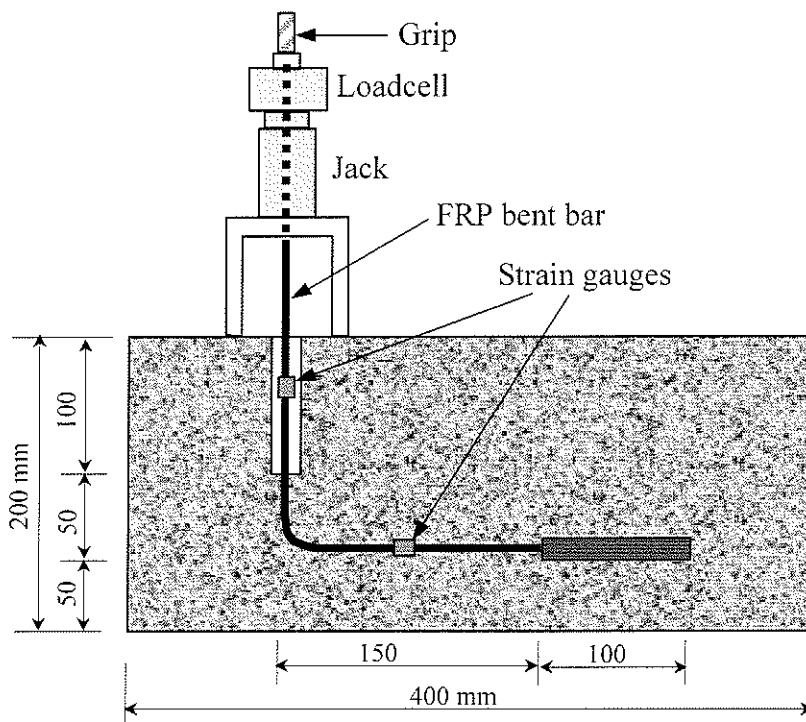


Figure 3-4. Test setup by Maruyama *et al.* (1993)

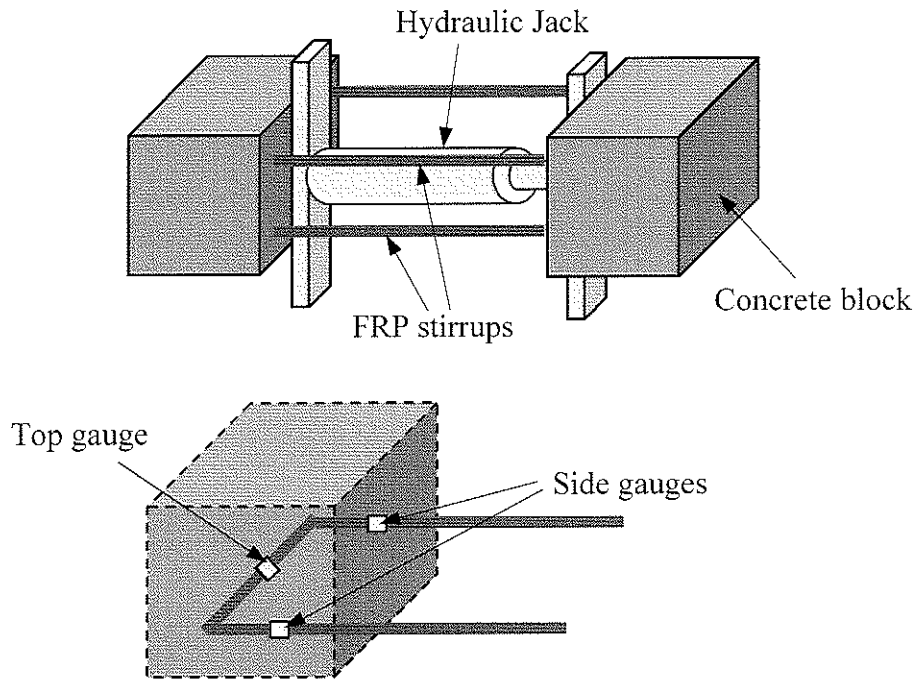


Figure 3-5. Details of specimens by Currier *et al.* (1994)

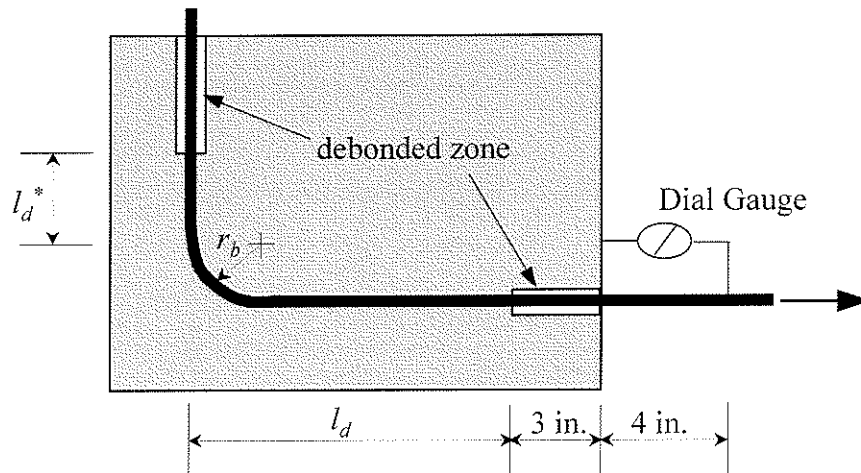


Figure 3-6. Details of specimens by Ehsani *et al.* (1995)

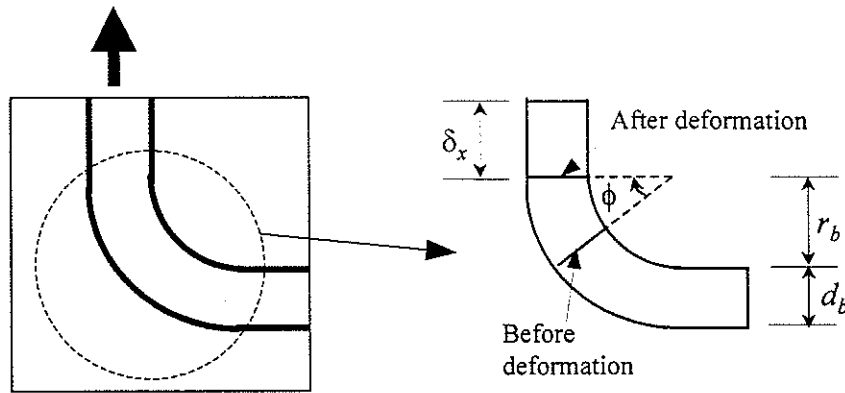


Figure 3-7. Model of bent bar in concrete by Nakamura and Higai (1995)

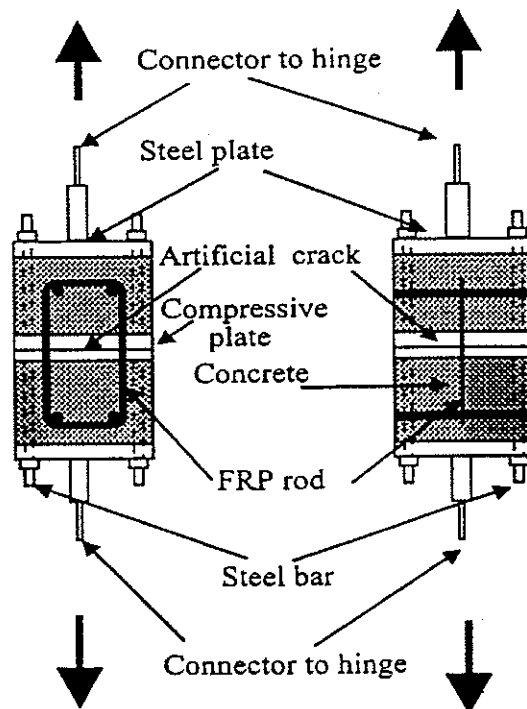


Figure 3-8. Test setup by Ueda *et al.* (1995)

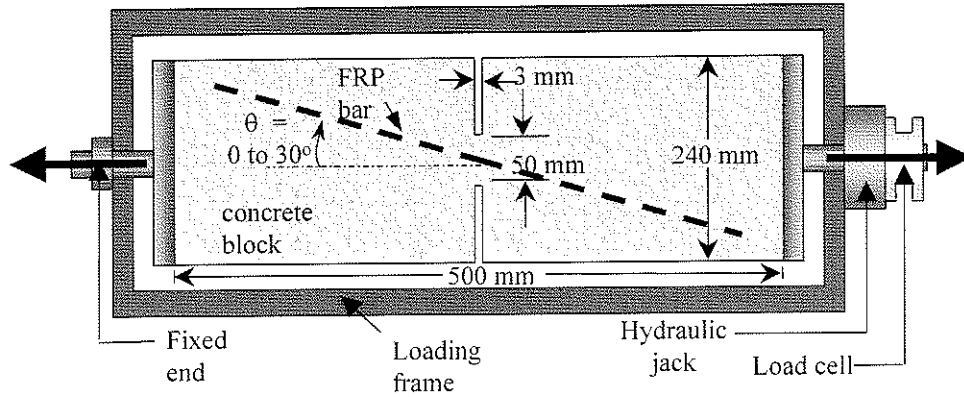


Figure 3-9. Details of specimens and test setup by Maruyama *et al.* (1989)

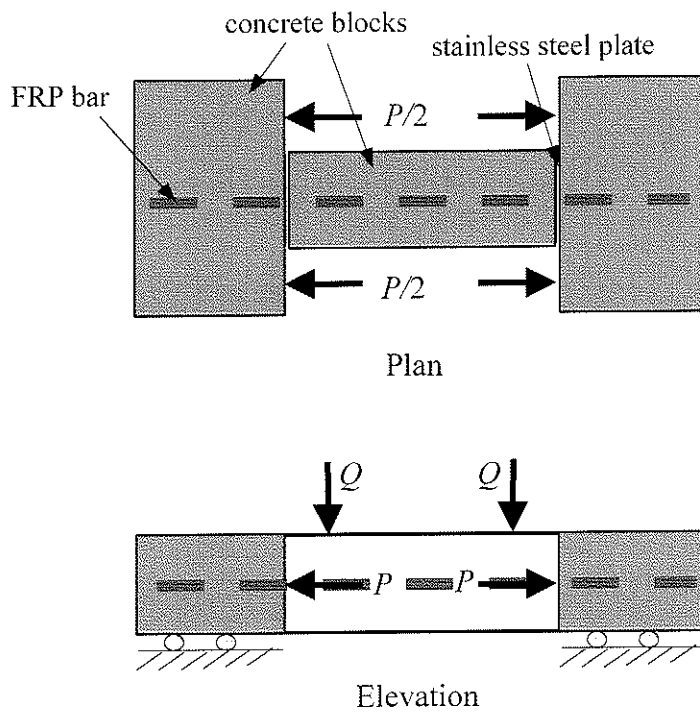


Figure 3-10. Test setup by Kanemastu *et al.* (1993)

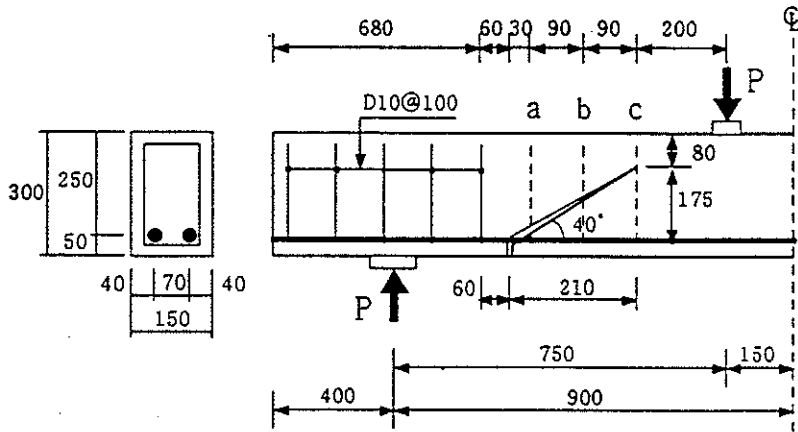


Figure 3-11. Details of specimens by Zhao *et al.* (1995)

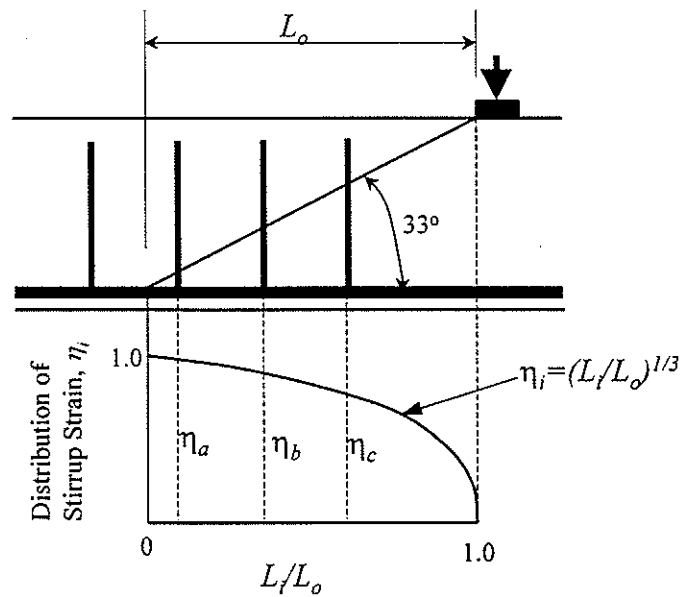


Figure 3-12. Model of stirrup strain distribution by Zhao *et al.* (1995)

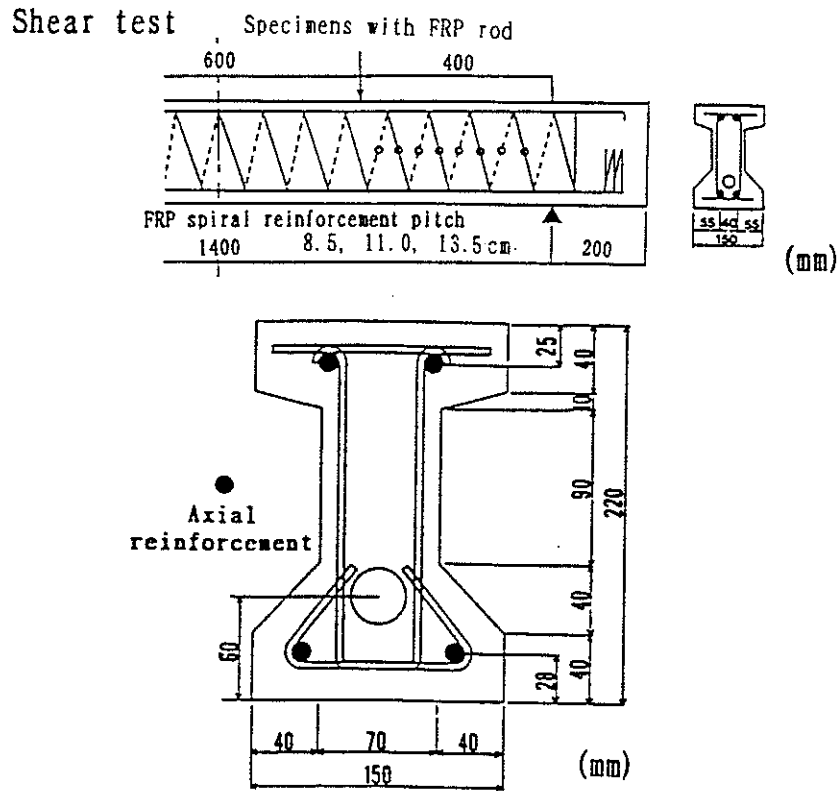


Figure 3-13. Details of specimens by Yonekura *et al.* (1993)

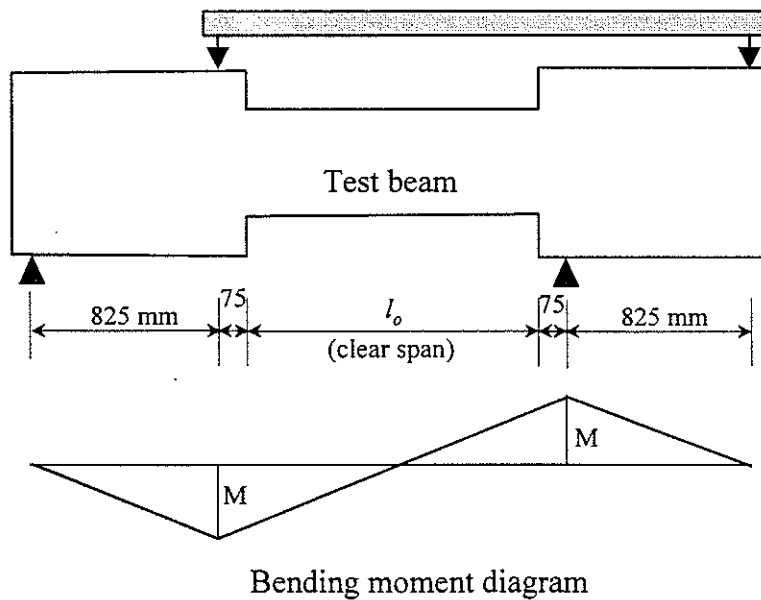


Figure 3-14. Outline of specimens and test setup by Nagasaka *et al.* (1993)

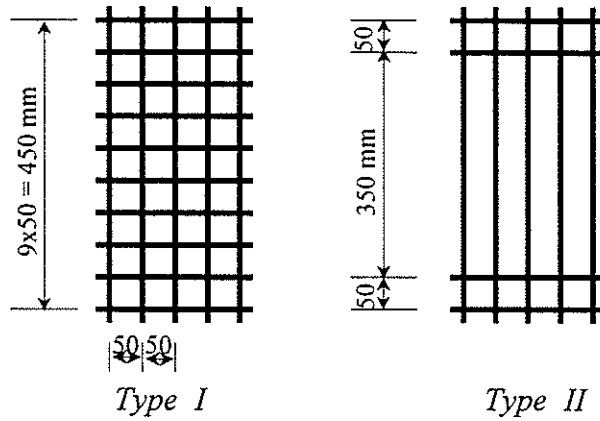


Figure 3-15. CFRP grids used by Erki and Bakht (1996)

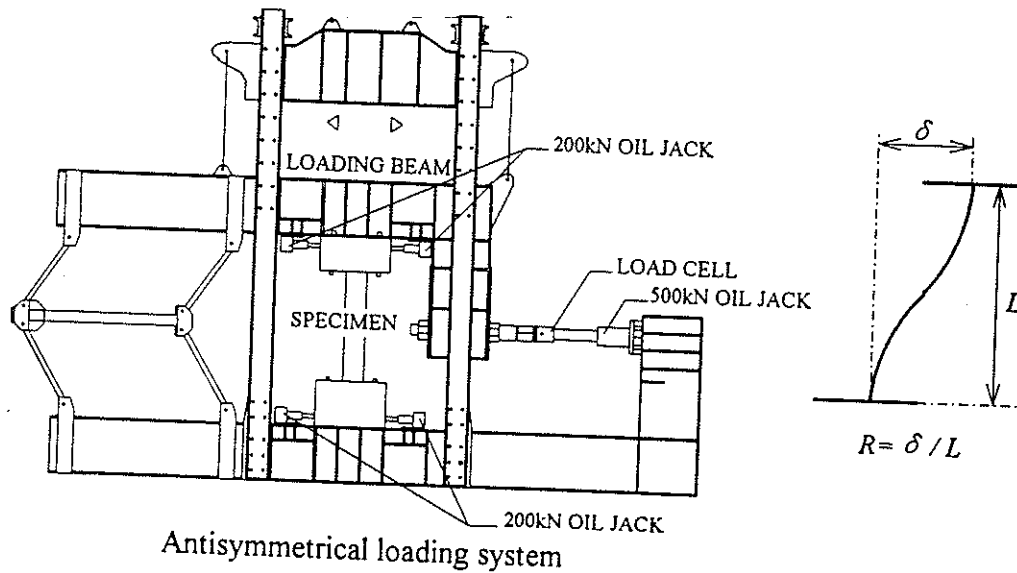
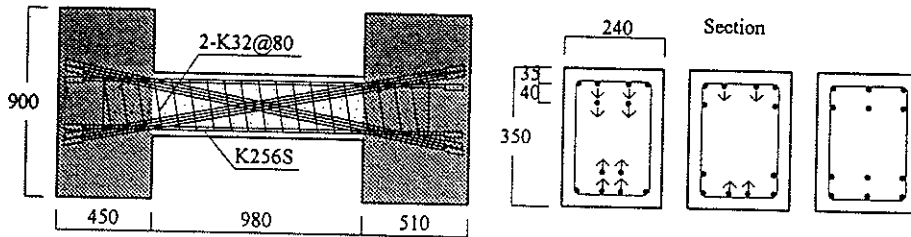


Figure 3-16. Details of specimens and test setup by Sonobe *et al.* (1995)

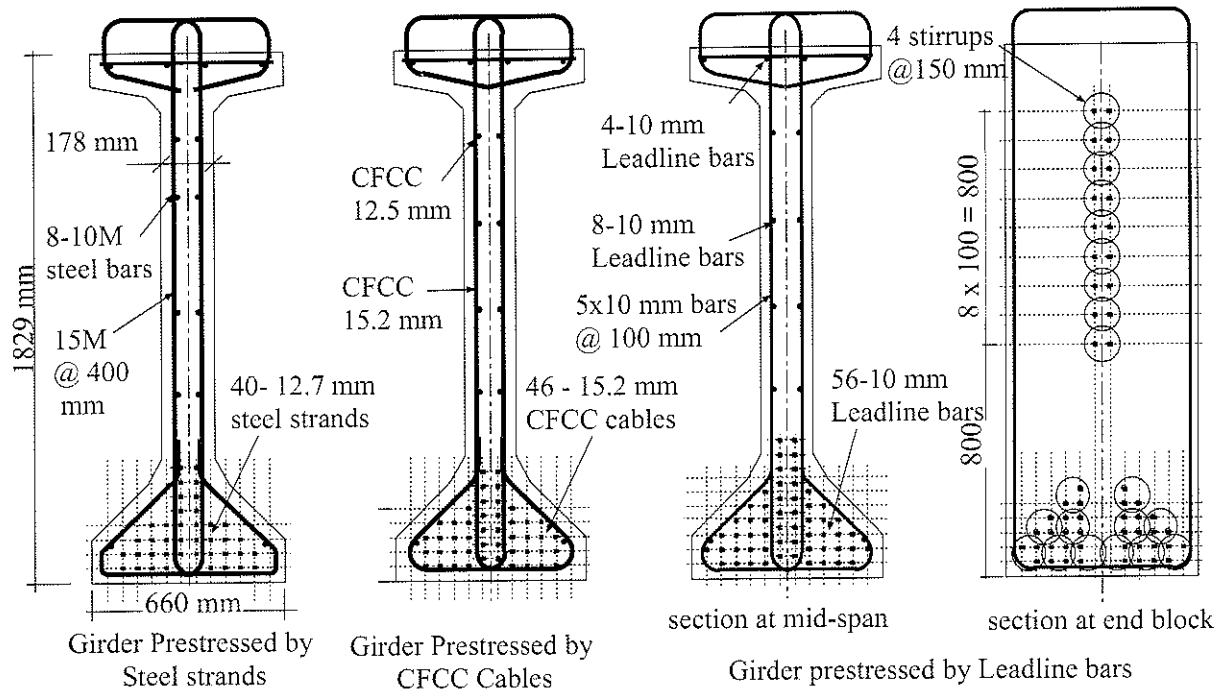


Figure 3-19. Cross-section of the Taylor bridge girders (Rizkalla *et al.* 1998)

Chapter 4

The Experimental Program

4.1 General

The main objective of the experimental program is to examine the structural performance of FRP stirrups as shear reinforcement for concrete structures.

The first phase, Phase I, is designed to evaluate the strength capacity of a single FRP stirrup as influenced by bending of the FRP bars to achieve the appropriate anchorage and the effect of the diagonal shear cracks which have an angle with the direction of the fibres. Eighty-six specially designed specimens were tested to examine the bend effect on the stirrup capacity. Seven specimens reinforced with steel stirrups were tested as control specimens. The variables considered are the type of material, bar diameter, configuration of the stirrup anchorage, embedment length, and tail length of the stirrups. Ten additional specimens reinforced with FRP stirrups with variable angles were specially designed and tested to examine the effect of the diagonal cracks on the stirrup capacity. Two specimens reinforced with steel stirrups were also tested as control specimens.

The second phase, Phase II, comprised ten large-scale reinforced concrete beams tested to failure to investigate the modes of failure and the ultimate carrying capacity of the FRP stirrups in the beam-action mechanism. The shear deformation, crack width, and stirrup strain were examined. The ten beams included four beams reinforced with carbon FRP stirrups, four beams reinforced with glass FRP, one beam reinforced with steel stirrups and one control beam without shear reinforcement. The variables considered in the second phase were the material of the stirrups, material of the flexural reinforcement, and stirrup spacing.

This chapter presents details of the specimens' configuration, fabrication, test setups and the instrumentation used to monitor the response at the different limit states during the test. This chapter also provides detailed characteristics of the materials used in this study based on testing of control specimens.

4.2 Materials

Two types of FRP stirrups were used as shear reinforcement, carbon FRP (CFRP) and glass FRP (GFRP). CFRP reinforcement is characterized by having the highest elastic modulus of commercially available FRP material; however, it has the smallest tensile strain at failure. GFRP reinforcement is characterized by having the lowest tensile elastic modulus; however, it exhibits the highest ultimate tensile strain among the different types of FRP. GFRP reinforcement is also considered to be the most economical FRP material. The different types of FRP bars used as shear reinforcement in this program are shown in Figure 4-1. Steel and CFRP strands were used as flexural reinforcement. The

characteristics of the CFRP, GFRP and steel reinforcement used in this study are presented in the following sections and summarized in Table 4-1.

4.2.1 CFRP Leadline

Leadline bars are produced by Mitsubishi Chemical, Japan (Mitsubishi Chemical Corporation, 1992). Leadline bars are manufactured using linearly oriented Dialead coal-tar-pitch-based continuous carbon fibres and epoxy resin. The bar has a rectangular cross-section (10x5mm) with a 1-mm epoxy-resin coat to protect the fibre core from any UV radiation or chemical attack. The effective diameter, d_e , of the Leadline bar used in this study was 7.0 mm with a cross-sectional area of 38.5 mm².

The stress-strain relationship of the Leadline is linearly elastic up to failure, as reported by the manufacturer and as measured by standard tension tests. Six straight Leadline bars were tested in tension to evaluate the elastic modulus and the strength parallel to the fibres. The tension specimens were anchored using 300-mm-long 19-mm-diameter steel pipes filled with epoxy. Strain gauges and extensometers were used to monitor the strain during the test. The average tensile stress and strain at ultimate were 1730 MPa and 1.26 percent, respectively. The average tensile elastic modulus of the Leadline bars, based on linear regression analysis up to failure, was 137 GPa. A typical stress-strain relationship for the Leadline bar is shown in Figure 4-2.

The CFRP Leadline stirrups were delivered prefabricated. The carbon fibres were present in the form of stirrups prior to the curing process. Two different configurations of the Leadline stirrups were used in this program, as shown in Figure 4-3(a) and Table 4-2.

The inside bend radius, r_b , of the Leadline stirrups, was either 20 mm or 50 mm, which corresponds to a r_b/d_e ratio of 3.0 or 7.0, respectively.

4.2.2 CFRP CFCC

Carbon-fibre-composite cables (CFCC) were also used in this program as shear reinforcement. CFCC bars are produced by Tokyo Rope, Japan (Tokyo Rope MFG. Co., Ltd., 1993). Three different sizes were used, 7.5-mm seven-wire cable, 5-mm solid cable and 5-mm seven-wire cable. The CFCC bars are manufactured using PAN carbon (Besfight HTA) fibres and modified epoxy resin. Table 4-1 shows the geometrical and material characteristics of the CFCC bars used in this program. Several tension tests were conducted to evaluate the tensile strength parallel to the fibre and the elastic modulus. The results of these tests are given in Table 4-1. The stress-strain relationship of the CFCC bars is linearly elastic up to failure with an elastic modulus varying from 137 to 143 GPa.

The CFCC stirrups were delivered prefabricated. It was reported that the pre-pregnated strands were bent over metal bars to the required bend radius and then the epoxy resin matrix was heated to harden. This process was evidenced by the flattened zone at the bend location. The dimensions of the two different configurations of the CFCC stirrups used in this program are given in Figure 4-3(b) and Table 4-2. The inside bend-radius to bar-diameter ratio (r_b/d_e) of the CFCC stirrups ranged between 3.2 and 4.8.

Fifteen-mm, 7-wire CFCC strands were used as flexural reinforcement for two beams tested in Phase II. The CFCC strands used had a guaranteed strength of 1750 MPa with a

tensile elastic modulus of 137 GPa. The geometrical and mechanical properties of the CFCC strand are given in Table 4-1.

4.2.3 GFRP C-BAR™

GFRP stirrups, commercially known as C-BAR, were also used in this program. The C-BAR stirrups are produced by Marshall Industries Composites Inc., Lima, Ohio, USA. C-BAR reinforcing bar is manufactured through a hybrid pultrusion process with proper deformation of the surface material that is made from ceramic fibres embedded in Urethane modified vinylester. The inner core is composed of unidirectional fibres embedded in recycled polyethylene terephthalate (PET) resin material. The nominal diameter of the C-BAR bar used in this program is 12 mm with a cross-sectional area of 113 mm².

The mechanical properties of the 12-mm C-BAR reinforcing bar are given in Table 4-1. The values given in Table 4-1 are based on an extensive experimental program conducted by Rizkalla *et al.* (1997). The stress–strain relationship of the C-BAR bar is linearly elastic up to failure with an elastic modulus of 41 GPa. The average tensile stress at ultimate was 640 MPa as reported by Rizkalla *et al.* (1997). However, the guaranteed tensile strength of the 12-mm C-BAR bar is 713 MPa, according to the manufacturer. A typical stress–strain relationship for the C-BAR reinforcing bar is shown in Figure 4-2.

The C-BAR stirrups were delivered prefabricated. The C-BAR bars were bent during the curing process of the impregnated glass fibres. The curing process included a heating process that could affect the strength capacity of the bend section. The dimensions of the

different configurations of the C-BAR stirrups used in this program are given in Figure 4-3(c) and Table 4-2. The inside bend radius of the C-BAR stirrups used in this program was 50 mm, which corresponds to a r_b/d_e ratio of 4.0.

4.2.4 Steel

The steel stirrups used in this program as shear reinforcement in the control specimens were made of 6.35-mm-diameter deformed steel bars. The steel stirrups had the configuration shown in Figure 4-3(d) and were delivered pre-bent by Cowin Steel Co., Winnipeg, Manitoba. The nominal yield stress of the 6.35-mm steel bars is 600 MPa. Three straight steel bars were tested in tension to determine the stress–strain relationship of the steel bar. Tension tests showed that the yield stress of the 6.35-mm steel bar was 660 MPa, based on the 0.2% proof stress, and the tensile elastic modulus was 206 GPa. A typical stress–strain diagram for the 6.35-mm steel bar is shown in Figure 4-2.

Fifteen-mm, 7-wire steel strands were used as flexural reinforcement for eight beams tested in Phase II. Three 1.0-m-long steel strands were tested in tension to evaluate the tensile properties of the steel strands. The steel strands used had a yield strength of 1590 MPa and an ultimate strength of 1860 MPa with a tensile elastic modulus of 200 GPa.

4.2.5 Concrete

Concrete was provided by a commercial supplier (Perimeter Concrete Ltd.) and all the specimens for phase I and II were cast in place in the laboratory. The concrete had a 10-mm maximum aggregate size and a 100-mm slump. The water/cement ratio was

approximately 0.40 and the cement content was 330 kg/m³. The mix proportion by weight was 1 (CSA type 10 normal Portland cement) : 3.0 (coarse aggregate) : 2.9 (fine aggregate). The target compressive strength of the concrete was 35 MPa after 28 days. Twelve concrete cylinders were cast from each batch. Six cylinders were tested in compression, three on the day of testing of each beam, according to ASTM C39-96. The stress-strain relationship of the concrete was also determined on the day of testing according to ASTM C468-87a using three concrete cylinders. The average compressive strength of the concrete cylinders ranged between 33 and 54 MPa at the time of testing. Figure 4-4 shows the stress-strain diagrams for two different batches of the concrete used. The tensile strength of the concrete was measured using the splitting test for three concrete cylinders on the same day as compression testing according to ASTM C496-90. The average tensile strength, based on the split-cylinder test, ranged from 3.0 MPa to 4.0 MPa.

4.3 Experimental Phase I

Phase I was conducted to evaluate the strength capacity of a single FRP stirrup as affected by

- a- the bend section of the FRP stirrup, "*bend effect*"
- b- the angle of inclination of the shear crack, "*kink effect*"

4.3.1 Test Specimens

Two types of panel specimens were specially designed and tested in this phase. The first type of panel specimen, designated as a *bend* specimen, was designed to investigate the bend effect on the strength capacity of FRP stirrups. The second type of panel specimen, designated as a *kink* specimen, was designed to investigate the kink effect on the strength capacity of FRP stirrups.

4.3.1.1 Bend specimens

Ninety-three specially designed specimens using different types of CFRP, GFRP and steel stirrups were fabricated. The configuration and dimensions of a typical specimen are shown in Figure 4-5. The embedment length within the blocks was varied by using different lengths of plastic tube for debonding as shown in Figure 4-5. The dimensions of each concrete block were 200 x 250 x 200 mm, 300 x 300 x 150 mm or 500 x 300 x 150 mm, according to the dimensions of the stirrup used. The free length of the stirrup between the two blocks was kept constant at 200 mm. The variables considered in this phase are as follows:

1. The material type of the stirrups. Three types of FRP material were used, CFRP Leadline stirrups, CFCC stirrups and GFRP C-BAR stirrups. Steel stirrups were also tested as control specimens.
2. The effective bar diameter, d_e ($\sqrt{4A_b / \pi}$). The effective bar diameter was determined based on the nominal cross-sectional area of the FRP bar. Table 4-1 gives the d_e values for the different FRP bars used in this program.

3. The bend radius, r_b . Different bend radii were used in this program. The bend-radius to effective-bar-diameter, r_b/d_e , ratio was varied between 3.0 and 7.0.
4. The embedment length, l_d . The embedment length was varied, as shown in Figure 4-5, between 25 and 350 mm.
5. The configuration of the stirrup anchorage. Two types of stirrup anchorage were used, as shown in Figure 4-5; type A anchorage with standard hook and a tail length, l_d^* , and type B anchorage with continuous end.
6. The tail length, l_d^* . The tail length, defined in Figure 4-5, was varied between 3 and 20 times the nominal bar diameter, d_b .

Detailed information about the tested bend specimens is given in Tables 4-3 through 4-6. Tables 4-3, 4-4 and 4-5 give the details of the bend specimens reinforced with Leadline, CFCC and C-BAR stirrups, respectively. Table 4-6 gives the details of the control specimens reinforced with steel stirrups.

The bend specimens were fabricated in groups of 6 to 22 specimens. The concrete was cast in wooden forms specially made for the blocks anchoring the FRP stirrup. The specimens were tested within 21 to 40 days after casting of the concrete. The average compressive strength of the concrete after 28 days was 45 MPa.

4.3.1.2 Kink specimens

Ten specially designed specimens using different types of CFRP and GFRP were fabricated. An additional two specimens reinforced with steel stirrups were tested as control specimens. The configuration and dimensions of a typical specimen are shown in

Figure 4-6. Each specimen was reinforced with two stirrups at angle θ with the central axis of the panel, as shown in Figure 4-6. The dimensions of the panel were kept constant for all the tested specimens. The variables of this experimental phase were as follows:

1. Type of material. Two types of FRP material were used, CFRP Leadline stirrups and GFRP C-BAR stirrups.
2. Angle of inclination θ . Five different inclination angles were used, 25 degrees, 35 degrees, 45 degrees, 53 degrees and 60 degrees.

Detailed information about the tested kink specimens is given in Table 4-7. The dowel strength of CFRP and GFRP bars used in this experimental phase was evaluated by direct shear test, illustrated in Figure 4-7. The direct shear test was conducted according to the “*test method for shear properties of continuous fibre reinforcing materials (JSCE-E540-1995)*” proposed by JSCE (1997).

4.3.2 Test setup

4.3.2.1 Bend specimens

The test setup, shown in Figure 4-8, consisted of a 500-kN hydraulic jack, used to apply the relative displacement between the two concrete blocks and a 75-kip (333-kN) load cell to measure the applied load. Steel plates (100 x 100 mm) and plaster bags were placed in front of the load cell and the hydraulic jack in order to distribute the applied load on the applied surface. The two blocks were placed on top of steel rollers to minimize the friction forces between the blocks and testing bed. Electrical strain gauges

and/or 50-mm extensometers were attached to each leg of the stirrup. Two 300-mm extensometers (PI gauges) were attached to the sides of the concrete blocks to monitor the relative displacement between the blocks. A 16-channel data acquisition system using a 16-bit Validyne A/D card was used to record the readings of the load cell, strain gauges, and extensometers.

4.3.2.2 Kink specimens

The test setup, shown in Figure 4-9, consisted of two 500-kN hydraulic jacks connected to the same air compressor using a T-hose connection and two 75-kip (333-kN) load cells to measure the applied load. Steel plates (100 x 100 mm) and plaster bags were placed in front of the load cells and the hydraulic jacks in order to distribute the applied load on the applied surface. The specimen was placed on the top of steel rollers to minimize the friction forces between the specimen and testing bed. Electrical strain gauges were attached to the stirrups in the direction of the fibres at the location of the artificial crack. 100-mm extensometer (PI gauge) was attached to the top surface of the specimen, as shown in Figure 4-9, to monitor the opening of the artificial crack. The readings of the load cells, strain gauges and the extensometer were recorded using a 16-channel data acquisition system.

4.4 Phase II

Phase II was undertaken to investigate the modes of failure and the ultimate carrying capacity of concrete beams reinforced with FRP stirrups. The shear deformation in terms

of crack width and relative slide along crack sides were also examined. In this experimental phase, CFRP and GFRP bars were used as shear reinforcement in the form of vertical stirrups. Steel and CFRP strands were used as flexural reinforcement to investigate the effect of the elastic modulus on the shear behaviour.

4.4.1 Test specimens

A total of ten specially designed beams were tested. Four beams were reinforced with CFRP Leadline stirrups, four beams with GFRP C-BAR stirrups, one beam with steel stirrups and a control beam without shear reinforcement. The cross-section of the tested beams was a T-section with a total depth of 560 mm and a flange width of 600 mm as shown in Figure 4-10. Eight beams were reinforced for flexure with six 15-mm, 7-wire steel strands with high yield strength. Two beams were reinforced for flexure with seven 15-mm 7-wire CFCC strands. All beams were designed to fail in shear while the flexural reinforcement was within the elastic range to simulate the linear behaviour of FRP. The beam without shear reinforcement was used as a control beam to account for all concrete contributions, including the dowel action of the steel strands used for flexural reinforcement, which are normally weaker in dowel action than conventional steel reinforcement. Each beam consisted of a 5.0-meter simply supported span with 1.0-meter projections from each end to avoid bond-slip failure of the flexural reinforcement. Spiral reinforcement was used at the beam end to provide confinement for the concrete around the reinforcing bars and therefore enhance their bond characteristics. The shear span was taken as 1.50 m, corresponding to a shear span-to-depth ratio of 3.2. Only one shear span

was reinforced with FRP stirrups, while the other shear span was reinforced with double 6.35-mm-diameter closely spaced steel stirrups, as shown in Figure 4-10. Control beam SS-2 was constructed using double 6.35-mm-diameter steel stirrups spaced at $d/2$ in the two shear spans, while control beam SN-0 had no shear reinforcement in the two shear spans. The variables considered in this phase are as follows:

1. The material type of stirrups. Two types of FRP material were used, CFRP Leadline stirrups and GFRP C-BAR stirrups. The FRP stirrups used in the beam specimens consisted of two single-legged stirrups tied together using plastic ties, as shown in Figure 4-11. Beams reinforced with 6.35-mm-diameter steel stirrups were also tested as control specimens. The steel stirrups used in the beam specimens have the same configuration as the GFRP stirrups. However, they were produced as a continuous bar (Figure 4-3). The properties of the FRP bars used as stirrups in the beam specimens are given in Table 4-1.
2. The stirrup spacing, s . The stirrup spacings used for the FRP stirrups were $d/2$, $d/3$ and $d/4$, where d is the effective beam depth ($d = 470$ mm).
3. The material type of flexural reinforcement. Steel strands were used to reinforce eight beams reinforced for shear by CFRP, GFRP and steel stirrups to evaluate the FRP stirrup contribution to the shear capacity. CFRP strands were used to reinforce two beams reinforced for shear by CFRP and GFRP stirrups to study the effect of using FRP as flexural reinforcement on the various shear components.

Detailed information about the tested beam specimens is given in Table 4-8. The designation of the beams uses the first letter either S or C, for beams reinforced with Steel strands or CFRP CFCC strands for flexure. The designation of the beams uses the second

letter either N, S, C or G, for beams with No shear reinforcement, Steel stirrups, CFRP stirrups or GFRP stirrups, respectively. The number in the beam designation of 2, 3 or 4, refers to the stirrup spacings $d/2$, $d/3$ or $d/4$; respectively.

4.4.2 Fabrication of the Beams

A casting bed was constructed to fabricate two beams at the same time, as shown in Figure 4-12. Before the concrete was cast, the wooden form was lubricated and the reinforcement cage, including the FRP stirrups, was assembled and tied in place. A special system of spreader beams was used to ensure the straightness of the reinforcing strands used as flexural reinforcement. Two cubic meters of concrete were provided by a commercial supplier with a target compressive strength of the concrete of 35 MPa after 28 days. The average compressive strength of the concrete, based on testing three standard cylinders, is given in Table 4-8 for each beam. The beams were taken out of the form, using two overhead cranes of 1.0-ton capacity, by lifting the beams at two points 1.0 m from the beam ends. The beams were tested after at least 28 days from the date of casting.

4.4.3 Test Setup

The beams were tested using two concentrated loads, 2.0 m apart. The load was applied using stroke control with a rate of 0.3 mm/min up to the shear cracking load and thereafter at a rate of 0.6 mm/min up to failure. A closed-loop MTS 1000-kN cyclic loading testing machine was used to apply the load. The range used for testing was 1000

kN for load and 150 mm for stroke. The beams were simply supported on rollers at each end of the beam, the rollers resting on concrete blocks, as shown in Figure 4-13. The load was applied through steel I-beams on the full width of the beam. Plaster pads were used at the loading locations and at the bearings to distribute the load evenly. The widths of the loading I-beams and the support plate were 75 and 100 mm, respectively, as shown in Figure 4-13. The beams were laterally braced at the location of the supports. The beams were painted with whitewash to enhance visibility of the cracks.

4.4.4 Instrumentation

Instrumentation of the beams included Linear Voltage Displacement Transducers (LVDTs) for deflection measurement, displacement gauges (PI gauges) for strain measurements on the concrete surface and electric strain gauges attached to the reinforcement. Detailed descriptions of the instrumentation are shown in Figure 4-14 for beam SN-0, Figure 4-15 for beams SS-2, SC-2 and SG-2, Figure 4-16 for beams SC-3 and SG-3, CC-3 and CG-3, and Figure 4-17 for beams SC-4 and SG-4.

Electrical strain gauges produced by Tokyo Sokki Kenkyujo Co. Ltd., Japan, of type FLA-5-11 and a resistance of 120 ohms, were installed on the flexural and shear reinforcement. The strain gauges were glued to the steel bars using M-Bond 200 and to the FRP stirrups using a two-compound epoxy, commercially known as AE-10. The strain gauges were covered by a waterproof coating to protect them from water and damage during casting the concrete. Nine strain gauges were installed on the steel strands used as flexural reinforcement, as shown in Figure 4-14(a). Strain gauges were also

installed on the FRP stirrups, located within a distance $2d$ from the applied load, as shown in Figures 4-14(a) to 4-17(a). Fifty-mm PI gauges were attached to the top surface of the beam at four different locations, as shown in Figures 4-14(b) to 4-17(b), to measure the strain in the concrete. A 500-mm PI gauge was attached to the concrete surface at the level of the bottom strand in the constant moment zone. The 500-mm gauge length was long enough to measure several flexural cracks and provide a representative average strain for the concrete. Two-hundred-mm PI gauges were mounted on the web surface in three directions at different locations in the shear span, as shown in Figure 4-18, to evaluate the shear deformations in terms of the shear crack width and the slide along the crack. The shear deformations of the other shear span were measured using demec-point stations, as shown in Figures 4-15(b), 4-16(b) and 4-17(b).

Displacement and strain readings were recorded during the test, using two data acquisition systems having a total capacity of 48 channels, at a rate of 1 sample per 2 seconds. The load and stroke of the cross-head of the machine were recorded. The deflections at midspan and at the loading points were monitored using LVDTs of 125-mm stroke. Cracking behaviour was monitored in terms of crack pattern and propagation of the cracks. The tests were videotaped up to failure to capture the progressive damage of the beam at the moment of failure.

Table 4-1. Properties of FRP and steel bars used in the experimental program

Material type	CFRP Leadline	CFRP CFCC				GFRP C-BAR	steel	
		U - 5.0	7-wire	7-wire	7-wire		bar	strand
Used for	shear	shear	shear	Shear	flexure	Shear	shear	flexure
nominal diameter d_b (mm)	rect. sec. (5x10mm)	5.0	5.0	7.5	15	12.0	6.35	15
nominal area A_b (mm ²)	38.48	15.20	10.10	30.40	113.6	113	31.67	140
effective diameter d_e (mm)	7.0	4.40	3.59	6.22	12.0	12.0	6.35	13.4
guaranteed strength (MPa)	1800	1842	1782	1875	1750	713	600 [#]	1590 [#]
ultimate tensile strength	1730 ^{##}	2170 ^{##}	1810 ^{##}	1910 ^{##}	2200 ^{##}	640 ^{##}	660 ^{##}	1860
elastic modulus E (GPa)	137	143	137	137	137	41	206	200
maximum strain ϵ_u (%)	1.26	1.52	1.32	1.40	1.60	1.56	2.0	4.0

[#] yield strength

^{##} Based on tension tests

Table 4-2. Dimensions of stirrups used in the experimental program

Stirrup ID	CFRP Leadline		CFRP CFCC				GFRP C-BAR			steel		
	1	2 [#]	3	4	5	6	7 [#]	8	9	10	11 [#]	12 ^{##}
d_b	Rect. 10x5	Rect. 10x5	5.0 7-wire	5.0 U	7.5 7-wire	7.5 7-wire	12	12	12	6.35	6.35	10
d_s	510	510	510	510	510	700	520	700	700	510	510	700
b_s	150	105	150	150	150	67.5	124	124	175	150	90	175
r_b	20.0	50	15	15	20	30	50	50	50	20	40	50
l_d^*	lapped	120	45	45	45	160	135	135	135	45	160	135

All dimensions in mm

[#] used in beam specimens

^{##} epoxy coated stirrups made of 10-mm-diameter, 440-MPa-yield-strength conventional mild steel bars were used for bend specimens only.

Table 4-3. Details of bend specimens: CFRP Leadline stirrups

material type	nominal diameter d_b mm	effective diameter d_e mm	bend radius		tail length		l_d mm	stirrup anchorage type		
			r_b mm	r_b/d_e	l_d^* mm	l_d^*/d_e				
Leadline stirrups	rectangular section 10 x 5 mm	7.0	21	3	21	3	$r_b+d_b^{***}$	A		
					42	6	r_b+d_b			
							150			
					63	9	r_b+d_b			
					84	12	r_b+d_b			
							150			
					120	17	r_b+d_b	B		
							r_b+d_b			
					---		100			
							150	A		
					50	7	21		3	r_b+d_b
										150
							42		6	r_b+d_b
										150
							63		9	r_b+d_b
							150			
					84	12	r_b+d_b			
							150			
					120	18				r_b+d_b
									150 ^{##}	
									250	
				300	B					
				350						
				r_b+d_b						
				---		100	B			
						150 ^{##}				
Leadline straight ^{###}	10 x 5	7.0	----	-----	----	----	150	-----		
							300			

^{##} d_b is the nominal bar diameter for round bars or strands and is taken as the height of the section in the direction of the bend in case of bars with rectangular section ($d_b = 5.0$ mm for Leadline stirrups), as illustrated below

^{##} reported for both type A and type B specimen configurations

^{###} bond tests of straight Leadline bar

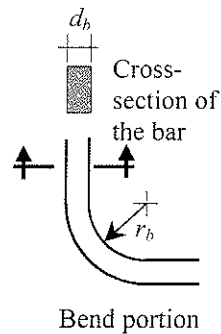


Table 4-4. Details of bend specimens: CFRP CFCC stirrups

material type	nominal diameter d_b mm	Effective diameter d_e mm	bend radius		tail length		l_d mm	stirrup anchorage type		
			r_b mm	r_b/d_e	l_d^* mm	l_d^*/d_b				
CFCC stirrups	5 mm 7-wire	3.59	15	4.2	45	9	r_b+d_b	A		
							80			
							150 [#]			
					-----	-----	r_b+d_b	B		
							80			
							150 [#]			
	5 mm single wire	4.40	15	3.4	45	9	r_b+d_b	A		
							80			
							150 [#]			
					-----	-----	r_b+d_b	B		
							80			
							150 [#]			
	7.5 mm 7 wire	6.22	20	3.2	45	6	r_b+d_b	A		
							80			
							150			
			-----	-----	22.5	3	-----	-----	r_b+d_b	A
									100	
									150	
			-----	-----	45	6	-----	-----	r_b+d_b	
									100	
									150	
-----			-----	67.5	9	-----	-----	r_b+d_b		
								100		
								150		
-----			-----	30	4.8	90	12	r_b+d_b		
								100		
								150		
-----	-----	150	20	-----	-----	r_b+d_b				
						100				
						150				
---	---	---	---	---	---	r_b+d_b	B			
						100				
						150				

[#] reported for both type A and type B specimen configurations

Table 4-5. Details of bend specimens: GFRP C-BAR™ stirrups

Material type	nominal diameter d_b mm	effective diameter d_e mm	bend radius		tail length		l_d mm	stirrup anchorage type	no. of specimens tested
			r_b mm	r_b/d_e	l_d^* mm	l_d^*/d_b			
C-BAR stirrups	12	12.0	50	4.0	72	6	r_b+d_b	A	2
							r_b+d_b		2
							100		2
					145	12	150	B	2
							250		6
							r_b+d_b		3
							100		1
					-----	-----	150	B	2
							250		10
							-----		-----

Table 4-6. Details of bend specimens: steel stirrups

Material type	nominal diameter d_b mm	effective diameter d_e mm	bend radius		tail length		l_d mm	stirrup anchorage type	no. of specimens tested
			r_b mm	r_b/d_e	l_d^* mm	l_d^*/d_b			
Steel Stirrups	6.35	6.35	20	3.0	40	6	r_b+d_b	A	1
							80		1
							150		1
	10 ^{###}	10	40	4.0	-----	-----	r_b+d_b	B	---
							150 [#]		1
							r_b+d_b		3

[#] reported for both type A and type B specimen configurations

^{###} epoxy coated stirrups made of 10-mm-diameter, 440-MPa-yield-strength conventional mild steel bars were used for bend specimens only.

Table 4-7. Details of kink specimens

material type	nominal diameter d_b (mm)	effective diameter d_e (mm)	angle of inclination θ
steel	6.35	6.35	0*
			30
			45
			90**
Leadline	rect. (10x5)	7.0	0*
			25
			35
			45
			53
			60
			90**
C-BAR	12	12.0	0*
			25
			35
			45
			53
			60
			90**

* uniaxial tension tests

** direct shear tests

Table 4-8. Details of beam specimens

Beam ID	Flexural reforc.	stirrups	E_{fv}/E_s	f_{fv} MPa	spacing s	shear rft ratio $\rho_v = A_v/b.s$	$\rho_{fv} E_{fv}/E_s$ %	$\rho_{fv} f_{fv}$ MPa	f'_c MPa
SN-0	6 15-mm 7-wire steel strands	-----				-----			54
SS-2		Steel [#]		660 ^{**}	$d/2^*$	0.40 %		2.64	54
SC-2		CFRP [#]			$d/2$	0.24 %	0.168	4.32	54
SC-3		Leadline	0.70	1800 ^{##}	$d/3$	0.36 %	0.252	6.48	54
SC-4					$d/4$	0.47 %	0.329	8.46	51
SG-2		GFRP [#]			$d/2$	0.71 %	0.149	5.06	54
SG-3		C-BAR	0.21	713 ^{##}	$d/3$	1.05%	0.220	7.49	33
SG-4					$d/4$	1.40%	0.294	9.98	33
CC-3		7 15-mm CFCC strands	Leadline	0.70	1800	$d/3$	0.36%	0.252	6.48
CG-3	C-BAR		0.21	713	$d/3$	1.40%	0.294	9.98	50

[#] 2-branch stirrups, shown in Figure 4-10 for the FRP stirrups and Figure 4-3 for the steel stirrups, dimensions of the stirrups used are given in Table 4-2

^{##} tensile strength of FRP bar in the direction of the fibres

* d is the effective beam depth = 470 mm

** yield strength

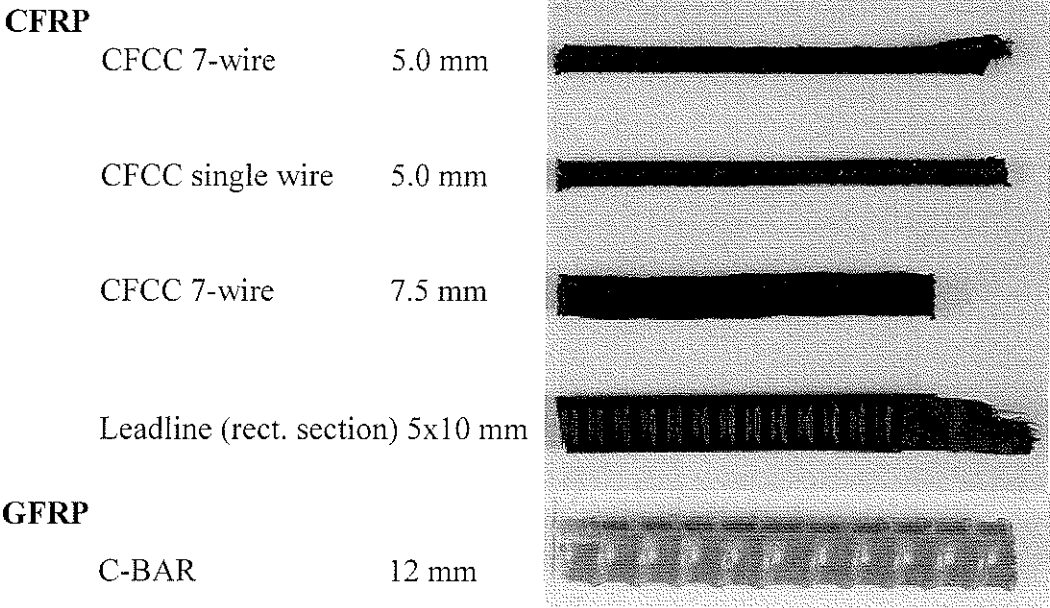


Figure 4-1. Carbon and Glass FRP bars used for the stirrups

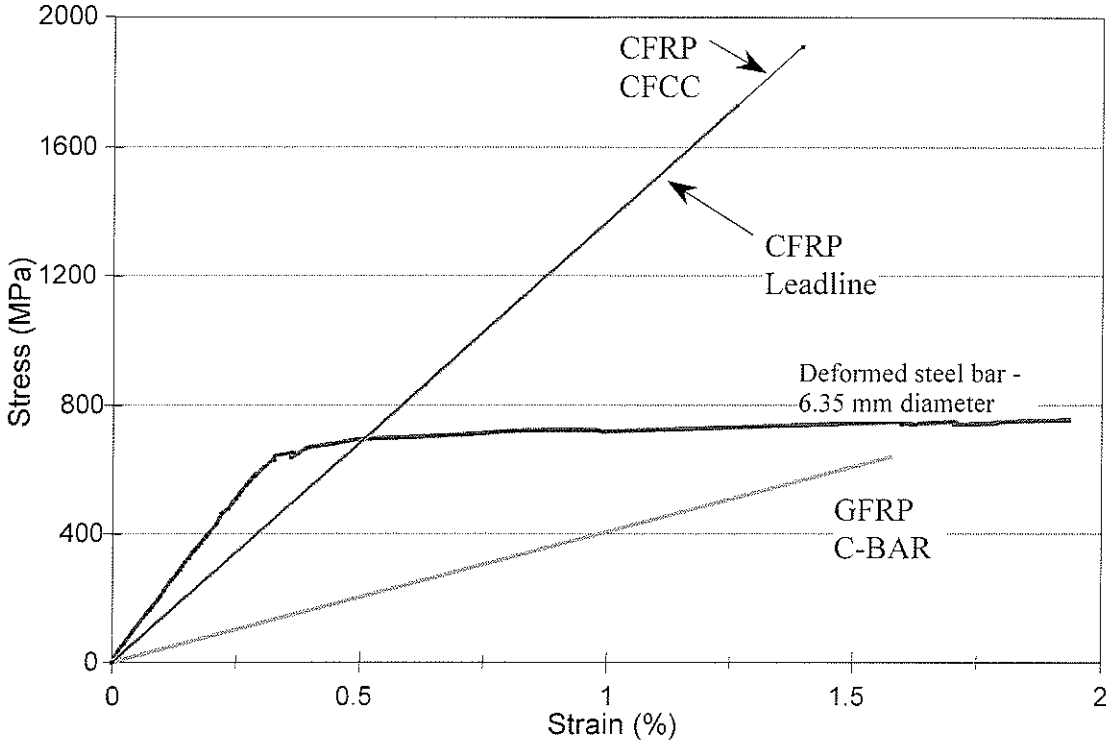


Figure 4-2. Stress-strain relationships of reinforcing bars used as stirrups in this program

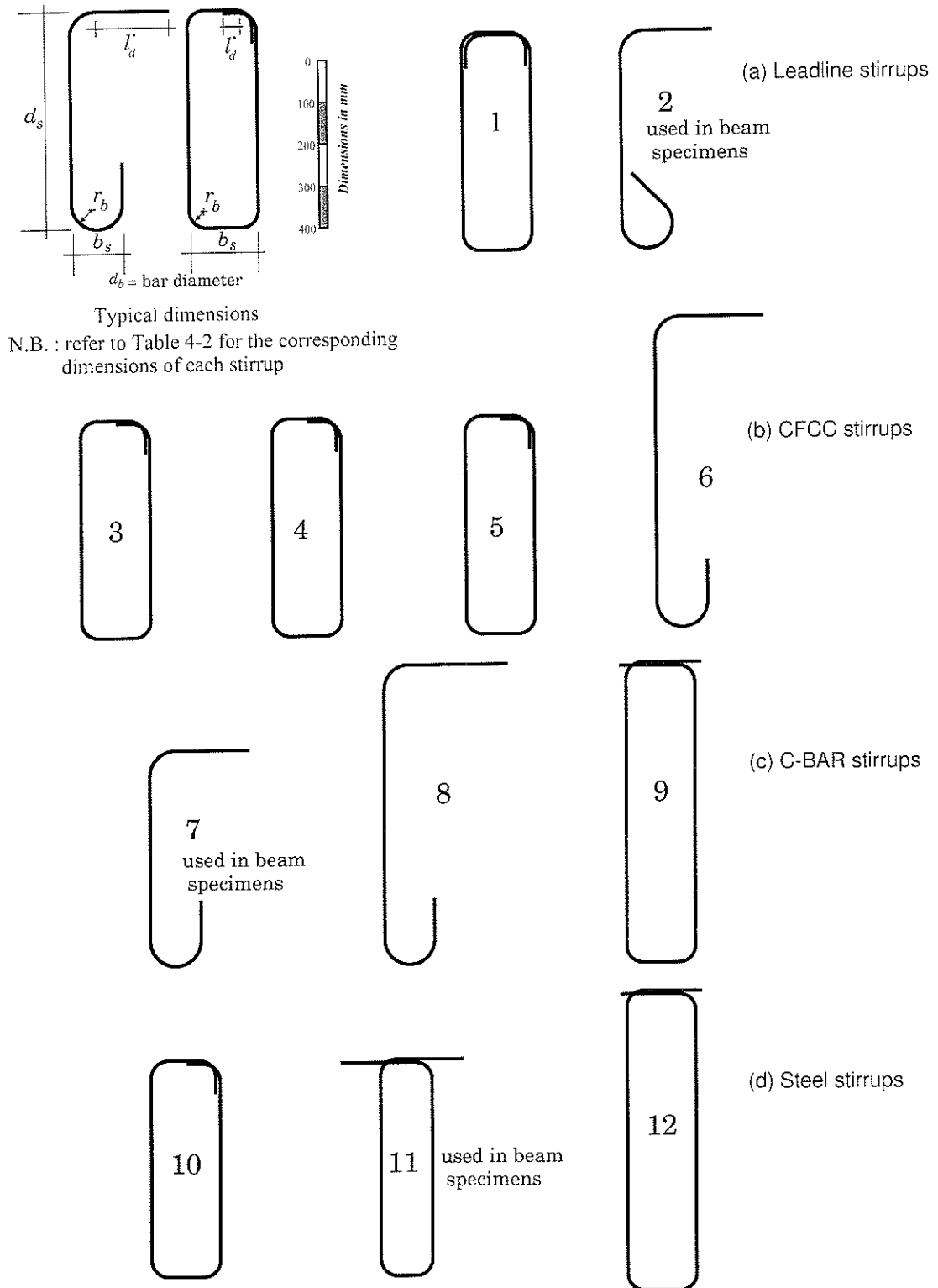


Figure 4-3. Configuration of stirrups used in the experimental program

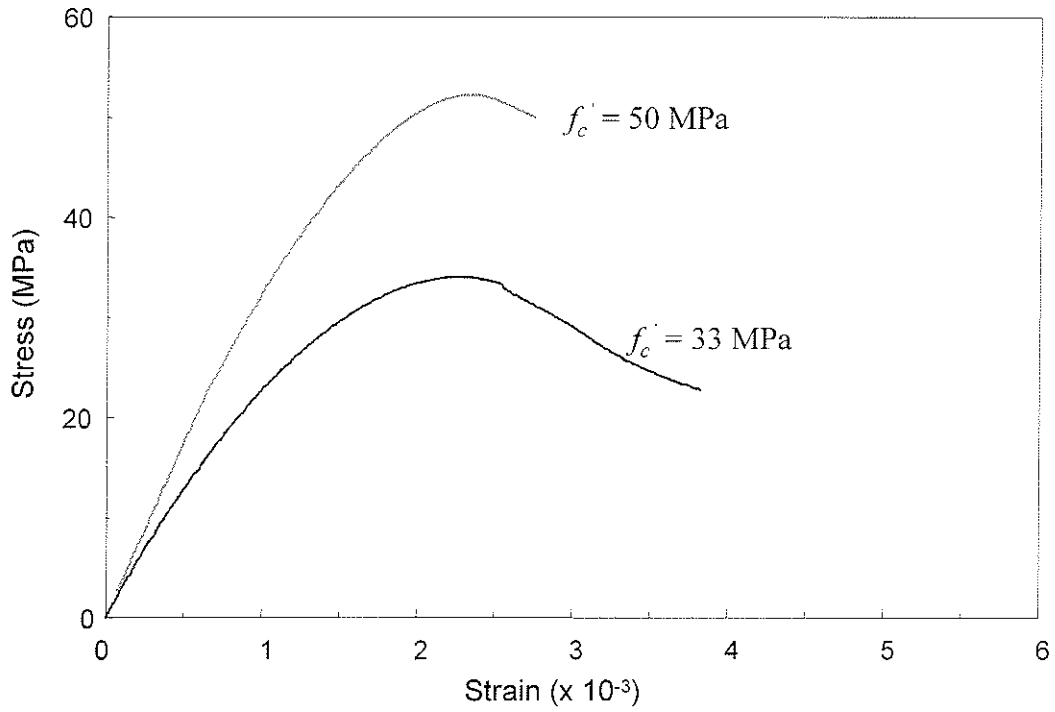


Figure 4-4. Stress-strain diagrams of different batches of concrete

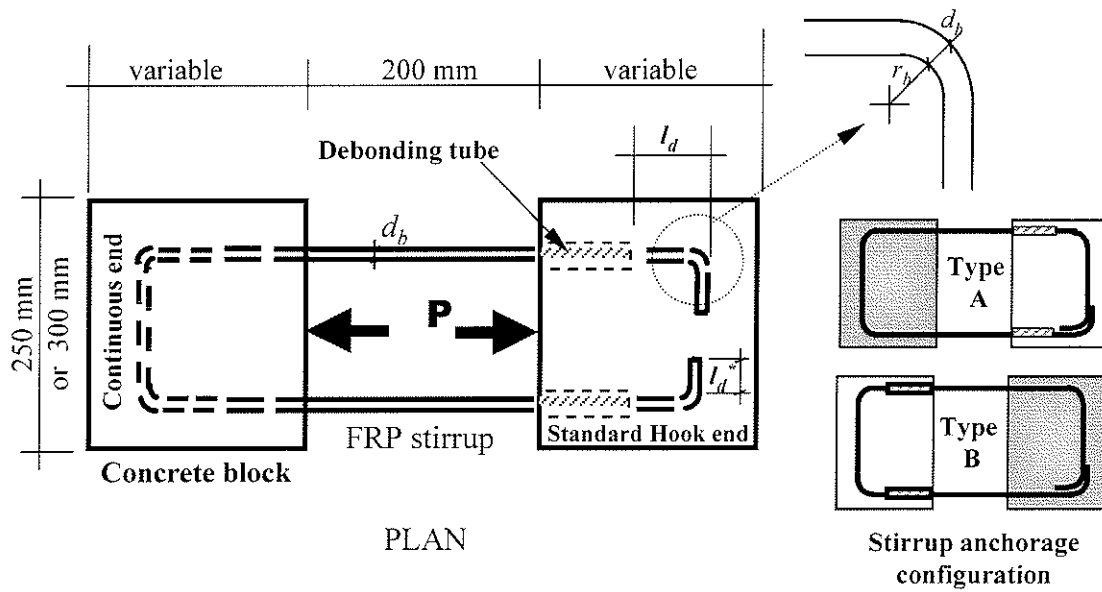


Figure 4-5. Details of bend specimens

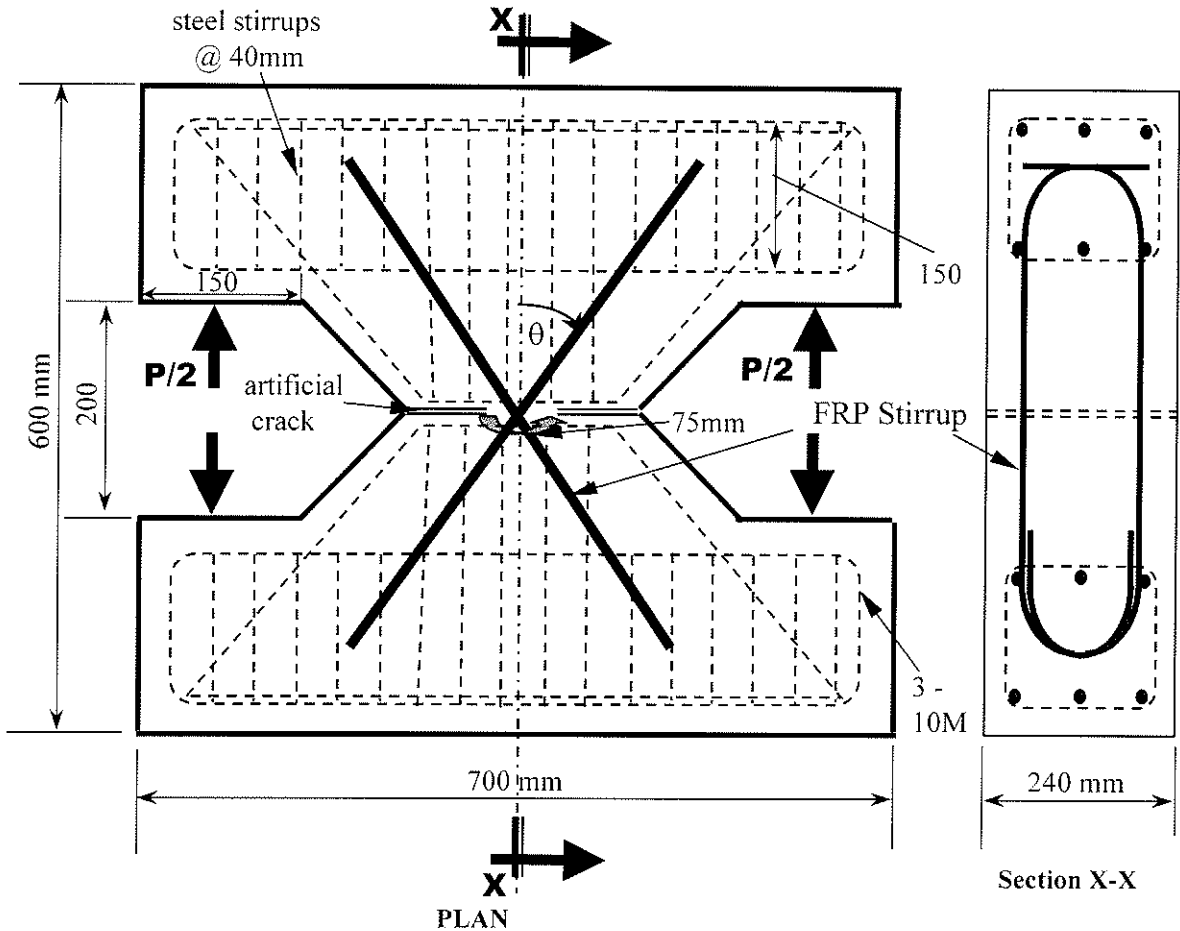


Figure 4-6. Details of kink specimens

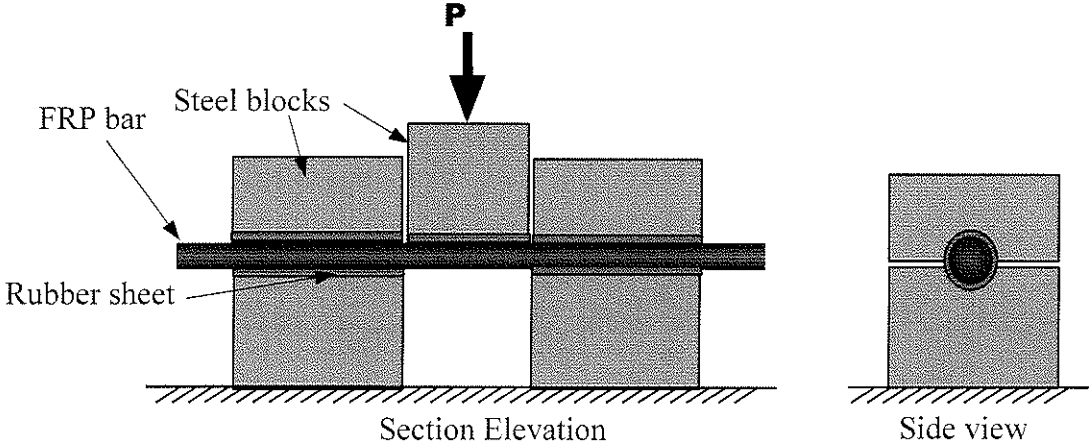


Figure 4-7. Description of the direct shear test setup

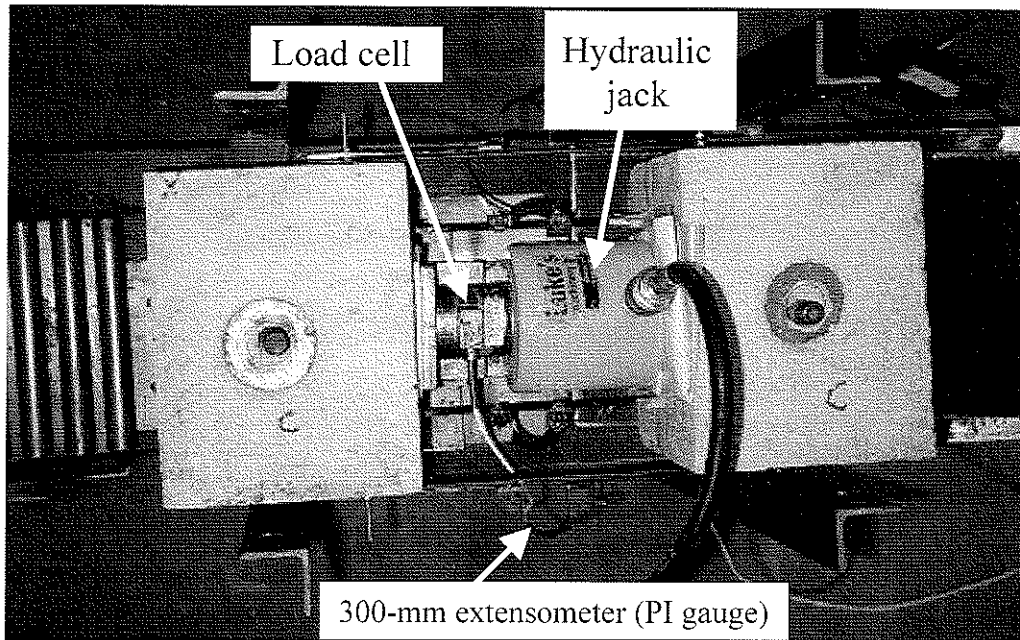


Figure 4-8. Test setup: bend specimens

100-mm extensometer
(PI gauge)

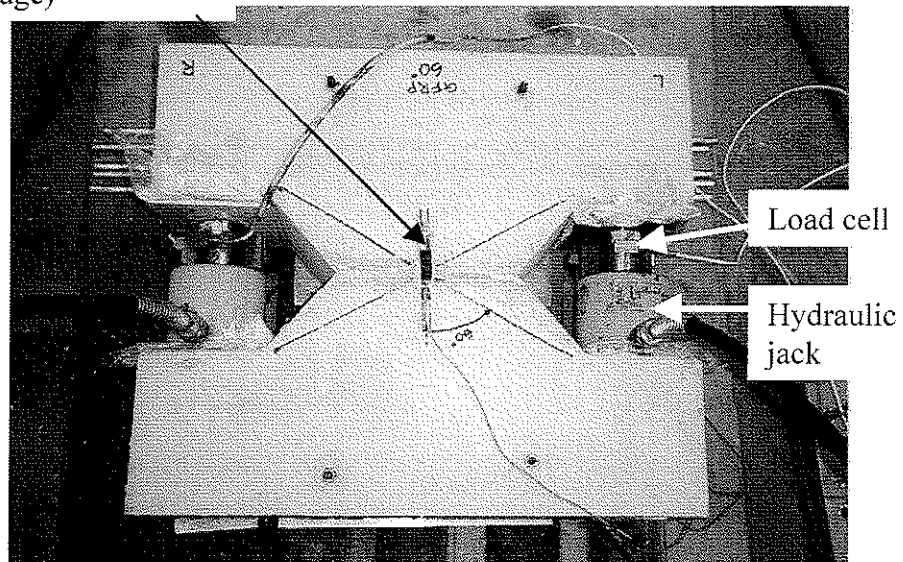


Figure 4-9. Test setup: kink specimens

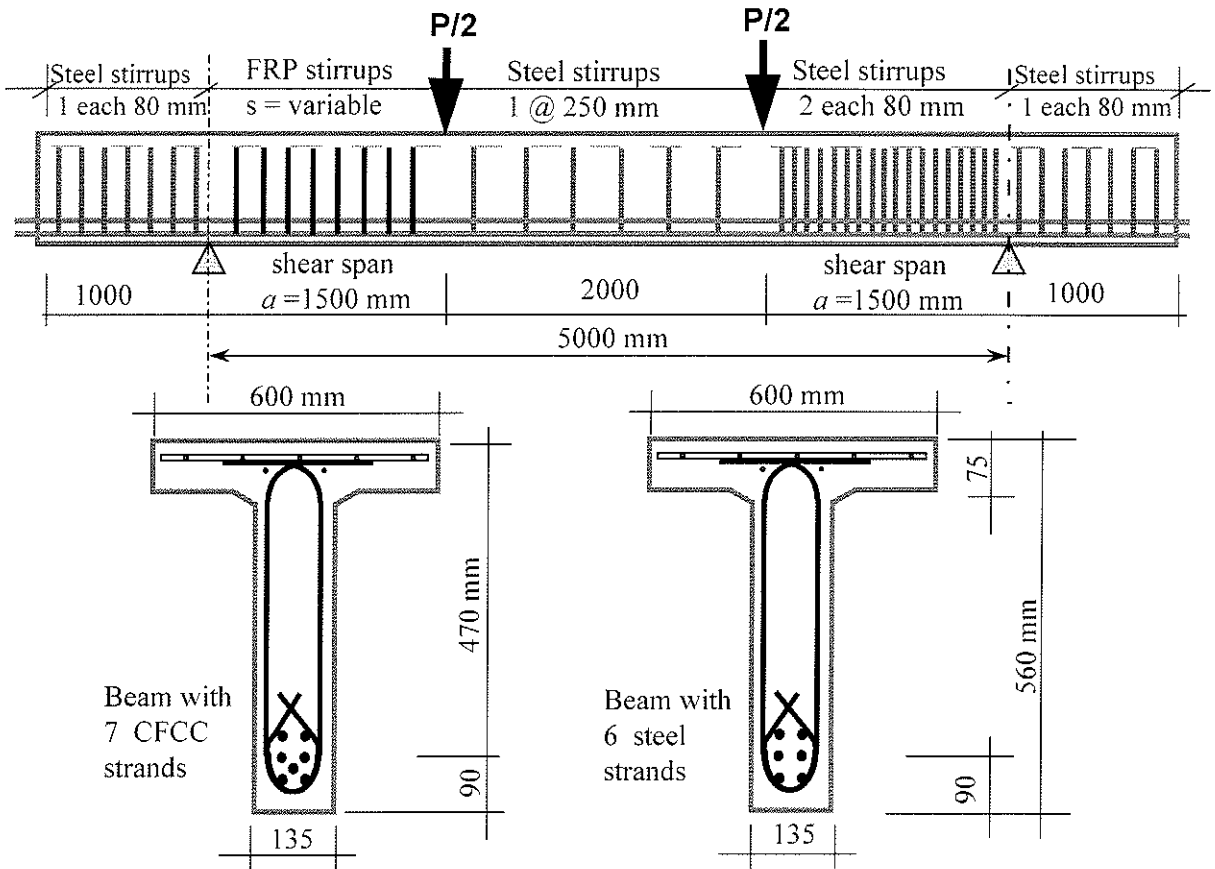


Figure 4-10. Details of beam specimens

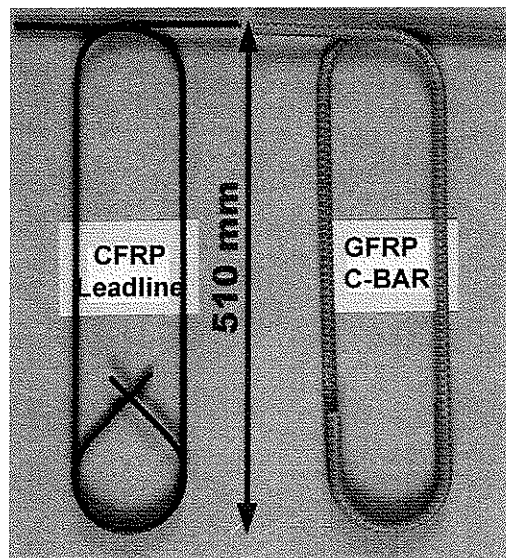


Figure 4-11. Configuration of FRP stirrups used in beam specimens

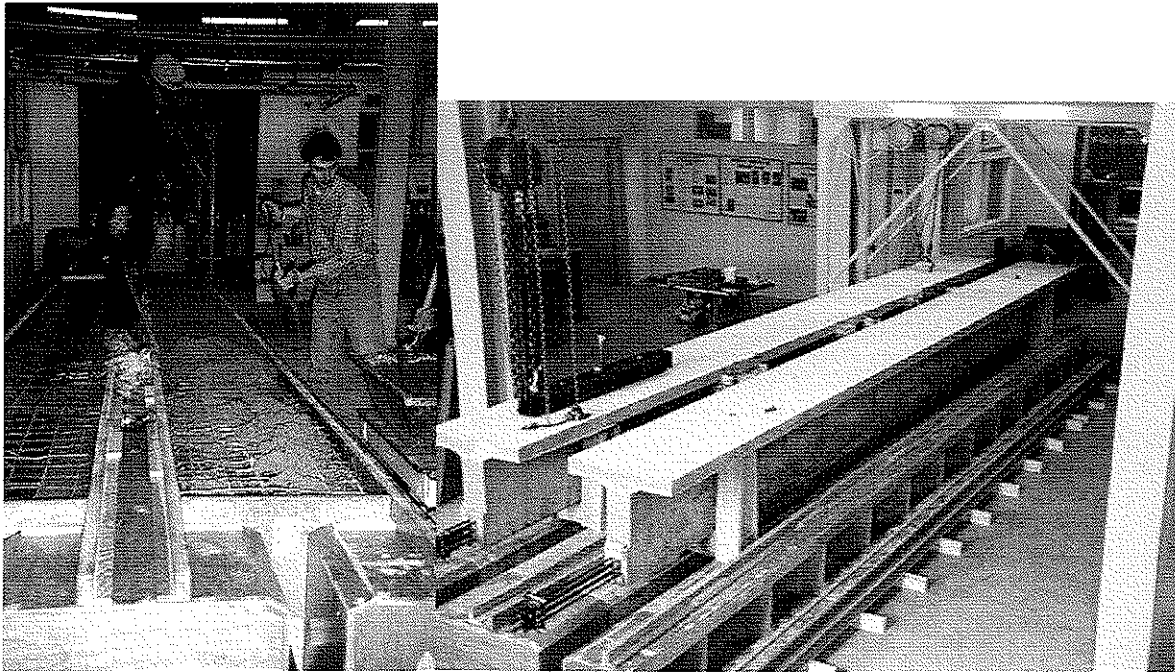


Figure 4-12. Casting bed for beam specimens

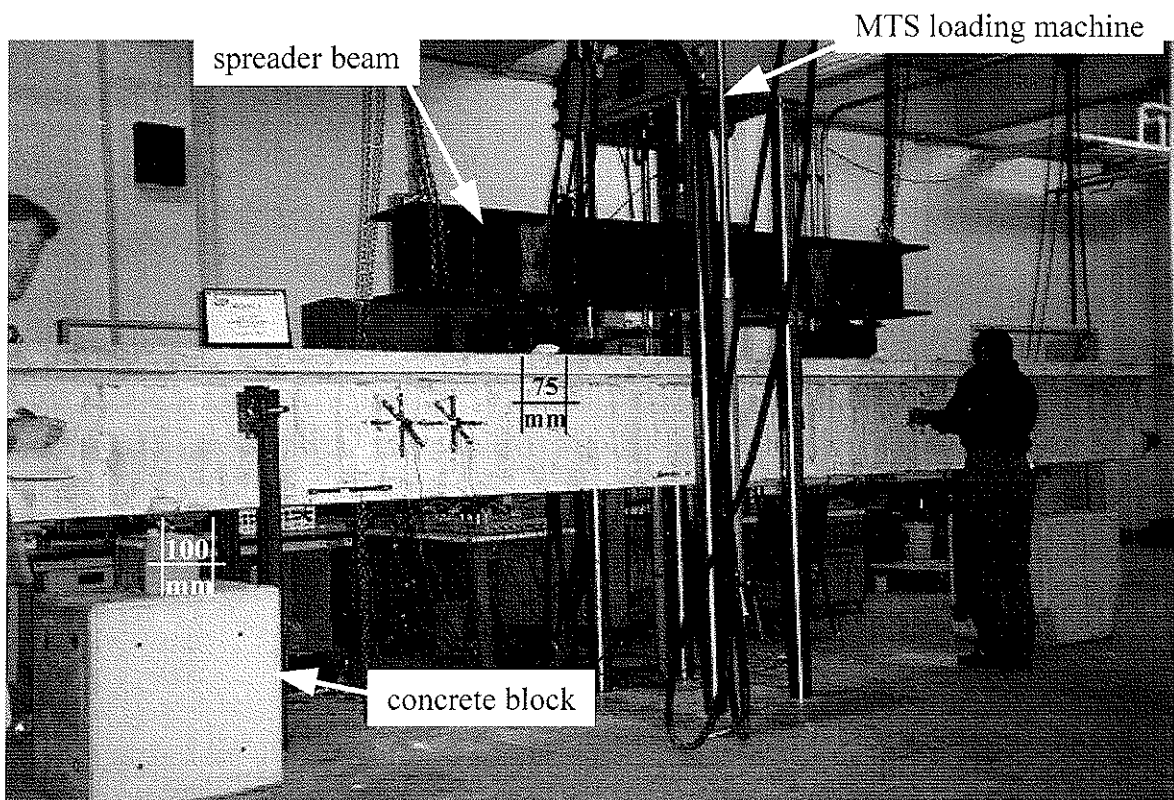


Figure 4-13. Test setup of beam specimens

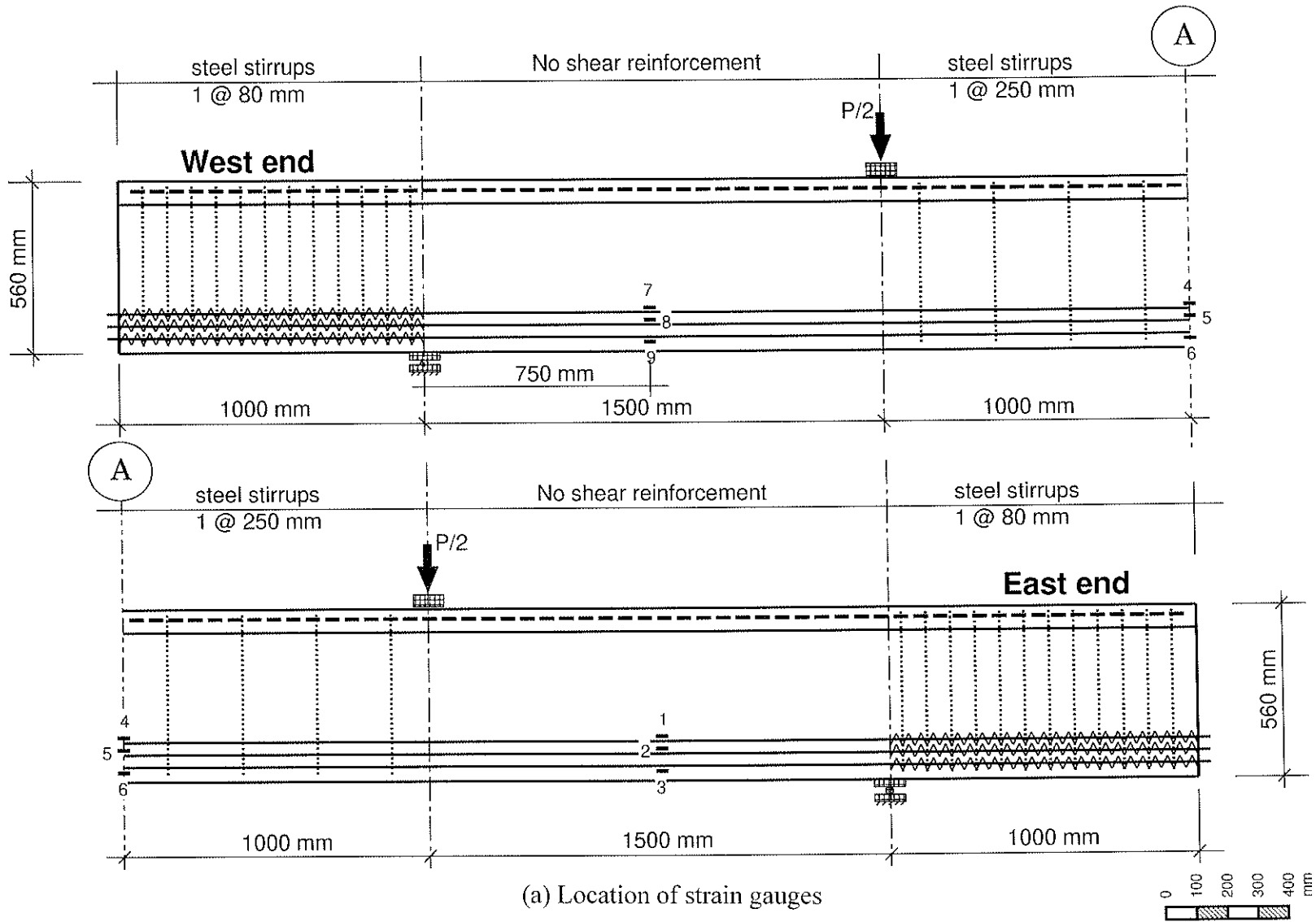
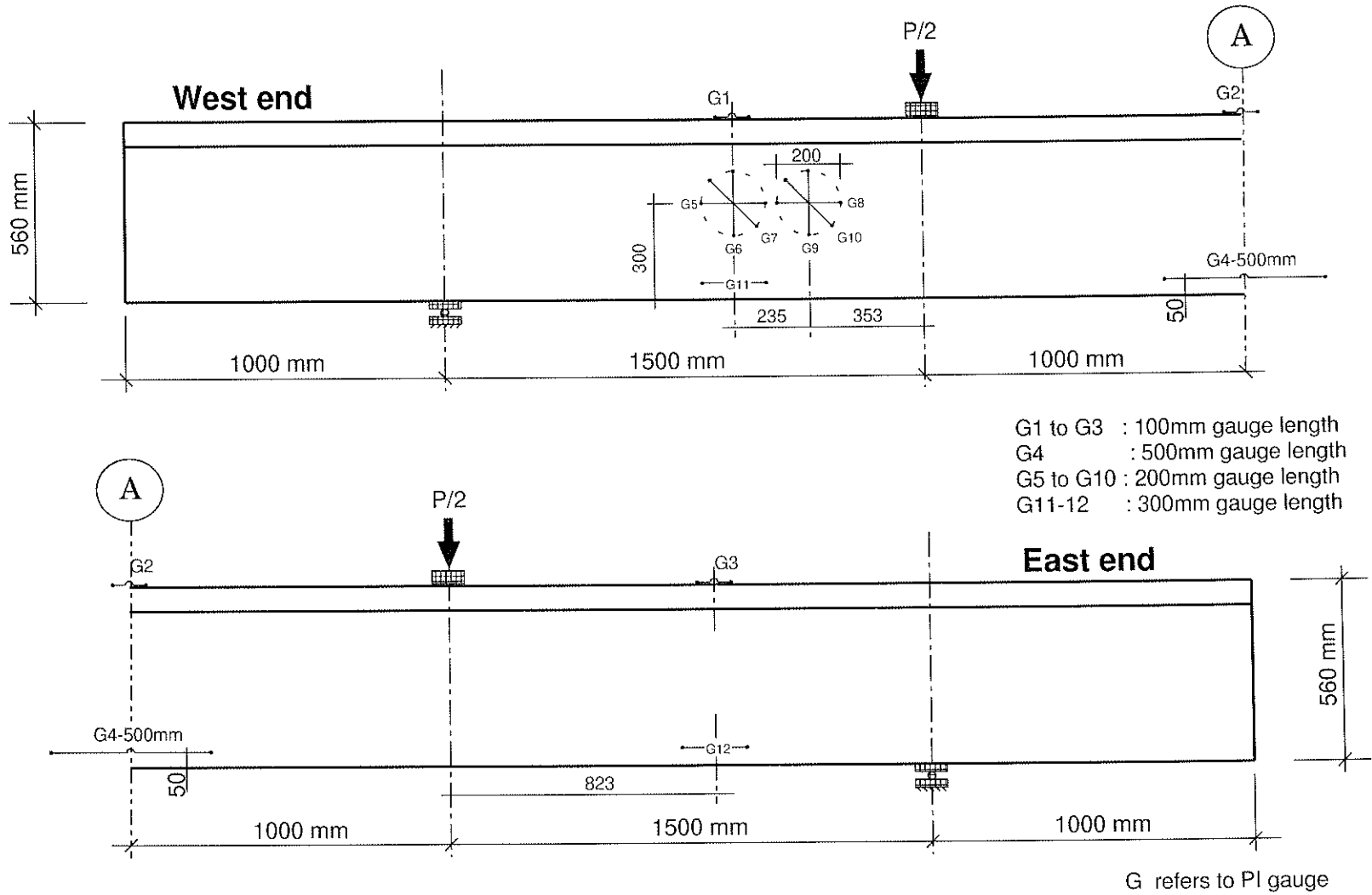


Figure 4-14. Instrumentation of beam SN-0



(b) Location of PI and demec gauges

Figure 4-14(cont'd). Instrumentation of beam SN-0

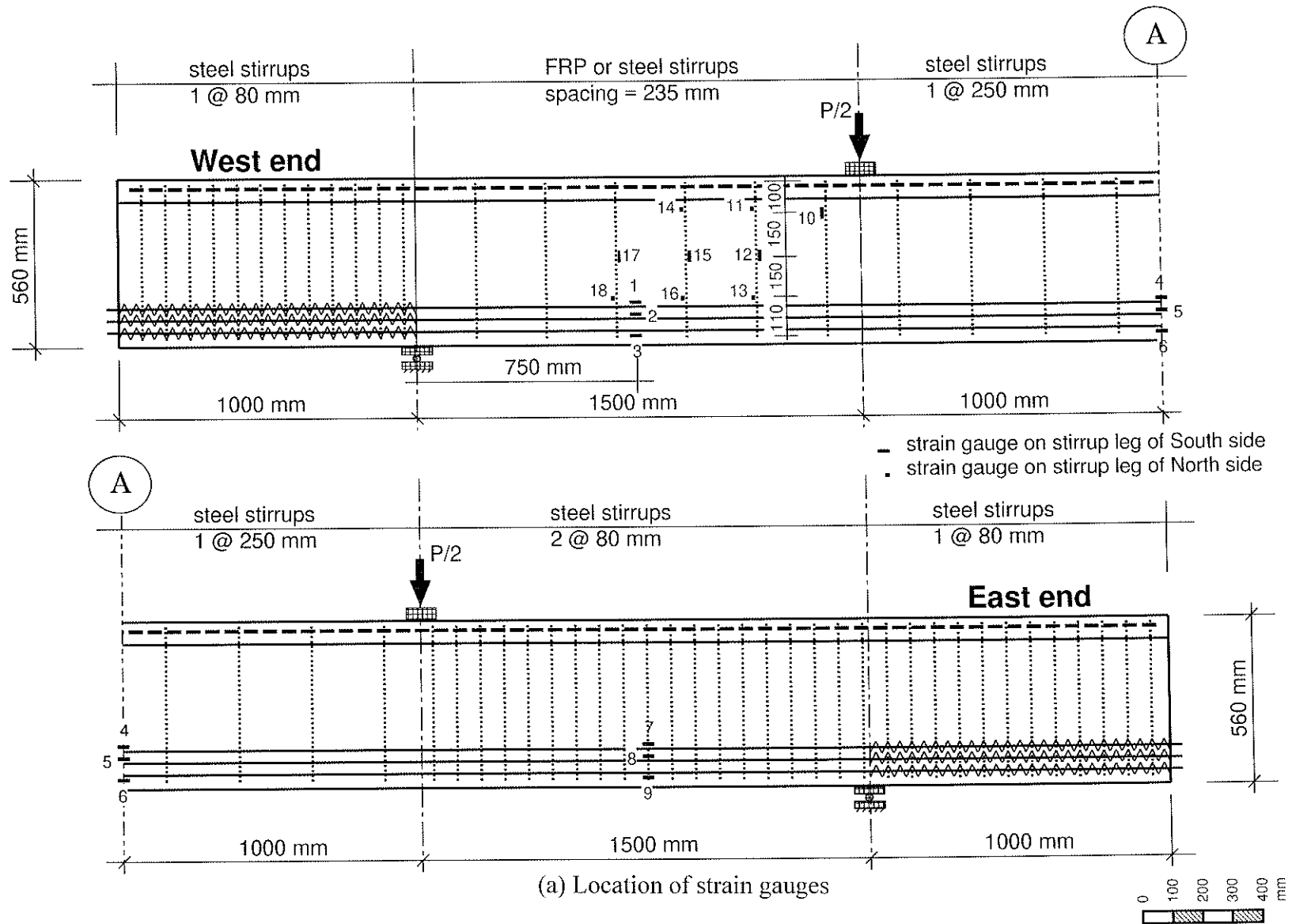
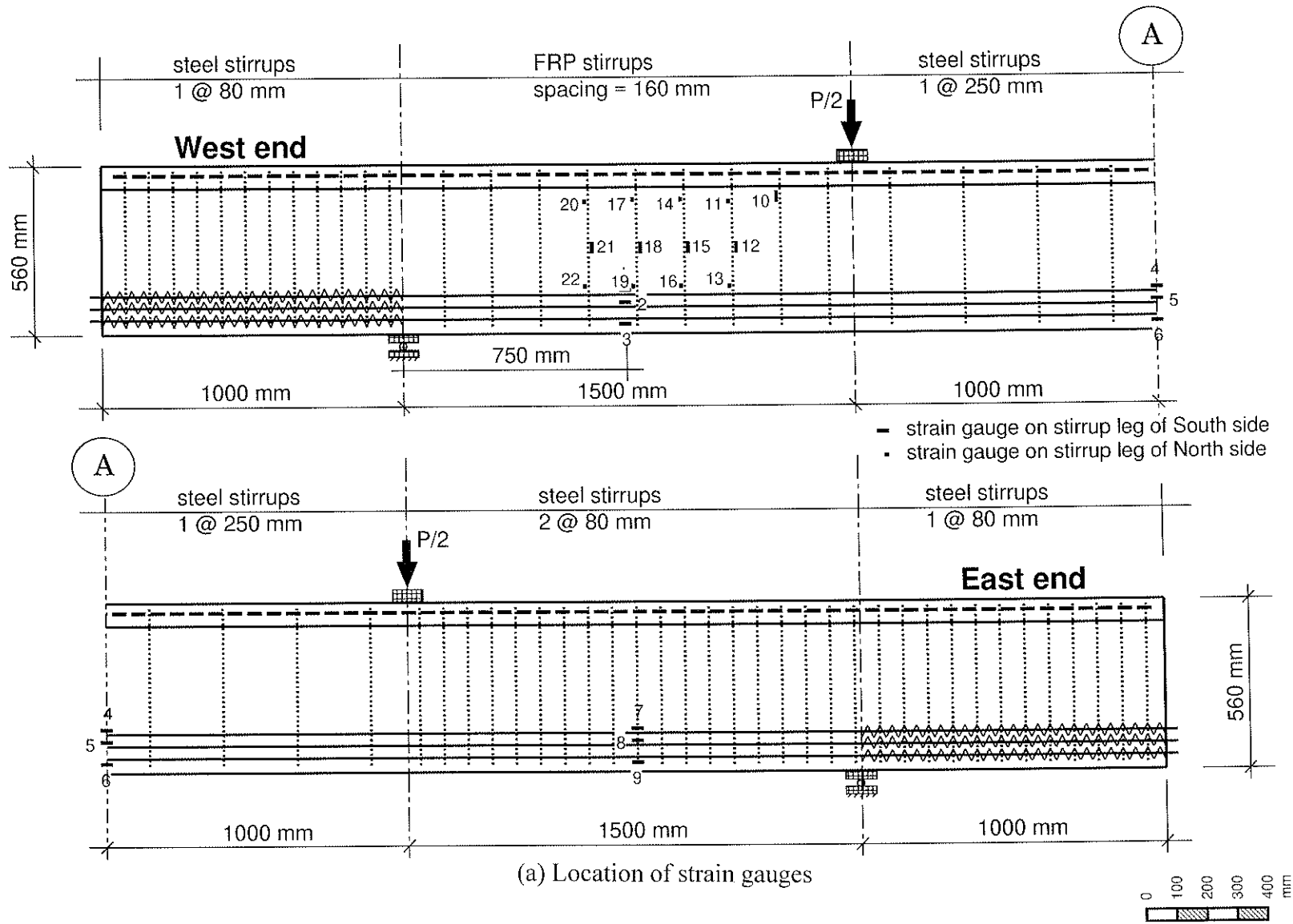
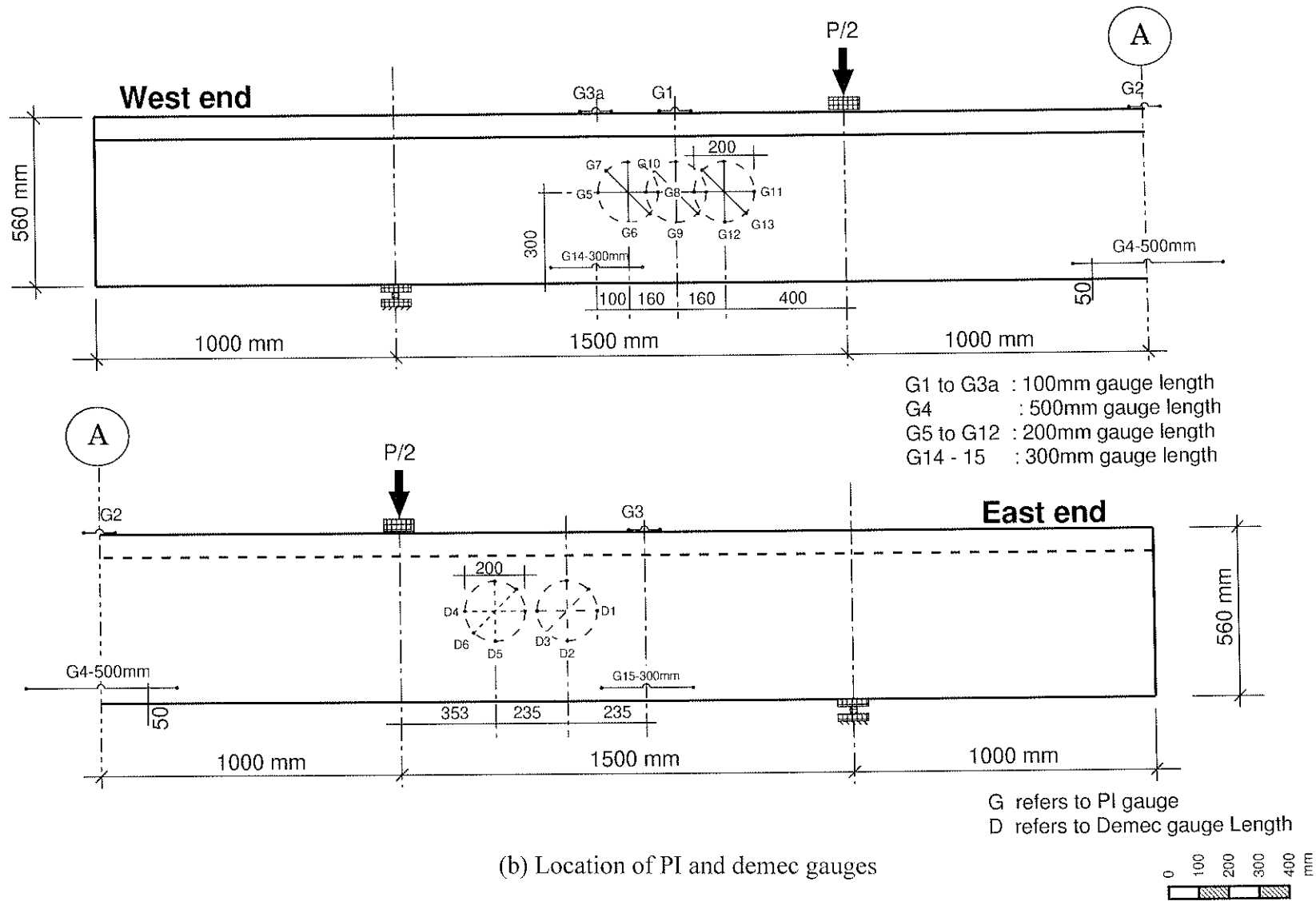


Figure 4-15. Instrumentation of beam SS-2, SC-2 and SG-2



(a) Location of strain gauges

Figure 4-16. Instrumentation of beam SC-3, SG-3, CC-3 and CG-3



(b) Location of PI and demec gauges

Figure 4-16(cont'd). Instrumentation of beam SC-3, SG-3, CC-3 and CG-3

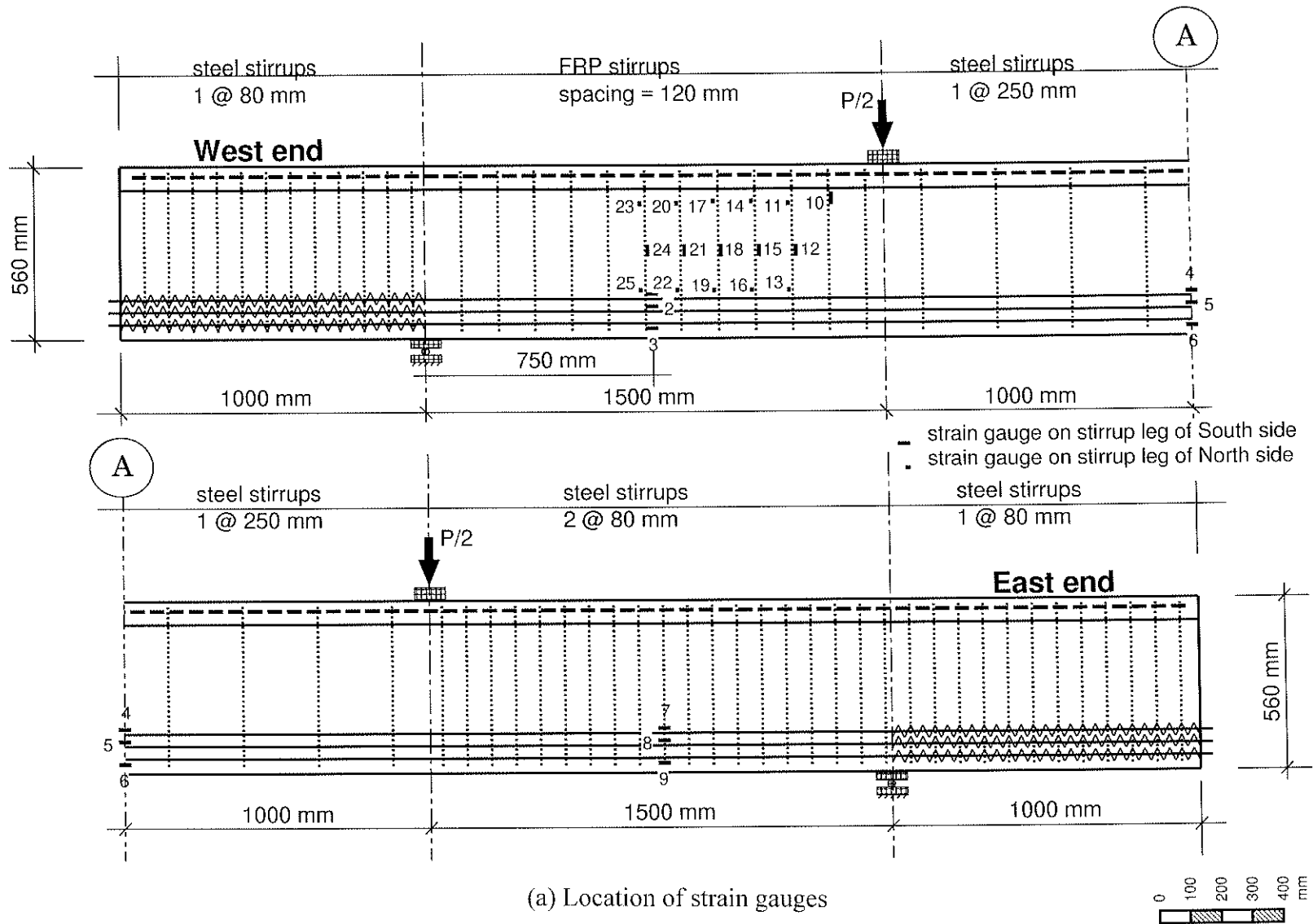
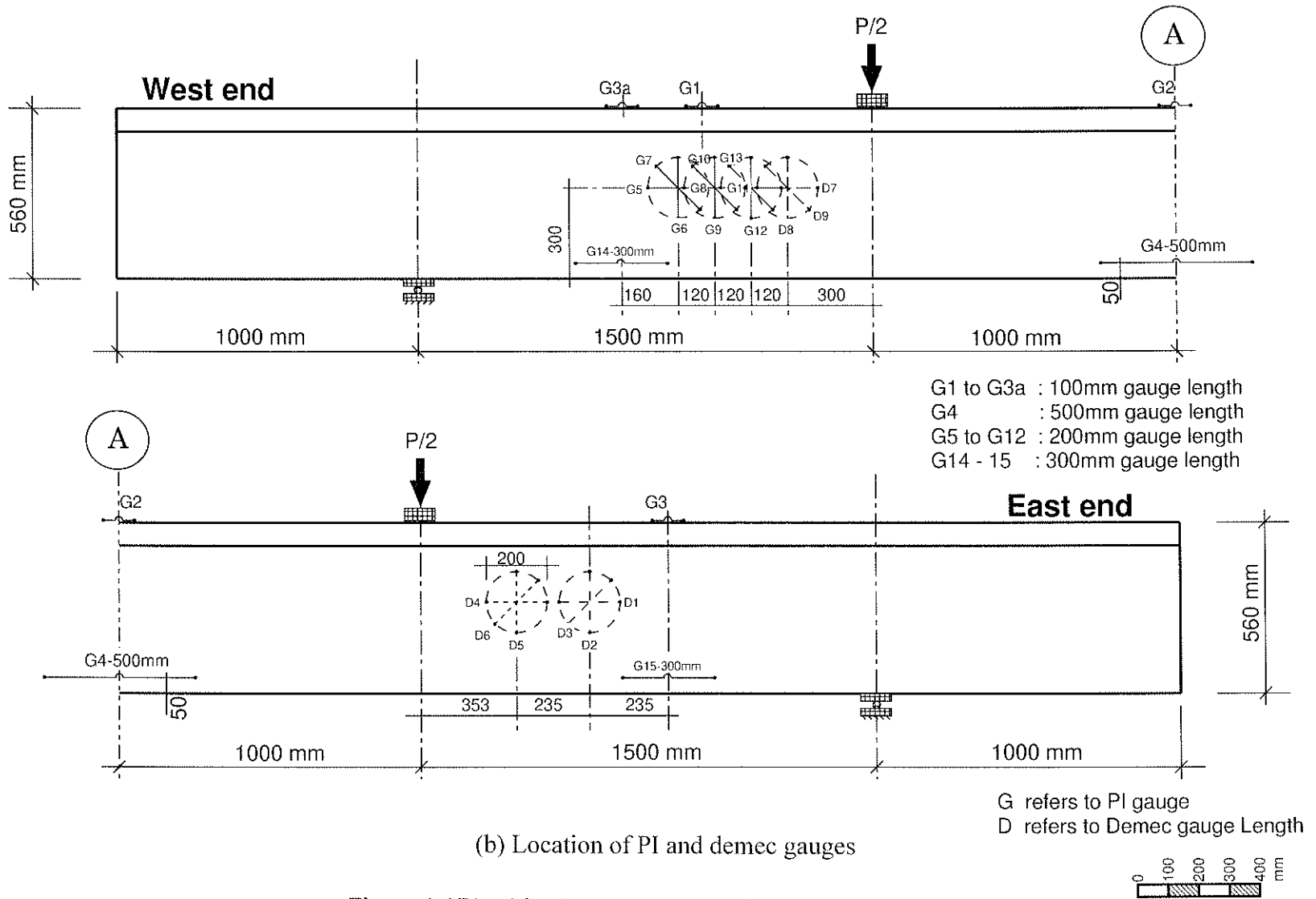


Figure 4-17. Instrumentation of beam SC-4, and SG-4



(b) Location of PI and demec gauges

Figure 4-17(cnt'd). Instrumentation of beam SC-4, and SG-4

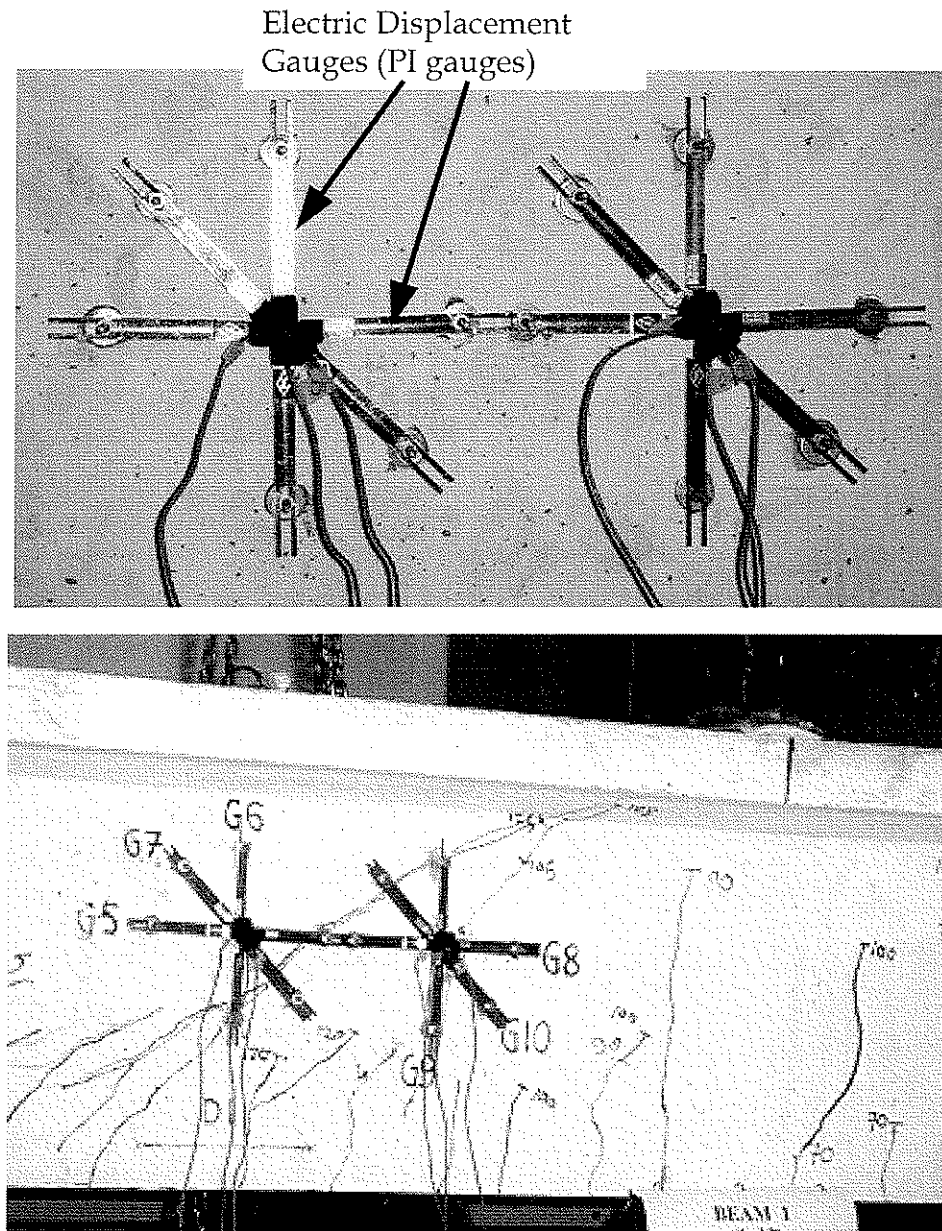


Figure 4-18. Instrumentation for shear cracks and deformation

Chapter

5

Experimental Results and Analysis:

Phase I Panel Specimens

5.1 General

The experimental program was undertaken to examine the structural performance of FRP stirrups for shear reinforcement of concrete structures. In the first phase of the experimental program, 86 panel specimens were tested to evaluate the bend capacity of the FRP stirrups. Seven specimens reinforced with steel stirrups were also tested as control specimens. In addition, twelve panel specimens, specially designed to investigate the kink effect, were tested. The variables considered in the bend tests were the material type of the stirrups, the bar diameter, the configuration of the stirrup anchorage, the embedment length and the tail length beyond the bend portion. The variables considered in the kink specimens were the material type of the stirrups and the angle between the stirrup and the shear crack. Three types of FRP reinforcement were used in this experimental phase, carbon FRP Leadline stirrups, carbon fibre composite cables (CFCC) stirrups and Glass FRP C-BAR stirrups.

This chapter discusses test results for 113 panel specimens tested to evaluate the capacity of a single FRP stirrup as influenced by the bend and kink effects. Test results of bend specimens were used to determine the strength reduction of the FRP stirrups at the bend zone. Test results of kink specimens were used to determine the strength reduction of the FRP stirrups at the shear crack location. Test results of bend and kink specimens were also used to assess the available equations proposed by other researchers presented in chapter 3. The chapter also provides design guidelines and equations for the strength capacity of FRP stirrups as affected by the bend and kink effects.

5.2 Bend capacity

Test results for 101 bend-specimens tested in this study are given in Tables 5-1, 5-2, 5-3 and 5-4 including the ultimate strength based on the measured strain in the stirrup at the failure, and the failure mode. The observed modes of failure are illustrated in Figure 5-1 and designated in Tables 5-1 through 5-4 as follows:

R-S: rupture of the FRP stirrups at the straight portion between the concrete blocks

R-B: rupture of the FRP stirrups at the bend

R-D: rupture of the FRP stirrups at the end of the debonded length inside the concrete block

S: slippage of the bonded part of the stirrup

S-RB: slippage of the bonded part of the stirrup, followed by rupture at the bend

R-BD: rupture of some fibres at the bend and others at the end of the debonded length

In the following sections, the test results are discussed for each type of stirrups and consequently the effect of the following parameters on the stirrup capacity are studied:

- a- bend radius, r_b ;
- b- embedment length, l_d ;
- c- stirrup anchorage; and
- d- tail length, l_d^* .

5.2.1 CFRP Leadline stirrups

For the different values of bend radius, r_b , failure always occurred at the bend zone as a result of bond failure between the fibres and the outer resin coating of the bar, as shown in Figure 5-2. Figure 5-2 also shows a bend specimen with a Leadline stirrup after splitting of the concrete to examine the failure at the bend. None of the tested Leadline stirrups achieved the guaranteed tensile strength parallel to the fibres, which is 1800 MPa (Mitsubishi Chemical Corporation, 1992). The strength at the bend was as low as 35 percent of the guaranteed tensile strength parallel to the fibres, as given in Table 5-1. The bend capacity was influenced by the embedment length l_d , the tail length l_d^* and the anchorage type. As the embedment length l_d of the bend increased, the stirrup capacity increased and achieved as high as 78 and 98 percent of the guaranteed tensile strength parallel to the fibres for Leadline stirrups of r_b/d_e ratios of 3.0 and 7.0, respectively. An increase of the tail length l_d^* of type A anchored stirrups resulted in an increase in the bend capacity for the Leadline stirrups with r_b/d_e of 3.0. It can be seen in Table 5-1 that using sufficient tail length for the type A anchored stirrups resulted in a stirrup capacity

higher than that of the type B anchored stirrups. An increase of the tail length did not affect the bend capacity for the Leadline stirrups with r_b/d_e of 7.0.

An average bond strength of 8.7 MPa for Leadline bars was determined based on the bond tests. Failure of these specimens occurred due to bond failure between the fibres and the outer resin coating of the bar.

5.2.2 CFRP CFCC stirrups

For the 7.5mm-CFCC stirrups with a r_b/d_e ratio of 3.2 it was noticed that, regardless the embedment length l_d used, failure occurred at the bend, as shown in Figure 5-3. However, for the longest embedment length l_d used (150 mm), the measured strength was found to be equal to the guaranteed tensile strength parallel to the fibres, f_{fu} . For the smallest embedment length of r_b+d_b , the measured strength was only 43 percent of the guaranteed strength parallel to the fibres. Failure modes of smaller diameter CFCC stirrups are listed in Table 5-2. The guaranteed tensile strength values of the CFCC bars are given in Table 4-1 and range between 1782 MPa and 1875 MPa. It should be mentioned that the measured ultimate tensile strength parallel to the fibres for CFCC bars based on tension tests is always higher than the guaranteed value, f_{fu} , reported by the manufacturer (Abdelrahman *et al.* 1995). The strength at the bend could be as low as 42 percent of the tensile strength parallel to the fibres, as given in Table 5-2. Results indicated that for a sufficient embedment length of 150 mm or more, the CFCC stirrup with r_b/d_e of 3.0 can develop the full strength parallel to the fibres.

For the 7.5 mm CFCC stirrups with a r_b/d_e ratio of 4.8, the bend capacity ranges from 42 to 100 percent of the guaranteed tensile strength parallel to the fibres. It can be seen in

Table 5-2c that the bend capacity of the 7.5 mm CFCC with a r_b/d_e ratio of 4.8 was greater than that of the stirrups with a r_b/d_e ratio of 3.2, and was greatly influenced by the tail length l_d^* . Results indicated that the embedment length, l_d , required for the CFCC stirrup with r_b/d_e of 4.8 to develop the full strength parallel to the fibres depends on the anchorage type and the tail length l_d^* . Using a sufficient tail length of 90mm (15 times the effective bar diameter, d_e) for the type A anchored stirrups resulted in a bend capacity approximately equal to the strength parallel to the fibres and higher than the bend capacity of the type B anchored stirrups.

An increase in the bend radius, r_b , resulted in an increase in the strength capacity of the CFCC stirrups. For the same tail length l_d^* of 45 mm ($7d_e$), the CFCC stirrup with a r_b/d_e ratio of 4.8 had a bend capacity of 62 percent of the tensile strength parallel to the fibres, while the CFCC stirrups with a r_b/d_e of 3.2 had a bend capacity of 43 percent of the tensile strength parallel to the fibres. The bend radius, r_b , is an important factor in improving the capacity of FRP stirrups, as will be discussed in detail in section 5.3.

5.2.3 GFRP C-BAR™ stirrups

Failure of the C-BAR specimens occurred either at the bend or at the straight portion of the stirrups, due to localized imperfections inside the FRP bar. At these points of imperfection, some of the fibres within the bar are not straight, but have a “wave” configuration. Waving of the fibres was observed in the bend portion as well as the straight portions of the stirrup, as shown in Figure 5-4. This resulted in the failure of some stirrups along the straight portion despite the fact that they were designed to fail at the bend. Therefore, the tensile strength of the FRP bar has been greatly reduced, as

given in Table 5-3. The reduction in the ultimate capacity of the stirrups was between 58 and 79 percent of the guaranteed tensile strength parallel to the fibres. The guaranteed strength parallel to the fibres of the 12-mm GFRP bar is 713 MPa, as reported by the manufacturer.

The strength at the bend of the C-BAR stirrups could be as low as 48 percent of the guaranteed tensile strength parallel to the fibres, as shown in Table 5-3.

5.2.4 Steel stirrups

Failure of the steel specimens occurred by yielding either at the bend or at the straight portion of the stirrups. The failure of the type A anchored stirrups (standard hook) initiated by slip at the hook before yielding at the bend. The observed stress at failure was equal to or greater than the nominal yield strength of the steel bars, as shown in Table 5-4. It was also observed that all the tested stirrups showed excessive deformation prior to failure.

5.3 Effect of bend radius on bend capacity

In general, test results indicated that a decrease in the bend radius, r_b , reduces the bend capacity. The strength reduction is attributed to the stress concentration at the bend section. The radii of the bend used in this study ranged between 3.0 and 7.0 times the effective bar diameter d_e .

To establish a relationship between the bend radius, r_b , and the bend capacity, f_{bend} , the relationship is presented in dimensionless form with respect to the effective bar diameter,

d_e , and the guaranteed strength, f_{fuv} , parallel to the fibres, respectively, as shown in Figure 5-5. Figure 5-5 indicates that the bend capacity varies greatly for the same type of reinforcing fibre. For instance, an increase in the bend radius of the CFCC stirrups might result in a strength capacity equal to the strength parallel to the fibres. On the other hand, it can be seen for the Leadline stirrups that the bend radius does not significantly affect the strength capacity of the stirrup. It is also shown in Figure 5-5 that there is a variation in the bend capacity, f_{bend} , for the same bend radius, r_b . This is attributed to the fact that the bend capacity is significantly affected by the tail length, l_d^* , as discussed in section 5.6.

The JSCE research committee on CFRM¹ (1997) has proposed the following equations for the determination of the strength capacity of the bend, f_{bend} :

$$\frac{f_{bend}}{f_{fuv}} = 0.09 \frac{r_b}{d_e} + 0.3 \leq 1.0 \quad (5-1)^2$$

$$\frac{f_{bend}}{f_{fuv}} = 0.05 \frac{r_b}{d_e} + 0.3 \leq 1.0 \quad (5-2)$$

where f_{fuv} is the guaranteed tensile strength of the FRP bar parallel to the fibres, r_b is the bend radius and d_e is the bar diameter which equals the nominal bar diameter, d_b , for bars with circular cross-section and equals $\sqrt{4A_b/\pi}$ for FRP bars with non-circular cross-section. Equation (5-1) is the regression equation that gives the average of all available test data, while equation (5-2) is the recommended design equation that provides an adequate margin of safety. Equations (5-1) and (5-2) are compared to the test results of

¹ continuous fibre reinforced materials

the current investigation in Figure 5-5(a). As shown in Figure 5-5(a), equation (5-1) gives a reasonable average for test results of CFCC stirrups only. It is also shown in Figure 5-5(a) that equation (5-2) can be used as a design tool for both the CFCC and C-BAR stirrups; however, it overestimates the bend capacity of the Leadline stirrups. It should be mentioned that equations (5-1) and (5-2) do not include the effect of the tail length l_d^* on the bend capacity and the tail length used to develop these equations is not reported in the JSCE recommendation (1997).

The following equations (5-3) and (5-4) were also proposed by Nakamura and Higai (1995) and Ishihara *et al.* (1997), respectively, to determine the strength capacity of the bend:

$$\frac{f_{bend}}{f_{fuw}} = \frac{r_b}{d_e} \ln \left(1 + \frac{d_e}{r_b} \right) \quad (5-3)^3$$

$$\frac{f_{bend}}{f_{fuw}} = \frac{1}{\lambda} \ln(1 + \lambda) \quad (5-4a)^3$$

$$\ln \lambda = 0.90 + 0.73 \ln \frac{d_e}{r_b} \quad (5-4b)^3$$

Equations (5-3) and (5-4) are compared to the test results of the current investigation, as shown in Figure 5-5(b). It is evident from Figure 5-5(b) that equations (5-3) and (5-4) overestimate the bend capacity of FRP stirrups tested in the current investigation. Therefore, these equations are not recommended for use in any future design codes or specifications.

² refer to section 3.5.1.1 in chapter 3

³ refer to equations (3-1) and (3-2) in chapter 3

Based on test results of bend specimens, it is proposed to use a minimum bend radius-to-bar diameter ratio, r_b/d_e , of 4.0 for the CFCC and the C-BAR stirrups and 7.0 for the Leadline stirrups, in order to achieve a stirrup capacity of 50 percent of the strength parallel to the fibres, or higher. A sufficient tail length should be provided beyond the bend, as discussed in section 5.2.5.

5.4 Effect of embedment length on FRP stirrup capacity

In general, test results indicated that a decrease in the embedment length, l_d , reduces the stirrup stress at failure, f_{fv} . The strength reduction is attributed to a reduction of the bonded length leading to exposure of the bend portion of the stirrup to the load. For CFCC stirrups, with d_b ranging from 5 to 7.5 mm, it is proposed that a 150 mm embedment length is sufficient to eliminate direct stressing of the bend portion of the stirrups; therefore, the guaranteed strength parallel to the fibres can be fully developed.

To establish a relation between the embedment length, l_d , and the stirrup stress at failure, f_v , the relationship is presented in dimensionless format with respect to the effective bar diameter, d_e , and the guaranteed strength parallel to the fibres, f_{fv} , respectively, as shown in Figures 5-6, 5-7 and 5-8. This relationship indicates that the reduction in the strength starts below a certain value of l_d/d_e ratio for each type of stirrup. This value was found to be in the range of 20 for the CFCC type A stirrups and 16 for type B stirrups. Using the value of l_d/d_e of 5.0 typically provided at the bend, the measured average strength for CFCC stirrups using type A and B were 50 and 74 percent, respectively, as shown in Figure 5-6. Figure 5-7 indicates that the limiting value for l_d/d_e for the Leadline stirrups

to achieve the guaranteed strength parallel to fibres, f_{fu} , is 42. Using a small development length could reduce the strength to 40 percent, as shown in Figure 5-7.

The following equations can be used to evaluate the stirrup stress at failure, f_{fv} , with smaller embedment lengths than the recommended values:

CFRP CFCC

$$0.52 \leq \frac{f_{fv}}{f_{fu}} = 0.35 + \frac{l_d}{30 d_e} \leq 1.00 \quad \text{Type A anchorage} \quad (5-5)$$

$$0.73 \leq \frac{f_{fv}}{f_{fu}} = 0.60 + \frac{l_d}{40 d_e} \leq 1.00 \quad \text{Type B anchorage} \quad (5-6)$$

CFRP Leadline

$$0.47 \leq \frac{f_{fv}}{f_{fu}} = 0.40 + \frac{l_d}{70 d_e} \leq 1.00 \quad (5-7)$$

It should be mentioned that for CFCC and Leadline stirrups, the proposed equation may be used for the various bend radii, r_b , as evident from Figure 5-7.

Test results of the C-BAR stirrups are presented in Figure 5-8. An increase in the embedment length, l_d , resulted in an increase in the stirrup capacity; however, there is no clear trend for the tested specimens as shown in Figure 5-8. Based on the reported bond stress of 21 MPa for the 12mm C-BAR bars (Rizkalla *et al.* 1997), it is predicted that stirrups will achieve the guaranteed strength parallel to the fibres for l_d values higher than 110 mm. Because of the “waving” imperfections in the C-BAR stirrups (Figure 5-4), none of the specimens reached the tensile strength parallel to the fibres. The ultimate capacity of the stirrup was always higher than or equal to the strength at the bend.

The following expression can be used as a failure criterion for C-BAR stirrups:

GFRP C-BAR

$$0.49 \leq \frac{f_{fv}}{f_{fuw}} = 0.24 + \frac{l_d}{20 d_e} \leq 0.80 \quad (5-8)$$

where f_{fv}/f_{fuw} is the bend capacity-to-tensile strength parallel to the fibres, and l_d/d_e is the embedment length-to-effective bar diameter ratio. Equation (5-8) is compared to test results in Figure 5-8.

5.5 Effect of stirrup anchorage on FRP stirrup capacity

A typical stirrup in a reinforced concrete beam has type A anchorage (overlapped) at the compression chord of the beam and type B anchorage (continuous) at the tension side, as illustrated in Figures 4-5, 4-10 and 5-8. The strength capacity of an FRP stirrup is governed by the lowest bend capacity of the two types of anchorage.

For an r_b/d_e ratio of 3.0, type A anchored Leadline stirrups with a minimum tail length, l_d^* , of 63 mm ($9d_e$) showed higher capacity than the type B anchored stirrups, as given in Table 5-1. Type B stirrups had a bend capacity of 40 percent of the guaranteed tensile strength parallel to the fibres, while type A stirrups had a capacity of 40 to 44 percent of the guaranteed tensile strength parallel to the fibres. For an r_b/d_e ratio of 7.0, type B stirrups had a capacity of 55 percent of the guaranteed strength, which is approximately equal to that of type A stirrups with a minimum tail length, l_d^* , of 42mm ($6d_e$).

Significant reduction in the stirrup capacity was observed in type A anchored CFCC stirrups with a standard tail length of $6d_b$, as compared to type B anchored CFCC stirrups, as shown in Figure 5-7. The strength reduction is attributed to possible slip at the bend leading to initiation of failure at a lower stress level. An increase in the tail length l_d^*

resulted in an increase in the stirrup capacity, as given in Table 5-2c for the test results of the 7.5mm CFCC stirrups. For a tail length-to-effective diameter ratio, l_d^*/d_e , higher than 13, the capacity of type A anchored stirrups is higher than that of type B anchored stirrups.

5.6 Effect of tail length on FRP stirrup capacity

For each bend radius, r_b , five Leadline stirrups with tail lengths, l_d^* , of $3d_e$, $6d_e$, $9d_e$, $12d_e$, and $18d_e$, were tested. For an r_b/d_e ratio of 7.0, the stress level at failure varied between 44 and 53 percent of the guaranteed tensile strength parallel to the fibres, as given in Table 5-1. For r_b/d_e of 3.0, the stress level at failure varied between 35 and 44 percent of the guaranteed tensile strength parallel to the fibres, as given in Table 5-1. Figure 5-9 shows the relationship between f_{bend}/f_{fiv} and l_d^*/d_e . It can be seen in Figure 5-9 that an increase in the tail length, l_d^* , resulted in a slight increase in the bend capacity. A tail length of 70 mm ($10d_e$) is sufficient to develop a bend capacity of 40 and 50 percent of the guaranteed tensile strength parallel to the fibres for r_b/d_e of 3.0 and 7.0, respectively. It can be seen in Table 5-2c for 7.5-mm-diameter CFCC stirrups that an increase in the tail length, l_d^* , of type A stirrups resulted in an increase in the stirrup capacity. Figure 5-10 shows the relationship between f_f/f_{fiv} and l_d^*/d_e for the 7.5-mm-diameter CFCC stirrups with three different values of the embedment length l_d of r_b+d_b , $16d_e$ and $24d_e$. This relationship indicates that the reduction in the strength starts below a certain value of l_d^*/d_e . This value was found to be in the range of 15 for the CFCC stirrups. Using a small tail length could reduce the strength to as low as 42 percent, as shown in Figure 5-

10. The following equation can be used to evaluate the bend capacity of CFCC stirrups, f_{bends} , with smaller tail lengths than the limiting value:

$$\frac{f_{bend}}{f_{tuv}} = 0.24 + \frac{l_d^*}{17 d_e} \leq 1.00 \quad (5-9)$$

A minimum tail length of 70 mm ($11d_e$) is recommended for the CFCC stirrups to develop at least 75 percent of the guaranteed tensile strength parallel to the fibres.

The tail length of the GFRP stirrups tested in this study was either $6d_e$ or $12d_e$. It can be seen in Table 5-3 that failure might occur at the straight portion of the FRP stirrup even if the bend is directly exposed to the load. The observed imperfection “waving” in the GFRP stirrups made it inconclusive to study the effect of the tail length as the failure is expected at the “waving” imperfection. However, for all GFRP bend specimens, no slip was observed prior to rupture either at the bend or at the “waving” imperfection. The bend capacity of such a minimum tail length of $6d_e$ was found to be 48 percent (or higher) of the guaranteed tensile strength parallel to the fibres, which almost equals the average bend capacity of type B stirrups.

5.7 Detailing of FRP stirrups

Based on test results of bend specimens, certain limitations on the detailing of CFRP and GFRP stirrups were proposed in the preceding sections to achieve the highest possible strength capacity for the FRP stirrups. To establish unified guidelines for detailing of both CFRP and GFRP stirrups, the following limitations are proposed, as illustrated in Figure 5-11:

- a- The bend radius, r_b , should not be less than four times the effective bar diameter or 50 mm, whichever is greater.
- b- The tail length, l_d^* , should not be less than six times the effective bar diameter or 70 mm, whichever is greater.

5.8 Stirrup capacity at crack intersection

Test results of the 12 kink specimens tested in this study are given in Table 5-5, including the measured failure load and strain, ε_{fs} , in the stirrups at failure. All kink specimens failed either by rupture in FRP stirrups or yield of steel stirrups at the crack location. The measured strain at failure was determined according to the readings of the electric strain gauges attached to the bars in the direction of the fibres. The load transfer in the kink specimens can be modelled using the following models (Figure 5-11):

5.8.1 Model “A”: Full bond between the FRP stirrups and the concrete

This approach was adopted by Maruyama *et al.* (1989) and Nakamura and Higai (1995) to establish a relationship between the strength capacity of FRP stirrups and the shear crack angle. If full bond is assumed between the bars and the concrete, the stirrups will not be free to deform inside the concrete blocks, leading to a minimal crack opening displacement, w (Figure 5-12a). Therefore, the force equilibrium at the crack location is satisfied according to Figure 5-12(a), where the FRP stirrup is subjected to a tensile force, $F_{tension}$, and a shear force, F_{shear} .

For FRP bars, as reported in chapter 3, Maruyama *et al.* (1989) proposed the following equation:

$$\frac{f_{fv}}{f_{fuv}} = 1 - \frac{k_f}{100} \theta \quad (5-10)^4$$

where k_f is the reduction factor and has an average value of 2.1 for CFRP bars, 1.9 for AFRP bars and 1.3 for GFRP bars for θ values varies from zero to 30 degrees.

Also, Nakamura and Higai (1995) proposed the following equations:

$$\frac{f_{fv}}{f_{fuv}} = \frac{1}{\cos\theta + 6 \sin\theta \tan\theta} \quad \text{for rectangular sections} \quad (5-11)^5$$

$$\frac{f_{fv}}{f_{fuv}} = \frac{1}{\cos\theta + 8 \sin\theta \tan\theta} \quad \text{for circular sections} \quad (5-12)^4$$

It should be mentioned that equations (5-11) and (5-12) are based on a small kinking (debonding) length of $d_b \tan \theta$ that results in very small crack width (~ 0).

For steel sections subjected to tensile and shear stresses, the failure is governed by Von Mises's failure criterion, which is represented by the following equation:

$$f_{tension}^2 + 3f_{shear}^2 = f_{sy}^2 \quad (5-13)$$

where $f_{tension}$ is the applied tensile stress ($f_{tension} = f_{sv} \cos \theta$), f_{shear} is the applied shear stress ($f_{shear} = f_{sv} \sin \theta$), and f_{sy} is the yield strength of steel. Replacing $f_{tension}$ by $f_{sv} \cos \theta$ and f_{shear} by $f_{sv} \sin \theta$, equation (5-13) can be rewritten as follows:

$$\frac{f_{sv}}{f_{sv}} = \sqrt{\frac{1}{\cos^2\theta + 3\sin^2\theta}} \quad (5-14)$$

⁴ refer to equation (3-3) in chapter 3

The relationship between f_{fv}/f_{fiv} (or f_{sv}/f_{svv}) and the angle of the stirrups, θ , for kink specimens is shown in Figure 5-13. As demonstrated in Figure 5-13, an increase in the angle θ reduces the strength capacity of the FRP and steel stirrups. However, the rate of strength reduction in FRP stirrups is higher than the strength reduction rate of steel stirrups. Figure 5-13(a) shows that test results of steel stirrups follow the Von Mises's criterion. Test results of FRP stirrups are compared to predicted values by equations (5-10), (5-11) and (5-12) in Figure 5-13(a). As seen in Figure 5-13(a), equation (5-10) shows good prediction for GFRP C-BAR stirrups within the range of $\theta = 0$ to 30 degrees and very conservative prediction for CFRP Leadline stirrups. Equations (5-11) and (5-12) result in very conservative prediction for the strength capacity of GFRP and CFRP stirrups.

The following equation is given in a similar format to Von Mises's criterion to predict the failure stress for an FRP stirrup intersecting a crack with an angle $90-\theta$ (Figure 5-13b):

$$\frac{f_{fv}}{f_{fiv}} = \sqrt{\frac{1}{\cos^2\theta + 6\sin^2\theta}} \quad (5-15)$$

where f_{fiv} is the guaranteed tensile strength of FRP stirrup parallel to the fibres.

For design purposes, the following equation is proposed to provide safe prediction for the strength capacity of FRP bars as affected by the angle θ (Figure 5-13b):

$$\frac{f_{fv}}{f_{fiv}} = \sqrt{\frac{1}{\cos^2\theta + 12\sin^2\theta}} \quad (5-16)$$

⁵ refer to equation (3-4) and (3-5) in chapter 3

For an angle θ of 45 degrees, which is a typical shear crack angle in concrete beams, the average failure stress based on equation (5-15) is 53 percent of the guaranteed tensile strength parallel to the fibres. For the same angle θ of 45 degrees, equation (5-16) gives a design stress of 39 percent of the guaranteed tensile strength parallel to the fibres. As shown later in chapter 6 (section 6.4), the stresses in FRP stirrups used as shear reinforcement in concrete beams reached values higher than 53 percent of the guaranteed tensile strength parallel to the fibres. Therefore, the assumption of full bond between the FRP stirrup and the concrete (Model "A") represents the behaviour of FRP bars subject to combined shear and tension and does not represent the actual situation of an FRP stirrup in a reinforced concrete beam.

5.8.2 Model "B": Debonding length at the crack location

If the bond between the FRP stirrups and the concrete is lost for a long length, l_{db} , the stirrups can be modeled as truss members as shown in Figure 5-12(b). The figure also demonstrates force equilibrium at the crack location when the FRP stirrup is subjected to a tensile force, $F_{tension}$, and no shear force, F_{shear} . The predicted deformed shape according to the proposed model is also shown. The failure in this model is governed by the guaranteed tensile strength of the FRP stirrups parallel to the fibres. The stresses in the kink specimens at failure were determined according to Model "B" and are given in Table 5-5. The relationship between the stress at failure based on Model "B" and the stirrup angle θ is shown in Figure 5-14(a). It can be seen in Figure 5-14(a) that there is no clear trend for an increase or decrease in the stirrup stress with the variation of the

angle θ for both GFRP and CFRP stirrups. The average failure stress-to-guaranteed strength ratio was found to be 0.810 with a standard deviation of 0.102.

Figure 5-14(b) shows the relationship between the observed strain in the direction of the fibres of FRP stirrups at failure, ε_{fv} , and the stirrup angle, θ . It can be seen in Figure 5-14(b) that there is no clear trend for an increase or decrease in the observed strain at failure with the variation of the angle θ for both GFRP and CFRP stirrups. The average failure strain-to-ultimate strain in the direction of the fibres ratio was found experimentally to be 0.831 with a standard deviation of 0.062.

The average observed strain ratio (0.831) agrees with the average stress determined according to Model "B" (0.810), as shown in Figure 5-14. This indicates that Model "B" provides closer representation for the load transfer in kink specimens. Therefore, it can be concluded from Figure (5-14) that the failure of FRP stirrups is governed by an average tensile strength higher than 80 percent of the guaranteed strength parallel to the fibres.

5.9 Summary and conclusions

The current research included an extensive experimental program to investigate two major effects on the strength capacity of FRP stirrups. Test results of 101 panel specimens tested to evaluate the bend effect on FRP stirrup capacity, as well as 12 panel specimens tested to investigate the kink effect, were reported in this chapter. Table 5-5 and Figure 5-14 show that for kink specimens the stress in an FRP stirrup at failure could be as low as 65 percent of the guaranteed tensile strength parallel to the fibres.

Meanwhile, it is observed for bend tests (Tables 5-1 to 5-3) that the stress at failure could be as low as 35 percent of the guaranteed tensile strength parallel to the fibres. Therefore, the bend effect on strength capacity of FRP stirrups is more critical than the kink effect and would limit the contribution of FRP stirrups in beam action. The findings of the current investigation support the conclusion made by the author at the end of chapter 3 based on the review of the available research on the use of FRP as shear reinforcement. However, this conclusion has not been reported by any researcher in the literature. Design guidelines for the strength capacity and detailing of FRP stirrups were also provided in this chapter.

Table 5-1. Test results of bend specimens: CFRP Leadline stirrups

material type	bend radius		tail length		l_d mm	stirrup anchorage Type	stress at failure f_{fv} MPa	f_{fv}/f_{fvw}	mode of failure [#]
	r_b mm	r_b/d_c	l_d^* mm	l_d^*/d_c					
Leadline stirrups	20	3	21	3	$r_b+d_b^{##}$	A	632	0.35	S-RB
			42	6	r_b+d_b		639	0.35	S-R
					150		1404	0.78	R-D
			63	9	r_b+d_b		737	0.41	S-RB
			84	12	r_b+d_b		728	0.40	S-RB
					150		1168	0.65	R-B
			120	17	r_b+d_b		793	0.44	S-R
					r_b+d_b		715	0.40	R-B
					100		1335	0.74	R-D
					150		1242	0.69	R-B
			-----			B			
	50	7	21	3	r_b+d_b	A	1057	0.59	R-B
					150		797	0.44	R-B
			42	6	r_b+d_b		1235	0.69	R-B
					150		955	0.53	R-B
			63	9	r_b+d_b		1062	0.59	R-B
					150		813	0.45	R-B
			84	12	r_b+d_b		1053	0.58	R-B
					150		935	0.52	R-B
					r_b+d_b		962	0.53	R-B
				150	1149		0.64	R-B	
120			17	250	1638		0.91	R-S	
				300	1504		0.84	R-B	
				350	1763		0.98	R-S	
				r_b+d_b	981		0.55	R-B	
		-----			B				
		100	987	0.55	R-B				
		150	1176	0.65	R-B				
Leadline straight	bond test	-----	150	N/A	874	0.49	S		
			300		1106	0.61	S		

Failure modes:**R-S :** rupture along the straight portion between the concrete blocks**R-B :** rupture at the bend**R-D :** rupture at the end of the debonded length inside the concrete block**S :** slippage of the bonded part of the stirrup**S-RB :** slippage of the bonded part of the stirrup, followed by rupture at the bend**R-BD:** rupture of some fibres at the bend zone and others at the end of the debonded length^{##} $d_b = 5$ mm

Table 5-2. Test results of bend specimens: CFRP CFCC stirrups

(a) $d_b = 5$ mm (7-wire)

material type	bend radius		tail length		l_d mm	stirrup anchorage type	stress at failure, f_{fv} MPa	f_{fv}/f_{fiv}	mode of failure
	r_b mm	r_b/d_e	l_d^* mm	l_d^*/d_b					
CFCC stirrups	15	4.2	45	9	r_b+d_b	A	916	0.51	R-B
					80		1975	1.11	R-S
					150 [#]		2145	1.20	R-S
			-----		r_b+d_b	B	1455	0.82	R-B
					80		2156	1.21	R-S
					150 [#]		2145	1.20	R-S

(b) $d_b = 5$ mm (single wire)

material type	bend radius		tail length		l_d mm	stirrup anchorage Type	stress at failure, f_{fv} MPa	f_{fv}/f_{fiv}	mode of failure
	r_b mm	r_b/d_e	l_d^* mm	l_d^*/d_b					
CFCC stirrups	15	3.4	45	9	r_b+d_b	A	983	0.53	R-B
					80		1973	1.07	R-S
					150 [#]		1957	1.06	R-S
			-----		r_b+d_b	B	1187	0.64	R-B
					80		1949	1.06	R-S
					150 [#]		1957	1.06	R-S

(c) $d_b = 7.5$ mm (7-wire)

material type	bend radius		tail length		l_d mm	stirrup anchorage type	stress at failure, f_{fv} MPa	f_{fv}/f_{fiv}	mode of failure
	r_b mm	r_b/d_e	l_d^* mm	l_d^*/d_b					
CFCC stirrups	20	3.2	45	6	r_b+d_b	A	798	0.43	R-B
					80		1421	0.76	R-B
					150		1900	1.01	R-B
					r_b+d_b	A	789	0.42	R-B
			22.5 3		100		1352	0.72	S-R
					150		1590	0.85	S-R
					r_b+d_b		1159	0.62	R-B
			45 6		100		1641	0.88	S-R
					150		1729	0.92	S-R
					r_b+d_b	1475	0.79	R-B	
			67.5 9		100	1398	0.75	R-B	
					150	1768	0.94	R-S	
					r_b+d_b	1846	0.98	R-B	
			90 12		100	1867	0.99	R-D	
					150	1875	1.0	R-B	
					r_b+d_b	1902	1.01	R-B	
			150 20		100	1987	1.06	R-S	
					150	1912	1.04	R-S	
					r_b+d_b	1798	0.96	R-B	
			-----		100	1669	0.89	R-S	
					150	2068	1.10	R-S	

[#] reported for both type A and type B specimen configurations

Failure mode: (refer to Table 5-1)

Table 5-3. Test results of bend specimens: GFRP C-BAR™ stirrups

material type	bend radius		tail length		l_d mm	stirrup anchorage type	no. of specimens tested	stress at failure f_{fv} MPa	f_{fv}/f_{fvv}	mode of failure
	r_b mm	r_b/d_e	l_d^* mm	l_d^*/d_b						
C-BAR stirrups	50	4.0	72	6	r_b+d_b	A	2	442	0.62	R-B
								400	0.56	R-S
			145	12	r_b+d_b		6	345 [#]	0.48	R-B
								447	0.63	R-S
					100		2	416	0.58	R-D
					150		2	424	0.59	R-S
					250		2	450	0.63	R-D
							2	556	0.78	R-S
							2	517	0.73	R-S
			-----	r_b+d_b	B		10	347 [#]	0.49	R-B
							2	561	0.79	R-BD
								500	0.70	R-D
							1	586	0.82	Splitting ^{##}
							3	409	0.57	R-D
	511	0.72				R-D				
			3	301	0.42	R-D				

average value

failure by splitting of the concrete block, other specimens were designed to prevent this type of failure

Table 5-4. Test results of bend specimens: steel stirrups

material Type	nominal diameter d_b mm	bend radius		tail length		l_d mm	stirrup anchorage type	No. of tests	stress at failure f_{sv} MPa	f_{sv}/f_{svv}	mode of failure			
		r_b mm	r_b/d_e	l_d^* mm	l_d^*/d_b									
steel stirrups	6.35	20	3.0	40	6	r_b+d_b	A	1	593	0.99	Y-S			
									757	1.26	Y-S			
									770	1.28	Y-B			
						r_b+d_b		B	---	669	1.12	Y-S		
					150 [#]				1	770	1.28	Y-B		
				10 ^{##}	40	4.0		-----	r_b+d_b	B	3	555	1.26	Y-B

Failure modes:

Y-S : yield along the straight portion between the concrete blocks

Y-B : yield at the bend

reported for both type A and type B specimen configurations

epoxy coated stirrups made of 10-mm-diameter, 440-MPa-yield-strength conventional mild steel bars were used for bend specimens only.

Table 5-5. Test results of kink specimens

material type	nominal diameter d_b mm	effective diameter d_e mm	angle of stirrup θ	Failure load kN	Strain at failure ϵ_{fv} %	$\epsilon_{fv}/\epsilon_{fuv}$	Model (a)		Model (b)	
							$f_{fv}^{\#}$ MPa	f_{fv}/f_{fuv}	f_{fv}	$\frac{f_{fv}}{f_{fuv}}$
steel	6.35	6.35	0*	---	---		660 ^{###}	1.000	660	1.000
			30	66	---		520	0.788	600	0.910
			45	60	---		470	0.712	665	1.008
			90**	---	---		381	0.577	---	
Leadline	rect. (10x5)	7.0	0 ^s	---	1.31	1.000	1800	1.000	1800	1.000
			25	195	0.96	0.733	1267	0.704	1398	0.777
			35	197	1.13	0.863	1280	0.711	1563	0.868
			45	159	1.02	0.779	1033	0.574	1461	0.812
			53	145	1.20	0.916	942	0.523	1565	0.869
			60	129	n/a		838	0.466	1676	0.931
			90**	---	---		315	0.175	---	---
C-BAR	12	12.0	0 ^s	---	1.74	1.0	713	1.000	713	1.000
			25	188	1.40	0.805	420	0.589	463	0.650
			35	187	1.61	0.925	414	0.581	505	0.708
			45	149	1.39	0.799	331	0.464	468	0.656
			53	175	1.44	0.828	386	0.541	641	0.899
			60	150	n/a		332	0.465	664	0.931
			90**	---	---		207	0.290	---	

* based on uniaxial tension test

** based on direct shear test

^s guaranteed tensile strength, according to the manufacturer[#] $f_{fv} = \text{Load} / (4 \cdot a_{fv})$, where a_{fv} is the cross-sectional area of a stirrup (see sketch in Figure 5-12b)^{###} yield strength

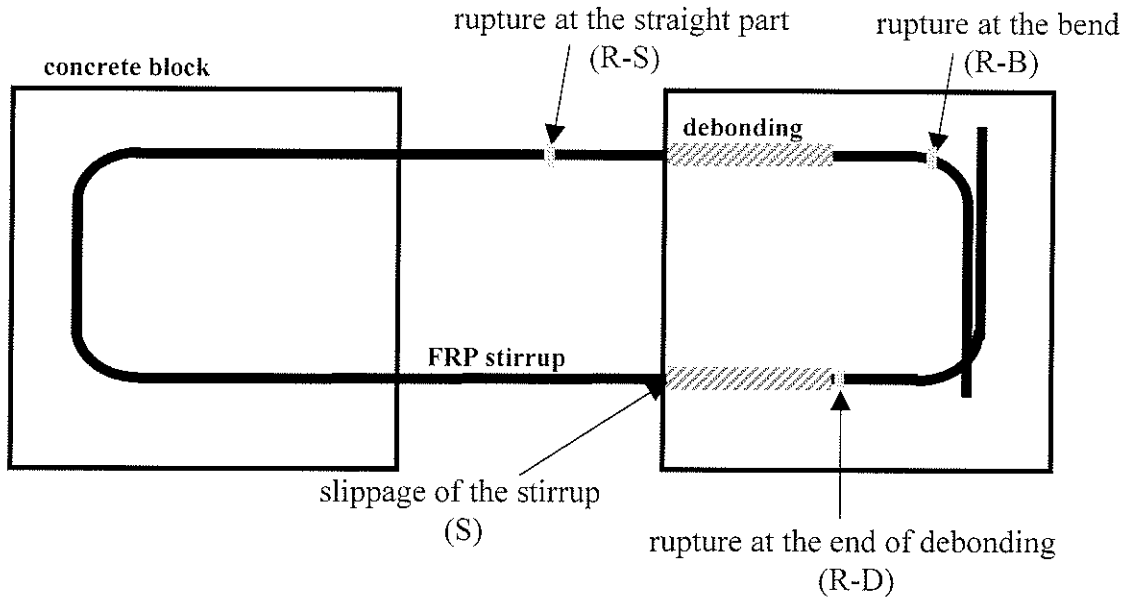


Figure 5-1. Failure modes of bend specimens

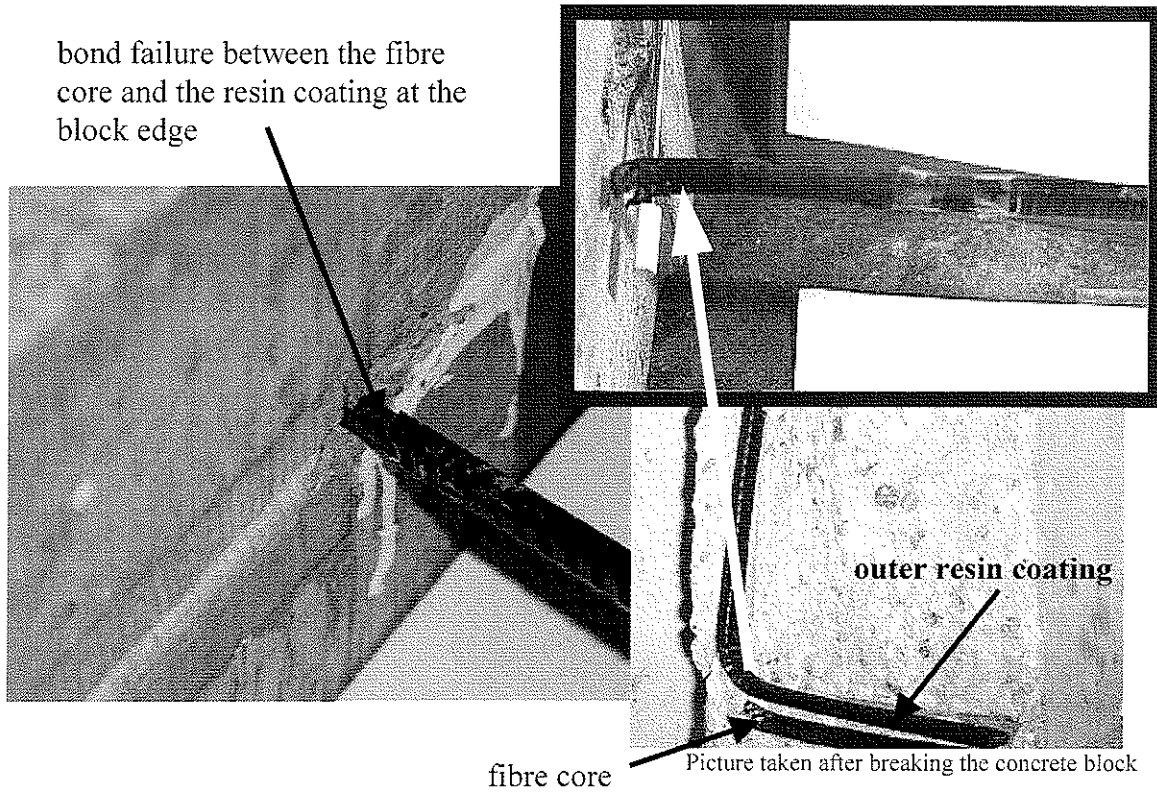


Figure 5-2. Failure at the bend - CFRP Leadline stirrups

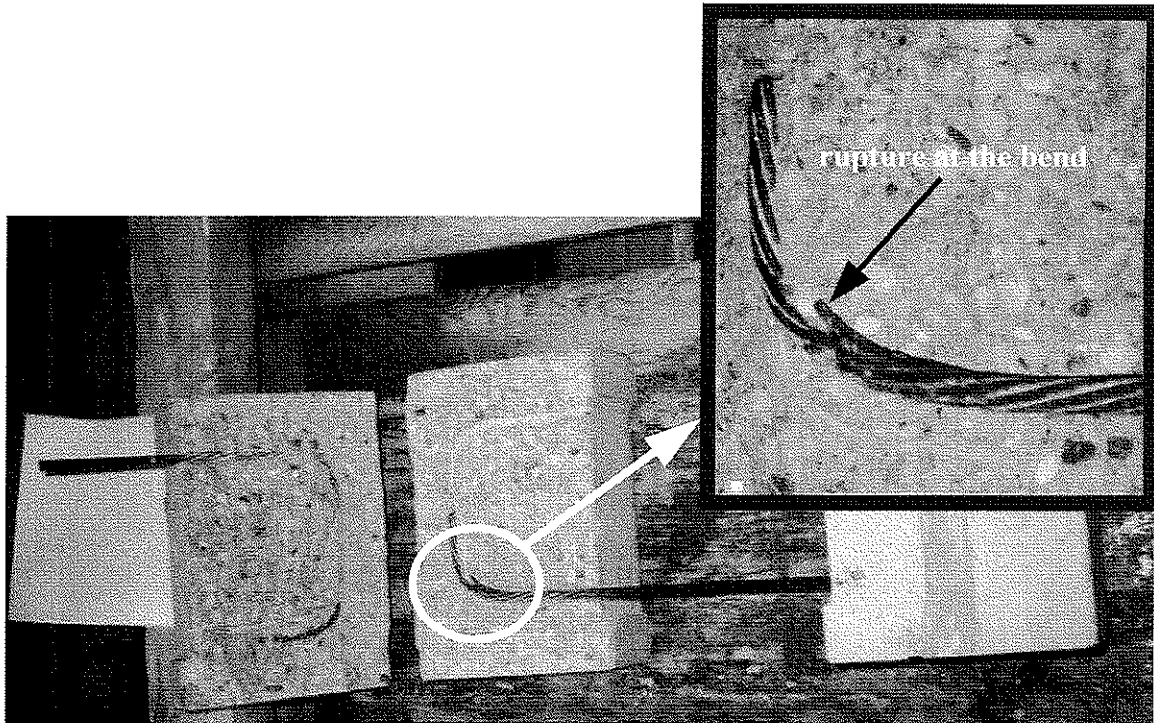


Figure 5-3. Failure at the bend - CFRP CFCC stirrups

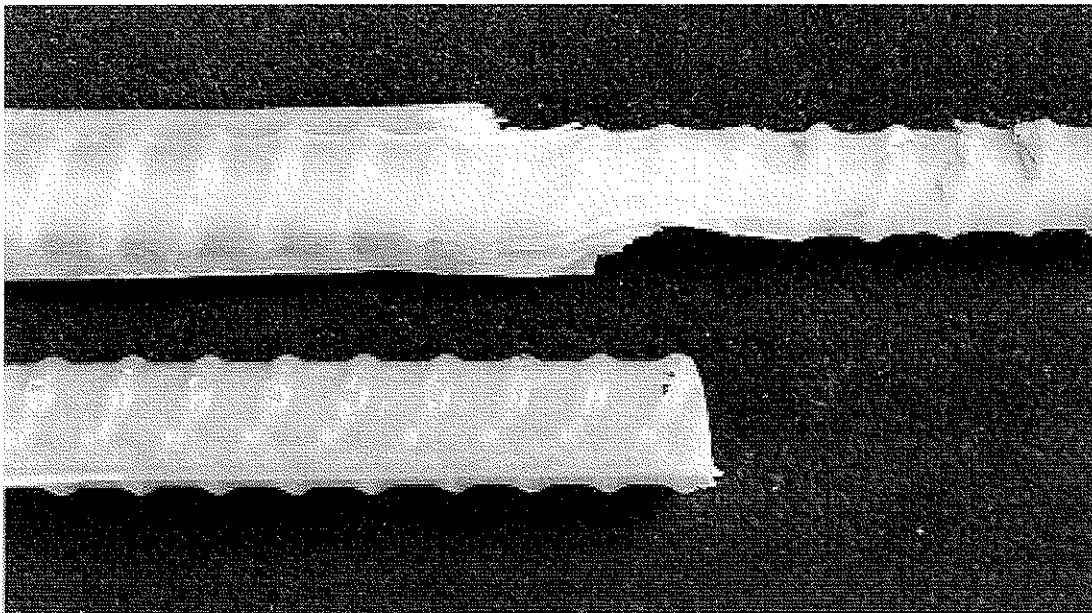
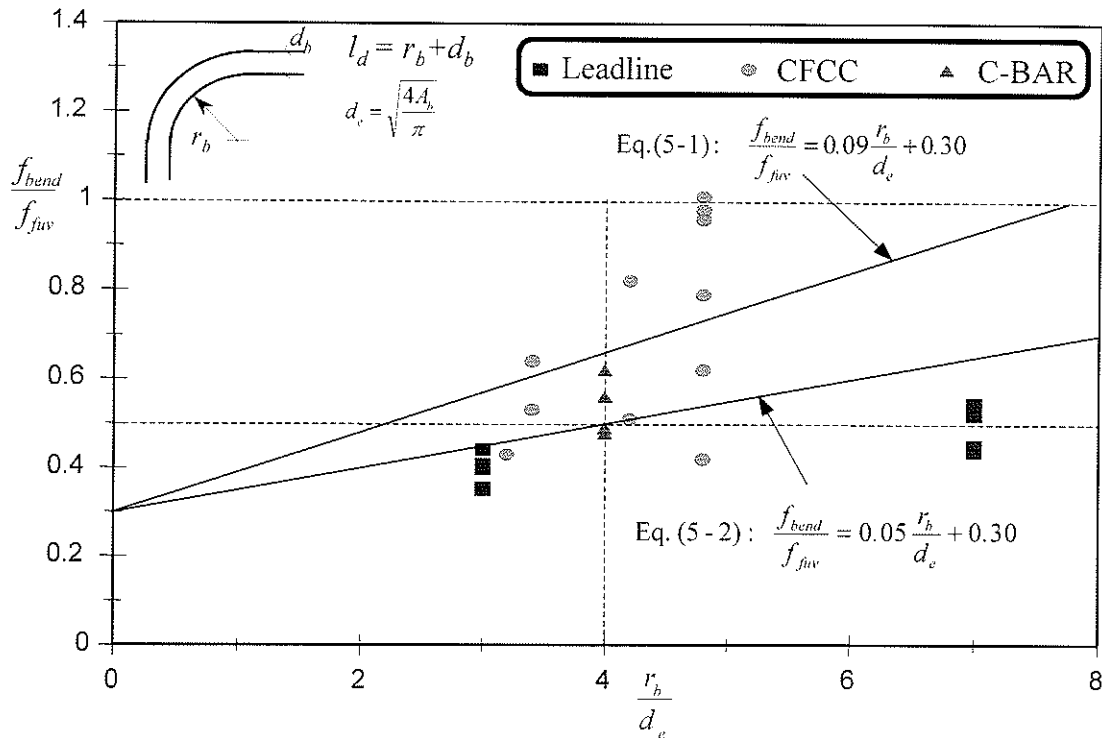
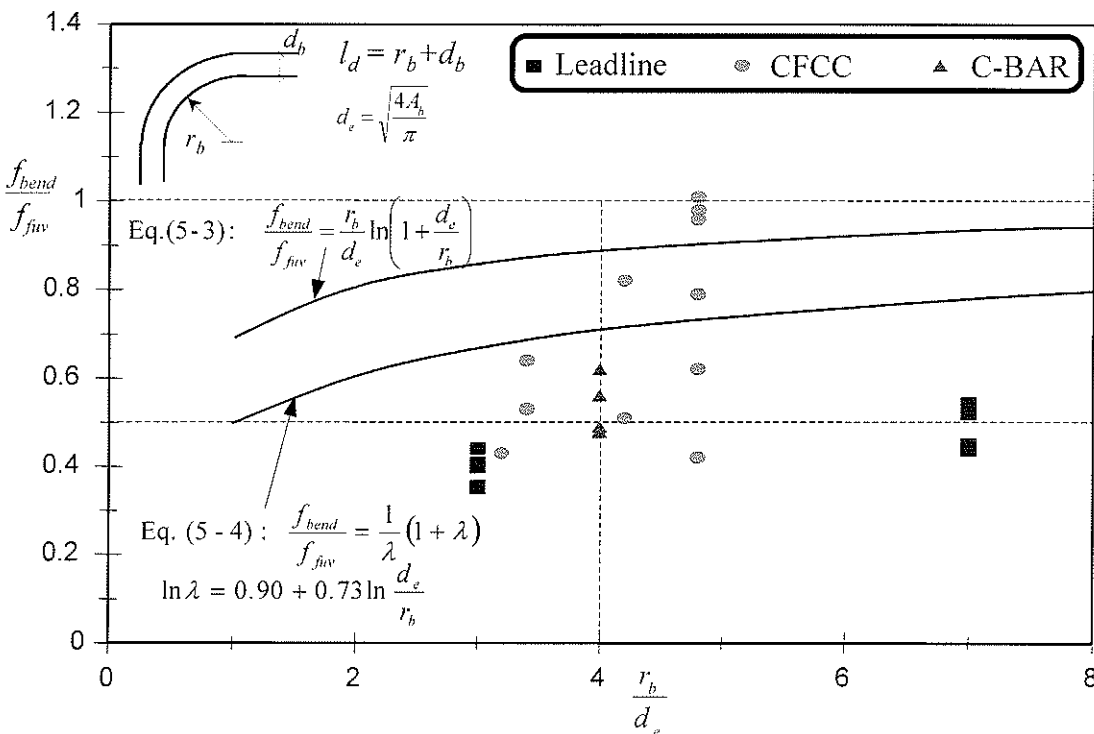


Figure 5-4. Failure of GFRP C-BAR™ stirrups due to "waving" of fibres



(a) Test results versus equations proposed by JSCE (1997)



(b) Test results versus equations proposed by Nakamura and Higai (1995; Eq. 5-3) and Ishihara *et al.* (1997; Eq. 5-4)

Figure 5-5. Effect of bend radius, r_b , on strength capacity of the bend, f_{bend}

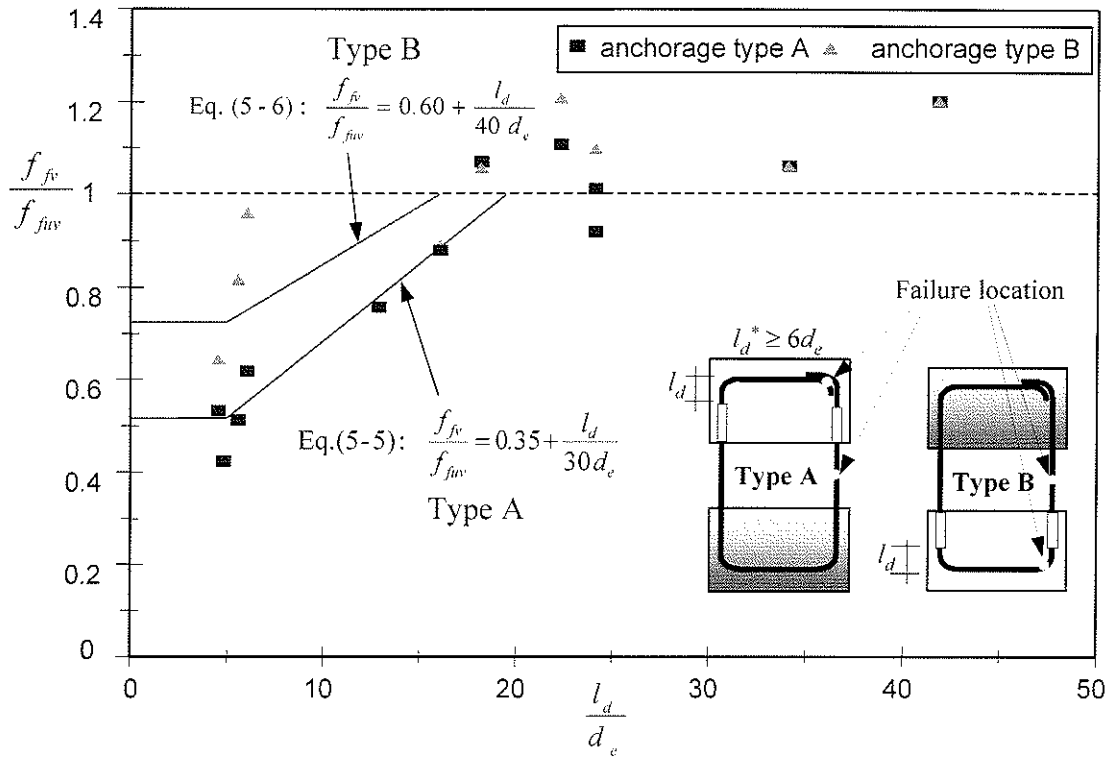


Figure 5-6. Effect of embedment length, l_d , on capacity of CFRP CFCC stirrups

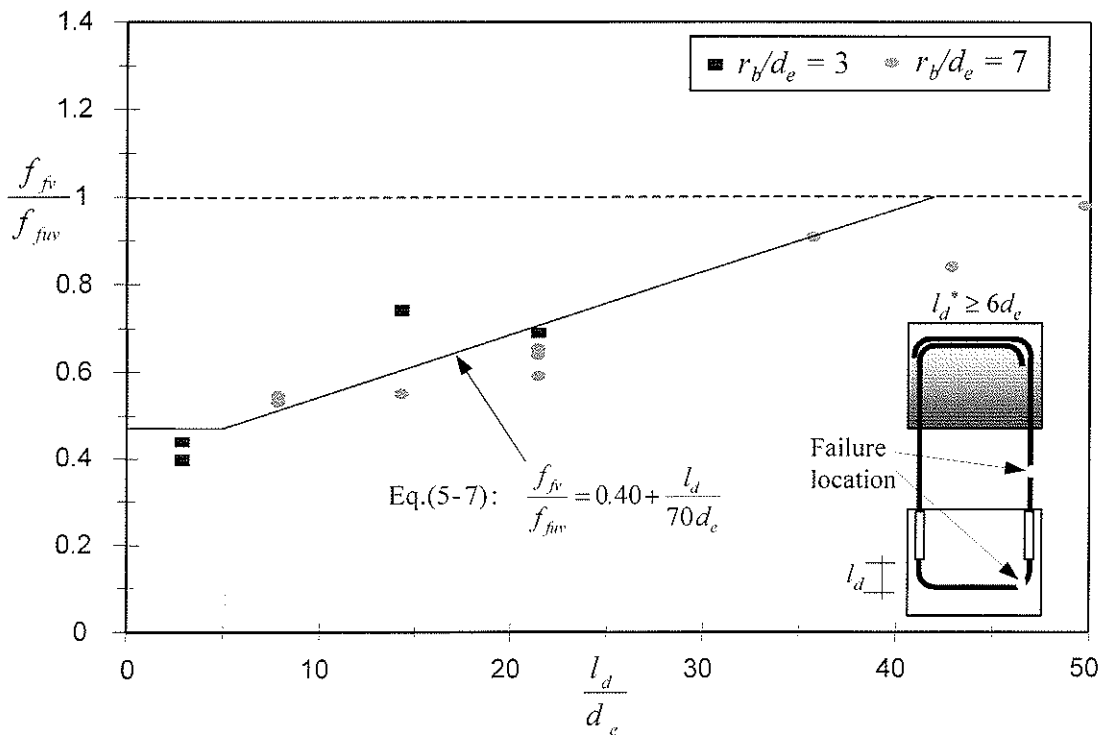


Figure 5-7. Effect of embedment length, l_d , on capacity of CFRP Leadline stirrups

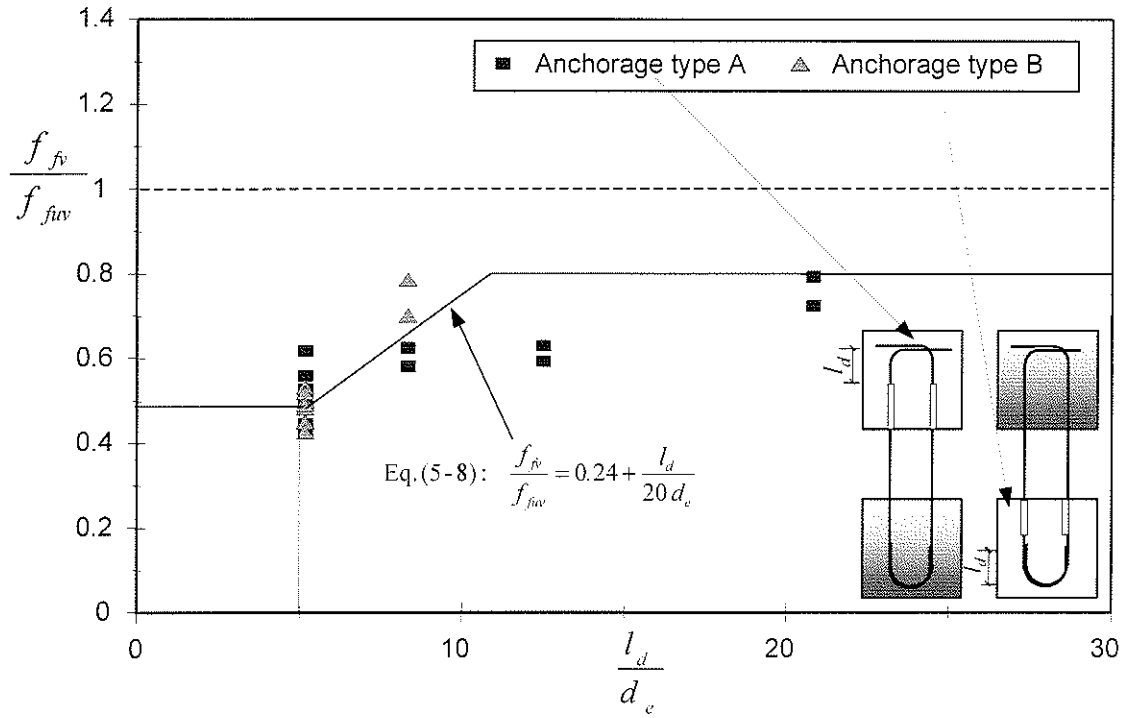


Figure 5-8. Effect of embedment length, l_d on capacity of GFRP C-BAR™ stirrups

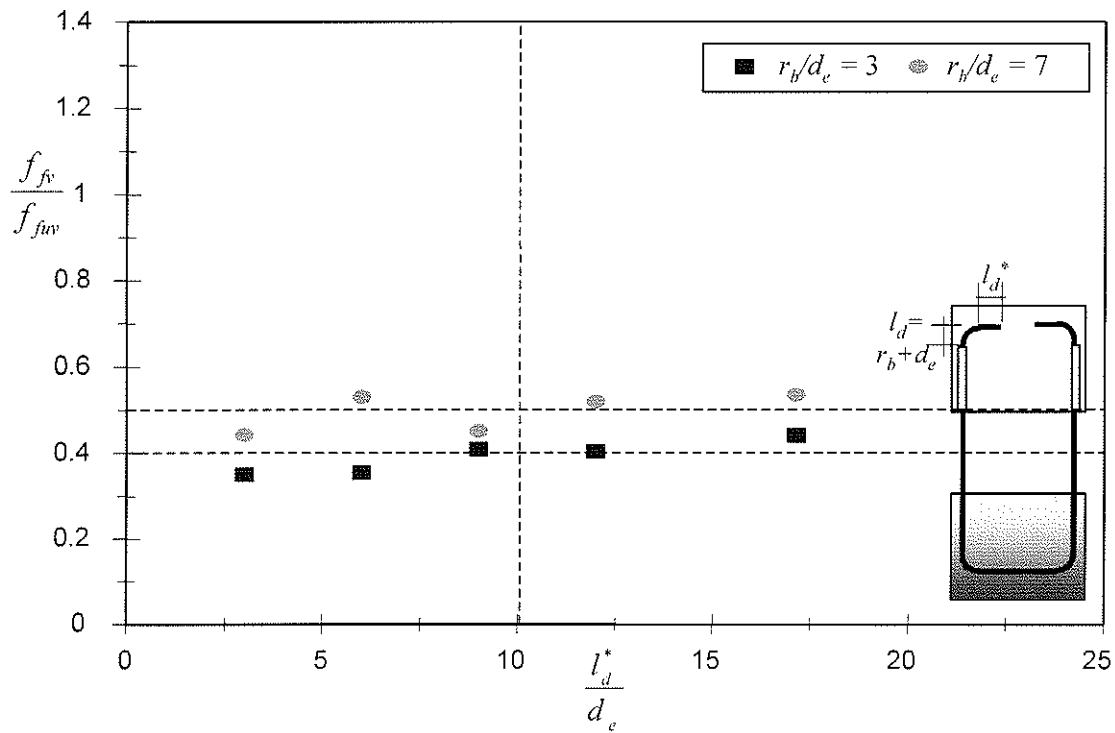


Figure 5-9. Effect of tail length, l_d^* , on bend capacity of CFRP Leadline stirrups

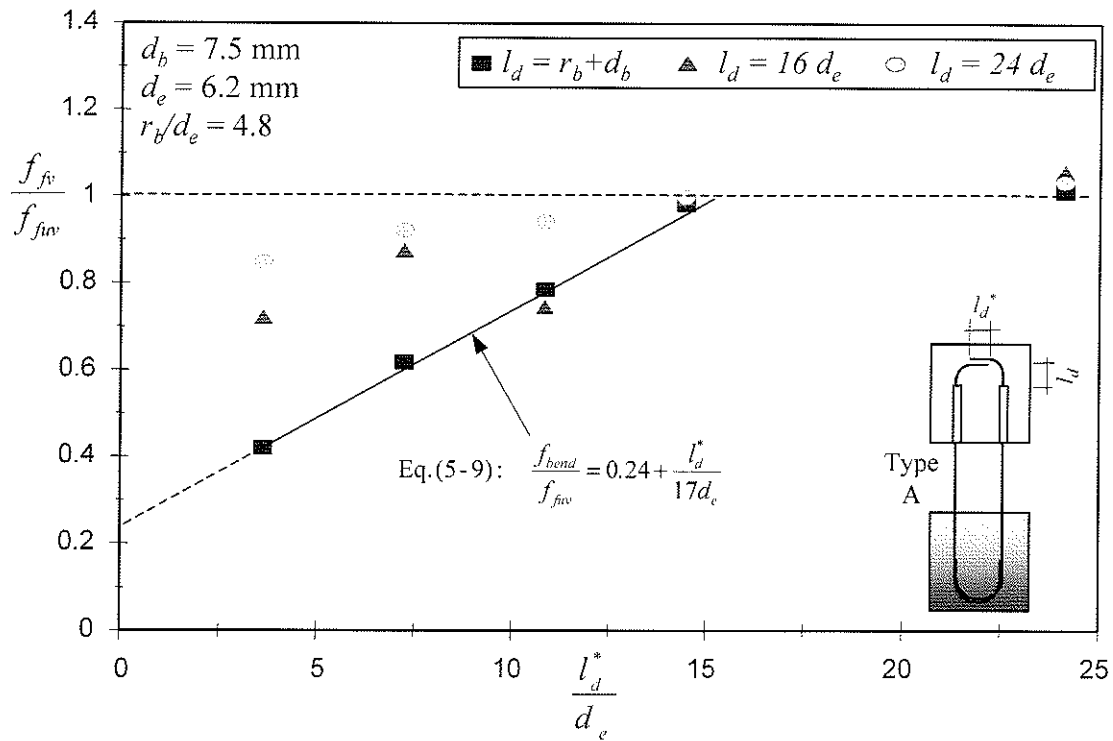


Figure 5-10. Effect of tail length l_d^* on capacity of CFRP CFCC stirrups

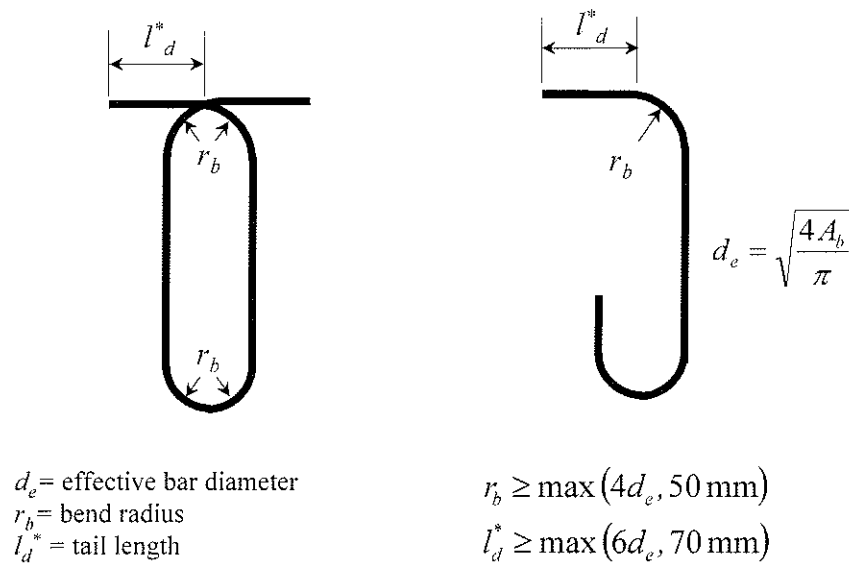


Figure 5-11. Detailing of FRP stirrups

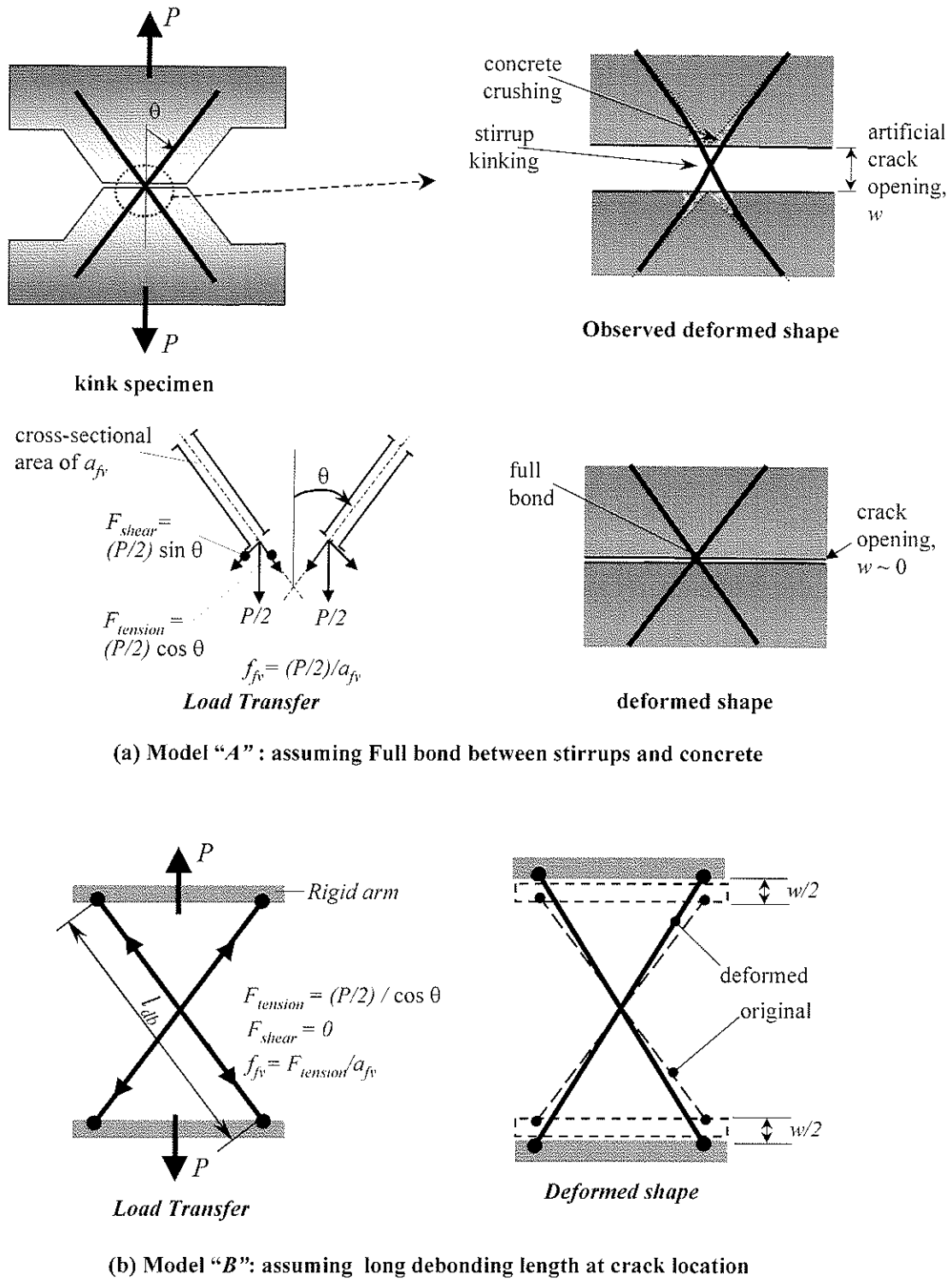
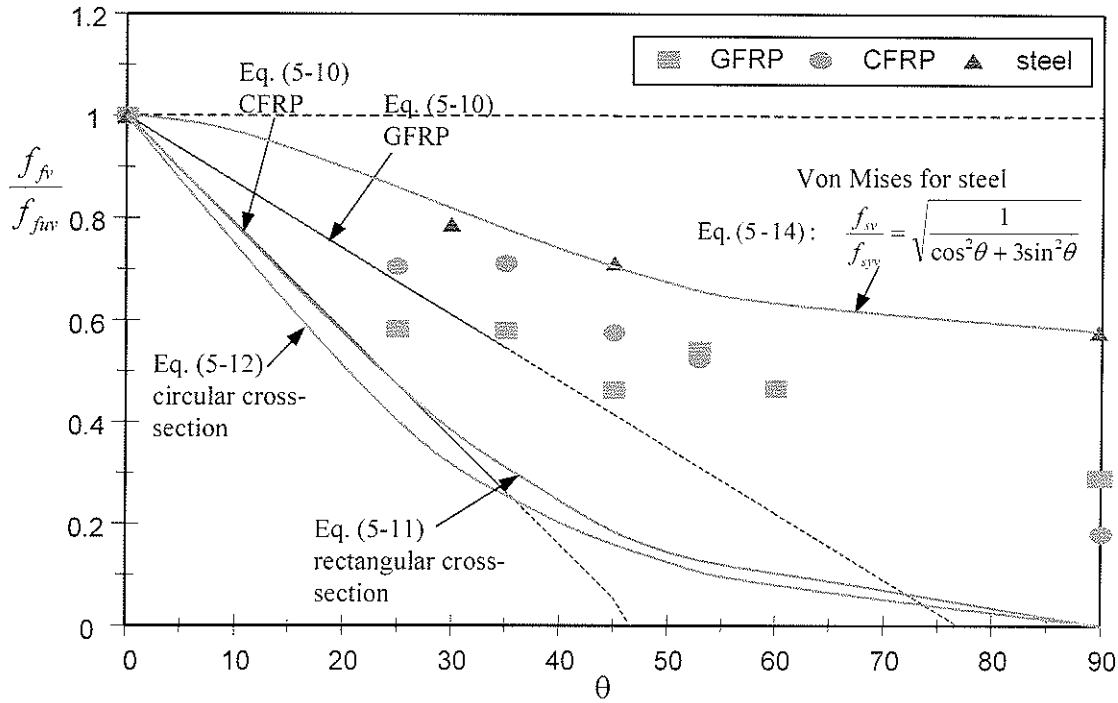
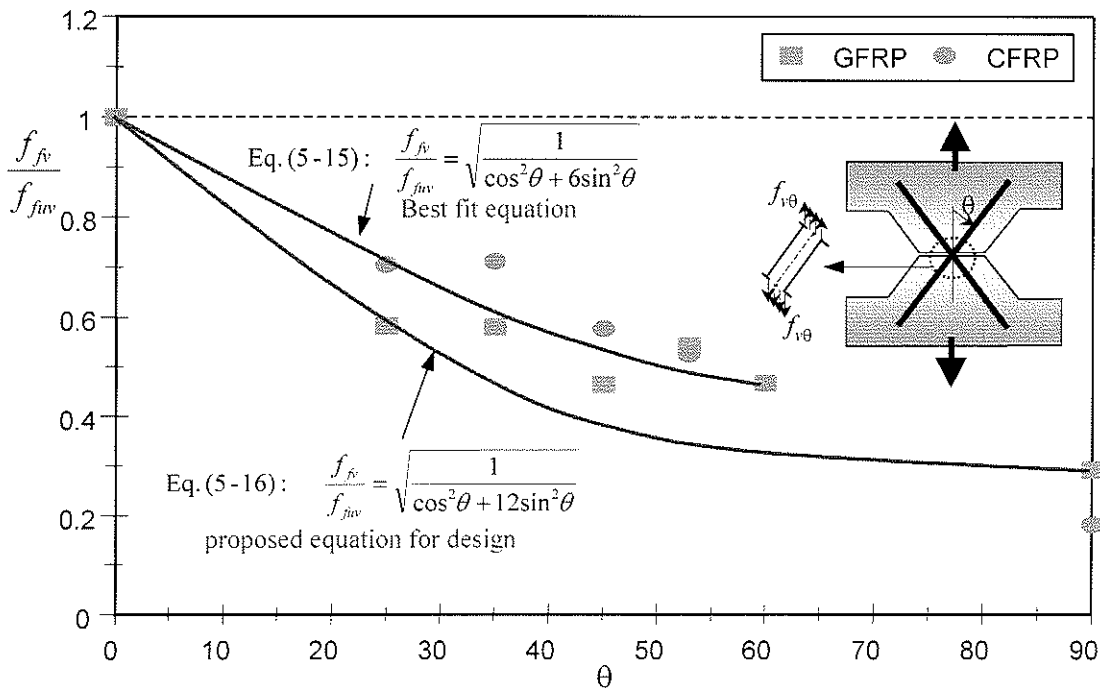


Figure 5-12. Kink specimens - Modelling of load transfer

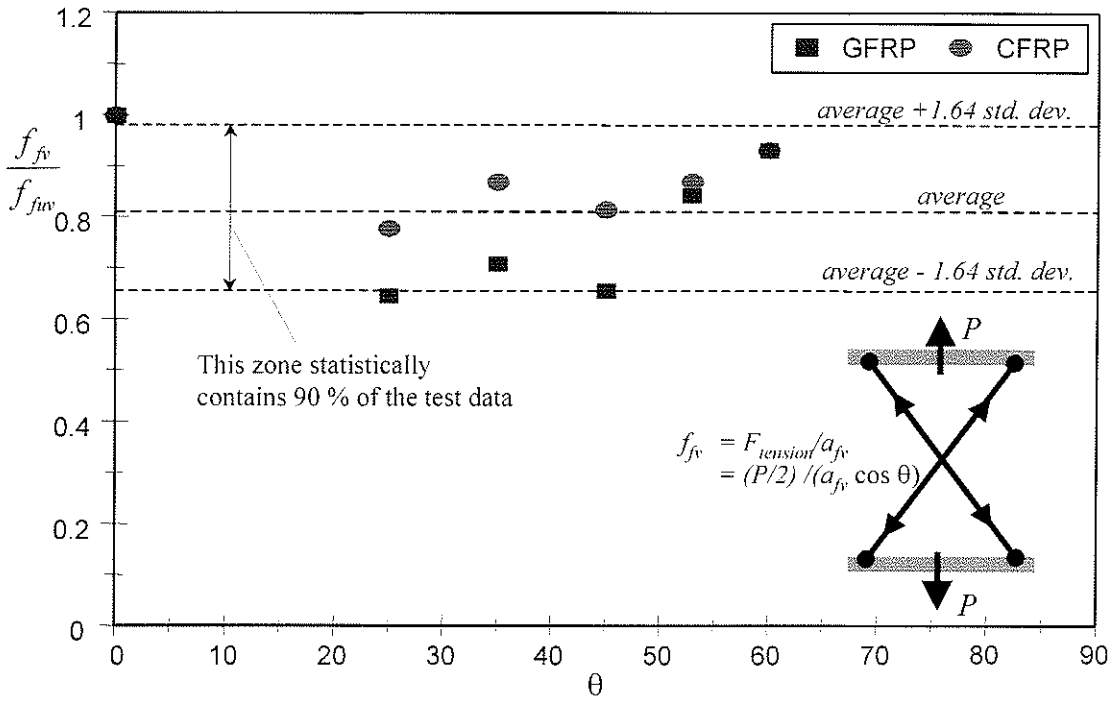


(a) Test results versus available equations in the literature

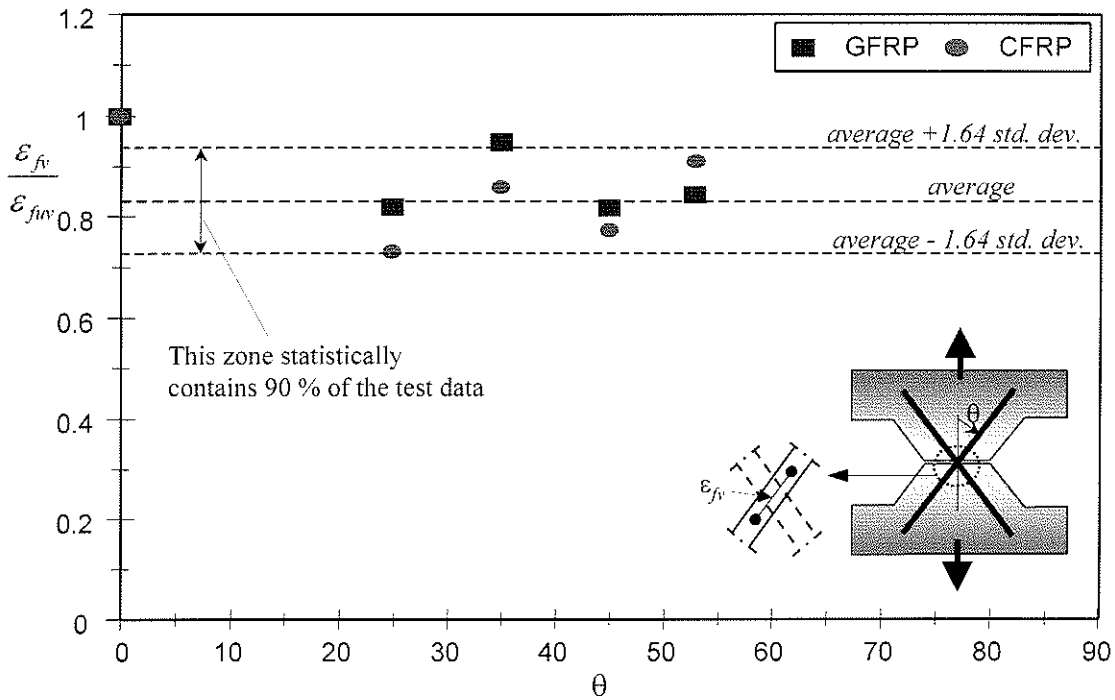


(b) Test results versus proposed equations

Figure 5-13. Effect of stirrup angle θ on capacity of FRP stirrups subject to combined shear and tension - Model "A"



(a) Stress in FRP stirrups at failure based on Model "B"



(b) Observed strain in FRP stirrups at failure, ϵ_{fv}

Figure 5-14. Effect of stirrup angle, θ , on capacity of FRP stirrups

Chapter

6

Experimental Results and Analysis:

Phase II Beam Specimens¹

6.1 General

The second phase of the experimental program consisted of testing concrete beams reinforced with FRP stirrups to investigate the modes of failure and the shear contribution of the FRP stirrups in beam action mechanism. Ten beam specimens were tested: four beams reinforced with carbon FRP stirrups, four beams reinforced with glass FRP, one reinforced with steel stirrups, and one without shear reinforcement. The variables considered in the second phase were the material type of the stirrups, the material type of the flexural reinforcement, and the stirrup spacing.

This chapter presents the test results for the ten beams tested in the second phase. The behaviour of beams reinforced with FRP stirrups is discussed in terms of shear cracking and failure mode. The measured strains in the FRP stirrups were used to evaluate the stirrup contribution to the shear resisting mechanism. The applied-shear-crack-width and

¹ All equations in chapter 6 use metric units (Newton, mm) unless otherwise specified

load–deflection relationships are also presented for all tested beams. The experimental results are compared to different analytical models used to predict the shear strength and behaviour of the tested beams. The analytical models used to predict the behaviour of the beams include simplified shear design methods and advanced shear theories. The shear design equations specified in the current ACI 318-95 code for concrete members reinforced with steel are used to predict the shear strength of the tested beams. In addition, several equations proposed by Japanese, Canadian and European code committees for concrete members reinforced with FRP and reported in chapter 3 are used. The beams were also analyzed using two well-established shear theories. The shear friction model (SFM) is used to predict the shear strength of beams reinforced with CFRP and GFRP stirrups. The modified compression field theory (MCFT) is used to predict the shear behaviour of beams reinforced with CFRP stirrups. The MCFT is also used to predict the average strain in stirrups and the shear crack width at any load level. Recommendations are given for the analysis of beams reinforced with FRP, using the SFM and the MCFT. Shear crack widths in tested beams are also predicted using equations available in the literature that are presented in chapter 2. The output of the shear models is examined against the results of the experimental program. Based on the findings of this investigation, a simple equation is proposed to predict the shear crack width in concrete beams reinforced with FRP stirrups.

6.2 General behaviour of beam specimens

A total of ten reinforced concrete beams were tested to failure, four beams reinforced with carbon FRP stirrups, four beams reinforced with glass FRP stirrups, one reinforced

with steel stirrups and a control beam without shear reinforcement. The variables considered in the beam specimens were the material type of the stirrups, the material type of the flexural reinforcement, and the stirrup spacing. The beams were reinforced for flexure with either six 15mm 7-wire steel strands or seven 15mm 7-wire CFRP strands. All the tested beams failed in shear before yielding of the steel strands or rupture of the CFRP strands. No slip of the flexural reinforcement was observed during any of the beam tests. Shear failure of the beams reinforced with FRP stirrups initiated either by rupture of the FRP stirrups at the bend (shear-tension failure) or by crushing of the concrete in the shear span (shear-compression failure). Failure of the control beam SS-2 occurred due to yielding of the steel stirrups.

A summary of the beam test results is presented in Table 6-1. The shear force at flexural cracking, the shear cracking load, the angle of the shear crack that caused the failure, the ultimate shear strength, the maximum stirrup strain at failure, the average stirrup strain at failure and the mode of failure, are given in Table 6-1 for each tested beam.

6.2.1 Shear cracking load

At the early stage of loading, flexural cracks were observed in the region of constant moment at different load levels, as given in Table 6-1. With a further increase in load, additional flexural cracks were formed in the shear spans between the applied load and the support. The shear cracking load was determined based on the following instrumentation data, in addition to the visual observation of cracks:

1. The strains in the stirrups measured by means of the strain gauges attached to the stirrups in the critical shear zone, as shown in Figures 4-15(a) to 4-17(a). A typical

relationship between the applied shear and the strains in FRP stirrups is given in Figure 6-1 for beam SC-4 reinforced with CFRP stirrups.

2. The concrete strains along the web by means of PI gauges G5 through G13, shown in Figure 4-15(b). A typical relationship between the applied shear and the average strains measured by PI gauges is given in Figure 6-2 for beam SC-4 reinforced with CFRP stirrups.
3. The top surface strain of the concrete within the shear span measured by means of the PI gauges G1 and G3, as shown in Figure 4-15(b). A typical relationship between the applied shear and the concrete strain within the shear span is given in Figure 6-3 for beam SC-4. The observed change in concrete strain from compression to tension is attributed to the shear carrying mechanism that varies during the different stages of the loading history, as illustrated in Figure 6-3.

The angle of shear crack reported in Table 6-1 was determined as the angle at which the shear crack intersects the mid-height of the shear depth jd . After shear cracking, the behaviour of the beams was influenced by the shear reinforcement. The behaviour of each beam is summarized in the following sections.

6.2.2 Beams reinforced with steel strands for flexure

6.2.2.1 Control beams

Two control beams reinforced with six 15-mm steel strands for flexure were tested: beam SN-0 without shear reinforcement and beam SS-2 with 6.35-mm-diameter steel

stirrups spaced at $d/2$ in the two shear spans. Only one shear span was instrumented using PI-gauges and electrical strain gauges to monitor the shear cracking behaviour and the strain in the steel stirrups. The shear cracking patterns for beams SN-0 and SS-2 are shown in Figures 6-4 and 6-6, respectively, while Figures 6-5 and 6-7 show the two beams at failure.

Only one major shear crack was observed in SN-0, as shown in Figure 6-4. With a further increase in load, the shear crack width increased dramatically until it reached a value of 8 mm prior to failure. From a serviceability point of view, the shear force, V_{cr} , at the initiation of the first shear crack is always considered as the shear capacity of a concrete beam without shear reinforcement. After shear cracking, the load was transmitted in the shear span by means of the shear resistance of the concrete in the compression zone, V_{cs} , and the dowel resistance of the longitudinal reinforcement, V_{dl} . The beam failed in a diagonal tension mode, as shown in Figure 6-5. Shear failure occurred within the instrumented shear span.

With a further increase in load after flexural cracking, several shear cracks occurred within the shear span in beam SS-2 and propagated diagonally towards the loading point. Beam SS-2 had five shear cracks in the shear span at the crack stabilization stage, as shown in Figure 6-6. Failure of beam SS-2 initiated by yielding of one steel stirrup intersecting with the shear crack, followed by yielding of another stirrup. With a further increase in the load, excessive shear deformation and crack width were observed as the steel stirrups experienced strain hardening. Finally, failure of the beam occurred by rupture of one steel stirrup at a high strain level, followed by rupture of another stirrup

and crushing of the concrete at the tip of the shear crack, as shown in Figure 6-7. Shear failure of the beam occurred in the non-instrumented shear span.

6.2.2.2 Beams reinforced with CFRP stirrups

Three beams reinforced with 10x5-mm CFRP stirrups for shear and six 15-mm steel strands for flexure were tested: beam SC-2 with CFRP stirrups spaced at $d/2$, beam SC-3 with CFRP stirrups spaced at $d/3$, and beam SC-4 with CFRP stirrups spaced at $d/4$. Only one shear span was reinforced with FRP stirrups. The shear cracking patterns for beams SC-2, SC-3 and SC-4 are shown in Figures 6-8, 6-10 and 6-12, respectively; while Figures 6-9, 6-11 and 6-13 show the three beams at failure.

Beams SC-2, SC-3 and SC-4 had three, four and four shear cracks, respectively, in the FRP reinforced shear span at the crack stabilization stage, as shown in Figures 6-8, 6-10 and 6-12. Failure of the three beams initiated by rupture of one CFRP stirrup at the bend, followed by failure of other stirrups at their anchorage at the bottom reinforcement and crushing of the concrete at the tip of the shear crack, as shown in Figures 6-9, 6-11 and 6-13. Rupture of the CFRP stirrup occurred at the bend zone away from its intersection with the shear crack. Loss of bond between the inner fibre core and the outer resin coating was observed in the stirrup that failed by rupture, as shown in Figure 6-9. Bond loss was also observed in the bend specimens, as mentioned in section 5.2.1.1. Failure of the three beams occurred in a fraction of a second after the rupture of the CFRP stirrup at the bend zone, as observed by video recording of the instant of failure.

6.2.2.3 Beams reinforced with GFRP stirrups

Three beams reinforced with 12-mm-diameter GFRP stirrups for shear and six 15-mm steel strands for flexure were tested: beam SG-2 with GFRP stirrups spaced at $d/2$, beam SG-3 with GFRP stirrups spaced at $d/3$, and beam SG-4 with GFRP stirrups spaced at $d/4$. Only one shear span was reinforced with FRP stirrups. The shear cracking patterns for beams SG-2, SG-3 and SG-4 are shown in Figures 6-14, 6-16 and 6-18, respectively; while Figures 6-15, 6-17 and 6-19 show the three beams at failure.

Beams SG-2, SG-3 and SG-4 had three, five and five shear cracks, respectively, in the FRP reinforced shear span at the crack stabilization stage, as shown in Figures 6-14, 6-16 and 6-18. Failure of beam SG-2 initiated by rupture of one GFRP stirrup at the bend, followed by failure of another stirrup at its anchorage at the bottom reinforcement and crushing of the concrete at the tip of the shear crack, as shown in Figure 6-15. Rupture of the GFRP stirrup occurred at the bend zone away from its intersection with the shear crack. Failure of beams SG-3 and SG-4 initiated by the propagation of the shear cracks diagonally towards the load, therefore reducing the depth of the compression zone. The decrease in the depth of the compression zone coupled with the relatively low-strength concrete caused the concrete under the loading point and in the web to crush before rupture of the GFRP stirrups, as shown in Figures 6-17 and 6-19. This type of failure was less brittle than the shear failure that occurred due to rupture of the FRP stirrups, as observed in beams SC-2, SC-3, SC-4 and SG-2. As given in Table 6-1, beams SG-3 and SG-4 had similar ultimate shear strength despite the variation in stirrup spacing. The maximum shear force, V_{test} , carried by both beams SG-3 and SG-4 was about 312 kN. As the load was applied using stroke control and with a further increase in the stroke, the

applied load started to decrease and finally the beams failed at a shear of about 290 kN. The reduction in the load with further increase in the deformation may be attributed to concrete softening prior to failure by crushing. Examination of the beam after failure showed that the GFRP stirrups were intact and supporting the crushed concrete in the web.

6.2.3 Beams reinforced with CFRP strands for flexure

6.2.3.1 Beam reinforced with CFRP stirrups

Beam CC-3 was reinforced with seven 15-mm CFRP strands for flexure and had 10x5-mm CFRP Leadline stirrups spaced at $d/3$ in one of the shear spans and closely spaced steel stirrups in the other shear span. The beam had four shear cracks in the FRP reinforced shear span at the crack stabilization stage, as shown in Figure 6-20. Shear cracks in beam CC-3 were deeper than in case of beams reinforced with steel strands, and propagated towards mid-depth of the flange, as shown in Figure 6-20. Failure of beam CC-3 initiated by rupture of one CFRP stirrup at the bend, followed by failure of two stirrups at their anchorage at the bottom reinforcement and crushing of the concrete at the tip of the shear crack, as shown in Figure 6-21. Similar to beam SC-3 reinforced with steel strands for flexure, rupture of the CFRP stirrup occurred at the bend zone away from its intersection with the shear crack. Loss of bond between the inner fibre core and the resin coating was also observed in the stirrup failed by rupture. After failure, the CFRP strands held the two pieces of the beam, as shown in Figure 6-21.

6.2.3.2 Beam reinforced with GFRP stirrups

Beam CG-3 was reinforced with seven 15-mm CFRP strands for flexure and had 12-mm GFRP C-BAR stirrups spaced at $d/3$ in one of the shear spans and closely spaced steel stirrups in the other shear span. The beam had five shear cracks in the FRP reinforced shear span at the crack stabilization stage, as shown in Figure 6-22. Shear cracks in beam CG-3 were deeper than in case of beams reinforced with steel strands, and propagated towards the mid-depth of the flange, as shown in Figure 6-22. Failure of beam CG-3 initiated by rupture of one CFRP stirrup at the bend, followed by failure of two stirrups at their anchorage at the bottom reinforcement and crushing of the concrete at the tip of the shear crack, as shown in Figure 6-23. Rupture of the GFRP stirrup occurred at the bend zone away from its intersection with the shear crack. After failure, the CFRP strands held the two pieces of the beam, as shown in Figure 6-23.

6.2.4 Load–deflection characteristics

Figures 6-24(a) and 6-24(b) show the applied load versus deflection measured at midspan and at the loading point, respectively. The load–deflection relationship was greatly affected by the presence of the shear reinforcement. It can be seen in Figure 6-24(a) that the beam with no shear reinforcement showed higher deflection than other beams at the same load level. The presence of shear reinforcement in the shear span reduced the midspan deflection due to partial restraining of the shear deformation. However, the variation of the stirrup material and spacing did not significantly affect the load–deflection characteristics, as shown in Figures 6-24(a) and 6-24(b). This is attributed to the fact that the tested beams had a span-to-depth ratio of 10.6 and therefore the flexural

deformations were the dominant component of the beam deflection. Despite the fact that all beams had the same amount of flexural reinforcement, there is a difference in behaviour between beams reinforced with steel strands and beams reinforced with CFRP strands (Figure 6-24b). This is attributed to the relatively lower elastic modulus of the CFRP strands in comparison to steel strands.

6.3 Failure modes

As intended, all the tested beams failed in shear. In general, the observed mode of failure was either shear–tension or shear–compression.

Shear–tension failure occurred due to rupture of the FRP stirrups at the bend or yielding of the steel stirrups. The shear–rupture failure initiated by rupture of one FRP stirrup at the bend zone. After rupture of one stirrup, the remaining components of the carrying mechanism could not resist the applied shear force and, consequently, the beam failed in shear. The other FRP stirrups contributing to resisting the applied shear were fractured at their anchorage to the bottom reinforcement, as shown in Figures 6-11 and 6-13. The shear–rupture mode was a sudden and brittle type of failure. The beam with steel stirrups had a shear–yield mode. The concrete compressive strength of the beams that had a shear–tension failure ranged from 51 to 54 MPa.

Shear–compression failure occurred due to crushing of the concrete under the loading point and in the web, as shown in Figures 6-17 and 6-19. The concrete compressive strength of the beams that had a shear–compression failure was 33 MPa. The failure initiated by extension of the shear cracks towards the loading point, thereby reducing the depth of the compression zone. Based on the shear–crack-width relationship, the load–

deflection relationship and the visual inspection of the beams, concrete softening was believed to occur prior to failure. The shear-compression mode was a less brittle type of failure. The same ultimate load was observed for beams SG-3 and SG-4 that failed in shear-compression, despite the different stirrup spacing. Concrete softening was also observed prior to failure in the shear span reinforced with closely spaced steel stirrups. However, the relatively low stiffness of the FRP stirrups and therefore higher shear crack widths and depths caused the failure to occur in the shear span with FRP stirrups.

6.4 Contribution of FRP stirrups

The contribution of the FRP stirrups to the shear resisting mechanism in concrete beams was evaluated based on each of the following:

- a- Strain measurement of the FRP stirrups based on the readings of the electric strain gauges
- b- Stirrup effectiveness, based on the gain in the shear strength of a beam with FRP stirrups as compared with a similar beam without shear reinforcement

6.4.1 Strain in FRP stirrups

The strains in the FRP stirrups located within a distance of one-half the shear span, $a/2$, were measured up to failure using electric strain gauges as described in chapter 4. The average strains of the FRP stirrups in each beam were determined based on the strain gauge readings. The maximum strain in the stirrups observed at the ultimate load is given in Table 6-1 for tested beams. The maximum strain in the stirrups was always less

than the ultimate strain capacity parallel to the fibres, ε_{fv} . The average strain in the stirrups at the ultimate load, ε_{fv} (or ε_{sv}), based on the readings of all the strain gauges is also given in Table 6-1. For beams that failed in the shear–tension mode, the average stirrup strain at ultimate, ε_{fv} , was higher than the ultimate strain based on the bend capacity, ε_{bend} (Table 6-1), except for beam SC-4 with closely spaced CFRP stirrups. For beams that failed in the shear–compression mode, the average stirrup strain at ultimate, ε_{fv} , was less than the ultimate strain based on the bend capacity, ε_{bend} , as the FRP stirrups did not fail by rupture and therefore were not fully utilized in these beams.

The shear versus average strain in stirrups for the beams reinforced with CFRP stirrups are shown in Figure 6-25. The shear versus average strain in stirrups for the beams reinforced with GFRP stirrups are shown in Figure 6-26. It is evident from Figures 6-25 and 6-26 that an increase in the shear reinforcement ratio resulted in reduction in the average strain in FRP stirrups at the same load level. To investigate the effect of the low elastic modulus of FRP stirrups on the stirrup strain, Figure 6-27 shows the shear reinforcement ratio multiplied by the elastic modulus ratio, $\rho_{fv} \frac{E_{fv}}{E_s}$, versus the average strain in the stirrups at an applied shear of 175 kN. A shear level of 175 kN was selected to ensure that the shear cracks were stabilized in all beams and the maximum strain in steel stirrups did not exceed the yield strain. The broken lines in Figure 6-27 present the trend of beams reinforced with CFRP and GFRP stirrups. By extending the lines in Figure 6-27 towards a shear reinforcement ratio of 0.40, it can be seen that a beam reinforced with CFRP or GFRP stirrups with $\rho_{fv} \frac{E_{fv}}{E_s} = \rho_{sv} = 0.4$ shows less stirrup strain than observed in the beam reinforced with steel stirrups. Therefore, it can be

concluded that the stirrup strain is not directly proportional to the modular ratio, E_{fv}/E_s , and is influenced by other factors such as bond characteristics of the FRP stirrups.

The effect of flexural reinforcement on the average strain in FRP stirrups is shown in Figure 6-28(a) and 6-28(b) for beams reinforced with CFRP and GFRP stirrups, respectively. Figure 6-28(a) shows that the use of CFRP strands for flexure did not have significant effect on the strains in the FRP stirrups. It should be noted that the behaviour of the beams reinforced with GFRP stirrups (Figure 6-28b) is affected not only by the CFRP longitudinal reinforcement but also by the variation in the concrete strength, f_c' . A detailed discussion of the effect of shear reinforcement and flexural reinforcement on shear cracking and deformations is given in section 6.5.

The average strain in the stirrups was used to determine the contribution of the stirrups to the shear carrying capacity, based on the stress–strain relationship of the FRP material. The contribution of the FRP stirrups to the shear resisting mechanism can be determined based on the stirrup strain as follows:

$$V_{sf} = n_{fv} A_{fv} \varepsilon_v E_{fv} \quad (6-1)$$

where n_{fv} is the number of FRP stirrups intersecting the shear crack that caused the failure. It was observed in the experimental program that for beams with stirrups spaced at $d/2$, $d/3$ and $d/4$, the corresponding number of stirrups intersecting the shear crack was 2, 3 and 4; respectively. This observation agrees with the 45-deg truss model, where $n_{fv}s = d \tan \theta = d$. Equation (6-1) can be rewritten in the following format:

$$V_{sf} = \frac{A_{fv}}{b_w s} \varepsilon_{fv} E_{fv} b_w (n_{fv} s) = (\rho_{fv} f_{fv}) b_w d \quad (6-2)$$

where f_{fv} is the stress in the stirrups corresponding to a strain of ε_{fv} and is determined according to the stress–strain relationship of the stirrup material and ρ_{fv} is the shear reinforcement ratio for the beam under consideration ($\rho_{fv} = A_{fv}/b.s$). The stress index, $\rho_{fv}f_{fv}$, given in equation (6-2) is plotted versus stirrup strain in Figure 6-29 for each beam to characterize the capability of the stirrups to resist shear in beam action. The $\rho_{fv}f_{fv}$ versus stirrup strain relationships for the beams reinforced with FRP stirrups spaced at $d/2$, $d/3$ and $d/4$ are shown in Figures 6-29(a), 6-29(b) and 6-29(c), respectively. The solid lines in Figure 6-29 end at the bend capacity of the FRP stirrups, f_{bend} , while the broken lines extend to the guaranteed tensile strength of the FRP parallel to the fibres, f_{fv} . The $\rho_{sv}f_{sv}$ versus stirrup strain relationship for the control beam reinforced with steel stirrups spaced at $d/2$ is also shown in Figure 6-29.

As a consequence, the stirrup contribution V_{sf} can be determined based on the average stirrup strain and the mechanical and geometric properties of the stirrups using the concept of smeared reinforcement in the concrete beam. Therefore, the stirrup contribution can be computed as follows:

1. The characteristic stress $\rho_{fv}f_{fv}$ can be determined from Figure 6-29 at any load level, based on the corresponding stirrup strain given from Figures 6-25, 6-26 and 6-28.
2. Applying the characteristic stress $\rho_{fv}f_{fv}$ to equation (6-2), the contribution of the stirrups to the shear resisting mechanism can be evaluated.

The relationships between the applied shear and the components of the shear resisting mechanism V_c and V_{sf} are presented in Figures 6-30, 6-31 and 6-32 for the beams reinforced with steel strands and with stirrups spaced at $d/2$, $d/3$ and $d/4$, respectively.

The relationships between the applied shear and the components of the shear resisting mechanism V_{cf} and V_{sf} are presented in Figures 6-33(a) and 6-33(b) for the beams reinforced with CFRP strands and with CFRP and GFRP stirrups, respectively.

It can be seen in Figures 6-30, 6-31 and 6-32 that for the beams reinforced with steel strands, the concrete contribution component, V_c , at any load level was higher than or equal to the shear force at the initiation of the first shear crack, V_{cr} . In addition, the concrete contribution component, V_c , at failure was always higher than the shear force at the initiation of the first shear crack, V_{cr} . Therefore, it can be concluded that the inclusion of the FRP stirrups in concrete beams contributes to the shear carrying capacity in two different ways:

1. Creating the stirrup contribution component V_{sf}
2. Enhancing the concrete contribution component V_c by:
 - a- controlling the shear cracks and thereby improving the shear resisted by aggregate interlock, V_{av} ; and
 - b- preventing the splitting of the concrete at the longitudinal reinforcement level, thereby improving the shear resisted by the dowel action, V_{dl}

For the beams reinforced with CFRP strands for flexure, Figures 6-33(a) and 6-33(b) show that the concrete contribution, V_{cf} , at any load level up to failure was less than the concrete contribution, V_c , for the corresponding beams reinforced with steel strands. This behaviour indicates that the use of FRP flexural reinforcement in concrete beams results in wider cracks, smaller depth of the compression zone and less dowel contribution, leading to reduction in the concrete contribution to the shear carrying mechanism, V_{cf} .

6.4.2 Effectiveness of FRP stirrups

The shear capacity of a concrete beam without shear reinforcement, V_{cr} , is always measured as the applied load which causes the initiation of the first shear crack. After this stage, the shear crack width increases dramatically. The contribution of the FRP stirrups to the shear carrying capacity of concrete beams was evaluated based on the difference between the measured shear strength, V_{test} , and the measured shear at the initiation of the first crack, V_{cr} . The term “ $V_{test}-V_{cr}$ ” also includes the stirrup effectiveness in enhancing the concrete contribution to the shear carrying capacity. Based on the traditional 45-degree truss model, and as observed in the beams tested in this experimental program, the effective stirrup capacity at failure, f_{fve} , can be determined as follows:

$$f_{fve} = \frac{(V_{test} - V_{cr})s}{A_{fv} d} \quad (6-3)$$

where A_{fv} is the area of the FRP stirrups, s is the stirrup spacing, and d is the effective beam depth. Figure 6-34 shows the effective stress in FRP stirrups at failure for the different spacing values, s , used in this study. Test results indicate that the effective capacity of FRP stirrups in beam action might be as low as 50 percent of the strength parallel to the fibres, provided that shear failure occurs due to rupture of the FRP stirrups. For closely spaced stirrups, there is a higher chance for the diagonal cracks to intersect the bend zone of the stirrups, leading to a lower contribution of the FRP stirrups, as evident from Figure 6-34. For beams reinforced with CFRP strands for flexure, the effective stirrup stress is less than the corresponding beam reinforced with steel strands. This can be attributed to the observed low values of the concrete contribution, V_{cf} , in comparison to the concrete contribution, $V_c (=V_{cr})$, in equation (6-3). The effect of FRP

longitudinal reinforcement on the concrete contribution, V_{cf} , is discussed in detail in chapter 7.

6.5 Shear cracking

Shear cracking behaviour of the beams was examined within the shear span. In general, the stirrups act as crack initiators for most of the flexural cracks that are first initiated in the shear span. With a further increase in load, the flexural cracks propagate diagonally with a varying angle towards the loading point. The characteristics of the shear crack width and distribution as influenced by the type of the shear reinforcement are discussed in the following sections.

6.5.1 Crack pattern

In general, shear cracks are characterized by irregular distribution as compared to flexural cracks in the constant moment zone. Shear cracking irregularity is attributed to the minor cracks that link the major shear cracks, as shown in Figures 6-6, 6-8, 6-10, ... etc. In the current study, shear cracks were identified as the cracks that run continuously from the tension side to the compression flange of the beam. It was observed that shear cracks initiated with a steep angle at the tension side of the beam and approached the compression flange at a flat angle.

Examination of shear cracking of the tested beams showed that:

1. The angle of the shear cracks in the beams with stirrups ranged between 42 and 46 degrees, as given in Table 6-1. This range of shear crack angles is typical for

reinforced concrete beams. The material type and spacing of the stirrups did not affect the shear crack angle. However, they affected the crack pattern and the crack width, as discussed in the following sections.

2. *The control beam* reinforced with steel stirrups had uniform crack distribution. This is attributed to the good bond characteristics of steel stirrups.
3. *Beams with CFRP Leadline stirrups* had non-uniform crack distribution and the lowest number of shear cracks among the tested beams. This is attributed to the poor bond characteristics of Leadline bars, as was also observed in the bend tests of Leadline stirrups. It was observed that the beams with small stirrup spacing show better distribution of shear cracks.
4. *Beams with C-BAR stirrups* had a uniform distribution of shear cracks. This is attributed to the fact that the bond characteristics of the GFRP reinforcing bars are better than those of the steel rebars, as reported by Rizkalla *et al.* (1997).
5. *Beams reinforced with CFRP strands for flexure* (Figures 6-20 and 6-22) had similar distribution and number of shear cracks at crack stabilization, compared to the corresponding beams reinforced with steel strands (Figures 6-10 and 6-16). However, the shear cracks were longer and extended to the flange in beams reinforced with CFRP strands for flexure, as shown in Figures 6-20 and 6-22. This is attributed to the relatively low elastic modulus of the CFRP strands in comparison to that of the steel strands.

6.5.2 Crack width

The monitoring data of the PI gauges mounted on the web were used to calculate the width of the shear cracks passing through PI-gauge stations and the slide displacement along the shear cracks, as illustrated in Figure 6-35. For a typical PI-gauge station and considering the PI gauges in diagonal and vertical directions, the summation of shear crack widths Σw and the slide displacement along the cracks can be determined as follows:

$$\begin{aligned}\Sigma w &= (\sqrt{2}\Delta_D - \Delta_V - 0.5l_g\varepsilon_{ct})\sin\theta + (\Delta_V - 0.5l_g\varepsilon_{ct})\cos\theta \\ \text{slide} &= (\sqrt{2}\Delta_D - \Delta_V - 0.5l_g\varepsilon_{ct})\cos\theta - (\Delta_V - 0.5l_g\varepsilon_{ct})\sin\theta\end{aligned}\quad (6-4)$$

where θ is the measured crack angle to the horizontal axis of the beam, l_g is the gauge length ($l = 200$ mm), ε_{ct} is maximum tensile strain of concrete ($\varepsilon_{ct} = 0.1 \times 10^{-3}$), and $\Delta_H, \Delta_V, \Delta_D$ are the displacements measured by the PI gauges, as described in Figure 6-35. Similar equations can be used to determine the shear crack width by considering either Δ_D and Δ_H or Δ_V and Δ_H . All beams had three or four PI-gauge stations in the shear critical zone, as shown in Figures 4-14 through 4-17. The summation of the shear crack widths, Σw , was determined using equation (6-4) for all the PI-gauge stations mounted on the web in the shear critical zone. The shear crack width per crack, w , was determined based on the number of shear cracks passing within the PI-gauge station. In general, the calculated shear crack width, based on the measurements of the PI-gauge station containing the crack that caused the failure, was the highest among all the PI-gauge stations in the shear span, and therefore was used to characterize the cracking behaviour of the beam.

The shear versus crack width relationships for the beams reinforced with CFRP stirrups are shown in Figure 6-36, compared with the control beams. The shear versus crack width for the beams reinforced with GFRP stirrups are shown in Figure 6-37, compared with the control beams. For beams reinforced with FRP stirrups, it can be seen in Figures 6-36 and 6-37 that low values of crack width were observed for beams with a higher shear reinforcement ratio ρ_{fv} .

The shear crack width at any load level is predicted to be proportional to the elastic modulus and the bond characteristics of the stirrups. As mentioned before, the GFRP stirrups have the lowest elastic modulus and the best bond characteristics in comparison with the steel and CFRP stirrups. For beams reinforced with GFRP stirrups, Figure 6-37 shows that the beam with a shear reinforcement ratio of $\rho_{fv} = 0.71$ percent behaves similarly to the one with a steel shear reinforcement ratio of $\rho_{sv} = 0.40$ percent. This indicates that an increase in the shear reinforcement ratio ρ_{fv} of 80 percent ($= \frac{0.71 - 0.40}{0.40}$) minimizes the effect of the low modular ratio ($E_{fv}/E_s = 41/200 = 0.21$) due to the good bond characteristics of GFRP stirrups. It is shown in Figure 6-36 that the beam with 0.4% steel stirrups falls between the two beams with CFRP stirrups of 0.36% and 0.47%. Therefore, it can be concluded that the beam with CFRP stirrups can have similar behaviour as beams with steel stirrups due to relatively high elastic modulus ratio for CFRP material ($E_{fv}/E_v = 137/200 = 0.69$). For the same stirrup spacing of $d/2$, Figure 6-38 shows the shear versus crack width for three beams reinforced with CFRP, GFRP, and steel stirrups. It can be seen that high values of crack width were observed for the beam with CFRP stirrups, even though the stiffness index $E_{fv}\rho_{fv}$ is higher for this beam than the one reinforced with GFRP stirrups. In general, it can be concluded that the beams

reinforced with GFRP stirrups performed well despite the very low elastic modulus of the GFRP material.

For beams with GFRP stirrups spaced at $d/3$ and $d/4$, the shear crack width remained almost constant at a shear force of 250 kN and up to failure, as shown in Figure 6-37. Similar behaviour was observed by the strains in the GFRP stirrups. It was also observed that the flexural cracks under the loading point became wider at the same load level and up to failure. This is attributed to the fact that the concrete under the loading point and in the web started to soften and absorbed more energy, causing an energy release in the zone of shear cracks.

Figure 6-39(a) and 6-39(b) show the shear versus crack width relationship for beams reinforced with CFRP strands for flexure, compared with the corresponding beams reinforced with steel strands. For beams with CFRP stirrups, Figure 6-39(a) shows that the use of CFRP strands as longitudinal reinforcement in beam CC-3 resulted in an insignificant increase in the shear crack width at the same load level in comparison to beam SC-3 reinforced with steel strands. For beams with GFRP stirrups, the beam CG-3 with CFRP strands resulted in wider shear cracks at low load levels, as shown in Figure 6-39(b). It should be mentioned that there are two factors affecting the shear crack width, the longitudinal reinforcement and the concrete strength, f'_c . While beam CG-3 was reinforced with CFRP strands for flexure and had f'_c of 50 MPa, beam SG-3 was reinforced with steel strands and had f'_c of 33 MPa. Because of the difference in concrete strength, the effect of CFRP longitudinal reinforcement on the cracking behaviour cannot be deduced from Figure 6-39(b).

6.5.3 Crack width versus stirrup strain

It is well established by many researchers (Leonhardt 1979 and Beeby 1979) and many design codes (ACI 318-95, EuroCode-2 and CSA23.3-94) that the crack width in reinforced concrete members is directly proportional to the strain in the reinforcing bars. A typical expression for crack width calculation takes the following form;

$$w = k_1 k_2 (f_s / E_s) \quad (6-5)$$

where f_s is the stress in the steel reinforcing bars, E_s is the elastic modulus of the steel reinforcement, and the coefficients k_1 , k_2 depend on the bond characteristics of reinforcing bars and the concrete cover. Design guidelines for concrete members reinforced with FRP (JSCE 1997, ACI 1998) recommended the use of the original code equations for calculation of crack width in concrete members reinforced with conventional steel. However, a recent investigation by Joh *et al.* (1997) on bond cracking performance of concrete beams reinforced with FRP showed that the use of original code equations overestimates the flexural crack width in concrete beams reinforced with FRP. Joh *et al.* (1997) attributed this observation to the effect of the low elastic modulus of FRP reinforcement on the strain distribution around the crack.

The relationship between the shear crack width and the average strain in stirrups is shown in Figures 6-40 and 6-41 for beams reinforced with CFRP stirrups and for beams reinforced with GFRP stirrups, respectively. As shown in Figures 6-40 and 6-41, there is an insignificant effect of the shear reinforcement ratio and the material type of longitudinal reinforcement on the relationship between the crack width and the stirrup strain. Therefore, the relationship between the crack width and the stirrup strain for CFRP and GFRP stirrups can be expressed by the average curve presented in Figures

6-40 and 6-41, respectively. The average curves in Figures 6-40 and 6-41 are drawn by calculating the average stirrup strain that corresponds to each value of the shear crack width for all beams shown in the figure. The relationship between the shear crack width and the stirrup strain for CFRP and GFRP stirrups is compared in Figure 6-42 to the corresponding relationship for steel stirrups, as observed in beam SS-2. It can be seen in Figure 6-42 that at the same strain level in stirrups, beams reinforced with GFRP stirrups showed a smaller crack width than beams reinforced with steel and CFRP stirrups. It should be mentioned that GFRP stirrups have bond characteristics similar to those of steel stirrups, as indicated by the similar shear crack pattern in beams reinforced with GFRP and steel stirrups. Therefore, it can be concluded that the shear crack width is affected by the low elastic modulus of the GFRP stirrups.

The effect of the elastic modulus on crack width can be explained by considering a concrete block reinforced with either a steel bar or an FRP bar, as shown in Figure 6-43. It is assumed that the steel and FRP bars have the same cross-sectional area, A , and the same bond characteristics. The stress distribution along the reinforcing bar inside the concrete block is shown in Figure 6-43. For the same strain level, ε_s , in the reinforcing bar, the force in the FRP bar is less than that in the steel bar. Therefore, the strain distribution at the crack location is predicted for the FRP bar to be different than that for the steel bar. It can be also shown that the length of lost bond, l_{db} , and the crack width, w ($=\varepsilon_s l_{db}$), in the concrete block reinforced with the FRP bar are smaller than those in the concrete block reinforced with the steel bar, as illustrated in Figure 6-43. This indicates that for the same strain level in reinforcing bars, the crack width in members reinforced

with FRP having a relatively low elastic modulus might be smaller than the crack width in members reinforced with steel.

6.6 Analytical Prediction

Different analytical models were used to predict the shear strength and behaviour of the tested beams. The analytical models used to predict the behaviour of the beams included simplified shear design equations and advanced shear theories. The shear design equations specified in the current ACI 318-95 code for concrete members reinforced with steel were used to predict the shear strength of the tested beams. In addition, design equations proposed by different task committees in Canada, Europe and Japan for concrete members reinforced with FRP and reported in chapter 3, were used. The beams were also analyzed using two well-established shear theories. The shear friction model (SFM) was used to predict the shear strength of beams reinforced with CFRP and GFRP stirrups. The modified compression field theory (MCFT) was used to predict the shear behaviour of beams reinforced with CFRP stirrups. The MCFT was also used to predict the average strain in stirrups and the shear crack width at any load level. Shear crack widths in tested beams were also calculated using equations available in the literature and presented in chapter 2. The output of the shear models was examined against the results of the experimental program. The suitability of the current shear models and theories that were mainly derived for members reinforced with steel, was investigated. Recommendations are given for the analysis of beams reinforced with FRP, using the SFM and the MCFT. In addition, a simple equation is proposed to predict the shear crack width in concrete beams reinforced with FRP stirrups.

6.6.1 Shear models in design codes and guidelines

The shear strengths of the ten tested beams were predicted using shear equations given by the following design codes (or guidelines):

- a- The ACI 318-95 building code for concrete members reinforced with steel: Equations (2-27), (2-28), (2-29), (2-32) and (2-33) were used. The design stress, f_{syw} , used in equation (2-32) for steel stirrups was assumed to be the tensile strength parallel to the fibres, f_{fiw} , for FRP stirrups.
- b- The JSCE recommendation for design and construction of concrete structures using FRP (1997): Equations (3-27), (3-28), (3-29) and (3-31) were used.
- c- The Japanese Building Research Institute (BRI) recommendations for design of concrete structures using FRP (sonobe *et al.* 1997): Equation (3-36) was used. The bend capacity of FRP stirrups used in tested beams, required for equation (3-36), was determined based on the bend tests reported in chapter 5.
- d- The new Canadian Highway Bridge Design Code - Section 16 Fibre-reinforced Structures (CHBDC 1998) : Equations (3-39) and (3-40) along with equation (2-39b) were used.
- e- The European guidelines – Eurocrete Project (Clarke *et al.* 1996): Equations (3-41) and (3-42) were used to modify the shear design equations (2-48) and (2-49) of the British Standard BS8110.

The predicted shear stress, $v_n = V_n / b_w d$, was determined based on the nominal shear strength, V_n , using a value of 1.0 for all material and safety factors ($\phi, \gamma_b, \gamma_m, \dots$). The shear strengths of the control beams SN-0 and SS-2 were predicted using the original

ACI, JSCE, BRI, CHBDC and BS8100 code equations for concrete members reinforced with steel. The code equations for members reinforced with steel are given in chapter 2. The shear stresses, v_n , calculated using the different code models are compared to test results in Figure 6-44. The numerical values shown in Figure 6-44 are given in detail in Table 6-2. It is evident from Figure 6-44 that all code models except the BRI model resulted in a conservative prediction for the control beams SN-0 and SS-2. Although the BRI model resulted in conservative prediction for the shear strength of the control beam reinforced with steel stirrups (SS-2), it overestimated the shear strength of the control beam without shear reinforcement (SN-0). Figure 6-44(a) shows that the current ACI shear model resulted in unsafe prediction for the shear strengths of beams reinforced with FRP stirrups. The JSCE and the CHBDC models greatly underestimated the shear strength of beams reinforced with FRP stirrups (Figures 6-44b and 6-44d), because both models use very low stirrup strain at ultimate in their equations. Due to the fact that the Eurocrete model uses a slightly higher stirrup strain at ultimate, the predicted shear strengths of beams reinforced with FRP stirrups (Figure 6-44e) were less conservative than those of the JSCE and CHBDC models. Also, the BRI model (Figure 6-44c) showed good prediction and less conservative shear strengths when compared to the JSCE and CHBDC, since it uses the experimentally evaluated bend capacity of FRP to limit the stirrup strain at ultimate. To develop a proposal for design equations for the shear strength of concrete beams reinforced with FRP, test results of 126 beams from experimental programs carried out by various researchers, including the beams tested in the current investigation, were used. The selected beams cover a wide range for the parameters affecting the shear strength of concrete beams reinforced with FRP. The

detailed properties of the selected beams are reported in chapter 3. Derivation and reliability assessment of the proposed model are presented in chapter 7.

6.6.2 Shear friction model (SFM)

As described in chapter 2, the SFM is based on the action of shear and longitudinal reinforcement crossing a shear crack plane. Stirrups and longitudinal reinforcement provide a clamping force, thereby increasing the friction force that can be transferred across a crack along a potential failure plane. The procedure and results for the analysis of beams tested in this experimental program using the SFM are presented in the following sections.

6.6.2.1 Analysis procedure

The shear strength of a concrete beam can be determined by considering all possible failure planes between the inside edge of the support plate and the inside edge of the load plate, as shown in Figure 6-45. The plane with the lowest calculated shear resistance value gives the governing shear strength of the beam. According to the SFM, the shear resistance corresponding to a potential failure plane can be determined as follows:

$$\frac{V_n}{C_w} = 0.5k^2 \left[\sqrt{\frac{T}{0.25k^2 C_w} + \cot^2 \theta} - \cot \theta \right] (1 + \cot^2 \theta) - \frac{T}{C_w} \cot \theta + \frac{T_v}{C_w} \leq \frac{7.0}{f'_c} \quad (6-6)$$

where C_w is the limiting force in concrete web based on overall depth h ($C_w = f'_c b_w h$), T is the tensile force in the longitudinal reinforcement corresponding to a shear force of $V=V_n$, θ is the angle of the potential failure plane, k is the shear-friction factor ($k =$

2. $1/f_c^{1-0.4}$), T_v is the ultimate load capacity of stirrups crossing the potential failure plane, b_w is the web width of the beam and h is the overall depth of the beam, as shown in Figure 6-46. As given by equation (6-6), V_u/C_w should not exceed $7.0/f_c'$ to avoid shear failure initiated by crushing of the concrete.

The SFM requires the examination of all possible failure planes between the inside edge of the support plate and the inside edge of the load plate. Selected potential failure planes are shown in Figures 6-45(a) to 6-45(j) for all beams tested in the second experimental phase. The analysis procedure was performed for each potential failure plane, according to the following steps:

1. Determine the angle of the potential failure plane, θ , the characteristic force $C_w = f_c' b_w h$, and the shear-friction factor k . It should be mentioned that the force C_w is determined for the area of the web, $b_w h$, ignoring the effect of the flange of the T-beams tested in this study.
2. Determine the strength capacity of the stirrups corresponding to the potential failure plane. The stress in the stirrups at failure, f_v , is taken as the yield strength, f_{syv} , in the case of steel stirrups and is determined based on the embedment of the bend for FRP stirrups, as described in the following text. As shown in Figure 6-46, the embedment lengths, l_{d1} , l_{d2} , ... etc. are determined based on the intersection of the potential failure plane with the FRP stirrups. The lowest embedment length l_{dmin} , is used to characterize the potential failure plane. The strength capacity of the FRP stirrups, f_{fv} , is determined according to the following equations (6-7) and (6-8) for CFRP and GFRP stirrups, respectively:

$$0.47 \leq \frac{f_{fv}}{f_{syv}} = 0.40 + \frac{l_{dmin}}{70 d_e} \leq 0.8 \quad (6-7)$$

$$0.49 \leq \frac{f_{fv}}{f_{fuv}} = 0.24 + \frac{l_{dmin}}{20 d_e} \leq 0.8 \quad (6-8)$$

Equations (6-7) and (6-8) were proposed based on the experimental results of the bend tests, described in section 5.4. A limitation on the FRP stirrup capacity, f_{fv} , of $0.8 f_{fuv}$ is imposed on equation (6-7) to account for the kink effect at crack intersection as concluded in chapter 5 (section 5.8).

3. The contribution of the stirrups, T_v , is determined as $\Sigma A_v f_v$, where ΣA_v is the total cross-sectional area of the stirrups crossing the potential failure plane, and f_v is the strength capacity of the stirrups as determined in step 2.
4. Determine the tensile force in the longitudinal forces, T , by considering the moment equilibrium at point A for the applied forces (Figure 6-46). Therefore, the tensile force, T , can be determined as a function of V_n using the following equation:

$$T = \frac{x_a}{y_{CT}} V_n - \frac{(x_1 + (x_1 + s) + (x_1 + 2s))}{y_{CT}} A_v f_v \quad (6-9)$$

where x_a , y_{CT} , x_1 and s are defined in Figure 6-46.

5. Apply C_w , k , T , θ and T_v to equation (6-6). The equation can be solved, as indicated in appendix A, to determine shear strength, V_n , corresponding to the potential shear plane.

A numerical example of this analysis procedure is given in Appendix A for beam SC-3. The results of the SFM for the ten tested beams are summarized in Table 6-3. Table 6-3 gives the values for the different parameters for each potential failure plane along with the predicted shear strength, V_n , and the predicted mode of failure. The governing failure plane with the lowest V_n is highlighted in Figures 6-45(a) to 6-45(j) and is indicated in bold-face letters in Table 6-3.

6.6.2.2 Analysis results and discussion

The observed test results for the beam specimens are compared with the results of the SFM in Table 6-3 and Figure 6-47. Figure 6-47 shows the measured-to-predicted shear strength ratio, V_{test}/V_n , for all tested beams. As shown in Figure 6-47, the SFM predicted very well the shear strength of beams reinforced with steel strands for flexure that failed in shear-rupture (or shear-yield) mode. As is evident from Table 6-3 and Figure 6-45, the SFM resulted in a good estimate for the shear crack angle and the number of stirrups intersecting the failure plane.

The SFM predicted the failure of beams with FRP stirrups by rupture of the stirrups at the bend, as indicated by the intersection of the predicted failure planes with the stirrups at the bend location (Figure 6-45). The failure of all analyzed beams reinforced with FRP stirrups was governed by a stirrup stress f_{fv} (column 9 of Table 6-1) equal to the bend capacity that corresponds to a l_d/d_e ratio of 5.0, according to equations (6-7) and (6-8). It was observed in the experimental program that using a small stirrup spacing increases the chance for shear cracks to intersect the bend zone and consequently causes significant reduction of the stirrup capacity in beam action, f_{fve} . Figure 6-48 shows the relationship between the f_{fve}/f_{fv} ratio and the s/d ratio as predicted by the SFM and as observed in the experimental program for beams that failed in a shear-rupture mode. As shown in Figure 6-48, the analytical results of the SFM follow the same trend observed in the experimental program. It can be concluded that the effect of the spacing of FRP stirrups on the shear strength of concrete beams can be captured using the SFM. The SFM, along with the proposed failure criteria of a single FRP stirrup, given by equations (6-7) and

(6-8), can predict extremely well the shear-rupture strength of the concrete beams reinforced with FRP stirrups.

For the two beams that failed in the shear-compression mode, the SFM predicts the failure mode as shear rupture at a higher load level, as indicated in Table 6-3. Equation (6-6) includes a limit for V_n as $7.0C_w/f_c'$ ($\equiv 7.0b_w h$) to avoid the shear-compression mode. However, this limit results in even higher shear strength for the beams, as given for potential failure plane no. 1 of beams SG-3 and SG-4 in Table 6-3. The corresponding limits in the ACI 318-95 code, CSA23.3-94 and BS8110-85 are $0.833\sqrt{f_c'}b_w d$, $\sqrt{f_c'}b_w d$, and $5.0b_w d$, respectively. The ultimate shear strengths as determined by these codes for beam SG-3 range from 57 to 69 percent of that predicted by the SFM. Therefore, the upper limit of the SFM provided by equation (6-6) does not provide a conservative prediction when compared to current code limits and requires further research.

For beams reinforced with CFRP strands for flexure, the SFM underestimated the shear strength of the two tested beams, as shown in Figure 6-49. This may be attributed to the effect of the low elastic modulus of the CFRP reinforcement on the shear-friction characteristics, represented by the factor k ($2.1f_c'^{-0.4}$). To account for the effect of the low elastic modulus of FRP reinforcement, a modification for the shear-friction factor, k , is proposed as follows:

$$k = 2.1f_c'^{-0.4} \left(\frac{E_{fl}}{E_s} \right)^{1.3} \quad (6-10)$$

where E_{fl} is the elastic modulus of the FRP longitudinal reinforcement and E_s is the elastic modulus of steel ($E_s = 200$ GPa). The use of proposed equation (6-10) in the SFM resulted in a good prediction for the two beams reinforced with CFRP strands, as shown

in Table 6-3 and Figure 6-49. However, extensive research is needed to investigate the shear-friction behaviour in concrete members reinforced with FRP as main reinforcement and to establish a more generalized relationship between the shear-friction factor, k , and E_f for different types of FRP reinforcement.

Finally, it can be concluded that the use of proposed equations (6-7) and (6-8) as a failure criterion for FRP stirrups in the SFM provides an excellent analytical model for the predicted behaviour of beams reinforced with FRP stirrups. However, the limit imposed on the SFM to avoid shear-compression failure for beams reinforced with either steel or FRP has to be re-investigated. Although the proposed equation (6-10) for the shear-friction factor, k , resulted in a reasonable prediction of the shear strength of beams reinforced longitudinally with FRP, further refinement of the theory is recommended to account for the effect of using FRP as longitudinal reinforcement.

6.6.3 Modified compression field theory (MCFT)

As described in chapter 2, the MCFT is considered as a rational theory to predict the behaviour of any concrete element subjected to a biaxial stress field. The MCFT uses the equilibrium equations (section 2.3.2), the compatibility conditions and the stress-strain relationships for concrete and reinforcement to determine the average stresses, the average strains and the crack angle θ at any load level up to failure.

6.6.3.1 Analysis procedure

As mentioned in section 2.3.2, Felber (1990) implemented a computer program “RESPONSE” to predict the behaviour of a beam section subjected to shear and bending moment using the MCFT. The “RESPONSE” program requires the following input data:

1. The concrete compressive strength, f_c' , the corresponding strain ϵ_c' , the concrete tensile strength, f_{cr} , and the tension stiffening factors α ($=\alpha_1\alpha_2$, as given in equation 2-12). The values of f_c' , ϵ_c' , and f_{cr} used in the analysis of the tested beams are based on the standard material tests described in chapter 4. As specified by Collins and Mitchell (1991), the factors α_1 and α_2 are taken as 0.7 for 7-wire bonded strands and 1.0 for static loading, respectively.
2. The parameters needed to describe the stress–strain relationships of the longitudinal reinforcement. Figure 6-50 shows the stress–strain relationships used for modelling the steel and CFRP strands used as longitudinal reinforcement.
3. The parameters needed to describe the stress–strain relationships of the shear reinforcement. The “RESPONSE” program limits the elastic modulus of the stirrups to between 100 and 200 GPa. Therefore it is not possible to model a beam section reinforced with GFRP stirrups since E_{gfrp} equals 41 GPa. The “RESPONSE” program also limits the tensile strength of shear reinforcement to 1000 MPa. Therefore, the behaviour of beams reinforced with CFRP stirrups is predicted up to this stress level. The stress–strain relationships for modelling the steel and CFRP stirrups used as shear reinforcement are shown in Figure 6-51.
4. The crack spacings in the longitudinal direction, s_{ml} , and in the transverse direction, s_{mv} , are determined using equations (2-16) and (2-17).

5. For integration purposes and as recommended by the “RESPONSE” user manual, the beam section is divided into three layers, as shown in Figure 6-52.
6. The location in the web where the longitudinal strain, ε_x , is considered for shear analysis of the beam. For the beams analyzed in the current investigation, the longitudinal strain, ε_x , is considered at the mid-shear depth, jd , as illustrated in Figure 2-6.
7. The shear span, a (= moment-to-shear ratio, M/V), is taken as 1.50 m.

Five beams were analyzed using the MCFT to predict the shear strength and behaviour in terms of the average stirrup strains and the shear crack width at any load level up to failure. The beams analyzed in the current investigation include beams tested in the second experimental phase and reinforced with steel or CFRP stirrups. These beams have the following designations: SS-2, SC-2, SC-3, SC-4 and CC-3. The input files for the “RESPONSE” program used to perform the MCFT analysis are given in Appendix B.

6.6.3.2 Analysis results and discussion

The shear versus the average stirrup strain as predicted by the MCFT is compared to test results in Figure 6-53 for beam SS-2 reinforced with steel stirrups. Similar graphs for beams reinforced with CFRP stirrups are shown in Figures 6-54 to 6-57. Due to the limitation of the “RESPONSE” program for f_{fv} (=1000 MPa), the behaviour of beams reinforced with CFRP stirrups was predicted up to a strain level, ε_{fv} , of 0.73% ($\equiv 1000/E_{fv}$). It is shown in Figures 6-54 to 6-57 that there is good agreement between the test results and the prediction using the MCFT. The shear strength of the beam reinforced with steel stirrups is defined as the shear force at the yielding of the steel

stirrups, V_y , and is determined based on the load level corresponding to a sudden change in the behaviour, as shown in Figure 6-53. For a beam with CFRP stirrups, it is proposed to use the bend capacity of the CFRP stirrups as a failure criterion. As determined using the bend tests (Table 6-1), the bend strength of the CFRP stirrups used in beam specimens equals 960 MPa, corresponding to a stirrup strain, ε_{fs} , of 0.70 %. The shear strength, V_n , of a beam reinforced with CFRP stirrups is therefore assumed to be the shear force corresponding to an average stirrup strain of 0.70 %, and is determined for beams analyzed using the MCFT as shown in Figures 6-54 to 6-57. Figure 6-58 shows the measured-to-predicted shear strength ratio, V_{test}/V_n , for beams analyzed using the MCFT. As shown in Figure 6-58, the MCFT along with the proposed failure criterion resulted in good and conservative prediction for the shear strength of beams reinforced for shear with CFRP stirrups and reinforced with either steel or CFRP strands for flexure. It was observed in the experimental program that using small stirrup spacing increases the chance for shear cracks to intersect the bend zone and consequently causes significant reduction of the stirrup capacity in beam action, f_{fve} . Figure 6-59 shows the relationship between the f_{fve}/f_{fiv} ratio and the s/d ratio as predicted by the MCFT and as observed in the experimental program for beams reinforced with CFRP stirrups. As shown in Figure 6-59, the analytical results of the MCFT follow the same trend observed in the experimental program. It can be concluded that the effect of the spacing of FRP stirrups on the shear strength of concrete beams can be evaluated using the MCFT.

The shear crack width is determined according to the MCFT using the following equations, as given in chapter 2 (section 2.3.2):

$$w = \varepsilon_1 s_m \theta \quad (6-11)$$

$$s_{m\theta} = 1 / \left(\frac{\sin \theta}{s_{ml}} + \frac{\cos \theta}{s_{mv}} \right) \quad (6-12)$$

$$s_{ml} = 2 \left(c_l + \frac{s_l}{10} \right) + 0.25k_1 \frac{d_{bl}}{\rho_{sl}} \quad (6-13)$$

$$s_{mv} = 2 \left(c_v + \frac{s_v}{10} \right) + 0.25k_1 \frac{d_{bv}}{\rho_{sv}} \quad (6-14)$$

where $s_{m\theta}$ is the diagonal crack spacing and s_{ml} and s_{mv} are the crack spacings indicative of the crack control characteristics of the longitudinal and transverse reinforcement, respectively. The shear versus crack widths for beams SS-2 and SC-3 analyzed using the MCFT are compared to the test results in Figures 6-60 and 6-61, respectively. The corresponding graphs for other tested beams are given in Appendix C. As demonstrated in Figures 6-60 and 6-61, the MCFT did not give a good prediction for the shear crack width. This is attributed to the overestimation of the crack spacings s_{ml} and s_{mv} calculated using equations (6-13) and (6-14).

Finally, it can be concluded that the use of the bend capacity of CFRP stirrups as a failure criterion for the MCFT analysis of beams provides good and conservative prediction for the shear strength of beams reinforced with CFRP stirrups. The MCFT also results in good prediction for the shear behaviour in terms of the average strain in CFRP stirrups. However, the equations used to estimate the crack spacings s_{ml} and s_{mv} result in an overestimation of the shear crack width at any load level. The computer program "RESPONSE" needs adjustment to accommodate the use of GFRP reinforcement with low elastic modulus.

6.6.4 Estimation of shear crack width

As shown in Figures 6-60 to 6-62, the MCFT overestimates the shear crack width in beams reinforced with steel or FRP stirrups, for reasons given above. The shear crack width in concrete beams reinforced with conventional steel rebars has not been as extensively investigated as has the flexural crack width. However, the following equations are provided by Placas and Regan (1971) and Hassan (1991) to predict the shear crack width in concrete beams reinforced with steel stirrups:

$$w = \frac{s \sin \alpha}{10^6 \rho_{sv} (f'_c)^{1.3}} \left(\frac{V - V_{cr}}{b_w d} \right) \quad \text{units : lb, in.} \quad (6-15)^2$$

$$w = \frac{1.8 S_d d_b}{10^6 (f'_c / 19.6)^{2.3} \rho_{sv}^{1.3}} \quad (6-16)^3$$

$$S_d = 8 \times 10^3 \varepsilon_{sv} + 2 \times 10^6 \varepsilon_{sv}^2$$

where V_{cr} is the shear cracking load and is predicted using the ACI equation (2-29) for $V_{c(aci)}$, α is the angle of the stirrups ($\alpha = 90^\circ$ for vertical stirrups), S_d is the slip of stirrup, ε_{sv} is the measured stirrup strain at the load level under consideration and d_b is the bar diameter of the stirrup. It should be noted that equation (6-16) cannot be considered as a direct procedure for crack width estimation as it requires measured strain data.

The shear crack widths predicted using equations (6-15) and (6-16) are compared to test results for beam SS-2 in Figure 6-60. Figure 6-60 shows that equation (6-15) resulted in relatively good estimate for the shear crack width compared with equation (6-16) and the MCFT. Shear crack widths determined according to equation (6-15) are compared to test results for beams SC-3 and SG-3 in Figures 6-61 and 6-62, respectively. The corresponding graphs for all tested beams are given in Appendix C. It is shown in

² Equation (2-55)

Figures 6-61 and 6-62 that equation (6-15) underestimated the shear crack width in beams reinforced with FRP stirrups due to the relatively low elastic modulus of the stirrups. A regression analysis using test results was conducted to provide an appropriate modification for equation (6-15) to account for the effect of the low elastic modulus of FRP stirrups. The following equation is proposed to estimate the shear crack width in beams reinforced with FRP stirrups.

$$w = \frac{s}{10^6 \rho_{fv} \left(\frac{E_{fv}}{E_s} \right) (f'_c)^{1.3}} \left(\frac{V - V_c}{b_w d} \right) \quad \text{units : lb, in.} \quad (6-17a)$$

$$w = \frac{27.6 s}{10^6 \rho_{fv} \left(\frac{E_{fv}}{E_s} \right) (f'_c)^{1.3}} \left(\frac{V - V_c}{b_w d} \right) \quad \text{units : N, mm} \quad (6-17b)$$

The shear crack widths predicted using proposed equation (6-17) are compared to test results for beams SC-3 and SG-3 in Figures 6-61 and 6-62, respectively. The corresponding graphs for all tested beams are given in Appendix C. Figures 6-61 and 6-62 and all other graphs in Appendix C show that the proposed equation (6-17) predicted well the shear crack width in beams reinforced for shear with FRP stirrups and reinforced with either steel or CFRP strands for flexure. Furthermore, the modification introduced in equation (6-17) resulted in a conservative estimate for the shear crack width in comparison to the original equation (6-15).

³ Equation (2-57)

6.7 Summary

Test results for the ten beams tested in the second experimental phase are presented in this chapter. The behaviour of beams reinforced with FRP stirrups were investigated in terms of shear cracking and failure mode. The contribution of FRP stirrups to the shear resisting mechanism in concrete beams was evaluated based on the strain measurement in the stirrups and the stirrup effectiveness concept. The effects of FRP longitudinal reinforcement on the concrete contribution, V_{cf} , and the shear crack width were investigated based on the test results. The behaviour of tested beams was predicted using the available code models, the shear friction model (SFM), and the modified compression field theory (MCFT). The predicted behaviour in terms of shear strength, stirrup strains, and crack width, was compared with the test results. Recommendations were made to adapt the SFM and MCFT for the analysis of concrete beams reinforced with FRP. Shear crack widths in tested beams were also predicted using equations available in the literature. Based on the findings of this investigation, a simple equation is proposed to predict the shear crack width in concrete beams reinforced with FRP stirrups.

Table 6-1. Test results of beam specimens

Beam ID	Flexural reforc.	stirrups	$\varepsilon_{fuv} = f_{fuv}/E_{fv}$ %	$\varepsilon_{bend} = f_{bend}/E_{fv}$ %	Spacing s	f_c MPa	Shear at flexural cracking kN	Shear cracking force V_{cr} kN	Angle of major crack θ deg	Ultimate shear V_{test} kN	$v_{test} = V_{test}/bd$ MPa	max stirrup strain at failure %	average stirrup strain at failure ε_v %	Mode of failure [#]
SN-0	6 15-mm 7-wire steel strands	-----				54	37.0	67.5	40	186.5	1.064**			DT
SS-2		Steel	2.0	---	$d/2^*$	54	37.0	70.0	42	272.5	4.295	0.95	0.44	SY
SC-2		CFRP	1.31	0.63	$d/2$	54	34.0	75.0	44	277.5	4.374	1.05	0.77	SR
SC-3		Leadline			$d/3$	54	34.0	75.0	44	341.0	5.374	1.04	0.71	SR
SC-4					$d/4$	51	34.0	75.0	45	375.5	5.918	0.80	0.55	SR
SG-2		GFRP	1.74	0.85	$d/2$	54	34.0	75.0	42	292.0	4.602	1.20	0.91	SR
SG-3		C-BAR			$d/3$	33	25.0	65.0	45	312.5	4.925	0.83	0.53	SC
SG-4					$d/4$	33	25.0	65.0	42	311.5	4.909	0.78	0.48	SC
CC-3		7 15-mm CFCC strands	Leadline	1.31	0.63	$d/3$	50	26.0	67.5	45	305	4.807	0.90	0.65
CG-3	C-BAR		1.74	0.85	$d/3$	50	26.0	67.5	46	304.5	4.799	1.07	0.85	SR

* d is the effective beam depth = 470 mm

** The shear cracking load is considered as the ultimate shear capacity for the control beam SN-0 without shear reinforcement

DT : diagonal tension failure

SY : shear failure initiated by yielding of the steel stirrups

SR : shear failure initiated by rupture of the FRP stirrups

SC : shear compression failure

f_{bend} : bend capacity of FRP stirrups, determined based on bend tests (chapter 5)

f_{fuv} : guaranteed strength in the direction of the fibres

E_{fv} : elastic modulus of the FRP stirrups

Table 6-2. Measured versus calculated ultimate shear stress for beams tested in experimental phase II

Beam ID	v_{test} MPa	ACI		JSCE		BRI		CHBDC		Eurocrete	
		v_n MPa	$\frac{v_{test}}{v_n}$	v_n MPa	$\frac{v_{test}}{v_n}$	<i>calc.</i> MPa	$\frac{v_{test}}{v_n}$	v_n MPa	$\frac{v_{test}}{v_n}$	v_n MPa	$\frac{v_{test}}{v_n}$
(1)	(2)	(3)	(4)	(5)	(6)	(7)	(8)	(9)	(10)	(11)	(12)
SN-0	1.064	1.100	0.970	1.003	1.061	1.381	0.770	0.969	1.098	0.976	1.090
SS-2	4.295	3.756	1.143	3.294	1.304	2.605	1.648	2.572	1.670	3.267	1.314
SC-2	4.374	5.316	0.823	1.583	2.762	2.282	1.916	1.479	2.956	1.806	2.421
SC-3	5.374	6.020	0.893	1.707	3.149	2.474	2.173	1.636	3.284	2.196	2.448
SC-4	5.918	5.852	1.011	1.774	3.337	2.585	2.289	1.706	3.469	2.602	2.274
SG-2	4.602	6.020	0.765	1.547	2.974	1.917	2.401	1.405	3.275	1.706	2.698
SG-3	4.925	4.721	1.0432	1.367	3.604	1.630	3.022	1.362	3.617	2.048	2.405
SG-4	4.909	4.721	1.040	1.447	3.394	1.730	2.837	1.329	3.694	2.405	2.041
CC-3	4.807	5.791	0.831	1.384	3.479	2.259	2.131	1.423	3.384	2.033	2.369
CG-3	4.799	5.791	0.831	1.357	3.546	1.831	2.629	1.393	3.454	1.917	2.511

- 1 Equations (2-27), (2-28), (2-29), (2-32) and (2-33) were used in the current investigation.
- 2 Equations (3-27), (3-28), (3-29) and (3-31) were used in the current investigation.
- 3 Equation (3-36) was used in the current investigation.
- 4 Equations (3-39) and (3-40) along with equation (2-39b) were used in the current investigations.
- 5 Equations (3-41) and (3-42) were used to modify the shear design equations (2-48) and (2-49) of the British standard BS8110.

Table 6-3. Shear friction analysis of tested beams

Beam ID	$C_w = f_c' b_w h$ kN	shear friction factor k	failure plane ID	angle of the plane θ	Contribution of stirrups					Tension in long. reinf. T kN	shear strength V_n kN	Failure mode**
					no. of stirrups	ΣA_v mm ²	l/d_c	f_v MPa	T_v kN			
(1)	(2)	(3)	(4)	(5)	(6)	(7)	(8)	(9)	(10)	(11)	(12)	(13)
Beam SN-0	4082.4	0.426	1	21.6	---	---	---	---	---	3.27 V_n	69.8	DT
			test*	40								67.5***
Beam SS-2	4082.4	0.426	1	43.9	2	253.36	---	660	167.2	3.29 V_n -61.3	302.3	SY
			2	46.8	1	126.7	---	660	83.6	2.09 V_n -44.1	280.2	SY
			3	35.3	2	253.36	---	660	167.2	2.09 V_n -132.	297.9	SY
			4	40.2	2	253.36	---	660	167.2	1.56 V_n -135.	314.1	SY
			5	53.5	1	126.7	---	660	83.6	0.99 V_n -42.4	240.7	SY
			test	42	2							257.5#
Beam SC-2	4082.4	0.426	1	44.7	2	153.9	5.0	849	130.6	3.29 V_n -47.9	283.0	SR
			2	46.8	1	77.0	35.7	1440	110.9	3.18 V_n -58.3	287.6	SR
			3	44.7	2	153.9	5.0	849	130.6	3.18 V_n -104.	292.1	SR
			4	35.3	2	153.9	23.8	1332	205.0	2.08 V_n -162.	334.1	SR
			5	46.5	2	153.9	5.0	849	130.6	1.62 V_n -43.0	322.5	SR
			6	51.6	2	153.9	5.0	849	130.6	1.07 V_n -41.9	318.8	SR
			test	44	2							277.5
Beam SC-3	4082.4	0.426	1	55.6	2	153.9	5.0	849	130.6	3.32 V_n -31.9	370.5	SR
			2	46.2	2	153.9	23.8	1332	205.0	3.27 V_n -111.	346.9	SR
			3	44.1	3	230.8	5.0	849	196.0	2.98 V_n -85.5	336.4	SR
			4	36.0	4	307.8	5.0	849	261.3	3.00 V_n -168.	342.9	SR
			5	44.1	3	230.8	5.0	849	196.0	2.24 V_n -85.4	364.5	SR
			6	42.9	3	230.8	7.7	917	211.7	1.41 V_n -153.	373.9	SR
			test	44	3							341.0
Beam SC-4	3855.6	0.436	1	54.2	2	153.9	23.8	1332	205.0	3.32 V_n -83.1	407.4	SR
			2	46.5	3	230.8	17.2	1162	268.2	3.30 V_n -141.	385.6	SR
			3	52.3	3	230.8	5.0	849	196.0	3.10 V_n -64.0	389.8	SR
			4	44.1	4	307.8	5.0	849	261.3	3.12 V_n -126.	372.4	SR
			5	37.8	5	384.7	5.0	849	326.6	3.13 V_n -208.	384.0	SR
			6	43.9	4	307.8	5.4	859	264.4	1.37 V_n -179.	435.1	SR
			test	45	4							375.5
Beam SG-2	4052.4	0.426	1	43.9	2	452.0	5.0	349	157.7	3.29 V_n -57.9	296.1	SR
			2	46.8	1	226.0	20.9	570	128.9	3.18 V_n -67.8	306.3	SR
			3	43.1	2	452.0	5.0	349	157.7	3.18 V_n -126.	302.9	SR
			4	35.3	2	452.0	13.9	570	257.6	2.08 V_n -206.	338.2	SR
			5	43.1	2	452.0	5.0	349	157.7	1.69 V_n -62.0	330.4	SR
			6	50.1	2	452.0	5.0	349	157.7	1.12 V_n -58.9	346.6	SR
			test	42	2							292.0

* observed test results : failure crack angle and number of stirrups intersecting the crack for beams failed in shear rupture mode and ultimate shear capacity

** DT : diagonal tension failure

SY : shear failure initiated by yielding of the steel stirrups

SR : shear failure initiated by rupture of the FRP stirrups

SC : shear compression failure

*** observed shear cracking load

observed shear load at yield of steel stirrups

Table 6-3(cont'd). Shear friction analysis of tested beams

Beam ID	$C_w = f_c b_w h$ kN	shear friction factor k	failure plane ID	angle of the plane θ	Contribution of stirrups					Tension in long. reinf. T kN	shear strength V_n kN	Failure mode**	
					no. of stirrups	ΣA_s mm ²	l/d_c	f_v MPa	T_v kN				
(1)	(2)	(3)	(4)	(5)	(6)	(7)	(8)	(9)	(10)	(11)	(12)	(13)	
Beam SG-3	2494.8	0.519	1	85.4	0	---	---	---	0	3.38 V_n	529.2	SC	
			2	72.3	0	---	---	---	0	3.28 V_n	522.5	SC	
			3	55.6	2	452.0	5.0	349	157.7	3.32 V_n -38.5	363.7	SR	
			4	46.2	2	452.0	13.9	570	257.6	3.27 V_n -138.	360.7	SR	
			5	42.5	3	678.0	5.0	349	236.6	3.05V_n-119.	334.2	SR	
			6	34.5	4	904.0	5.0	349	315.5	3.09 V_n -231.	355.2	SR	
			7	42.5	3	678.0	5.0	349	326.6	2.31 V_n -119.	430.2	SR	
			8	42.9	3	678.0	4.5	349	326.6	1.41 V_n -171.	482.1	SR	
			<i>test*</i>	see Figure 6-1									312.5
Beam SG-4	2494.8	0.519	1	87.6	0	---	---	---	0	3.38 V_n	529.2	SC	
			2	76.5	0	---	---	---	0	3.32 V_n	529.2	SC	
			3	54.2	2	452.0	13.9	570	257.6	3.32 V_n -104.	420.8	SR	
			4	46.5	3	678.0	10.0	535	362.6	3.30 V_n -191.	425.4	SR	
			5	50.7	3	678.0	5.0	349	236.6	3.15 V_n -89.2	381.8	SR	
			6	42.5	4	904.0	5.0	349	315.5	3.18V_n-173.	379.2	SR	
			7	36.3	5	1130.	5.0	349	394.4	3.22 V_n -284.	402.4	SR	
			8	43.9	4	904.0	3.2	349	315.5	1.37 V_n -214.	476.0	SR	
			<i>test</i>	see Figure 6-1									311.5
Beam CC-3	3780.0	0.439	1	55.6	2	153.9	5.0	849	130.6	3.32 V_n -31.9	366.3	SR	
			2	46.2	2	153.9	23.8	1332	205.0	3.27 V_n -111.	343.4	SR	
			3	44.1	3	230.8	5.0	849	196.0	2.98V_n-85.4	333.2	SR	
			4	36.0	4	307.8	5.0	849	261.3	3.00 V_n -168.	340.4	SR	
			5	44.1	3	230.8	5.0	849	196.0	2.24 V_n -85.4	361.5	SR	
			6	42.9	3	230.8	7.67	917	211.7	1.41 V_n -153.	371.7	SR	
		0.387 ^{##}	1	55.6	2	153.9	5.0	849	130.6	3.32 V_n -31.9	305.2	SR	
			2	46.2	2	153.9	23.8	1332	205.0	3.27 V_n -111.	296.5	SR	
			3	44.1	3	230.8	5.0	849	196.0	2.98V_n-85.4	288.2	SR	
			4	36.0	4	307.8	5.0	849	261.3	3.00 V_n -168.	302.2	SR	
			5	44.1	3	230.8	5.0	849	196.0	2.24 V_n -85.4	316.5	SR	
			6	42.9	3	230.8	7.67	917	211.7	1.41 V_n -153.	340.1	SR	
			<i>test</i>	45	3							305.0	SR
Beam CG-3	3780.0	0.439	1	55.6	2	452.0	5.0	349	157.7	3.32 V_n -38.5	385.4	SR	
			2	46.2	2	452.0	13.9	570	257.6	3.27 V_n -138.	377.6	SR	
			3	42.5	3	678.0	5.0	349	236.6	3.05V_n-119.	349.6	SR	
			4	34.5	4	904.0	5.0	349	315.5	3.09 V_n -231.	368.4	SR	
			5	42.5	3	678.0	5.0	349	236.6	2.31 V_n -119.	383.6	SR	
			6	42.9	3	678.0	4.5	349	236.6	1.41 V_n -171.	399.0	SR	
		0.387 ^{##}	1	55.6	2	452.0	5.0	349	157.7	3.32 V_n -38.5	323.9	SR	
			2	46.2	2	452.0	13.9	570	257.6	3.27 V_n -138.	329.4	SR	
			3	42.5	3	678.0	5.0	349	236.6	3.05V_n-119.	305.7	SR	
			4	34.5	4	904.0	5.0	349	315.5	3.09 V_n -231.	330.4	SR	
			5	42.5	3	678.0	5.0	349	236.6	2.31 V_n -119.	339.2	SR	
			6	42.9	3	678.0	4.5	349	236.6	1.41 V_n -171.	366.3	SR	
			<i>test</i>	46	3							304.5	SR

^{##} shear friction factor, k , determined by equation (6-10) to account for the effect of E_{ft} .

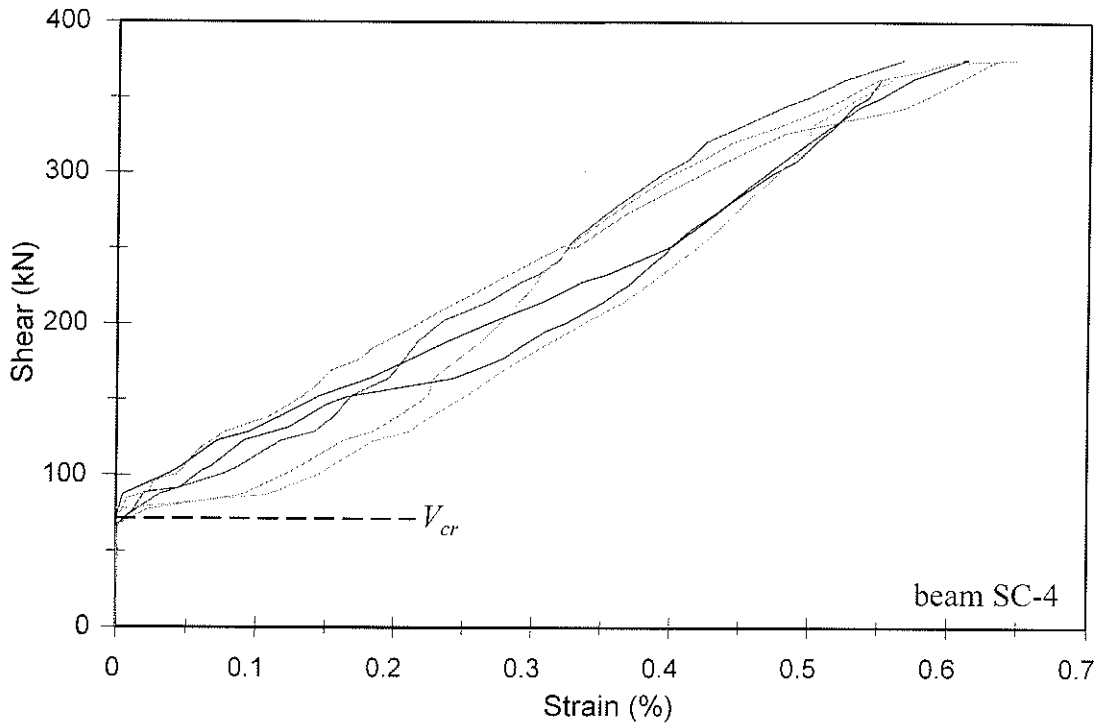


Figure 6-1. Typical shear versus strain in FRP stirrups: beam specimens

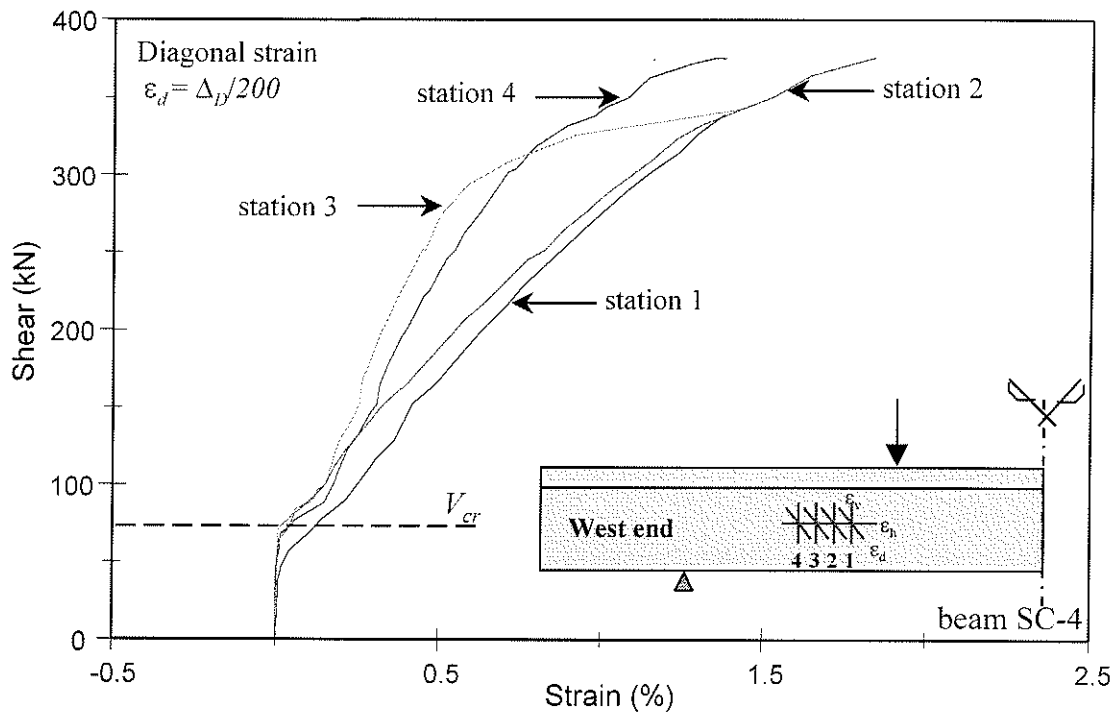
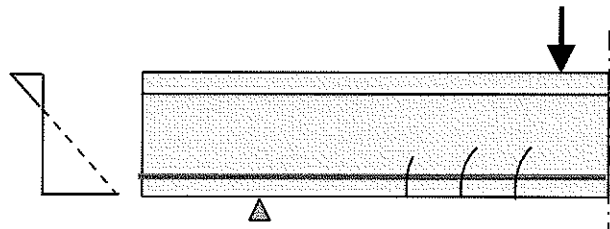
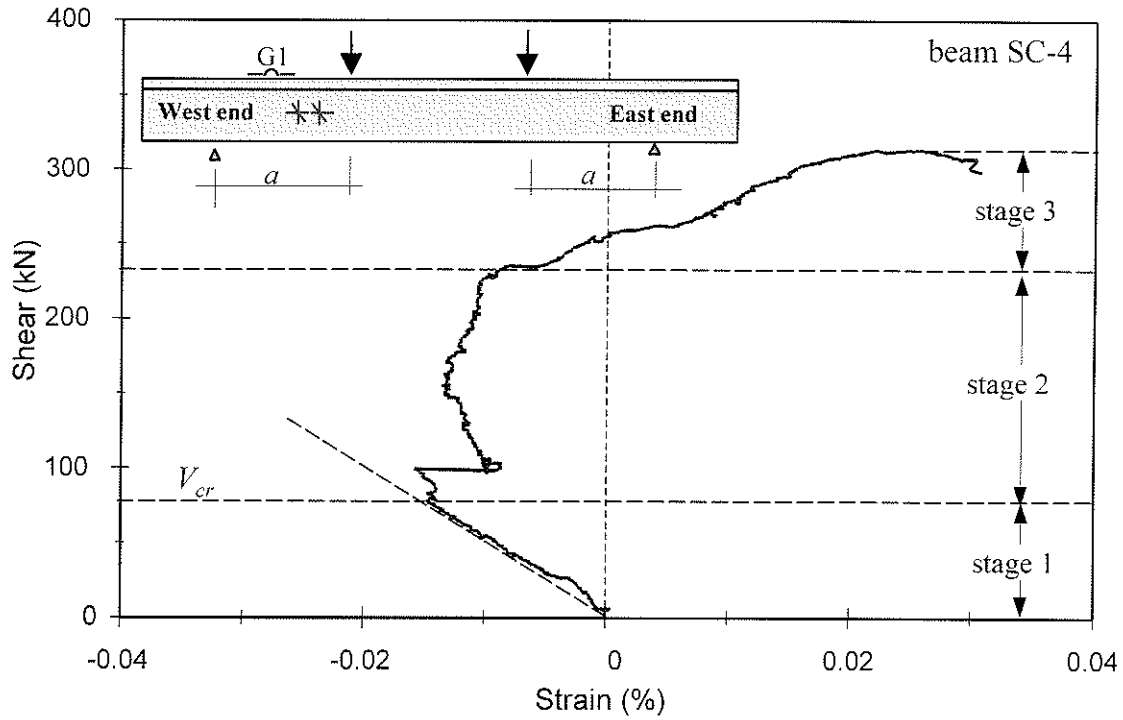
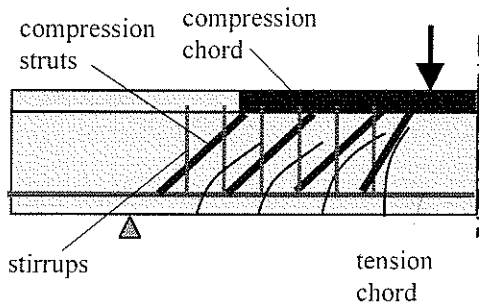


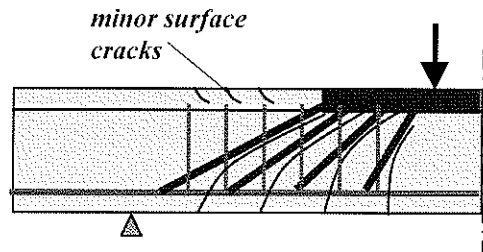
Figure 6-2. Typical shear versus average strains in the web: beam specimens



Stage 1: uncracked or flexural cracks only
(strain compatibility)



Stage 2: stabilization of shear cracks
(truss mechanism)



Stage 3: Excessive shear cracks
(variable angle truss mechanism)

Figure 6-3 Typical shear versus top strain in the shear span: beam specimens

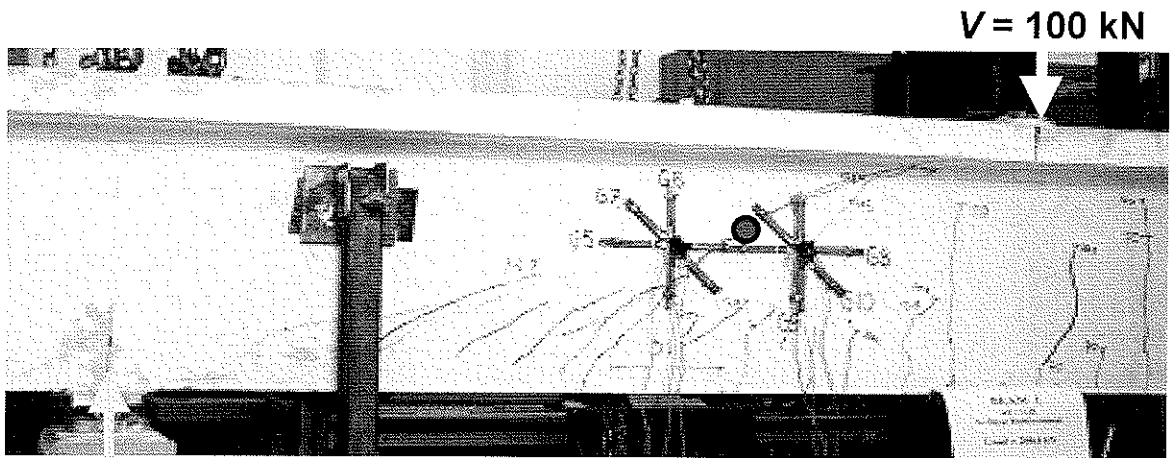


Figure 6-4. Shear cracking of beam SN-0

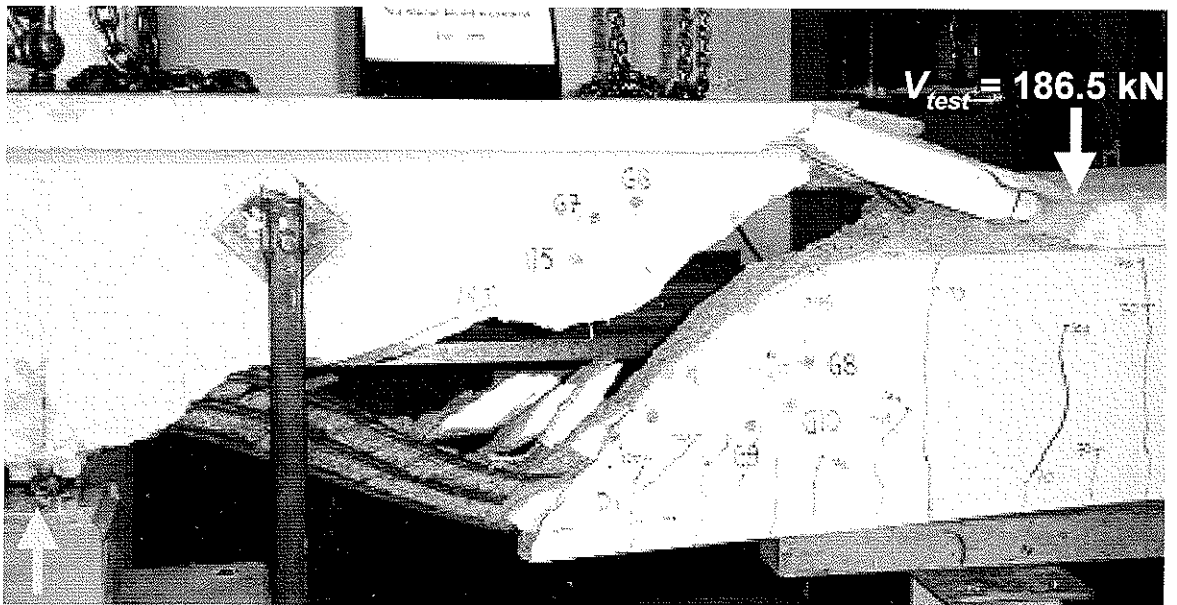


Figure 6-5. Beam SN-00 at failure

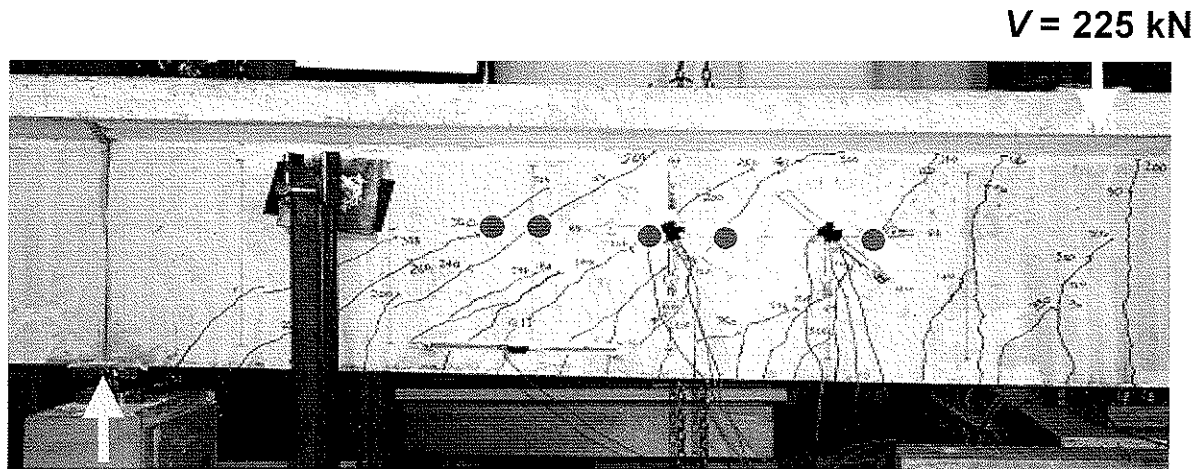


Figure 6-6. Shear cracking of beam SS-2

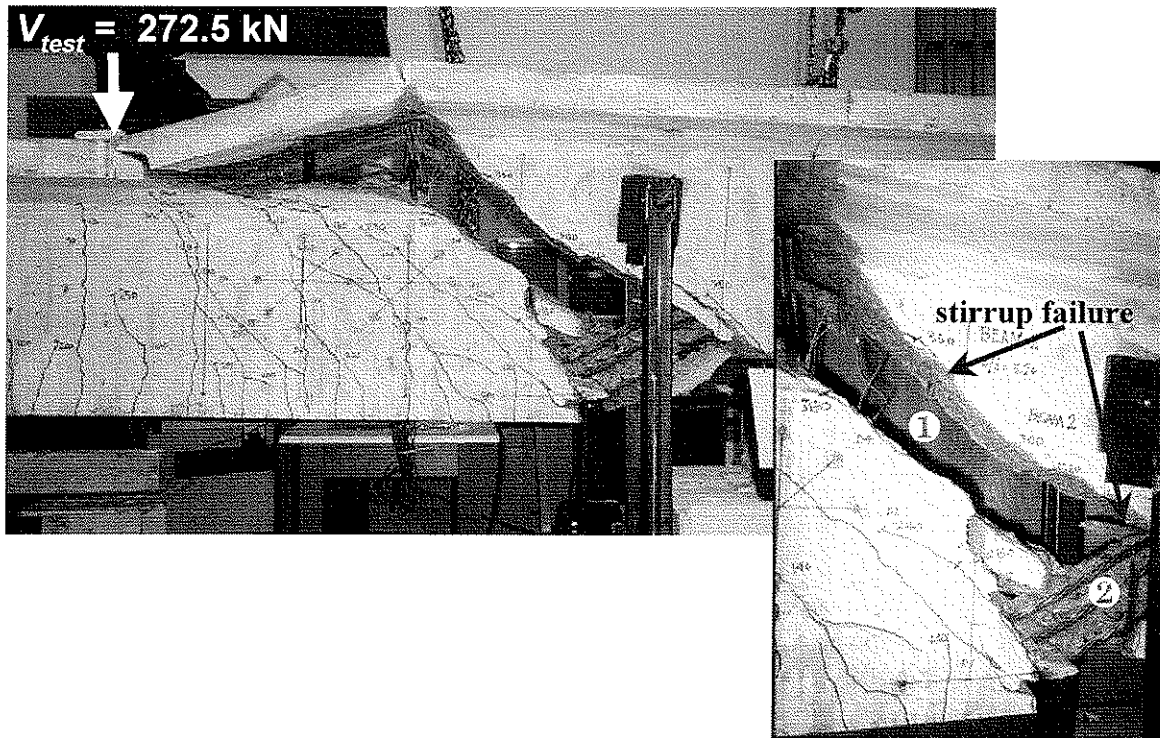


Figure 6-7. Beam SS-2 at failure

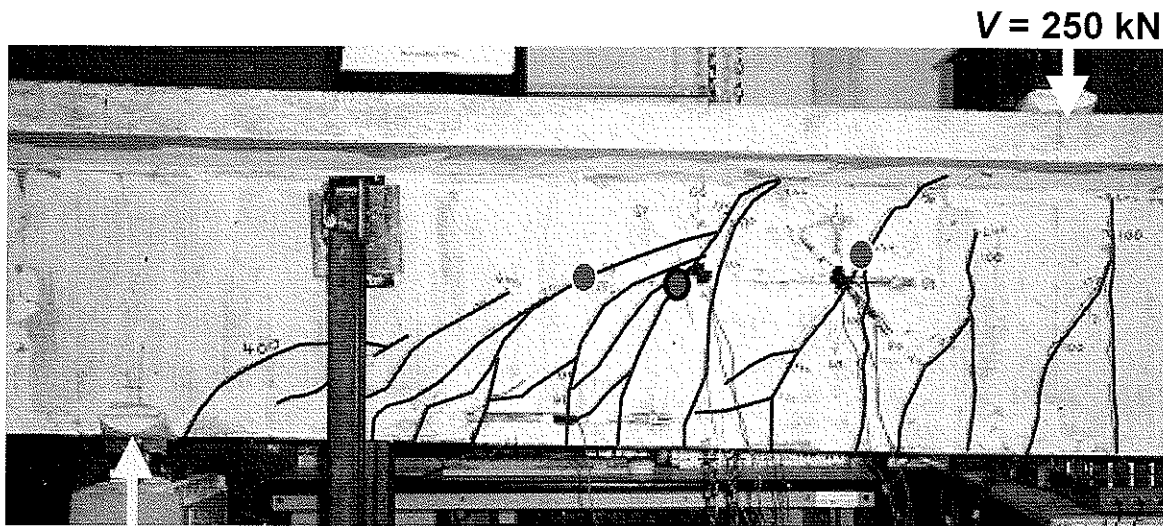


Figure 6-8. Shear cracking of beam SC-2

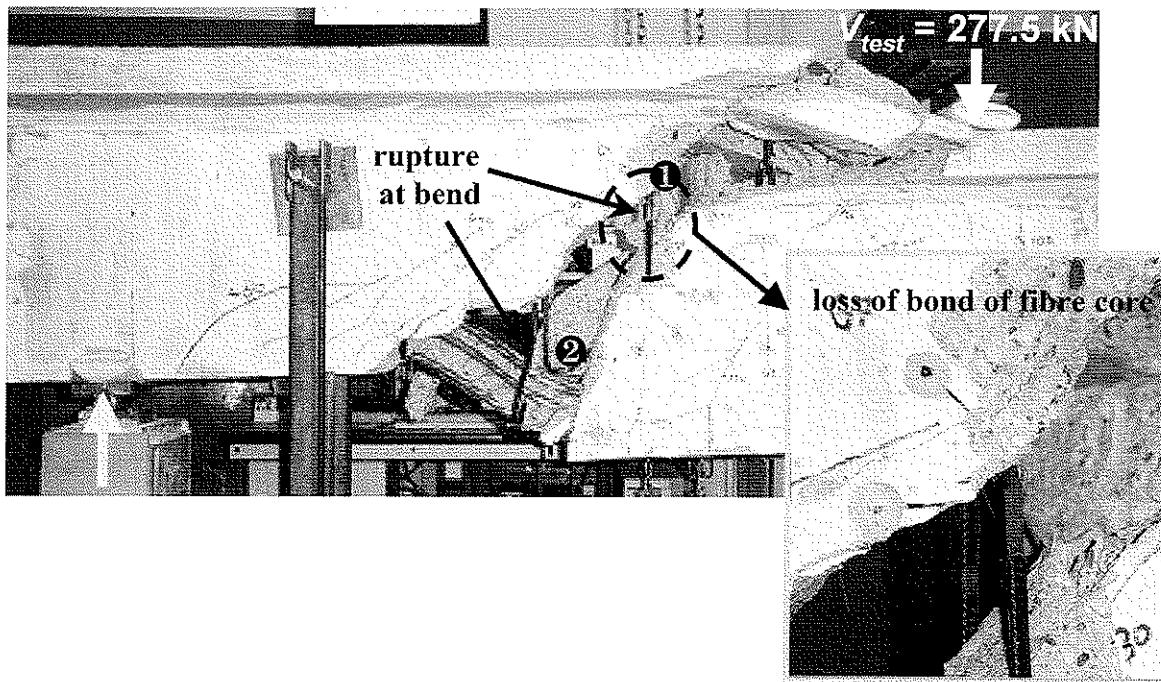


Figure 6-9. Beam SC-2 at failure

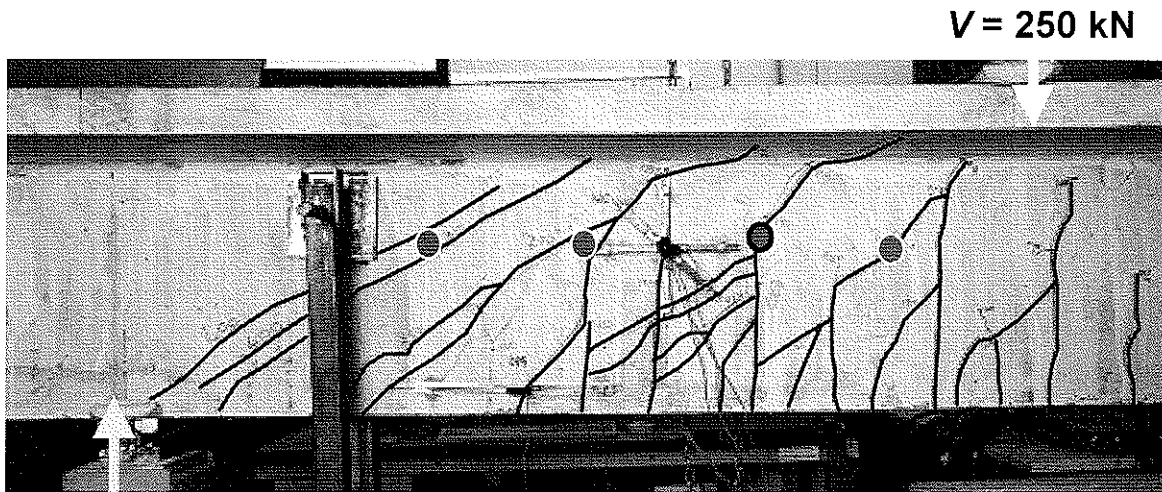


Figure 6-10. Shear cracking of beam SC-3

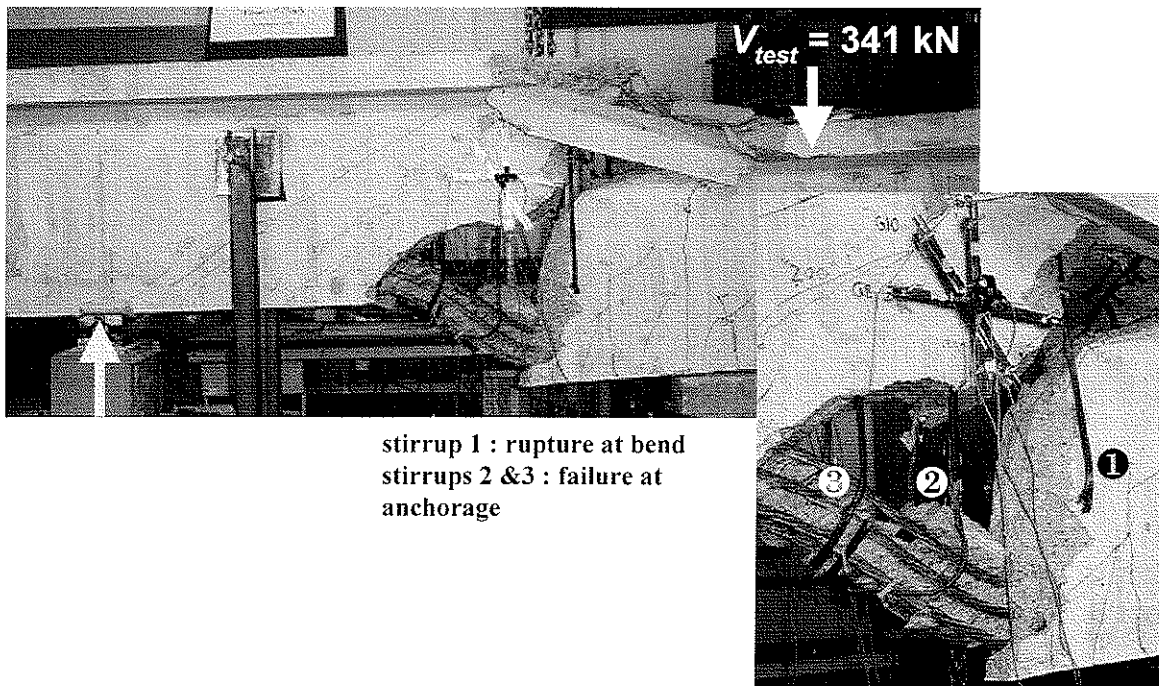


Figure 6-11. Beam SC-3 at failure

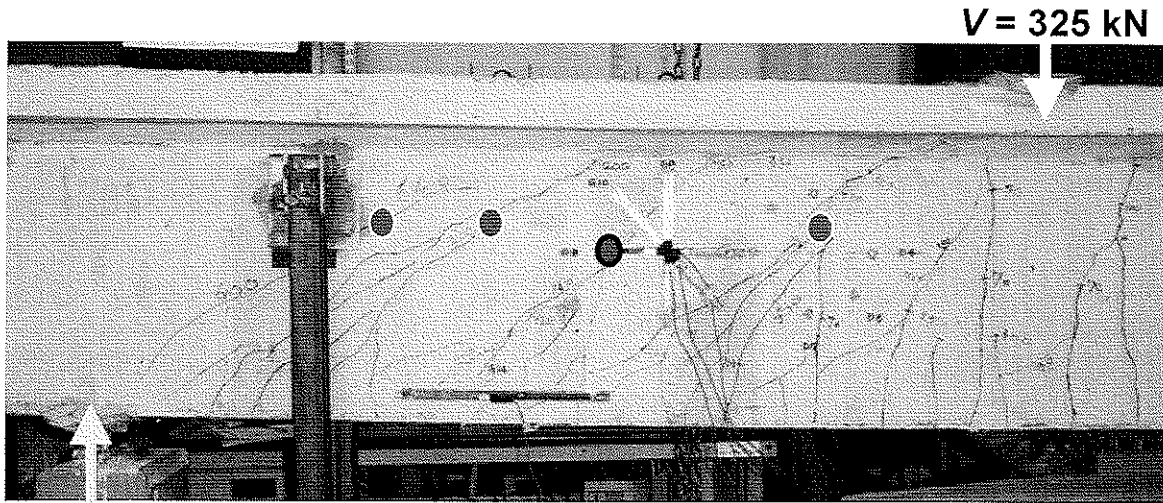


Figure 6-12. Shear cracking of beam SC-4

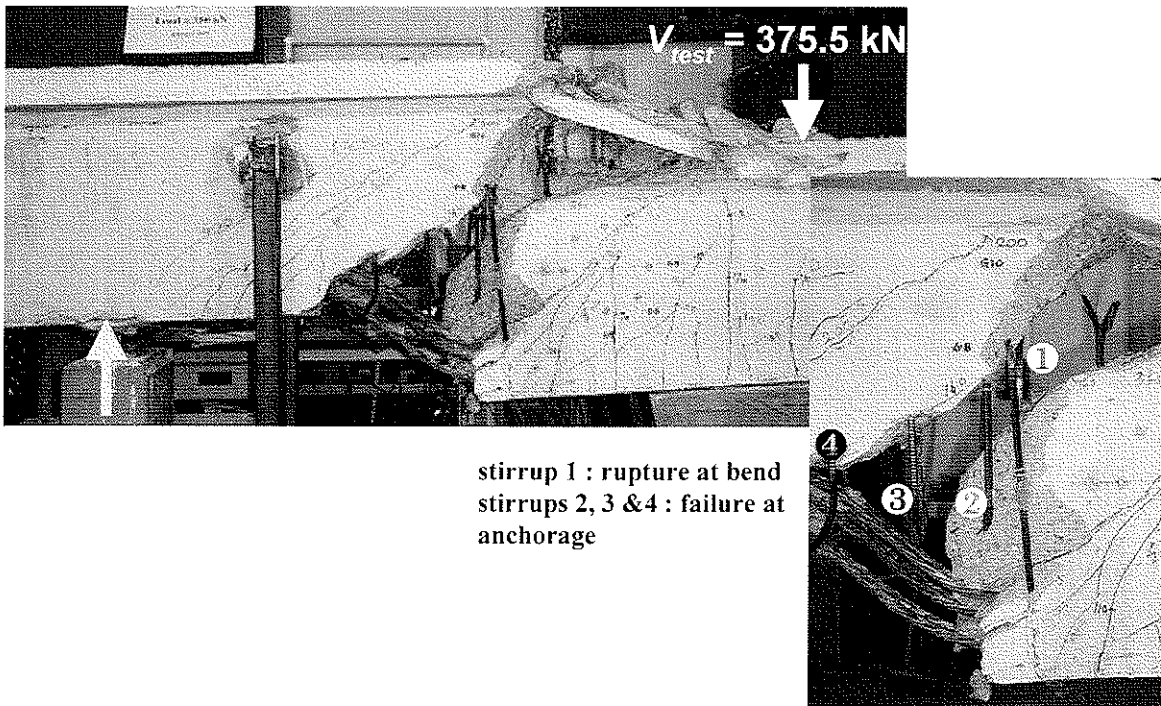


Figure 6-13. Beam SC-4 at failure

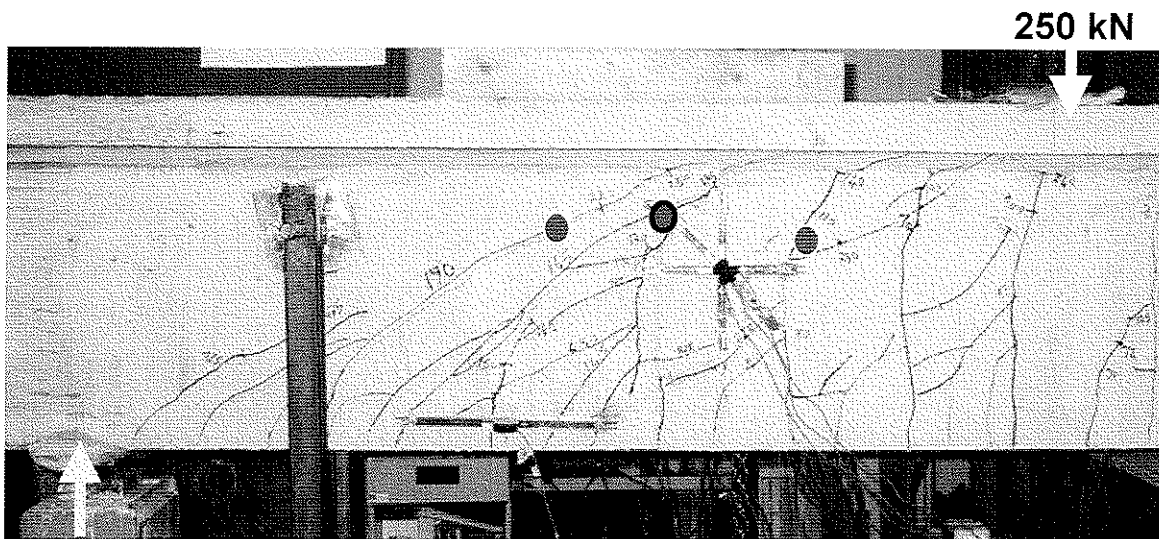


Figure 6-14. Shear cracking of beam SG-2

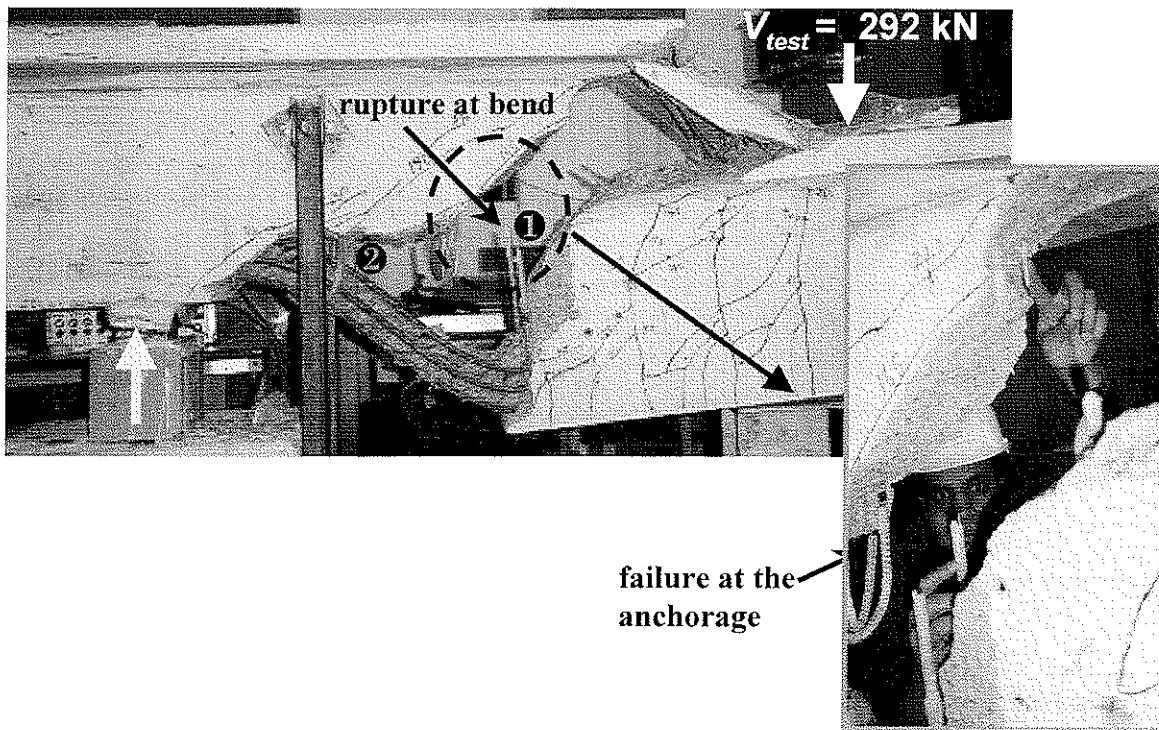


Figure 6-15. Beam SG-2 at failure

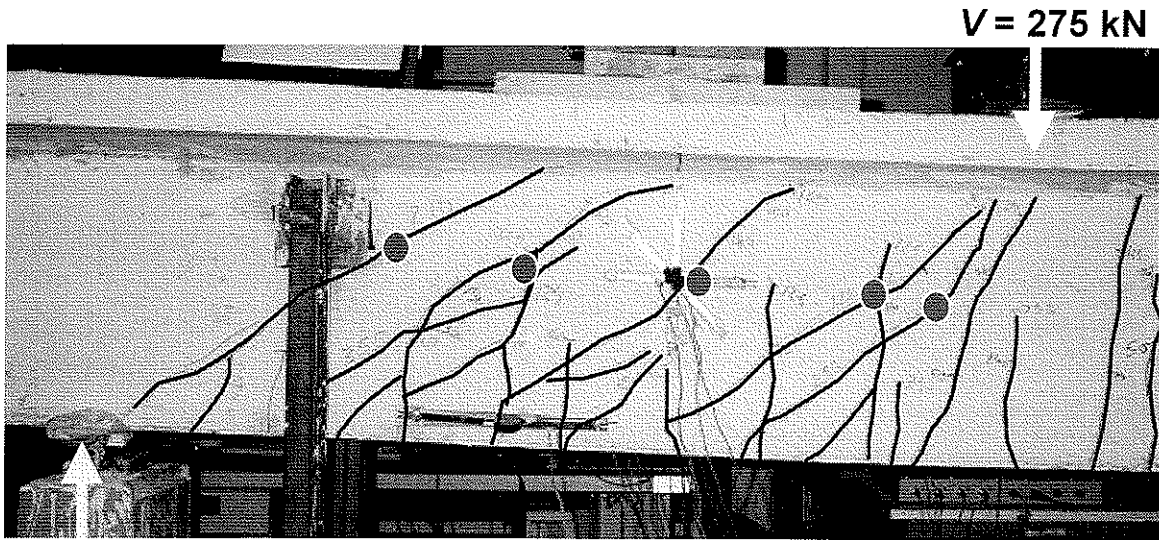


Figure 6-16. Shear cracking of beam SG-3

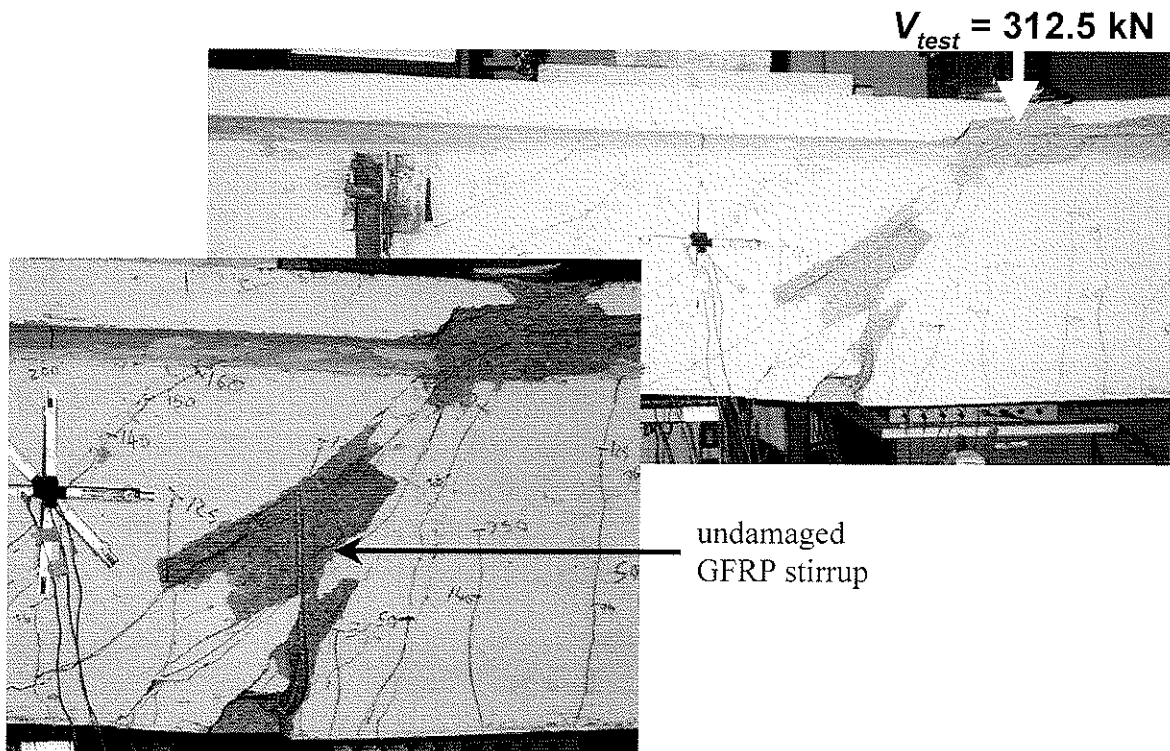


Figure 6-17. Beam SG-3 at failure

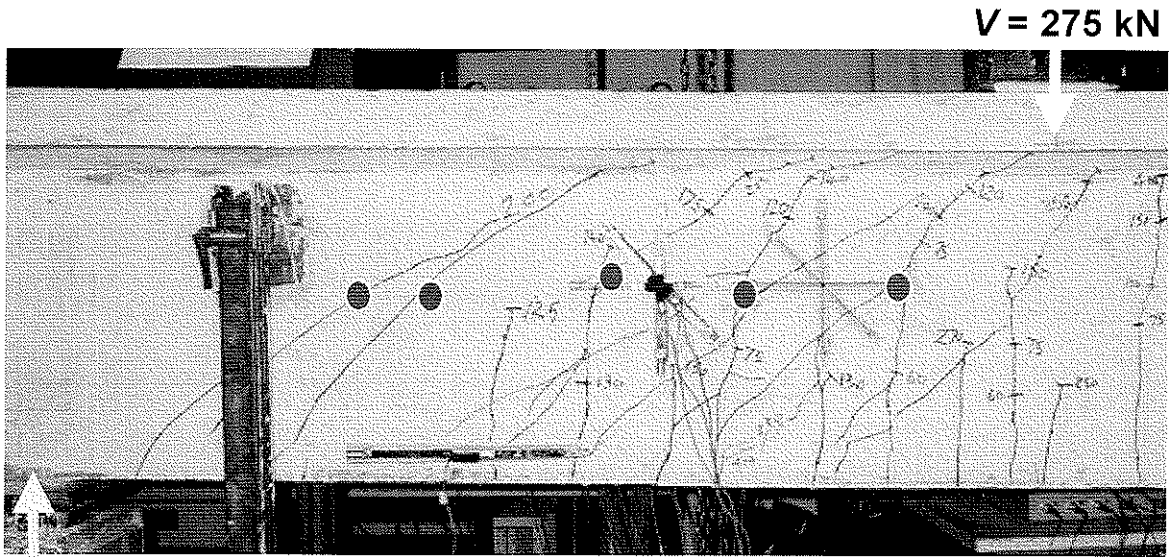


Figure 6-18. Shear cracking of beam SG-4

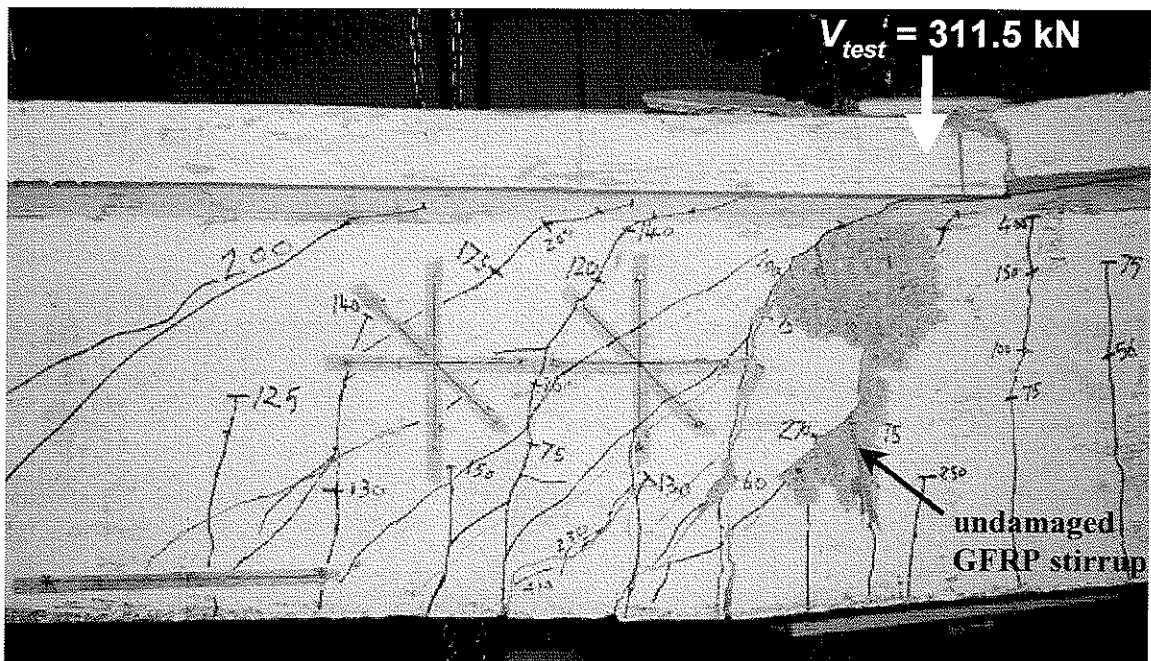


Figure 6-19. Beam SG-4 at failure

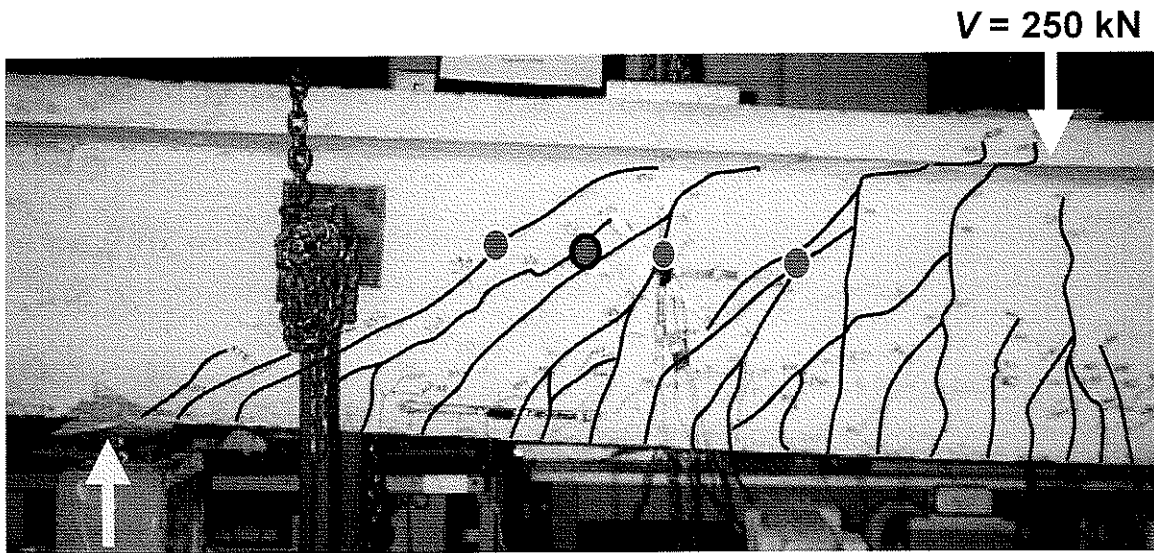


Figure 6-20. Shear cracking of beam CC-3

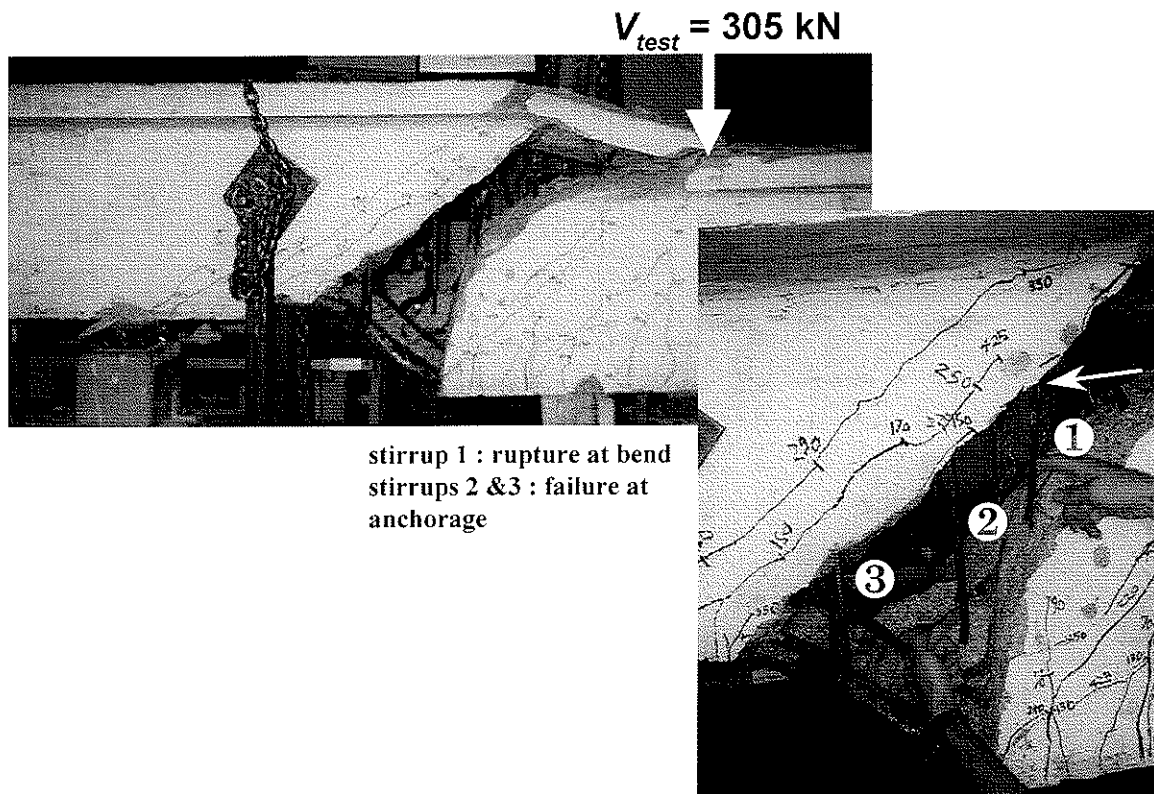


Figure 6-21. Beam CC-3 at failure

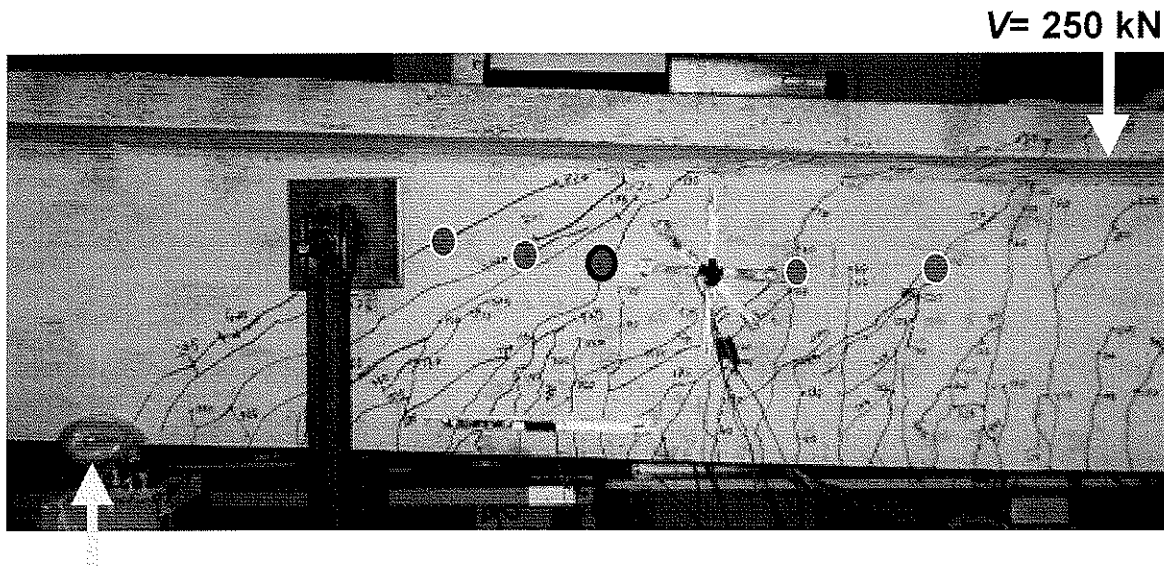


Figure 6-22. Shear cracking of beam CG-3

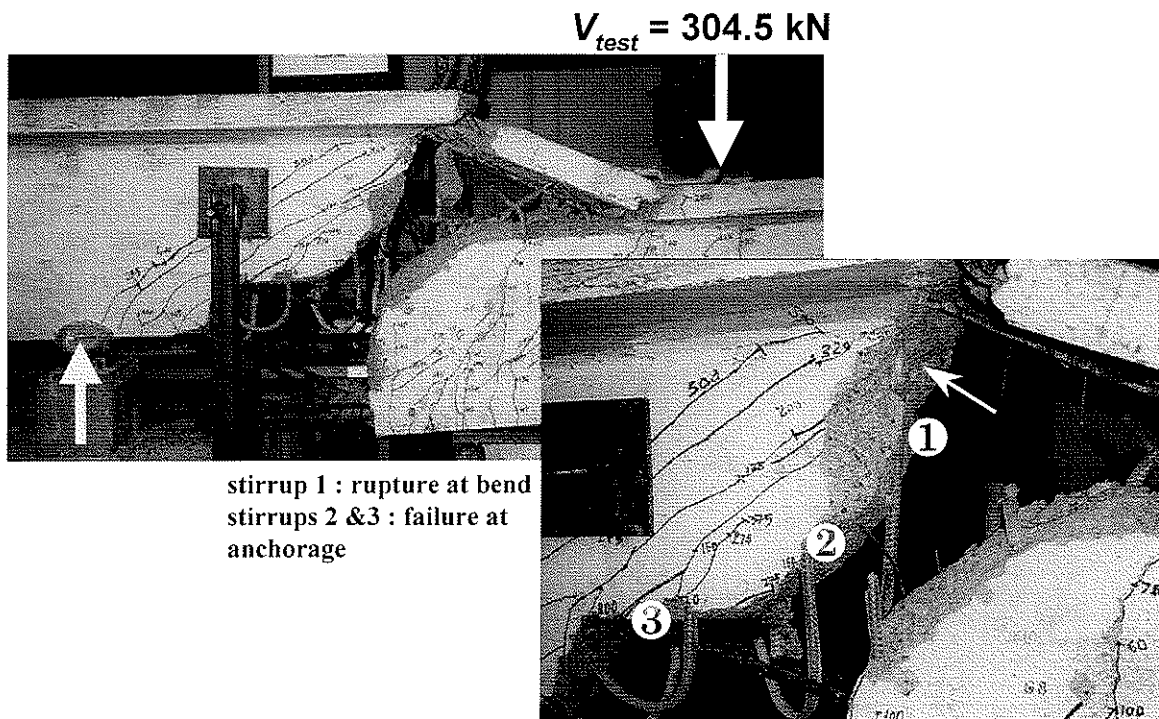
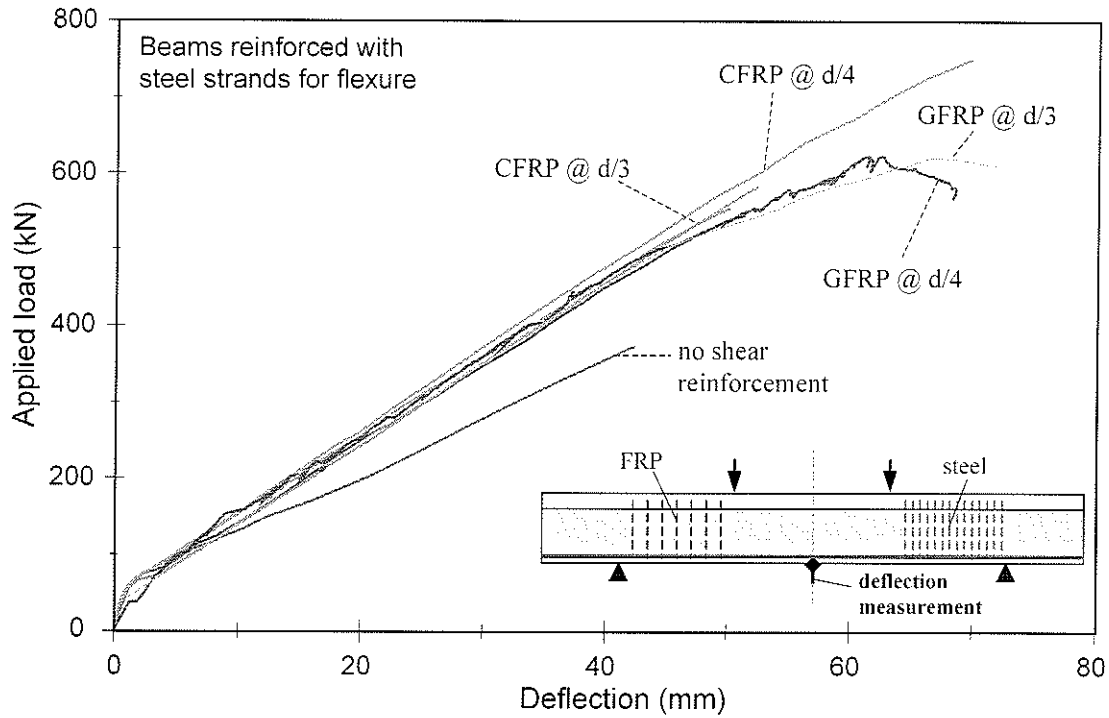
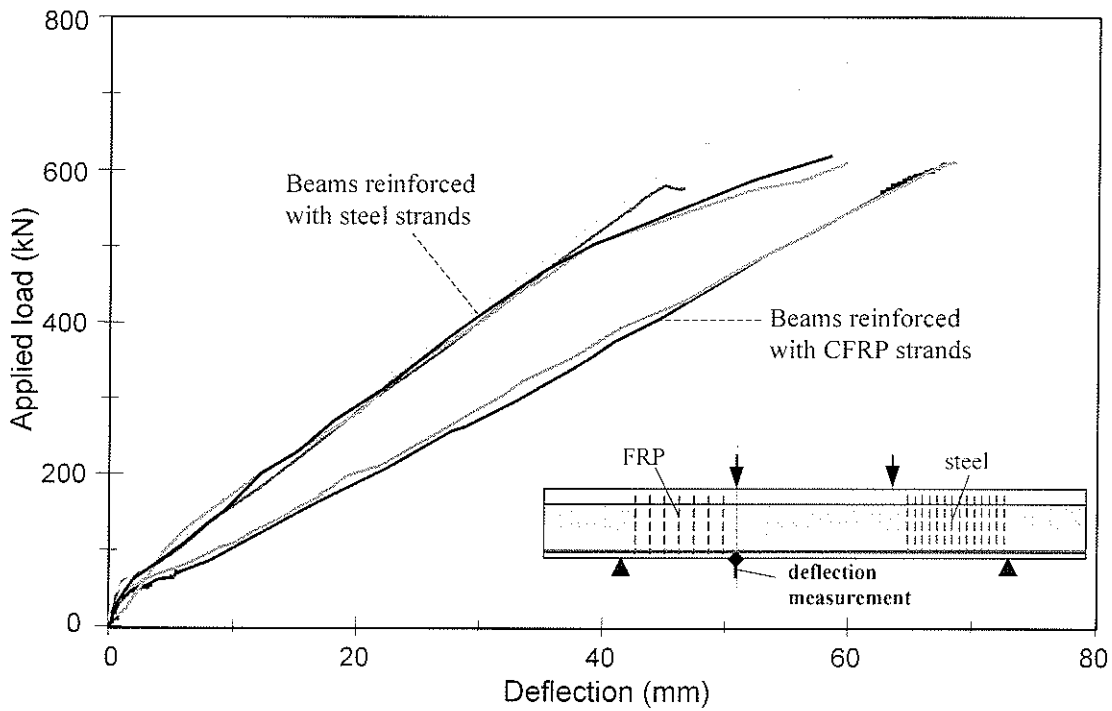


Figure 6-23. Beam CG-3 at failure



(a) Applied load versus deflection measured at midspan



(b) Applied load versus deflection measured at loading point

Figure 6-24. Load–deflection relationships: beam specimens

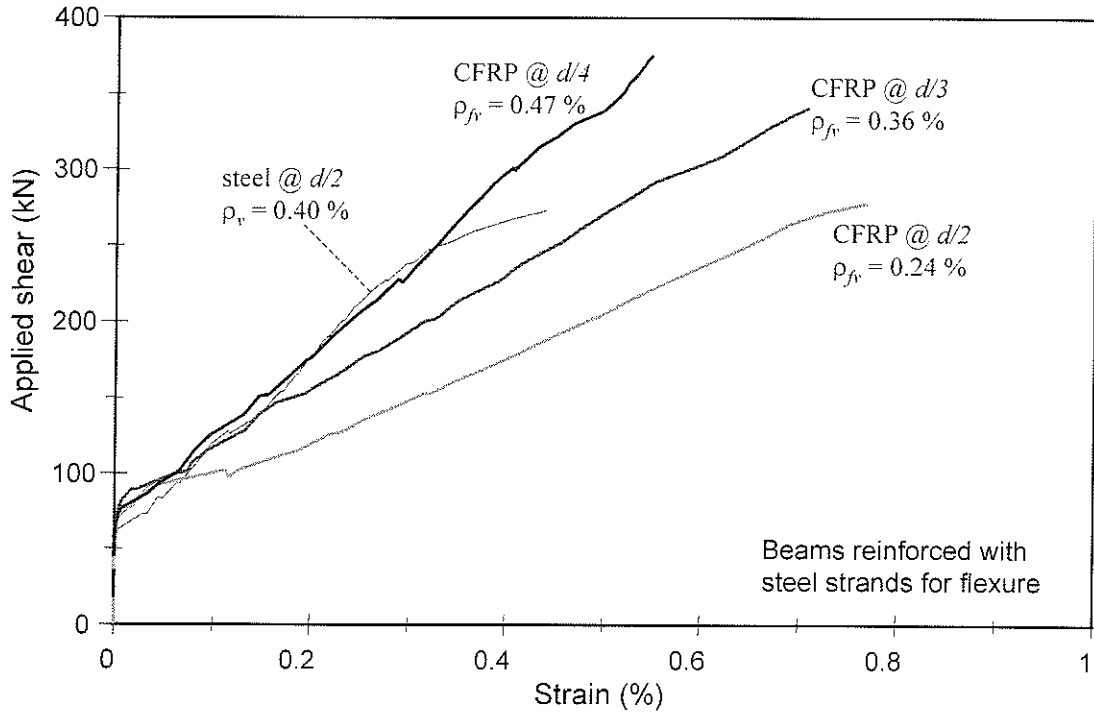


Figure 6-25. Applied shear versus average strain in stirrups: beams reinforced with CFRP stirrups

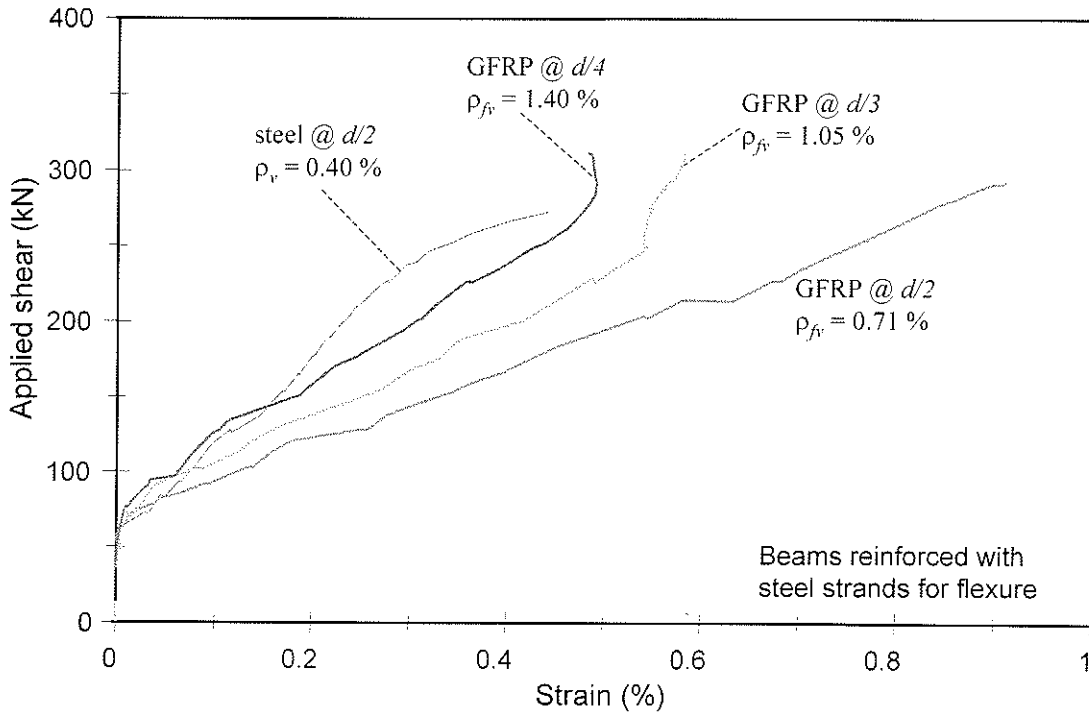


Figure 6-26. Applied shear versus average strain in stirrups: beams reinforced with GFRP stirrups

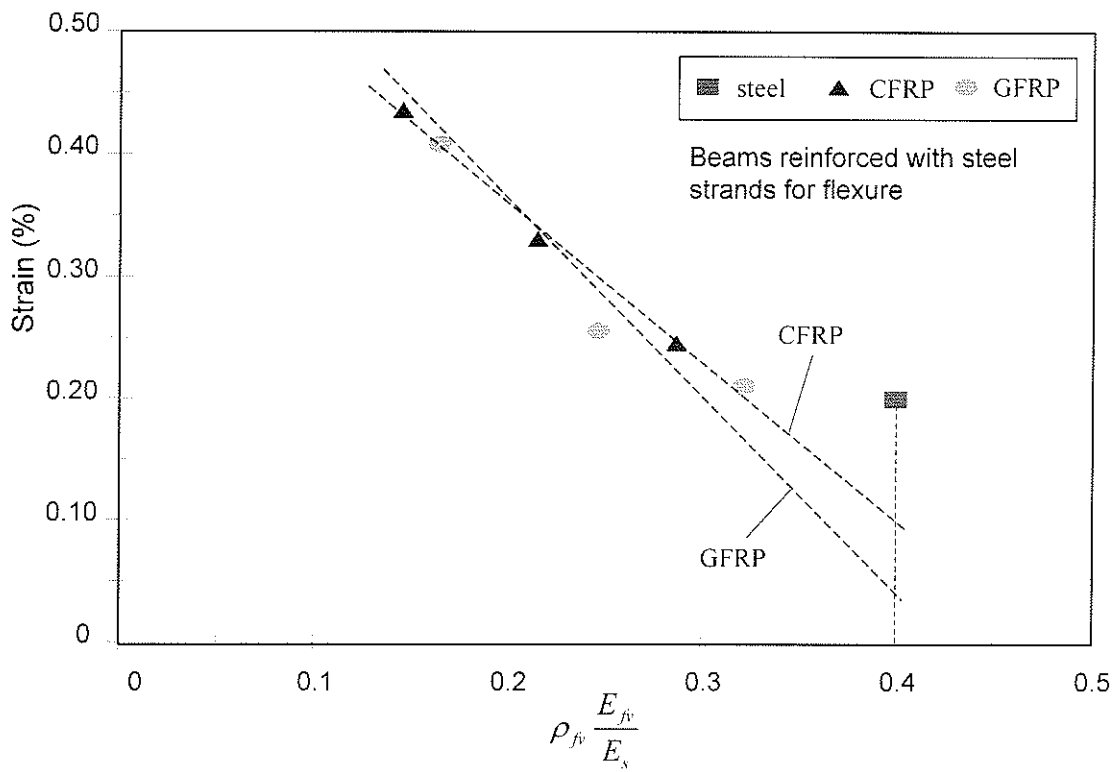
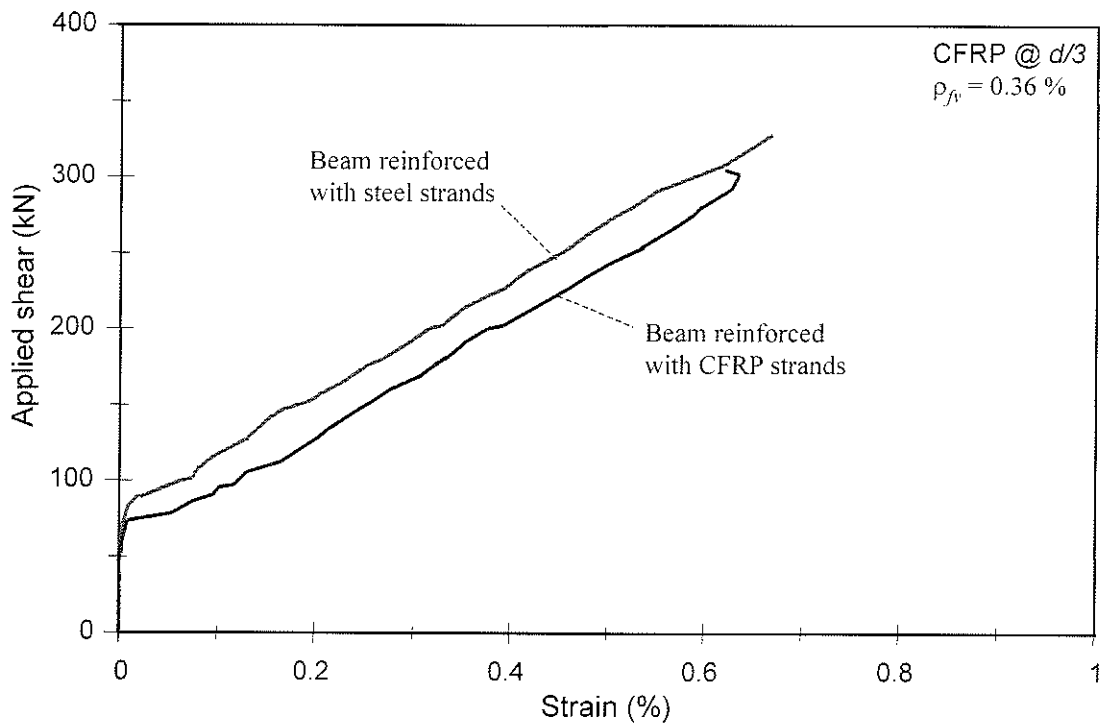
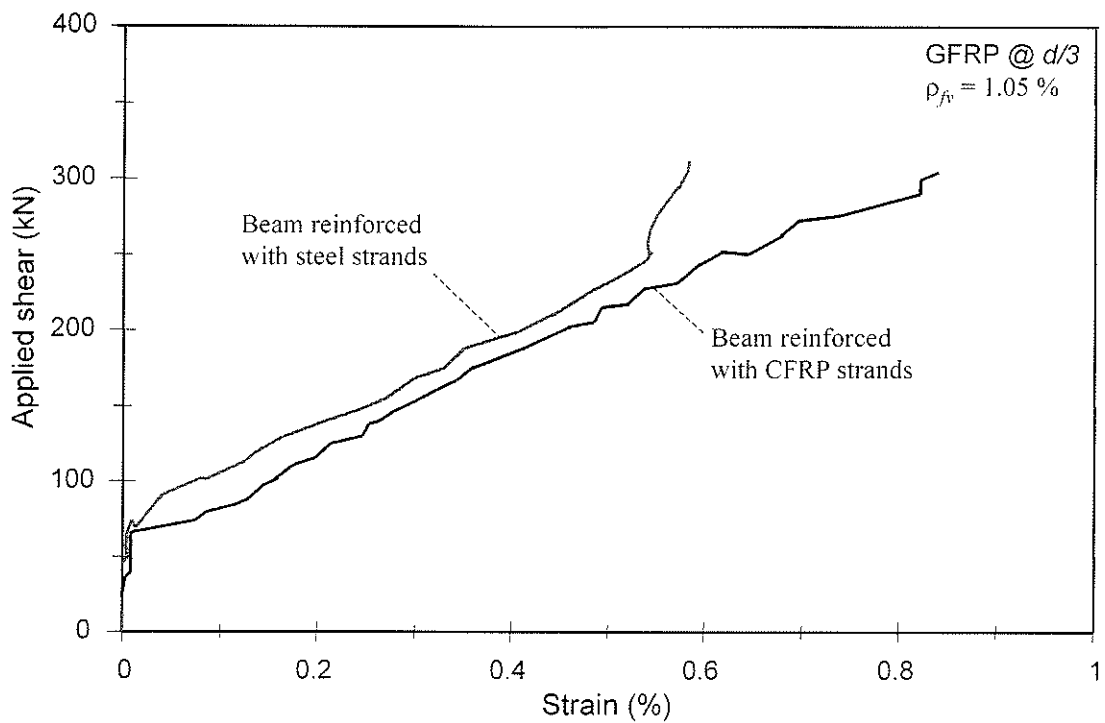


Figure 6-27. Shear reinforcement ratio versus stirrup strain at applied shear, $V = 175$ kN



(a) Beams reinforced with CFRP stirrups



(b) Beams reinforced with GFRP stirrups

Figure 6-28. Effect of flexural reinforcement on average strain in FRP stirrups

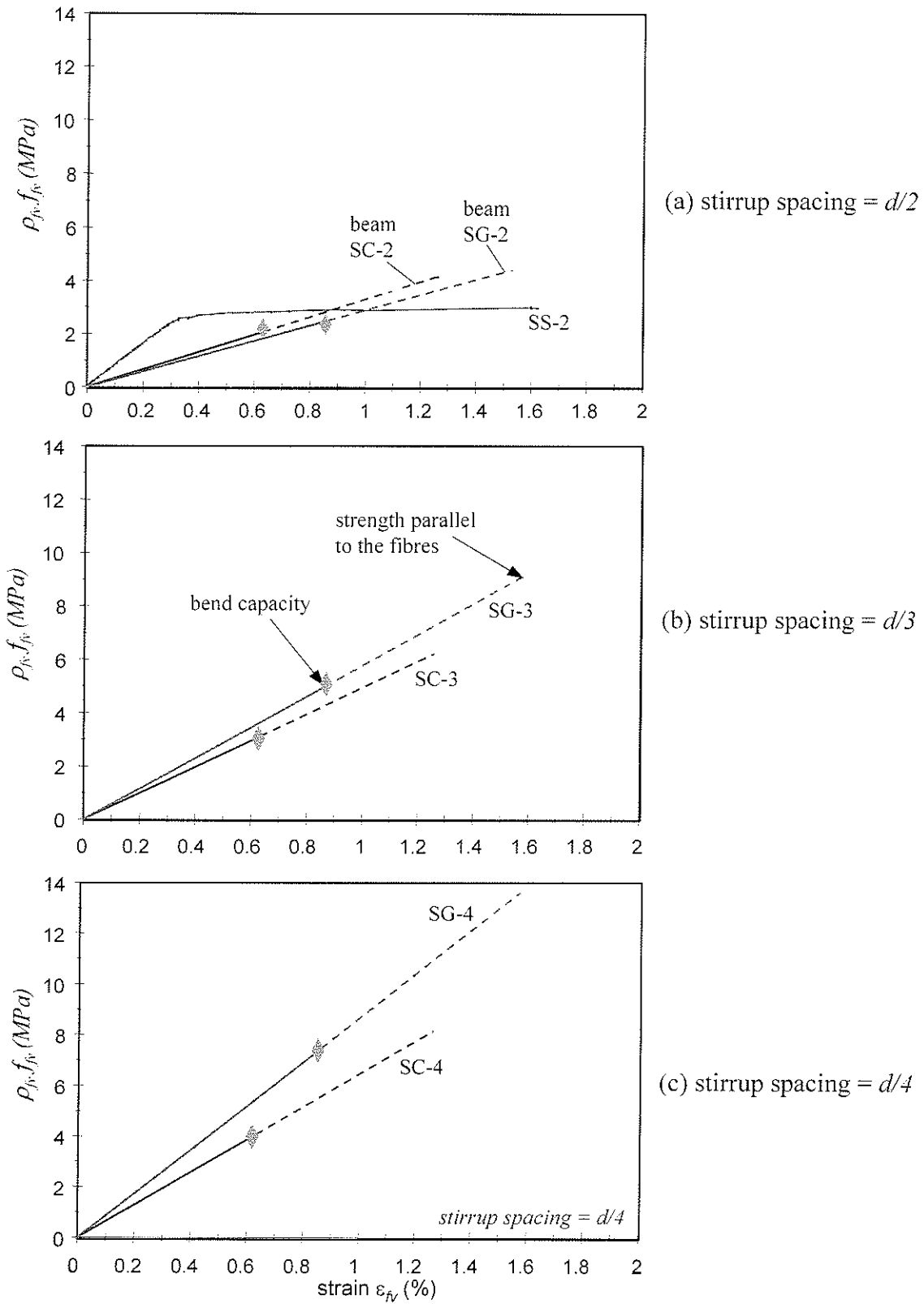


Figure 6-29. Characteristic stirrup stress $\rho_{f_v} f_{f_v}$ versus stirrup strain: beam specimens

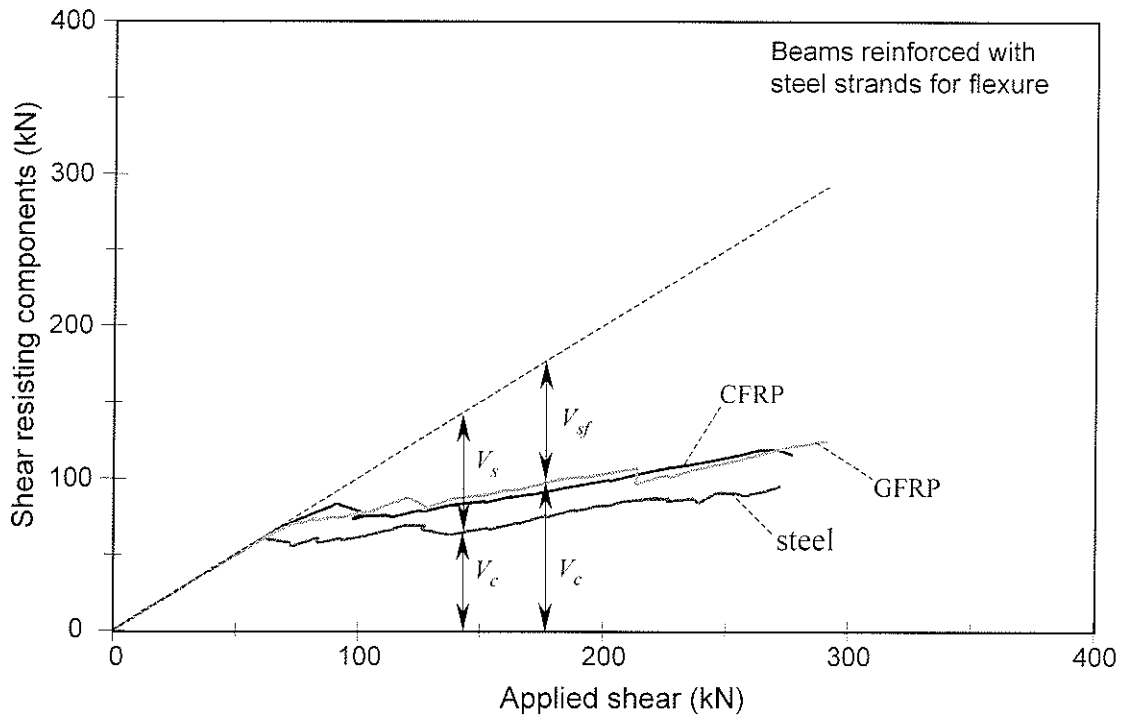


Figure 6-30. Applied shear versus shear resisting components: beams with stirrup spacing = $d/2$

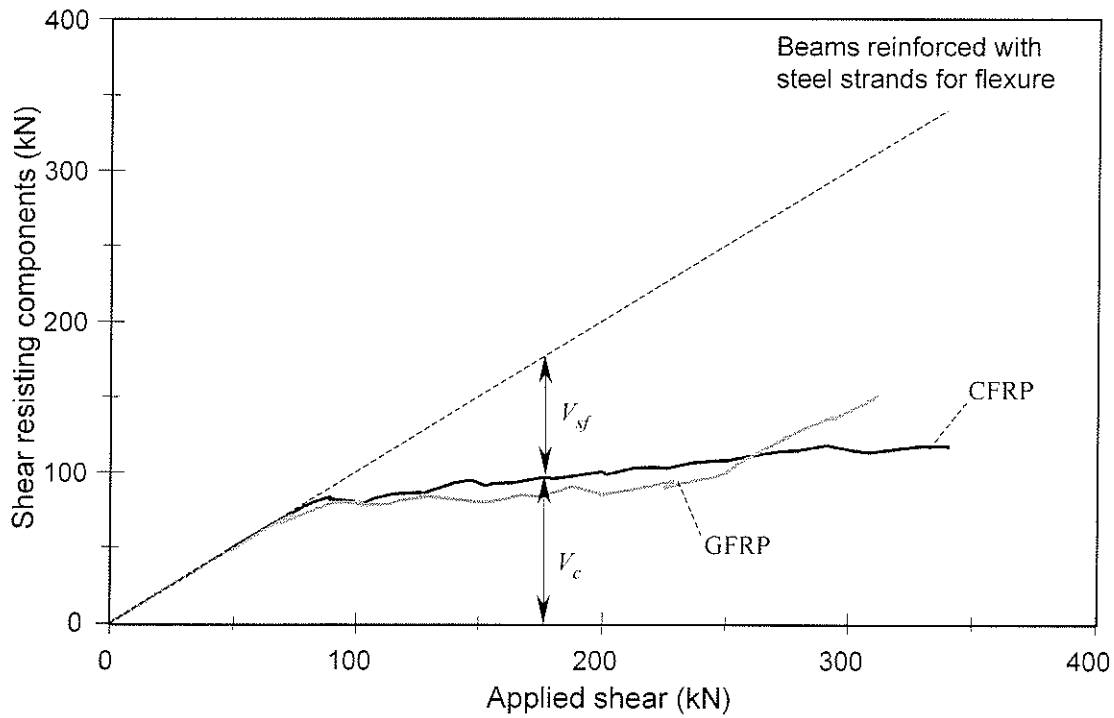


Figure 6-31. Applied shear versus shear resisting components: beams with stirrup spacing = $d/3$

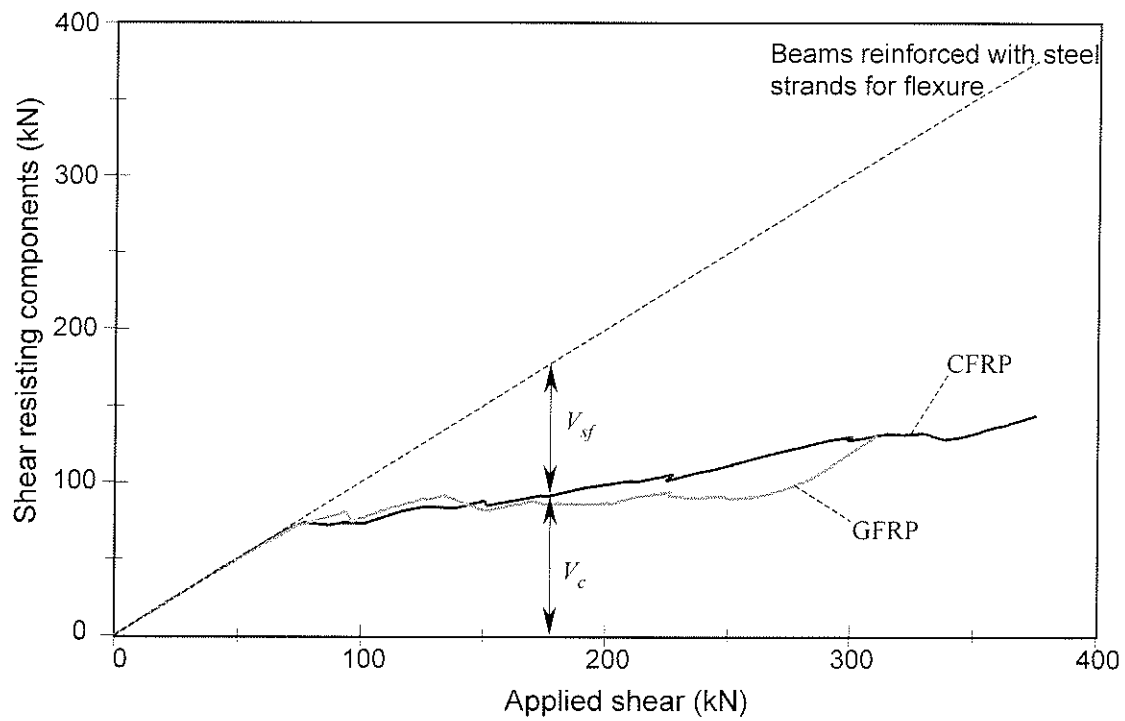
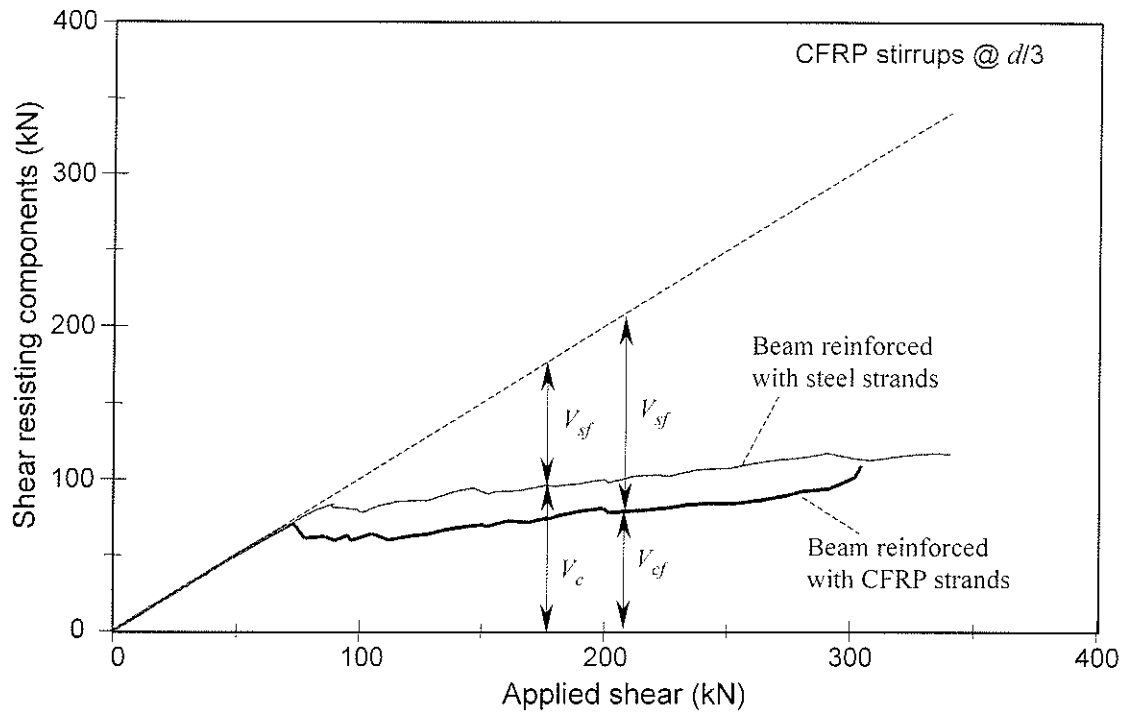
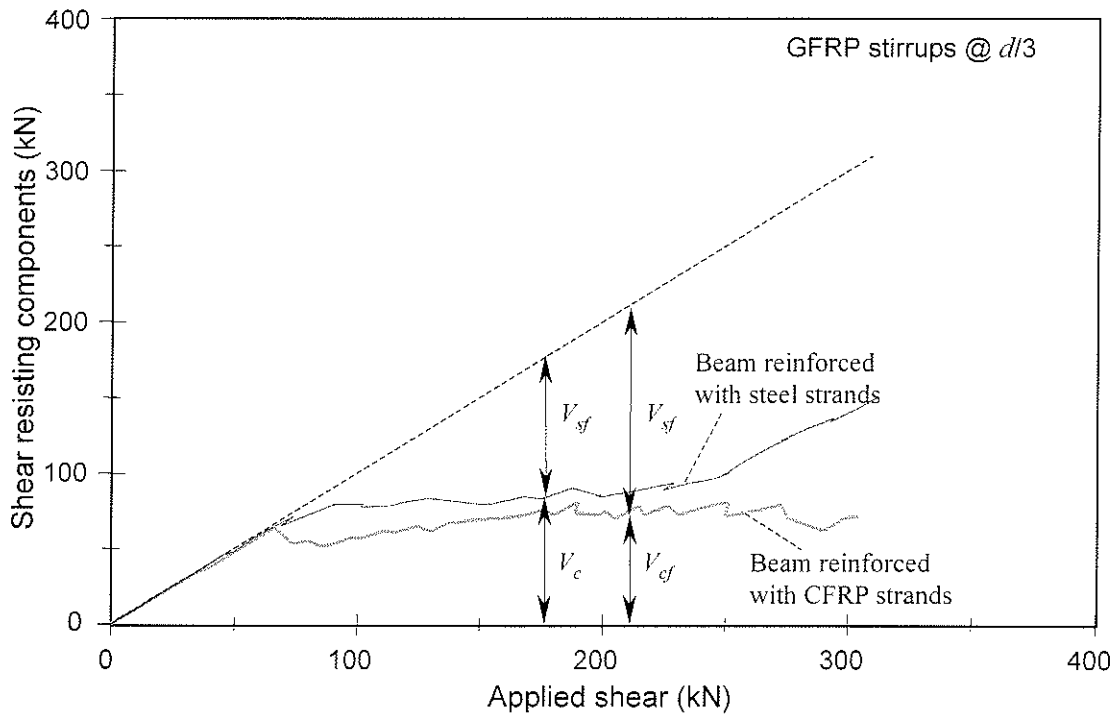


Figure 6-32. Applied shear versus shear resisting components: beams with stirrup spacing = $d/4$



(a) Beams reinforced with CFRP stirrups



(b) Beams reinforced with GFRP stirrups

Figure 6-33. Effect of flexural reinforcement on shear resisting components

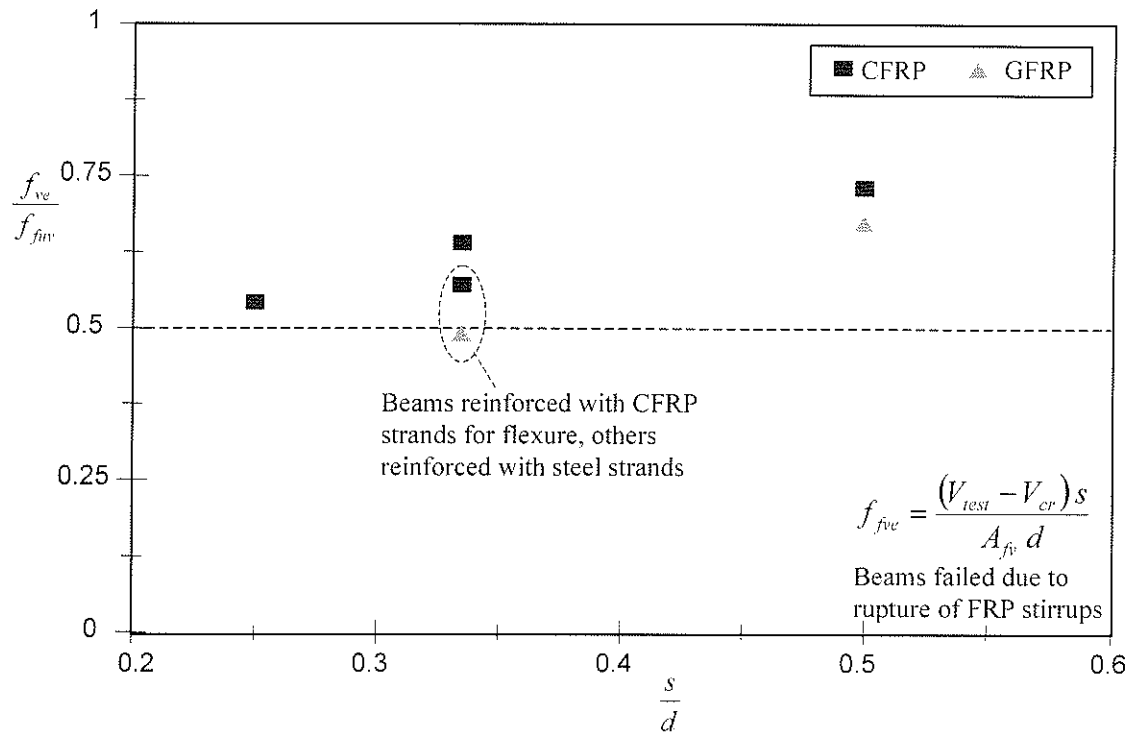
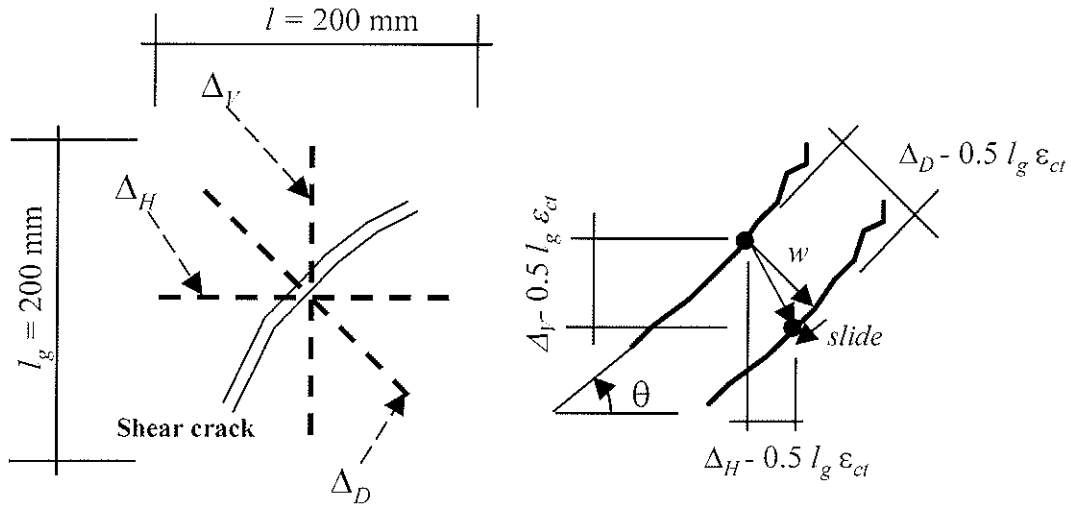


Figure 6-34. Effect of stirrup spacing on effective capacity of FRP stirrups



Typical PI-gauge station in the shear span

Figure 6-35. Determination of shear crack width

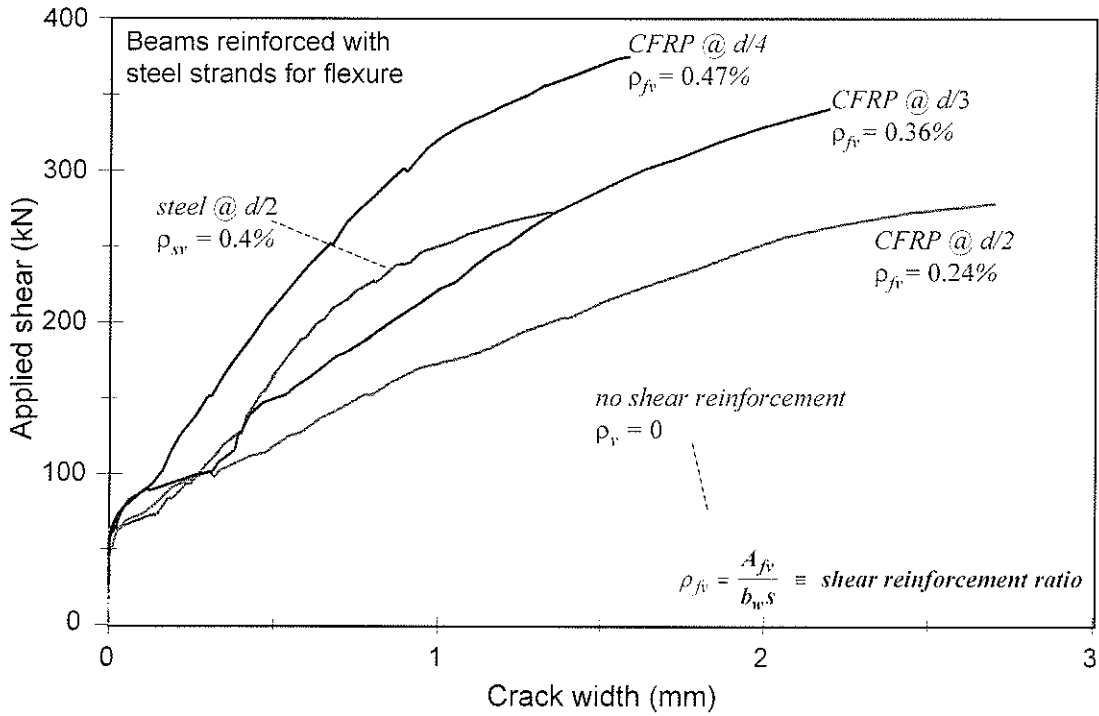


Figure 6-36. Applied shear versus crack width: beams reinforced with CFRP stirrups

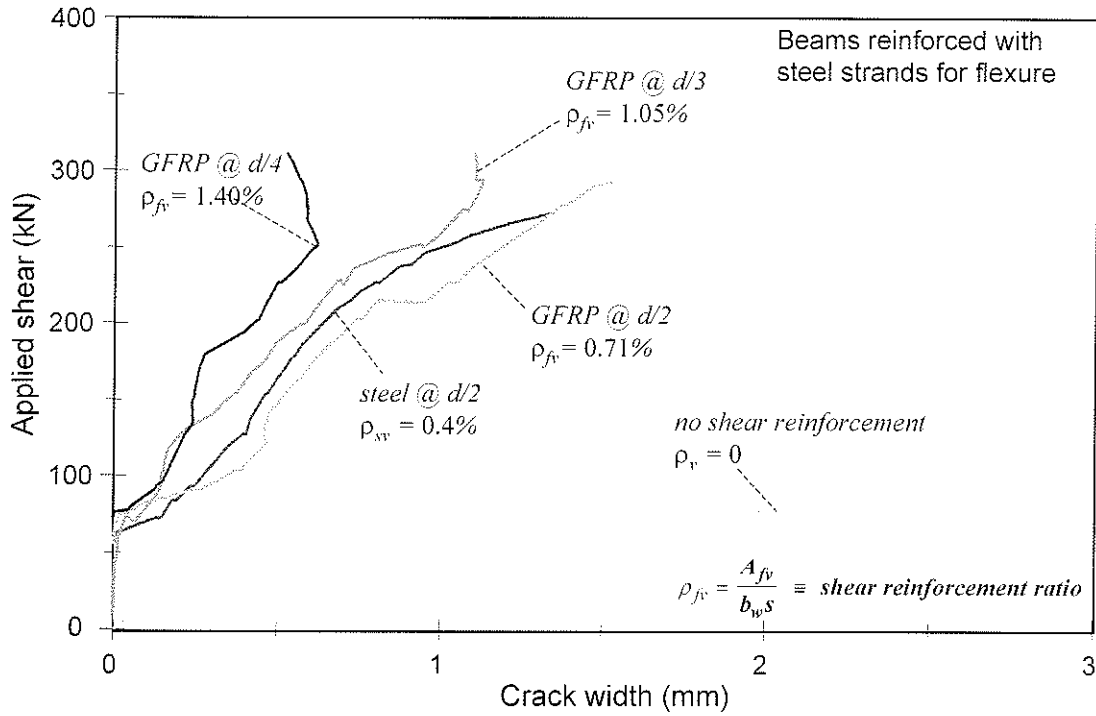


Figure 6-37. Applied shear versus crack width: beams reinforced with GFRP stirrups

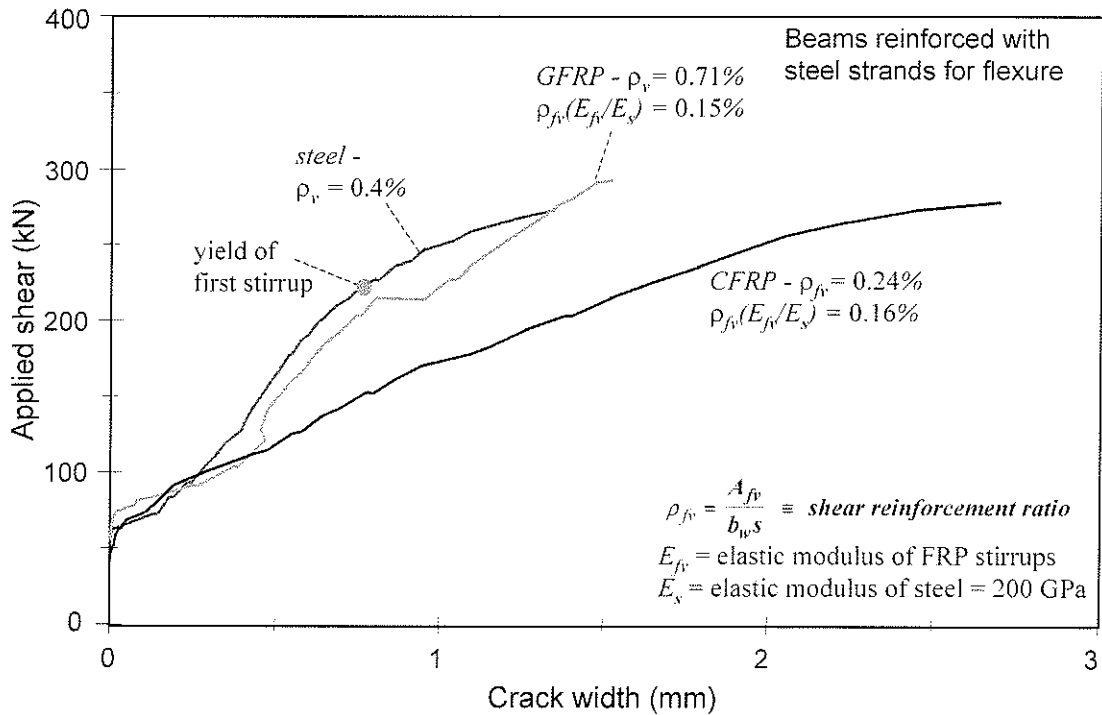
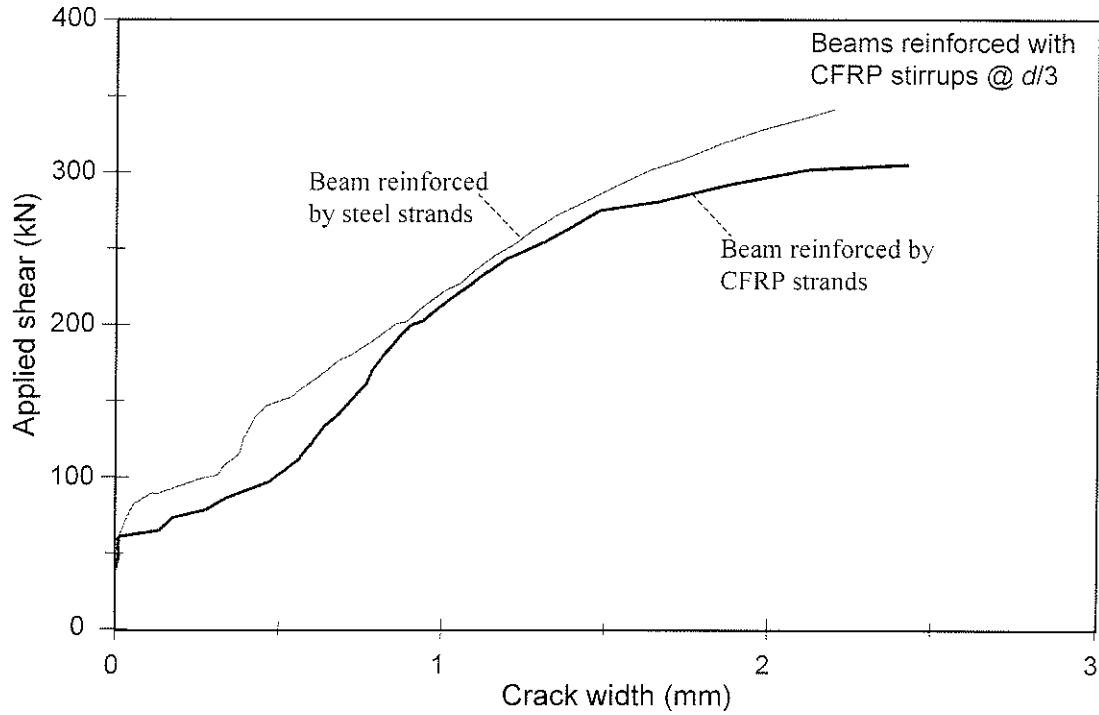
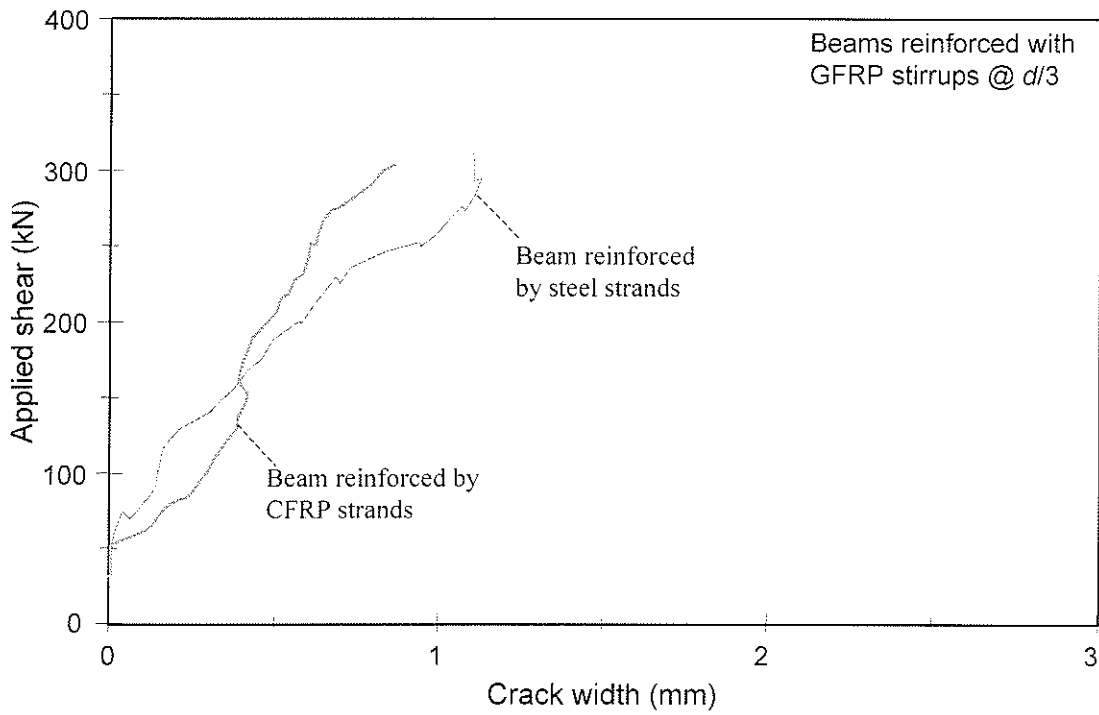


Figure 6-38. Applied shear versus crack width: beams reinforced with stirrups spaced at $d/2$



(a) Beams reinforced with CFRP stirrups



(b) Beams reinforced with GFRP stirrups

Figure 6-39. Effect of flexural reinforcement on shear crack width - beam specimens

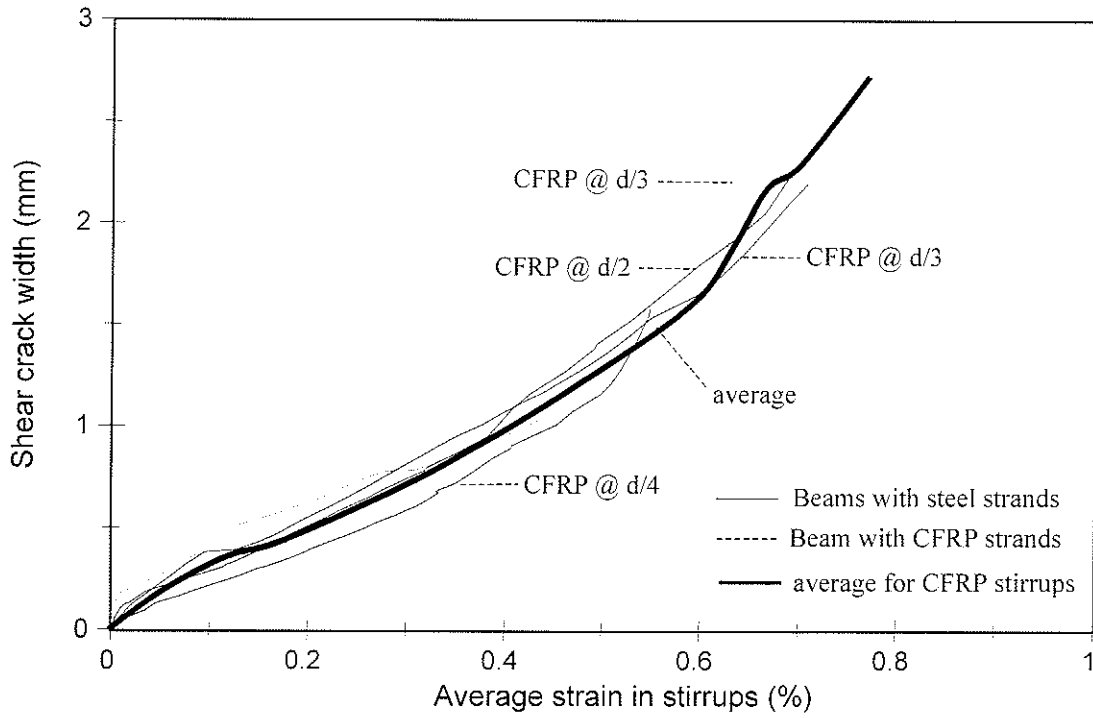


Figure 6-40. Shear crack width versus average strain in stirrups - beams reinforced with CFRP stirrups

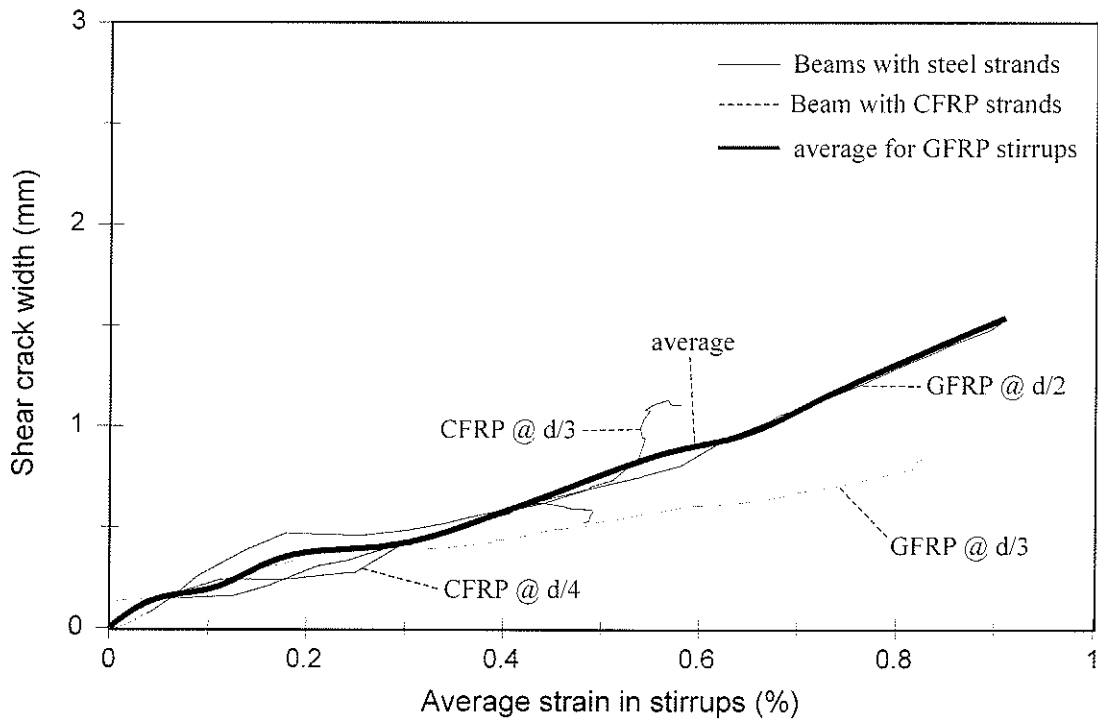


Figure 6-41. Shear crack width versus average strain in stirrups - beams reinforced with CFRP stirrups

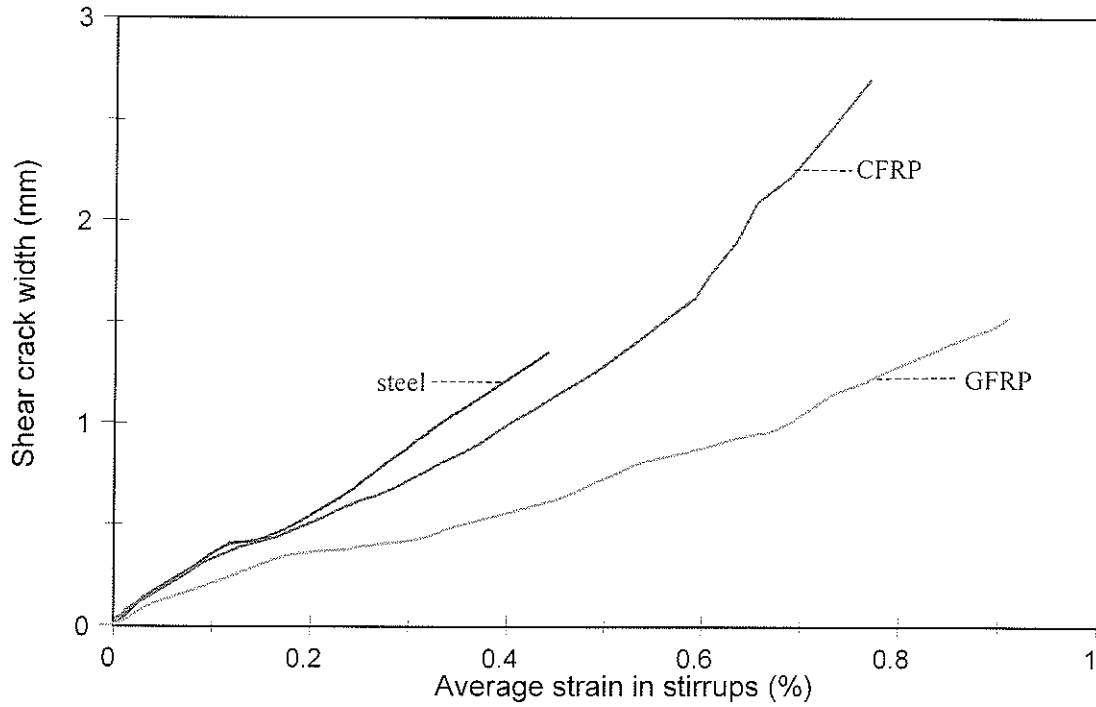


Figure 6-42. Effect of stirrup material on shear crack width

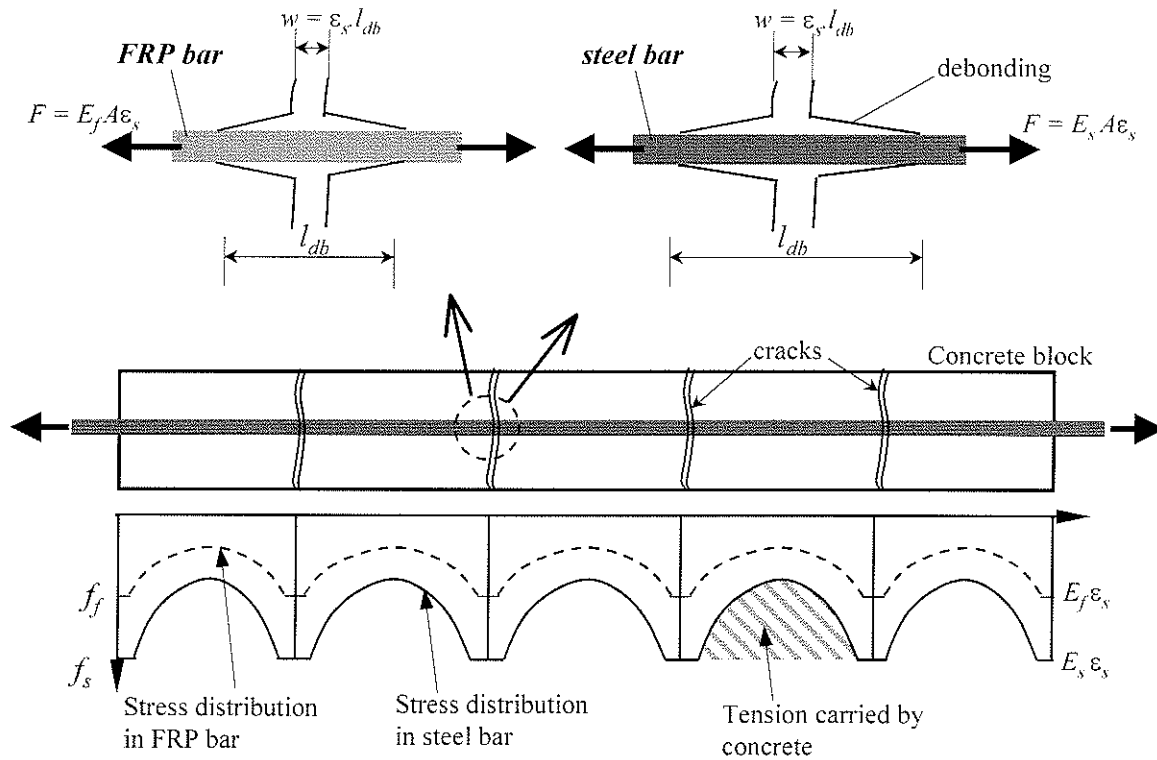


Figure 6-43. Effect of elastic modulus of reinforcing bar on crack width

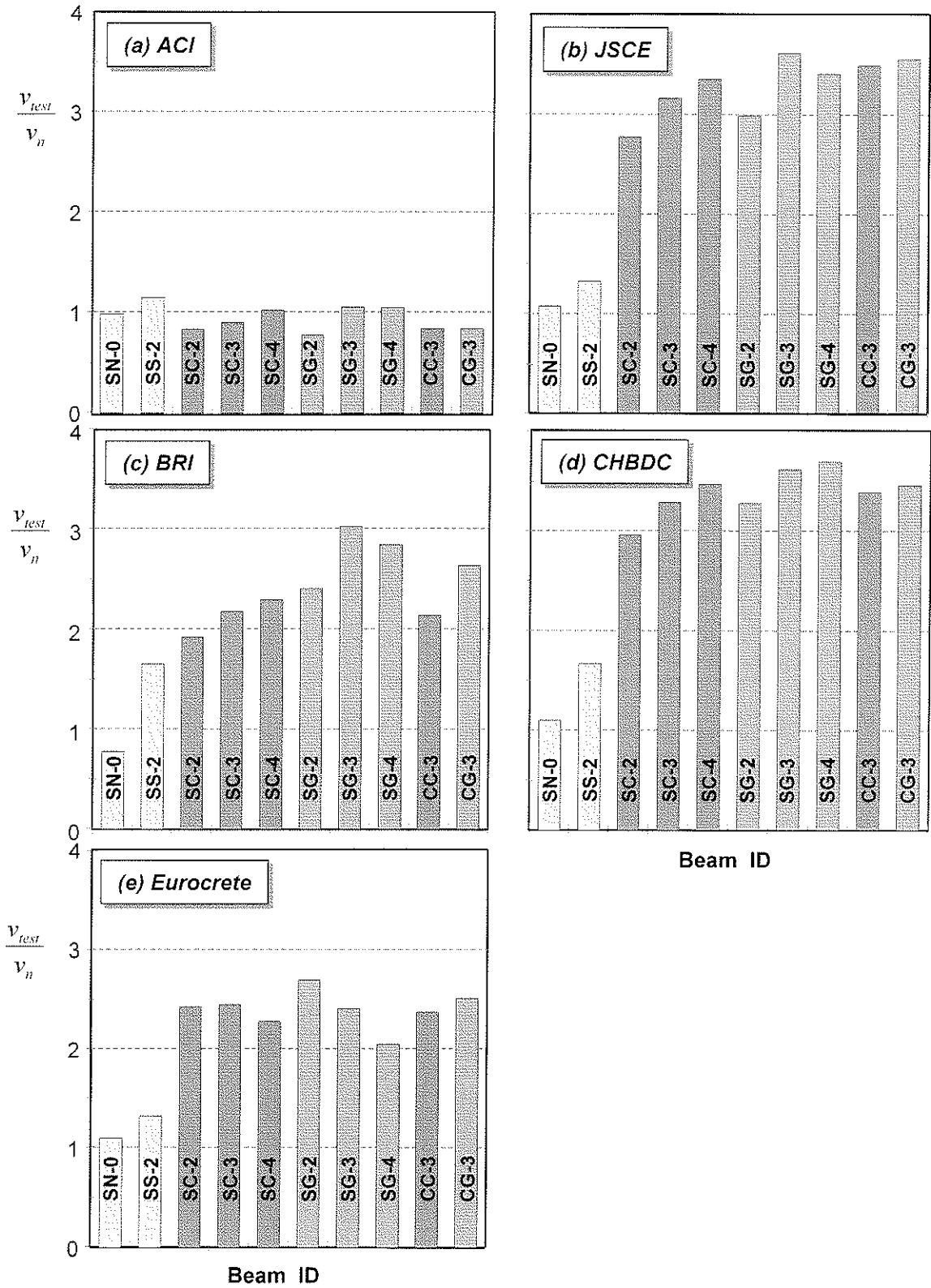


Figure 6-44. Measured ultimate shear stress versus calculated from : (a) ACI318-95 Code (1995), (b) JSCE model (1997), (c) BRI model (1997), (d) CHBDC Code (1998), and (e) Eurocrete model (1996); for tested beams

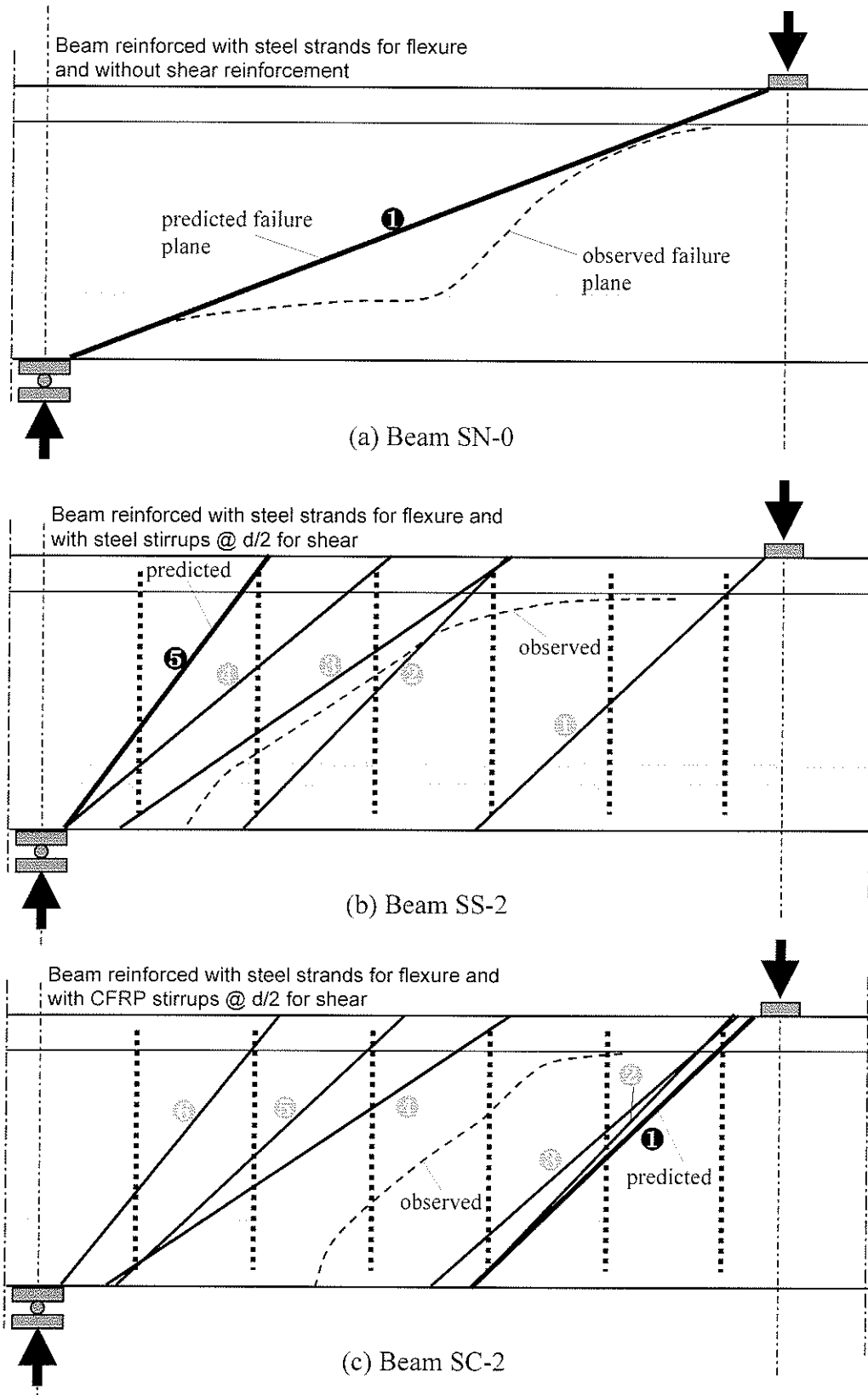


Figure 6-45. Potential failure planes in beams analyzed using shear friction model (SFM)

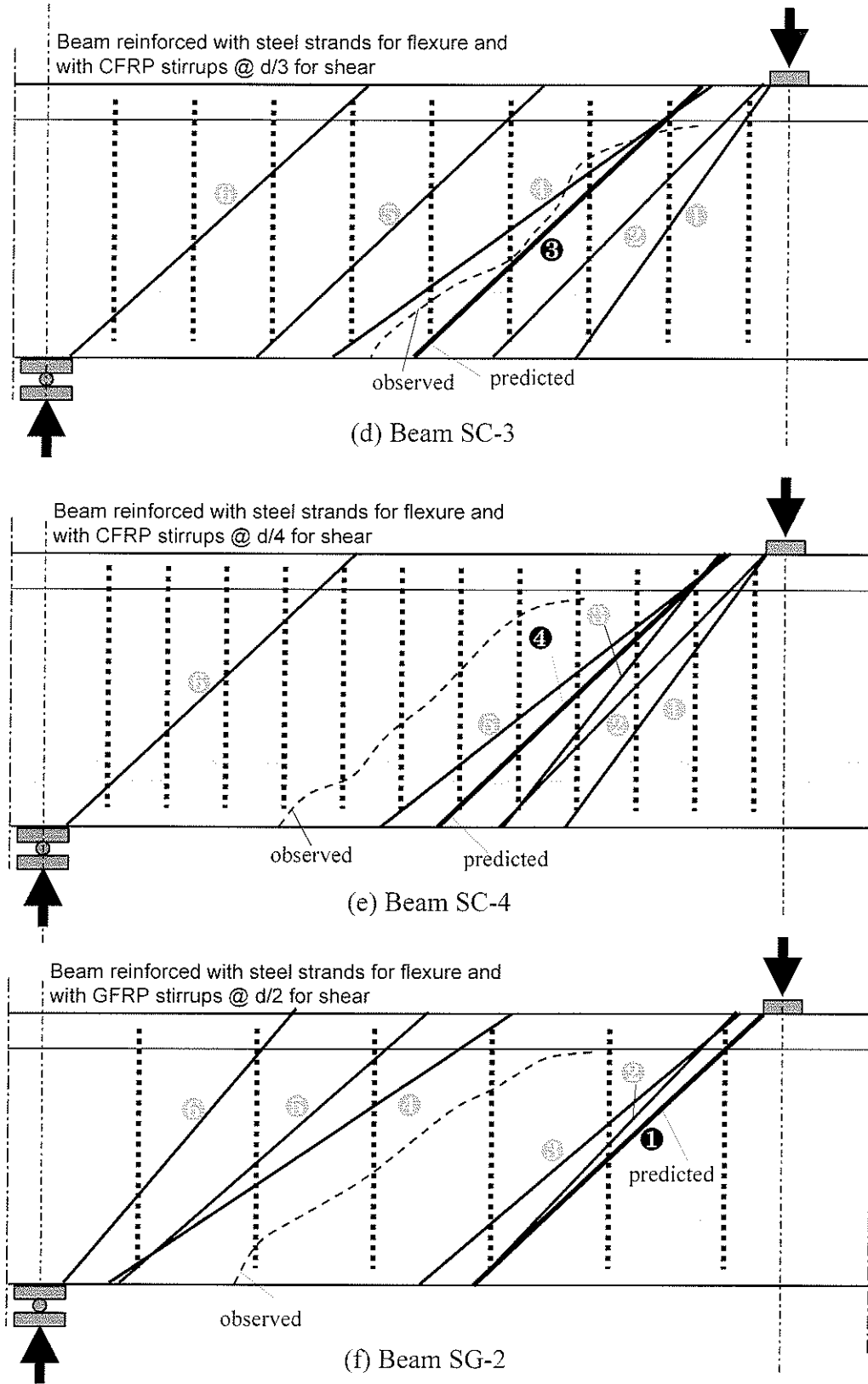


Figure 6-45(cont'd). Potential failure planes in beams analyzed using shear friction model (SFM)

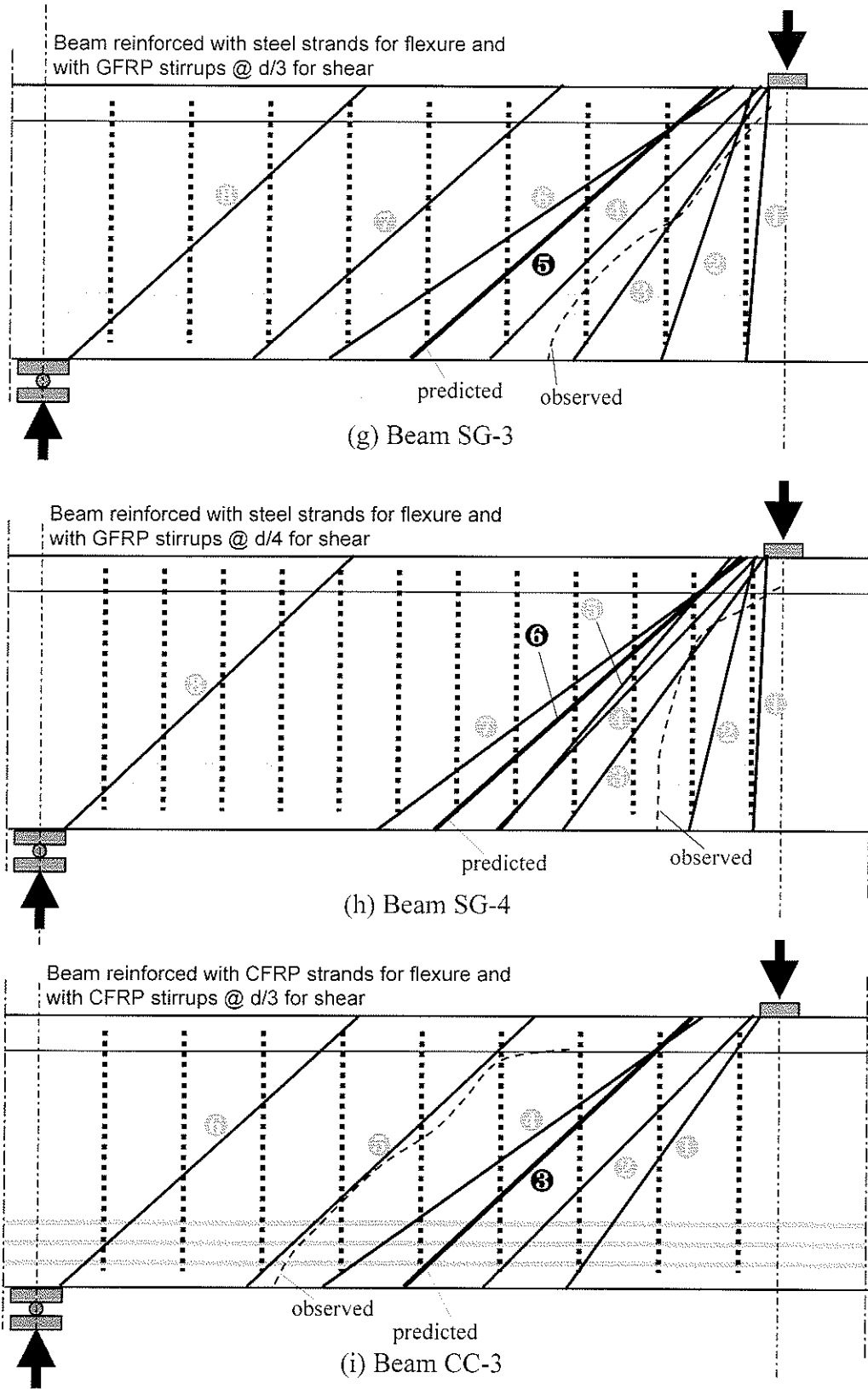


Figure 6-45(cont'd). Potential failure planes in beams analyzed using shear friction model (SFM)

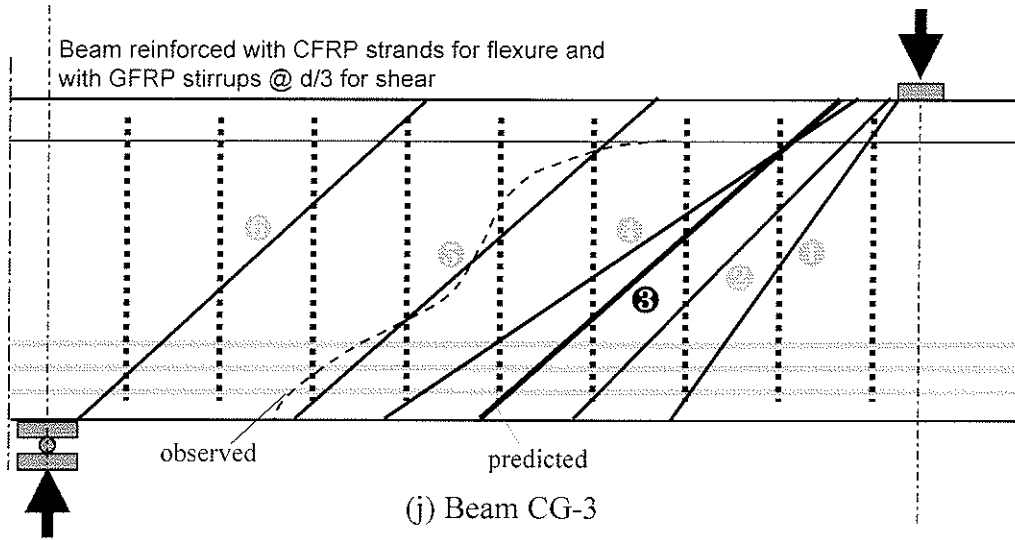


Figure 6-45(cont'd). Potential failure planes in beams analyzed using shear friction model (SFM)

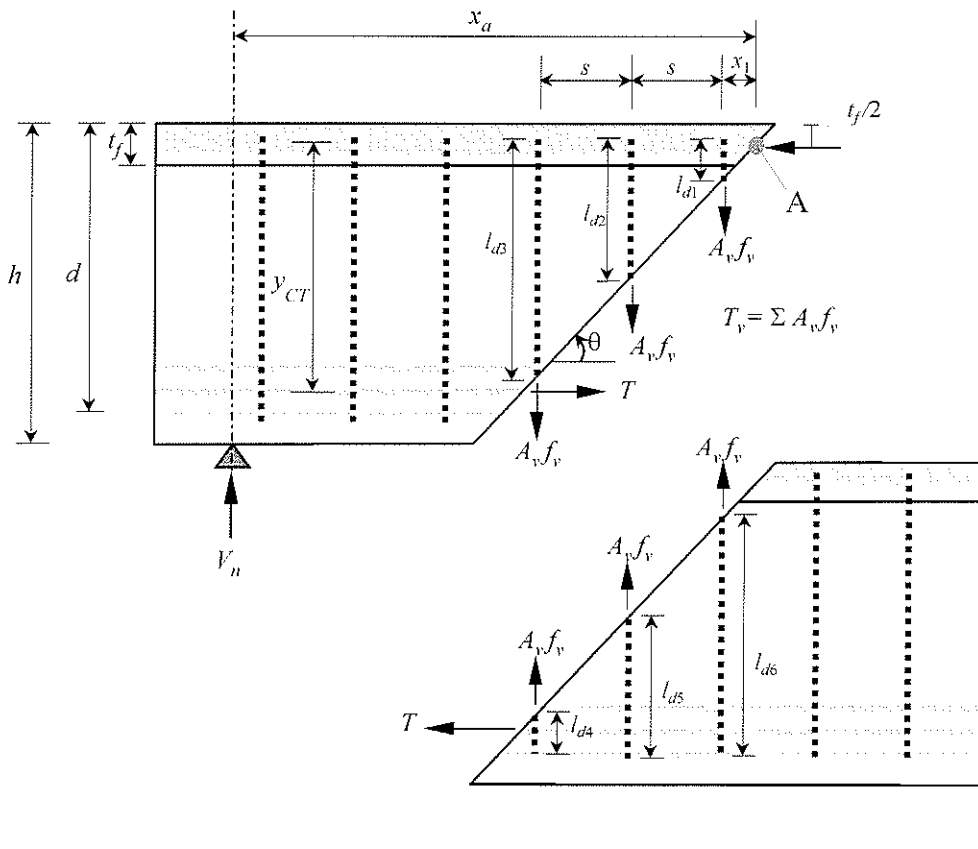


Figure 6-46. Internal forces at a potential failure plane: SFM

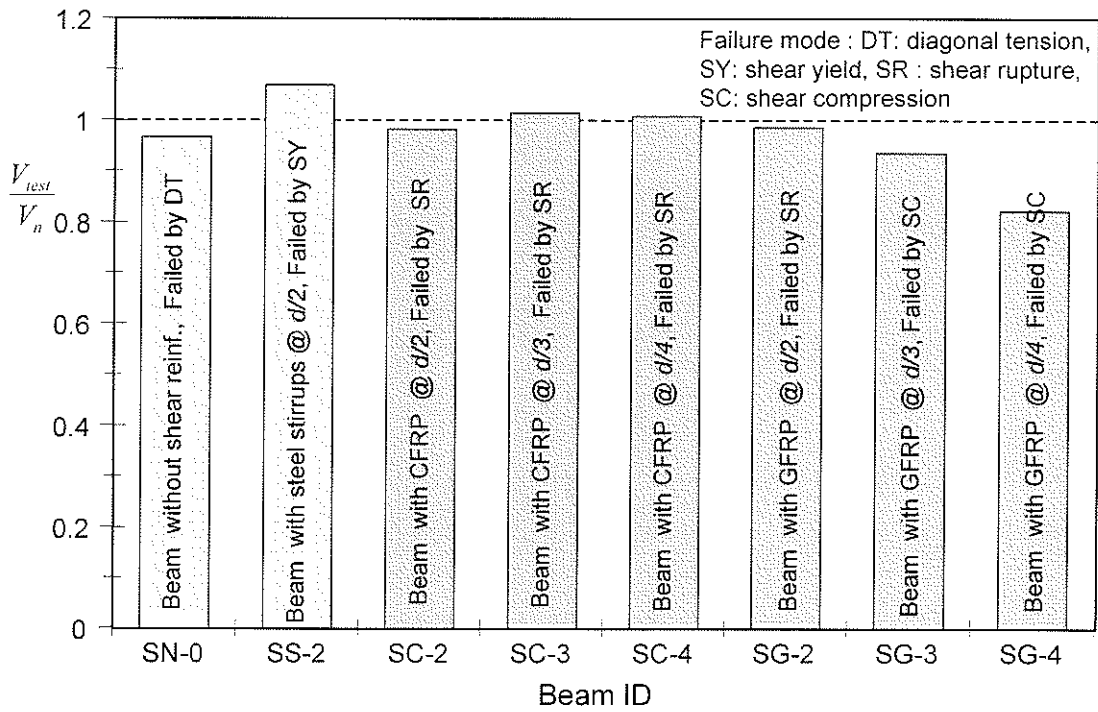


Figure 6-47. Measured shear strength versus calculated using the SFM for beams reinforced with steel strands

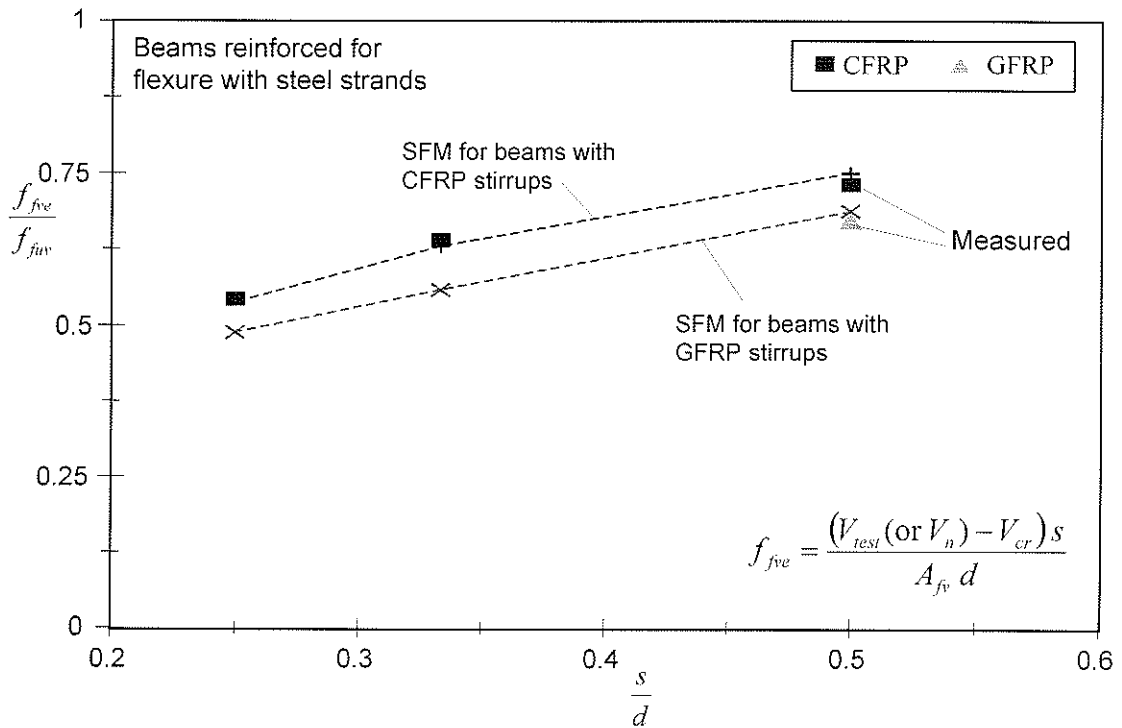


Figure 6-48. Effect of stirrup spacing on effective capacity of FRP stirrups in beam action: Measured versus SFM

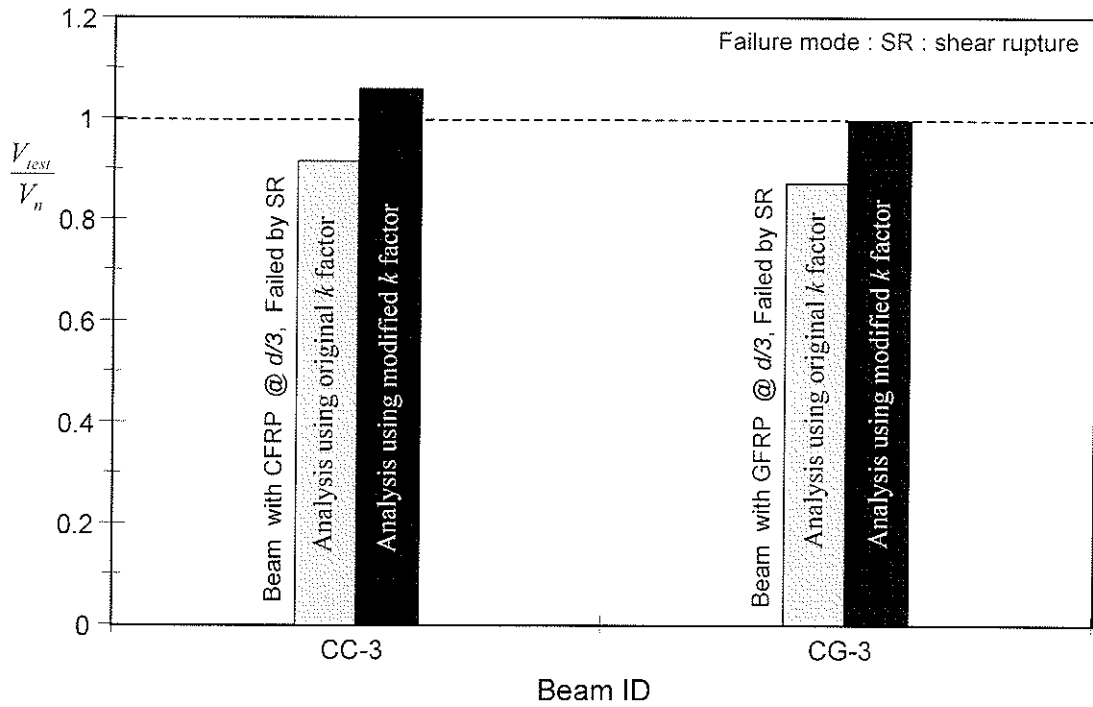


Figure 6-49. Measured shear strength versus calculated using the SFM for beams reinforced with CFRP strands

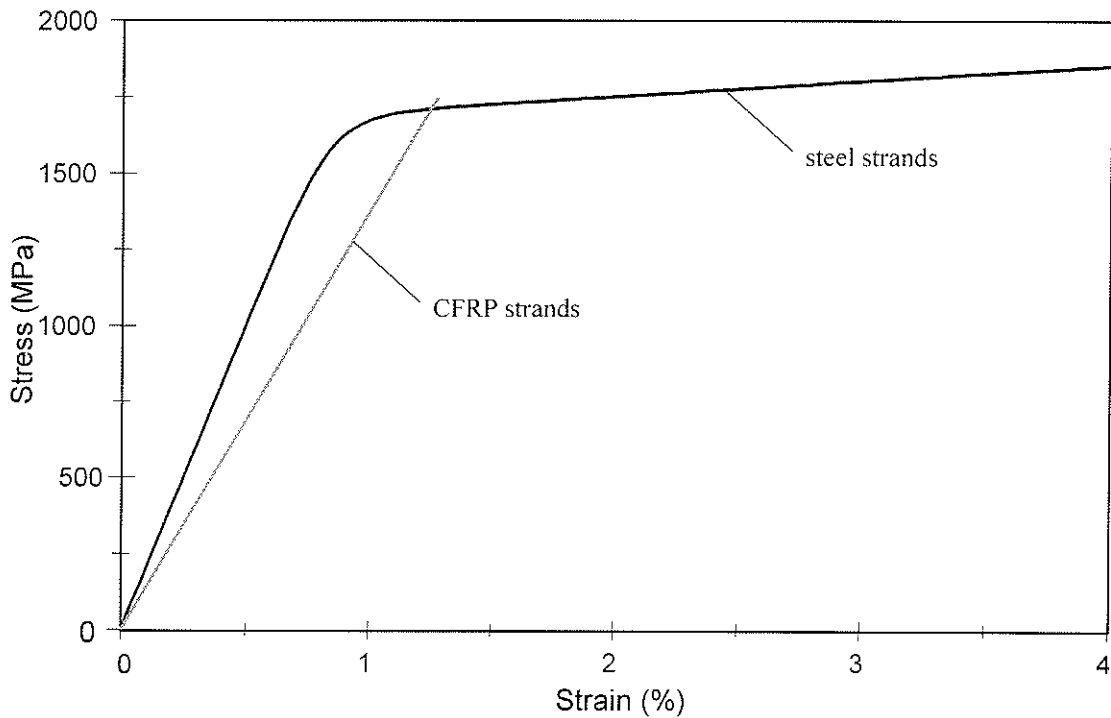


Figure 6-50. Stress-strain relationships used to model the longitudinal reinforcement for the Modified compression field theory (MCFT)

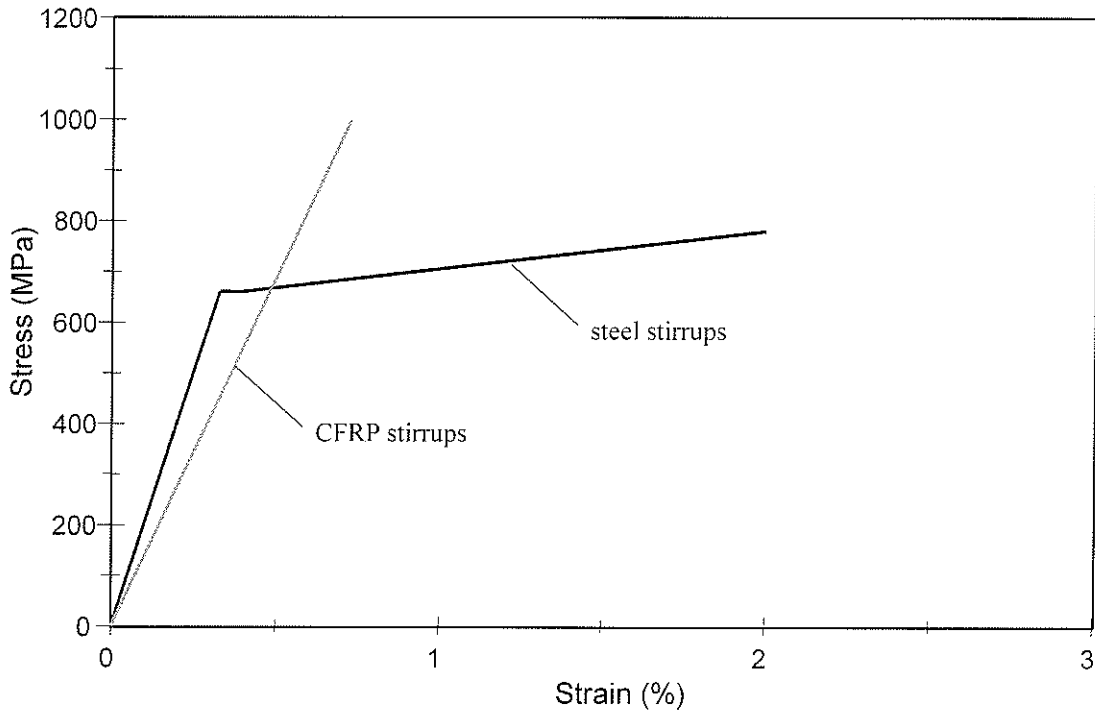


Figure 6-51. Stress-strain relationships used to model the shear reinforcement for the MCFT

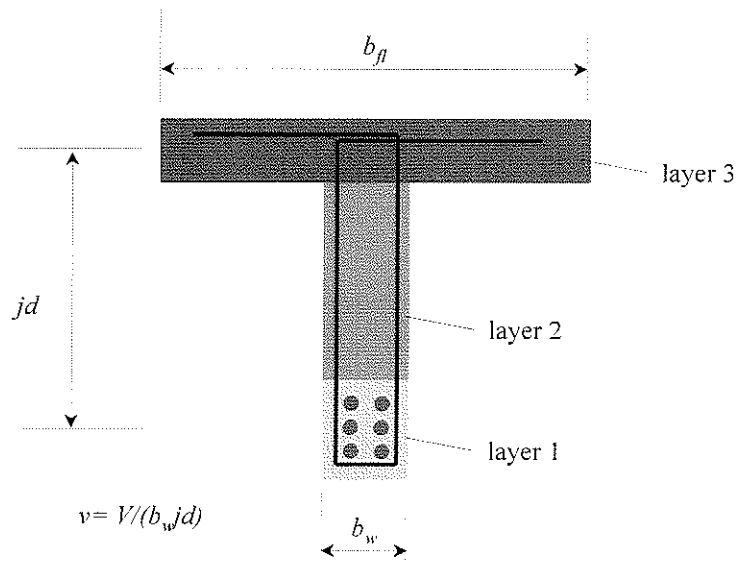


Figure 6-52. Modelling of the beam section as three concrete layers for the MCFT

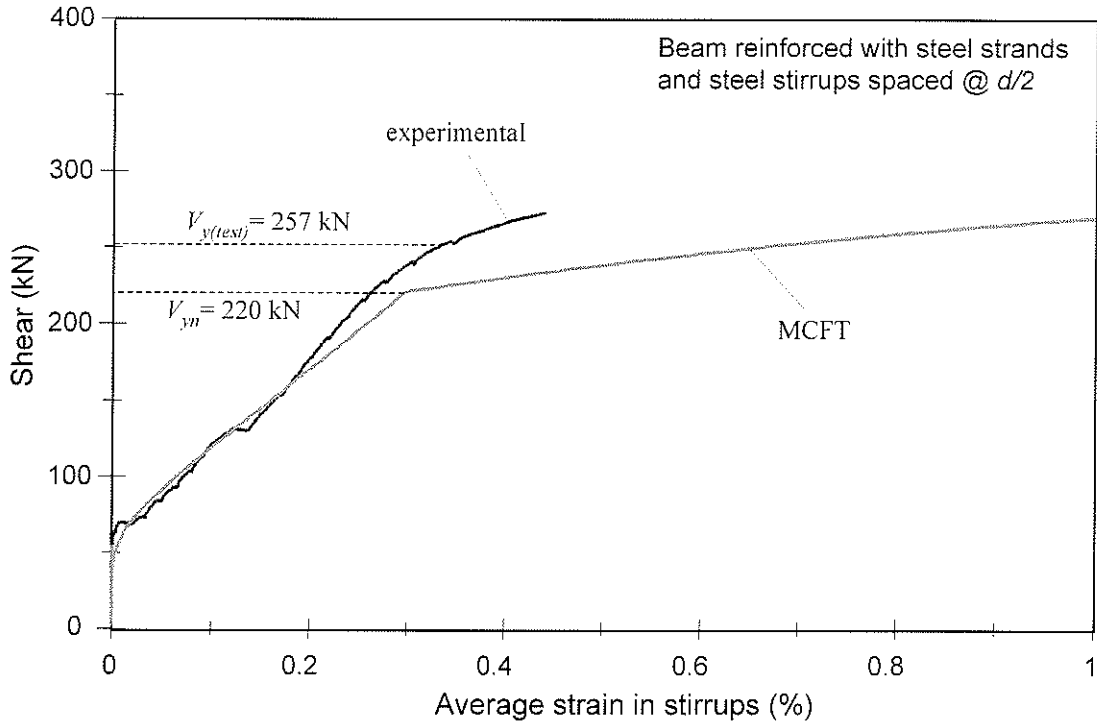


Figure 6-53. Shear versus average strain in stirrups as predicted using MCFT for beam SS-2

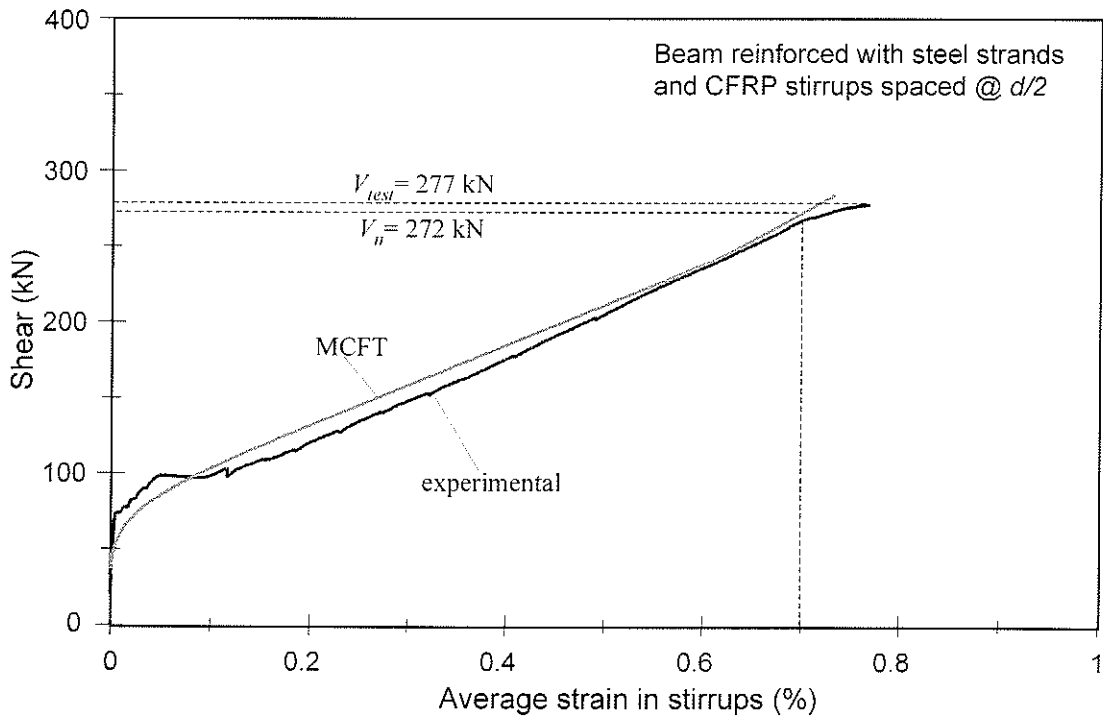


Figure 6-54. Shear versus average strain in stirrups as predicted using MCFT for beam SC-2

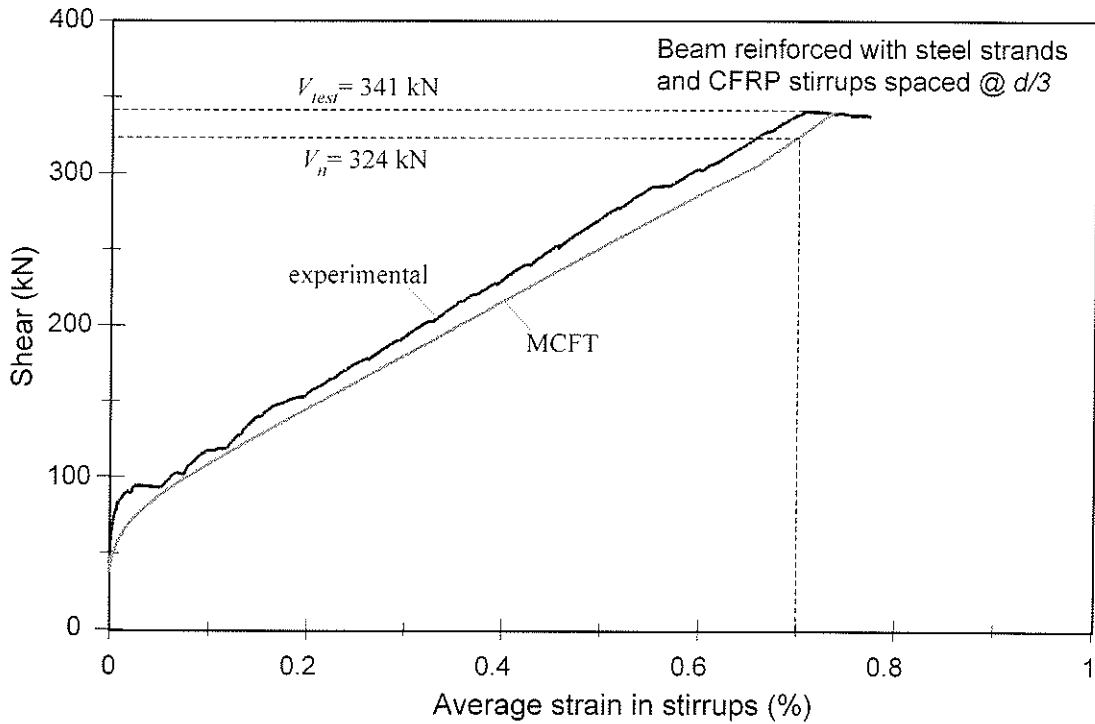


Figure 6-55. Shear versus average strain in stirrups as predicted using MCFT for beam SC-3

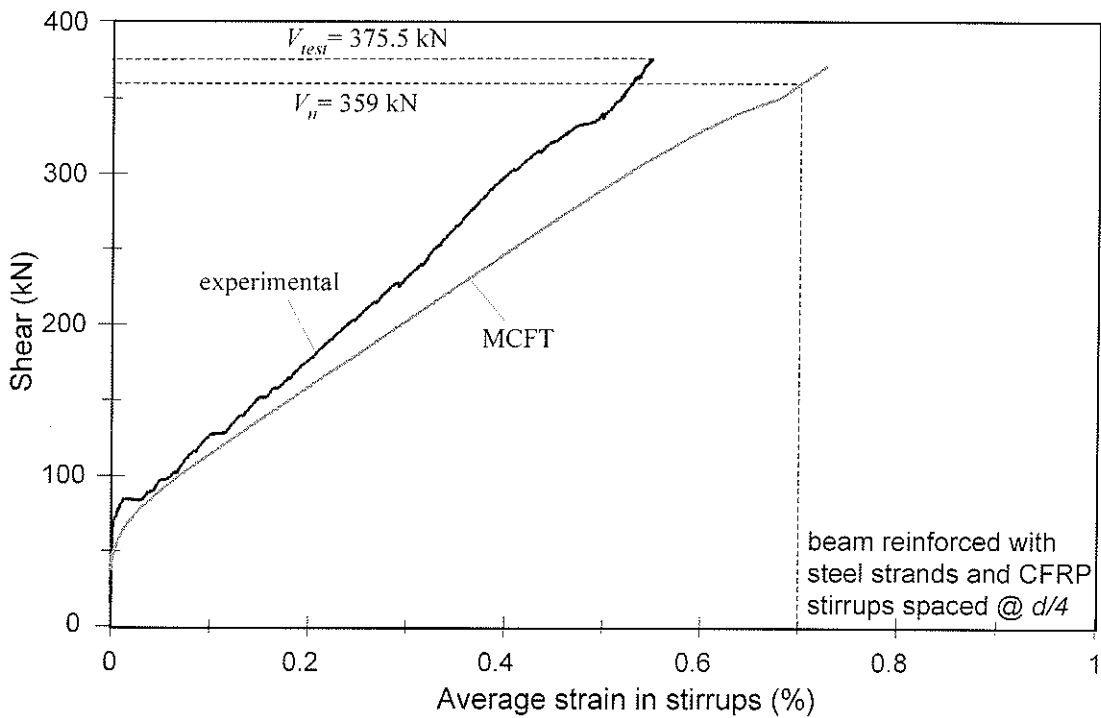


Figure 6-56. Shear versus average strain in stirrups as predicted using MCFT for beam SC-4

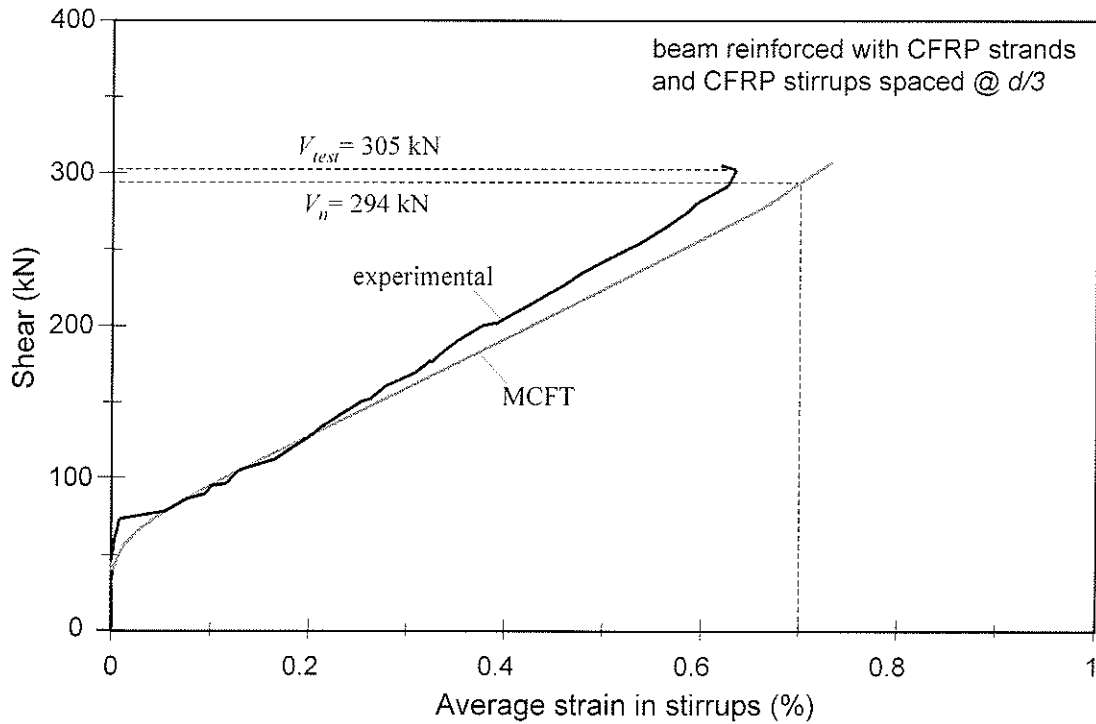


Figure 6-57. Shear versus average strain in stirrups as predicted using MCFT for beam CC-3

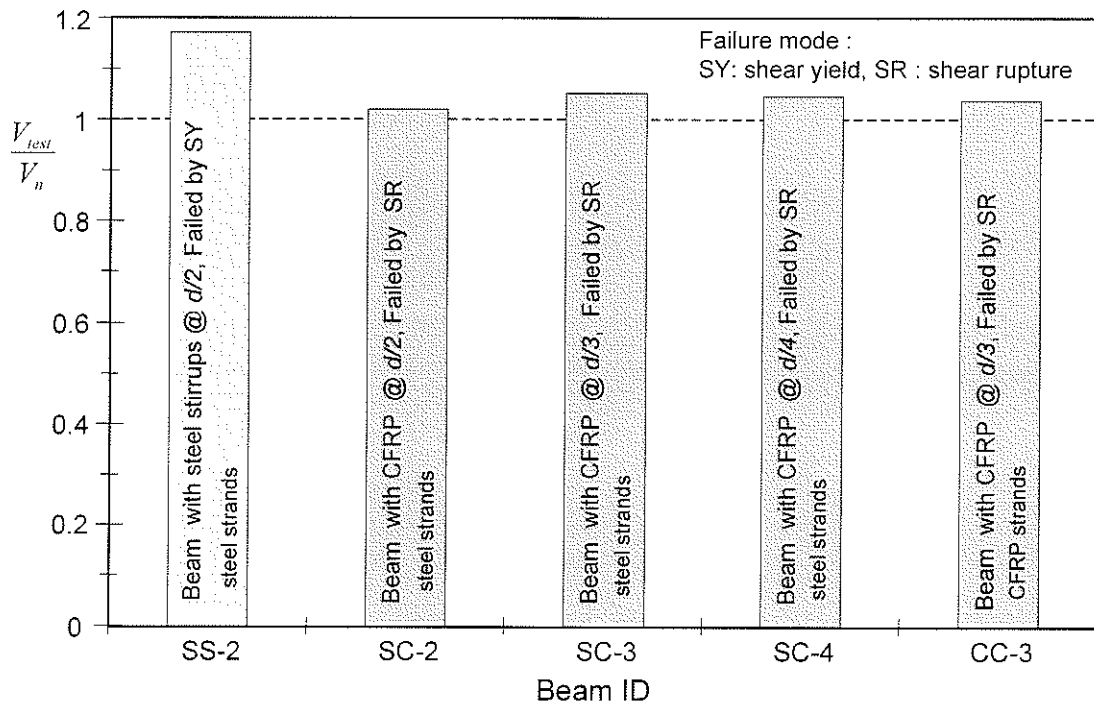


Figure 6-58. Measured shear strength versus calculated using the MCFT for beams reinforced with steel or CFRP stirrups

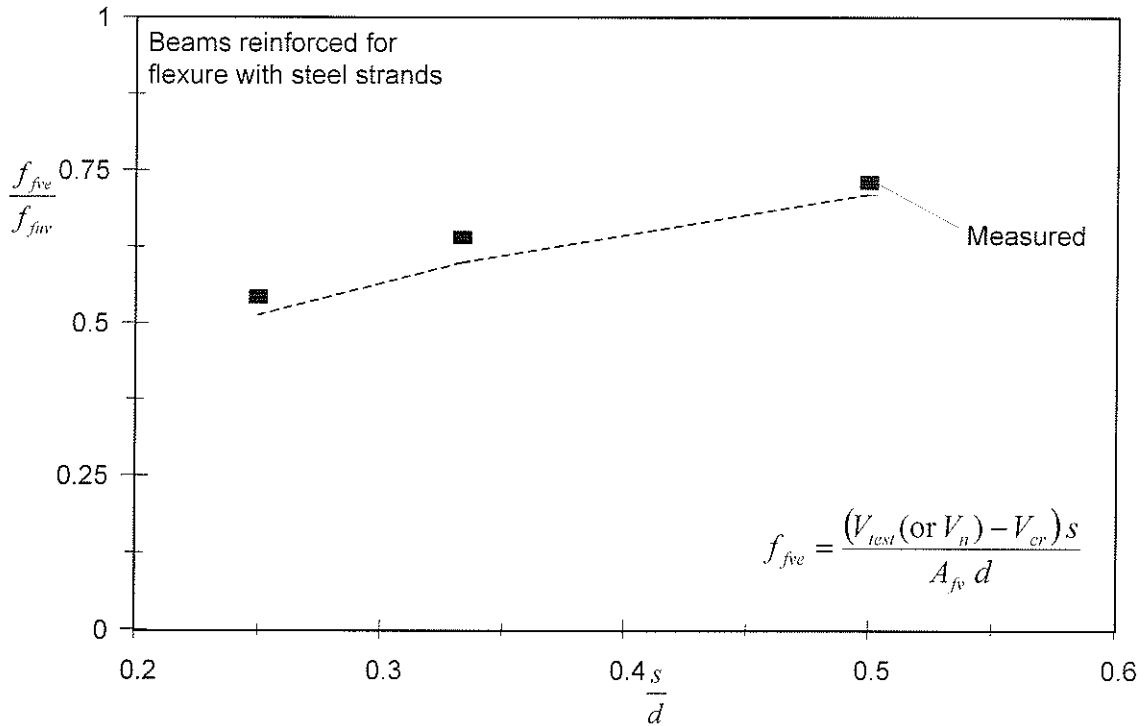


Figure 6-59. Effect of stirrup spacing on effective capacity of CFRP stirrups in beam action: Measured versus MCFT

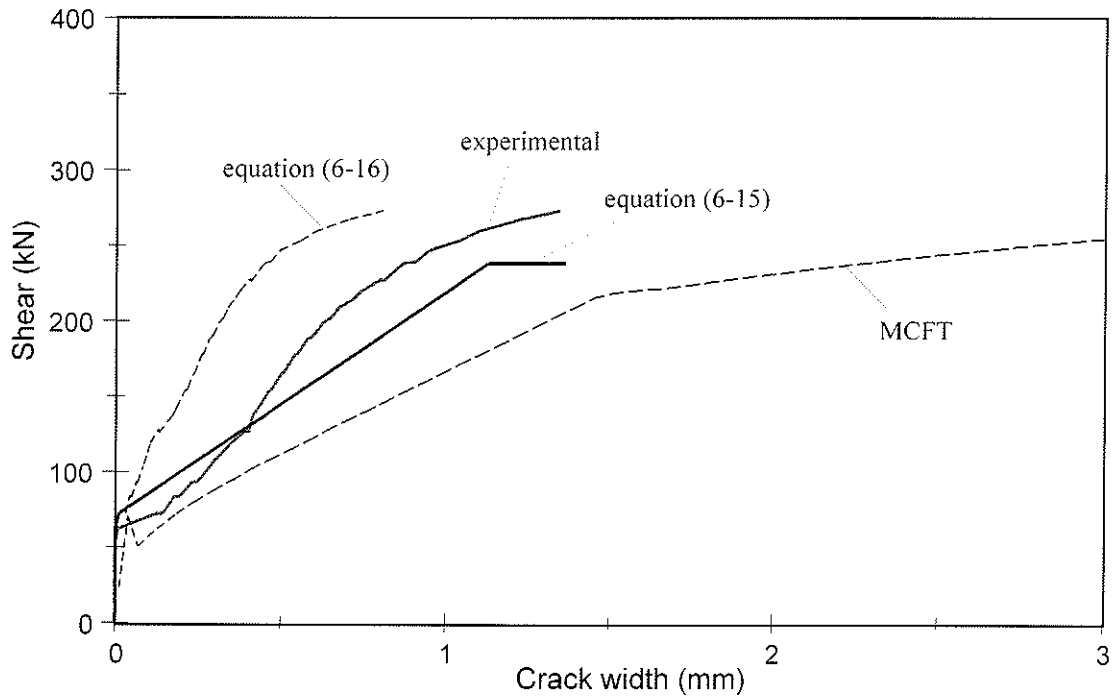


Figure 6-60. Measured versus predicted shear crack width for beam SS-2

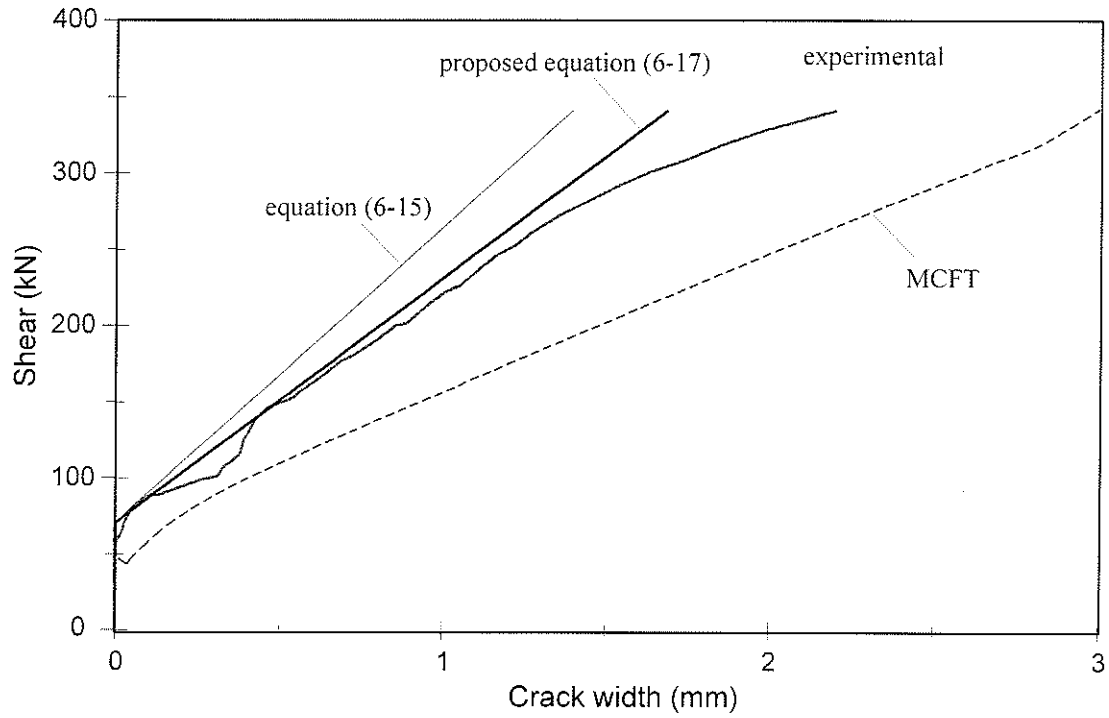


Figure 6-61. Measured versus predicted shear crack width for beam SC-3

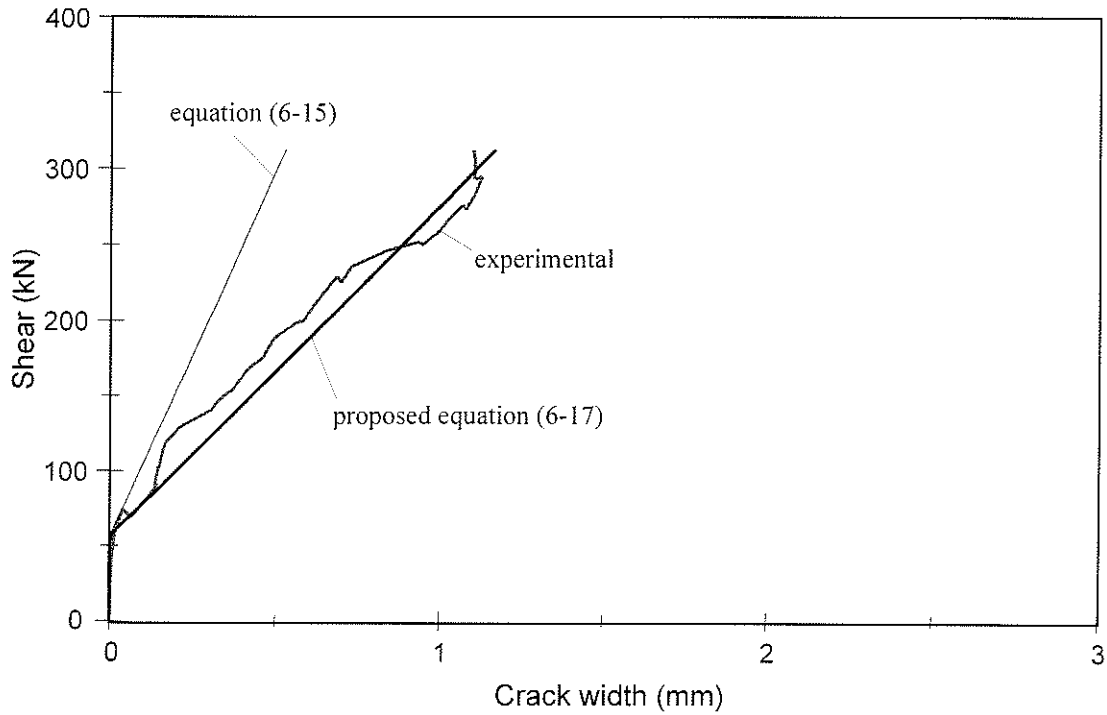


Figure 6-62. Measured versus predicted shear crack width for beam SG-3

Chapter 7

Proposed Provision for FRP Shear Reinforcement of Concrete Beams

7.1 General

This chapter proposes design guidelines for concrete beams reinforced with FRP shear reinforcement and FRP or steel longitudinal reinforcement. Test results of 126 beams, reinforced with FRP and failed in shear, including the beams tested in the second experimental phase of the current study were used to examine the current shear design provisions. It was found that the current shear design provisions in several codes provided for steel shear reinforcement are not safe for FRP reinforcement.

Design guidelines are provided in a convenient format for the current development of design codes for the use of FRP as shear reinforcement in concrete structures. The design guidelines consist of three sections. The first section proposes shear design equations for concrete beams reinforced with FRP using the American Concrete Institute (ACI) design approach. The second section proposes shear design equations for concrete beams reinforced with FRP using the Canadian Standard Association (CSA) design approaches. A minimum FRP shear reinforcement ratio is also proposed. The proposed modifications to the ACI and CSA code equations are found to be very reliable in predicting most of the

test results reported in the literature. The third section proposes strain limits for the FRP stirrups to control the shear crack width in concrete beams.

7.2 Proposed provision based on ACI design approach

This section introduces a design provision for concrete beams reinforced with FRP shear reinforcement and FRP or steel longitudinal reinforcement based on the shear design approach adopted in the current ACI 318-95 code. The primary parameters affecting the shear strength of concrete beams reinforced with FRP are investigated using extensive test data available in the literature. Based on the influence of each parameter, appropriate modifications to the shear design equations to the current ACI 318-95 code are suggested. The proposed equations account for different modes of shear failure of concrete beams reinforced with FRP. A rational approach is undertaken to propose an expression for the minimum FRP shear reinforcement required for concrete beams. The recommended design equations along with the requirement for minimum shear reinforcement should provide a reliable contribution to the current development of design codes for concrete members reinforced with FRP.

7.2.1 Background and basic remarks

The shear design provision in the current ACI 318-95 code follows the traditional “concrete plus stirrup contribution” concept, where the factored shear force due to applied loads should not exceed:

$$\begin{aligned} V_d &= \phi V_n \\ V_n &= V_c + V_s \end{aligned} \quad (7-1)^1$$

$$V_c = \frac{1}{7} \left\{ \sqrt{f'_c} + 120 \rho_{st} \frac{V_n d}{M_n} \right\} b_w d \quad (7-2)^2$$

$$V_s = \frac{A_{sv} \cdot f_{yv} d}{s} \quad (7-3)^3$$

where V_d is the design shear force, and ϕ is the strength reduction factor with a value of 0.85.

According to the ACI-ASCE committee (1973), the concrete contribution to the shear strength, V_c , is determined by equation (7-2), which was originally proposed for the diagonal tension cracking, V_{cr} .

As is known from preceding studies by Bazant and Kim (1984) and Russo and Puleri (1997), the concrete contribution, V_c , consists of:

- a- a component V_1 , which reflects the beam action that arises from the transmission of a tensile force into the steel bars by means of bond stresses; and
- b- a component V_2 which reflects what is known as arch action, since it arises from an arch-like variation in the distance between the compressive resultant, C , carried by the concrete strut, and the tensile resultant, T , carried by the longitudinal reinforcement.

The component V_1 depends on the shear transfer along the crack and the dowel resistance of the longitudinal reinforcement. It is suggested by Bazant and Kim (1984) that a rational expression of the concrete contribution, V_c , should include V_1 as a function of

¹ ACI 318-95 code equation [11-2]

² ACI 318-95 code equation [11-5]

$\sqrt{f'_c}$ and ρ_{sl} , and V_2 as a function of ρ_{sl} and $a/d (= M_u/V_u d)$. The ACI equation (7-2) for V_c can be rewritten as follows:

$$V_c = V_1 + V_2 = \frac{1}{7} \sqrt{f'_c} b_w d + \frac{120}{7} \rho_{sl} \frac{V_u d}{M_u} b_w d \quad (7-4)$$

Despite the fact that the ACI equation (7-2) does not fulfill these requirements for V_1 , it gives a conservative prediction for the concrete contribution to the ultimate shear strength of concrete members.

The stirrup contribution, V_s , given by equation (7-3), is determined based on the 45-degree truss model assuming that all the stirrups crossing the shear crack reach yield and hence equation (7-1) governs the shear–yield (shear–tension) mode of failure. To avoid shear failure initiated by crushing of the concrete before utilizing the full capacity of shear reinforcement, ACI 318-95 limits V_s to $\frac{2}{3} \sqrt{f'_c} b_w d$; hence, the upper bound condition of ACI equation (7-1) for shear–compression failure may be rewritten as follow:

$$\left. \begin{aligned} V_d &= \phi V_n \\ V_n &= V_c + \left\{ \frac{2}{3} \sqrt{f'_c} b_w d \right\} \end{aligned} \right\} (7-5)^4$$

7.2.2 Available experimental results

A total of 126 beams from experimental programs carried out by various researchers, including the beams tested in the current investigation, are reported in Tables 7-1 to 7-4.

³ ACI 318-95 code equation [11-15]

The selected beams were reinforced with FRP as shear and/or flexural reinforcement.

The beams were classified into four groups:

Group	Reinforcement		Details are shown in
	flexure	shear	
A	FRP	None	Table (7-1)
B	FRP	FRP	Table (7-2)
C	Steel	FRP	Table (7-3)
D	FRP	Steel	Table (7-4)

The detailed dimensions, material properties, maximum shear force at failure, V_{test} , and observed mode of failure for the 126 beams are given in Tables 7-1 to 7-4. The following are the ranges of the parameters of test data used to establish the proposed model:

Effective depth of the member:	150	$< d <$	500 mm
Shear span-to-depth ratio:	1.2	$< a/d <$	4.3
Concrete compressive strength:	23	$< f'_c <$	84 MPa
Flexural reinforcement ratio:	0.5%	$< \rho_l <$	4.6%
Elastic modulus of flexural reinforcement:	29	$< E_l <$	200 GPa
Shear reinforcement ratio:	0.04%	$< \rho_{fv} <$	1.5%
Elastic modulus of shear reinforcement:	31	$< E_v <$	145 GPa
Shear reinforcement capacity:	0.7	$< \rho_{fv} f_{fv} <$	20 MPa

⁴ ACI 318-95 code section 11.5.4.3

All selected beams failed in shear, either by rupture of the stirrups (shear-rupture) or concrete crushing (shear-compression). The mode of failure for most of the reported beams is given by the corresponding reference. Complete details of the selected beams can be found in chapters 3 and 6 and in the work of the original investigators as given in column (2) of Tables 7-1 to 7-4.

7.2.3 Influence of major factors

It is well known that the shear strength of concrete beams is affected by many factors, such as: a) the longitudinal reinforcement ratio, ρ_{sl} ; b) the concrete compressive strength f_c ; c) the shear span-to-depth ratio a/d (or M/Vd); and d) the shear reinforcement index $\rho_{sv}f_{sv}$.

For beams reinforced with FRP, other parameters are found to affect the ultimate shear strength of concrete beams. These factors are: a) the strength reduction of FRP stirrups due to bending the bars into a stirrup configuration; b) the presence of cracks at an angle with the direction of the fibres; c) the relatively lower magnitude of the elastic modulus of the longitudinal reinforcement, E_{fl} ; and d) the low elastic modulus of the shear reinforcement, E_{fv} .

The effect of these parameters on the ultimate shear strength of concrete beams reinforced with FRP is discussed in the following sections, based on the available experimental results. Each individual parameter is evaluated by proper separation of other parameters. The effect of FRP flexural reinforcement on ultimate shear strength of concrete beams without shear reinforcement is based on the results of "Group A" beams. The effect of using FRP stirrups is based on the results of "Group C" beams, which are

reinforced with FRP as shear reinforcement and with steel as flexural reinforcement. The effect of longitudinal reinforcement on the concrete contribution, V_c , is based on “Group B” and “Group D” beams reinforced with FRP for flexure.

7.2.3.1 Beams without shear reinforcement

The ultimate shear capacity of reinforced concrete beams without shear reinforcement is determined in the ACI 318-95 code according to equation (7-2) which was mainly derived based on the load corresponding to initiation of shear cracks. The test results of beams reinforced with FRP as longitudinal reinforcement without shear reinforcement, “Group A”, are compared to the prediction according to the ACI equation. The strength reduction factor in equation (7-1), ϕ , is set to 1.00 for direct comparison with the measured shear strengths of “Group A” beams. The ratio $V_{test}/V_{c(aci)}$ versus the relative elastic modulus of the longitudinal reinforcement (E_{fr}/E_s) and the stiffness index $\rho_{fr}(E_{fr}/E_s)$ are shown in Figures 7-1(a) and 7-1(b), respectively. It is evident from Figures 7-1(a) and 7-1(b) that the relatively low elastic modulus of FRP used as longitudinal reinforcement does not influence the prediction of the shear strength as provided by the ACI equation (7-1). This finding may be attributed to the fact that the second term in the ACI equation restated in equation (7-4) is a function of the reinforcement ratio, ρ_p , and contributes to the nominal shear strength, $V_{c(aci)}$, by a relatively small amount ranging from 3 to 20 percent. Therefore, the ACI equation (7-1) can be safely used for beams with FRP longitudinal reinforcement and without shear reinforcement. Behaviour of concrete slabs reinforced with FRP reinforcement (Michaluk *et al.* 1998) could be different due to the small depth in comparison with the test data used in the current study.

7.2.3.2 FRP Stirrups

The contribution of FRP stirrups to the shear strength of reinforced concrete beams is affected by the strength capacity of the bend. It is observed in the first experimental phase of the current study that the bend capacity could be as low as 35 percent of the strength of the FRP bar parallel to the fibres. Test results of “Group C” beams reinforced with steel for flexure that failed by rupture of FRP stirrups were examined to determine the FRP stirrup contribution to the shear strength. The concrete contribution, V_c , was calculated using equation (7-2) since these beams were reinforced with steel as longitudinal reinforcement. The effective stress in the FRP stirrups at ultimate, f_{fv} , is evaluated using the following expression;

$$f_{fv} = \frac{s}{A_{fv}d} (V_{test} - V_{c(aci)}) \quad (7-6)$$

The ratio of effective stress in the FRP stirrups at ultimate, f_{fv} , to the guaranteed tensile strength parallel to the fibres, f_{fiv} , is compared to $\rho_{fv}f_{fiv}$ and $\rho_{fv}(E_{fv}/E_s)$ in Figures 7-2(a) and 7-2(b), respectively, for “Group C” beams that failed in shear-rupture. The parameter $\rho_{fv}f_{fiv}$ is selected in Figure 7-2(a) to emphasize the effect of the nominal capacity of the stirrups, while $\rho_{fv}(E_{fv}/E_s)$ is selected in Figure 7-2(b) to reflect the effect of the stiffness of the FRP stirrups. It can be seen in Figures 7-2(a) and 7-2(b) that there is no clear trend to identify the variation of f_{fv} , as affected by $\rho_{fv}f_{fiv}$ or $\rho_{fv}(E_{fv}/E_s)$. Based on the available test results shown in Figure 7-2, an average value for $\chi = f_{fv}/f_{fiv}$ of 0.60 with a standard deviation of 0.07 is obtained. Therefore, a factor χ is recommended to determine the contribution of FRP stirrups, V_{sf} , as follows:

$$V_{sf} = \chi f_{fiv} \frac{A_{fv}d}{s} \quad (7-7)$$

For design purposes and based on the following statistical expression given in equation (7-8), the strength reduction factor, χ , is selected to be 0.4 to ensure that more than 95 percent of beams reinforced with FRP for shear show an effective stirrup stress at ultimate, f_{fv} , higher than 40 percent of the guaranteed tensile strength parallel to the fibres, f_{fiw} . The χ factor is based on the following equation:

$$\chi = \left(\frac{f_{fv}}{f_{fiw}} \right)_{av.} - 2.0 * \sigma = 0.40 \quad (7-8)$$

where σ is the standard deviation for the ratio f_{fv}/f_{fiw} , and the coefficient “2.0” reflects the 95 percent confidence level.

7.2.3.3 Concrete contribution to shear strength of beams reinforced with FRP

The contribution of the concrete to the shear resisting mechanism of concrete beams is the summation of three components: the shear carried by the uncracked compression zone, the aggregate interlock and the dowel action of the longitudinal reinforcement. The use of FRP as longitudinal reinforcement negatively affects the concrete contribution due to its low elastic modulus and low dowel resistance. The low elastic modulus of the longitudinal reinforcement results in greater crack depth and a consequently smaller area of concrete in the compression zone. In addition, the use of FRP results in wider cracks and minimizes the aggregate interlock component. To evaluate the effect of the elastic modulus of the longitudinal reinforcement, E_{fl} , on the concrete contribution for beams reinforced with FRP, the concrete contribution, V_{cf} , is estimated based on the test results as follows:

$$V_{cf} = V_{test} - \chi f_{fiw} \frac{A_{fv} d}{s} \quad (7-9)$$

The ratio $V_{cf}/V_{c(aci)}$ is plotted for “Group B” and “Group D” beams reinforced with FRP as longitudinal reinforcement and failed in shear–rupture, in Figures 7-3(a) and 7-3(b) using a strength reduction factor χ of 0.6 and 0.4, respectively. For the sake of simplicity, we assume that $V_{cf}/V_{c(aci)}$ depends on $(E_{fr}/E_s)^n$, recognizing that the scatter of test data makes it impossible to calibrate any more refined dependence. Based on the test results given in Figure 7-3(a), the shear strength of beams reinforced with FRP stirrups and longitudinal reinforcement and failed in shear–rupture mode can be predicted using the following proposed equation:

$$V_n = V_{cf} + V_{sf} \quad (7-10)$$

$$V_{cf} = V_{c(aci)} \left(\frac{E_{fr}}{E_s} \right)^n \quad (7-11)$$

where $n = 0.5$, $V_{c(aci)}$ is the concrete contribution to the nominal shear strength of concrete beams, determined by the ACI equation (7-1), and V_{sf} is the contribution of FRP stirrups as given by equation (7-7) where $\chi = 0.40$. Figure 7-3(b) shows that equation (7-10) provides a safe prediction for shear strength of beams reinforced with FRP and failed in shear–rupture mode.

7.2.4 Maximum shear strength of beams reinforced with FRP

The shear strength of a reinforced concrete beam is limited by rupture of the stirrups or concrete crushing in the web. While the shear–rupture mode in FRP reinforced beams is governed by equation (7-10), there is a need to provide a limit for the shear–compression failure. The shear failure initiated by crushing of the web occurs when the compressive strain in the concrete strut exceeds f_{2max} , which is a function of the concrete compressive

strength, f_c' , and the transverse tensile strain ε_1 as given by equation (2-10) and shown in Figure 2-4e. Increasing the tensile strain, ε_1 , reduces the compressive strength, f_{2max} . The transverse tensile strain, ε_1 , is affected by many factors such as the shear reinforcement ratio ρ_v , the longitudinal reinforcement ratio, ρ_l , and the elastic moduli of both types of reinforcement E_v and E_l . The current ACI approach does not consider the shear reinforcement ratio, ρ_{sv} , or the longitudinal reinforcement ratio, ρ_{sl} , for beams reinforced with steel, as is evident from equation (7-5). To provide a design equation that is compatible with the ACI code approach, a modification of equation (7-5) is introduced to account for the presence of FRP reinforcement. Group B and C beams reinforced with FRP as shear reinforcement and failed in shear-compression are analyzed to provide the proper modification for the ACI equation. The shear-compression resistance, V_{comp} , was estimated as follows:

$$V_{comp} = V_{test} - V_{c(aci)} \left(\frac{E_{fl}}{E_s} \right)^{0.5} \quad (7-12)$$

The ratio $V_{comp} / \left(\frac{2}{3} \sqrt{f_c'} b_w d \right)$ is plotted versus the elastic moduli ratio of the longitudinal reinforcement E_{fl} and the stirrups E_{fv} for Group B and C beams that failed in shear-compression in Figures 7-4(a) and 7-4(b), respectively. It is evident from Figure 7-4(a) that no trend can be drawn for the variation of the shear-compression load as influenced by the elastic modulus, E_{fl} . Based on the test results given in Figure 7-4(b), a limit for the shear-compression failure of beams reinforced with FRP can be estimated using the following proposed equation:

$$V_{n_{max}} = V_{c(aci)} \left(\frac{E_{fr}}{E_s} \right)^n + \left\{ \frac{2}{3} \sqrt{f'_c} b_w d \right\} \left(\frac{E_{fr}}{E_s} \right)^m \quad (7-13)$$

where $n = 0.5$ and $m = 0.5$. It should be mentioned that ACI equation for $V_{n_{max}}$ (equation 7-5) is also provided to control shear crack width as proposed by the ASCE-ACI Task Committee (1973). Therefore, the use of E_{fr}/E_s to modify $V_{n_{max}}$ in equation (7-13) provides further control of shear cracks in concrete beams reinforced with FRP stirrups with low elastic modulus.

Therefore, design of beams reinforced with FRP should be based on:

$$\phi_f V_n \geq V_u \quad (7-14)$$

where V_n is the nominal shear strength based on the minimum of equations (7-10) and (7-13), V_u is the factored shear force due to applied loads and ϕ_f is the strength reduction factor for members reinforced with FRP.

7.2.5 Prediction of shear failure mode

The shear strength of beams reinforced with FRP can be determined as the minimum of V_n provided by equations (7-10) and (7-13), respectively. Equation (7-10) provides the limit for the shear-rupture failure, while equation (7-13) provides the limit for the shear-compression failure. The capacity of FRP stirrups controls the type of failure of concrete beams reinforced with FRP. It is evident from equation (7-10) that the shear-rupture failure is affected by the FRP stirrup capacity, conservatively estimated using a strength reduction factor χ of 0.4. As is evident from equation (7-13), the shear-compression failure is a function of the square root of the concrete compressive strength, f'_c , and the

square root of the ratio E_{fr}/E_s . The relative stirrup capacity with respect to the concrete strength and the modular ratio, $\rho_{fr}(\chi f_{fr})/\sqrt{f'_c(E_{fr}/E_s)}$ versus V_{test} for Group B and C beams reinforced with FRP as shear reinforcement is shown in Figure 7-5. In Figure 7-5, beams that failed by rupture of FRP stirrups (shear-rupture) are differentiated from other beams that failed by concrete crushing (shear-compression). It is evident from the trend shown in Figure 7-5 that an increase of the stirrup capacity results in an increase of the ultimate shear capacity in the case of shear-rupture failure. However, further increase in the stirrup capacity above a certain level results in no further increase in the shear strength of concrete beams as shear-compression becomes the governing mode of failure. The critical value of $\rho_{fr}(\chi f_{fr})/\sqrt{f'_c(E_{fr}/E_s)}$ factor is found to be 1.0, which corresponds to $\rho_{fr}(f_{fr})/\sqrt{f'_c(E_{fr}/E_s)}$ of 2.5. For values of $\rho_{fr}(f_{fr})/\sqrt{f'_c}$ less than 2.5, the failure mode is expected to be shear-rupture; and for values higher than 2.5, the failure mode is expected to be shear-compression.

7.2.6 Minimum shear reinforcement

Minimum shear reinforcement is required to prevent sudden shear failure upon formation of the first diagonal tension cracking. It is also required to provide adequate control of the diagonal tension cracks at the service load level. The 1995 ACI code requires a minimum amount of shear reinforcement for nonprestressed members reinforced with steel, as given by the following equation:

$$\rho_{sv_{min}} = \frac{A_{sv_{min}}}{b_w s} = \frac{0.345}{f_{sv}} \quad (7-15)$$

The minimum amount of shear reinforcement is required by the ACI code in reinforced concrete members where the factored shear force, V_u , exceeds one-half the design shear strength, ϕV_c , provided by the concrete.

It is demonstrated by Figure 7-1 that the shear strength of a beam without shear reinforcement which equals the diagonal tension cracking load, V_{cr} , is the same for beams reinforced with steel or FRP reinforcement and can be safely taken as $V_{c(aci)}$. However, the use of FRP in reinforced concrete beams may result in a concrete contribution, V_{cf} , less than the shear cracking force V_{cr} . Therefore, for FRP reinforced beams without shear reinforcement, additional shear reinforcement is required to provide shear strength higher than the diagonal tension cracking load. The additional shear reinforcement proposed to provide shear resistance is given by the following equation:

$$V_{s_{min}} = V_{c(aci)} \left(1 - \sqrt{E_f / E_s} \right) \quad (7-16)$$

Based on equation (7-16), the proposed amount of minimum FRP shear reinforcement is:

$$\rho_{fv_{min}} = \frac{V_{s_{min}}}{\chi f_{fv}} \geq \frac{0.345}{\chi f_{fv}} \quad (7-17)$$

Equation (7-17) is examined using the available test results of Group B beams reinforced with FRP as longitudinal and shear reinforcement. Figure 7-6(a) shows the diagonal tension cracking stress, v_{cr} , which is equivalent to $v_{c(aci)}$, versus the measured ultimate shear stress, v_{test} . It is evident from Figure 7-6(a) that for all 72 beams in Group B, except one, the measured shear strength exceeded the predicted diagonal tension cracking load. Figure 7-6(b) shows the required minimum shear reinforcement $\rho_{fv_{min}}$ versus the provided

ρ_{fv} for Group B beams. It is evident from Figure 7-6(b) that most of Group B beams satisfy the proposed requirement for minimum shear reinforcement (equation 7-17). Therefore, it can be concluded that satisfying equation (7-17) for minimum shear reinforcement provides a nominal shear strength higher than the diagonal tension cracking load. The minimum amount of FRP shear reinforcement should be provided where the factored shear force, V_u , exceeds one-half of the concrete contribution in beams reinforced with FRP, $\phi_f V_{cf}$.

7.2.7 Reliability of the proposed provisions

The proposed revisions to the ACI provisions for shear design of beams reinforced with FRP are given by equations (7-10), (7-13) and (7-17). The proposed equations have been used to predict the shear strength of Group B beams reinforced with FRP longitudinal and stirrups and Group C beams reinforced with FRP stirrups. It should be mentioned that the extensive data used to develop the proposed equations utilized only results for beams with identified failure modes, which are only 60 percent of the total reported in Tables 7-2 and 7-3. The predicted shear strength, $v_n = V_u/bd$, was based on the minimum V_u , as proposed by equations (7-10) and (7-13) and compared to the measured shear strength v_{test} in Figures 7-7(a) and 7-8(a) for Group B and Group C beams, respectively. The calculated values $v_n = V_u/bd$ shown in Figures 7-7(b) and 7-8(b) are according to current ACI code (equation 7-1, where f_{syv} is assumed to be f_{fv}). The other codes including JSCE, BRI, CHBDC and the Eurocrete project recommendations are shown in Figures 7-7(c,d,e,f) and 7-8(c,d,e,f); respectively. The equations used for these codes are given in Chapter 3 (section 3.5). The calculated shear stress v_n was based on the nominal shear

strength, V_n , using unit value for all material and safety factors (ϕ , γ_b , γ_m , ...). The numerical values predicted in Figures 7-7 and 7-8 are given in detail in Tables 7-5 and 7-6. The 45-degree broken lines in Figures 7-7 and 7-8 correspond to the exact prediction, while other straight lines statistically bound 90 percent of the data points, as given by:

$$\text{slope of the bounding lines} = \left(v_{test} / v_n \right)_{av.} \pm 1.64 * \sigma \quad (7-18)$$

where σ is the standard deviation for the v_{test}/v_n ratio.

It is observed that direct application of the current ACI code equations to available test data results in an unsafe prediction for the shear strength of concrete beams reinforced with FRP. Both JSCE and CHBDC models greatly underestimate the shear strength, due to the fact that both models use the same expression for very low stirrup strain at ultimate (equations 3-29, 3-40) and hence lead to very conservative values when compared to the measured data. The recommended Eurocrete project (equations 3-41 and 3-42) underestimates the shear strength for the shear-rupture failure mode since the recommended stirrup strain at ultimate is relatively low compared to the experimental results. In addition, the Eurocrete project overestimates the shear strength for the shear-compression failure mode as it does not introduce an expression to limit the shear-compression failure. The BRI design model (equations 3-36) shows good prediction when compared to the JSCE, CHBDC and Eurocrete models, since it requires the experimental evaluation of the bend capacity of FRP stirrups. The proposed revisions to the ACI code result in better distribution for the measured-to-calculated ratio, as shown in Figures 7-7 and 7-8. The relatively good performance of the proposed equations is attributed to the fact that they account for the various factors affecting shear strength of

beams reinforced with FRP, and differentiate between the two different shear failure modes.

The six design methods are compared in Tables 7-7 and 7-8, using the ratio of measured to calculated shear strength, v_{test}/v_n , for 72 beams of Group B and the 28 beams of Group C, respectively. As is evident from Table 7-7, the proposed method shows a COV value of 0.20 and 0.22 for Group B and Group C beams, respectively, which are the lowest of all other available methods. It should be mentioned that statistical studies conducted by Sarsam and Al-Musawi (1992) on 154 beams reinforced with conventional steel reinforcement showed that the current ACI equations provide an average of 1.39 and a COV of 0.24 for the ratio of measured to calculated shear strength. Therefore, the results presented in Tables 7-7 and 7-8 suggest that the proposed equations are quite reliable.

The proposed equations are relatively simple and do not increase the computational effort over other recommended methods. Since the application of a factor to equations (7-10) and (7-13) leaves unchanged the COV value (given by STD-to-AVG ratio), the proposed equations provide a design method making more uniform prediction than other models. The proposed value for the strength reduction factor ϕ_f in equation (7-14) is 0.8, which is smaller than lowest v_{test}/v_n as reported in Tables 7-7 and 7-8. Therefore, equation (7-14) results in a reasonably conservative design formula for the shear strength of beams reinforced with FRP.

7.3 Proposed provision based on CSA design approach

This section introduces a design provision for concrete beams reinforced with FRP shear and/or flexural reinforcement based on the shear design approaches adopted in the current

CSA 23.3-94 code. It is suggested to use consistent design approaches in the ACI and CSA codes for concrete members reinforced with FRP. The rational approach used to modify the current ACI shear equations was also used to revise the current CSA 23.3 shear equations.

The following sections provide two shear design provisions for concrete beams reinforced with FRP, based on:

- a- the simplified method of the CSA 23.3-94 code
- b- the general method of the CSA 23.3-94 code

It should be mentioned that the CHBDC (1998) proposes a shear design provision for concrete members reinforced with FRP, based on the general method of the CSA code. However, it is shown in the previous section that the CHBDC equations result in very conservative design for beams reinforced with FRP.

An expression for the minimum FRP shear reinforcement is also proposed. The proposed design equations were used to predict the shear strength of the Group B and C beams reported in Tables 7-3 and 7-4.

7.3.1 Proposed design guidelines based on the simplified method

The simplified method in the CSA 23.3-94 is based on the 45-degree truss model with an effective depth of d . The design shear strength can be determined using equations (2-35), (2-36) and (2-37) for beams reinforced with steel. The approach used to modify the shear design method of the ACI 318-95, code as proposed by equations (7-10) and (7-13), was used to modify the simplified method in the CSA 23.3-94 code, as follows:

$$V_d = V_{cfd} + V_{sfd} \quad (7-19)$$

$$V_{cfd} = 0.2\lambda\phi_c\sqrt{f'_c}b_wd\left(\frac{E_{fr}}{E_s}\right)^n \quad d \leq 300 \text{ mm} \quad (7-20)$$

$$V_{cfd} = \frac{260}{1000+d}\lambda\phi_c\sqrt{f'_c}b_wd\left(\frac{E_{fr}}{E_s}\right)^n \geq 0.1\lambda\phi_c\sqrt{f'_c}b_wd\left(\frac{E_{fr}}{E_s}\right)^n \quad d > 300 \text{ mm}$$

$$V_{sfd} = \phi_f\chi f_{frv}\frac{A_{frv}d}{s} \leq 0.8\lambda\phi_c\sqrt{f'_c}b_wd\left(\frac{E_{frv}}{E_s}\right)^m \quad (7-21)$$

where $n = 0.5$, $\chi = 0.4$, $m = 0.5$, λ equals 1.0 for normal density concrete, ϕ_c is the material safety factor for concrete ($\phi_c = 0.60$) and ϕ_f is the material safety factor for FRP. It is recommended to use a material safety factor, ϕ_f , equals to 0.85 and 0.75 for CFRP and GFRP, respectively, as proposed by the CHBDC (1998).

7.3.2 Proposed design guidelines based on the general method

The general method in CSA 23.3-94 is based on the MCFT; however, it is formulated in the form of a concrete contribution plus stirrup contribution approach. The design shear strength can be determined using equations (2-39) and (2-40) and (2-37) for beams reinforced with steel. The approach used to modify the shear design method of the ACI 318-95 code, as proposed by equations (7-10) and (7-13), was used to modify the general method in the CSA 23.3-94 code, as follows:

$$V_d = V_{cfd} + V_{sfd} \leq 0.25 f'_c b_w jd \left(\frac{E_{frv}}{E_s}\right)^m \quad (7-22)$$

$$V_{cfd} = 1.3 \lambda \phi_c \beta \sqrt{f'_c} b_w jd \quad (7-23)$$

$$V_{sfd} = \frac{\phi_f A_{frv} \chi f_{frv}}{s} jd \cot \theta \quad (7-24)$$

where $m=0.5$, $\chi=0.5$, β and θ are determined from Figure 2-8 for sections with shear reinforcement, where v_f is the factored shear stress ($v_f = V_u/b_wjd$) and ε_{fx} is the longitudinal strain of FRP flexural reinforcement, which can be estimated as:

$$\varepsilon_{fx} = \frac{M_u / jd + 0.5V_u \cot \theta}{E_{fl} A_{fl}} \quad (7-25)$$

where M_u is the moment at the critical section, A_{fl} is the cross-sectional area of longitudinal FRP reinforcement in the flexural tension side of the beam and E_{fl} is the elastic modulus of longitudinal FRP reinforcement.

The proposed equation (7-23) for V_{cfd} was not modified similarly to the proposed equation for the ACI code (equation 7-11). This is because the factor β in equation (7-23) accounts for the relatively high strain in the FRP longitudinal reinforcement, ε_{fx} , that is determined using equation (7-25).

There is no direct solution to find the shear strength of a beam using the general method. First, the applied shear load V_u has to be assumed and then the design shear strength V_d can be determined by equation (7-22). This process is iterated until V_u equals V_d .

7.3.3 Minimum shear reinforcement

The CSA 23.3-94 code uses equation (2-38) for minimum shear reinforcement for concrete beams reinforced with steel. The approach used to modify the minimum shear reinforcement expression of the ACI 318-95 code as proposed by equation (7-17) was used to modify the CSA 23.3-94 code equation, as follows:

$$\rho_{f_{min}} = \frac{V_{c(csa)} \left(1 - \sqrt{E_{fl} / E_s}\right) b_w d}{\chi f_{fu}} \geq \frac{0.06 \sqrt{f'_c}}{\chi f_{fu}} \quad (7-26)$$

where $V_{c(csa)}$ is determined using equation (2-36) taking $\phi_c = 1.0$.

Equation (7-26) was examined with the available test results of Group B beams reinforced with FRP as longitudinal and shear reinforcement. Figure 7-9(a) shows the diagonal tension cracking stress, v_{cr} , which is equivalent to $v_{c(csa)}$, versus the measured ultimate shear stress, v_{test} . It is evident from Figure 7-9(a) that for all 72 beams in Group B, the measured shear strength exceeded the predicted diagonal tension cracking load. Figure 7-9(b) shows the required minimum shear reinforcement $\rho_{fv, min}$ versus the provided ρ_{fv} for Group B beams. It is evident from Figure 7-9(b) that most of Group B beams satisfy the proposed requirement for minimum shear reinforcement (equation 7-26). Therefore, it can be concluded that satisfying equation (7-26) for minimum shear reinforcement provides a nominal shear strength higher than the diagonal tension cracking load. The minimum amount of FRP shear reinforcement should be provided where factored shear force V_u exceeds one-half of the concrete contribution in beams reinforced with FRP, V_{cfd} , determined using equation (7-20).

7.3.4 Reliability of the proposed provisions

The proposed provisions for the CSA shear design for beams reinforced with FRP are given by equations (7-19), and (7-22). Equation (7-19) is derived based on the simplified method in the CSA 23.3-94 code, while equation (7-22) is derived based on the general method in the CSA 23.3-94 code.

The proposed equations have been used to predict the shear strength of Group B beams reinforced with FRP longitudinal and stirrups and Group C beams reinforced with FRP stirrups. The predicted shear strength, $v_n = V_n/bd$, was compared to the measured shear

strength v_{test} in Figures 7-10 and 7-11 for Group B and C beams, respectively. The calculated values $v_n = V_n/bd$ shown in Figures 7-10(a) and 7-11(a) were according to the proposed simplified method (equation 7-19). The values $v_n = V_n/bd$ shown in Figures 7-10(b) and 7-11(b) were calculated according to the proposed general method (equation 7-22). The calculated shear stress v_n was based on the nominal shear strength, V_n , using values of 1.0 for all material safety factors (ϕ_c and ϕ_f). The numerical values predicted in Figures 7-10 and 7-11 are given in detail in Tables 7-9 and 7-10. The 45-degree broken lines in Figures 7-10 and 7-11 correspond to the exact prediction, while other straight lines statistically bound 90 percent of the data points, as given by equation (7-19).

It can be observed from Figures (7-10) and (7-11) that the proposed simplified method results in more uniform distribution for the measured versus calculated shear strength of beams reinforced with FRP than the proposed general method. This is attributed to the fact that the proposed general method overestimates the shear strength for the shear-compression failure mode which is given by the limit imposed on equation (7-22).

The two proposed design methods and the current CHBDC method are compared in Tables 7-11 and 7-12 using the measured-to-calculated shear strength, v_{test}/v_n , for 72 beams of Group B and the 28 beams of Group C, respectively. While the proposed simplified method results in the lowest average for the v_{test}/v_n ratio, it shows a COV value of 0.2 and 0.24 for Group B and Group C beams, respectively, which are the lowest of all other methods. It is also evident from Tables 7-11 and 7-12 that the proposed simplified method is more reliable than other methods, since it results in a narrower distribution around the average for the v_{test}/v_n ratio.

It is recommended to use a material safety factor, ϕ_f , equal to 0.85 and 0.75 for CFRP and GFRP, respectively, as proposed by the CHBDC (1998). It should be mentioned that the CSA 23.3-94 code uses a relatively low material safety factor, ϕ_c (= 0.60). The use of the recommended values for the material safety factors in equation (7-19) results in a lower bound for the v_{est}/v_n ratio, which is higher than 1.00. Therefore, equation (7-19) of the proposed simplified method results in a reasonably conservative design formula for shear strength of concrete beams reinforced with FRP. In addition, the proposed simplified method does not increase the computational effort as given in the proposed general method. Therefore, the proposed simplified method is recommended for the current development of CSA design codes for concrete members reinforced with FRP.

7.4 Proposed provision for serviceability requirement

The control of crack widths at service load level is an important serviceability criterion for reinforced concrete structures. Investigation of the shear crack width in concrete beams reinforced with FRP has not been reported in the available literature. Therefore, the test results of the second experimental phase of the current study are the only available data for shear cracking behaviour in concrete beams reinforced with FRP. These test results were used to provide design guidelines for the serviceability requirement. The following section introduces the observed relationship between the shear crack width and the stirrup strain for tested beams, as influenced by the mechanical properties of the stirrup material. Provisions for the serviceability requirement to control shear crack widths in concrete beams reinforced with FRP stirrups are proposed.

The control of crack widths at the service load level is an important serviceability criterion for reinforced concrete structures. Although current design codes include provisions for the control of the widths of tensile and flexural cracks in beams reinforced with steel, none of these codes introduces provisions for shear cracks. However, the previous version of the CEB-FIP Model Code-78 (1978) contains provisions for shear cracks based on the recommendation of Leonhardt (1977), as given by equation (2-56). The CEB-FIP code assumes that the width of inclined cracks is a function of the stress in the stirrups, which in turn is a function of $(V-V_c)$. The current ACI code (1995) uses an indirect approach to control shear crack widths, based on the recommendation of the ASCE-ACI Committee 426 (1973). As mentioned in section 2.6.1, the ASCE-ACI Committee 426 (1973) concluded that it may be possible to control crack widths at service loads by limiting the value of $V_s (=V_u-V_c)$ at the ultimate load. Thus, for steel stirrups of a yield strength of 420 MPa and a load factor of 1.6 and an upper limit on the stirrup contribution, V_s/b_wd , of $2\sqrt{f'_c}/3$, the stirrup stress, $f_{sv,ser}$, at service load 1.0(D+L) will be about 220 MPa ($\epsilon_{sv,ser} = 0.11\%$), corresponding to a maximum shear crack width of about 0.33 mm (0.013 in.).

The relationship between the shear crack width and the stirrup strain observed in beam tests is shown in Figure 7-12 for a crack width range of 0 to 1.0 mm. For the beam reinforced with steel stirrups, the measured shear crack width corresponding to a stirrup strain of 0.11 % was 0.35 mm (0.014 in.), as shown in Figure 7-12. Therefore, there is good agreement between the measured crack width and the specified crack width at the service load according to the ASCE-ACI Committee 426.

The current ACI code (1995) limits the crack width for members reinforced with steel to 0.33 mm (0.013 in.). As FRP reinforcement is generally considered to be non-corroding, the maximum crack width could be relaxed when reinforcement corrosion is the primary reason for crack width limitation. The CHBDC (1998), JSCE (1997) and ACI Committee 440 (1998) take into account the aesthetic point of view only and set the maximum allowable crack width to 0.51 mm (0.020 in.) for concrete members reinforced with FRP. It is observed for beams reinforced with CFRP stirrups that the average strain in the stirrups corresponding to a shear crack width of 0.51 mm is 0.2 %, as shown in Figure 7-12. The corresponding strain value for beams reinforced with GFRP stirrups is 0.35 %, as shown in Figure 7-12. It should be noted that for the beam reinforced with steel stirrups, the average strain in the stirrups corresponding to a crack width of 0.51 mm is 0.18 %.

The average strain in the stirrups at service load level can be estimated based on the 45-degree truss model using the following equation:

$$\varepsilon_{v_{ser}} = \frac{s (V_{ser} - V_c)}{A_v d E_v} \quad (7-27)$$

where A_v is the cross-sectional area of the stirrup, E_v is the elastic modulus of the stirrups, d is the effective beam depth, s is the stirrup spacing, V_{ser} is the unfactored shear force at service load level and V_c is the concrete contribution to the shear resisting mechanism. The concrete contribution, $V_c (= V_{c(aci)})$, can be determined using equations (7-2) for beams reinforced with steel as longitudinal reinforcement. For beams reinforced with FRP as longitudinal reinforcement, the concrete contribution, $V_c (= V_{cf})$, can be determined using equation (7-11).

To control shear crack widths in concrete beams reinforced with FRP stirrups, it is recommended to limit the strain in CFRP and GFRP stirrups at the service load level to 0.2 % and 0.35 %, respectively. Therefore, equation (7-27) can be rewritten as follows:

$$\varepsilon_{fv_{ser}} = \frac{s (V_{ser} - V_c)}{A_{fv} d E_{fv}} \leq \begin{matrix} 0.0020 & \text{for CFRP stirrups} \\ 0.0035 & \text{for GFRP stirrups} \end{matrix} \quad (7-28)$$

The use of equation (7-28) to limit the strain in FRP stirrups satisfies the serviceability requirement to control the shear crack width. The manufacturer of the GFRP stirrups (Marshall industries composites, 1997) recommends that C-BAR GFRP bars can be designed for 25 % of the ultimate tensile strength (a strain of 0.43 %) at the service load level to satisfy the durability requirements in a highly alkaline environment. The proposed limitation on the strain in GFRP stirrups given by equation (7-28) satisfies these durability requirements.

7.5 Design example

Appendix D gives a design example for shear in a concrete beam reinforced with FRP reinforcement. The concrete beam considered in this example is designed according to the proposed shear design provisions based on the ACI and CSA approaches, as given in sections 7.2 and 7.3. The beam is also designed to satisfy the proposed serviceability requirements given in section 7.5.

Table 7-1. Basic data for 20 test beams reinforced with FRP bars for flexure and having no shear reinforcement

Beam	Ref. ID	b_w mm	d mm	a/d	f_c MPa	Flex. reinf.		Shear reinforcement				$v_{test} = V_{test}/bd$ MPa	Mode of failure	
						ρ_f %	E_{ff} GPa	ρ_{fv} %	f_{fv} MPa	f_{hend} MPa	E_{fv} GPa			
(1)	(2)	(3)	(4)	(5)	(6)	(7)	(8)	(9)	(10)	(11)	(12)	(13)	(14)	
Group A	1	Vijay <i>et al.</i>	150	264.5	1.89	44.8	1.43	54	---				1.129	DT
	2	(1996)	150	264.5	1.89	31	0.64	54	---				1.129	DT
	3	Zhao <i>et al.</i>	150	250	3	34.3	1.51	105	---				1.200	DT
	4	(1995)	150	250	3	34.3	3.03	105	---				1.227	DT
	5		150	250	3	34.3	2.27	105	---				1.080	DT
	6	Duranovi <i>et al.</i>	150	210	3.65	38.1	1.36	45	---				1.679	DT
	7	(1997)	150	210	3.65	32.9	1.36	45	---				1.394	DT
	8	Nagasaka <i>et al.</i>	250	253	1.78	34.1	1.9	56	---				1.784	DT
	9	(1993)	250	253	1.78	22.9	1.9	56	---				1.318	DT
	10	Nakamura <i>et al.</i>	300	150	4	22.7	1.34	29	---				0.736	DT
	11	(1995)	300	150	4	27.8	1.79	29	---				0.808	DT
	12		200	325	2.15	44.6	0.7	137	---				1.509	S
	13		200	325	3.23	44.5	0.7	137	---				1.887	S
	14		200	325	4.31	45.0	0.7	137	---				1.811	S
	15	Tottori and	200	325	2.77	46.9	0.86	192	---				2.264	S
	16	Wakui (1993)	200	325	3.23	46.9	0.86	192	---				1.434	S
	17		200	325	4.31	46.9	0.86	192	---				1.207	S
	18		200	325	2.15	46.9	0.92	58	---				2.339	S
	19		200	325	3.23	46.9	0.92	58	---				0.951	S
	20		200	325	4.30	46.9	0.92	58	---				0.724	S

column (5) a is the shear span
 column (14) DT = diagonal tension failure ST = shear failure by rupture of FRP or yield of steel
 SC = shear failure by concrete crushing
 S = shear failure (type of failure was not identified in the corresponding reference)

Table 7-2. Basic data for 72 test beams reinforced with FRP bars for flexure and FRP stirrups for shear

Beam	Ref. ID	b_w mm	d mm	a/d	f_c MPa	Flex. reinf.		Shear reinforcement				$v_{test} = V_{test}/bd$ MPa	Mode of failure	
						ρ_f %	E_f GPa	ρ_{fv} %	f_{fv} MPa	f_{bend} MPa	E_{fv} GPa			
(1)	(2)	(3)	(4)	(5)	(6)	(7)	(8)	(9)	(10)	(11)	(12)	(13)	(14)	
Group B	1	Vijay <i>et al.</i>	150	264.5	1.89	44.8	1.43	54	0.93	655	248	54	3.196	ST
	2	(1996)	150	264.5	1.89	44.8	1.43	54	0.62	655	248	54	2.899	ST
	3		150	264.5	1.89	31	0.64	54	0.93	655	248	54	3.105	ST
	4		150	264.5	1.89	31	0.64	54	0.62	655	248	54	3.108	ST
	5	Alsayed <i>et al.</i>	200	309.5	3.23	35.5	1.37	36	0.21	565	n/a	42	1.107	ST
	6	(1996, 1997)	200	309.5	3.23	39.5	1.37	36	0.21	565	n/a	42	0.936	ST
	7		200	309	2.36	35.7	1.3	43	0.4	565	n/a	42	1.762	ST
	8		150	250	3	34.3	3.03	105	0.42	1100	n/a	39	3.013	SC
	9	Zhao <i>et al.</i>	150	250	3	34.3	3.03	105	0.42	1300	n/a	100	3.357	SC
	10	(1995)	150	250	3	34.3	2.27	105	0.42	1100	n/a	39	3.099	SC
	11		150	250	2	34.3	1.51	105	0.42	1100	n/a	39	3.288	SC
	12		150	250	4	34.3	1.51	105	0.42	1100	n/a	39	1.955	SC
	13	Duranovi <i>et al.</i>	150	210	3.65	39.8	1.36	45	0.35	1000	n/a	45	3.110	ST
	14	(1997)	150	210	2.44	39.8	1.36	45	0.35	1000	n/a	45	4.225	ST
	15		250	253	1.19	28.9	1.9	56	0.5	1285	903	112	3.893	ST
	16		250	253	1.19	34.0	1.9	56	1	1285	903	112	4.917	ST
	17		250	253	1.19	32.8	1.9	56	1.48	1285	903	112	5.677	ST
	18		250	253	1.78	28.9	1.9	56	0.5	1285	903	112	3.226	ST
	19		250	253	1.78	28.9	1.9	56	1	1285	903	112	4.374	ST
	20		250	253	1.78	28.9	1.9	56	1.48	1285	903	112	4.467	SC
	21		250	253	2.37	32.8	1.9	56	0.5	1285	903	112	2.513	ST
	22		250	253	2.37	32.8	1.9	56	1	1285	903	112	3.629	ST
	23		250	253	1.78	33.4	1.9	56	0.5	1373	824	60	3.179	ST
	24		250	253	1.78	34.7	1.9	56	1	1373	824	60	4.296	SC
	25		250	253	1.78	33.4	1.9	56	0.5	716	481	44	2.683	ST
	26	Nagasaka <i>et al.</i>	250	253	1.78	33.4	1.9	56	1	716	481	44	3.846	ST
	27	(1993)	250	253	1.78	34.7	1.9	56	0.5	1354	608	46	2.776	ST
	28		250	253	1.78	36.0	1.9	56	1	1354	608	46	3.614	ST
	29		250	253	1.78	23.5	1.9	56	1	1285	903	112	3.273	SC
	30		250	253	1.78	22.5	1.9	56	1.48	1285	903	112	3.505	SC
	31		250	253	2.37	24.3	1.9	56	1	1285	903	112	2.885	SC
	32		250	253	2.37	22.9	1.9	56	1.48	1285	903	112	3.024	SC
	33		250	253	1.78	22.5	1.9	56	1	1373	824	60	3.009	SC
	34		250	253	1.78	22.5	1.9	56	1.48	1373	824	60	3.211	SC
	35		250	253	1.78	23.5	1.9	56	1	716	481	44	3.009	SC
	36		250	253	1.78	23.5	1.9	56	1.48	716	481	44	3.350	SC
	37		250	253	1.78	39.5	1.9	56	1.48	1285	903	112	4.622	SC
	38		250	253	2.37	39.2	1.9	56	1.48	1285	903	112	3.583	SC
	39		200	250	3	35.4	1.61	29	0.35	828	544	31	1.668	ST
	40	Nakamura and	200	250	3	33.4	1.61	29	0.35	828	649	31	2.001	ST
	41	Higai (1995)	200	250	3	35.2	1.61	29	0.18	828	544	31	1.124	ST
	42		200	250	3	35.2	1.61	29	0.18	828	649	31	1.324	ST

Table 7-2 (cont'd). Basic data for 72 test beams reinforced with FRP bars for flexure and FRP stirrups for shear

Beam ID	Ref. ID	b_w mm	d mm	a/d	f'_c MPa	Flex. reinf.		Shear reinforcement				$v_{test} = V_{test}/bd$ MPa	Mode of failure	
						ρ_f %	E_f GPa	ρ_{fv} %	f_{uv} MPa	f_{bend} MPa	E_{fv} GPa			
(1)	(2)	(3)	(4)	(5)	(6)	(7)	(8)	(9)	(10)	(11)	(12)	(13)	(14)	
Group B	43	Tottori and Wakui (1993)	200	325	3.23	44.4	0.7	137	0.15	716	n/a	40	1.584	S
	44		200	325	3.23	44.7	0.7	137	0.15	716	n/a	40	1.63	S
	45		200	325	3.23	44.9	0.7	137	0.07	1511	n/a	69	1.305	S
	46		200	325	2.15	44.6	0.7	137	0.07	1413	n/a	110	2.490	S
	47		200	325	3.23	44.8	0.7	137	0.07	1413	n/a	110	1.283	S
	48		200	325	4.31	44.6	0.7	137	0.07	1413	n/a	110	1.132	S
	49		200	325	3.23	45.0	0.7	137	0.04	2040	n/a	144	1.509	S
	50		200	325	3.23	44.7	0.7	140	0.06	1746	n/a	137	1.660	S
	51		200	325	3.23	44.7	0.7	140	0.10	1746	n/a	137	2.415	S
	52		200	325	3.23	39.4	0.7	140	0.12	1089	n/a	58	1.585	S
	53		200	325	3.23	39.4	0.92	58	0.09	1236	n/a	58	1.283	S
	54		200	325	3.23	39.4	0.92	58	0.13	1236	n/a	58	1.509	S
	55		200	325	3.23	39.4	0.92	58	0.23	1236	n/a	58	2.037	S
	56		200	325	3.23	39.4	0.92	58	0.12	1089	n/a	58	1.653	S
	57		200	325	3.23	39.4	0.92	58	0.12	1089	n/a	58	1.207	S
	58		200	325	3.23	57.8	0.92	58	0.12	1089	n/a	58	1.653	S
	59		200	325	3.23	39.4	0.92	58	0.04	1746	n/a	137	1.328	S
	60		150	250	2.5	35.5	0.55	94	0.12	1283	n/a	94	1.543	S
	61		150	250	2.5	37.6	0.55	94	0.24	1283	n/a	94	2.197	S
	62		150	250	2.5	34.3	1.05	94	0.12	1283	n/a	94	1.903	S
63	150	250	2.5	34.2	2.11	94	0.12	1283	n/a	94	2.158	S		
64	300	500	2.5	31.9	0.53	94	0.06	1283	n/a	94	1.069	S		
65	150	260	3.08	42.2	3.08	63	0.13	1766	n/a	53	1.547	S		
66	200	250	2	77.5	0.93	137	0.28	1864	n/a	53	5.209	S		
67	200	250	3	82.5	0.93	137	0.38	1864	n/a	53	3.443	S		
68	200	250	3	84.2	0.93	137	0.15	1766	n/a	137	3.885	S		
68	200	250	3	84.2	0.93	137	0.27	1864	n/a	53	2.806	S		
70	200	250	3	82.5	0.93	137	0.12	1766	n/a	137	3.659	S		
71	Shehata*	135	470	3.2	50	1.25	137	0.36	1800	860	137	4.815	ST	
72	(1999)	135	470	3.2	50	1.25	137	1.05	713	346	41	4.812	ST	

* Basic data and test results of beams are reported in chapters 4 and 6

column (5) a is the shear span

column (14) DT = diagonal tension failure ST = shear failure by rupture of FRP or yield of steel

SC = shear failure by concrete crushing

S = shear failure (type of failure was not identified in the corresponding reference)

Table 7-3. Basic data for 28 test beams reinforced with FRP stirrups for shear and steel bars for flexure

Beam	Ref. ID	b_w mm	d mm	a/d	f_c MPa	Flex. reinf.		Shear reinforcement				$v_{test} = V_{test}/bd$ MPa	Mode of failure	
						ρ_l %	E_s GPa	ρ_{fv} %	f_{fv} MPa	f_{bond} MPa	E_{fv} GPa			
(1)	(2)	(3)	(4)	(5)	(6)	(7)	(8)	(9)	(10)	(11)	(12)	(13)	(14)	
Group C	1	Alsayed <i>et al</i> ¹⁹⁹⁷	200	310	2.36	35.7	0.99	200	0.40	565	n/a	42	2.330	ST
	2	Nagasaka <i>et al.</i> (1993)	250	253	1.78	26.0	1.89	184	1	716	481	44	3.288	SC
	3		250	253	1.78	25.3	1.89	184	0.5	1285	544	112	2.792	SC
	4		250	253	1.78	25.4	1.89	184	1	1285	649	112	3.645	SC
	5		250	253	1.78	27.6	1.89	184	1.48	1285	544	112	3.8	SC
	6	Nakamura and Higai (1995)	200	250	3	34.7	1.72	180	0.23	828	649	31	1.929	ST
	7		200	250	3	34.4	1.72	180	0.23	828	903	31	2.127	ST
	8		200	250	3	35.6	1.72	180	0.14	828	903	31	1.596	ST
	9		200	250	3	35.8	1.72	180	0.14	828	903	31	1.596	ST
	10	Tottori and Wakui (1993)	200	285	2.11	37.2	4.07	206	0.54	602	n/a	36	4.044	S
	11		200	285	2.11	37.2	4.07	206	0.27	602	n/a	36	3.890	S
	12		200	285	3.16	35.3	4.07	206	0.54	602	n/a	36	2.977	S
	13		200	285	3.16	35.3	4.07	206	0.27	602	n/a	36	2.409	S
	14		200	285	3.16	35.3	4.07	206	0.18	602	n/a	36	2.065	S
	15		200	285	4.21	31.4	4.07	206	0.27	602	n/a	36	2.031	S
	16		200	325	3.23	42.2	0.86	192	0.41	602	n/a	36	2.430	S
	17		200	325	3.23	71.6	0.86	192	0.41	602	n/a	36	2.551	S
	18		200	325	4.31	50.6	0.86	192	0.41	602	n/a	36	2.309	S
	19		200	325	4.31	65.7	0.86	192	0.41	602	n/a	36	2.354	S
	20	150	250	2.5	29.4	2.06	206	0.12	1283	n/a	94	2.825	S	
	21	150	260	3.08	38.8	2.98	206	0.13	1766	n/a	53	2.176	S	
	22	200	250	3.2	40.7	4.65	206	0.38	1278	n/a	64	3.836	S	
	23	Shehata* (1999)	135	470	3.2	54	1.32	200	0.24	1800	860	137	4.374	ST
	24		135	470	3.2	54	1.32	200	0.36	1800	860	137	5.374	ST
	25		135	470	3.2	51	1.32	200	0.47	1800	860	137	5.918	ST
	26		135	470	3.2	54	1.32	200	0.71	713	346	41	4.602	ST
	27		135	470	3.2	33	1.32	200	1.05	713	346	41	4.925	SC
	28		135	470	3.2	33	1.32	200	1.4	713	346	41	4.909	SC

* Basic data and test results for these beams are reported in chapters 4 and 6

Table 7-4. Basic data for 6 test beams reinforced with FRP bars for flexure and steel stirrups for shear

Beam	Ref. ID	b_w mm	d mm	a/d	f_c MPa	Flex. reinf.		Shear reinforcement				$v_{test} = V_{test}/bd$ MPa	Mode of failure	
						ρ_l %	E_f GPa	ρ_{fv} %	f_{sv} MPa	f_{bond} MPa	E_s GPa			
(1)	(2)	(3)	(4)	(5)	(6)	(7)	(8)	(9)	(10)	(11)	(12)	(13)	(14)	
Group D	1	Alsayed <i>et al</i> ¹⁹⁹⁷	200	309	2.36	35.2	1.30	43	0.35	286	---	200	1.675	ST
	2	Yonekura <i>et al.</i> (1993)	70	180	2.67	62	1.81	145	1.69	183	---	200	7.778	SC
	3		70	180	2.67	59.8	2.44	145	1.69	183	---	200	8.214	SC
	4	Nagasaka (1993)	250	253	1.78	38.2	1.9	56	0.8	1432	---	206	4.281	SC
	5	Nakamura and Higai (1995)	200	250	3	38.6	1.61	29	0.21	370	---	180	1.543	ST
	6		200	250	3	37.1	1.61	29	0.13	370	---	180	1.095	ST

Table 7-5. Measured and calculated ultimate shear stress for Group B beams, reinforced with FRP bars for flexure and FRP stirrups for shear

Beam	Ref. ID	v_{test} MPa	Proposed		ACI		JSCE		BRI		CHBDC		Eurocrete	
			v_n	$\frac{v_{test}}{v_n}$	v_n	$\frac{v_{test}}{v_n}$	v_n	$\frac{v_{test}}{v_n}$	v_n	$\frac{v_{test}}{v_n}$	v_n	$\frac{v_{test}}{v_n}$	v_n	$\frac{v_{test}}{v_n}$
			MPa	MPa	MPa	MPa	MPa	MPa	MPa	MPa	MPa	MPa	MPa	MPa
(1)	(2)	(3)	(4)	(5)	(6)	(7)	(8)	(9)	(10)	(11)	(12)	(13)	(14)	(15)
1	Vijay <i>et al.</i> (1996)	3.20	2.89	1.11	5.55	0.58	1.09	2.94	2.68	1.19	1.15	2.78	2.01	1.59
2		2.90	2.19	1.32	5.15	0.56	1.02	2.84	2.57	1.13	1.08	2.68	1.59	1.82
3		3.11	2.38	1.31	4.57	0.68	0.69	4.49	1.95	1.59	0.85	3.64	1.83	1.70
4		3.11	2.07	1.50	4.57	0.68	0.65	4.75	1.84	1.69	0.81	3.82	1.41	2.21
5	Alsayed <i>et al.</i> (1996, 97)	1.11	0.87	1.27	2.12	0.52	0.66	1.68	n/a	n/a	0.80	1.38	0.84	1.32
6		0.94	0.89	1.05	2.16	0.43	0.69	1.36	n/a	n/a	0.84	1.11	0.84	1.11
7		1.76	1.33	1.32	3.18	0.55	0.73	2.40	n/a	n/a	0.85	2.06	1.06	1.66
8	Zhao <i>et al.</i> (1995)	3.01	2.46	1.23	4.91	0.61	1.44	2.09	n/a	n/a	1.20	2.52	1.62	1.86
9		3.36	2.91	1.15	4.91	0.68	1.66	2.02	n/a	n/a	1.48	2.27	2.26	1.48
10		3.10	2.42	1.28	4.87	0.64	1.29	2.40	n/a	n/a	1.13	2.74	1.51	2.05
11		3.29	2.42	1.36	4.87	0.68	1.11	2.96	n/a	n/a	1.10	2.98	1.37	2.40
12		1.96	2.38	0.82	4.81	0.41	1.11	1.76	n/a	n/a	0.95	2.07	1.37	1.42
13	Duranovi <i>et al.</i> (1997)	3.11	1.85	1.68	4.45	0.70	0.85	3.65	n/a	n/a	0.90	3.44	1.13	2.76
14		4.23	1.87	2.26	4.48	0.94	0.85	4.96	n/a	n/a	0.90	4.67	1.13	3.76
15	Nagasaka <i>et al.</i> (1993)	3.89	3.12	1.25	4.63	0.84	1.06	3.66	3.79	1.03	1.10	3.55	2.21	1.76
16		4.92	3.50	1.40	5.00	0.98	1.30	3.79	4.56	1.08	1.37	3.59	3.65	1.35
17		5.68	3.44	1.65	4.92	1.15	1.40	4.06	4.87	1.17	1.35	4.21	5.00	1.14
18		3.23	3.07	1.05	4.54	0.71	1.06	3.03	2.98	1.08	1.00	3.24	2.21	1.46
19		4.37	3.19	1.37	4.54	0.96	1.21	3.60	3.48	1.26	1.15	3.80	3.62	1.21
20		4.47	3.19	1.40	4.54	0.98	1.33	3.37	3.85	1.16	1.27	3.53	4.79	0.93
21		2.51	3.08	0.82	4.78	0.53	1.12	2.25	2.67	0.94	1.06	2.37	2.25	1.12
22		3.63	3.37	1.08	4.78	0.76	1.28	2.84	3.17	1.15	1.23	2.96	3.65	0.99
23		3.18	2.66	1.20	4.86	0.65	1.02	3.11	2.79	1.14	0.96	3.30	1.60	1.99
24		4.30	2.70	1.59	4.95	0.87	1.16	3.71	3.19	1.35	1.11	3.88	2.35	1.83
25		2.68	1.97	1.36	4.59	0.58	0.98	2.73	2.50	1.07	0.92	2.91	1.39	1.93
26		3.85	2.35	1.64	4.86	0.79	1.08	3.55	2.73	1.41	1.03	3.75	1.94	1.98
27		2.78	2.43	1.14	4.95	0.56	1.00	2.77	2.63	1.06	0.94	2.94	1.42	1.95
28		3.61	2.48	1.46	5.04	0.72	1.12	3.22	2.94	1.23	1.07	3.37	2.00	1.81
29		3.27	2.89	1.13	4.11	0.80	1.12	2.93	3.27	0.99	1.04	3.15	3.57	0.92
30		3.51	2.83	1.24	4.03	0.87	1.20	2.93	3.61	0.97	1.12	3.13	4.24	0.83
31		2.89	2.91	0.99	4.13	0.70	1.13	2.55	2.92	0.99	1.06	2.73	3.57	0.81
32		3.02	2.83	1.07	4.02	0.75	1.21	2.51	3.25	0.93	1.13	2.68	4.27	0.71
33		3.01	2.20	1.37	4.03	0.75	0.98	3.07	2.73	1.10	0.89	3.37	2.26	1.33
34		3.21	2.20	1.46	4.03	0.80	1.05	3.06	2.99	1.07	0.97	3.32	2.99	1.07
35	3.01	1.98	1.52	4.11	0.73	0.95	3.18	2.35	1.28	0.95	3.18	1.86	1.62	
36	3.35	1.98	1.69	4.11	0.81	1.01	3.32	2.52	1.33	0.93	3.62	2.39	1.40	
37	4.62	3.71	1.24	5.27	0.88	1.51	3.06	4.25	1.09	1.48	3.12	5.00	0.92	
38	3.58	3.68	0.97	5.21	0.69	1.50	2.38	3.72	0.96	1.48	2.43	5.00	0.72	
39	Nakamura and Higai (1995)	1.67	1.52	1.10	3.84	0.43	0.69	2.41	1.43	1.16	0.81	2.06	0.92	1.82
40		2.00	1.51	1.32	3.82	0.52	0.68	2.95	1.43	1.40	0.79	2.55	0.92	2.18
41		1.12	0.94	1.20	2.39	0.47	0.66	1.71	1.31	0.86	0.77	1.46	0.78	1.44
42		1.32	0.94	1.41	2.39	0.55	0.66	2.02	1.34	0.99	0.77	1.72	0.78	1.70

Table 7-5 (cont'd). Measured and calculated ultimate shear stress for Group B beams, reinforced with FRP bars for flexure and FRP stirrups shear

Beam	Ref. ID	v_{test} MPa	Proposed		ACI		JSCE		BRI		CHBDC		Eurocrete	
			v_n	$\frac{v_{test}}{v_n}$	v_n	$\frac{v_{test}}{v_n}$	v_n	$\frac{v_{test}}{v_n}$	v_n	$\frac{v_{test}}{v_n}$	v_n	$\frac{v_{test}}{v_n}$	v_n	$\frac{v_{test}}{v_n}$
			MPa	MPa	MPa	MPa	MPa	MPa	MPa	MPa	MPa	MPa	MPa	MPa
(1)	(2)	(3)	(4)	(5)	(6)	(7)	(8)	(9)	(10)	(11)	(12)	(13)	(14)	(15)
43		1.58	1.24	1.28	2.04	0.78	0.80	1.97	n/a	n/a	0.82	1.92	0.84	1.89
44		1.63	1.24	1.31	2.05	0.80	0.81	2.02	n/a	n/a	0.83	1.97	0.84	1.95
45		1.31	1.26	1.04	2.08	0.63	0.80	1.63	n/a	n/a	0.82	1.59	0.83	1.58
46		2.49	1.22	2.04	1.97	1.26	0.81	3.06	n/a	n/a	0.84	2.97	0.86	2.91
47		1.28	1.21	1.06	1.95	0.66	0.81	1.57	n/a	n/a	0.84	1.53	0.86	1.50
48		1.13	1.20	0.94	1.94	0.58	0.81	1.39	n/a	n/a	0.84	1.35	0.86	1.32
49		1.51	1.15	1.31	1.82	0.83	0.81	1.87	n/a	n/a	0.83	1.82	0.84	1.80
50		1.66	1.23	1.34	2.00	0.83	0.82	2.02	n/a	n/a	0.84	1.97	0.87	1.91
51		2.41	1.54	1.57	2.76	0.88	0.85	2.85	n/a	n/a	0.88	2.73	0.94	2.56
52		1.59	1.31	1.21	2.24	0.71	0.78	2.03	n/a	n/a	0.79	2.01	0.86	1.85
53		1.28	0.96	1.34	2.06	0.62	0.63	2.04	n/a	n/a	0.77	1.66	0.69	1.85
54	Tottori and	1.51	1.15	1.32	2.54	0.60	0.64	2.37	n/a	n/a	0.78	1.93	0.72	2.09
55	Wakui	2.04	1.62	1.25	3.73	0.55	0.65	3.12	n/a	n/a	0.80	2.55	0.79	2.57
56	(1993)	1.65	1.03	1.60	2.25	0.73	0.63	2.61	n/a	n/a	0.78	2.12	0.72	2.31
57		1.21	1.03	1.17	2.25	0.54	0.63	1.90	n/a	n/a	0.78	1.55	0.72	1.69
58		1.65	1.14	1.46	2.44	0.68	0.72	2.28	n/a	n/a	0.94	1.76	0.72	2.31
59		1.33	0.79	1.67	1.65	0.80	0.63	2.11	n/a	n/a	0.77	1.72	0.70	1.90
60		1.54	1.23	1.26	2.44	0.63	0.65	2.36	n/a	n/a	0.75	2.05	0.80	1.92
61		2.20	1.87	1.18	4.01	0.55	0.69	3.16	n/a	n/a	0.80	2.74	0.95	2.32
62		1.90	1.24	1.53	2.46	0.77	0.81	2.34	n/a	n/a	0.77	2.49	0.97	1.97
63		2.16	1.29	1.67	2.53	0.85	1.04	2.08	n/a	n/a	0.97	2.22	1.18	1.83
64		1.07	0.89	1.20	1.62	0.66	0.51	2.08	n/a	n/a	0.69	1.54	0.62	1.73
65		1.55	1.51	1.03	3.32	0.47	1.07	1.44	n/a	n/a	0.90	1.71	1.11	1.40
66		5.21	3.22	1.62	6.60	0.79	1.21	4.32	n/a	n/a	1.15	4.52	1.08	4.81
67		3.44	3.93	0.88	7.41	0.46	1.26	2.73	n/a	n/a	1.23	2.80	1.15	3.01
68		3.89	2.20	1.76	4.05	0.96	1.27	3.05	n/a	n/a	1.25	3.11	1.16	3.36
69		2.81	2.82	1.00	5.58	0.50	1.22	2.29	n/a	n/a	1.17	2.40	1.05	2.68
70		3.66	1.98	1.85	3.50	1.05	1.24	2.95	n/a	n/a	1.20	3.05	1.10	3.31
71	Shehata	4.82	3.39	1.42	5.79	0.83	1.38	3.48	2.26	2.13	1.42	3.38	2.03	2.37
72	(1999)	4.81	3.03	1.59	5.79	0.83	1.36	3.55	1.83	2.63	1.39	3.45	1.92	2.51
Total no. of beams				72		72		72		34*		72		72
AVG				1.33		0.71		2.73		1.22		2.68		1.85
STD				0.27		0.17		0.79		0.35		0.82		0.72
COV (= STD/AVG)				0.20		0.24		0.29		0.29		0.31		0.39
no. of unconservative predictions** (< 1.0)				7		69		0		8		0		8

The BRI is applied for beams with a reported value for the bend strength of FRP stirrups.

** indicates the number of beams (out of the total number) for which $v_{test} < v_n$.

Table 7-6. Measured and calculated ultimate shear stress for Group C beams, reinforced with FRP stirrups for shear and steel bars for flexure

Beam	Ref. ID	v_{test} MPa	Proposed		ACI		JSCE		BRI		CHBDC		Eurocrete	
			v_n	$\frac{v_{test}}{v_n}$	v_n	$\frac{v_{test}}{v_n}$	v_n	$\frac{v_{test}}{v_n}$	<i>calc.</i>	$\frac{v_{test}}{v_n}$	v_n	$\frac{v_{test}}{v_n}$	v_n	$\frac{v_{test}}{v_n}$
			MPa	MPa	MPa	MPa	MPa	MPa	MPa	MPa	MPa	MPa	MPa	MPa
(1)	(2)	(3)	(4)	(5)	(6)	(7)	(8)	(9)	(10)	(11)	(12)	(13)	(14)	(15)
1	Alsayed ¹⁹⁹⁷	2.33	1.82	1.28	3.16	0.74	1.18	1.98	n/a	n/a	1.15	2.02	1.40	1.66
2	Nagasaka <i>et al.</i> (1993)	3.29	2.51	1.31	4.31	0.76	1.61	2.05	2.38	1.38	1.50	2.19	2.30	1.43
3		2.79	1.71	0.82	2.87	0.66	1.36	1.68	1.48	1.00	1.01	1.90	1.43	1.08
4		3.64	1.71	1.07	2.87	0.86	1.36	1.89	1.51	1.11	1.01	2.11	1.43	0.91
5		3.80	1.41	1.07	2.11	0.86	1.32	1.73	1.43	1.02	1.06	1.51	1.36	0.81
6	Nakamura and Higai (1995)	1.93	1.42	1.13	2.11	0.67	1.32	1.41	1.45	1.30	1.06	1.50	1.36	1.35
7		2.13	3.41	1.24	4.26	0.74	1.66	1.57	2.78	1.41	1.69	1.65	2.59	1.49
8		1.60	3.42	1.13	4.26	0.76	1.93	1.21	3.28	1.12	1.79	2.04	3.99	1.18
9		1.60	3.56	1.13	4.44	0.76	2.20	1.21	3.74	1.10	2.11	1.80	4.68	1.18
10	Tottori and Wakui (1993)	4.04	2.51	1.61	4.47	0.90	1.71	2.37	n/a	n/a	1.64	2.47	1.85	2.18
11		3.89	1.86	2.09	2.84	1.37	1.61	2.42	n/a	n/a	1.51	2.58	1.73	2.25
12		2.98	2.38	1.25	4.34	0.69	1.67	1.78	n/a	n/a	1.41	2.11	1.85	1.61
13		2.41	1.72	1.40	2.70	0.89	1.58	1.53	n/a	n/a	1.38	1.75	1.73	1.39
14		2.07	1.51	1.37	2.16	0.96	1.54	1.35	n/a	n/a	1.34	1.54	1.69	1.22
15		2.03	1.62	1.25	2.60	0.78	1.51	1.34	n/a	n/a	1.22	1.66	1.71	1.18
16		2.43	1.95	1.24	3.42	0.71	1.02	2.39	n/a	n/a	0.88	2.75	1.11	2.19
17		2.55	2.24	1.14	3.71	0.69	1.23	2.08	n/a	n/a	1.11	2.30	1.11	2.30
18		2.31	2.03	1.14	3.50	0.66	1.08	2.13	n/a	n/a	0.95	2.42	1.11	2.08
19		2.35	2.17	1.08	3.64	0.65	1.19	1.98	n/a	n/a	1.07	2.20	1.11	2.12
20		2.18	1.94	1.12	3.28	0.66	1.54	1.42	n/a	n/a	1.24	1.76	1.57	1.39
21		2.83	1.54	1.84	2.46	1.15	1.27	2.22	n/a	n/a	1.08	2.62	1.43	1.98
22		3.84	3.08	1.25	5.41	0.71	1.87	2.05	n/a	n/a	1.55	2.47	2.03	1.89
23	Shehata (1999)	4.37	2.80	1.56	5.32	0.82	1.58	2.76	2.28	1.92	1.48	2.96	1.81	2.42
24		5.37	3.59	1.50	6.02	0.89	1.71	3.15	2.47	2.17	1.64	3.28	2.20	2.45
25		5.92	4.38	1.35	5.85	1.01	1.77	3.34	2.59	2.29	1.71	3.47	2.60	2.27
26		4.60	3.15	1.46	6.02	0.76	1.55	2.97	1.92	2.40	1.41	3.27	1.71	2.70
27		4.93	2.63	1.88	4.72	1.04	1.37	3.60	1.63	3.02	1.36	3.62	2.05	2.40
28		4.91	2.63	1.87	4.72	1.04	1.45	3.39	1.73	2.84	1.33	3.69	2.41	2.04
Total no. of beams				28		28		28		14*		28		28
AVG				1.34		0.83		2.11		1.72		2.34		1.76
STD				0.30		0.17		0.69		0.71		0.66		0.54
COV (= STD/AVG)				0.22		0.21		0.33		0.41		0.28		0.31
no. of unconservative predictions** (< 1.0)				1		23		0		0		0		2

* The BRI is applied for beams with a reported value for the bend strength of FRP stirrups.

** indicates the number of beams (out of the total number) for which $v_{test} < v_n$.

Table 7-7. Comparison between measured, v_{test} , and calculated, v_n , shear strength for Group B beams, reinforced with FRP bars for flexure and FRP stirrups for shear

Design method	Proposed	ACI	JSCE	BRI	CHBDC	Eurocrete
(1)	(2)	(3)	(4)	(5)	(6)	(7)
Total no. of beams	72	72	72	34*	72	72
Average (AVG)	1.33	0.72	2.73	1.22	2.68	1.85
Standard deviation (STD)	0.27	0.17	0.79	0.35	0.82	0.72
COV (= STD/AVG)	0.20	0.24	0.29	0.29	0.31	0.39
Range- Low	0.82	0.41	1.36	0.86	1.11	0.71
High	2.26	1.26	4.96	2.63	4.67	4.81
<u>High</u>	2.76	3.07	3.65	3.06	4.21	6.77
<u>Low</u>						
No. of unconservative predictions** (< 1.0)	7	69	0	8	0	8

* The BRI is applied for beams with a reported value for the bend strength of FRP stirrups.

** indicates the number of beams (out of the total number) for which $v_{test} < v_n$.

Table 7-8. Comparison between measured, v_{test} , and calculated, v_n , shear strength for Group C beams, reinforced with FRP stirrups for shear and steel bars for flexure

Design method	Proposed	ACI	JSCE	BRI	CHBDC	Eurocrete
(1)	(2)	(3)	(4)	(5)	(6)	(7)
Total no. of beams	28	28	28	14*	28	28
Average (AVG)	1.34	0.83	2.11	1.72	2.34	1.76
Standard deviation (STD)	0.30	0.17	0.69	0.71	0.66	0.54
COV (= STD/AVG)	0.22	0.21	0.33	0.41	0.28	0.31
Range- Low	0.82	0.65	1.21	1.00	1.50	0.81
High	2.09	1.37	3.60	3.02	3.69	2.70
<u>High</u>	2.56	2.12	2.98	3.02	2.46	3.33
<u>Low</u>						
No. of unconservative predictions** (< 1.0)	1	23	0	0	0	2

*The BRI is applied for beams with a reported value for the bend strength of FRP stirrups.

** indicates the number of beams (out of the total number) for which $v_{test} < v_n$.

Table 7-9. Measured and calculated ultimate shear stress for Group B beams - CSA design approaches

Beam	Ref. ID	v_{test} MPa	simplified method		general method	
			v_n MPa	$\frac{v_{test}}{v_n}$	v_n MPa	$\frac{v_{test}}{v_n}$
(1)	(2)	(3)	(4)	(5)	(6)	(7)
1	Vijay <i>et al.</i> (1996)	3.20	3.14	1.02	2.08	1.53
2		2.90	2.32	1.25	1.68	1.73
3		3.11	2.90	1.07	1.98	1.57
4		3.11	2.21	1.41	1.49	2.09
5	Alsayed <i>et al.</i> (1996, 97)	1.11	0.98	1.13	0.82	1.34
6		0.94	1.01	0.93	0.85	1.09
7		1.76	1.44	1.22	1.08	1.63
8	Zhao <i>et al.</i> (1995)	3.01	2.69	1.12	2.70	1.12
9		3.36	3.03	1.11	2.81	1.19
10		3.10	2.69	1.15	2.24	1.38
11		3.29	2.69	1.22	2.28	1.44
12		1.96	2.69	0.73	1.65	1.19
13	Duranovi <i>et al.</i> (1997)	3.11	1.99	1.56	1.41	2.20
14		4.23	1.99	2.12	1.41	2.99
15	Nagasaka <i>et al.</i> (1993)	3.89	3.14	1.24	2.43	1.61
16		4.92	4.12	1.19	3.77	1.30
17		5.68	4.04	1.40	6.57	0.86
18		3.23	3.14	1.03	2.25	1.44
19		4.37	3.80	1.15	3.73	1.17
20		4.47	3.80	1.18	5.79	0.77
21		2.51	3.18	0.79	2.07	1.21
22		3.63	4.04	0.90	3.76	0.96
23		3.18	3.16	1.01	2.19	1.45
24		4.30	3.22	1.33	4.00	1.07
25		2.68	2.05	1.31	1.90	1.41
26		3.85	2.79	1.38	2.39	1.61
27		2.78	2.89	0.96	2.32	1.20
28		3.61	2.95	1.23	3.96	0.91
29		3.27	3.42	0.96	4.71	0.70
30		3.51	3.35	1.05	4.51	0.78
31		2.89	3.48	0.83	4.86	0.59
32		3.02	3.38	0.89	4.59	0.66
33		3.01	2.59	1.16	3.31	0.91
34		3.21	2.59	1.24	3.31	0.97
35		3.01	2.34	1.29	2.25	1.34
36		3.35	2.34	1.43	2.95	1.14
37		4.62	4.44	1.04	5.56	0.83
38		3.58	4.42	0.81	5.57	0.64
39	Nakamura and Higai (1995)	1.67	1.62	1.03	1.24	1.35
40		2.00	1.60	1.25	1.22	1.64
41		1.12	1.03	1.09	0.88	1.27
42		1.32	1.03	1.28	0.88	1.50

Table 7-9 (cont'd). Measured and calculated ultimate shear stress for Group B beams – CSA design approaches

Beam	Ref. ID	v_{test} MPa	simplified method		general method	
			v_n MPa	$\frac{v_{test}}{v_n}$	v_n MPa	$\frac{v_{test}}{v_n}$
(1)	(2)	(3)	(4)	(5)	(6)	(7)
43		1.58	1.51	1.05	1.12	1.41
44		1.63	1.51	1.08	1.12	1.45
45		1.31	1.53	0.86	1.14	1.15
46		2.49	1.47	1.69	1.24	2.01
47		1.28	1.47	0.87	1.10	1.16
48		1.13	1.47	0.77	0.93	1.21
49		1.51	1.42	1.06	1.09	1.38
50		1.66	1.50	1.11	1.13	1.47
51		2.41	1.80	1.34	1.24	1.95
52		1.59	1.55	1.02	1.13	1.40
53		1.28	1.11	1.16	0.83	1.54
54	Tottori and	1.51	1.30	1.16	0.95	1.59
55	Wakui	2.04	1.78	1.15	1.24	1.64
56	(1993)	1.65	1.19	1.39	0.88	1.88
57		1.21	1.19	1.02	0.88	1.37
58		1.65	1.33	1.24	1.00	1.65
59		1.33	0.95	1.40	0.78	1.70
60		1.54	1.44	1.07	0.93	1.65
61		2.20	2.08	1.06	1.30	1.69
62		1.90	1.42	1.34	1.17	1.63
63		2.16	1.42	1.52	1.54	1.40
64		1.07	0.98	1.09	0.82	1.31
65		1.55	1.62	0.95	1.68	0.92
66		5.21	3.57	1.46	2.46	2.12
67		3.44	4.31	0.80	2.52	1.37
68		3.89	2.59	1.50	1.77	2.19
69		2.81	3.21	0.88	1.90	1.48
70		3.66	2.36	1.55	1.70	2.15
71	Shehata	4.82	3.53	1.36	2.35	2.05
72	(1999)	4.81	3.60	1.34	2.50	1.92
Total no. of beams				72		72
AVG				1.16		1.41
STD				0.24		0.43
COV (= STD/AVG)				0.21		0.31
no. of unconservative predictions* (< 1.0)				14		13

* indicates the number of beams (out of the total number) for which $v_{test} < v_n$.

Table 7-10. Measured and calculated ultimate shear stress for Group C beams – CSA design approaches

Beam ID	Ref. ID	v_{test} MPa	simplified method		general method		
			v_n MPa	$\frac{v_{test}}{v_n}$	v_n MPa	$\frac{v_{test}}{v_n}$	
(1)	(2)	(3)	(4)	(5)	(6)	(7)	
1	Alsayed ¹⁹⁹⁷	2.33	2.08	1.12	1.71	1.36	
2	Nagasaka <i>et al.</i> (1993)	3.29	2.94	1.12	3.26	1.01	
3		2.79	3.58	0.78	3.62	0.77	
4		3.64	4.03	0.90	5.08	0.72	
5		3.80	4.20	0.90	5.53	0.69	
6	Nakamura and Higai (1995)	1.93	1.95	0.99	1.75	1.11	
7		2.13	1.95	1.09	1.74	1.22	
8		1.60	1.66	0.96	1.55	1.03	
9		1.60	1.66	0.96	1.55	1.03	
10	Tottori and Wakui (1993)	4.04	2.53	1.60	2.86	1.42	
11		3.89	1.87	2.07	2.30	1.69	
12		2.98	2.50	1.19	2.72	1.10	
13		2.41	1.84	1.31	2.06	1.17	
14		2.07	1.62	1.27	1.98	1.04	
15		2.03	1.77	1.14	1.98	1.02	
16		2.43	2.26	1.08	1.53	1.59	
17		2.55	2.64	0.97	1.71	1.49	
18		2.31	2.38	0.97	1.47	1.57	
19		2.35	2.57	0.92	1.57	1.50	
20		2.18	2.13	1.02	2.25	0.97	
21		2.83	1.70	1.66	1.68	1.68	
22		3.84	3.19	1.20	3.41	1.12	
23		Shehata (1999)	4.37	2.98	1.47	2.36	1.86
24	5.37		3.76	1.43	2.78	1.93	
25	5.92		4.55	1.30	3.01	1.97	
26	4.60		3.33	1.38	2.54	1.81	
27	4.93		3.10	1.59	2.93	1.68	
28	4.91		3.10	1.59	3.39	1.45	
Total no. of beams				28		28	
AVG				1.21		1.32	
STD				0.30		0.37	
COV (= STD/AVG)				0.24		0.28	
no. of unconservative predictions* (< 1.0)				9		4	

* indicates the number of beams (out of the total number) for which $v_{test} < v_n$.

Table 7-11. Comparison between measured, v_{test} , and calculated, v_n , shear strength for Group B beams – CSA and CHBDC design approaches

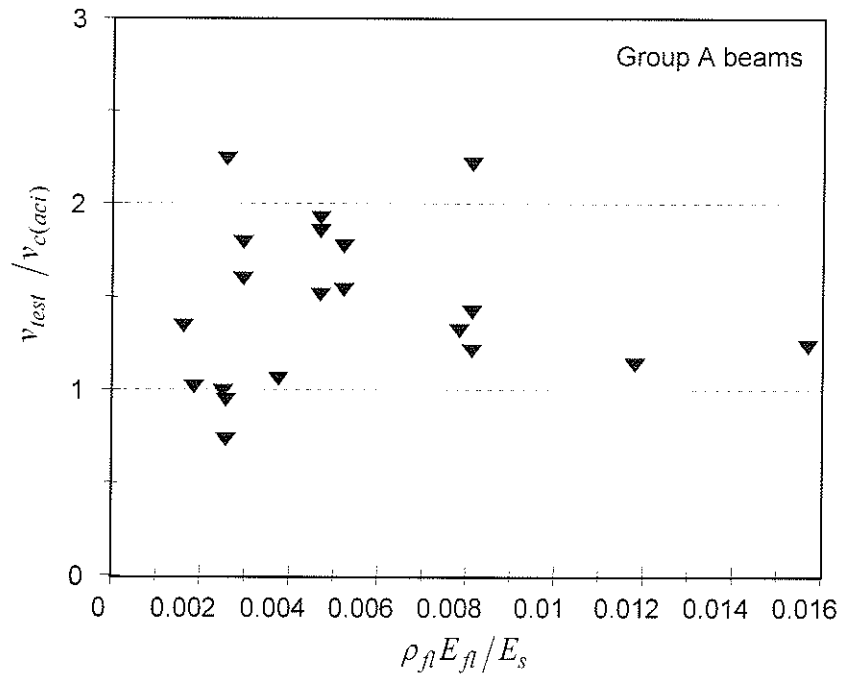
Design method	proposed simplified method	proposed general method	current CHBDC
(1)	(2)	(3)	(4)
Total no. of beams	72	72	72
Average (AVG)	1.16	1.41	2.68
Standard deviation (STD)	0.24	0.43	0.82
COV (= STD/AVG)	0.21	0.31	0.31
Range- Low	0.73	0.59	1.11
High	2.12	2.99	4.67
<u>High</u>	2.90	5.07	4.21
Low			
No. of unconservative predictions* (< 1.0)	14	13	0

* indicates the number of beams (out of the total number) for which $v_{test} < v_n$.

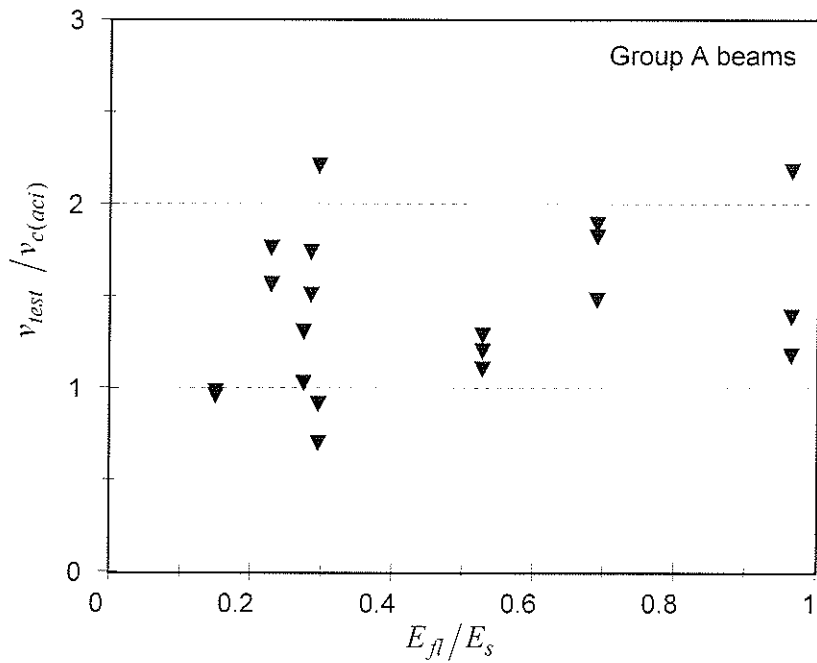
Table 7-12. Comparison between measured, v_{test} , and calculated, v_n , shear strength for Group C beams – CSA and CHBDC design approaches

Design method	proposed simplified method	proposed general method	current CHBDC
(1)	(2)	(3)	(6)
Total no. of beams	28	28	28
Average (AVG)	1.21	1.32	2.34
Standard deviation (STD)	0.30	0.37	0.66
COV (= STD/AVG)	0.24	0.28	0.28
Range- Low	0.78	0.69	1.50
High	2.08	1.97	3.69
<u>High</u>	2.67	2.86	2.46
Low			
No. of unconservative predictions* (< 1.0)	9	4	0

* indicates the number of beams (out of the total number) for which $v_{test} < v_n$.

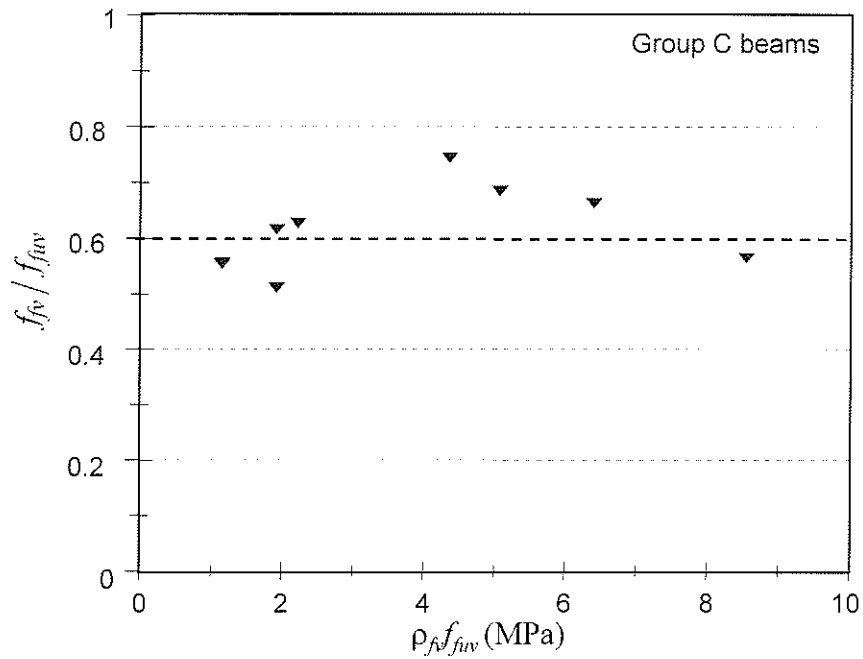


(a) Effect of $\rho_{fl} E_{fl} / E_s$

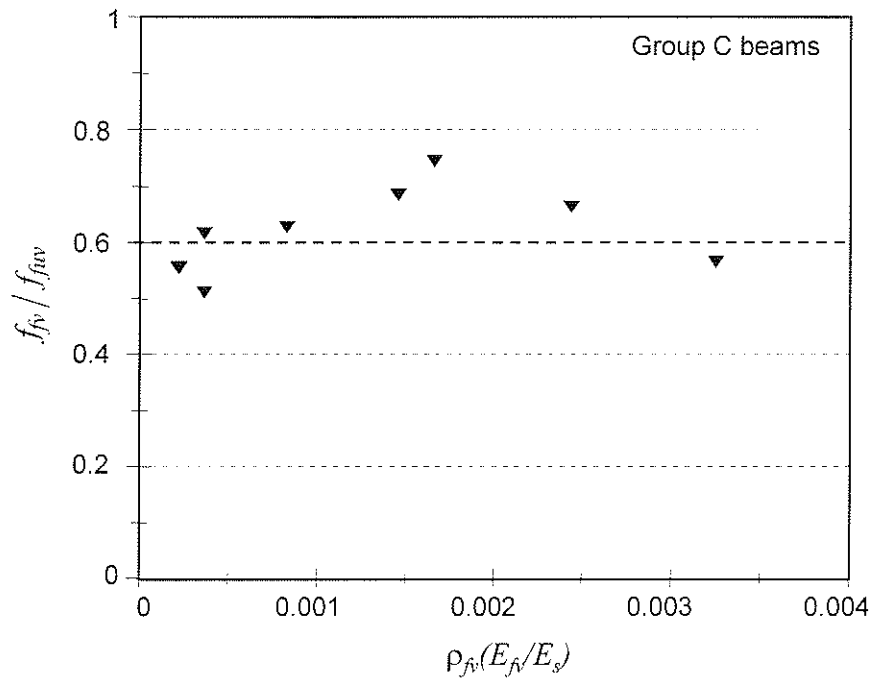


(b) Effect of E_{fl} / E_s

Figure 7-1. Effect of FRP longitudinal reinforcement on shear strength of beams without shear reinforcement

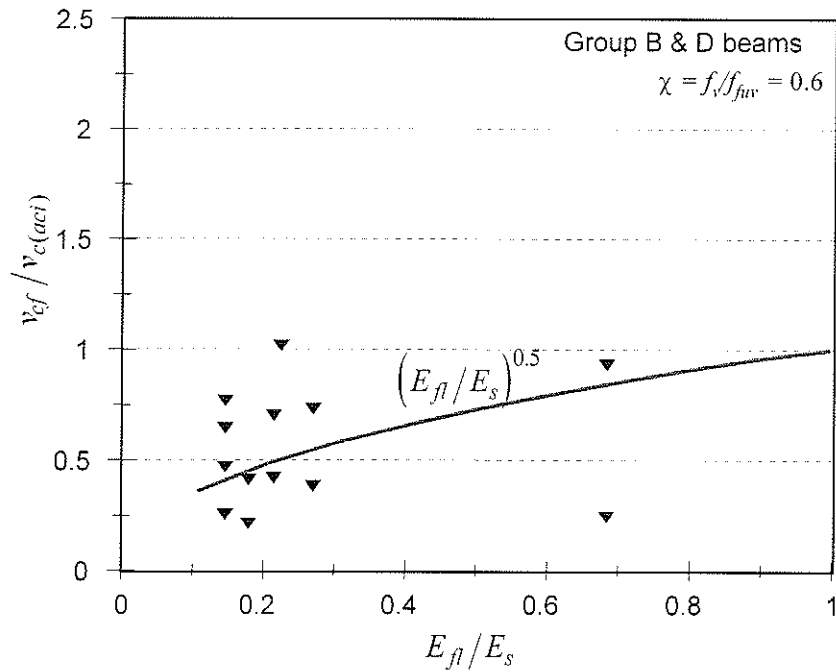


(a) variation with $\rho_{fv} f_{fuv}$

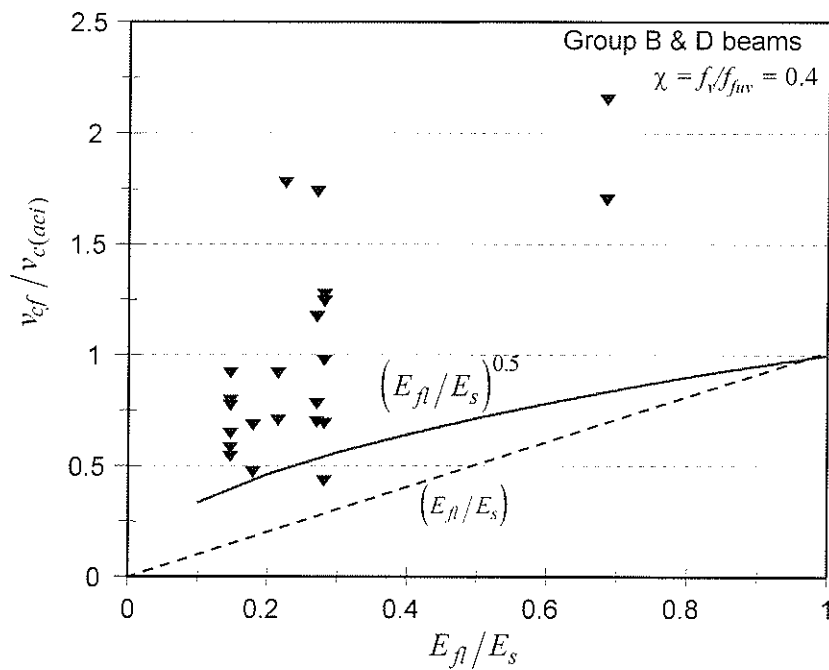


(b) variation with $\rho_{fv} (E_{fv} / E_s)$

Figure 7-2. Effective stirrup stress at ultimate in beams reinforced with FRP stirrups

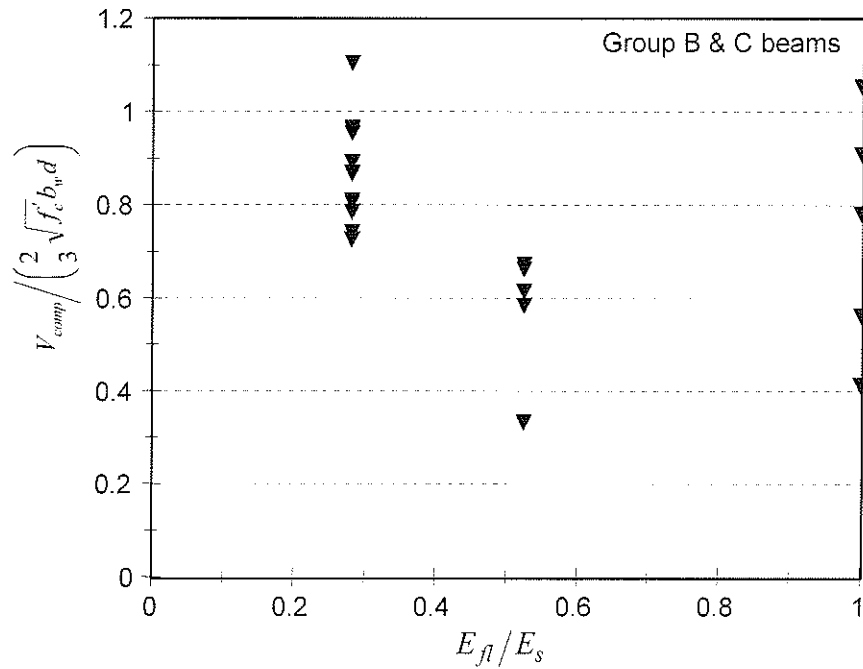


(a) based on average stirrup contribution

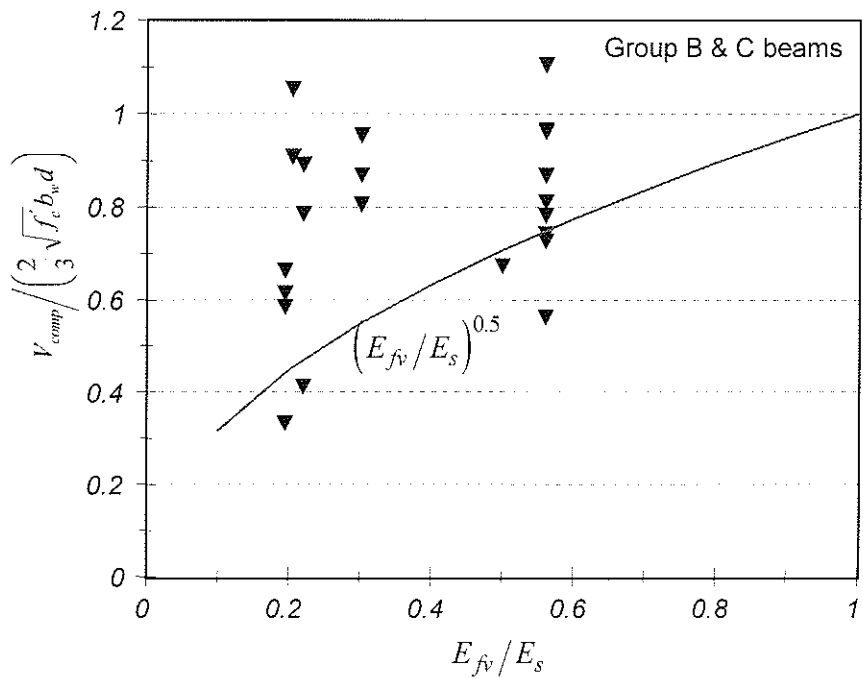


(b) based on safe stirrup contribution

Figure 7-3. Evaluation of concrete contribution to the shear strength of beams reinforced with FRP



(a) effect of E_{f1}



(b) effect of E_{fv}

Figure 7-4. Shear strength of beams reinforced with FRP and governed by shear-compression mode of failure

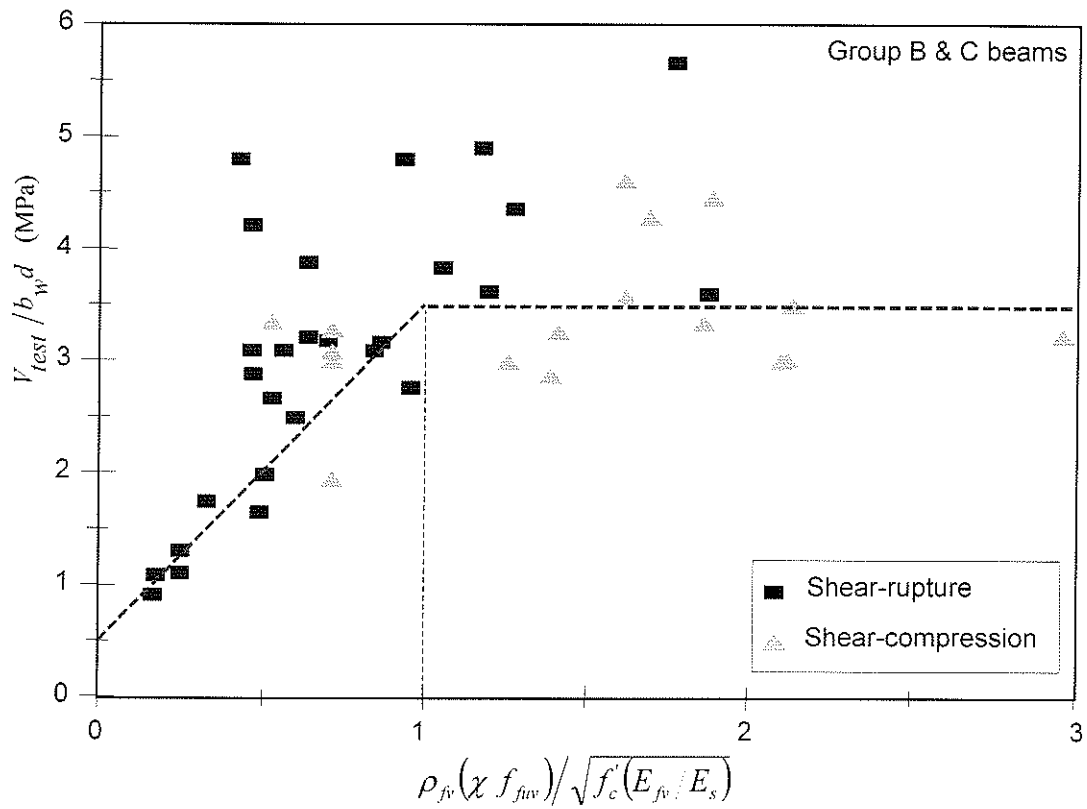
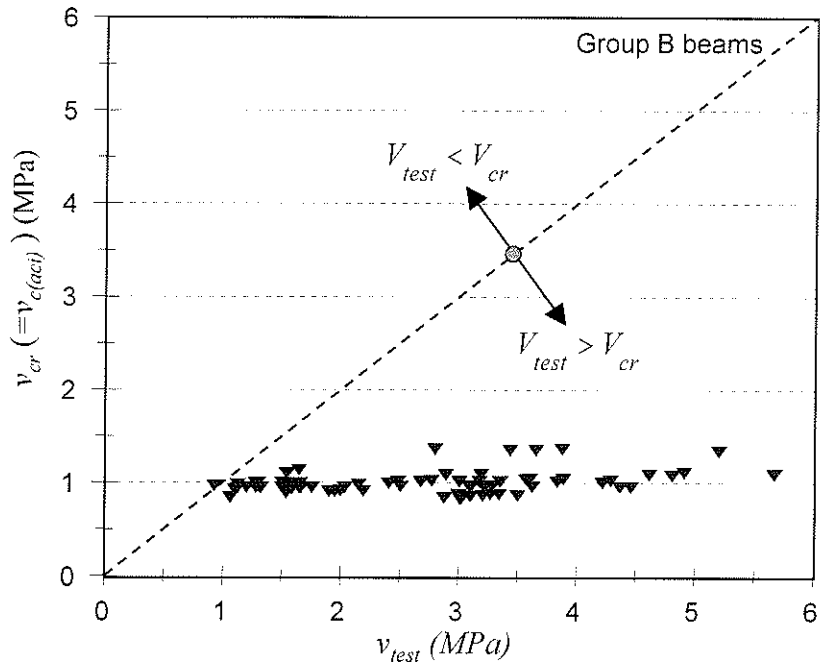
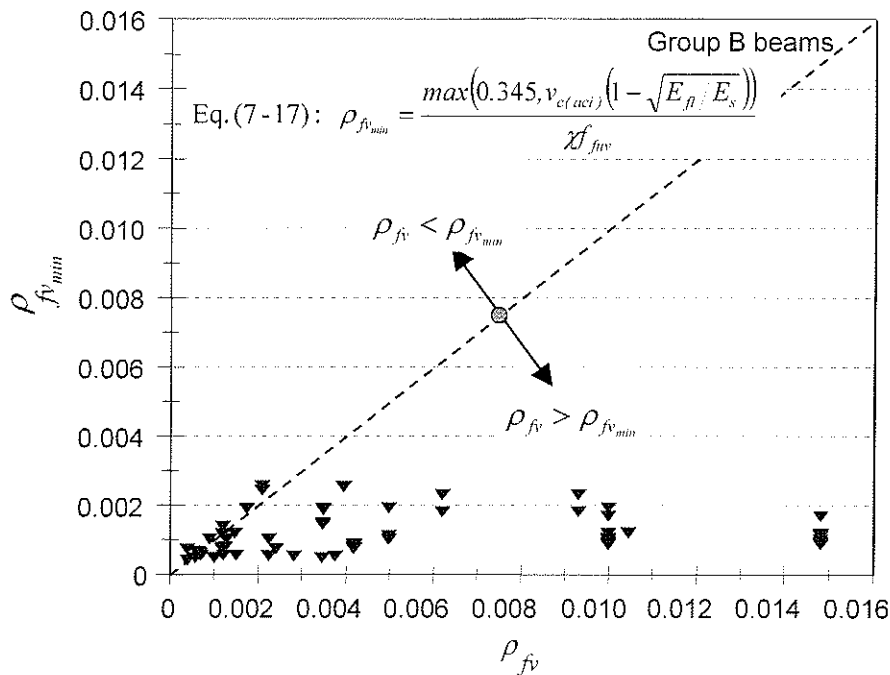


Figure 7-5. Shear-rupture failure versus shear-compression failure



(a) diagonal tension cracking stress, $v_{cr}(v_{c(aci)})$ versus measured shear capacity, v_{test}



(b) proposed ρ_{fvmin} versus provided ρ_{fv}

Figure 7-6. Requirement of minimum shear reinforcement: ACI approach

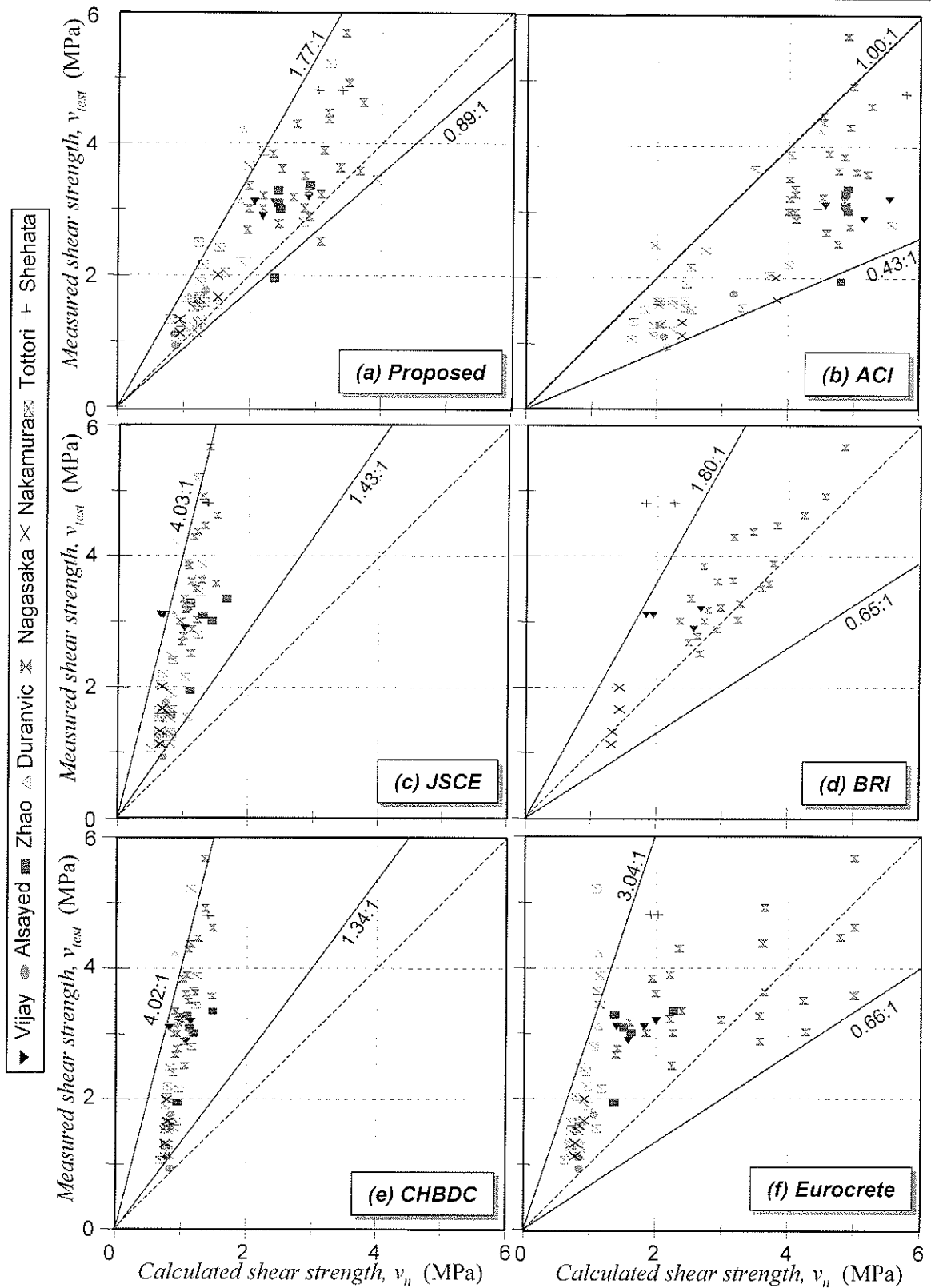


Figure 7-7. Measured ultimate shear stress versus calculated from : (a) Proposed Design equations (7-10) and (7-13), (b) ACI318-95 Code (1995), (c) JSCE method 1 (1997), (d) BRI method (1997), (e) CHBDC Code (1998), and (f) Eurocrete project (1996); for beams reinforced with FRP for shear and flexure and tested by many researchers

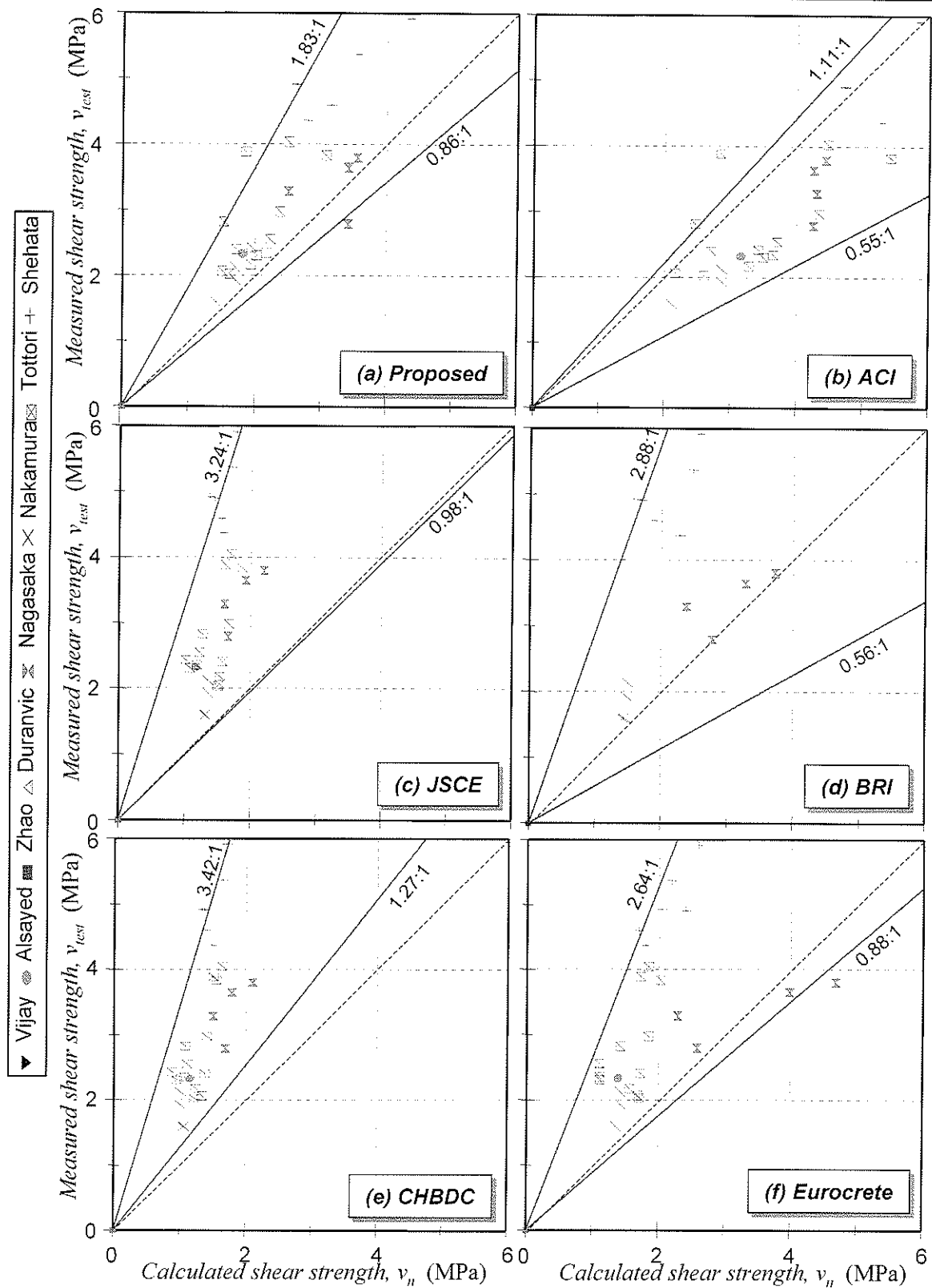
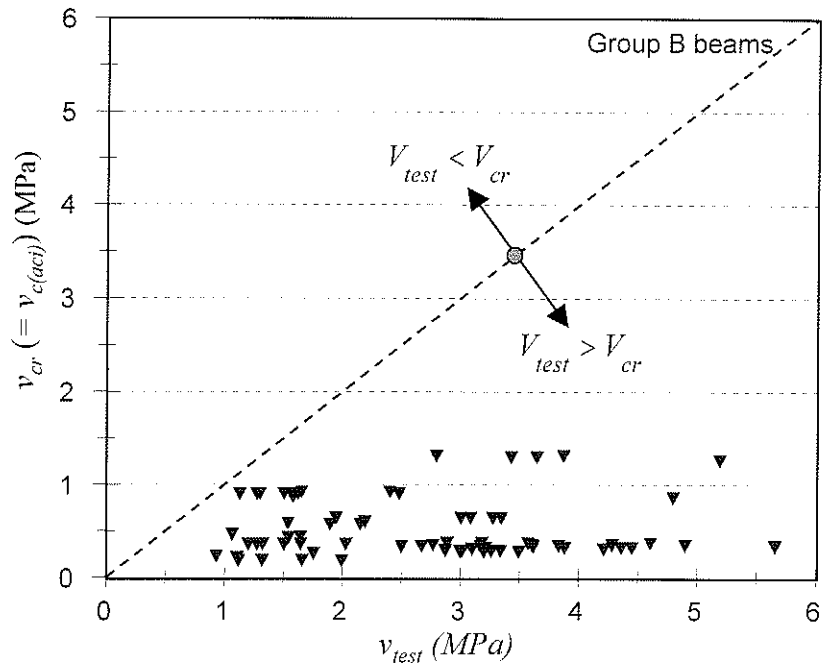
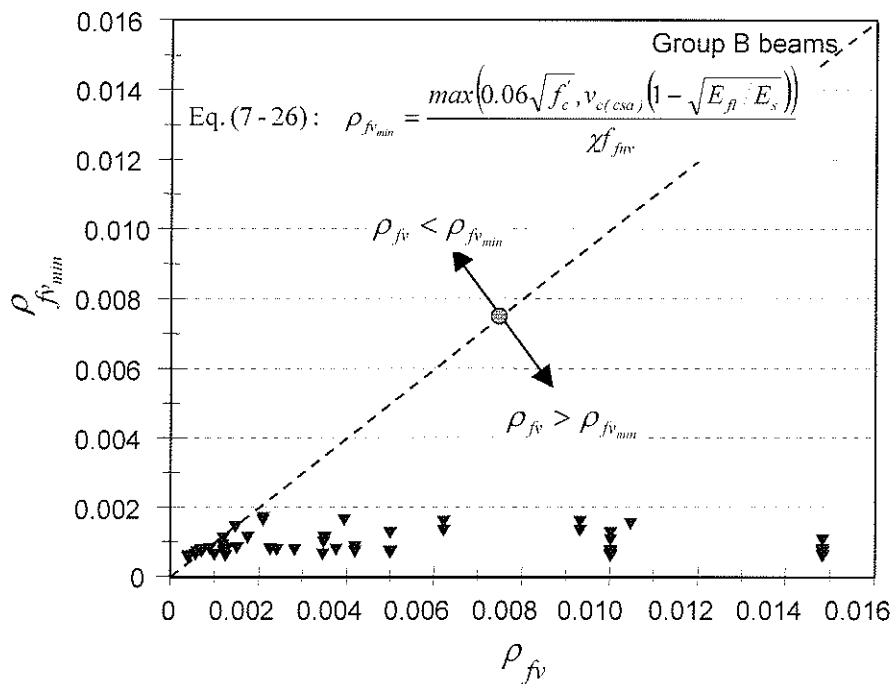


Figure 7-8. Measured ultimate shear stress versus calculated from : (a) Proposed Design equations (7-10) and (7-13), (b) ACI318-95 Code (1995), (c) JSCE method 1 (1997), (d) BRI method (1997), (e) CHBDC Code (1998), and (f) Eurocrete project (1996); for beams reinforced with FRP for shear and steel for flexure and tested by many researchers



(a) diagonal tension cracking stress, $v_{cr}(v_{c(aci)})$ versus measured shear capacity, v_{test}



(b) proposed ρ_{fvmin} versus provided ρ_{fv}

Figure 7-9. Requirement of minimum shear reinforcement: CSA approach

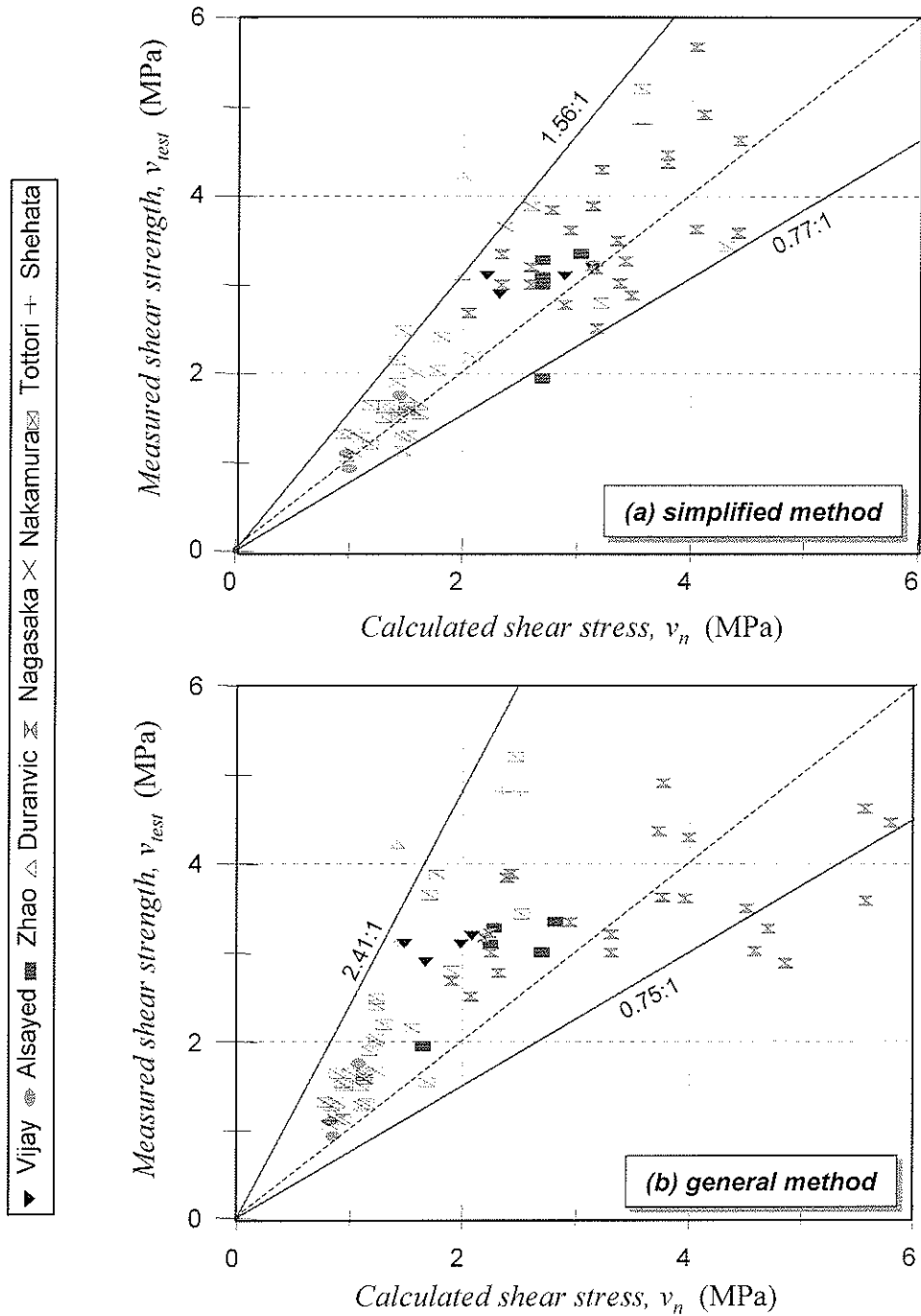


Figure 7-10. Measured ultimate shear stress versus calculated from proposed design equations based on: (a) the simplified method in the CSA23.3-94 code (equation 7-18), and (b) the general method in the CSA23.3-94 code (equation 7-21); for beams reinforced with FRP for shear and flexure and tested by many researchers

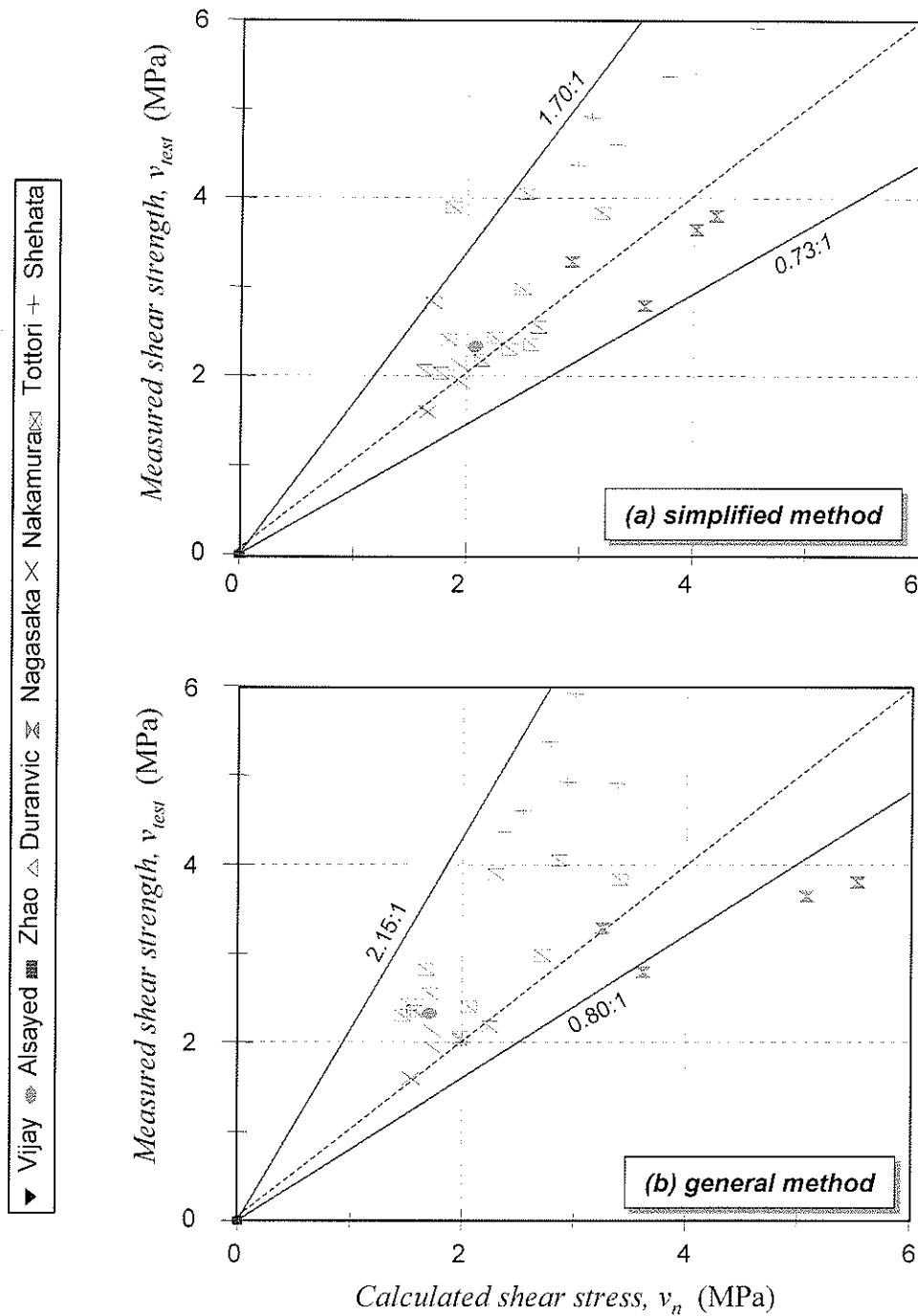


Figure 7-11. Measured ultimate shear stress versus calculated from proposed design equations based on: (a) the simplified method in the CSA23.3-94 code (equation 7-18), and (b) the general method in the CSA23.3-94 code (equation 7-21); for beams reinforced with FRP for shear and steel for flexure and tested by many researchers

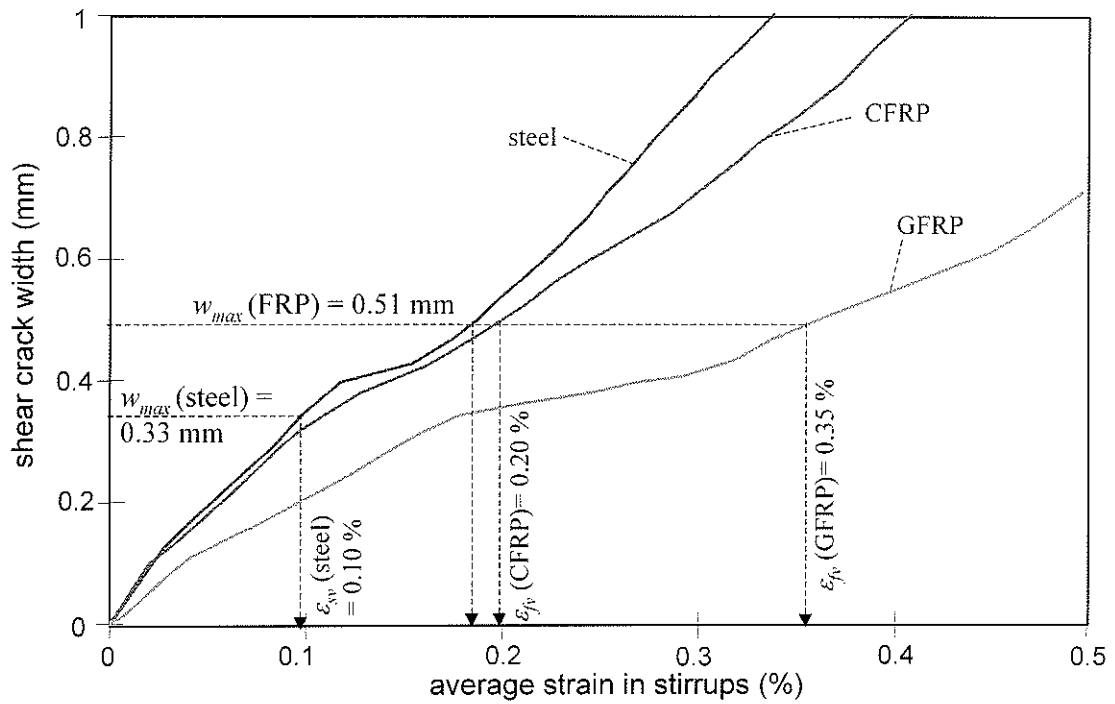


Figure 7-12. Serviceability requirement: shear crack width versus average strain in stirrups

Chapter

8

Summary and Conclusions

8.1 Summary

The current study has investigated the performance of FRP stirrups as shear reinforcement for concrete structures. The scope of the study consisted of an experimental investigation and an analytical investigation. Based on the findings of the experimental and analytical investigations, design guidelines are proposed to use FRP as shear reinforcement for concrete structures. The research also includes proposed analytical models to predict the shear strength and behaviour of concrete beams reinforced with FRP.

The experimental program consisted of two phases. The first experimental phase, Phase I, was designed to evaluate the strength capacity of a single FRP stirrup as influenced by bending of the FRP bars to achieve the appropriate anchorage and by the diagonal shear cracks that have an angle to the direction of the fibres. Three types of FRP reinforcement were used in this program, carbon FRP Leadline stirrups, carbon fibre composite cables (CFCC) stirrups and Glass FRP C-BAR stirrups. One hundred and thirteen specially designed specimens were tested. These specimens included 94 bend specimens tested to

evaluate the bend capacity of the FRP stirrups, and ten kink specimens tested to investigate the kink effect due to diagonal orientation with respect to the direction of the fibres. Seven bend specimens and two kink specimens reinforced with steel stirrups were also tested as control specimens. The test results of the bend specimens were compared to different equations available in the literature to evaluate the strength capacity of FRP stirrups as influenced by the bend. Two analytical models were used to predict the behaviour of FRP stirrups in kink specimens. The first model “Model A” assumes full bond between the FRP stirrups and the concrete, while the second model “Model B” assumes debonding length for FRP stirrups at their intersection with the inclined crack.

The second experimental phase, Phase II, comprised ten reinforced concrete beams tested to failure to investigate the modes of failure and the ultimate carrying capacity of the FRP stirrups in the beam action mechanism. The shear deformation, crack width, and stirrup strain were examined. The ten beams included four beams reinforced with carbon FRP stirrups, four beams reinforced with glass FRP, one beam reinforced with steel stirrups and one control beam without shear reinforcement. The variables considered in the second phase were the material of the stirrups, material of the flexural reinforcement, and the stirrup spacing. Two types of FRP stirrups were used as shear reinforcement: carbon FRP (CFRP) and glass FRP (GFRP). Steel and CFRP strands were used as flexural reinforcement for concrete beams. All the beams failed in shear, either by rupture of FRP stirrups at the bend or crushing of the concrete under the load and in the web.

The analytical phase included analysis of the test results to describe the various factors affecting the strength capacity of the FRP stirrups. The test results for the beam specimens were compared to different analytical models used to predict the shear strength and

behaviour of beams reinforced with FRP. The analytical models used to predict the behaviour of the beams included simplified shear design methods and recently developed shear theories. The shear design equations specified in the current ACI 318-95 code for concrete members reinforced with steel were used to predict the shear strength of the tested beams. In addition, shear equations proposed by Japanese, Canadian and European task committees for concrete members reinforced with FRP were used. The beams were also analyzed using two well-established shear theories: the shear friction model (SFM) and the modified compression field theory (MCFT). Shear crack widths in the tested beams were also predicted using equations available in the literature. The predictions of the shear models were compared with the results of the experimental program. Based on the test results of the beam specimens tested in this study and an additional 118 beams tested by others, design guidelines are proposed to assist code writers in establishing design specifications for the use of FRP as shear reinforcement in concrete structures.

8.2 Conclusions

The current study has shown that FRP stirrups can be effectively used for shear reinforcement in concrete structures. However, certain issues should be considered for the design of concrete members reinforced with FRP stirrups. The findings of the current study are summarized in the following sections.

8.2.1 Strength of a single FRP stirrup

Based on the test results and analysis of the 101 bend specimens and 12 kink specimens, the following conclusions are reached:

1. The test procedure used to examine the bend capacity of FRP stirrups is simple and easy to perform. It is recommended to adopt this procedure as a standard ASTM test method for FRP stirrups and bent bars.
2. Failure in the CFRP Leadline stirrups is mainly due to bond failure between the fibres and the outer resin coating. This behaviour was observed for the CFRP Leadline stirrups used to reinforce the bend and beam specimens.
3. The bond strength of the CFRP Leadline bar was determined based on bond tests as 8.7 MPa. The bond strength of the CFRP Leadline bar was found to be less than that of the CFRP CFCC and GFRP C-BAR reinforcement reported in the literature.
4. Failure of the C-BAR stirrups occurred either at the bend or at the straight portion of the stirrup, due to the “waving” imperfection in the C-BAR stirrups. However, the strength capacity of the C-BAR stirrups was found to be equal to or greater than 48 percent of the guaranteed strength parallel to the fibres, as reported by the manufacturer.
5. A decrease in the embedment length, l_d , of the stirrup increases the possibility of failure at the bend zone of the stirrup, resulting in an average strength as low as 35 percent of the strength in the direction of the fibres.
6. An embedment length-to-diameter ratio, l_d/d_e , of 20 for the CFRP CFCC stirrups with standard hook and minimum tail length l_d^* of $6d_e$, 16 for the CFRP CFCC stirrups with

continuous anchorage and 42 for the CFRP Leadline stirrups, is sufficient to develop the full guaranteed strength parallel to the fibres. For an embedment length-to-diameter ratio of less than the limiting values, the strength can be predicted using the equations proposed in chapter 5.

7. The tail length, l_d^* , of the type A stirrups did not significantly affect the strength capacity of CFRP Leadline and GFRP C-BAR stirrups. Type A anchored CFRP CFCC stirrups with a tail length-to-diameter ratio, l_d^*/d_e , of 15 or greater developed the full guaranteed strength in the direction of the fibres.
8. The following limitations are proposed for detailing of FRP stirrups and to achieve a stirrup capacity of at least 50 percent of the guaranteed strength parallel to the fibres:
 - a- The bend radius, r_b , should not be less than four times the effective bar diameter or 50 mm, whichever is greater.
 - b- The tail length, l_d^* , should not be less than six times the effective bar diameter or 70 mm, whichever is greater.
9. Test results of kink specimens were compared to equations available in the literature to determine the diagonal tensile strength of FRP stirrups. The available equations, that assume full bond between the concrete and the FRP stirrups, did not show good agreement with test results. Two equations were proposed to determine the diagonal tensile strength of FRP stirrups as influenced by the crack angle, θ .
10. The average measured strain at failure was found to be higher than 80 percent of the ultimate strain in the direction of the fibres for both CFRP and GFRP stirrups.
11. It was shown that for kink specimens the stress in an FRP stirrup at failure could be as low as 65 percent of the guaranteed tensile strength parallel to the fibres. Meanwhile, it

was observed for bend tests that the stress at failure could be as low as 35 percent of the guaranteed strength in the direction of the fibres. Therefore, the bend effect on the strength capacity of FRP stirrups is more critical than the kink effect and should be used to limit the contribution of FRP stirrups in beam action.

8.2.2 Behaviour of FRP stirrups in beam action

Based on the test results of the ten beam specimens tested in the second experimental phase, the following conclusions are reached:

12. All tested beams failed in shear. The beams that failed in the shear–compression mode due to crushing of the concrete gave more warning before failure than those that failed in the shear–rupture mode. This is attributed to the softening of the concrete that occurred prior to failure.
13. For beams reinforced with steel strands for flexure, the concrete contribution component, V_c to the shear resisting mechanism, at any load level, was higher than the shear force at the initiation of the first shear crack, V_{cr} .
14. Beams reinforced with CFRP strands for flexure, showed less concrete contribution, V_c , than beams reinforced with steel strands. This is attributed to the wide cracks, small depth of the compression zone and less dowel contribution associated with the use of FRP as longitudinal reinforcement.
15. Using a small stirrup spacing to increase the shear strengths of concrete beams, increases the chance for shear cracks to intersect the bend zone of FRP stirrups and consequently causes a significant reduction of the effectiveness of FRP stirrups.

16. Test results indicated that the effective capacity of FRP stirrups in beam action might be as low as 50 percent of the guaranteed strength parallel to the fibres, provided that the failure occurs due to rupture of FRP stirrups.
17. The use of FRP as shear reinforcement in concrete beams did not affect the observed load level of initiation of the first diagonal crack. The angle of shear cracks in concrete beams reinforced by FRP stirrups varied between 42 to 46 degrees. These values are typical for reinforced concrete beams.
18. The shear deformations are affected not only by the elastic modulus of the stirrup material but also by other factors such as the bond characteristics of the stirrups. The beams reinforced with GFRP C-BAR stirrups showed a better distribution of shear cracks than those reinforced with CFRP Leadline stirrups.
19. The use of CFRP strands for flexure resulted in a slight increase in the shear crack width at the same load level in comparison to beams reinforced with steel strands.
20. For the same strain level in the stirrups, the crack width in concrete beams reinforced with CFRP or GFRP stirrups was found to be smaller than the crack width in concrete beams reinforced with steel stirrups.
21. The variation in the stirrup material and spacing does not significantly affect the load-deflection characteristics of test beams with span-to-depth ratios greater than 10.
22. The relatively inexpensive GFRP stirrups can be a good alternative for shear reinforcement in concrete structures.

8.2.3 Analysis of beam specimens

Based on the analysis of the beam specimens using the simplified shear design methods and the recently developed shear theories, the following conclusions are made:

23. The direct application of the current ACI 318 code to concrete beams reinforced with FRP overestimates the shear strength.
24. The shear equations in the available design guidelines for concrete members reinforced with FRP greatly underestimate the shear strength of tested beams. This is mainly attributed to the fact that the recommended equations are based on low values of stirrup strains to satisfy the serviceability requirement, while they are formulated to predict the ultimate limit shear strength.
25. The shear friction model (SFM) introduced by Loov (1998), used to predict the shear strength of the ten concrete beams tested in the current study, provides an excellent analytical model for the prediction of the behaviour of beams reinforced with FRP stirrups. However, the limit imposed on the SFM to avoid the shear–compression failure has to be re-evaluated for beams reinforced with either steel or FRP. Although the proposed equation for the shear friction factor, k , resulted in good prediction for the shear strength of beams reinforced longitudinally with FRP, further development for the theory is recommended to account for the effect of using FRP as longitudinal reinforcement.
26. The use of the bend capacity of CFRP stirrups as a failure criterion for the MCFT analysis of beams provides a reasonably conservative prediction for the shear strength of beams reinforced with CFRP stirrups. The MCFT also results in good prediction for

the shear behaviour in terms of the average strain in CFRP stirrups. However, the MCFT overestimates the shear crack width in concrete beams reinforced with CFRP or steel stirrups. The computer program “RESPONSE” used to apply the MCFT analysis needs certain adjustment for GFRP reinforcement with a low elastic modulus.

27. A simplified method for the estimation of shear crack width in concrete beams reinforced with FRP as shear reinforcement and/or FRP or steel as longitudinal reinforcement is proposed.

8.2.4 Design guidelines

Based on the test results of the beam specimens tested in the current study and an additional 118 beams tested by others, design guidelines are proposed to establish design specifications for the use of FRP as shear reinforcement in concrete structures:

28. The most significant factors affecting the shear strength of concrete beams reinforced with FRP were found to be the elastic modulus of FRP and the strength reduction of FRP stirrups due to bend and kink effects.
29. The shear strength of beams reinforced with FRP without shear reinforcement can be predicted by the current ACI equation for V_c , as long as the diagonal tension cracking is considered as the ultimate limit state. This is not the case for slabs reinforced by FRP due to their small depth-to-span ratio.
30. The concrete contribution to the shear strength of concrete beams reinforced with FRP for shear and flexure can be estimated using $V_{c(aci)}$ and a multiplier factor based on the square root of the ratio E_f/E_s , where E_s is the reference elastic modulus ($E_s = 200$ GPa).

31. The FRP stirrups should be designed for 40 percent of the guaranteed strength parallel to the fibres to account for the strength reduction due to the bend effect.
32. In the case of shear failure initiated by crushing of the concrete, the ultimate shear capacity of concrete beams reinforced with FRP is proposed to be proportional to the square root of E_{fv}/E_s .
33. The shear-rupture failure mode might be distinguished from the shear-compression failure mode by means of the parameter $\rho_{fv}(f_{uv})/\sqrt{f'_c(E_{fv}/E_s)}$. For values of $\rho_{fv}(f_{uv})/\sqrt{f'_c(E_{fv}/E_s)}$ of 2.5 or less, shear-rupture may occur, and for values higher than 2.5, a shear-compression failure is expected.
34. The effect of the various factors are compiled into the proposed revisions to ACI as given in equations (7-10) and (7-13). The proposed equations make it possible to assess the ultimate shear strength of concrete beams reinforced with FRP more accurately than other considered methods, although maintaining the same level of computational effort as the current ACI code.
35. Similar equations are proposed based on the shear design approaches currently adopted in the CSA 23.3-94 code. The proposed equation (7-19) based on the simplified CSA 23.3 approach was found to be more reliable and precise than those equations based on the general method.
36. Expressions for minimum shear reinforcement in concrete beams reinforced with FRP (equation (7-17) for ACI code and equation (7-26) for CSA code) are proposed to ensure that the shear strength exceeds the shear cracking load.

37. Strain limits for CFRP and GFRP stirrups are proposed to control the shear crack width in concrete beams. The proposed limits provides appropriate limit for the shear crack width at service load level.

8.3 Recommendations for future work

Based on the findings and conclusions of the current study, the following recommendations are made for future research in FRP shear reinforcement:

1. The concrete contribution in concrete beams reinforced with FRP bars for flexure needs further investigation. Experimental programs to evaluate the effect of the elastic modulus of longitudinal reinforcement on the shear behaviour of concrete beams are recommended.
2. Research is needed for more refinement of the currently available rational shear theories to incorporate the FRP as reinforcement in concrete structures.
3. Improvement in the fabrication of FRP stirrups should be considered to minimize the strength reduction due to the bend portions.
4. The behaviour of concrete beams prestressed by FRP and reinforced with FRP or steel for shear should be considered for future investigations.

REFERENCES

1. ACI Committee 318, 1995; "Building Code Requirements for Reinforced Concrete and Commentary," ACI 318M-95/ACI 318RM-95, American Concrete Institute, Detroit.
2. ACI 440R-96, 1996; "State-of-the-Art Report on Fiber Reinforced Plastic Reinforcement for Concrete Structures," American Concrete Institute, Detroit, Michigan, 68 p.
3. ACI Committee 440, 1998; "Provisional Design Recommendations for Concrete with FRP Bars," Draft 2, reviewed in the ACI Fall Convention, L.A., Oct. 1998.
4. AIJ 1987; "Data for Ultimate Strength Design of Reinforced Concrete Structures," Architectural Institute of Japan, pp. 52-55.
5. Alsayed, S., Y. Al-Salloum, T. Almusallam, and M. Amjad, 1996; "Evaluation of Shear Stresses in Concrete Beams Reinforced by FRP Bars," Proceedings of the Second International conference on Advanced Composite Materials for Bridges and Structures (ACMBS-II), Montreal, Québec, August, pp. 173-179.
6. Alsayed, S., Y. Al-Salloum, and T. Almusallam, 1997; "Shear Design of GFRP Bars," Proceeding of the Third International Symposium on Non-Metallic (FRP) Reinforcement for Concrete Structures, Sapporo, Japan, Oct.1997, Vol.2, pp. 285-292.
7. ASCE-ACI Committee 426, 1973; "Shear Strength of Reinforced Concrete Members", ASCE Proceedings, Vol. 99, ST6, June, pp. 1091-1188.

8. ASCE-ACI Committee 445 on Shear and Torsion, 1998; "Recent Approaches to Shear Design of Structural Concrete," *Journal of Structural Engineering*, ASCE, Vol. 124, No. 12, December, pp. 1375-1417.
9. ASTM C39-96, 1996; "Standard Test Method for Compressive Strength of Cylindrical Concrete Specimens," developed by ASTM Subcommittee C09.61, 5 p.
10. ASTM C496-96, 1996; "Standard Test Method for Splitting Tensile Strength of Cylindrical Concrete Specimens," developed by ASTM Subcommittee C09.61, 4 p.
11. Bank, L. and A. Shapira, 1997; "Structural and Construction Aspects of Novel Multidirectional Reinforcements for Concrete," Proceeding of the Third International Symposium on Non-Metallic (FRP) Reinforcement for Concrete Structures, Sapporo, Japan, Oct.1997, Vol.2, pp. 623-630.
12. Bazant, Z. and J. Kim, 1984; "Size Effect in Shear Failure of Longitudinally Reinforced Beams," *ACI Journal*, V. 81, No. 5, Sept.-Oct., pp. 456-468.
13. Bedard, C., 1992; "Composite Reinforcing Bars: Assessing Their Use in Construction," *Concrete International*, Vol. 14, No. 1, pp. 55-59.
14. Beeby, A., 1979; "The Prediction of Crack Widths in Hardened Concrete," *The Structural Engineer Journal*, Vol. 57A, No.1, Jan., pp. 9-17.
15. Bhide, S., and M. Collins, 1989; "Influence of axial tension on the shear capacity of reinforced concrete members," *ACI Structural Journal*, V. 86, No. 5, Sept.-Oct., pp. 570-581.
16. Canadian Highway Bridge Design Code (CHBDC), 1998; "Fibre Reinforced Structures," Section 16, Final Draft, Feb. 1998.

17. Canadian Standards Association (CSA), 1994; "Design of Concrete Structures for Buildings (CAN-A23.3-94)", Rexdale, Ontario, 220 p.
18. CHBDC Technical Subcommitte No. 16, 1996; "Design Provisions for Fibre Reinforced Structures in the Canadian Highway Bridge Design Code," Proceedings of the Second International conference on Advanced Composite Materials for Bridges and Structures (ACMBS-II), Montreal, Québec, August, pp. 391-406.
19. Comite Euro-International Du Beton (CEB), 1978; "CEB-FIP Model Code for Concrete Structures", 420 p.
20. Choi, I., J. Niwa, and T. Tanabe, 1997; "Predicted Shear resisting Mechanism of FRP Reinforced Concrete Beams by Lattice Model," Proceeding of the Third International Symposium on Non-Metallic (FRP) Reinforcement for Concrete Structures, Sapporo, Japan, Oct.1997, Vol.2, pp. 301-308.
21. Clark, A., 1951; "Diagonal Tension in Reinforced Concrete Beams," *ACI Structural Journal*, Vol.48, No.10, October, pp. 145-155.
22. Clarke, J., 1996; "FRP Reinforced Concrete Structures," Proceedings of the Second International conference on Advanced Composite Materials for Bridges and Structures (ACMBS-II), Montreal, Québec, August, pp. 41-48.
23. Clarke, J., 1993; "Alternative Materials for the Reinforcement and Prestressing of Concrete," 1st edition, Blackie Academic & Professional, Great Britain, 204 p.
24. Collins, M., 1972; "Torque-Twist Characteristics of Reinforced Concrete Beams," Symposium on Inelsticity and Non-Linearity in Structural Concrete, University of Waterloo Press, pp. 211-231.

-
25. Collins, M., 1978; "Towards a Rational Theory for RC Members in Shear," *Journal of the Structural Division*, ASCE, Vol. 104, No. ST4, April, pp. 649-666.
 26. Collins, M., D. Mitchell, P. Adebar, and F. Vecchio, 1996; "A General Shear Design Method," *ACI Structural Journal*, Vol.93, No.1, January-February, pp. 36-45.
 27. Currier, J., C. Fogstad, D. Walrath, and C. Dolan, 1994; "Bond Development of Thermoplastic FRP Shear Reinforcement Stirrups," Proceedings of the Third Materials Engineering Conference, ASCE, San Diego, CA, pp. 592-597.
 28. Duranovic, N., K. Pilakoutas, and P. Waldron, 1997; "Tests on Concrete Beams Reinforced with Glass Fibre Reinforced Plastic Bars," Proceeding of the Third International Symposium on Non-Metallic (FRP) Reinforcement for Concrete Structures, Sapporo, Japan, Oct.1997, Vol.2, pp. 479-486.
 29. Ehsani, M., H. Saadatmanesh, and S. Tao, 1995; "Bond of Hooked Glass Fiber Reinforced Plastic (GFRP) Reinforcing Bars to Concrete," *ACI Materials Journal*, Vol. 92, No. 4, July-August, pp. 391-400.
 30. Erki, M.A., and B. Bakht, 1996; "Non-Metallic Shear Reinforcement for Reinforced Concrete Beams," Proceedings of the 24th Annual Conference, Canadian Society of Civil Engineering, CSCE, 29May-1June, Edmonton, Alberta, pp. 159-165.
 31. Eurocode No. 2, 1992; "Design of Concrete Structures - Part 1 : General rules and rules for buildings," European Committee for Standardization, Lausanne, 253 p.
 32. Eurocrete Project, 1996; "Modification of Design Rules to Incorporate Non-ferrous Reinforcement" prepared by J.L. Clarke, D. P. O'Regan, and C. Thirugnanendran, January 1996, 34 p.

-
33. Fam, A., S. Rizkalla, and G. Tadros, 1997; "Behaviour of CFRP for Prestressing and Shear Reinforcements of Concrete Highway Bridges," *ACI Structural Journal*, Vol.94, No.1, January-February, pp. 77-86.
34. Felber, A., 1990; "RESPONSE: A Program to Determine the Load-Deformation Response of Reinforced Concrete Sections," M.Sc. thesis, Department of Civil Engineering, University of Toronto, 148 p.
35. Fickelhorn, M., 1990; "Editorial," *Materials and Structures Journal*, RILEM, vol. 23, No. 137, pp. 317.
36. Gilstrap, J., C. Burke, D. Dowden, and C. Dolan, 1997; "Development of FRP Reinforcement Guidelines for Prestressed Concrete Structures," *Journal of Composites for construction*, ASCE, Vol.1, No.3, November 1997, pp. 131-139.
37. Hassan, H., *et al.*, 1991; "Displacement at Shear Crack in Beams with Shear Reinforcement under Static and Fatigue Loadings," Proceedings of JSCE, No.433, V-15, August 1991, pp. 215-222.
38. Hutchinson, R., A. Abdelrahman, and S. Rizkalla, 1997; "Shear Strengthening Using CFRP Sheets for Prestressed Concrete Bridge Girders in Manitoba, Canada," Proceedings of the Second International Conference on Composites in Infrastructure, Tucson, Arizona, Jan. 1998, pp. 261-275.
39. Ishihara, K., T. Obara, Y. Sato, T. Ueda, and Y. Kakuta, 1997; "Evaluation of Ultimate Strength of FRP Rods at Bent-Up Portion," Proceeding of the Third International Symposium on Non-Metallic (FRP) Reinforcement for Concrete Structures, Sapporo, Japan, Oct.1997, Vol.2, pp. 27-34.

-
40. Japanese Society of Civil Engineers, JSCE, 1993; "State-of-the-Art Report on Continuous Fiber Reinforcing Materials," Concrete Engineering Series 3, Edited by A. Machida, 164 p.
41. Japanese Society of Civil Engineers, JSCE, 1997; "Recommendation for Design and Construction of Concrete Structures using Continuous Fibre Reinforcing Materials," Concrete Engineering Series 23, Edited by A. Machida, 325 p.
42. Joh, O., Z. Wang, and Y. Goto, 1997; "Experimental Study on Bond Cracking Performance of FRP Reinforced Concrete," Proceeding of the Third International Symposium on Non-Metallic (FRP) Reinforcement for Concrete Structures, Sapporo, Japan, Oct.1997, Vol.2, pp. 431-438.
43. Kanematsu, H., Y. Sato, T. Ueda, and Y. Kakuta, 1993; "A Study on Failure Criteria of FRP Rods Subject to Tensile and Shear Force," FIP Symposium '93, Kyoto, Japan, Oct. 17-20, pp. 743-750.
44. Kani, G., M. Huggins, and R. Wittkopp, 1979; "Kani on Shear in Reinforced Concrete," Department of Civil Engineering, University of Toronto, Toronto, 225 p.
45. Krauthammer, T., 1992; "Minimum Shear Reinforcement Based on Interface Shear Transfer," *ACI Structural Journal*, Vol.89, No.1, January-February, pp. 99-105.
46. Kriski, W. and R. Loov, 1996; "Strength of Beams Based on Shear-Friction," Proceedings of the 24th Annual Conference, Canadian Society of Civil Engineering, CSCE, May29-June 1, Edmonton, Canada, Vol. IIa, pp. 537-547.
47. Leonhardt, F., 1977; "Crack Control in Concrete Structures," IABSE Surveys No. S-4/77, Zurich, 26 p.

-
48. Loov, R., 1998; "Review of A23.3-94 Simplified Method of Shear Design and Comparison with Results Using Shear Friction," *Canadian Journal of Civil Engineering*, Vol. 25, No. 3, June, pp. 437-450.
49. Machida, A., 1996; "Designing Concrete Structures with Continuous Fiber Reinforcing Materials," Keynote lecture, First International Conference on Composites in Infrastructure, ICCI'96, 15-17 January, 15 p.
50. Machida, A., Y. Kakuta, Y. Tsuji, H. Seki, and T. Uomoto, 1995; "Initatives in Developing the Specifications for Design and Construction of Concrete Structures Using FRP in Japan," Non-Metallic (FRP) Reinforcement for Concrete Structures, Proceedings of the Second International RILEM Symposium (FRPRCS-2), Edited by L. Taerwe, E & FN SPON, Great Britain, pp. 627-635.
51. Mallick, P., 1993; "Fiber-Reinforced Composites, Manufacturing and Design," 2nd Edition, Marcel Dekker Inc., USA, 566 p.
52. Marshall Industries Composites, 1997; "C-BAR Composite Reinforcing Rods: The Future of Concrete Reinforcement," Product Manual, USA, 6 p.
53. Maruyama, K., T. Yoshida, T. Mukai, and C. Hashimoto, 1986; "Some Considerations on Shear Behaviour of Reinforced Concrete Beams," Transactions of the Japan Concrete Institute, Vol.8, pp. 275-282.
54. Maruyama, K., and W. Zhao, 1996; "Size Effect in Shear Behaviour of FRP Reinforced Concrete Beams," Proceedings of the Second International conference on Advanced Composite Materials for Bridges and Structures (ACMBS-II), Montreal, Québec, August, pp. 227-234.

-
55. Maruyama, T., M. Honma, and H. Okamura, 1989; "Experimental Study on the Diagonal Tensile Characteristics of Various Fibre Reinforced Plastic Rods," Transactions of the Japan Concrete Institute, Vol.11, pp. 193-198.
56. Maruyama, T., M. Honma, and H. Okamura, 1993; "Experimental Study on Tensile Strength of Bent Portion of FRP Rods," American Concrete Institute, ACI SP-138, edited by A. Nanni and C.W. Dolan, pp. 163-176.
57. Mattock, A. and N. Hawkins, 1972; "Shear Transfer in Reinforced Concrete - Recent Research," *PCI Journal*, Vol.17, No. 2, March-April 1972, pp. 55-75.
58. Michaluk, C., S. Rizkalla, G. Tadros, and B. Benmokrane, 1998; "Flexural Behaviour of One-Way Concrete Slabs Reinforced by FRP Reinforcements," *ACI Structural Journal*, Vol. 95, No. 3, May-June, pp. 353-365.
59. Mitsubishi Chemical Corporation, 1992; "Leadline Carbon Fiber Tendons/Bars," Product Manual, Japan, 75 p.
60. Miyata, S., S. Tottori, T. Terada, and K. Sekijima, 1989; "Experimental Study on Tensile Strength of FRP Bent Bar," Transaction of the Japan Concrete Institute, vol. 11, pp. 185-192.
61. Mostofinjad, D., and A. Razaqpur, 1997; "Critical Analysis of Current Shear Design Methods for FRP Reinforced Concrete Beams," Proceeding of the Third International Symposium on Non-Metallic (FRP) Reinforcement for Concrete Structures, Sapporo, Japan, Oct.1997, Vol.1, pp. 159-166.
62. Mphonde, A., 1989; "Use of Stirrup Effectiveness in Shear Design of Concrete Beams," *ACI Structural Journal*, Vol. 86, No.5, September-October, pp. 541-545.

63. Murphy, J., 1998; "Reinforced Plastics Handbook," 1st edition, Elsevier Science Publishers Ltd., Great Britain, 541 p.
64. Naaman, A., and S. Park, 1997; "Shear Behaviour of Concrete Beams Prestressed with CFRP Tendons: Preliminary Tests Evaluation," Proceeding of the Third International Symposium on Non-Metallic (FRP) Reinforcement for Concrete Structures, Sapporo, Japan, Oct.1997, Vol.2, pp. 679-686.
65. Nagasaka, T., H. Fukuyama, and M. Tanigaki, 1993; "Shear Performance of Concrete Beams Reinforced with FRP Stirrups," American Concrete Institute, ACI SP-138, edited by A. Nanni and C. Dolan, pp. 789-811.
66. Najjar, S., K. Pilakoutas, and P. Waldron, 1997; "Finite Element Analysis of GFRP Reinforced Concrete Beams," Proceeding of the Third International Symposium on Non-Metallic (FRP) Reinforcement for Concrete Structures, Sapporo, Japan, Oct.1997, Vol.2, pp. 519-526.
67. Nakai, H., H. Asai, S. Kumagai, and M. Okano, 1993; "Shearing Property of Prestressed Concrete Beams using Continuous Fiber Reinforcement Materials," FIP Symposium '93, Kyoto, Japan, Oct. 17-20, Vol.II, pp. 789-796.
68. Nakamura, H., and T. Higai, 1995a; "Evaluation of Shear strength of RC Beam Section Based on Extended Modified Compression Field Theory," Concrete Library International, Proceedings of Japan Society of Civil Engineers, No.25, June 1995, pp. 93-105.
69. Nakamura, H., and T. Higai, 1995b; "Evaluation of Shear Strength of Concrete Beams Reinforced with FRP," Concrete Library International, Proceedings of Japan Society of Civil Engineers, No.26, December 1995, pp. 111-123.

-
70. Nielsen, M., 1984; "Limit Analysis and Concrete Plasticity," Prentice-Hall, Inc., Englewood Cliffs, New Jersey, 421 p.
71. Niwa, J., 1983; "Design Equation for Shear Capacity of Deep Beams based on FEM Analysis," Proceedings of Japan Concrete Institute, 2nd Colloquim on Shear Analysis of RC Structures, pp. 119-126.
72. Niwa, J., Y. Hirai, and T. Tanabe, 1997; "Size Effect in the Shear Strength of Concrete Beams Reinforced with FRP Rods," Proceeding of the Third International Symposium on Non-Metallic (FRP) Reinforcement for Concrete Structures, Sapporo, Japan, Oct.1997, Vol.2, pp. 293-300.
73. Okumura, K., H. Saito, H. Akiyama, and H. Nakamura, 1993; "Mechanical Properties of Concrete Structures Reinforced by CFRP Rods as Shear Reinforcement," FIP Symposium '93, Kyoto, Japan, Oct. 17-20, Vol.II, pp. 819-826.
74. Pang, X., and T. Hsu, 1992; "Constitutive Laws of Reinforced Concrete in Shear," Research Report UHCEE 92-1, Department of Civil Engineering, University of Houston, 188 p.
75. Pang, X., and T. Hsu, 1995; "Behaviour of Reinforced Concrete Membrane Elements in Shear," *ACI Structural Journal*, Vol.92, No.6, November-December, pp. 665-679.
76. Pang, X., and T. Hsu, 1996; "Fixed Angle Softened Truss Model for Reinforced Concrete," *ACI Structural Journal*, Vol.93, No.2, March-April, pp. 197-207.
77. Placas, A., and P. Regan, 1971; "Shear Failure of Reinforced Concrete Beams," *ACI Journal*, Vol.68, No. 10, October, pp. 763-773.

-
78. Rizkalla, S., and G. Tadros, 1994; "A Smart Highway Bridge in Canada," *Concrete International*, Vol. 16, No. 6, pp. 42-44.
79. Rizkalla, S., *et al.*, 1997; "Material Properties of C-BARTM Reinforcing Rods," Research report submitted to Reichhold Chemicals Inc., 80 p.
80. Russo, G., and G. Puleri, 1997; "Stirrup Effectiveness in Reinforced Concrete Beams under Flexure and Shear," *ACI Structural Journal*, Vol. 94, No. 3, May-June, pp. 227-238.
81. Sarsam, K., and J. Al-Musawi, 1992; "Shear Design of High- and Normal Strength Concrete Beams with Web Reinforcement," *ACI Structural Journal*, Vol. 89, No. 6, November-December, pp. 658-664.
82. Sato, Y., T. Ueda, and Y. Kakuta, 1993; "Analytical Evaluation of Shear Resisting Behaviour of Concrete Beams Reinforced with FRP Rods As Shear Reinforcement," *Transactions of the Japan Concrete Institute*, Vol.15, pp. 319-324.
83. Sato, Y., T. Ueda, and Y. Kakuta, 1994; "Analytical Evaluation of Shear Resisting Behaviour of Prestressed Concrete Beams Reinforced with FRP Rods," *Transactions of the Japan Concrete Institute*, Vol.16, pp. 425-430.
84. Sato, Y., T. Ueda, and Y. Kakuta, 1995; "Ultimate Shear capacity of Concrete Beams Reinforced with FRP Rods," *Non-Metallic (FRP) Reinforcement for Concrete Structures, Proceedings of the Second International RILEM Symposium (FRPRCS-2)*, Edited by L. Taerwe, E & FN SPON, Great Britain, pp. 337-343.
85. Shehata, E., A. Abdelrahman, G. Tadros, and S. Rizkalla, 1997; "FRP for Large Span Highway Bridge in Canada," *Recent Advances in Bridge Engineering*, Edited by Urs Meier and R. Betti, Zurich, Switzerland, pp. 251-258.

-
86. Sonobe, Y., T. Kanakubo, M. Fujisawa, M. Tanigaki, and T. Okamoto, 1995; "Structural Performance of Concrete Beams Reinforced with Diagonal FRP Bars," Non-Metallic (FRP) Reinforcement for Concrete Structures, Proceedings of the Second International RILEM Symposium (FRPRCS-2), Edited by L. Taerwe, E & FN SPON, Great Britain, pp. 344-351.
87. Sonobe, Y., H. Fukuyama, T. Okamoto, N. Kani, K. Kimura, K. Kobayashi, Y. Masuda, Y. Matsuzaki, S. Mochizuki, T. Nagasaka, A. Shimizu, H. Tanano, M. Tanigaki, and M. Teshigawara, 1997; "Design Guidelines of FRP Reinforced Concrete Buildings Structures," *Journal of Composites for Construction*, ASCE, Vol.1, No.3, August, pp. 90-115.
88. Tokyo Rope MFG. Co., Ltd., 1993; "Technical Data on Carbon Fiber Composite Cables (CFCC)," Product Manual, Japan, 65 p.
89. Tomaszewicz, A., and G. Markeset, 1997; "Shear Transfer in Concrete Reinforced with FRP bars," Proceeding of the Third International Symposium on Non-Metallic (FRP) Reinforcement for Concrete Structures, Sapporo, Japan, Oct.1997, Vol.2, pp. 325-332.
90. Tottori, S., and H. Wakui, 1993; "Shear Capacity of RC and PC Beams Using FRP Reinforcement," American Concrete Institute, ACI SP-138, edited by A. Nanni and C.W. Dolan, pp. 615-631.
91. Ueda, T., Y. Sato, Y. Kakuta, A. Imamura, and H. Kanematsu, 1995; "Failure Criteria for FRP Rods Subjected to a Combination of Tensile and Shear Forces," Non-Metallic (FRP) Reinforcement for Concrete Structures, Proceedings of the Second International RILEM Symposium (FRPRCS-2), Edited by L. Taerwe, E & FN SPON, Great Britain, pp.26-33.

-
92. Vecchio, F., and M. Collins, 1981; "Stress-Strain Characteristics of Reinforced Concrete in Pure Shear," IABSE Colloquium on Advanced Mechanics of Reinforced Concrete, Delft, Netherlands, pp. 211-225.
93. Vecchio, F., and M. Collins, 1982; "The Response of Reinforced Concrete to In-Plane Shear and Normal Stresses," Publication No. 82-03, Department of Civil Engineering, University of Toronto, Toronto, 332 pp.
94. Vecchio, F., and M. Collins, 1986; "The Modified Compression Field Theory for Reinforced Concrete Elements Subjected to Shear," *ACI Structural Journal*, Vol.83, No.2, March-April, pp. 219-231.
95. Vecchio, F., and M. Collins, 1988; "Predicting the Response of Reinforced Concrete Beams Subjected to Shear Using Modified Compression Field Theory," *ACI Structural Journal*, Vol.85, No.3, May-June, pp. 258-268.
96. Vijay, P., S. Kumar, and H. GangaRao, 1996; "Shear and Ductility Behaviour of Concrete Beams Reinforced with GFRP Bars," Proceedings of the Second International conference on Advanced Composite Materials for Bridges and Structures (ACMBS-II), Montreal, Québec, August, pp. 217-226.
97. Yokoi, K., H. Shima, and H. Mizuguchi, 1992; "Applicability of Shear Strength Equations for RC Beams to Concrete Beams Reinforced with FRP Rods," Transactions of the Japan Concrete Institute, Vol.14, pp. 247-252.
98. Yonekura, A., E. Tazawa, and H. Nakayama, 1993; "Flexural and Shear Behaviour of Prestressed Concrete Beams Using FRP Rods as Prestressing Tendons," American Concrete Institute, ACI SP-138, edited by A. Nanni and C.W. Dolan, pp. 525-548.

99. Zhao, W., K. Maruyama, and H. Suzuki, 1995; "Shear Behaviour of Concrete Beams Reinforced by FRP Rods as Longitudinal and Shear Reinforcement," Non-Metallic (FRP) Reinforcement for Concrete Structures, Proceedings of the Second International RILEM Symposium (FRPRCS-2), Edited by L. Taerwe, E & FN SPON, Great Britain, pp. 352-359.

Appendix A

Sample calculation using shear friction model

Sample calculations using the shear friction model (SFM) are presented in this appendix for beam SC-3. Beam SC-3 was reinforced for flexure using steel strands and for shear using CFRP Leadline stirrups spaced at $d/3$.

Beam data:

Dimensions: $b_w = 135 \text{ mm}$, $d = 470 \text{ mm}$, $h = 560 \text{ mm}$

Concrete strength: $f_c' = 54 \text{ MPa}$

Flexural reinforcement: steel strands $A_{st} = 780 \text{ mm}^2$

Shear reinforcement: CFRP Leadline stirrups $A_{fv} = 76.94 \text{ mm}^2$, $s = 160 \text{ mm}$, $f_{fv} = 1800 \text{ MPa}$.

Used equations:

Equation used to determine the stirrup capacity as affected by the embedment length, l_d :

$$0.47 \leq \frac{f_{fv}}{f_{fv}} = 0.40 + \frac{l_d}{70 d_e} \leq 0.8 \quad (\text{A-1})^1$$

Equation used to determine the shear friction factor, k :

$$k = 2.1 f_c'^{-0.4} \quad (\text{A-2})$$

Equation used to determine the force, T , in the flexural reinforcement:

¹ Chapter 5, equation (6-7)

$$T = \frac{x_a}{y_{CT}} V_n - \frac{(x_1 + (x_1 + s) + (x_1 + 2s))}{y_{CT}} A_v f_v \quad (\text{A-3})^2$$

Equation used to determine the shear strength, V_n :

$$\frac{V_n}{C_w} = 0.5k^2 \left[\sqrt{\frac{T}{0.25k^2 C_w} + \cot^2 \theta} - \cot \theta \right] (1 + \cot^2 \theta) - \frac{T}{C_w} \cot \theta + \frac{T_v}{C_w} \leq \frac{7.0}{f_c'} \quad (\text{A-4})^3$$

Potential failure planes:

Six planes are assumed to be the most favorable failure planes, as shown in Figure A-1.

The sample calculations are given in this appendix for planes no. ② and ③.

Plane no. ②:

1. The angle of the plane: $\theta = \tan^{-1}(500/480) = 46.2$ degrees

$$C_w = f_c' b_w h = 54.0 * 135 * 560 / 1000 = 4082.4 \text{ kN}$$

$$\text{Using equation (A-2): } k = 2.1 * 54^{-0.4} = 0.426$$

2. As shown in Figure A-2, the lowest embedment length $l_d = 166.7$ mm,

$$l_d / d_e = 166.7 / 7 = 23.8$$

Using equation (A-1):

$$f_{fv} = 1800 * (0.4 + 23.8 / 70) = 1332 \text{ MPa}$$

3. The total number of stirrups intersecting the failure plane is 2.

$$\text{The stirrup contribution: } T_v = 76.94 * 2 * 1332 / 1000 = 205 \text{ kN}$$

4. Determination of the tensile force, T :

- a. As shown in Figure A-2: $x_a = 1414$ mm, $x_1 = 154$ mm and $y_{CT} = 433$ mm

² Chapter 6, equation (6-9)

³ Chapter 6, equation (6-6)

b. Using equation (A-3):

$$T = 1414 V_n / 433 - 76.94 * 1332 * (154 + (154 + 160)) / 433 = 3.27 V_n - 111. \text{ kN}$$

5. Applying θ , C_w , k , T_v and T to equation (A-4). The governing equation (A-4) can be reduced to the following polynomial:

$$563.8 \left(\frac{V_n}{C_w} \right)^2 - 47.335 \left(\frac{V_n}{C_w} \right) - 0.048892 = 0 \quad (\text{A-5})$$

Equation (A-5) was solved to determine V_n :

$$V_n = 0.0849797 C_w = 346.9 \text{ kN}$$

Plane no. ③:

1. The angle of the plane: $\theta = \tan^{-1}(465/480) = 44.1$ degrees

$$C_w = f_c b_w h = 54.0 * 135 * 560 / 1000 = 4082.4 \text{ kN}$$

$$\text{Using equation (A-2): } k = 2.1 * 54^{-0.4} = 0.426$$

2. As shown in Figure A-3, the lowest embedment length $l_d = 35$ mm,

$$l_d / d_e = 35 / 7 = 5.0$$

Using equation (A-1):

$$f_{fr} = 1800 * (0.4 + 5.0 / 70) = 849 \text{ MPa}$$

3. The total number of stirrups intersecting the failure plane is 3.

$$\text{The stirrup contribution: } T_v = 76.94 * 3 * 849 / 1000 = 196.0 \text{ kN}$$

4. Determination of the tensile force, T :

a. As shown in Figure A-3: $x_d = 1289$ mm, $x_1 = 29$ mm and $y_{CT} = 433$ mm

b. Using equation (A-3):

$$T = 1414 V_n / 433 - 76.94 * 849 * (29 + (29 + 160) + (29 + 2 * 160)) / 433$$

$$= 2.98V_n - 85.5 \text{ kN}$$

5. Applying θ , C_w , k , T_v and T to equation (A-4). The governing equation (A-4) can be reduced to the following polynomial:

$$473.1 \left(\frac{V_n}{C_w} \right)^2 - 36.960 \left(\frac{V_n}{C_w} \right) - 0.167207 = 0 \quad (\text{A-6})$$

Equation (A-6) was solved to determine V_n :

$$V_n = 0.08241617 C_w = 336.4 \text{ kN}$$

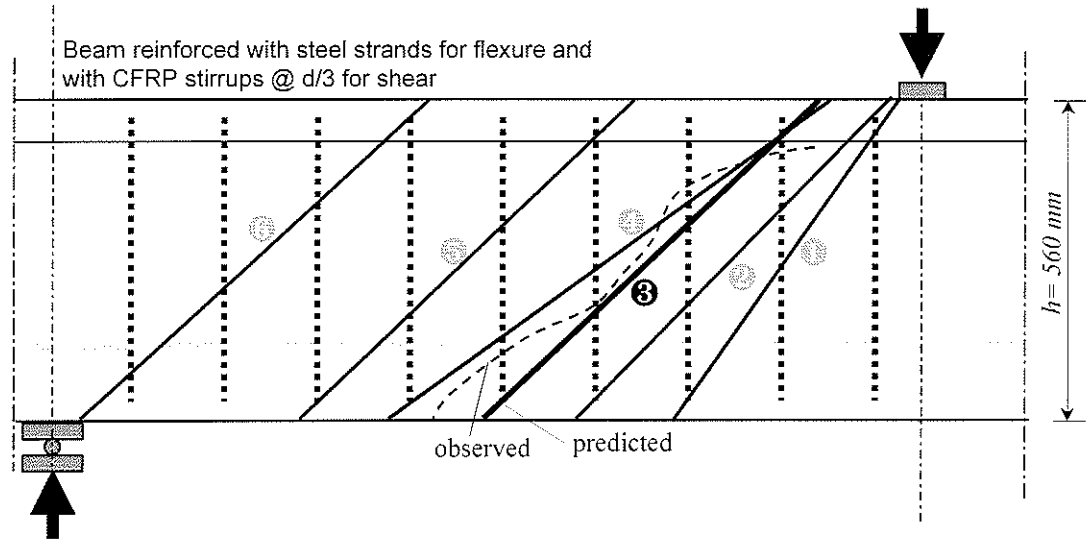


Figure A-1. Potential failure planes for beam SC-3

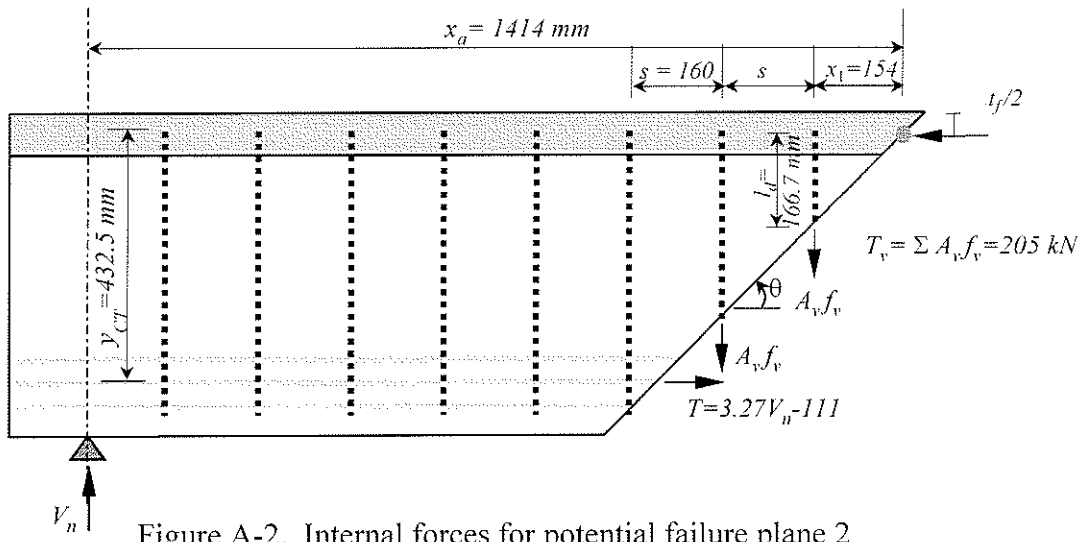


Figure A-2. Internal forces for potential failure plane 2

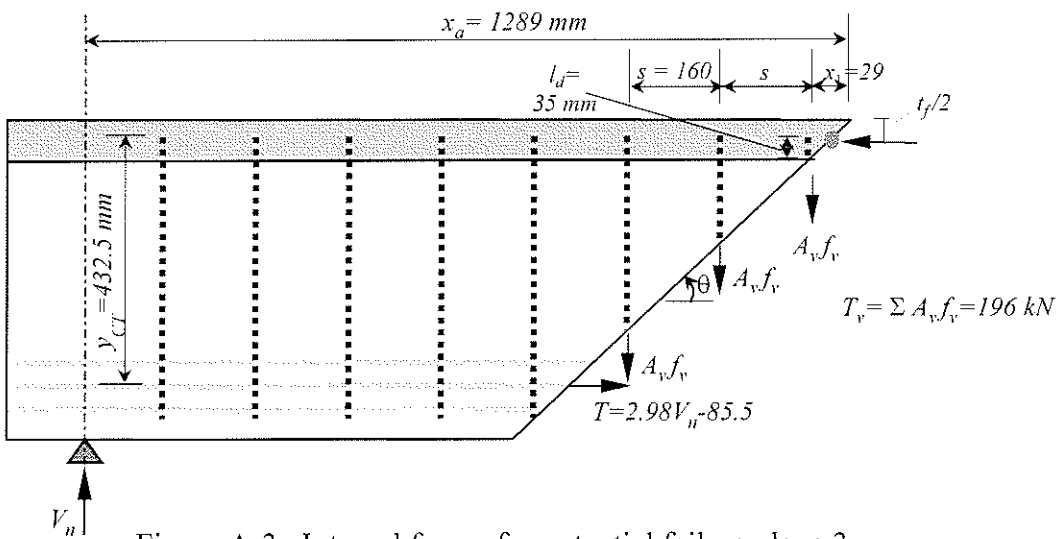


Figure A-3. Internal forces for potential failure plane 3

Appendix B
Input data for the MCFT analysis

The input files for the “RESPONSE” program used to perform the MCFT analysis are given in for the following beams:

- 1) beam SS-2 : reinforced for flexure using steel strands and for shear using steel stirrups spaced at $d/2$, where d is the effective beam depth.
- 2) beam SC-2 : reinforced for flexure using steel strands and for shear using CFRP stirrups spaced at $d/2$.
- 3) beam SC-3 : reinforced for flexure using steel strands and for shear using CFRP stirrups spaced at $d/3$.
- 4) beam SC-4 : reinforced for flexure using steel strands and for shear using CFRP stirrups spaced at $d/4$.
- 5) beam CC-3 : reinforced for flexure using CFRP strands and for shear using CFRP stirrups spaced at $d/3$.

Beam SS-2

Response Version 1 Data-File

Copyright 1990 A. Felber

Name of Section: Beam SS-2

Units M/U 'Metric/U.S.Customary': M

Number of Concrete Types (1-5): 1

Type	f'c	ec'	fcR	Tension Stiffening
Number	[Mpa]	[Milli-Strain]	[Mpa]	Factor
1	54.00	-2.000	4.12	0.70

Number of Rebar Types (1-5): 2

Type	Elastic Modulus	fy	esh	esrupt	fu
Number	[Mpa]	[Mpa]	{---Milli-Strain--}	[Mpa]	[Mpa]
1	200000	400	20.000	40.000	400
2	200000	660	4.000	20.000	780

Number of Tendon Types (1-5): 1

Type	[Ramberg-Osgood-Factors--]			Elastic Modulus	fpu	esrupt
Number	A	B	C	[Mpa]	[Mpa]	[Ms]
1	0.025	118.000	10.000	200000	1860	40.000

Height of Section: 560 mm

Distance to Moment Axis: 280 mm

Shear Y/N 'Yes/No': Y

Web width (bw) : 135 mm

Shear depth (jd) : 432 mm

Distance to web strain ex : 300 mm

Distance to center of web : 242 mm

Longitudinal crack spacing: 300 mm

Maximum Aggregate size : 10 mm

Stirrups Y/N 'Yes/No': Y

Transverse crack spacing : 300 mm

Area of Stirrups (Av) : 127 mm²

Stirrup Spacing (s) : 235 mm

Stirrup (Rebar) Type : 2

Number of Concrete Layers (1-20): 3

Layer	y	bottom width	top width	height	Type
Number	[mm]	[mm]	[mm]	[mm]	Number
1	0	135	135	180	1
2	180	135	135	305	1
3	485	600	600	75	1

Number of Rebar Layers (0-10) : 1

Layer	y	Area	Type
Number	[mm]	[mm ²]	Number
1	523	200	1

Number of Tendon Layers (0-10) : 3

Layer	y	Area	Prestrain	Type
Number	[mm]	[mm ²]	[Milli-Strain]	Number
1	50	280	0.000	1
2	90	280	0.000	1
3	130	280	0.000	1

Consider displaced Concrete Y/N: N

Thermal & Shrinkage Strains Y/N : N

Initial Strains Y/N : N

Beam SC-2

Response Version 1 Data-File

Copyright 1990 A. Felber

Name of Section: Beam SC-2

Units M/U 'Metric/U.S.Customary': M

Number of Concrete Types (1-5): 1

Type	f'c	ec'	fcr	Tension Stiffening
Number	[Mpa]	[Milli-Strain]	[Mpa]	Factor
1	54.00	-2.000	4.12	0.70

Number of Rebar Types (1-5): 2

Type	Elastic Modulus	fy	esh	esrupt	fu
Number	[Mpa]	[Mpa]	[---Milli-Strain--]	[Mpa]	[Mpa]
1	200000	400	20.000	40.000	400
2	137000	1000	7.300	8.759	1200

Number of Tendon Types (1-5): 1

Type	[Ramberg-Osgood-Factors--]			Elastic Modulus	fpu	esrupt
Number	A	B	C	[Mpa]	[Mpa]	[Ms]
1	0.025	118.000	10.000	200000	1860	40.000

Height of Section: 560 mm

Distance to Moment Axis: 280 mm

Shear Y/N 'Yes/No': Y

Web width (bw) : 135 mm

Shear depth (jd) : 432 mm

Distance to web strain ex : 300 mm

Distance to center of web : 242 mm

Longitudinal crack spacing: 300 mm

Maximum Aggregate size : 10 mm

Stirrups Y/N 'Yes/No': Y

Transverse crack spacing : 200 mm

Area of Stirrups (Av) : 77 mm²

Stirrup Spacing (s) : 235 mm

Stirrup (Rebar) Type : 2

Number of Concrete Layers (1-20): 3

Layer	y	bottom width	top width	height	Type
Number	[mm]	[mm]	[mm]	[mm]	Number
1	0	135	135	180	1
2	180	135	135	305	1
3	485	600	600	75	1

Number of Rebar Layers (0-10) : 1

Layer	y	Area	Type
Number	[mm]	[mm ²]	Number
1	523	200	1

Number of Tendon Layers (0-10) : 3

Layer	y	Area	Prestrain	Type
Number	[mm]	[mm ²]	[Milli-Strain]	Number
1	50	280	0.000	1
2	90	280	0.000	1
3	130	280	0.000	1

Consider displaced Concrete Y/N: N

Thermal & Shrinkage Strains Y/N : N

Initial Strains Y/N : N

Beam SC-3

Response Version 1 Data-File
 Copyright 1990 A. Felber
 Name of Section: Beam SC-3
 Units M/U 'Metric/U.S.Customary': M
 Number of Concrete Types (1-5): 1

Type	f'c	ec'	fcR	Tension Stiffening
Number	[Mpa]	[Milli-Strain]	[Mpa]	Factor
1	54.00	-2.000	4.12	0.70

 Number of Rebar Types (1-5): 2

Type	Elastic Modulus	fy	esh	esrupt	fu
Number	[Mpa]	[Mpa]	[---Milli-Strain--]	[Mpa]	[Mpa]
1	200000	400	20.000	40.000	400
2	137000	1000	7.300	8.759	1200

 Number of Tendon Types (1-5): 1

Type	[Ramberg-Osgood-Factors--]			Elastic Modulus	fpu	esrupt
Number	A	B	C	[Mpa]	[Mpa]	[Ms]
1	0.025	118.000	10.000	200000	1860	40.000

 Height of Section: 560 mm
 Distance to Moment Axis: 280 mm
 Shear Y/N 'Yes/No': Y
 Web width (bw) : 135 mm
 Shear depth (jd) : 432 mm
 Distance to web strain ex : 300 mm
 Distance to center of web : 242 mm
 Longitudinal crack spacing: 300 mm
 Maximum Aggregate size : 10 mm
 Stirrups Y/N 'Yes/No': Y
 Transverse crack spacing : 200 mm
 Area of Stirrups (Av) : 77 mm²
 Stirrup Spacing (s) : 160 mm
 Stirrup (Rebar) Type : 2
 Number of Concrete Layers (1-20): 3

Layer	y	bottom width	top width	height	Type
Number	[mm]	[mm]	[mm]	[mm]	Number
1	0	135	135	180	1
2	180	135	135	305	1
3	485	600	600	75	1

 Number of Rebar Layers (0-10) : 1

Layer	y	Area	Type
Number	[mm]	[mm ²]	Number
1	523	200	1

 Number of Tendon Layers (0-10) : 3

Layer	y	Area	Prestrain	Type
Number	[mm]	[mm ²]	[Milli-Strain]	Number
1	50	280	0.000	1
2	90	280	0.000	1
3	130	280	0.000	1

 Consider displaced Concrete Y/N: N
 Thermal & Shrinkage Strains Y/N : N
 Initial Strains Y/N : N

Beam SC-4

Response Version 1 Data-File
 Copyright 1990 A. Felber
 Name of Section: Beam SC-4
 Units M/U 'Metric/U.S.Customary': M
 Number of Concrete Types (1-5): 1

Type	f'c	ec'	fcr	Tension Stiffening
Number	[Mpa]	[Milli-Strain]	[Mpa]	Factor
1	51.00	-2.000	4.12	0.70

Number of Rebar Types (1-5): 2

Type	Elastic Modulus	fy	esh	esrupt	fu
Number	[Mpa]	[Mpa]	[---Milli-Strain--]	[Mpa]	[Mpa]
1	200000	400	20.000	40.000	400
2	137000	1000	7.300	8.759	1200

Number of Tendon Types (1-5): 1

Type	[Ramberg-Osgood-Factors--]			Elastic Modulus	fpu	eprupt
Number	A	B	C	[Mpa]	[Mpa]	[Ms]
1	0.025	118.000	10.000	200000	1860	40.000

Height of Section: 560 mm
 Distance to Moment Axis: 280 mm
 Shear Y/N 'Yes/No': Y

Web width (bw) : 135 mm
 Shear depth (jd) : 432 mm
 Distance to web strain ex : 300 mm
 Distance to center of web : 242 mm
 Longitudinal crack spacing: 300 mm
 Maximum Aggregate size : 10 mm

Stirrups Y/N 'Yes/No': Y

Transverse crack spacing : 200 mm
 Area of Stirrups (Av) : 77 mm²
 Stirrup Spacing (s) : 120 mm
 Stirrup (Rebar) Type : 2

Number of Concrete Layers (1-20): 3

Layer	y	bottom width	top width	height	Type
Number	[mm]	[mm]	[mm]	[mm]	Number
1	0	135	135	180	1
2	180	135	135	305	1
3	485	600	600	75	1

Number of Rebar Layers (0-10) : 1

Layer	y	Area	Type
Number	[mm]	[mm ²]	Number
1	523	200	1

Number of Tendon Layers (0-10) : 3

Layer	y	Area	Prestrain	Type
Number	[mm]	[mm ²]	[Milli-Strain]	Number
1	50	280	0.000	1
2	90	280	0.000	1
3	130	280	0.000	1

Consider displaced Concrete Y/N: N
 Thermal & Shrinkage Strains Y/N : N
 Initial Strains Y/N : N

Beam CC-3

Response Version 1 Data-File
 Copyright 1990 A. Felber
 Name of Section: Beam CC-3
 Units M/U 'Metric/U.S.Customary': M
 Number of Concrete Types (1-5): 1

Type	f'c	ec'	fcr	Tension Stiffening
Number	[Mpa]	[Milli-Strain]	[Mpa]	Factor
1	50.00	-2.000	4.12	0.70

 Number of Rebar Types (1-5): 2

Type	Elastic Modulus	fy	esh	esrupt	fu
Number	[Mpa]	[Mpa]	[---Milli-Strain--]	[Mpa]	[Mpa]
1	200000	400	20.000	40.000	400
2	137000	1000	7.300	8.759	1200

 Number of Tendon Types (1-5): 1

Type	[Ramberg-Osgood-Factors--]	Elastic Modulus	fpu	eprupt
Number	A B C	[Mpa]	[Mpa]	[Ms]
1	0.000 50.000 20.000	137000	2000	40.000

 Height of Section: 560 mm
 Distance to Moment Axis: 280 mm
 Shear Y/N 'Yes/No': Y
 Web width (bw) : 135 mm
 Shear depth (jd) : 432 mm
 Distance to web strain ex : 300 mm
 Distance to center of web : 242 mm
 Longitudinal crack spacing: 300 mm
 Maximum Aggregate size : 10 mm
 Stirrups Y/N 'Yes/No': Y
 Transverse crack spacing : 200 mm
 Area of Stirrups (Av) : 77 mm²
 Stirrup Spacing (s) : 160 mm
 Stirrup (Rebar) Type : 2
 Number of Concrete Layers (1-20): 3

Layer	y	bottom width	top width	height	Type
Number	[mm]	[mm]	[mm]	[mm]	Number
1	0	135	135	180	1
2	180	135	135	305	1
3	485	600	600	75	1

 Number of Rebar Layers (0-10) : 1

Layer	y	Area	Type
Number	[mm]	[mm ²]	Number
1	523	200	1

 Number of Tendon Layers (0-10) : 3

Layer	y	Area	Prestrain	Type
Number	[mm]	[mm ²]	[Milli-Strain]	Number
1	50	280	0.000	1
2	90	280	0.000	1
3	130	280	0.000	1

 Consider displaced Concrete Y/N: N
 Thermal & Shrinkage Strains Y/N : N
 Initial Strains Y/N : N

Appendix C

Measured versus predicted shear crack width

The figures presented in Appendix C compare test results to the different methods used to predict the shear crack width in tested beams reinforced using FRP stirrups. Detailed discussion of observed shear versus shear crack width relationships can be found in section 6.5.2. The different methods used to predict the shear crack width, as indicated in Figures C-1 to C-9, are:

1. The modified compression field theory (MCFT): The shear crack width is determined according to the MCFT using the following equations (section 2.3.2):

$$w = \varepsilon_1 s_{m\theta} \quad (\text{C-1})$$

$$s_{m\theta} = 1 / \left(\frac{\sin \theta}{s_{ml}} + \frac{\cos \theta}{s_{mv}} \right) \quad (\text{C-2})$$

$$s_{ml} = 2 \left(c_l + \frac{s_l}{10} \right) + 0.25 k_1 \frac{d_{bl}}{\rho_{sl}} \quad (\text{C-3})$$

$$s_{mv} = 2 \left(c_v + \frac{s_v}{10} \right) + 0.25 k_1 \frac{d_{bv}}{\rho_{sv}} \quad (\text{C-4})$$

where ε_1 is the principal tensile strain, $s_{m\theta}$ is the diagonal crack spacing and s_{ml} and s_{mv} are the crack spacings indicative of the crack control characteristics of the longitudinal and transverse reinforcement; respectively. The principal tensile strain, ε_1 , is determined according to the MCFT using the computer program "RESPONSE" (section 6.6.3).

2. Equation (C-5) proposed by Hassan (1991):

$$w = \frac{1.8 S_d d_b}{10^6 (f'_c / 19.6)^2 \rho_{sv}^{1.3}} \quad (\text{C-5})^1$$

$$S_d = 8 \times 10^3 \varepsilon_{sv} + 2 \times 10^6 \varepsilon_{sv}^2$$

¹ Equation (2-55)

where S_d is the slip of stirrup, ε_{sv} is the measured stirrup strain at the load level under consideration and d_b is the bar diameter of the stirrup. It should be noted that equation (C-5) cannot be considered as a direct procedure for crack width estimation as it requires measured strain data.

3. Equation (C-6) proposed by Placas and Regan (1971):

$$w = \frac{s \sin \alpha}{10^6 \rho_{sv} (f'_c)^{1.3}} \left(\frac{V - V_{cr}}{b_w d} \right) \quad \text{units : lb, in.} \quad (\text{C-6})^2$$

where V_{cr} is the shear cracking load and is predicted using the ACI equation (2-27) and α is the angle of the stirrups ($= 90^\circ$ for vertical stirrups).

- 4) Equation (C-7)³ proposed for beams reinforced using FRP stirrups:

$$w = \frac{s}{10^6 \rho_{fv} \left(\frac{E_{fv}}{E_s} \right) (f'_c)^{1.3}} \left(\frac{V - V_c}{b_w d} \right) \quad \text{units : lb, in.} \quad (\text{C-7a})^3$$

$$w = \frac{27.6 s}{10^6 \rho_{fv} \left(\frac{E_{fv}}{E_s} \right) (f'_c)^{1.3}} \left(\frac{V - V_c}{b_w d} \right) \quad \text{units : N, mm} \quad (\text{C-7b})^3$$

where V_c is determined using equation (2-27) for beams reinforced for flexure using steel and using equation (7-11) for beams reinforced for flexure using FRP, E_{fv} is the elastic modulus of the FRP shear reinforcement and E_s is the elastic modulus of steel ($= 200$ GPa).

² Equation (2-57)

³ Equation (6-17)

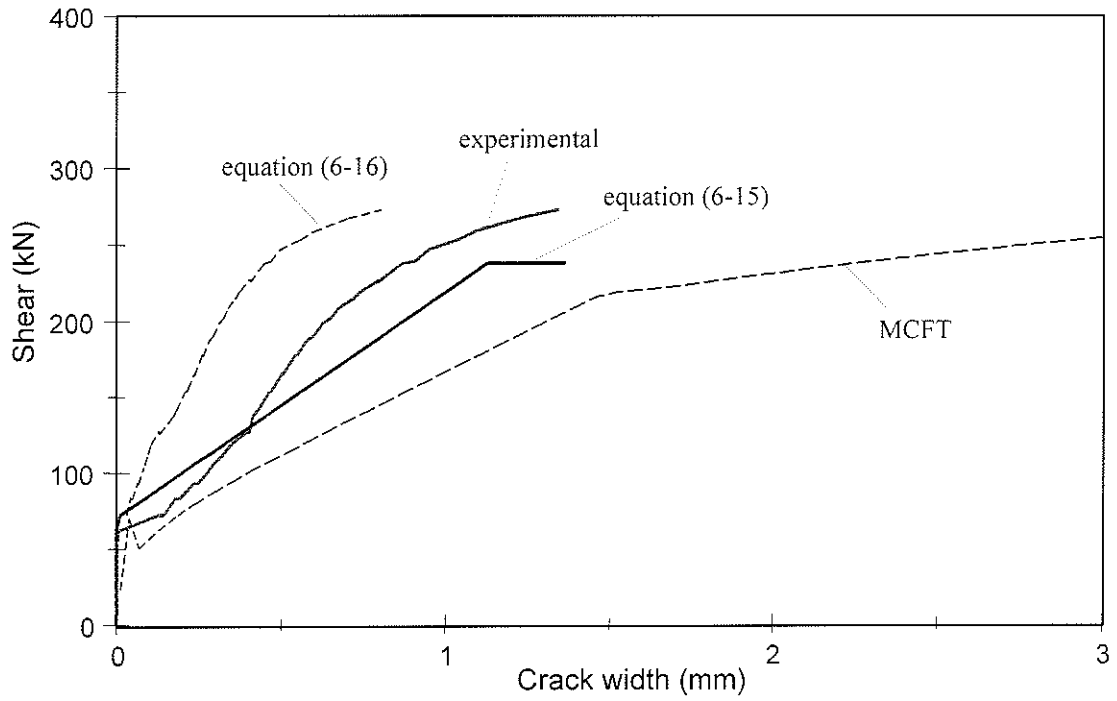


Figure C-1. Measured versus predicted shear crack width for beam SS-2

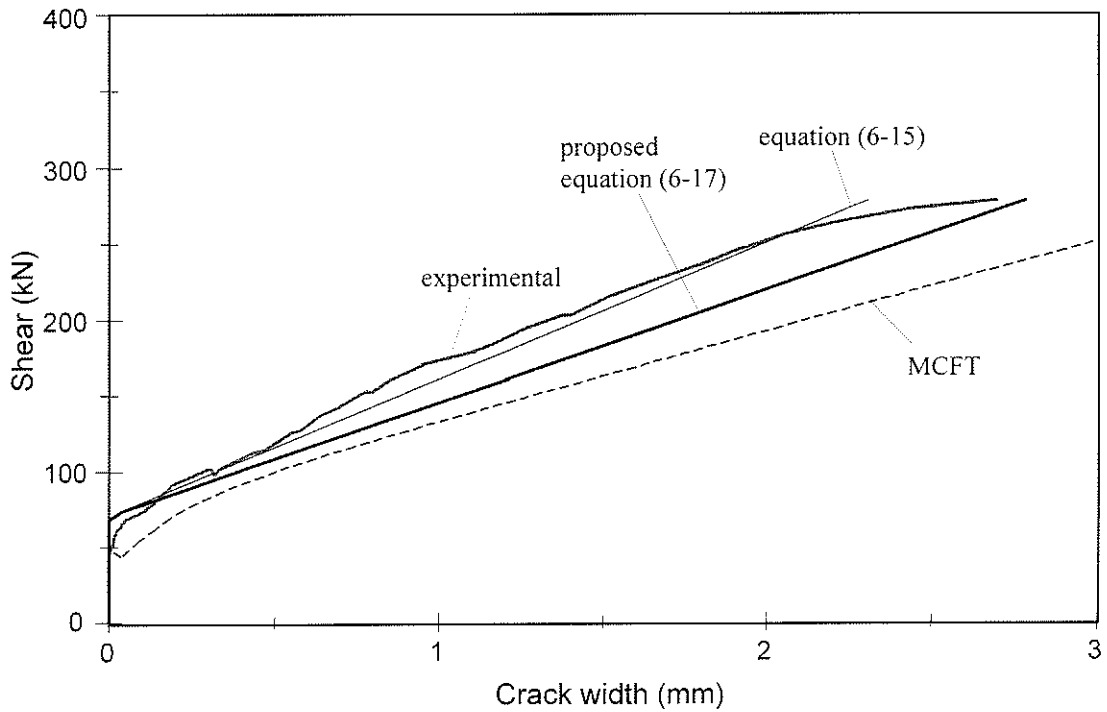


Figure C-2. Measured versus predicted shear crack width for beam SC-2

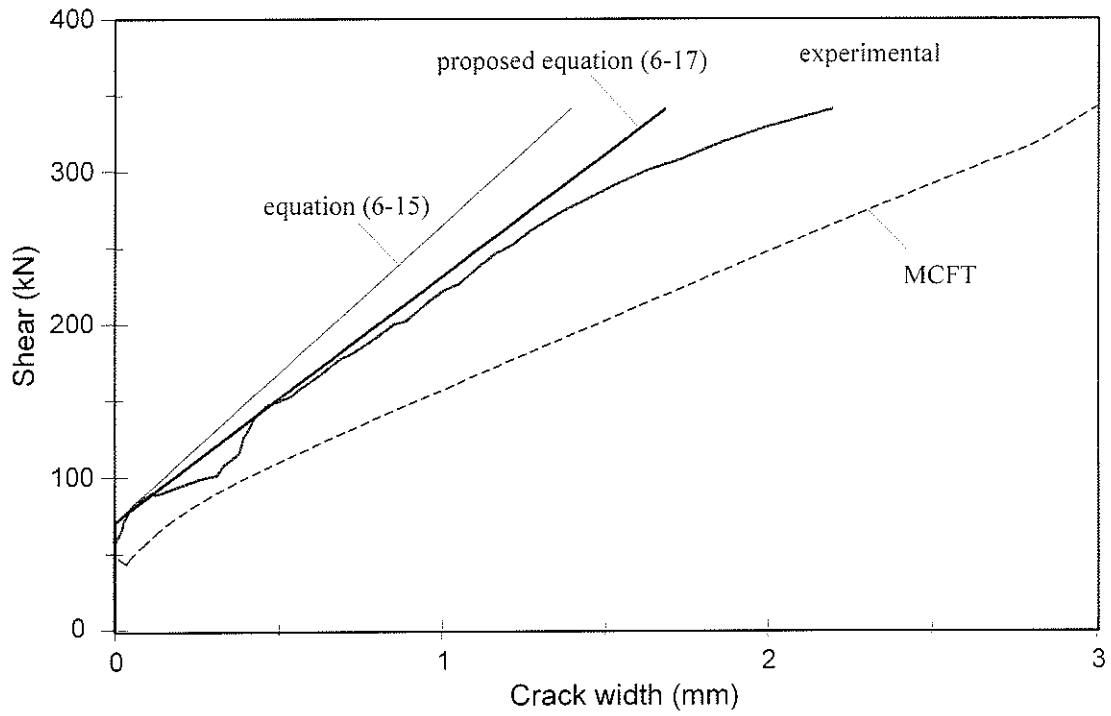


Figure C-3. Measured versus predicted shear crack width for beam SC-3

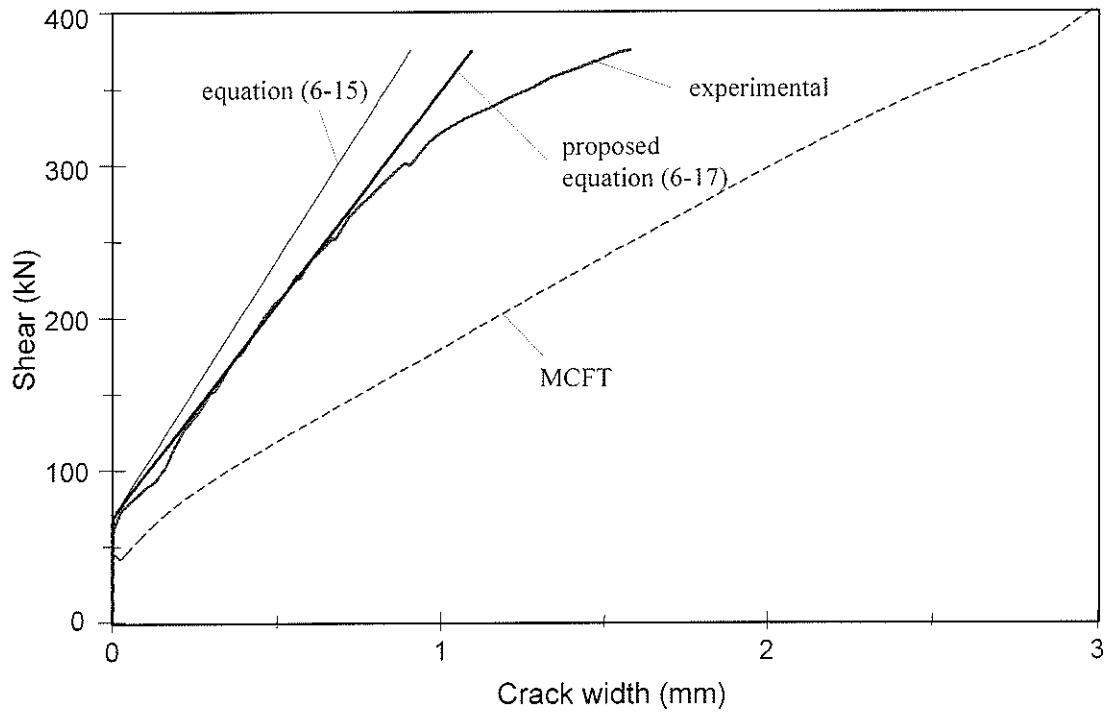


Figure C-4. Measured versus predicted shear crack width for beam SC-4

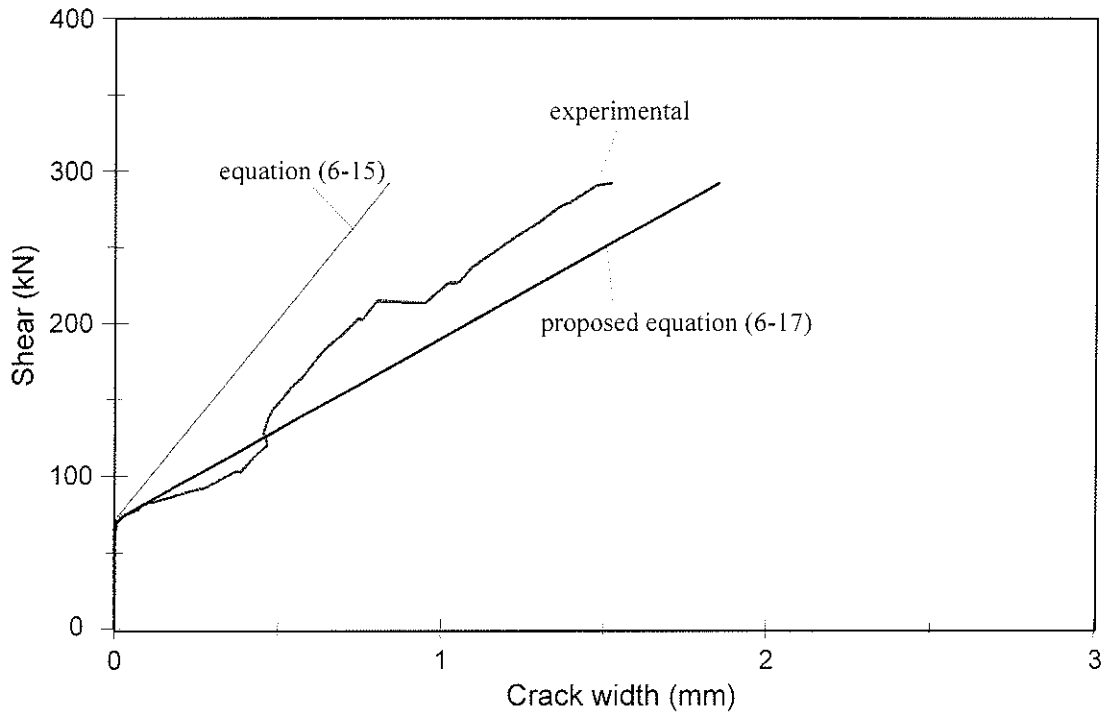


Figure C-5. Measured versus predicted shear crack width for beam SG-2

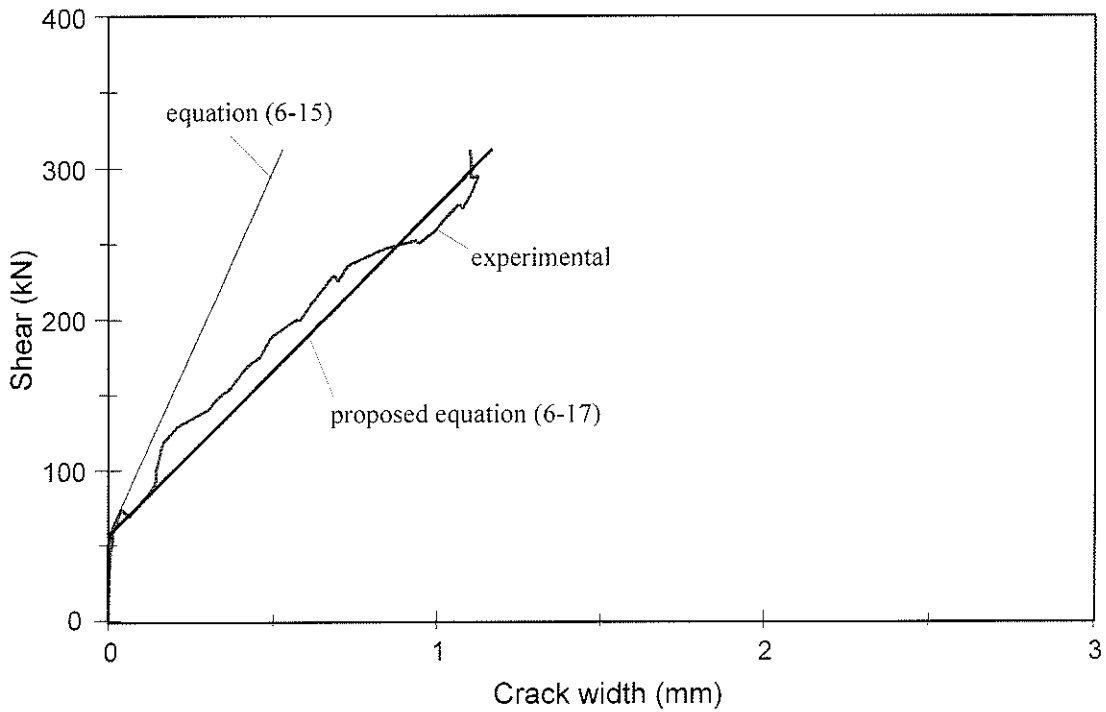


Figure C-6. Measured versus predicted shear crack width for beam SG-3

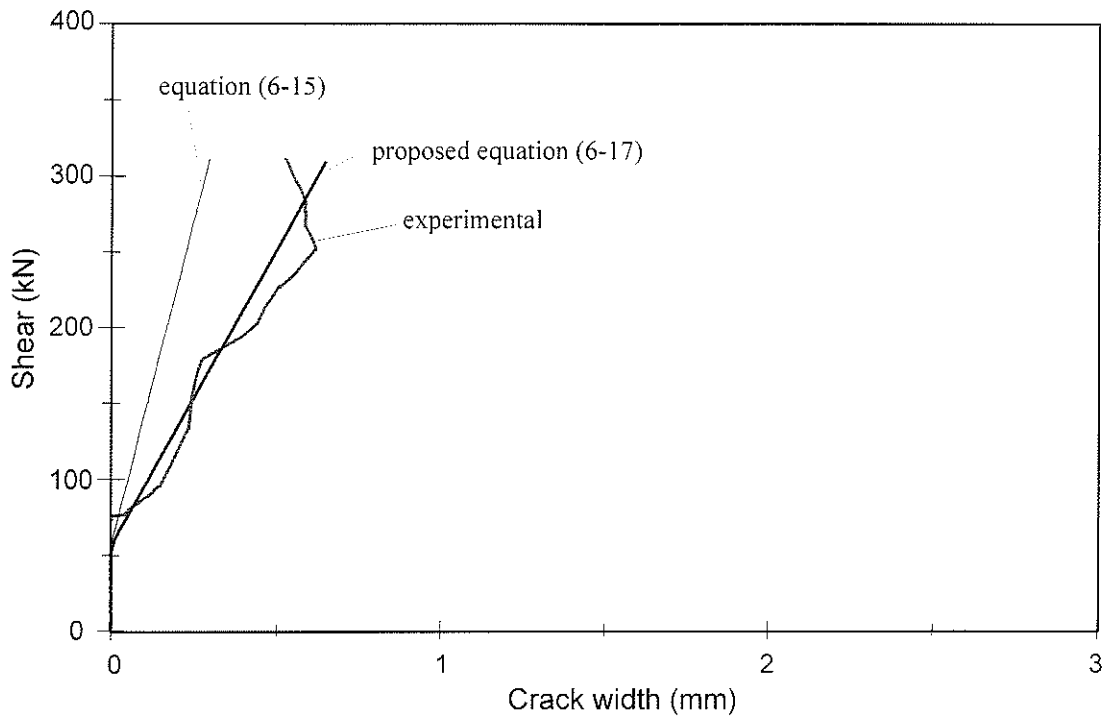


Figure C-7. Measured versus predicted shear crack width for beam SG-4

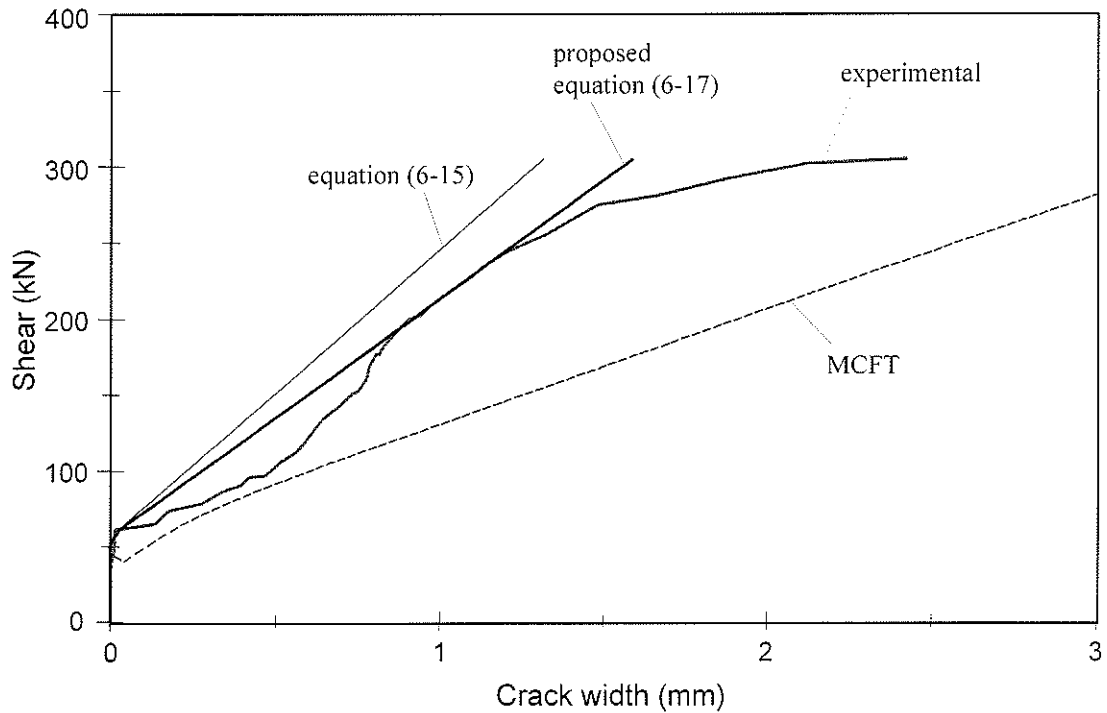


Figure C-8. Measured versus predicted shear crack width for beam CC-3

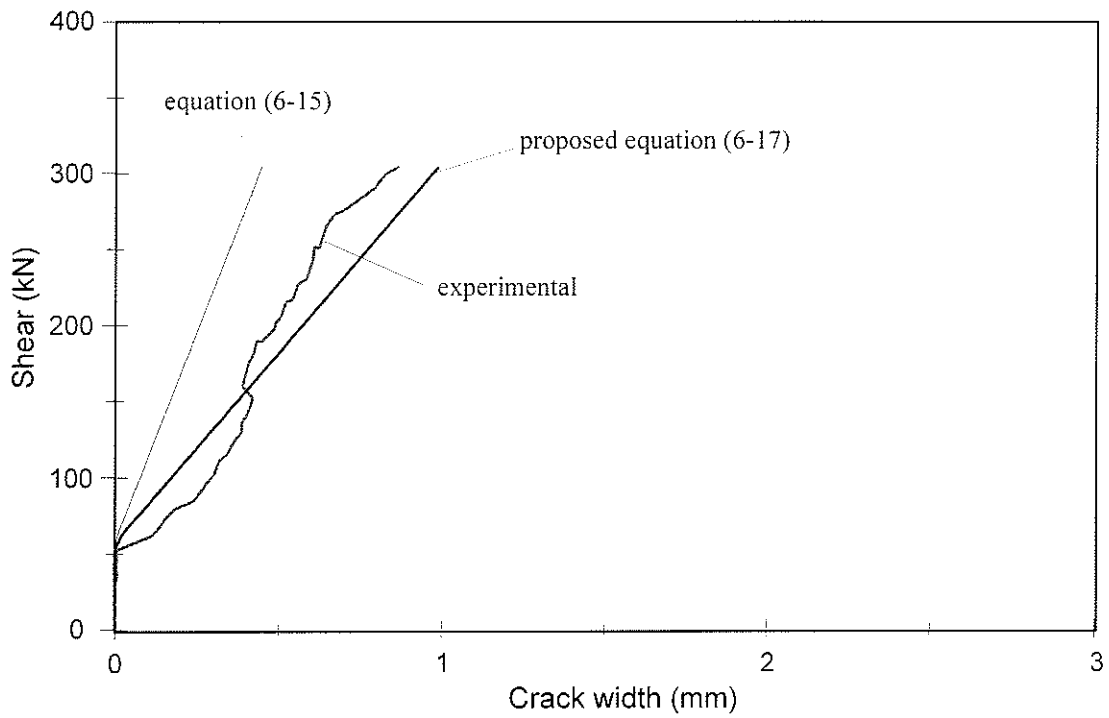


Figure C-9. Measured versus predicted shear crack width for beam CG-3

Appendix D
Design Example

The following example demonstrates the use of the proposed ACI and CSA shear provisions for the design of a concrete beam reinforced with FRP.

Example:

A normal weight concrete beam ($f_c' = 40$ MPa) needs to carry a service live load of 30 kN/m (assuming 50% is sustained) plus its own weight over a 6.7 m single span. The beam cross-section and longitudinal reinforcement are given in Figure D-1. Determine the required amount of shear reinforcement using GFRP C-BAR stirrups

Solution:

Given:

Dimensions: $b_w = 300$ mm, $d = 600$ mm, $h = 660$ mm, span = 6700 mm

Concrete strength: $f_c' = 40$ MPa

Flexural reinforcement: $A_{fl} = 1988$ mm², $\rho_{fl} = A_{fl}/b_w d = 0.01104$, $E_{fl} = 44.8$ GPa

Shear reinforcement: $f_{fv} = 713$ MPa; for #10 and #12 GFRP stirrups

$E_{fv} = 41$ GPa

Design according to proposed ACI provision:

Calculate dead loads: $w_d = 0.30 * 0.66 * 23.5 = 4.65$ kN/m

Calculate factored loads: $w_u = 1.4w_d + 1.7w_l = 1.4 * 4.65 + 1.7 * 30 = 57.5$ kN/m

Calculate factored shear and moment at critical section:

$$V_u = w_u (\text{span}/2 - a) = 57.5 * (6.7/2 - 0.70) = 152.4 \text{ kN}$$

$$M_u = w_u * \text{span}/2 * a - w_u a^2/2$$

$$= 57.5 * 6.7/2 * 0.70 - 57.5 * (0.70)^2/2 = 120.8 \text{ kN.m}$$

Calculate concrete contribution (equations 7-2 and 7-11):

$$V_{c(aci)} = \frac{1}{7} \left\{ \sqrt{f_c'} + 120 \rho_{fl} \frac{V_u d}{M_u} \right\} b_w d = 188.4 \text{ kN}$$

$$V_{cf} = V_{c(aci)} \left(\frac{E_{fl}}{E_s} \right)^{0.5} = 188.4 * \left(\frac{44.8}{200} \right)^{0.5} = 89.2 \text{ kN}$$

Determine the need for shear reinforcement:

$$\phi_f V_{cf} = 0.8 * 89.2 = 71.4 \text{ kN} < V_u$$

∴ shear reinforcement is needed

Determine minimum shear reinforcement (equation 7-17):

$$V_{sf_{min}} = V_{c(aci)} \left(1 - \sqrt{E_{fl}/E_s} \right) = 188.4 \left(1 - \sqrt{44.8/200} \right) \\ = 99.2 \text{ kN}$$

$$\rho_{fv_{min}} = \frac{V_{sf_{min}}}{\chi f_{fv}} \frac{b_w d}{b_w d} = \frac{99200}{0.4 * 713} \frac{300 * 600}{300 * 600} = 0.00193 \\ > \frac{0.345}{\chi f_{fv}} = \frac{0.345}{0.4 * 713} = 0.00121$$

Determine required shear reinforcement:

$$V_{sf} = V_u / \phi_f - V_{cf} = 152.4 / 0.8 - 89.2 = 101.3 \text{ kN}$$

using equation (7-7)

$$V_{sf} = \lambda f_{fv} \frac{A_{fv} d}{s}$$

take $s = 200 \text{ mm}$

$$A_{fv} = 101300 * 200 / (0.4 * 713 * 600) = 118.4 \text{ mm}^2$$

use GFRP C-BAR stirrups #10 (2 legs); $A_{fv} = 156 \text{ mm}^2$

Check shear reinforcement ratio:

$$\rho_{fv_{min}} = \frac{156}{200 * 300} = 0.0026 > \rho_{fv_{min}} = 0.00193$$

⇒ o.k.

Check shear-compression mode (equation 7-13):

$$\begin{aligned} V_{n_{max}} &= V_{cf} + \left\{ \frac{2}{3} \sqrt{f'_c} b_w d \right\} \left(\frac{E_{fv}}{E_s} \right)^{0.5} \\ &= 89.2 + \left\{ \frac{2}{3} \sqrt{40} * 300 * 600 \right\} \left(\frac{41}{200} \right)^{0.5} \\ &= 432.8 \text{ kN} > V_u / \phi_f = 190.5 \text{ kN} \end{aligned}$$

⇒ o.k.

Check serviceability requirement :

$$\begin{aligned} \text{sustained service load } w_{ser} &= w_d + 0.50 * w_l \\ &= 4.65 + 0.3 * 30 \\ &= 19.65 \text{ kN/m} \end{aligned}$$

$$\begin{aligned}
 V_{ser} &= w_{ser} (span/2 - a) \\
 &= 19.65 * (6.7/2 - 0.70) = 52.1 \text{ kN}
 \end{aligned}$$

$$V_{ser} = 52.1 \text{ kN} < V_{cf} = 89.2 \text{ kN} \quad \Rightarrow \text{o.k.}$$

\therefore the beam is not cracked in shear under service load level

Design according to the proposed simplified CSA provision:

Calculate dead loads: $w_d = 0.30 * 0.66 * 23.5 = 4.65 \text{ kN/m}$

Calculate factored loads: $w_u = 1.25w_d + 1.5w_l = 1.25 * 4.65 + 1.5 * 30 = 50.8 \text{ kN/m}$

Calculate factored shear and moment at critical section:

$$V_u = w_u (span/2 - a) = 50.8 * (6.7/2 - 0.70) = 134.6 \text{ kN}$$

$$M_u = w_u * span/2 * a - w_u * a^2/2$$

$$= 50.8 * 6.7/2 * 0.70 - 50.8 * (0.70)^2/2 = 106.7 \text{ kN.m}$$

Calculate concrete contribution (equation 7-20):

$$\begin{aligned}
 V_{cd(csa)} &= \frac{260}{1000 + d} \lambda \phi_c \sqrt{f'_c} b_w d \\
 &= \frac{260}{1000 + 600} * 0.6 * \lambda \sqrt{40} * \frac{300 * 600}{1000} = 111.0 \text{ kN}
 \end{aligned}$$

$$V_{cfd} = V_{cd(csa)} \left(\frac{E_{fl}}{E_s} \right)^{0.5} = 111.0 \left(\frac{44.8}{200} \right)^{0.5} = 52.5 \text{ kN}$$

Determine the need for shear reinforcement:

$$V_{cf} = 52.5 \text{ kN} < V_u$$

∴ shear reinforcement is needed

Determine minimum shear reinforcement (equation 7-26):

$$\begin{aligned} V_{sf_{min}} &= V_{c(\text{CSA})} \left(1 - \sqrt{E_f/E_s}\right) \\ &= 111.0 * \left(1 - \sqrt{44.8/200}\right) = 97.4 \text{ kN} \end{aligned}$$

$$\begin{aligned} \rho_{fv_{min}} &= \frac{V_{sf_{min}}}{\chi f_{fu}} \frac{b_w d}{s} = \frac{97400}{0.4 * 713} \frac{300 * 600}{600} = 0.00190 \\ &> \frac{0.06 \sqrt{f'_c}}{\chi f_{fu}} = \frac{0.06 \sqrt{40}}{0.4 * 713} = 0.00133 \end{aligned}$$

Determine required shear reinforcement:

$$V_{sfd} = V_u - V_{cfd} = 134.6 - 52.5 = 82.1 \text{ kN}$$

using equation (7-21)

$$V_{sfd} = \phi_f \chi f_{fu} \frac{A_{fv} d}{s}$$

take $s = 200 \text{ mm}$

$$A_{fv} = 82100 * 200 / (0.75 * 0.4 * 713 * 600) = 127.9 \text{ mm}^2$$

use GFRP C-BAR stirrups #10 (2 legs); $A_{fv} = 156 \text{ mm}^2$

Check shear reinforcement ratio:

$$\rho_{fv_{min}} = \frac{156}{200 * 300} = 0.0026 > \rho_{fv_{min}} = 0.00193 \Rightarrow \text{o.k.}$$

Check shear-compression mode:

$$\begin{aligned}
 V_{n_{max}} &= V_{cfd} + \left\{ 0.8 \lambda \phi_c \sqrt{f'_c} b_w d \right\} \left(\frac{E_{fv}}{E_s} \right)^{0.5} \\
 &= 52.5 + \left\{ 0.8 * 0.6 * \sqrt{40} * 300 * 600 \right\} \left(\frac{41}{200} \right)^{0.5} \\
 &= 247.5 \text{ kN} > V_u = 134.6 \text{ kN}
 \end{aligned}$$

⇒ o.k.

Check serviceability requirement :

$$\begin{aligned}
 \text{sustained service load } w_{ser} &= w_d + 0.50 * w_l \\
 &= 4.65 + 0.50 * 30 \\
 &= 19.65 \text{ kN/m}
 \end{aligned}$$

$$V_{ser} = 19.65 * (6.7/2 - 0.70) = 52.1 \text{ kN}$$

$$V_{ser} = 52.1 \text{ kN} < V_{cf} = 87.6 \text{ kN} \quad \Rightarrow \text{o.k.}$$

∴ the beam is not cracked in shear under service load level

Detailing of stirrups

The stirrup detailing is provided according to the proposed guidelines in section 5.7. The 10-mm GFRP C-BAR stirrups should have a bend radius of $4d_b$ (40 mm), and a tail length of 70 mm beyond the bend. The configuration of the stirrups is shown in Figure D-1.

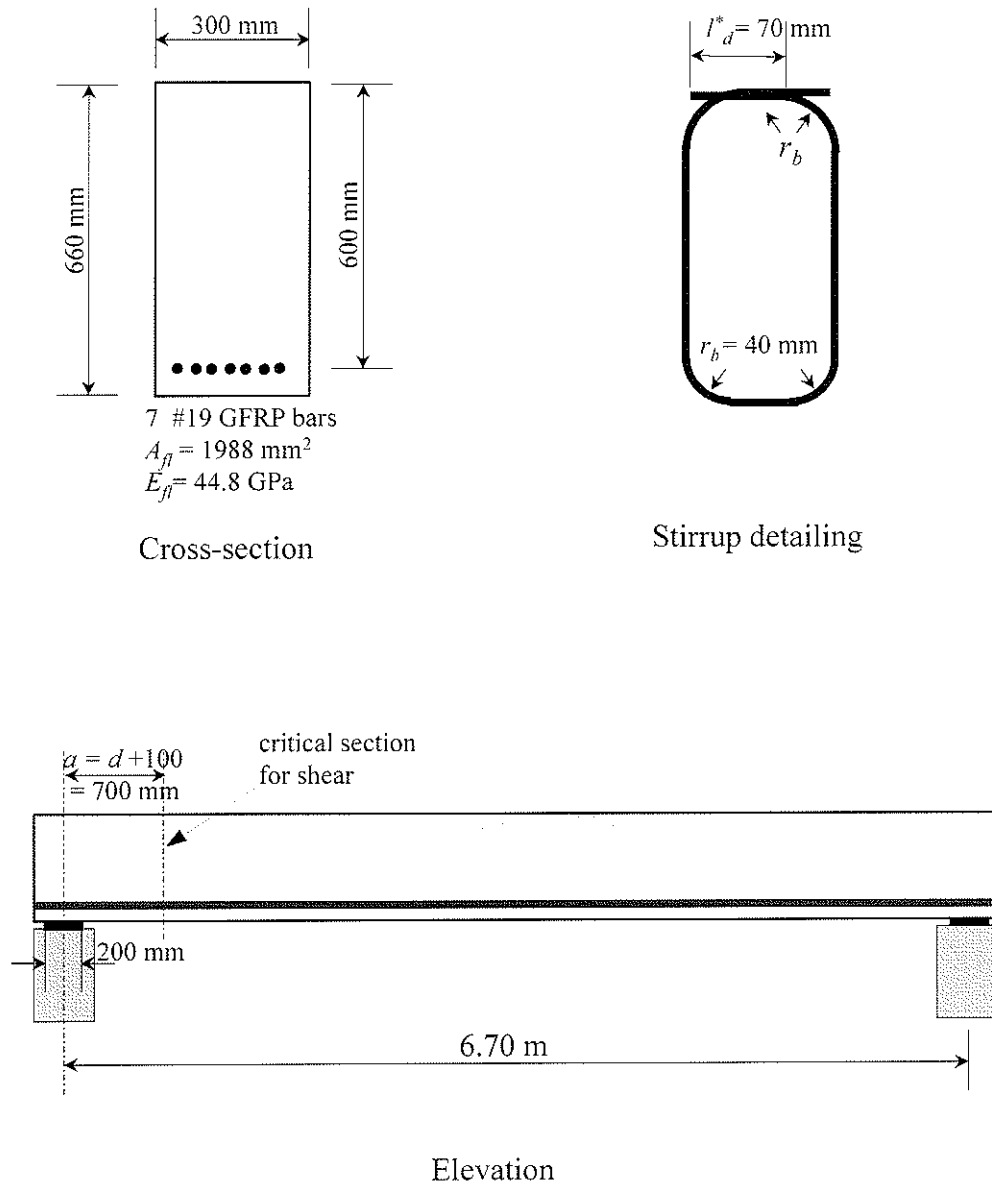


Figure D-1. Dimensions and details of the beam